frontiers | Research Topics

Improving memory deficits in alzheimer's disease

Edited by
Ralf J. Braun, Fushun Wang, Valentina Echeverria Moran and Shijun Xu

Published in
Frontiers in Aging Neuroscience

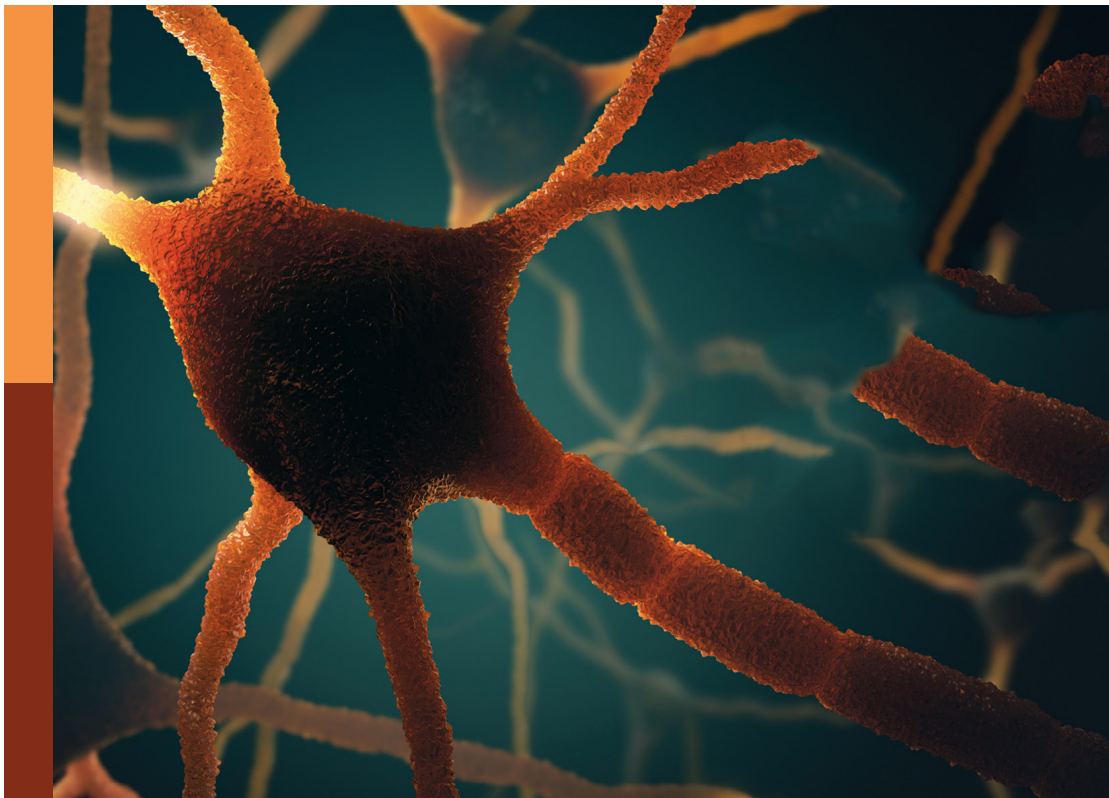

ISSN 1664-8714
ISBN 978-2-83250-919-7
DOI 10.3389/978-2-83250-919-7

About Frontiers

Frontiers is more than just an open access publisher of scholarly articles: it is a pioneering approach to the world of academia, radically improving the way scholarly research is managed. The grand vision of Frontiers is a world where all people have an equal opportunity to seek, share and generate knowledge. Frontiers provides immediate and permanent online open access to all its publications, but this alone is not enough to realize our grand goals.

Frontiers journal series

The Frontiers journal series is a multi-tier and interdisciplinary set of open-access, online journals, promising a paradigm shift from the current review, selection and dissemination processes in academic publishing. All Frontiers journals are driven by researchers for researchers; therefore, they constitute a service to the scholarly community. At the same time, the *Frontiers journal series* operates on a revolutionary invention, the tiered publishing system, initially addressing specific communities of scholars, and gradually climbing up to broader public understanding, thus serving the interests of the lay society, too.

Dedication to quality

Each Frontiers article is a landmark of the highest quality, thanks to genuinely collaborative interactions between authors and review editors, who include some of the world's best academicians. Research must be certified by peers before entering a stream of knowledge that may eventually reach the public - and shape society; therefore, Frontiers only applies the most rigorous and unbiased reviews. Frontiers revolutionizes research publishing by freely delivering the most outstanding research, evaluated with no bias from both the academic and social point of view. By applying the most advanced information technologies, Frontiers is catapulting scholarly publishing into a new generation.

What are Frontiers Research Topics?

Frontiers Research Topics are very popular trademarks of the *Frontiers journals series*: they are collections of at least ten articles, all centered on a particular subject. With their unique mix of varied contributions from Original Research to Review Articles, Frontiers Research Topics unify the most influential researchers, the latest key findings and historical advances in a hot research area.

Find out more on how to host your own Frontiers Research Topic or contribute to one as an author by contacting the Frontiers editorial office: frontiersin.org/about/contact

Improving memory deficits in alzheimer's disease

Topic editors

Ralf J. Braun — Danube Private University, Austria
Fushun Wang — Nanjing University of Chinese Medicine, China
Valentina Echeverria Moran — Bay Pines VA Healthcare System, Veterans Health Administration, United States Department of Veterans Affairs, United States
Shijun Xu — Chengdu University of Traditional Chinese Medicine, China

Citation

Braun, R. J., Wang, F., Moran, V. E., Xu, S., eds. (2022). *Improving memory deficits in alzheimer's disease*. Lausanne: Frontiers Media SA.
doi: 10.3389/978-2-83250-919-7

Table of contents

frontiers | Frontiers in Aging Neuroscience

TYPE Editorial
PUBLISHED 21 November 2022
DOI 10.3389/fnagi.2022.1066598

OPEN ACCESS

EDITED BY
Agustin Ibanez,
Latin American Brain Health Institute (BrainLat), Chile

REVIEWED BY
Juan C. Melendez,
University of Valencia, Spain

*CORRESPONDENCE
Fushun Wang
13814541138@163.com

SPECIALTY SECTION
This article was submitted to Alzheimer's Disease and Related Dementias, a section of the journal Frontiers in Aging Neuroscience

RECEIVED 11 October 2022
ACCEPTED 09 November 2022
PUBLISHED 21 November 2022

CITATION
Wang F, Braun RJ, Echeverria V and Xu S (2022) Editorial: Improving memory deficits in Alzheimer's disease. *Front. Aging Neurosci.* 14:1066598. doi: 10.3389/fnagi.2022.1066598

Editorial: Improving memory deficits in Alzheimer's disease

Fushun Wang[1]*, Ralf J. Braun[2], Valentina Echeverria[3,4] and Shijun Xu[5]

[1]Institute of Brain and Psychological Sciences, Sichuan Normal University, Chengdu, China, [2]Research Area Neurodegenerative Diseases, Center for Biosciences, Faculty of Medicine/Dental Medicine, Danube Private University, Krems an der Donau, Austria, [3]Bay Pines VA Healthcare System, Veterans Health Administration, United States Department of Veterans Affairs Bay Pines, Bay Pines, FL, United States, [4]Facultad de Medicina, Universidad San Sebastián, Concepción, Chile, [5]School of Pharmacy, Chengdu University of Traditional Chinese Medicine, Chengdu, China

KEYWORDS

Alzheimer's disease (AD), astrocyte, glymphatic system, memory, stress, cognitive deficit

Editorial on the Research Topic
Improving memory deficits in Alzheimer's disease

Alzheimer's disease (AD) is one of the most prevalent dementia causes, and accounts for > 80% of cases in the elderly. In addition, the incidence rate of AD is increasing, especially in people that suffered COVID-19. It is estimated that there will be over 150 million people with dementia across the world in 2050. This will put an immense pressure on social economic and healthcare and decrease the quality of life of the global population. The causes of the AD are still far from clear, despite many advances in recent years showing a prominent role of inflammation and the immune system. The most prominent symptom of AD is a progressive deterioration of cognitive functions, which includes working memory and long-term episodic memory. These impairments result in a wide range of devastating problems ranging from difficulties in simple daily lives to a complete loss of independent living and premature death.

Memory is affected by many factors, including both cognitive and emotional factors. Many studies have suggested that emotion arousal can enhance memory in both normal adults and AD patients (Nashiro and Mather, 2011; Kumfor et al., 2014). Previous studies in our lab have found that monoamine neuromodulators are the major substances for emotional arousal (Gu et al., 2018). And many studies showed that emotion related memory performance, central monoaminergic function and sympathetic nerve activity were lower in patients with dementia of the Alzheimer type (Corona et al., 1989). In addition, the monoamines can affect the function of astrocytes as well as the glymphatic system (Gu et al., 2019). It is found that chronic stress related monoamine neuromodulators such as norepinephrine can impair the function of glymphatic system and lead to tau accumulation and thus AD, while sleep can help the clearance function of the glymphatic system (Nedergaard and Goldman, 2020). In addition, the control of the cholinergic system with modulators of the nicotinic acetylcholine receptors with nicotine derivatives such as Cotinine to reduce neuroinflammation

and control stress resilience are new avenues explored (Echeverria et al., 2016).

Glymphatic system is modulated by stress and related monoamine neuromodulators, such as norepinephrine, dopamine and serotonin as well as choline, and affects the clearance of Aβ and tau protein (Iliff et al., 2015). In contrast, impairment of glymphatic system might be the major reason for AD (Nedergaard and Goldman, 2020). The glymphatic system is a recently found network that functions to clean up the protein metabolite and cell debris in the extracellular milieu, which plays a pivot role controlling inflammation and maintenance of brain homeostasis (Rasmussen et al., 2018). The structure of the glymphatic system has been recently defined with immunofluorescence staining of the meninges in the whole brain of mice (Louveau et al., 2015).

The discovery of the cerebral glymphatic system has provided a revolutionary perspective to elucidate the pathophysiological mechanisms of many neurodegenerative disorders (Mestre et al., 2020). The glymphatic system is regarded as a pivot supplementary system for blood circulation, which helps maintain homeostasis by removing large molecular substances produced by cell death or metabolism, and inducing immune reactions (Wen et al., 2022). Indeed, it is recently found that the impaired protein degradation and accumulation of inflammatory molecules as well as accumulation of ROS (reactive oxygen species) and autophagy might be the mechanisms of cognitive deterioration in the progression of AD (Li et al., 2021).

However, the treatment is far from effective, except that early prevention can alleviate the progressive deterioration of serious cognitive abilities. Searching for effective therapeutic approaches are critically important for the early diagnosed patients. The aim of this Research Topic is to collect recent studies on early diagnosis of AD by measuring memory performance and novel therapeutic approaches targeted at preventing memory loss in AD. As the brain abnormalities underlying memory deficits in AD are complex and multifactorial, we encouraged submissions investigating a wide range of therapeutic targets in patients and animal models. Our topic includes 12 papers describing new therapeutic approaches as follows.

In the experimental paper titled "*Attenuation of HECT-E3 ligase expression rescued memory deficits in 3xTg-AD mice,*" Suresh et al. studied the role of HECT-E3 ligases pathways in the context of AD pathogenesis by measuring the expressions of HECT-E3 ligases and their effects on inflammasome in autophagy. They found that M01 treatment reversed the HECT-E3 ligases induced working memory deficits of 3xTg-AD mice in T-maze and Morris water maze. In addition, the expression of the NLRP3 inflammasome protein were decreased together with the improved memory performance. They suggested that modulation of HECT-E3 ligase expression might be a strategy to treat early memory deficits in AD by decreasing NLRP3 activity and increasing the autophagy pathway.

In the experimental study, Zhao et al. introduced another paper titled "*Dihydroartemisinin Ameliorates Learning and Memory in Alzheimer's disease through Promoting Autophagosome-Lysosome Fusion and Autolysosomal Degradation for Aβ Clearance.*" In the paper, the authors investigated the effects of Dihydroartemisinin (DHA) on autophagy, which plays a pivot role in removing the damaged cell components, as well as the removal of toxic protein aggregates intracellularly and extracellularly to prevent AD. In this study, the authors found that DHA treatment can promote the clearance of Aβ fibrils, improve autophagy dysfunction, and have a multi-target effect on the neuropathological process, memory, and cognitive deficits of AD.

Jia et al. from University of Toronto reported one experimental paper, titled "*Inhibition of Rac1 in ventral hippocampal excitatory neurons improves social recognition memory and synaptic plasticity.*" In the paper, the authors probed into the effects of Rac1 in AD, which is critically involved in the regulation of the actin cytoskeleton, neuronal structure, synaptic plasticity and memory, and they found that the reduction of Rac1 hyperactivity in ventral hippocampal excitatory neurons improves social recognition memory in APP/PS1 mice.

In the experimental paper titled, "*Dihuang-Yinzi Alleviates Cognition Deficits via Targeting Energy-related Metabolism in an Alzheimer Mouse model as Demonstrated by Integration of Metabolomics and Network Pharmacology*," Han et al. introduced a kind of Chinese herb, named Dihuang-Yinzi (DHYZ), which has been used to treat AD and other neurodegenerative diseases for centuries. It is suggested energy metabolism disturbance and the consequent ROS overproduction play a key and pathogenic role in the onset and progression of Alzheimer's disease (AD). In the present study, the authors provided a novel, comprehensive and systematic insight into the therapeutic efficacy of DHYZ against AD *via* ameliorating energy-related metabolism.

In the experimental study, Shi et al. investigated the phosphodiesterase 4 (PDE4) dependent cAMP signaling in cognitive impairment associated with AD. They introduced the paper titled "*Phosphodiesterase-4D knockdown in the prefrontal cortex alleviates memory deficits and synaptic failure in mouse model of Alzheimer's disease*," which demonstrated that RNA interference (iRNA)-mediated PDE4D knockdown in the prefrontal cortex ameliorated memory loss, which is associated with synaptic failure in AD by its antioxidant, antiapoptotic and neuroprotective properties.

Ryou et al. reported an experimental study in the paper titled "*Intermittent Hypoxia Training Prevents Deficient Learning-Memory Behavior in Mice Modeling Alzheimer's disease: A Pilot Study.*" The authors used a mouse model of AD to investigate the effects of normobaric intermittent hypoxia training (IHT) on learning-memory behavior, and the results suggested that IHT diminishes Aβ accumulation in cerebral cortex and hippocampus, and increases the level of cerebrocortical brain-derived neurotrophic factor (BDNF) in

a mouse model of AD-like pathology. They concluded that moderate normobaric IHT prevented spatial learning-memory decline and restored cerebrocortical BDNF contents despite ongoing Aβ accumulation in 3xTg-AD mice. This finding is in agreement with previous studies showing an amelioration of cognitive abilities and a decrease of neuroinflammatory factors in the brain of AD mice treated with cRaf inhibitors (Burgess and Echeverria, 2010).

In the experimental study, Park et al. reported their studies about neurophysiological changes after a 24-week multi-domain intervention program in the paper titled "*Functional Brain Changes Using Electroencephalography after a 24-week Multidomain Intervention Program to Prevent Dementia.*" They showed positive biological changes, including increased functional connectivity and higher global efficiency on QEEG after a multidomain intervention program.

Brain-gut axis has recently been found to be involved in many neurodegenerative diseases (Xu et al., 2022). In the paper titled "*Effects of Tempeh Probiotics on Elderly with Cognitive Impairment,*" Handajani et al. showed that probiotic supplement-based therapies that alter the composition of gut microbiota can help prevent cognitive decline.

Blume et al. from German introduced another paper titled "*Chronic PPARγ Stimulation Shifts Amyloidosis to Higher Fibrillarity but Improves Cognition.*" In the paper, the authors performed longitudinal β-amyloid positron emission tomography (Aβ-PET) imaging while treated the Aβ model mice with peroxisome proliferator-activated receptor gamma (PPARγ) agonist pioglitazone. And they found that the treatment rescued from increases of the Aβ-PET signal while promoting spatial learning and preservation of synaptic density.

In the experimental study, Zheng et al. designed a study to test the feasibility of using hybrid convolutional neural networks and long-short term memory (CNN-LSTM) modeling in the treatment of AD. In the report titled "*Predicted cognitive conversion in guiding early decision-tailoring on patients with cognitive impairment,*" the authors suggested that the utilization of deep learning modeling and featured longitudinal information might be a good therapeutic strategy for AD.

In another study, Yamashita et al. reported a paper titled "*Long-term Effect of Acetylcholinesterase Inhibitors on the Dorsal Attention Network of Alzheimer's disease Patients: A Pilot Study Using Resting-state Functional Magnetic Resonance Imaging.*" In the paper, the authors used resting-state functional magnetic resonance imaging (rs-fMRI) to probe into the physiological dynamics of functionally connected brain networks in AD. The study found that the negative correlation between the frontal cortex and the dorsal attention network may be a biomarker of the therapeutic effect of AChEIs for AD.

In another paper titled "*Precision repetitive transcranial magnetic stimulation over the left parietal cortex improves memory in Alzheimer's disease: A randomized, double-blind, sham-controlled study,*" Jia et al. introduced a study about the effect of precision repetitive transcranial magnetic stimulation (rTMS) over the left parietal cortex on the memory and cognitive function in Alzheimer's disease (AD). They found that the target site of left parietal cortex can improve AD patients' cognitive function, especially memory, providing a potential therapy (Burgess and Echeverria, 2010).

Altogether, this topic highlight potential new therapies targeting a broad range of brain processes at functional and molecular level to treat AD. We hope that this Research Topic will inspire scientist worldwide to advance basic and clinical research to find effective therapies to treat AD.

Author contributions

FW wrote the paper. RB, VE, and SX helped with the revision. VE helped with manuscript writing. All authors contributed to the article and approved the submitted version.

Funding

This study was supported by the grants from the project supported by National Natural Science Foundation of China, China (No. 82171392) and Fondecyt, ANID 1190264 (VE).

Conflict of interest

The authors declare that the research was conducted in the absence of any commercial or financial relationships that could be construed as a potential conflict of interest.

Publisher's note

References

Burgess, S., and Echeverria, V. (2010). Raf inhibitors as therapeutic agents against neurodegenerative diseases. *CNS Neurol. Disord. Drug Targets* 9, 120–127. doi: 10.2174/187152710790966632

Corona, G. L., Cucchi, M. L., Frattini, P., Santagostino, G., Schinelli, S., Romani, A., et al. (1989). Clinical and biochemical responses to therapy in Alzheimer's disease and multi-infarct dementia. *Eur. Arch. Psychiatry Neurol. Sci.* 239, 79–86. doi: 10.1007/BF01759579

Echeverria, V., Yarkov, A., and Aliev, G. (2016). Positive modulators of the alpha7 nicotinic receptor against neuroinflammation and cognitive impairment in Alzheimer's disease. *Prog. Neurobiol.* 144: 142–157. doi: 10.1016/j.pneurobio.2016.01.002

Gu, S., Gao, M., Yan, Y., Wang, F., Tang, Y. Y., and Huang, J. H. (2018). The neural mechanism underlying cognitive and emotional processes in creativity. *Front. Psychol.* 9, 1924. doi: 10.3389/fpsyg.2018.01924

Gu, S., Wang, F., Patel, N. P., Bourgeois, J. A., and Huang, J. H. (2019). A model for basic emotions using observations of behavior in drosophila. *Front. Psychol.* 10, 781. doi: 10.3389/fpsyg.2019.00781

Iliff, J. J., Goldman, S. A., and Nedergaard, M. (2015). Implications of the discovery of brain lymphatic pathways. *Lancet Neurol.* 14, 977–979. doi: 10.1016/S1474-4422(15)00221-5

Kumfor, F., Irish, M., Hodges, J. R., and Piguet, O. (2014). Frontal and temporal lobe contributions to emotional enhancement of memory in behavioral-variant frontotemporal dementia and Alzheimer's disease. *Front. Behav. Neurosci.* 8, 225. doi: 10.3389/fnbeh.2014.00225

Li, X., Wen, W., Li, P., Fu, Y., Chen, H., Wang, F., Dai, Y., and Xu, S. (2021). Mitochondrial protection and against glutamate neurotoxicity via Shh/Ptch1 signaling pathway to ameliorate cognitive dysfunction by Kaixin San in multi-infarct dementia rats. *Oxid. Med. Cell. Longev.* 2021, 5590745. doi: 10.1155/2021/5590745

Louveau, A., Smirnov, I., Keyes, T. J., Eccles, J. D., Rouhani, S. J., Eske, J. D., et al. (2015). Structural and functional features of central nervous system lymphatic vessels. *Nature*. 523, 337–341. doi: 10.1038/nature14432

Mestre, H., Mori, Y., and Nedergaard, M. (2020). The brain's glymphatic system: current controversies. *Trends Neurosci.* 43, 458–466. doi: 10.1016/j.tins.2020.04.003

Nashiro, K., and Mather, M. (2011). Effects of emotional arousal on memory binding in normal aging and Alzheimer's disease. *Am. J. Psychol.* 124, 301–312. doi: 10.5406/amerjpsyc.124.3.0301

Nedergaard, M., and Goldman, S. A. (2020). Glymphatic failure as a final common pathway to dementia. *Science*. 370, 50–56. doi: 10.1126/science.abb8739

Rasmussen, M. K., Mestre, H., and Nedergaard, M. (2018). The glymphatic pathway in neurological disorders. *Lancet Neurol.* 17, 1016–1024. doi: 10.1016/S1474-4422(18)30318-1

Wen, W., Li, P., Liu, P., Xu, S., Wang, F., and Huang, J. H. (2022). Post-translational modifications of BACE1 in Alzheimer's disease. *Curr. Neuropharmacol.* 20, 211–222. doi: 10.2174/1570159X19666210121163224

Xu, Q., Jiang, M., Gu, S., Zhang, X., Feng, G., Ma, X., et al. (2022). Metabolomics changes in brain-gut axis after unpredictable chronic mild stress. *Psychopharmacology (Berl)*. 239, 729–743. doi: 10.1007/s00213-021-05958-w

frontiers in Aging Neuroscience

ORIGINAL RESEARCH
published: 02 March 2020
doi: 10.3389/fnagi.2020.00047

Dihydroartemisinin Ameliorates Learning and Memory in Alzheimer's Disease Through Promoting Autophagosome-Lysosome Fusion and Autolysosomal Degradation for Aβ Clearance

Yueyang Zhao[1], Zhimin Long[1,2], Ya Ding[1], Tingting Jiang[1], Jiajun Liu[1], Yimin Li[1], Yuanjie Liu[1,2], Xuehua Peng[3], Kejian Wang[1,2], Min Feng[1] and Guiqiong He[1,2]**

[1]Neuroscience Research Center, Chongqing Medical University, Chongqing, China, [2]Department of Human Anatomy, Basic Medical School, Chongqing Medical University, Chongqing, China, [3]Wuhan Children's Hospital, Tongji Medical College, Huazhong University of Science & Technology, Wuhan, China

OPEN ACCESS

Edited by:
Ralf J. Braun,
Danube Private University, Austria

Reviewed by:
Christian Griñán-Ferré,
Bosch i Gimpera Foundation, Spain
Valentina Echeverria Moran,
Bay Pines VA Healthcare System,
United States

***Correspondence:**
Min Feng
minfeng@cqmu.edu.cn
Guiqiong He
guiqionghe@cqmu.edu.cn

Received: 22 October 2019
Accepted: 11 February 2020
Published: 02 March 2020

Citation:
Zhao Y, Long Z, Ding Y, Jiang T, Liu J, Li Y, Liu Y, Peng X, Wang K, Feng M and He G (2020) Dihydroartemisinin Ameliorates Learning and Memory in Alzheimer's Disease Through Promoting Autophagosome-Lysosome Fusion and Autolysosomal Degradation for Aβ Clearance. Front. Aging Neurosci. 12:47. doi: 10.3389/fnagi.2020.00047

Dihydroartemisinin (DHA) is an active metabolite of sesquiterpene trioxane lactone extracted from Artemisia annua, which is used to treat malaria worldwide. DHA can activate autophagy, which is the main mechanism to remove the damaged cell components and recover the harmful or useless substances from eukaryotic cells and maintain cell viability through the autophagy lysosomal degradation system. Autophagy activation and autophagy flux correction are playing an important neuroprotective role in the central nervous system, as they accelerate the removal of toxic protein aggregates intracellularly and extracellularly to prevent neurodegenerative processes, such as Alzheimer's disease (AD). In this study, we explored whether this mechanism can mediate the neuroprotective effect of DHA on the AD model *in vitro* and *in vivo*. Three months of DHA treatment improved the memory and cognitive impairment, reduced the deposition of amyloid β plaque, reduced the levels of Aβ40 and Aβ42, and ameliorated excessive neuron apoptosis in APP/PS1 mice brain. In addition, DHA treatment increased the level of LC3 II/I and decreased the expression of p62. After Bafilomycin A1 and Chloroquine (CQ) blocked the fusion of autophagy and lysosome, as well as the degradation of autolysosomes (ALs), DHA treatment increased the level of

Abbreviations: Aβ, Amyloid-β peptide; AD, Alzheimer's disease; AL, Autolysosome; ALs, Autolysosomes; AP, Autophagosome; APP, Amyloid-β protein precursor; APs, Autophagosomes; APS, Ammonium persulfate; BACE1, β-site APP cleaving enzyme; Bafi, Bafilomycin A1; Cathepsin B, CTSB; CQ, Chloroquine; Control, CTRL; DHA, dihydroartemisin; DMSO, Dimethyl sulfoxide; DNs, dark neurons; ECL, Enhanced chemiluminescebce; GSK-3, Glycogen synthase kinase-3; IDE, Insulin degrading enzyme; IHC, Immunohistochemistry; LAMP-1, lysosome associated membrane protein 1; LC3, microtubule-associated protein light chain 3; LTP, long-term potentiation; mTOR, mammalian target of rapamycin; NEP, Neprilysin; PAGE, Polyacrylamide; PBS, Phosphate buffered saline; PBST, PBS with 0.1% Tween-20; PS1, Presenilin 1; PVDF, Polyvinylidene difluride; Rab7, Ras-related protein 7;RAPA, rapamycin;RILP, Rab-interacting lysosomal protein; SDS-PAGE, SDS-polyacrylamide gel; SP, Senile Plaque; Tau, Tau protein; TEM, transmission electron microscopy; TEMED, Tetramethylenediamine; WB, Western blotting; WT, Wild type.

LC3 II/I and decreased the expression of p62. These results suggest that DHA treatment can correct autophagic flux, improve autophagy dysfunction, inhibit abnormal death of neurons, promote the clearance of amyloid-β peptide (Aβ) fibrils, and have a multi-target effect on the neuropathological process, memory and cognitive deficits of AD.

Keywords: Alzheimer's disease, amyloid-beta, dihydroartemisinin, autophagic flux, autolysosomal degradation, autophagosome-lysosome fusion, cognitive deficits

INTRODUCTION

Alzheimer's disease (AD) has been known as one of the neurodegenerative diseases, manifested by chronic and progressive memory and cognitive deficits (Luheshi et al., 2008). Histopathologically, AD manifests *via* synaptic abnormalities, neuronal degeneration as well as the deposition of extracellular amyloid plaques and intraneuronal neurofibrillary tangles, which lead to a decline in memory and other cognitive functions. Beta-amyloid peptide (Aβ), which is mainly produced by the abnormal shearing of amyloid precursor protein (APP) by β-secretase and γ-secretase, respectively, is the core of senile plaque (SP) and plays a key role in AD pathogenesis (Folch et al., 2018). Excessive production and degradation of Aβ in cells lead to an imbalance and accumulation of Aβ metabolism. The imbalance of Aβ metabolism further leads to form extracellular SPs and a series of pathological changes of AD. Aβ excessive formation and blocked degradation impel SP deposition in the brain that, subsequently, accelerate the occurrence of overactive microglia, excessive apoptotic neurons and cerebral atrophy (Selkoe and Hardy, 2016; Nixon, 2017). In recent years, it has been found that extracellular Aβ is only the result of its toxic effect on cells, and the accumulation of intracellular Aβ is the fundamental factor leading to the cytotoxic effects (Esquerda-Canals et al., 2017). The degradation of extracellular Aβ is mainly completed by the insulin-degrading enzyme (IDE) and enkephalinase (Yamamoto et al., 2013, 2014), while the degradation of intracellular Aβ is mainly transported to lysosome through endocytosis or autophagy (Thal, 2015). The autophagy-lysosomal system dysfunction could directly affect APP metabolism and promote β-amyloidogenesis (Nixon, 2017). Thus, maintaining the stability of the autophagy–lysosomal network and strengthening the degradation of Aβ peptides in the lysosomes digestion system might be a promising strategy for treating AD. Macroautophagy (hereafter referred to as autophagy) is the main form of autophagy, and its role in neurodegenerative diseases has attracted much attention. Autophagy in healthy neurons is characterized by its high efficiency and continuous activation but low level (Boland et al., 2008) that accelerates the clearance of toxic and damaged intraneuronal and extracellular protein aggregates in lysosomes digestion system (Fecto et al., 2014). While in AD, autophagosomes (APs) accumulate owing to the stimulation of initiation of autophagy and sluggish rate of APs formation associated with failure to achieve adequate lysosome fusion as well as digestion (Uddin et al., 2019). Autophagy increases in the early stage of AD, which can play a role in scavenging Aβ, but excessive autophagy itself can also lead to increased production of Aβ. With the development of AD, the clearance of Aβ decreased due to the fusion of APs and lysosomes. The accumulation of APs due to the inhibition of degradation led to the further increase of Aβ production (De Strooper and Karran, 2016; Esquerda-Canals et al., 2017). So it has been reported that autophagy acts as a "double-edged sword" in the development of AD (Martinet et al., 2009; Choi et al., 2018; Hamano et al., 2018).

Autophagy flux, the rate at which long-lived protein aggregates are degraded by autophagy (Klionsky et al., 2016), includes the whole autophagy process, including the formation of autophagy structure, the transport of substrate to lysosome, the degradation of substrate and the release of macromolecule substances back to the cytoplasm (Yoon and Kim, 2016). In AD, dysfunctional autophagic flux was characterized as accumulating levels of APs in dystrophic neurites, whereas APP, Aβ peptides, β-site APP cleaving enzyme (BACE1) protein, damaged mitochondria and Golgi fragments are rich and cannot be cleared away by endosomal–lysosomal degradation process (Yu et al., 2005; Joshi and Wang, 2015; Feng et al., 2017; Kerr et al., 2017; Nixon, 2017). Therefore, the accumulation of APs not only affects the clearance of Aβ in cells but also could be the place where Aβ is produced. With increasing clinical researches and observations on the etiology, pathogenesis and candidate drugs of AD, the drugs which can reduce the production of pathological Aβ and promote the degradation of Aβ will be a new direction for the development of anti-AD drugs. Thus, maintaining highly efficient autophagy flux in brain homeostasis for maintaining Aβ-related production and degradation balance might be a promising strategy to treat AD.

In recent years, Chinese herbal medicine has received great attention in maintaining the efficient flux of autophagy in the brain. Artemisinins, a class of sesquiterpene trioxane lactone agents extracted from the ancient Chinese *herb Artemisia annua L*, has been used effectively to treat malaria (Lam et al., 2018) with universally acknowledged safety records in clinical trials (Kloprogge et al., 2018; Lohy Das et al., 2018). The main mechanism by which artemisinin acts in the treatment of malaria is activating autophagy to change the membrane structure of the parasite and, subsequently, starving the parasite (Chen et al., 2000). However, whether artemisinin can treat AD by regulating autophagy or not remains unclear. Dihydroartemisinin (DHA), the active metabolite of artemisinin, exhibits an ample array of autophagic activities as a drug intervention in many diseases (Jia et al., 2014; Jiang et al., 2016; Zhang et al., 2017), but no such study of DHA for AD treatment has ever been reported. One research has shown that DHA could be liable to penetrate the brain-blood barrier (Xie et al., 2009). In addition, low doses of DHA have beneficial effects on brain diseases, for example,

experimental cerebral malaria in mice (Dormoi et al., 2013). In the present study, we used DHA to treat APP/PS1 double transgenic AD mice and AD model cells, intending to investigate whether DHA would maintain Aβ related production and degradation balance *via* promoting autophagy flux and exert a protective effect in AD. *In vitro* and *in vivo* results suggested that DHA alleviated memory deficits, decreased Aβ production and neuritic plaque formation, ameliorates the autophagy flux in the brains of AD mice. The multitarget-regulating effects of DHA on autophagic flux were verified in AD cell models pretreated with chloroquine (CQ) and bafilomycin A1. In brief, our data suggest that DHA is effective in the prevention and treatment of AD through promoting autophagosome-lysosome fusion and autolysosomal degradation in autophagic flux to clear Aβ.

MATERIALS AND METHODS

Chemicals

DHA (≥98%, Aladdin, Shanghai, China; **Figure 1**) was prepared and characterized in our laboratory according to previously described methods (Peters et al., 2003). DHA was dissolved in 10% dimethyl sulfoxide (DMSO, Amresco, USA) for oral treatment of mice. For cell treatments, DHA, bafilomycin A1 (Selleck, USA) and rapamycin (Gene Operation, USA) were dissolved in 100% DMSO as 50 mM stock solutions and stored for later use. CQ was dissolved in phosphate-buffered saline (PBS; 1× pH 7.4) as a 50 mM stock solution.

Animals and Cells

In our pre-experiments, five male mice and five female mice per group were taken to assess their behavioral and pathological changes in the AD pathological course. We preliminarily found that no significant difference can be noted in DHA-treated model mice across genders. Thus, we chose only male mice for this study. The experiments were carried out utilizing male APPswe/PSEN1dE9 double-transgenic (APP/PS1) mice and non-transgenic (wild type, WT) littermates that were purchased from the Biomedical Research Institute of Nanjing University (Nanjing, China). A number of qualitative qualification for mice: 201803104 and 201806178. The mice were housed from ages 3- to 9-months-old in a laminar flow rack exposed to a 12 h light/dark cycle, with free access to water and standard rodent chow. All experimental procedures were performed in accordance with the guidelines approved by the Animal Protection and Ethics Committee of Chongqing Medical University.

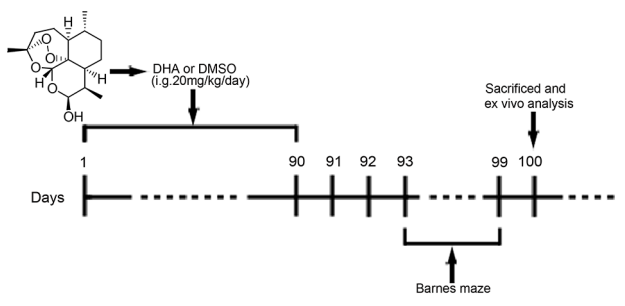

FIGURE 1 | Chemical structure of dihydroartemisinin (DHA) and experimental protocol scheme. Mice received intragastric (i.g.) treatments for 90 days until the beginning of the behavioral tests. From the 93rd day of the experimental protocol, the animals were subjected to Barnes maze tests. On the 100th day, the mice were euthanized for *in vivo* analysis.

Mouse neuroblastoma cell line Neuron-2a/APPswe (N2a-APP) cells and differentiated SH-SY5Y cells stably transfected with the APPswe gene (APP-SH-SY5Y) were gifts from Professor Zhifang Dong at the Laboratory of Translational Medical Research in Cognitive Development and Learning and Memory Disorders, Children's Hospital of Chongqing Medical University (Chongqing, China), and the APP-SH-SY5Y cells were confirmed to be human through STR profiling. The N2A-APP cells were maintained in 90% DMEM (Gibco/Thermo Fisher Scientific, Waltham, MA, USA) and 10% fetal bovine serum (FBS, Biological Industries, USA) with 100 μg/ml G418. The APP-SH-SY5Y cells were cultured in 90% DMEM with 10% FBS, 100 U/ml penicillin and 100 μg/ml streptomycin. All cells were maintained at 37°C in 5% CO_2 and 95% air (v/v).

Drug Treatment/Administration

At 6 months old, APP/PS1 mice and WT mice were randomly divided into the DHA-treated AD group, DMSO-treated AD group, and DMSO-treated WT group (15 per group) and were administered DHA (20 mg/kg/day, intragastric administration, once daily) or an equal amount of DMSO for 3 months. Pharmacological studies using a dosage of 20 mg/kg/day per mouse were based on the scope of safe doses for adults, children and pregnant women from related studies (Chairat et al., 2018; Kloprogge et al., 2018; Chotsiri et al., 2019) and the formulas in the Conversion of Animal Doses to Human Equivalent Doses FDA guidelines (U.S. Department of Health and Human Services, Center for Drug Evaluation and Research (CDER), 2005). In these studies, 3 months of treatment for 6-month-old APP/PS1 mice were in accordance with the initial stage of Aβ deposition in this mouse model Xiang et al., 2015), which might support the preventive potential of DHA treatment in AD. After 3 months of treatment, behavioral tests were initiated. The day after the final day of behavioral tests, the mice were euthanized, and the brains were removed for *ex vivo* experiments. The experimental protocol is shown in **Figure 1**. Because artemisinin and its derivatives were mainly metabolized in the liver (Gautam et al., 2009), the safety of DHA in mice for three months was reflected by the concentration of the serum GPT/ALT and GOT/AST B36 (**Supplementary Figure S1**) and was verified it drug safety.

Bafilomycin A1 was diluted to 1 nM for APP-SH-SY5Y cells and 50 nM for N2A-APP cells (Guo et al., 2017). CQ was diluted to 10 μM for APP-SH-SY5Y cells and 25 μM for N2A-APP cells (Xu et al., 2018). Rapamycin was diluted to 100 nM for APP-SH-SY5Y cells and N2A-APP cells (Xu et al., 2018). The final concentration of DMSO was <0.1%. The CON groups were treated with the same concentration of DMSO or PBS.

Cell Proliferation Assay

The cells were incubated in 96-well flat-bottom plates (1.0×10^4 cells/well) with 0, 0.05, 0.5, 1, 5 and 50 μM DHA for 24 h before

cell proliferation was assessed. Cell growth was analyzed using CCK-8 cell proliferation and cytotoxicity assay kit (Solarbio, Shanghai, China). Absorbance at 450 nm was measured using an ultra microplate reader (Thermo Scientific, USA).

Behavioral Tests

Spatial learning and memory were assessed using the Barnes maze task in accordance with Pompl et al. (1999) but with minor modifications (Souza et al., 2012). The Barnes maze consists of a flat, circular disk (122 cm diameter) with 18 circular holes (5 cm diameter) at equal distances around the perimeter and rising 100 cm above the floor. The escape box (13 × 29 × 14 cm) was kept under one hole. The mice learned the location of the escape box under the hole using spatial reference points fixed to the wall. Animals were trained in the Barnes maze on the first day for one trial. Training consisted of placing the animal in a black box and leaving it for a minute. Then, the black box was placed in the center of the Barnes maze. The black box was removed, and then the training began. The mice freely explored the maze to find the escape box under the hole. The maximum latency to finding the escape box was 300 s. The latency to reach the escape box and the number of wrong holes was measured. After the first day of training, the test began, and the data for two trials were recorded over the next 5 days. On the seventh day, the escape box was removed, each mouse was placed in the center of the maze. The number of attempts to find the escape box and the number of other holes was reported.

Preparation of Brain Tissue and Cells

At the end of treatment, the mice were euthanized by CO_2 inhalation. Mice (n = 16 per group) were perfused transcardially with 0.01 M PBS (pH 7.4). The left cerebral hemisphere was bluntly dissected to the hippocampus and cortex for ELISA, and the right cerebral hemisphere was prepared for histological staining and Western blotting (WB). The rest cerebral hemisphere was used for transmission electron microscopy (TEM).

For histological staining, excised brains were immersed in 4% paraformaldehyde overnight, 20% sucrose for 24 h and 30% sucrose for another 48 h. Then, the brains were embedded in optimum cutting temperature compound in a freezing microtome, and 10 μm-thick sections were cut with a freezing microtome (Leica, Germany).

For TEM, mice from each group were transcardially perfused with 0.01 M PBS, followed by 2.5% glutaraldehyde 4% paraformaldehyde in 0.01 M PBS. The brain was quickly stripped in an ice bath. Brain tissues (1 mm^3 thick) were cut from the hippocampal CA1 area and were fixed in 2.5% special glutaraldehyde solution for 2 h for TEM, washed several times with 0.01 M PBS, postfixed in 1% osmium tetroxide in 0.01 M PBS for 2 h and dehydrated with gradient alcohol. Tissue samples were embedded in Epon812 epoxy resin. Tissue blocks were then cut into 1-μm sections, placed on slides, stained with azure-methylene blue (Sino Chemical Co., Ltd., Zhengzhou, China), and visualized under a light microscope (Leica Microsystems, Wetzlar, Germany). The areas were selected from semi-thin sections and then cut into thin sections. The APP-N2a cells were prefixed in a 2.5% glutaraldehyde solution overnight at 4°C and postfixed in cold 1% aqueous osmium tetroxide for 1 h at 4°C. The samples were rinsed three times with PBS, dehydrated in a graded series of 25%–100% ethanol, embedded in fresh resin and polymerized at 60°C for 24 h. The samples were sectioned on a Leica EM UC6 ultramicrotome at 60–80 nm and collected on pioloform-coated Cu2*1 oval slot grids (Electron Microscopy Sciences, Hatfield, PA, USA).

TEM

After uranyl acetate/lead citrate double staining (Sansd Plastic Co., Ltd, Fujian, China), neurons, gliocytes and their ultrastructures in brain sections were observed by TEM (Philips, Amsterdam, Netherlands). For cells, the sections were subsequently examined under a Hitachi7500 transmission electron microscope (Philips, Amsterdam, Netherlands). The morphological ultrastructures and status of APs and lysosomes in cells were photographed for each group.

Histological Staining

For Thioflavin S staining, brain slices were mounted onto slides and washed three times with 0.01 M PBS for 5 min each. The washed brain slices were incubated in acetone for 10 min at room temperature, washed in 80% ethanol, 70% ethanol, and distilled water for 30 s, respectively. After that, slices were incubated in 0.1% $KMnO_4$ for 30 s and then washed with distilled water, 70% ethanol, and 80% ethanol for 30 s. Subsequently, Thioflavin S (0.1% in 80% ethanol) was dripped on the slides for 15 min at room temperature in the dark. Finally, the sections were covered with coverslips. They were then photographed using fluorescence microscopy.

For immunohistochemistry, brain sections were mounted onto slides for staining. The slices were incubated in 88% formic acid for 10 min and washed in 0.01 M PBS three times. Then, the slices were incubated in 3% H_20_2 peroxidase and citrate buffer (Bioss, Beijing, China; pH 6.0) for 30 min. Tissues were then blocked with 5% fetal calf serum (HyClone, Logan, Utah, UT, USA) in 0.3% Triton X-100 for 30 min at 37°C. Then, the tissues were incubated overnight at 4°C with the mouse monoclonal antibody 4G8 (1:200 dilution; Biolegend, USA). After rinsing, a biotinylated secondary antibody (1:200 dilution; Vector Laboratories, Burlingame, CA, USA) was added to tissue sections for 30 minutes at 37°C, followed by the avidin-biotin-peroxidase complex (Vectastain ABC kit; Vector Laboratories) according to the manufacturer's protocol. Immunoreactivity was visualized. Plaques were visualized by the ABC and diaminobenzidine (DAB) method and counted under microscopy at 40× magnification. A minimum of three washes with 0.01 M PBS was completed between steps.

To assess autophagic flux in response to DHA, autophagic agonists and antagonists were used, and a tandem mRFP-GFP-LC3 adenovirus (Hanheng Biotechnology Co Ltd., Shanghai, China) was transfected into cultured APP-SH-SY5Y cells for 24 h at an MOI of 50. On the 2nd day following transfection, 1 μM DHA, 100 nM rapamycin, 10 μM CQ, and 1 nM bafilomycin A1 were added to the corresponding groups for 24 h. After fixing the cells with PFA and DAPI staining, autophagy was observed

under a TCS-TIV confocal laser scanning microscope (Leica Microsystems). The tandem mRFP-GFP-LC3 protein showed both red (mRFP) and green (GFP) fluorescence at neutral pH and formed yellow (red+green) puncta that represent APs formation (Kimura et al., 2007). The relative ratio of positive dots near the nucleus vs. the total number of dots is an index of autophagic flux.

Western Blotting Analysis

Protein expression was analyzed by immunoblot analysis. Total protein extract was prepared using RIPA lysis buffer (Beyotime Biotechnology, Shanghai, China), which was supplemented with phenylmethanesulfonylfluoride (Beyotime Biotechnology, Shanghai, China) according to the manufacturer's instructions. Total protein concentration was determined using an enhanced BCA protein assay kit (Beyotime Biotechnology, Shanghai, China). Equal amounts of proteins were resolved using a 6%–12% SDS-PAGE gel kit (CWBIO, Beijing, China) and transferred onto polyvinylidene fluoride membranes (Millipore, USA). The membranes were incubated overnight at 4°C with the following primary antibodies: SQSTM1/p62 (#5114), LC3 (#3868), Rab7 (#9367), Cathepsin B/CTSB (#31718), ATG5 (DF6010), ATG12 (DF7937), ATG16L1 (DF3825), mammalian target of rapamycin (mTOR; AF6308), phospho-mTOR (Ser2448; AF3308), ULK1 (DF7588), phospho-ATG14 (Ser29; AF2320; all from Affinity Biosciences, USA); ATG14 (NBP2-36445, Novus Bio, USA); RILP (ab140188, Abcam, USA); Beclin1 (ab62557), Lamp1 (ab24170), APP (ab32136), BACE1 (ab183612), Presenilin 1/PS1 (ab76083), IDE (ab133561) and neprilysin/NEP (ab58968). After washing, the membranes were incubated for an hour at room temperature with horseradish peroxidase-conjugated secondary antibodies. The immunoblots were visualized using enhanced chemiluminescence WB detection kits and then visualized using a molecular imager with Image Lab software (Bio-Rad, CA, USA). Protein bands were also quantified with Image Lab software (Bio-Rad, CA, USA). Equal loading of proteins was verified by β-actin (#A5441, Sigma, USA) and GAPDH (AF7021, Affinity Biosciences, USA) immunoblot analysis. At least three separate experiments were performed with different lysates to confirm the changes in protein levels. List of effective concentrations of primary antibodies in Western blotting see **Supplementary Figure S2**.

ELISA

The levels of Aβ40 and Aβ42 were detected using ELISA kits by technicians who were blinded to the experimental groups. For the detection of Aβ40 and Aβ42 levels in cells, the cells were washed, trypsinized, and lysed in extraction buffer (1% CHAPS in TBS, pH 7.6). Intracellular Aβ40 and Aβ42 were then detected. The volume of the medium used was adjusted to the protein concentrations measured in total cell lysates. For the detection of soluble or insoluble Aβ40 and Aβ42 in the brains of WT and APP/PS1 mice, dissected tissue was homogenized in 5 volumes of extraction buffer (1% CHAPS in TBS, pH 7.6). Then, all mixtures were placed on ice for at least 3 h. The homogenates were centrifuged at 70,000 rpm for 20 min at 4°C, and the supernatants were diluted with EIA buffer contained in the kit for the analysis of soluble Aβ40 and Aβ42.

Statistical Analysis

All data are expressed as the mean ± standard error of the mean (SEM). Data were analyzed by GraphPad Prism 5 (GraphPad Software, Inc., La Jolla, CA, USA). For the examination of statistically significant differences between two groups, a two-sided, unpaired Student's *t*-test was used, and for multiple comparisons, a one-way ANOVA followed by the Newman–Keuls test was used. In the Barnes maze training, statistical analysis was performed using a two-way ANOVA followed by the Newman–Keuls test and one-way analysis of variance/Newman–Keuls test for the probe test. The main effects are presented only when the higher second-order interaction was not significant. Values of $p < 0.05$, $p < 0.01$, and $p < 0.001$ were considered statistically significant.

RESULTS

Oral DHA Alleviated Memory and Cognitive Deficits in APP/PS1 Double Transgenic Mice

After 3 months of treatment, the mice began the Barnes test, which evaluates spatial learning and memory. After the adaptive training on the first day, the latency to find the escape box and the number of wrong holes visited revealed the main effects of the next 5 days of training for the mice. Mice moving tracks in the CTRL group (**Figure 2A**), the AD group (**Figure 2B**), the AD-DHA group (**Figure 2C**) see in **Figure 2**. *Post hoc* comparisons showed that on the second (ANOVA: $F_{(3,20)} = 0.6152$, $p = 0.8610$) and third days ($F_{(3,20)} = 0.7752$, $p = 0.4654$), no change in the latency to find the escape box was observed between the groups. Moreover, no significance was noted in the number of wrong holes visited on the second ($F_{(3,20)} = 2.103$, $p = 0.1337$) or the third day ($F_{(3,20)} = 0.8793$, $p = 0.4213$). On the fourth, fifth and sixth days of training, DMSO-treated AD mice had significantly increased latency to find the escape box (+99.64%, 274.29%, and 163.59%, respectively; **Figure 2D**) and the number of wrong holes visited (+147.78%, 207.53%, and 166.37%, respectively; **Figure 2E**) when compared to WT mice. Treatment with DHA for AD mice significantly protected against these increases on the fourth, fifth and sixth days of training (−37.20%, 53.94%, and 55.23%, respectively; **Figure 2D**; −52.41%, 40.43% and, 40.56%, respectively; **Figure 2E**), when compared to those of the DMSO-treated AD mice.

In the probe test, one-way ANOVA followed by a Newman–Keuls *post hoc* test demonstrated that DMSO-treated AD mice had a decrease in the number of entries into the target hole (55.75%) and an increase in the number of entries into other holes (110.96%), when compared with that of WT mice, and DHA significantly enhanced the accuracy of finding escape holes (approximately 76%) and recognizing the wrong holes (48.92%; **Figures 2F,G**). Mice treated with DHA did not change their behavioral parameters when compared to those of the WT group (**Figures 2F,G**; $F_{(3,20)} = 6.003$, $p < 0.01$).

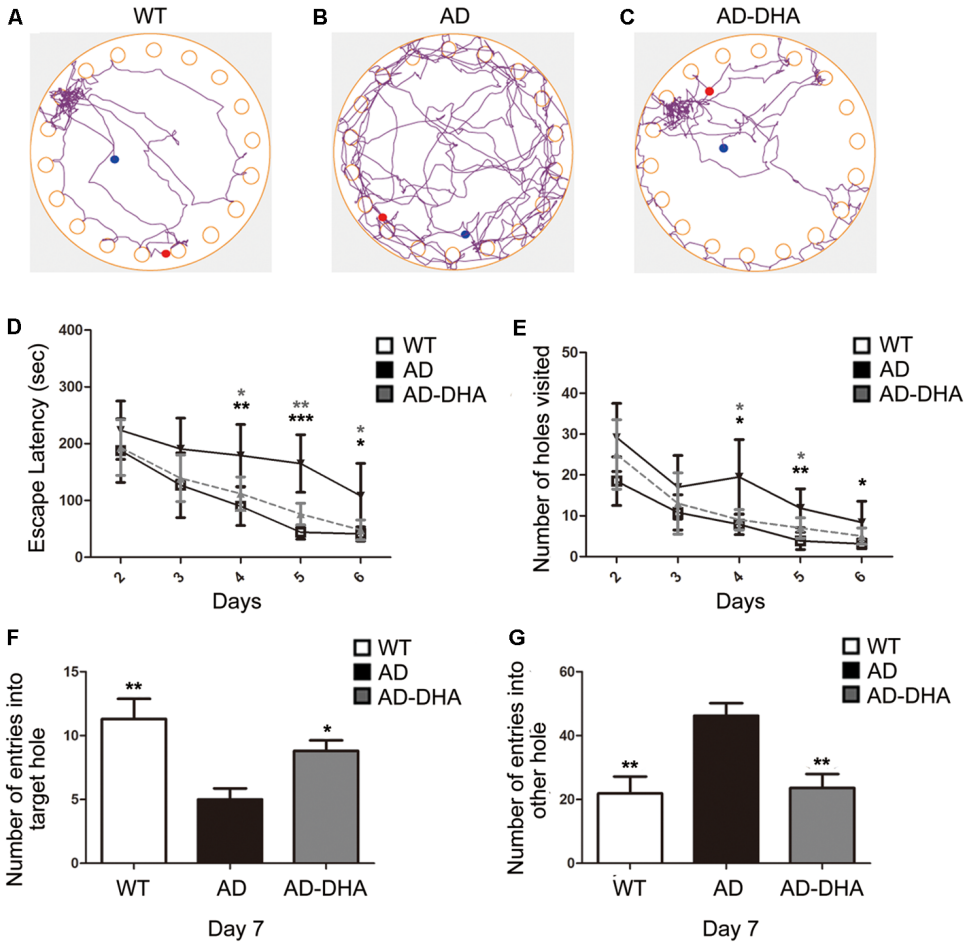

FIGURE 2 | Effect of DHA on APP/PS1 mice in the Barnes maze. Moving tracks of the CTRL group **(A)**, Alzheimer's disease (AD) group **(B)** and AD-DHA group mice **(C)**. Difference analysis of latency to find the escape box **(D)** and number of wrong holes visited **(E)** on training days, the number of entries into the target holes **(F)** and the other holes **(G)** on the test day in the Barnes maze test. Data are reported as the mean ± standard error of the mean (SEM) of ten animals per group. $^{*}p < 0.05$, $^{**}p < 0.01$, and $^{***}p < 0.001$ compared to the wild type (WT) group (Two-way ANOVA followed by the Newman–Keuls test for the training test and one-way analysis of variance/Newman–Keuls test for the probe test).

Oral DHA Decreased the Burden of Aβ Aggregations and SP Without the Participation of AD-Related Degradation Enzymes

Three mice per group were sacrificed after the behavioral tests to detect Aβ deposition by Thioflavin S staining (**Figures 3A,C**) and SP by immunohistochemistry (**Figures 3B,D**) in the cortex and hippocampus, respectively. Thioflavin S staining confirmed that the Aβ burden of both the cortex and hippocampus in the DHA-treated group were significantly lower than those in the DMSO-treated AD group (Newman–Keuls test; $p < 0.001$ in the cortex; $p < 0.05$ in the hippocampus). Anti-Aβ 4G8 antibody staining for immunochemistry ($p < 0.001$ in the cortex; $p < 0.01$ in the hippocampus) also showed that the quantities of SP in the cortex and hippocampus of the DHA-treated group were markedly reduced, which was consistent with the results of the Thioflavin S staining.

The Aβ40 and Aβ42 levels in the cortex and hippocampus of AD mice (**Figures 4A–F**). An ELISA assay revealed that DHA markedly reduced Aβ42 production in both the cortex and hippocampus (Newman–Keuls test; $P < 0.05$ in the cortex; $p < 0.01$ in the hippocampus; **Figures 4A,B**). The standard curve of mouse Aβ42 ELISA assay was shown in **Figure 4C**. Relative to the AD CTRL group, the burden of Aβ40 in the cortex was markedly downregulated ($p < 0.001$; **Figures 4D,E**) by oral DHA, while no significant change was found in the hippocampus of the DHA-treated group ($P > 0.05$). The standard curve of mouse Aβ40 ELISA assay was shown in **Figure 4F**.

Compared with the WT group, the expression of APP in the DMSO-treated AD group was significantly increased (Newman–Keuls test; $p < 0.001$; **Figures 4G,H**), whereas the treatment with DHA protected against the increase (+169.39% compared to WT, $p < 0.001$; +23.61% compared to AD, $p < 0.01$; **Figures 4G,H**). Significant differences in the expression of BACE1 were noted between the AD groups ($p < 0.05$;

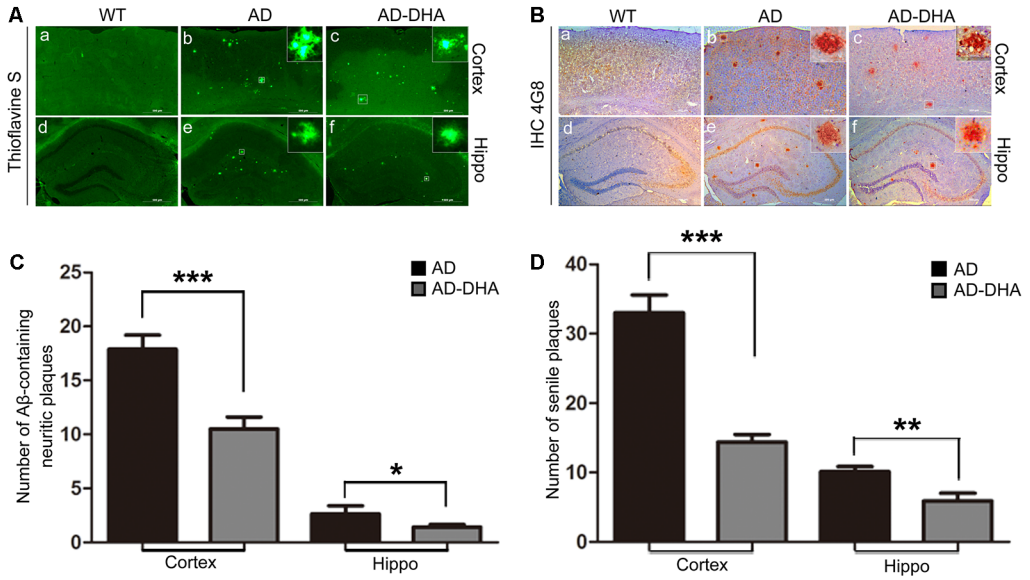

FIGURE 3 | Effects of DHA on Aβ aggregation and senile plaque (SP) deposition. The brains were prepared from mice treated with intragastric administration of DHA (20 mg/kg/day) or DMSO for 90 days. Thioflavin S staining **(Aa–f)** and immunohistochemistry **(Ba–f)** showed Aβ-containing neuritic plaques and SP in the cortex and hippocampus of WT mice, DMSO-treated AD mice, and DHA-treated AD mice. The number of Aβ aggregates **(C)** and the number of SP as determined by immunohistochemistry **(D)** in the cortex and hippocampus are illustrated as histograms. $n = 6$. $^{*}p < 0.05$, $^{**}p < 0.01$, and $^{***}p < 0.001$ compared to the DMSO-treated AD group. Student's unpaired *t*-test was performed for histological staining data and ELISA results. Scale bar = 500 μm.

Figures 4G,H). There were no significant differences in the expression of PS1 in the AD groups ($p > 0.05$; **Figures 4G,H**) after oral DHA treatment. There were no significant differences in the expression of IDE ($p > 0.05$; **Figures 4G,H**) or NEP ($p > 0.05$; **Figures 4G,H**) between the AD group and the AD-DHA group, although significant difference was noted in the protein expression of IDE between the WT group and the AD-DHA group ($p < 0.05$; **Figures 4G,H**).

Oral DHA Corrected Autophagy Dysfunction in AD Mice Model

In contrast with DMSO-treated AD mice, neuronal autophagy was markedly induced, and the AD-like pathological characteristics were evidently ameliorated in DHA-treated APP/PS1 mice, and there was no significant difference between DMSO-treated WT mice and DHA-treated AD mice (**Figures 5A–C**). In the CA1 hippocampus in DHA-treated APP/PS1 mice, neurons remained clear and intact (**Figure 5Aa**). Conversely, dark neurons (DNS; **Figure 5Ba**) and neurons with autophagic dysfunction (**Figure 5Bb**) emerged in the CA1 hippocampus of DMSO-treated APP/PS1 mice but did not emerge in the other two groups (**Figures 5Aa,Ca**). Membrane structures of mitochondria (**Figure 5Ab**) and Golgi apparatus (**Figure 5Ac**) were integral, cytoplasm in axons was clear (**Figure 5Ad**) and lipofuscins emerged (**Figure 5Ae**) in the CTRL group. In the subcellular ultrastructure of DMSO-treated AD mice, the edema of mitochondria (**Figure 5Bc**) and hydropic degeneration of the Golgi apparatus (**Figure 5Bd**) occurred. Axons were filled with aberrant myelin figures that damaged the basic structure of microtubules (**Figure 5Be**) and late APs were massively deposited around the nucleus (**Figure 5Bf**). In contrast, organelles such as mitochondria (**Figure 5Cb**) and Golgi bodies (**Figure 5Cc**), with the presence of APs with a double membrane that engulfed abnormal organelles (**Figure 5Cd**) and some granules of lipofuscin present (**Figure 5Cf**), maintained basically complete organelle structures in DHA-treated AD mice (**Figure 5C**) and WT mice (**Figure 5A**).

The ratio of LC3 II/I and the expression level of SQSTM/p62 were used as one of the measures of autophagic flux. The ratio of LC3 II/I was significantly upregulated and the degradation of SQSTM/p62 was significantly hampered in the DMSO-treated AD group, compared with the CTRL group ($p < 0.01$; **Figures 5D,E**). Oral DHA treatment increased the ratio of LC3 II/I (+65.98% AD vs. AD-DHA, $p < 0.01$; **Figures 5D,E**) and the blocked degradation of SQSTM/p62 ($p < 0.01$; **Figures 5D,E**) was significantly reverted in DHA-treated AD group, compared with the DMSO-treated AD group.

Expression of ATG5 ($p < 0.001$; **Figures 6A,B**) and ATG12 ($p < 0.001$; **Figures 6A,B**) were markedly decreased in the AD group compared with that of the WT group, which were protected by DHA treatment. Although there was no significant difference in the level of ATG16L1 between the WT and AD CTRL groups ($p > 0.05$), DHA treatment enhanced the expression of ATG16L1 in AD mice ($p < 0.01$; **Figures 6A,B**).

Expression of Beclin1 ($p < 0.001$; **Figures 6C,D**) and ATG14 ($p < 0.01$; **Figures 6C,D**) were markedly decreased in the AD group compared with that of the WT group, which were protected by DHA treatment. Conversely, no significant difference in p-ATG14 (Ser29) between the AD groups was noted ($p > 0.05$; **Figures 6C,D**). The levels of

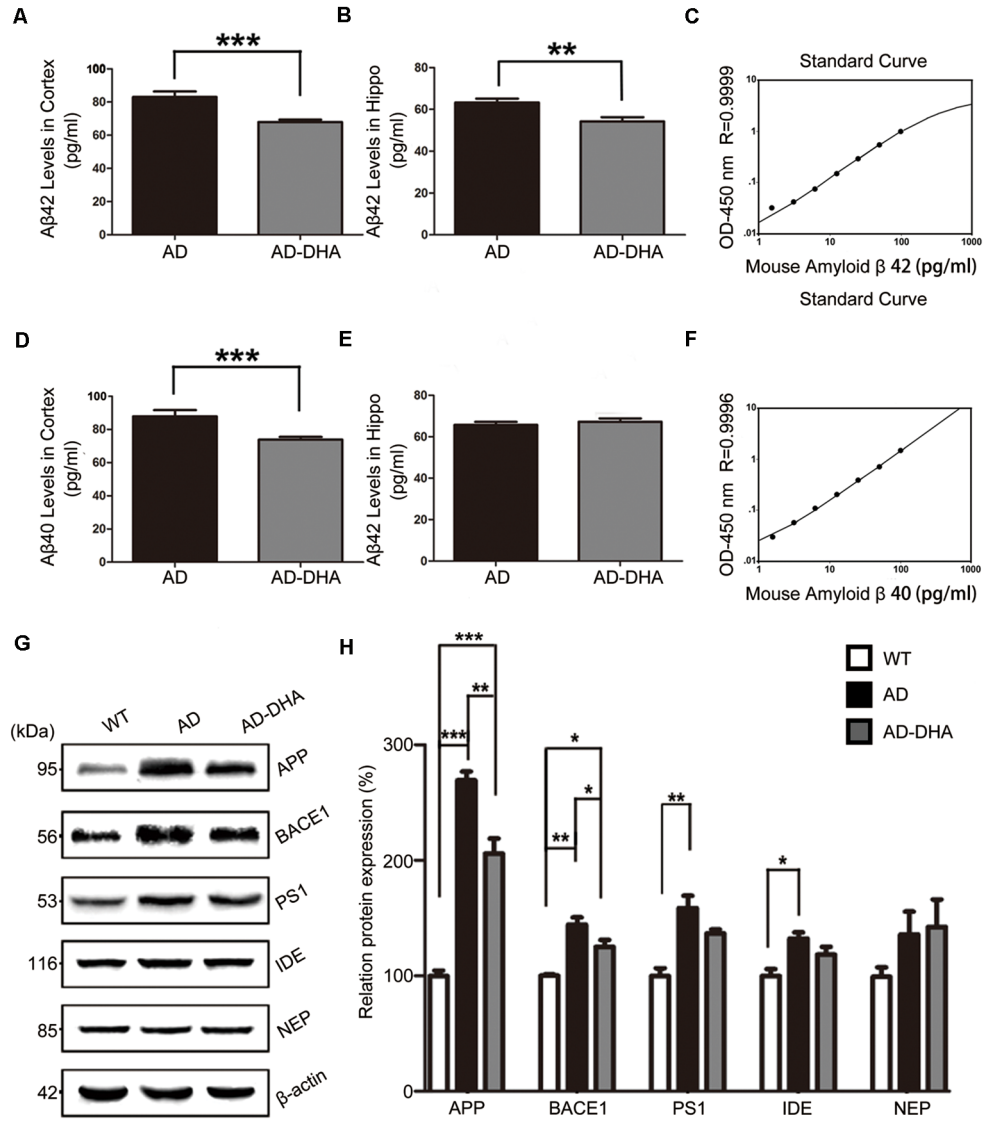

FIGURE 4 | Effects of DHA on eliminating Aβ40, Aβ42, APP, and β-site APP cleaving enzyme (BACE1). Protein levels of Aβ40 and Aβ42 in the hippocampus and cortex were detected by ELISA **(A–F)**. $^{**}p < 0.01$ and $^{***}p < 0.001$ compared to the DMSO-treated AD group. Protein levels of APP, BACE1, PS1, insulin-degrading enzyme (IDE) and NEP in extracts of whole brain tissue were detected by Western blotting (WB), shown in panel **(G)**. Quantification of the WB results are shown in panel **(H)**, and the results are shown as the mean values ± SD. $^{*}p < 0.05$, $^{**}p < 0.01$, and $^{***}p < 0.001$ between two groups. One-way analysis of variance/Newman–Keuls test was performed for all WB data.

Rab7 ($p < 0.05$; **Figures 6C,D**) were significantly upregulated and RILP ($p < 0.001$; **Figures 6C,D**) was downregulated by overexpression of APP/PS1 in the AD model, compared with that of the WT mice. As shown in **Figures 6C,D**, the effects of oral DHA upregulated the expression level of Rab7 ($p < 0.01$; **Figures 6C,D**) and RILP ($p < 0.001$; **Figures 6C,D**), compared with that of the DMSO-treated AD group.

The levels of Lamp1 ($p < 0.01$; **Figures 6E,F**) were significantly upregulated by overexpression of APP/PS1 in the AD model, while the expression of CTSB ($p < 0.05$; **Figures 6E,F**) was inhibited compared with that of the WT mice. Rather, as shown in **Figures 6E,F**, the effects of oral DHA significantly upregulated the levels of Lamp1 ($p < 0.001$), and CTSB ($p < 0.05$; **Figures 6E,F**).

The ratio of expression of phosphorylated/total mTOR was used as a measure for autophagy inhibition. Oral DHA treatment increased the p/t mTOR ratio (Newman–Keuls test; +100.81% AD vs. AD-DHA, $p < 0.01$; **Figures 6G,H**), suggesting rejuvenation in autophagic activity in AD mice. Expression of ULK1 ($p < 0.01$; **Figures 6G,H**) was markedly decreased in the AD group compared with that of the WT group, which were protected by DHA treatment. The ratio of expression of phosphorylated/total GSK3β was used as an indirect measure of GSK3β activity. Oral DHA treatment increased the p/t GSK3β

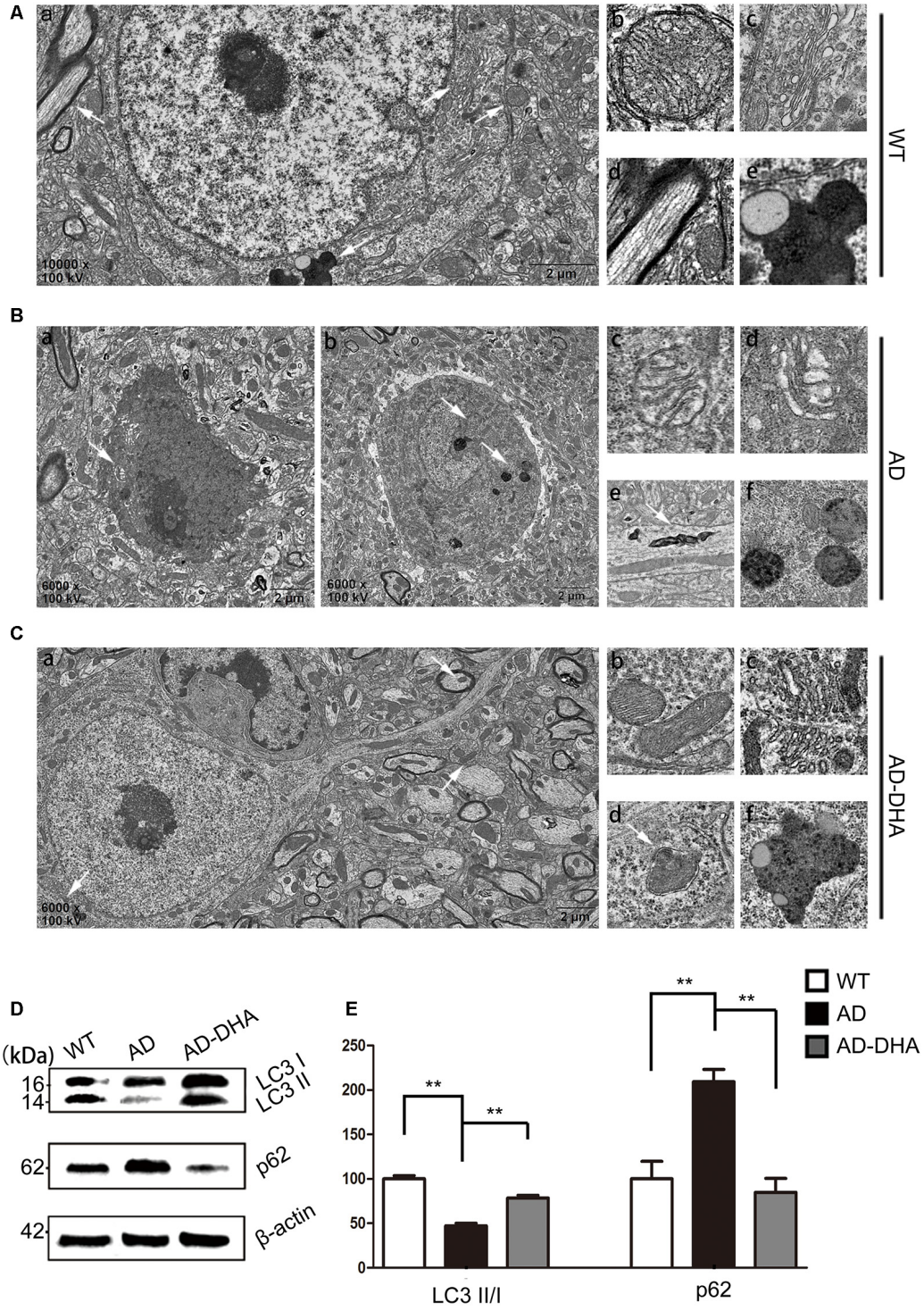

FIGURE 5 | Oral DHA protects the ultrastructures of hippocampal neurons and normalizes autophagic flux. **(Aa,Ba,b,Ca)** Low magnification images of CA1 hippocampal neurons in the three groups were detected by transmission electron microscopy (TEM). Normal mitochondria **(Ab)**, Golgi apparatus **(Ac)**, microtubules **(Ad)**, and granules of lipofuscin with lipid droplets **(Ae)** in the cytoplasm of neurons of WT mice (white arrows in **Aa**). Abnormal mitochondria **(Bc)**, Golgi fragments **(Bd)**, aberrant myelin figures **(Be)**, and late autophagosome deposits **(Bf)** in the neurons of the DMSO-treated AD group (white arrows in **Ba**). Intact mitochondria **(Cb)**, Golgi apparatus **(Cc)**, early autophagosomes **(Cd)**, and granules of lipofuscin with lipid droplets **(Cf)** in the cytoplasm of neurons of DHA-treated mice (white arrows in **Ca**). *Scale bars* **(Aa,Ba,b,Ca)**: 2 μm and **(Ab–e,Bc–f,Cb–f)**: 350 nm. Levels of LC3, p62, and β-actin in extracts of whole brain tissue were detected by WB **(D)**, and quantification of the results is shown in panel **(E)**. $^{**}p < 0.01$ between two groups. One-way analysis of variance/Newman–Keuls test was performed for all WB data.

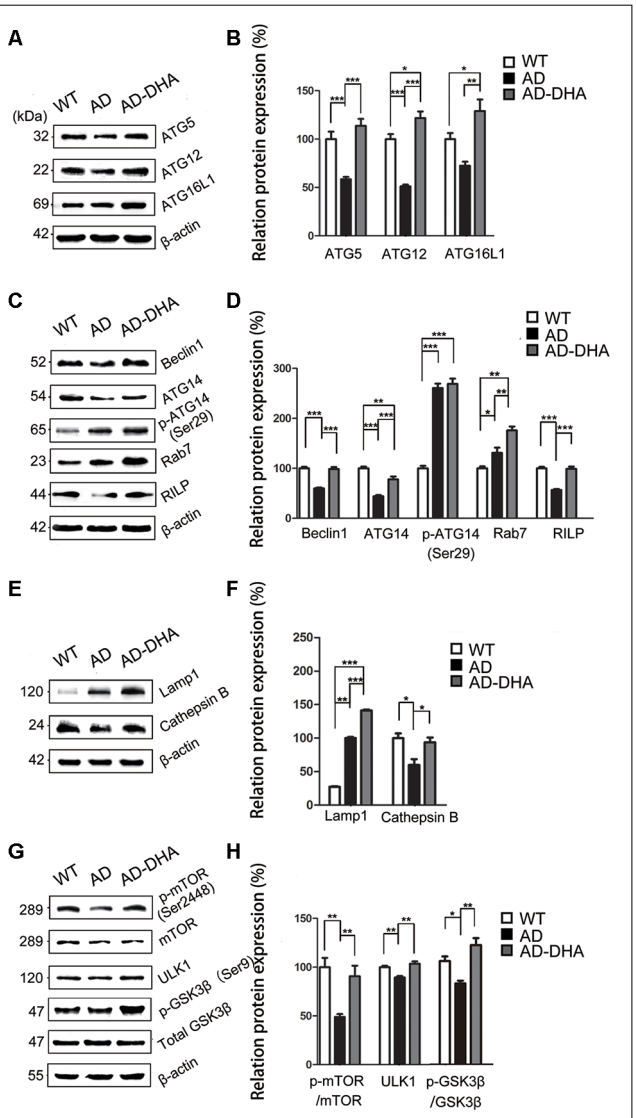

FIGURE 6 | DHA increases the basal level of autophagy. Protein levels of ATG5, ATG12, ATG16L1, Beclin1, ATG14, p-ATG14 (Ser29), Rab7, RILP, Lamp1, CTSB, p-mTOR(Ser2448), mammalian target of rapamycin (mTOR), ULK1, p-GSK3β (Ser9), GSK3β in extracts of whole brain tissue were detected by WB. Representative Western blots are presented in panels **(A,C,E,G)**, and quantification of the results is shown as the mean values ± SD in panels **(B,D,F,H)**. $^{*}p < 0.05$, $^{**}p < 0.01$, and $^{***}p < 0.001$ between two groups. One-way analysis of variance/Newman–Keuls test was performed for all WB data.

ratio (+approximately 47.28% AD vs. AD-DHA, $p < 0.01$; **Figures 6G,H**), suggesting decreased the enzyme activity of GSK3β in AD mice. The values of total and phosphorylated GSK3β are presented in **Figures 6G,H**.

Treatment With DHA Had Multitarget-Regulating Effects on Autophagy Flux in AD Model Cells

The cell viability was significantly inhibited in N2a-APP with 5 μM or 50 μM of DHA and APP-SH-SY5Y cells treated with 50 μM of DHA in 24 h. The relative rate was calculated using the following formula: each group/Control group × 100% (**Figures 7A,B**).

WB analysis of N2a-APP cells revealed a marked difference in the autophagic flux marker proteins, LC3 and p62, comparing levels in the CON group and DHA group with that of the CQ group, Bafi group, Bafi-DHA group, and CQ-DHA group (**Figures 7C,D**).

TEM analysis of N2a-APP cells and fluorescence microscopy analysis of APP-SH-SY5Y cells transfected with mRFP-GFP-LC3 adenoviruses showed a significant difference in key biomarkers of autophagy flux, APs, and lysosomes, comparing levels in the CON group and DHA-treated (DHA) group with that of the CQ-treated group, bafilomycin A1-treated (Bafi), Bafi-DHA-treated (Bafi-DHA) group, CQ-DHA-treated (CQ-DHA) group and positive CTRL group, which was the rapamycin (Rapa) group (**Figure 8**).

DHA treatment markedly increased the number of positive puncta (Newman–Keuls test; +295.2% CON vs. DHA, $p < 0.001$; **Figures 8Ab,c** for the CON group and Bb-c for the DHA group; **Figure 8H** for the histogram), suggesting an increase in the autophagic activity of APP-SH-SY5Y cells, which is in accordance with the TEM data comparing the CON group and DHA group (**Figure 8Aa** for the CON group and Ba for the DHA group; **Figure 8I** for the histogram). Moreover, the ratio of LC3 II/I increased (+51.0% CON vs. DHA, $p < 0.01$; **Figures 7C,D**) and the level of p62 decreased (−22.4% CON vs. DHA, $p < 0.05$; **Figures 7C,D**) with DHA treatment of N2a-APP cells, which is consistent with results comparing the AD mice with the AD-DHA mice groups (**Figures 7C,D**).

Bafilomycin A1 treatment significantly downregulated the ratio of positive puncta near the nucleus (Newman–Keuls test; −81.14% CON vs. Bafi, $p < 0.01$; **Figures 8Ab,c** for the CON group and Cb-c for the Bafi group; **Figure 8I** for the histogram), suggesting that the fusion between APs and lysosomes near the nucleus was impaired, and the increased number of positive puncta in the Bafi group compared with that of the CON group was not significantly different ($p > 0.05$; **Figures 8Ab,c,Cb,c,I** for the histogram). APs dyed dark gray, suggest that late APs accumulated in the cytoplasm after bafilomycin A1 treatment (**Figures 8Ca–c**). TEM results coincided with the results shown in **Figures 7C,D** that the ratio of LC3 II/I significantly increased when comparing the Bafi group with that of the CON group (+138.2% CON vs. Bafi, $p < 0.001$; **Figures 7C,D**). Not only the number of positive puncta (+107.4% Bafi vs. Bafi-DHA, $p < 0.01$; **Figures 8Cb,c,H**) but also the ratio of puncta near the nucleus markedly increased (+447.9% Bafi vs. Bafi-DHA, $p < 0.05$; **Figures 8Cb,c,Db,c,I**) in the Bafi-DHA group compared with that of the Bafi group. Furthermore, WB analysis showed that DHA treatment ameliorated the increase in the ratio of LC3 II/I induced by bafilomycin A1 ($p < 0.05$; **Figures 7C,D**) and downregulated the level of p62 in the Bafi-DHA group compared with that of the Bafi group ($p < 0.01$; **Figures 7C,D**).

CQ hindered APs degradation by lysosomes, which was manifested by the increased number of APs (Newman–Keuls test;

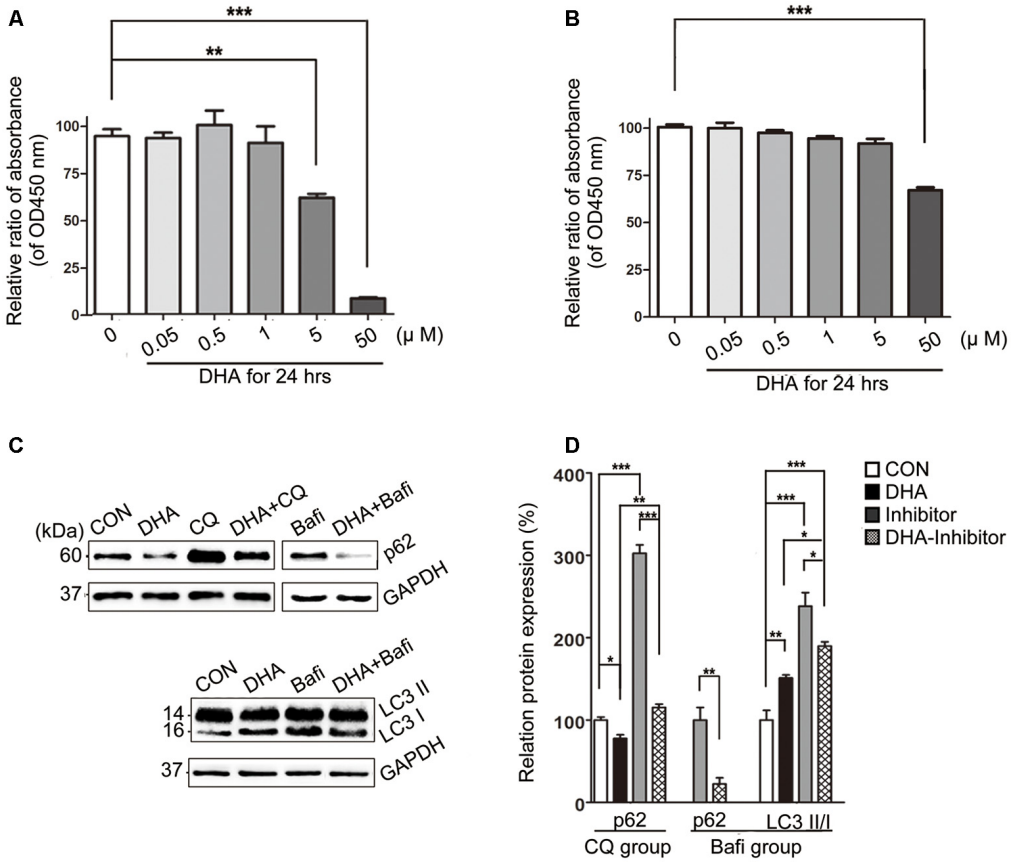

FIGURE 7 | DHA ameliorates the protein levels of autophagic fusion and degradation processes. **(A,B)** DHA reduced the cell viability in a dose-dependent manner both in N2a-APP cells and APP-SH-SY5Y cells. The data are presented as the means ± SEM and were analyzed by one-way ANOVA (Newman–Keuls test, $^{**}p < 0.01$, $^{***}p < 0.001$). **(C)** Protein levels of SQSTM/p62, LC3B I and LC3 II in cells in the CON group, DHA group, chloroquine (CQ) group, CQ-DHA group, Bafi group and Bafi-DHA group were detected by WB. Representative Western blots are presented in panels **(C)**, and quantification of the results is shown as the mean values ± SD in panels **(D)**. $^{*}p < 0.05$, $^{**}p < 0.01$, and $^{***}p < 0.001$ between two groups. One-way analysis of variance/Newman–Keuls test was performed for all WB data.

+130.8% CON vs. CQ, $p < 0.01$; **Figures 8Eb,c,H**), the increased ratio of positive puncta near the nucleus (Newman–Keuls test; +224.6% CON vs. CQ, $p < 0.001$; **Figures 8Eb,c,I**) and upregulation of p62 (Newman–Keuls test; +202.4% CON vs. CQ, $p < 0.001$; **Figures 7C,D**) compared with those of the CON group. Additionally, large lysosomes and APs dyed dark gray aggregated in the cytoplasm after CQ treatment (**Figure 8Ea**). Fluorescence microscopy analysis showed that DHA treatment not only further enhanced the production of APs in the CQ+DHA group (Newman–Keuls test; +67.44% CQ vs. CQ+DHA, $p < 0.05$; **Figures 8Eb,c,Fb,c,H**) but also increased the ratio of positive puncta away from the nucleus by 27.86% ($p < 0.01$; **Figure 8I**) compared with that of the CQ group, although the ratio was smaller than that of the DHA group (Newman–Keuls test; +87.97% DHA vs. CQ+DHA, $p < 0.01$; **Figures 8Bb,c,Fb,c,I**). WB data showed that DHA rescued the degradation dysfunction of p62 caused by CQ (Newman–Keuls test; −187.1% CQ vs. CQ+DHA, $p < 0.001$; **Figures 7C,D**). No large lysosomes were detected in the CQ+DHA group (**Figure 8Fa**).

DISCUSSION

The brain neuropathology of AD is characterized by synaptic abnormalities and neuronal degeneration, as well as extracellular Aβ deposition and intraneuronal neurofibrillary tangles, leading to a decline in memory and other cognitive functions (Ho et al., 2014). Recent studies have suggested that the molecular level of autophagic maintenance might be a suitable way to treat AD as well as some other neurodegenerative diseases, since it could not only prevent cell death but also effectively degrade pathological proteins, such as Aβ, p-Tau, α-synuclein, and glutamine repeats (Ghavami et al., 2014). Autophagy, as a lysosomal mediated process of cell self-processing, is closely related to the clearance of abnormal accumulation of AD-related proteins. However, a large number of studies have reported that there are dual roles for autophagy, which are degradation and secretion of AD Aβ peptide (Choi et al., 2018; Uddin et al., 2018). There are a large number of APs and autolysosomes (ALs) in the brain of AD patients, which are caused by the activation of autophagy on the one hand, the fusion obstacle between APs and lysosome,

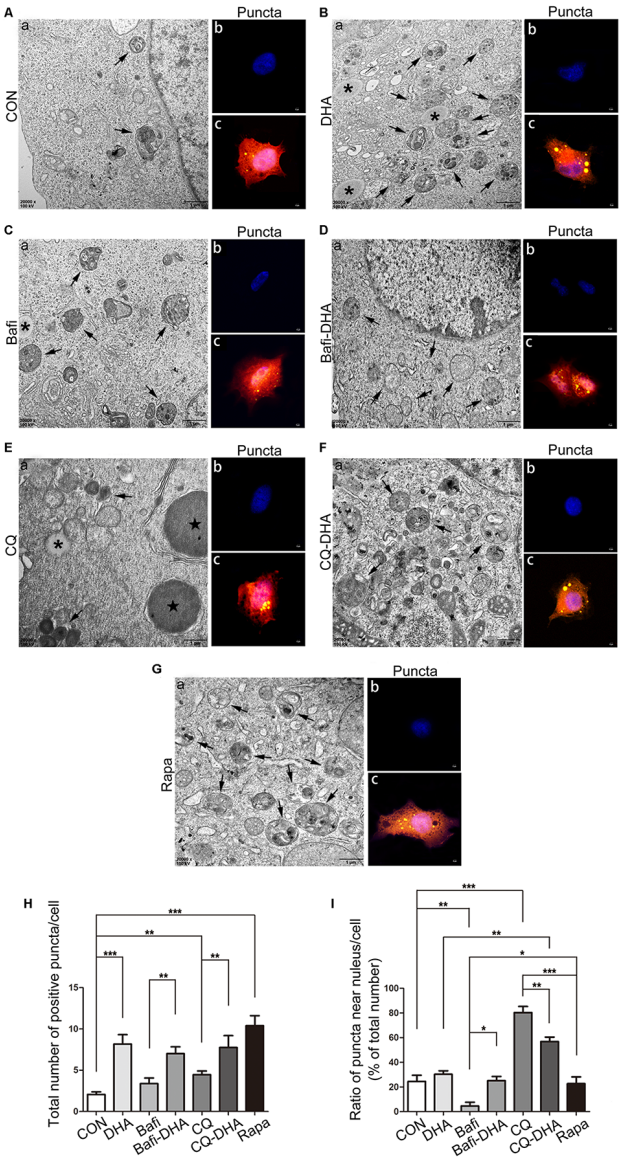

FIGURE 8 | DHA stimulated autophagosomes (APs) formation and affected autophagic flux morphology. **(Aa**,**Ba**,**Ca**,**Da**,**Ea**,**Fa**,**Ga)** High magnification images of APs (arrows in **Aa**,**Ba**,**Ca**,**Da**,**Ea**,**Fa**,**Ga**) and lysosomes (***Aa**,**Ba**,**Ca**,**Da**,**Ea**,**Fa**,**Ga**) or lipid droplets (★in **Aa**,**Ba**,**Ca**,**Da**,**Ea**,**Fa**,**Ga**) of N2a-APP cells in the seven groups were detected by TEM after treatment with DMSO **(Aa)**, DHA (1 μM, 24 h) **(Ba)**, bafilomycin A1(50 nM, 25 h) **(Ca)**, bafilomycin A1 (50 nM, 25 h) and DHA (1 μM, 24 h) **(Da)**, CQ (25 μM, 25 h) **(Ea)**, CQ (25 μM, 25 h) and DHA (1 μM, 24 h) **(Fa)**, rapamycin (100 nM, 24 h) **(Ga)**. **(Ab,c**,**Bb,c**,**Cb,c**,**Db,c**,**Eb,c**,**Fb,c**,**Gb,c)** APP-SH-SY5Y cells were transfected with a tandem mRFP-GFP-LC3 adenovirus for 24 h, followed by treatment with DHA (1 μM, 24 h) **(Bb,c)**, bafilomycin A1 (1 nM, 25 h) **(Cb,c)**, bafilomycin A1 (1 nM, 25 h) and DHA (1 μM, 24 h) **(Db,c)**, CQ (10 μM, 25 h) **(Eb,c)**, CQ (10 μM, 25 h) and DHA (1 μM, 24 h) **(Fb,c)** and rapamycin (100 nM, 24 h) **(Gb,c)**. APs were visualized in each group as yellow puncta under a confocal microscope. Scale bar (**Aa**,**Ba**,**Ca**,**Da**,**Ea**,**Fa,Ga)**: 1 μm and **(Ab,c,Bb,c,Cb-c,Db,c,Eb,c,Fb,c,Gb,c)**: 5 μm. **(H,I)** Positive puncta were counted, and the ratio of puncta near the nucleus in each cell was calculated. Randomly selected fields were counted, and the data are presented as the means ± SEM and were analyzed by one-way ANOVA (Newman–Keuls test, $^{*}p < 0.05$, $^{**}p < 0.01$, and $^{***}p < 0.001$ compared to CON group).

or the degradation reduction of ALs on the other hand. In the early stage of AD, autophagy can accelerate the clearance of denatured protein and promote the survival of neurons. With the development of AD, the aggregation of APs is increased and the clearance of ALs decreased. Therefore, it is of great scientific significance to study the dynamic changes of autophagy flux in the pathogenesis of AD and to find new targets for the prevention and treatment of AD.

DHA, the active metabolite of artemisinin, may meet the conditions for the induction of basal autophagy and correction of autophagic flux (Ho et al., 2014; Efferth, 2017; Lam et al., 2018). However, no study has mentioned the therapeutic effect of DHA in AD regarding the degradation of toxic aggregated proteins by inducing autophagy. Thus, it is vital to determine the potential effects and mechanisms of DHA treatment on AD. In the present study, Barnes maze test results showed that DHA administration by gastric perfusion for 3 months exhibited a protective effect on learning and memory impairment in the APP/PS1 double transgenic mice. Then we found that the diameters of SP were smaller and the densities of SP were lower in the DHA-treated group compared with those of the DMSO-treated group, which supports our assumption that DHA may prevent the aggregation of Aβ and deposition of SP. The main forms of Aβ in the brain are Aβ40 and Aβ42, the latter is more prone to amyloidosis and toxicity. To verify the potential effects of DHA on the levels of Aβ40 and Aβ42 in the cortex and hippocampus, ELISA results showed that the levels of Aβ42 in both the cortex and hippocampus and of Aβ40 in the cortex were markedly reduced by oral DHA, which indicates that DHA may normalize the burden of Aβ42 that acts as more harmful peptides prone to misfolding and aggregating, but not Aβ40, and plays a central role in the pathological course of AD (Querfurth and LaFerla, 2010; Lane et al., 2018). In addition, hippocampal neurons are more prone to protein aggregation than neurons in the cortex, which may suggest that this selective difference is closely related to the degradation rate of aggregated proteins; the degradation rate is based on cell- and region-specific autophagy activity and vulnerability of substrates to clearance *via* autophagy, possibly due to neuronal dependency on autophagic flux (Lumkwana et al., 2017). We found that the anti-Aβ42 effect of DHA on the cortex was more significant than that on the hippocampus, as well as the anti-Aβ40 effect of DHA on the cortex. Consequently, we considered that DHA exhibited neuroprotective effects in AD. The imbalance of Aβ metabolism leads to the formation of extracellular SPs and a series of pathological changes. Aβ is formed by the cleavage of APP protein by β- and γ-secretase, and BACE1 and PS1 are the active centers of β- and γ-secretases, respectively. In this study, the results showed that compared with the control group, the levels of APP and BACE1 protein were down-regulated after DHA treatment, indicating that Aβ production was reduced. Then we tested the degradation of Aβ. The degradation of extracellular Aβ is mainly completed by IDE and NEP (Yamamoto et al., 2018). However, our results showed that DHA treatment did not significantly change the levels of IDE and NEP proteins compared with the control group. While the degradation of intracellular Aβ is mainly transported to lysosome through endocytosis or autophagy, there

is increasing evidence that autophagy dysfunction accompanies the development of AD (Choi et al., 2018; Uddin et al., 2018). Dysfunction in the autophagy-lysosome pathway is closely related to the production, clearance and neurotoxicity of Aβ. In the current study, TEM results showed that there were a large number of normal neurons in the brain of DHA-treated mice as the WT mice. In addition, double-membraned APs enveloped organelles and cytosolic proteins instead of aberrant myelin accumulation occurred in DHA-treated neurons. At the same time, no DNs and neurons with autophagic dysfunction could be found in DHA-treated neurons. Therefore we speculate that autophagy could be markedly improved by DHA treatment in an AD mouse model. The levels of autophagy-associated proteins were assessed by WB to verify the hypothesis that oral DHA could protect against AD pathophysiology by inducing autophagy in AD-like neurons. We found that the level of SQSRM1/p62 increased and the ratio of LC3 II/I decreased in AD brains compared with that of WT brains, which indicates low autophagic activity and obstructed autophagic flux in AD pathogenesis (Boland et al., 2008). The relatively low level of LC3 II along with a high level of Aβ burden in AD mice brain might be explained by the lack of a potential protective role for LC3-associated endocytosis that downregulates the levels of neurotoxic Aβ (Heckmann et al., 2019).

We next investigated the mechanism by which DHA activates autophagy. The first step is autophagy initiation and APs formation. The levels of proteins associated with isolation of AP membranes from the ER, such as ULK1 and Atg14, proteins associated with the elongation of AP membranes, such as ATG12, ATG5, ATG16L1, and LC3. The second step is AL formation (via the fusion of APs and lysosomes), proteins associated with the ALs fusion, such as ATG14, p-ATG14, Rab7, and RILP. The third step is AL degradation: autophagy-encapsulated proteins are released by CTSB and CTSD degradation, and lysosomal acidification plays an important role in their degradation. The WB results showed that the expression of proteins involved in the early stage of autophagy, such as ATG5, ATG12 and ATG16L, were upregulated in DHA treated group, indicating that autophagy was activated. At the middle stage of autophagy, the levels of LC3 II/I were increased, and the p62 protein level was decreased, indicating that autophagy was induced by DHA treatment. ATG14 has been shown to form a complex with Beclin1 in the early stage of autophagy and promote the fusion of APs and lysosomes in the middle stage of autophagy (Diao et al., 2015). However, after treatment with DHA, the levels of Beclin1, ATG14, Rab7 and RILP proteins were significantly increased, indicating that DHA treatment not only activated autophagy but also promoted the fusion of autophagy and lysosome. Studies have shown that reducing the content of proteases in lysosomes and inhibiting the activity of lysosomal enzymes can lead to the accumulation of Aβ in cells. In addition, the endocytosis of Aβ can, in turn, reduce the function of lysosomes and affect the degradation of Aβ by lysosomes (Zheng et al., 2012; Lauritzen et al., 2016). The results of this study showed that the protein expression of the lysosomal protease CTSB and the lysosomal marker Lamp1 in the DHA-treated mice increased compared with that of the CRTL group, suggesting that DHA treatment can also increase the number of lysosomes and their degradation function.

GSK3β-TIP60-ULK1 pathway and mTOR/ ULK1 pathway are two classic autophagy activation pathways (Nie et al., 2016). In this study, WB showed that DHA inhibited the activity of mTOR, then activated ULK, indicating that DHA can also activate autophagy by inhibiting the mTOR/ ULK1 signaling pathway, but DHA does not activate autophagy by activating GSK3.

To clarify the potential mechanisms by which DHA affects autophagic flux, N2a-APP cells and APP-SH-SY5Y cells were treated with DHA, followed by treatment with bafilomycin A1, an autophagic fusion agonist, CQ, and autophagic degradation agonist, and rapamycin, an autophagic initiation antagonist. We found that DHA indeed accelerated the degradation of p62 in the cell model compared with that of the CON group. In addition, CQ treatment significantly hampered the degradation of p62 in the cell model, which was consistent with its inhibition of degradative enzyme activity (Homewood et al., 1972), and was markedly ameliorated by DHA treatment, which reversed the blocked degradation of aggregated proteins and damaged organelles in lysosomes. To detect the process of APs formation mediated by DHA, autophagic agonists and antagonist, TEM and shoots for puncta formation of fluorescent-tagged LC3 proteins in the cytoplasm under fluorescence microscopy were utilized (Klionsky et al., 2012). We found that a large number of lipid droplets and large lysosomes accumulated in the cytoplasm near the nucleus after CQ treatment. Increasing the accumulation of lysosomes indicates that APs and their contents could not be cleared smoothly by lysosomes, which was notably improved in the CQ-DHA group. The phenomenon was also detected by fluorescence microscopy in the CQ group and the CQ-DHA group, in which positive puncta that aggregated near the nucleus were corrected by DHA treatment. Then, we found that the reinforced degradation of p62 by DHA was not disrupted by bafilomycin A1, an autophagic degradation agonist that inhibits the transport of lysosomal protons and leads to blocking the fusion between APs and lysosomes (Klionsky et al., 2008). In addition, DHA not only upregulated the basal level of LC3 II in N2a-APP cells compared with that of the CON group but also reversed the accumulation of LC3 II caused by bafilomycin A1 treatment. Moreover, a mass of stacked APs dyed dark gray (indicating late APs) in the cytoplasm in the Bafi group were mostly replaced by APs dyed light gray (indicating early APs) in the Bafi-DHA group; however, a few late APs were still measured by TEM. The trend was also consistent with the trend in the Bafi group and the Bafi-DHA group under fluorescence microscopy. In addition, differences between the effects of DHA and rapamycin on autophagy mediation and the Aβ clearance are discussed in our study. Unlike rapamycin-induced initiation of autophagy to improve Aβ pathology (Majumder et al., 2011), DHA mainly contributes to maintaining the fusion and AL-digestion stage in autophagic flux as we described above. Moreover, we found that DHA helps clear Aβ42 levels in both the cortex and hippocampus and Aβ40 levels in the cortex of APP/PS1 mice, but rapamycin downregulates Aβ42 but not Aβ40 levels (Spilman et al., 2010), which indicates DHA may have a wider effect

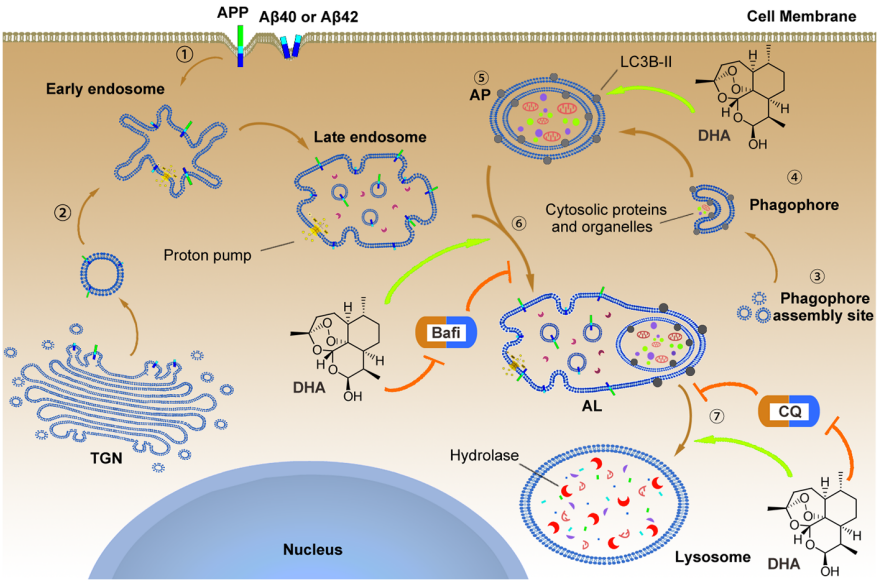

FIGURE 9 | The underlying mechanism by which DHA improves autophagic flux and clears Aβ40 and Aβ42. ①② APP, Aβ40 and Aβ42 can reach the early endosome either *via* the trans-Golgi network (TGN) or *via* the cell surface. ③④⑤ In parallel, normal autophagy is induced by the formation of APs that initiate at the phagophore assembly site; nucleation of the phagophore, sequestration of substrates, and expansion of the double membrane are involved in this process, which is markedly hindered in AD pathology. To reverse this process, DHA upregulated the levels of the Atg5-Atg12-Atg16L complex to facilitate LC3 lipidation (LC3 I) with phosphatidylethanolamine that was inhibited by AD-like pathogenesis ⑥⑦. In addition, the treatment of DHA protected against the bafilomycin A1-induced abnormal fusion of APs and late endosomes, ameliorated the CQ-mediated loss of lysosomal degradation function, and finally promoted the degradation of Aβ40 and Aβ42.

for Aβ clearance. Thus, based on the evidence above, we found that DHA treatment can contribute to the clearance of Aβ by maintaining autophagy flux *in vivo* and *in vitro* (**Figure 9**).

CONCLUSION

Overall, DHA treatment can ameliorate behavioral and biochemical deficits in an AD mouse model. The major mechanisms of the therapeutic effects of DHA involve enhancing autophagy, avoiding excessive neuronal death and recovering autophagic flux in AD models *in vivo* and *in vitro*. As AD is undoubtedly caused by multiple factors, and there are many pathological ongoing processes, including a shortage of neurotrophic factors, accumulation of aggregated proteins and progressive neuron loss, one might assume that effective treatment of this disease should include corrections to all these processes. This study demonstrated that DHA can prevent neurons death through raising the overall level of autophagy and maintaining the proper function of autophagy flux in the fusion and degradation stages that predominantly reduces the burden of pathological proteins (such as Aβ40, Aβ42, in this work) in AD models *in vivo* and *in vitro*. Hence, DHA, the active metabolite of *Artemisia annua*, might be a multifunctional molecule capable of correcting the pathology of this disease. Owing to the fact that DHA has been shown to be safe and versatile in many clinical trials worldwide, we suggest that the use of this compound might be considered a therapeutic treatment to reduce and/or prevent symptoms of AD in humans.

DATA AVAILABILITY STATEMENT

The datasets used and/or analyzed during the current study are available from the corresponding author upon reasonable request.

ETHICS STATEMENT

The animal study was reviewed and approved by the Ethics Committee of Chongqing Medical University.

AUTHOR CONTRIBUTIONS

GH, MF, and YZ conceived, designed and supervised the entire study. YZ performed the experiments, acquired data, analyzed data, and drafted the manuscript. YD, TJ, JL, and YLi participated in designing research studies, conducted experiments, acquired data, analyzed data and provided reagents. KW performed TEM, measured autophagic flux *in vivo* and *in vitro*, acquired and analyzed data. YLiu and XP conducted statistical analysis and generated the figures. ZL and GH reviewed and edited the manuscript. All authors have read and approved the final manuscript.

FUNDING

This study was supported by the National Natural Science Foundation of China (Nos. 81671257, 81371221, and 31600825), the Hubei Natural Science Foundation (2018CFB766) and

Yingyao Experimental Design Competition of School of Basic Medical Sciences (JCYY201611).

ACKNOWLEDGMENTS

We thank Professor Zhifang Dong (Ministry of Education Key Laboratory of Child Development and Disorders, Children's Hospital of Chongqing Medical University) for his team's assistance in performing the experiments.

SUPPLEMENTARY MATERIAL

The Supplementary Material for this article can be found online at: https://www.frontiersin.org/articles/10.3389/fnagi.2020.00047/full#supplementary-material.

REFERENCES

Boland, B., Kumar, A., Lee, S., Platt, F. M., Wegiel, J., Yu, W. H., et al. (2008). Autophagy induction and autophagosome clearance in neurons: relationship to autophagic pathology in Alzheimer's disease. *J. Neurosci.* 28, 6926–6937. doi: 10.1523/JNEUROSCI.0800-08.2008

Chairat, K., Jittamala, P., Hanboonkunupakarn, B., Pukrittayakamee, S., Hanpithakpong, W., Blessborn, D., et al. (2018). Enantiospecific pharmacokinetics and drug-drug interactions of primaquine and blood-stage antimalarial drugs. *J. Antimicrob. Chemother.* 73, 3102–3113. doi: 10.1093/jac/dky297

Chen, P. Q., Yuan, J., Du, Q. Y., Chen, L., Li, G. Q., Huang, Z. Y., et al. (2000). Effects of dihydroartemisinin on fine structure of erythrocytic stages of Plasmodium berghei ANKA strain. *Acta Pharmacol. Sin.* 21, 234–238.

Choi, M. Y., Han, K., and Kim, J. (2018). The role of autophagy in Alzheimer's disease: modeling and simulations. *Biophys. J.* 114:665a. doi: 10.1016/j.bpj.2017.11.3587

Chotsiri, P., Zongo, I., Milligan, P., Compaore, Y. D., Somé, A. F., Chandramohan, D., et al. (2019). Optimal dosing of dihydroartemisinin-piperaquine for seasonal malaria chemoprevention in young children. *Nat. Commun.* 10:480. doi: 10.1038/s41467-019-08297-9

De Strooper, B., and Karran, E. (2016). The cellular phase of Alzheimer's disease. *Cell.* 164, 603–615. doi: 10.1016/j.cell.2015.12.056

Diao, J., Liu, R., Rong, Y., Zhao, M., Zhang, J., Lai, Y., et al. (2015). ATG14 promotes membrane tethering and fusion of autophagosomes to endolysosomes. *Nature* 520, 563–566. doi: 10.1038/nature14147

Dormoi, J., Briolant, S., Pascual, A., Desgrouas, C., Travaillé, C., and Pradines, B. (2013). Improvement of the efficacy of dihydroartemisinin with atorvastatin in an experimental cerebral malaria murine model. *Malar. J.* 12:302. doi: 10.1186/1475-2875-12-302

Efferth, T. (2017). From ancient herb to modern drug: artemisia annua and artemisinin for cancer therapy. *Semin. Cancer Biol.* 46, 65–83. doi: 10.1016/j.semcancer.2017.02.009

Esquerda-Canals, G., Martíclúa, J., Roda, A. R., and Villegas, S. (2017). An intracellular amyloid-β/AβPP epitope correlates with neurodegeneration in those neuronal populations early involved in Alzheimer's disease. *J. Alzheimers Dis.* 59, 1–18. doi: 10.3233/JAD-170218

Fecto, F., Esengul, Y. T., and Siddique, T. (2014). Protein recycling pathways in neurodegenerative diseases. *Alzheimers. Res. Ther.* 6:13. doi: 10.1186/alzrt243

Feng, T., Tammineni, P., Agrawal, C., Jeong, Y. Y., and Cai, Q. (2017). Autophagy-mediated regulation of BACE1 protein trafficking and degradation. *J. Biol. Chem.* 292, 1679–1690. doi: 10.1074/jbc.m116.766584

Folch, J., Ettcheto, M., Petrov, D., Abad, S., Pedrós, I., Marin, M., et al. (2018). Review of the advances in treatment for Alzheimer disease: strategies for combating β-amyloid protein. *Neurologia* 33, 47–58. doi: 10.1016/j.nrl.2015.03.012

Gautam, A., Ahmed, T., Batra, V., and Paliwal, J. (2009). Pharmacokinetics and pharmacodynamics of endoperoxide antimalarials. *Curr. Drug Metabol.* 10, 289–306. doi: 10.2174/138920009787846323

Ghavami, S., Shojaei, S., Yeganeh, B., Ande, S. R., Jangamreddy, J. R., Mehrpour, M., et al. (2014). Autophagy and apoptosis dysfunction in neurodegenerative disorders. *Prog. Neurobiol.* 112, 24–49. doi: 10.1016/j.pneurobio.2013.10.004

Guo, F., He, X. B., Li, S., and Le, W. (2017). A central role for phosphorylated p38α in linking proteasome inhibition-induced apoptosis and autophagy. *Mol. Neurobiol.* 54, 7597–7609. doi: 10.1007/s12035-016-0260-1

Hamano, T., Hayashi, K., Shirafuji, N., and Nakamoto, Y. (2018). The implications of autophagy in Alzheimer's disease. *Curr. Alzheimer Res.* 15, 1283–1296. doi: 10.2174/1567205015666181004143432

Heckmann, B. L., Teubner, B. J. W., Tummers, B., Guy, C. S., Zakharenko, S. S., Green, D. R., et al. (2019). LC3-associated endocytosis facilitates β-amyloid clearance and mitigates neurodegeneration in murine Alzheimer's disease. *Cell* 178, 536.e14–551.e14. doi: 10.1016/j.cell.2019.05.056

Ho, W. E., Peh, H. Y., Chan, T. K., and Wong, W. S. F. (2014). Artemisinins: pharmacological actions beyond anti-malarial. *Pharmacol. Ther.* 142, 126–139. doi: 10.1016/j.pharmthera.2013.12.001

Homewood, C. A., Warhurst, D. C., and Peters, W. B. V. (1972). Lysosomes, pH and the anti-malarial action of chloroquine. *Nature* 235, 50–52. doi: 10.1038/235050a0

Jia, G., Kong, R., Ma, Z. B., Han, B., Wang, Y. W., Pan, S. H., et al. (2014). The activation of c-Jun NH2-terminal kinase is required for dihydroartemisinin-induced autophagy in pancreatic cancer cells. *J. Exp. Clin. Cancer Res.* 33:8. doi: 10.1186/1756-9966-33-8

Jiang, L. B., Meng, D. H., Lee, S. M., Liu, S. H., Xu, Q. T., Wang, Y., et al. (2016). Dihydroartemisinin inhibits catabolism in rat chondrocytes by activating autophagy via inhibition of the NF-κB pathway. *Sci. Rep.* 6:38979. doi: 10.1038/srep38979

Joshi, G., and Wang, Y. (2015). Golgi defects enhance APP amyloidogenic processing in Alzheimer's disease. *Bioessays* 37, 240–247. doi: 10.1002/bies.201400116

Kerr, J. S., Adriaanse, B. A., Greig, N. H., Mattson, M. P., Cader, M. Z., Bohr, V. A., et al. (2017). Mitophagy and Alzheimer's disease: cellular and molecular mechanisms. *Trends Neurosci.* 40, 151–166. doi: 10.1016/j.tins.2017.01.002

Kimura, S., Noda, T., and Yoshimori, T. (2007). Dissection of the autophagosome maturation process by a novel reporter protein, tandem fluorescent-tagged LC3. *Autophagy* 3, 452–460. doi: 10.4161/auto.4451

Klionsky, D. J., Abdelmohsen, K., Abe, A., Abedin, J., Abeliovich, H., Arozena, A. A., et al. (2012). Guidelines for the use and interpretation of assays for monitoring autophagy. *Autophagy* 8, 445–544. doi: 10.4161/auto.19496

Klionsky, D. J., Abdelmohsen, K., Abe, A., Abedin, M. J., Abeliovich, H., Acevedo Arozena, A., etal. (2016). Guidelines for the use and interpretation of assays for monitoring autophagy (3rd edition). *Autophagy* 12, 1–222. doi: 10.1080/15548627.2015.1100356

Klionsky, D. J., Elazar, Z., and Seglen PO, R. D. (2008). Does bafilomycin A1 block the fusion of autophagosomes with lysosomes. *Autophagy* 4, 849–950. doi: 10.4161/auto.6845

Kloprogge, F., Workman, L., Borrmann, S., Tékété, M., Lefèvre, G., Hamed, K., et al. (2018). Artemether-lumefantrine dosing for malaria treatment in young children and pregnant women: a pharmacokinetic-pharmacodynamic meta-analysis. *PLoS Med.* 15:e1002579. doi: 10.1371/journal.pmed.1002579

Lam, N. S., Long, X., Su, X. Z., and Lu, F. (2018). Artemisinin and its derivatives in treating helminthic infections beyond schistosomiasis. *Pharmacol Res.* 133, 77–100. doi: 10.1016/j.phrs.2018.04.025

Lane, C. A., Hardy, J., and Schott, J. M. (2018). Alzheimer's disease. *Eur. J. Neurol.* 25, 59–70. doi: 10.1111/ene.13439

Lauritzen, I., Pardossi-Piquard, R., Bourgeois, A., Pagnotta, S., Biferi, M. G., Barkats, M., et al. (2016). Intraneuronal aggregation of the β-CTF fragment of APP (C99) induces Aβ-independent lysosomal-autophagic pathology. *Acta Neuropathol.* 132, 257–276. doi: 10.1007/s00401-016-1577-6

Lohy Das, J., Rulisa, S., de Vries, P. J., Mens, P. F., Kaligirwa, N., Kaligirwa, N., et al. (2018). Population pharmacokinetics of artemether, dihydroartemisinin and lumefantrine in rwandese pregnant women treated for uncomplicated

plasmodium falciparum malaria. *Antimicrob. Agents Chemother.* 62:e00518-18. doi: 10.1128/AAC.00518-18

Luheshi, L. M., Crowther, D. C., and Dobson, C. M. (2008). Protein misfolding and disease: from the test tube to the organism. *Curr. Opin. Chem. Biol.* 12, 25–31. doi: 10.1016/j.cbpa.2008.02.011

Lumkwana, D., du Toit, A., Kinnear, C., and Loos, B. (2017). Autophagic flux control in neurodegeneration: progress and precision targeting—Where do we stand? *Prog. Neurobiol.* 153, 64–85. doi: 10.1016/j.pneurobio.2017.03.006

Majumder, S., Richardson, A., Strong, R., and Oddo, S. (2011). Inducing autophagy by rapamycin before, but not after, the formation of plaques and tangles ameliorates cognitive deficits. *PLoS One* 6:e25416. doi: 10.1371/journal.pone.0025416

Martinet, W., Agostinis, P., Vanhoecke, B., Dewaele, M., and De Meyer, G. R. (2009). Autophagy in disease: a double-edged sword with therapeutic potential. *Clin. Sci.* 116, 697–712. doi: 10.1042/cs20080508

Nie, T., Yang, S., Ma, H., Zhang, L., Lu, F., Tao, K., et al. (2016). Regulation of ER stress-induced autophagy by GSK3β-TIP60-ULK1 pathway. *Cell Death Dis.* 7:e2563. doi: 10.1038/cddis.2016.423

Nixon, R. A. (2017). Amyloid precursor protein and endosomal-lysosomal dysfunction in Alzheimer's disease: inseparable partners in a multifactorial disease. *FASEB J.* 31, 2729–2743. doi: 10.1096/fj.201700359

Peters, W., Fleck, S. L., Robinson, B. L., Stewart, L. B., and Jefford, C. W. (2003). The chemotherapy of rodent malaria. LX. The importance of formulation in evaluating the blood schizontocidal activity of some endoperoxide antimalarials. *Ann. Trop. Med. Parasitol.* 96, 559–573. doi: 10.1179/000349802125001744

Pompl, P. N., Mullan, M. J., Bjugstad, K., and Arendash, G. W. (1999). Adaptation of the circular platform spatial memory task for mice: use in detecting cognitive impairment in the APP(sw) transgenic mouse model for Alzheimer's disease. *J. Neurosci. Methods* 87, 87–95. doi: 10.1016/s0165-0270(98)00169-1

Querfurth, H. W., and LaFerla, F. M. (2010). Alzheimer's disease. *N. Engl. J. Med.* 362, 329–344. doi: 10.1056/NEJMra0909142

Selkoe, D., and Hardy, J. (2016). The amyloid hypothesis of Alzheimer's disease at 25 years. *EMBO Mol. Med.* 8, 595–608. doi: 10.15252/emmm.201606210

Souza, M. A., Magni, D. V., Guerra, G. P., Oliveira, M. S., Furian, A. F., Pereira, L., et al. (2012). Involvement of hippocampal CAMKII/CREB signaling in the spatial memory retention induced by creatine. *Amino Acids.* 43, 2491–2503. doi: 10.1007/s00726-012-1329-4

Spilman, P., Podlutskaya, N., Hart, M. J., Debnath, J., Gorostiza, O., Richardson, A., et al. (2010). Inhibition of mTOR by rapamycin abolishes cognitive deficits and reduces amyloid-beta levels in a mouse model of Alzheimer's disease. *PLoS One* 5:e9979. doi: 10.1371/journal.pone.0009979

Thal, D. R. (2015). Clearance of amyloid β-protein and its role in the spreading of Alzheimer's disease pathology. *Front. Aging Neurosci.* 7:25. doi: 10.3389/fnagi.2015.00025

Uddin, M. S., Mamun, A. A., Labu, Z. K., Hidalgo-Lanussa, O., Barreto, G. E., and Ashraf, G. M. (2019). Autophagic dysfunction in Alzheimer's disease: cellular and molecular mechanistic approaches to halt Alzheimer's pathogenesis. *J. Cell. Physiol.* 234, 8094–8112. doi: 10.1002/jcp.27588

Uddin, M. S., Stachowiak, A., Mamun, A. A., Tzvetkov, N. T., Takeda, S., Atanasov, A. G., et al. (2018). Autophagy and Alzheimer's disease: from molecular mechanisms to therapeutic implications. *Front. Aging Neurosci.* 10:04. doi: 10.3389/fnagi.2018.00004

U.S. Department of Health and Human Services, Center for Drug Evaluation and Research (CDER). (2005). Food and drug administration. guidance for industry: estimating the maximum safe starting dose in initial clinical trials for therapeutics in adult healthy volunteers, 7–19. Available online at: www.researchgate.net/publication/237342033_US_Department_of_Health_and_Human_Services_Food_and_Drug_Administration_Center_for_Drug_Evaluation_and_Research/citation/download.

Xiang, Y., Bu, X. L., Liu, Y. H., Zhu, C., Shen, L. L., Jiao, S. S., et al. (2015). Physiological amyloid-beta clearance in the periphery and its therapeutic potential for Alzheimer's disease. *Acta Neuropathol.* 130, 487–499. doi: 10.1007/s00401-015-1477-1

Xie, L. H., Li, Q., Zhang, J., and Weina, P. J. (2009). Pharmacokinetics, tissue distribution and mass balance of radiolabeled dihydroartemisinin in male rats. *Malar. J.* 8:112. doi: 10.1186/1475-2875-8-112

Xu, C., Wang, M., Song, Z., Wang, Z., Liu, Q., Jiang, P., et al. (2018). Pseudorabies virus induces autophagy to enhance viral replication in mouse neuro-2a cells in vitro. *Virus Res.* 248, 44–52. doi: 10.1016/j.virusres.2018.02.004

Yamamoto, N., Arima, H., Naruse, K., Kasahara, R., Taniura, H., Hirate, H., et al. (2013). Ketamine reduces amyloid beta-protein degradation by suppressing neprilysin expression in primary cultured astrocytes. *Neurosci. Lett.* 545, 54–58. doi: 10.1016/j.neulet.2013.04.016

Yamamoto, N., Ishikuro, R., Tanida, M., Suzuki, K., Ikeda-Matsuo, Y. and Sobue, K. (2018). Insulin-signaling pathway regulates the degradation of amyloid β-protein *via* astrocytes. *Neuroscience* 385, 227–236. doi: 10.1016/j.neuroscience.2018.06.018

Yamamoto, N., Tanida, M., Ono, Y., Kasahara, R., Fujii, Y., Ohora, K., et al. (2014). Leptin inhibits amyloid beta-protein degradation through decrease of neprilysin expression in primary cultured astrocytes. *Biochem. Biophys. Res. Commun.* 445, 214–217. doi: 10.1016/j.bbrc.2014.01.168

Yoon, S. Y., and Kim, D. H. (2016). Alzheimer's disease genes and autophagy. *Brain Res.* 1649, 201–209. doi: 10.1016/j.brainres.2016.03.018

Yu, W. H., Cuervo, A. M., Kumar, A., Peterhoff, C. M., Schmidt, S. D., Lee, J. H., et al. (2005). Macroautophagy--A novel β-amyloid peptide-generating pathway activated in Alzheimer's disease. *J. Cell Biol.* 171, 87–98. doi: 10.1083/jcb.200505082

Zhang, Z., Yao, Z., Zhao, S., Shao, J., Chen, A., Zhang, F., et al. (2017). Interaction between autophagy and senescence is required for dihydroartemisinin to alleviate liver fibrosis. *Cell Death Dis.* 8:e2886. doi: 10.1038/cddis.2017.255

Zheng, L., Cedazo-Minguez, A., Hallbeck, M., Jerhammar, F., Marcusson, J., and Terman, A. (2012). Intracellular distribution of amyloid beta peptide and its relationship to the lysosomal system. *Transl. Neurodegener.* 1, 19–26. doi: 10.1186/2047-9158-1-19

Conflict of Interest: The authors declare that the research was conducted in the absence of any commercial or financial relationships that could be construed as a potential conflict of interest.

frontiers in Aging Neuroscience

ORIGINAL RESEARCH
published: 29 June 2021
doi: 10.3389/fnagi.2021.693611

Precision Repetitive Transcranial Magnetic Stimulation Over the Left Parietal Cortex Improves Memory in Alzheimer's Disease: A Randomized, Double-Blind, Sham-Controlled Study

Yanli Jia[1†], Luoyi Xu[1†], Kehua Yang[1†], Yingchun Zhang[1], Xinghui Lv[1], Zhenwei Zhu[1], Zheli Chen[2], Yunlong Zhu[3], Lili Wei[1], Xia Li[4], Mincai Qian[2], Yuedi Shen[5], Weiming Hu[3] and Wei Chen[1,6,7]**

[1] Department of Psychiatry, Sir Run Run Shaw Hospital, Zhejiang University School of Medicine, Hangzhou, China, [2] Third People's Hospital of Huzhou, Huzhou, China, [3] The Third Hospital of Quzhou, Quzhou, China, [4] Department of Geriatric Psychiatry, Shanghai Mental Health Center, Shanghai Jiao Tong University School of Medicine, Shanghai, China, [5] School of Medicine, Hangzhou Normal University, Hangzhou, China, [6] Department of Psychology and Behavioral Sciences, Zhejiang University, Hangzhou, China, [7] Key Laboratory of Medical Neurobiology of Zhejiang Province, Hangzhou, China

Objective: We aim to study the effect of precision repetitive transcranial magnetic stimulation (rTMS) over the left parietal cortex on the memory and cognitive function in Alzheimer's disease (AD).

Methods: Based on the resting-state functional magnetic resonance imaging, the left parietal cortex site with the highest functional connectivity to the hippocampus was selected as the target of rTMS treatment. Sixty-nine AD patients were randomized to either rTMS or sham treatment (five sessions/week for a total of 10 sessions). The Mini-Mental State Examination (MMSE), 12-Word Philadelphia Verbal Learning Test (PVLT), and Clinical Dementia Rating (CDR) were assessed at baseline and after the last session.

Results: After a 2-week treatment, compared to patients in the sham group, those in the rTMS group scored significantly higher on PVLT total score and its immediate recall subscale score. Moreover, in the rTMS group, there were significant improvements after the 2-week treatment, which were manifested in MMSE total score and its time orientation and recall subscale scores, as well as PVLT total score and its immediate recall and short delay recall subscale scores. In the sham group, the PVLT total score was significantly improved.

Conclusion: The target site of the left parietal cortex can improve AD patients' cognitive function, especially memory, providing a potential therapy.

Keywords: precision rTMS, left parietal cortex, Alzheimer's disease, memory, cognition

OPEN ACCESS

Edited by:
Aurel Popa-Wagner, University of Medicine and Pharmacy of Craiova, Romania

Reviewed by:
Tianzhen Chen, Shanghai Jiao Tong University, China
Dominique Januel, Unité de Recherche Clinique (URC), EPS Ville Evrard, France

***Correspondence:**
Wei Chen
srrcw@zju.edu.cn
Weiming Hu
h1561@163.com

[†] These authors have contributed equally to this work

***Received:** 11 April 2021*
***Accepted:** 31 May 2021*
***Published:** 29 June 2021*

Citation:
Jia Y, Xu L, Yang K, Zhang Y, Lv X, Zhu Z, Chen Z, Zhu Y, Wei L, Li X, Qian M, Shen Y, Hu W and Chen W (2021) Precision Repetitive Transcranial Magnetic Stimulation Over the Left Parietal Cortex Improves Memory in Alzheimer's Disease: A Randomized, Double-Blind, Sham-Controlled Study. Front. Aging Neurosci. 13:693611. doi: 10.3389/fnagi.2021.693611

INTRODUCTION

Alzheimer's disease (AD), the most common subtype of dementia among elderly adults (Sosa-Ortiz et al., 2012; Fargo et al., 2014), is generally characterized by memory decline (the core symptom), language dysfunctions, mood and personality changes, loss of spatial and temporal orientation, and behavioral derangements, leading to impaired functioning in individuals' occupational and social domains (Lane et al., 2018). The global number of people with dementia was 4.38 million in 2016 (Nichols et al., 2019), which would be more than triple by 2050, according to the World Health Organization (WHO) (2017). Among them, individuals with AD accounted for 50–75% (Alzheimer's Disease International, 2019). Therefore, the financial burden caused by AD would also continue to increase substantially (Winblad et al., 2016).

Up to now, AD is mainly treated by focusing on decelerating cognition decline using clinically approved medications, such as cholinesterase inhibitors, including donepezil, rivastigmine, and galantamine, for mild and moderate AD (Birks, 2006), and memantine, a medication antagonizing the *N*-methyl-D-aspartate receptor, for moderate and severe AD (McShane et al., 2019). However, these medications can only be used for symptomatic treatment, with limited efficacy, and cannot prevent disease course (Fargo et al., 2014; Anand et al., 2017; Lane et al., 2018), and not all patients can tolerate it. In clinical trials, about 29% of patients in the active treatment group withdrew from the trial due to side effects, which was significantly higher than that in the placebo group (Birks, 2006). As a consequence, exploring some non-pharmacological therapeutic strategies is highly demanding.

Repetitive transcranial magnetic stimulation (rTMS) is an alternative therapeutic method that can non-invasively stimulate the brain in a rhythmic form through electromagnetic induction, thereby modulating cortical excitability and neural activity (Rossi et al., 2009; Valero-Cabré et al., 2017). Low-frequency rTMS decreases neural excitability in targeted cortical areas, whereas high frequency increases neural excitability (Gangitano et al., 2002). In healthy participants, rTMS could serve as possible modulators of cognitive function. For instance, subthreshold TMS (50% and 60% motor thresholds) applied over the right dorsolateral prefrontal cortex effectively modulated cognitive function (Bashir et al., 2020). Studies also showed that rTMS enhanced cognitive and motor functions of healthy old adults (Zimerman and Hummel, 2010). In 2008, the US Food and Drug Administration (FDA) approved rTMS for 4–6 weeks to clinically treat medication-resistant major depression (FDA approval K061053). Currently, rTMS has achieved preliminary results in improving cognitive function in AD patients. Meta-analysis studies revealed that high-frequency rTMS treatment positively affected cognitive function and global impression (Cheng et al., 2018; Dong et al., 2018; Lin et al., 2019). Another recent meta-analysis also revealed that compared with sham brain stimulation, high-frequency rTMS had short-term and long-term (lasting to 1 month after treatment) positive effects on the general cognition of AD patients (Chu et al., 2021). More concretely, significant improvements were found on language, including the accuracy of action naming and auditory sentence comprehension (Cotelli et al., 2006, 2008, 2011; Zhao et al., 2017), verbal and non-verbal agility (Devi et al., 2014), memory (Haffen et al., 2012; Zhao et al., 2017; Chu et al., 2021), and attention (Eliasova et al., 2014).

Regarding memory improvement, verbal working memory was significantly improved after 10 Hz rTMS with 100% resting motor threshold applied over the left prefrontal cortex in healthy participants (Ohn et al., 2008). A randomized, double-blind, and sham-controlled trial indicated that after a 6-week 20 Hz rTMS treatment applied over brain areas of parietal P3/P4 and posterior temporal T5/T6 consistent to the electroencephalogram 10–20 system (one session per day and 5 days per week for a total of 30 sessions), AD patients' memory in Montreal Cognitive Assessment increased significantly compared with their baseline, especially in patients with mild AD (Zhao et al., 2017). One case study using 10 Hz rTMS over the left prefrontal cortex (one session per day and 5 days per week for a total of 10 sessions) as an adjunct to AD treatment revealed that after 1 month of treatment, the patient performed better on episodic memory and speed processing tests (Haffen et al., 2012). Nevertheless, the studies focusing on memory improvement in AD patients are underrepresented. Moreover, most previous studies used comprehensive cognitive questionnaires to assess the efficacy, not specifically for memory, and reached inconsistent results (Liao et al., 2015; Cheng et al., 2018; Lin et al., 2019). Meanwhile, as we all know, memory decline is related to the hippocampus buried deep in the brain. However, the stimulus target is determined by the 5-cm rule, electroencephalogram 10–20 system, or magnetic resonance imaging navigation (Cheng et al., 2018), and the stimulus focality is limited only to the cerebral cortex (Thielscher and Kammer, 2004). It is difficult to directly stimulate the hippocampus or precisely stimulate it indirectly. Therefore, it is necessary to select a location in the cerebral cortex as the target of rTMS based on functional connectivity between the hippocampus and the cortex.

Although the hippocampus played a vital role in the process of memory encoding and retrieval (Battaglia et al., 2011), studies suggested that the interaction between brain regions underlying memory, rather than a single brain region such as the hippocampus, was the key to memory improvement (Kim et al., 2016), and interactions of the hippocampus with other locations in the cortical–hippocampal network were observed in a functional magnetic resonance imaging study (Spaniol et al., 2009). The parietal cortex, as a component of the cortical–hippocampal network, was related to the memory function, such as episodic memory and working memory (Berryhill, 2012), which was validated in several rTMS studies. In healthy participants, using rTMS to stimulate the lateral parietal target site, with the highest functional connectivity to the hippocampus, could modulate cortical–hippocampal networks and concomitantly manipulate associative memory (Wang et al., 2014). These findings could be reproduced. Using similar rTMS settings, Freedberg et al. (2019) found that hippocampal functional connectivity increased significantly and that this effect was specific to the hippocampal network. Moreover, theta-burst TMS treatment applied over the posterior inferior parietal

cortex might also serve as a potential therapy for specifically manipulating the encoding of new associative memory without influencing memory retrieval (Tambini et al., 2018). In AD patients, the integrity of the parietal memory network including the inferior parietal lobule was disrupted (Greene and Killiany, 2010; Hu et al., 2019). After a 2-week rTMS treatment (1,640 pulses, 20 Hz, 100 MT, one session per day and 5 days per week) applied over the left lateral parietal cortex, AD patients performed better on visual recognition memory and clock drawing test, indicating that high-frequency rTMS treatment could improve cognition and modulate functional connectivity of the brain network (Velioglu et al., 2021). Evidence also showed that in prodromal AD patients, a 2-week 20 Hz rTMS treatment applied over the precuneus enhanced their episodic memory and neural activity (Koch et al., 2018). Besides, the left hemisphere was selected due to the known role of the left lateral parietal cortex in memory retrieval (Wagner et al., 2005). Based on these findings, we select the left parietal cortex as the target site, instead of the common dorsolateral prefrontal cortex used in most previous studies (Liao et al., 2015), to improve episodic memory in addition to general cognition.

Herein, we recruit patients for a 2-week 10 Hz rTMS or sham treatment and adapt some evaluation scales to assess their memory and cognition. We have hypothesized that after a 2-week 10 Hz rTMS treatment based on the functional connectivity of cortical–hippocampal networks, AD patients' memory and cognition improved significantly compared to the baseline or sham group.

MATERIALS AND METHODS

Study Design

The study involved a double-blind, randomized, and sham-controlled trial, which was approved by the Ethics Committee of Sir Run Run Shaw Hospital, School of Medicine, Zhejiang University (number: 20170228-1), and was registered on the National Medical Research Platform of China (number: MR-33-20-004217)[1]. The patients were randomly assigned to either rTMS or sham treatment. The rTMS group patients received daily treatment sessions for 2 weeks (one session per day and 5 days per week for a total of 10 sessions), while the sham group patients received regular sham management. Neuropsychological assessments were performed at baseline and immediately after a 2-week treatment. The primary outcomes were the differences in the 12-Word Philadelphia Verbal Learning Test (PVLT) scores between the groups and between pre- and post-treatment. The secondary outcomes were the differences in the Mini-Mental State Examination (MMSE) scores.

Patients

A total of 103 patients with mild to moderate AD were recruited from outpatients and inpatients of the Sir Run Run Shaw Hospital, School of Medicine, Zhejiang University, Hangzhou, China, and underwent a standardized evaluation. The patients were screened from an ongoing follow-up project that aimed to treat AD by precision rTMS of the left parietal cortex. Patients were included if they (1) met the diagnostic criteria for probable AD according to the *Diagnostic and Statistical Manual of Mental Disorders*, fifth edition (DSM-5), criteria (American Psychiatric Association, 2013); (2) had a Clinical Dementia Rating (CDR) score between 0.5 and 2; and (3) were from 55 to 85 years old and right-handed. The exclusion criteria included: (1) severe liver, kidney, heart, and lung diseases; (2) history of head trauma, neurological disorders, psychiatric disorders, and/or substance abuse; (3) focal brain lesions on T1 or T2 images; (4) any rTMS contraindications (e.g., medical implants or devices, metal in the body, or epilepsies). Besides, for patients who used medications stably for more than 3 months, we continued the same medication types and doses during the 2-week rTMS sessions. All patients signed an informed consent form before the administration of the baseline assessment.

The patients were randomly assigned to groups with a single random number sequence that was used to produce a series of opaque and sealed envelopes. The envelope for each patient was opened by the rTMS therapist before the first treatment session.

MRI Data Acquisition

T1-weighted and resting-state functional magnetic resonance imaging (fMRI) data were acquired using a 3.0-T Siemens Prisma MRI scanner (GE Discovery MR750, GE Medical Systems, Milwaukee, WI, United States) equipped with an eight-channel head coil array. During scanning, all patients were instructed to keep their head and body motionless with their eyes open and not think about anything specific. The functional images were obtained axially using an echo-planar imaging (EPI) sequence with the following parameters: 240 volumes; repetition time (TR) = 2,000 ms; echo time (TE) = 30 ms; flip angle (FA) = 90°; field of view (FOV) = 220 mm × 220 mm; matrix = 64 × 64; and slice thickness = 3.2 mm with no gap. High-resolution anatomic three-dimensional T1-weighted images were obtained with the following parameters: 176 axial slices; TR = 8.1 ms; TE = 3.1 ms; FA = 8°; FOV = 250 mm × 250 mm; matrix = 250 × 250; and slice thickness = 1.0 mm with no gap.

rTMS Procedures

Each patient's stimulus target was precisely identified using personal maps of hippocampal resting-state functional connectivity obtained at baseline. According to the method developed by Wang et al. (2014), based on the personal map, the average hippocampus coordinate [Montreal Neurological Institute (MNI) coordinates: $x = -24$, $y = -18$, $z = -18$] was selected as the seed of whole-brain functional connection analysis to identify the left parietal site with the highest functional connectivity to the hippocampus. This is the local highest connectivity within a 15-mm radius of MNI coordinates $x = -47$, $y = -68$, $z = +36$ [an area including the inferior parietal lobule (supramarginal and angular gyrus) and Brodmann areas 39 and 40], and this site was designated as the target of rTMS treatment.

We applied rTMS treatment over the left lateral parietal site, guided by an online neuronavigation system (Brainsight 2, Rogue Research, Montreal, QC, Canada). The patients received 10 Hz

[1]http://114.255.48.20/login

rTMS treatments for 2 weeks (one session per day and 5 days per week for a total of 10 sessions). In every rTMS session, the patient was seated in a reclining armchair and was asked to keep the head still. The figure-of-eight coil (70-mm diameter) connected to a Magstim Rapid2 stimulator (Magstim Company, Whitland, Wales, United Kingdom) was held tangential to the target site with reference to a frameless infrared stereotactic system. The motor threshold was defined as the minimum TMS intensity that produced a motor evoked potential of at least 50 μV for at least 5 of 10 consecutive pulses at baseline. We determined the resting motor threshold by stimulating the left motor cortex, which required at least 5 of 10 consecutive pulses that must evoke contraction in the first dorsal interosseous muscle of the right hand when the patients kept the first dorsal interosseous muscles relaxed in both hands (Rossini et al., 2015). Each treatment included 800 pulses at 10 Hz and 100–110% motor threshold, and the stimulation lasted for 2 s, followed by a 28-s stimulation interval. The sham group received regular sham management such that the same coil was rotated 45° away from the brain scalp, with one wing of the coil being in contact with the scalp and the distance between the coil center and the target site being larger than 5 cm, and the patients would also perceive the same noise and sensation caused by the stimulation.

Blinding

Sham treatment produces the same noise and sensation, and patients were told that scalp discomfort and transient fatigability might occur during rTMS or sham sessions. All patients and neuropsychologists administering clinical assessments did not know whether the patients received rTMS or sham treatment; only the rTMS therapist knew the randomized treatment. After every treatment session, patients were asked how they felt about the treatment to confirm that they did not know which treatment they received.

Neuropsychological Assessments

All patients underwent several clinical assessments administered by a trained neuropsychologist at baseline and after the last (10th) session, including the following evaluation scales: the MMSE (Folstein et al., 1975); a brief screening questionnaire assessing cognitive impairment, including orientation, registration, recall, attention and calculation, and language ability to follow spoken and written commands; the PVLT (Bezdicek et al., 2014), a learning task consisting of three categories of words used to assess immediate, short delay, long delay, and distractor memory in AD patients; and the CDR (Hughes et al., 1982), a semi-structured diagnostic interview for the staging of clinical dementia in the elderly.

The primary outcome measure was the difference of the PVLT scores between the rTMS group and sham group and that between the baseline and post-treatment in both groups. The secondary outcome measure was the difference of the MMSE scores between the rTMS group and sham group and that between the baseline and post-treatment in both groups.

Sample Size and Power Analysis

In our pre-experiment, the mean increment in PVLT score from baseline to 2 weeks was 6.10 points (SD = 4.80) in the rTMS group and 1.80 points (SD = 3.58) in the sham group. A relatively conservative difference of 4.00 points (SD = 5.00) between the two groups was used to estimate the sample size. The statistical analysis showed that a total of 68 patients (34 per group) were sufficient to provide a power of approximately 90% at a 5% significance level. Considering the potential study dropout, the sample size was increased by 25%, to 43 patients per group.

Statistical Analyses

The statistics program SPSS version 22.0 (SPSS Inc., Chicago, IL, United States) was employed in this study, and all data were checked for normal distribution $p > 0.05$ in the Shapiro–Wilk test. Descriptive statistics for demographics and baseline measures in the two groups of participants were compared using Student's *t*-test or a non-parametric Mann–Whitney test for continuous data or a χ^2 test for categorical data. Within each group, a paired-sample two-tailed *t*-test was used to compare the mean scores at baseline and after the last (10th) session, and a Wilcoxon signed-rank test was utilized for non-parametric scores. Two-way ANOVA (group × scale) was applied to the mean scores after 2 weeks of 10 sessions between the two groups. Whenever a significant main effect was found, *post hoc* Student's *t*-test was employed for comparison. Meanwhile, repeated-measures ANOVA, using group as the between-group factor and time as the within-group factor, was performed to assess the effect of rTMS intervention. Two-sided *p*-values less than 0.05 were considered significant.

RESULTS

Screening, enrollment, and participation information are shown in **Figure 1**. Before randomization, 10 patients were excluded due to brain lesions and psychiatric disorders, five patients withdrew due to personal reasons, and two patients were not contactable. After randomization, eight patients in the rTMS group and nine patients in the sham group did not complete neuropsychological assessments at baseline or did not tolerate the rTMS/sham treatment due to adverse effects, i.e., scalp discomfort and transient fatigability.

Patients' Baseline Characteristics

A total of 69 patients completed the 2-week treatment, and 35 of them were assigned to the rTMS group, and others were assigned to the sham group. No significant differences were found between the two groups as to gender ($\chi^2 = 0.12$, $p = 0.733$), age ($t = -0.99$, $p = 0.325$), education level ($t = 0.15$, $p = 0.878$), medication using ($\chi^2 = 0.12$, $p = 0.726$), and neuropsychological assessments (MMSE, PVLT, and CDR scores, see **Table 1**).

Primary Outcomes

The mean PVLT scale scores after the 2-week treatment were significantly different between the two groups [group effect, $F = 4.43$, $p = 0.039$, mean square error (MSE) = 291.51; scale

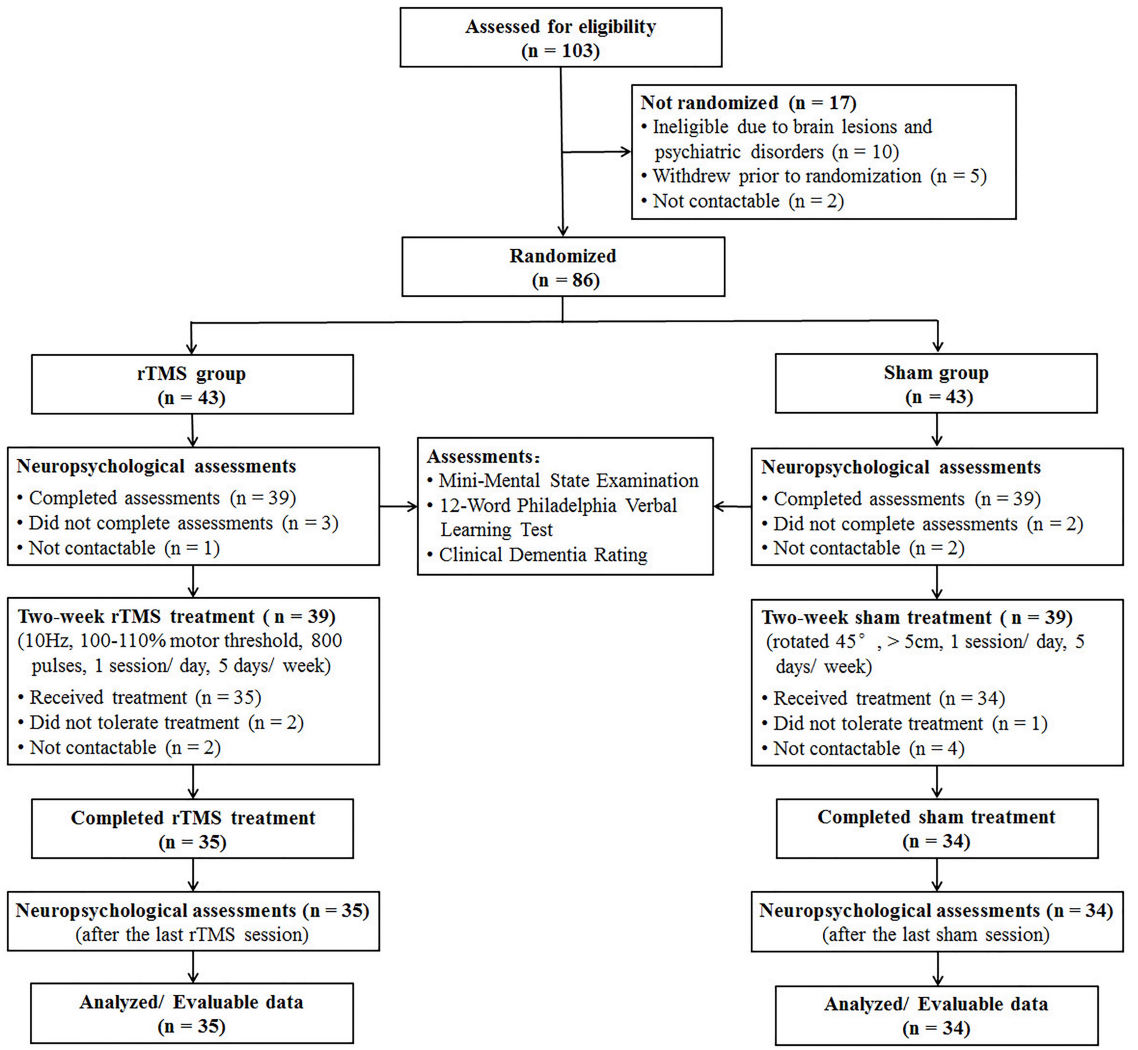

FIGURE 1 | CONSORT diagram of patients with Alzheimer's disease in a double-blind, sham-controlled study of rTMS.

effect, $F = 234.94$, $p < 0.001$, MSE = 3,888.96; group × scale interaction effect, $F = 5.38$, $p = 0.006$, MSE = 89.09]. Subsequent *post hoc* Student's *t*-test analysis demonstrated that patients in the rTMS group scored significantly higher than those in the sham group on the PVLT total score ($t = 2.10$, $p = 0.039$) and its immediate recall subscale score ($t = 2.38$, $p = 0.020$; see **Table 2**).

Within the rTMS group, we found some significant improvements after the 2-week treatment, which was manifested in the PVLT total score ($t = -6.99$, $p < 0.001$) and its immediate recall ($t = -7.19$, $p < 0.001$) and short delay recall ($t = -3.26$, $p = 0.003$) subscale scores. Within the sham group, the PVLT total score ($t = -2.57$, $p = 0.015$) was significantly improved (also see **Table 2**).

Meanwhile, the statistical results of repeated-measures ANOVA were also consistent with the above results. Repeated-measures ANOVA also showed a significant group effect ($F = 4.54$, $p = 0.041$, MSE = 1,045.07), time effect ($F = 53.24$, $p < 0.001$, MSE = 556.07), and group × time effect ($F = 10.33$, $p = 0.003$, MSE = 142.07) on the PVLT total score, and *post hoc* analysis revealed significant improvement in the rTMS group ($F = 48.79$, $p < 0.001$), in the sham group ($F = 6.60$, $p = 0.015$), and between the two groups after treatment ($F = 6.69$, $p = 0.014$). A significant group effect ($F = 4.47$, $p = 0.042$, MSE = 466.94), time effect ($F = 39.52$, $p < 0.001$, MSE = 232.97), and group × time effect ($F = 12.31$, $p = 0.001$, MSE = 88.97) were also found on its immediate recall subscale score, and *post hoc* analysis revealed significant improvement in the rTMS group ($F = 51.65$, $p < 0.001$) and between the two groups after treatment ($F = 7.43$, $p = 0.010$). A significant time effect was found on its short delay recall subscale score ($F = 7.88$, $p = 0.008$, MSE = 25.60), and *post hoc* analysis revealed a significant improvement in the rTMS group ($F = 10.63$, $p = 0.003$). Although there was a significant time effect on the long delay recall subscale score ($F = 7.06$, $p = 0.010$, MSE = 10.48), *post hoc* analysis revealed no significant improvement in either the rTMS group ($F = 3.19$, $p = 0.083$) or sham group ($F = 3.87$, $p = 0.058$). No significant

TABLE 1 | Baseline characteristics of AD patients.

Characteristics	rTMS group (n = 35)	Sham group (n = 34)	p-value
Age (years)	71.41 ± 8.85	73.41 ± 7.73	0.325
Female (%)	25 (71.43%)	23 (67.65%)	0.733
Education (years)	7.70 ± 5.26	7.50 ± 5.19	0.878
Medication (%)	20 (57.14%)	18 (52.94%)	0.726
MMSE	15.71 ± 5.60	15.62 ± 6.49	0.947
PVLT			
Immediate recall	13.94 ± 7.68	12.24 ± 8.65	0.389
Short delay recall	2.83 ± 3.21	2.56 ± 3.39	0.735
Long delay recall	1.97 ± 3.00	0.97 ± 1.99	0.107
Distractor recall	2.03 ± 1.54	1.53 ± 1.38	0.161
Intrusions	10.29 ± 11.02	8.21 ± 9.92	0.413
CDR	6.10 ± 3.03	6.63 ± 3.36	0.497

Means ± standard deviation. MMSE, Mini-Mental State Examination; PVLT, 12-Word Philadelphia Verbal Learning Test; CDR, Clinical Dementia Rating.

group effect (F = 1.26–1.31, p = 0.257–0.266, MSE = 3.71–256.96), time effect (F = 1.48–2.14, p = 0.149–0.228, MSE = 1.01–47.95), or group × time effect (F = 0.65–1.48, p = 0.228–0.424, MSE = 1.01–14.55) was found on other subscale scores.

Secondary Outcomes

Within the rTMS group, we found some significant improvements after the 2-week treatment, which was manifested in the MMSE total score (t = -3.43, p = 0.002) and its time orientation (t = -2.33, p = 0.026) and recall (z = -2.29, p = 0.026) subscale scores (also see **Table 2**).

Meanwhile, a significant time effect was found on MMSE total score (F = 10.08, p = 0.003, MSE = 36.03), and *post hoc* analysis revealed a significant improvement in the rTMS group (F = 11.77, p = 0.002). A significant group × time effect was found on its time orientation subscale scores (F = 4.25, p = 0.047, MSE = 2.65), and *post hoc* analysis revealed a significant improvement in the rTMS group (F = 5.44, p = 0.026). Although there was a significant time effect on attention and calculation subscale score (F = 4.17, p = 0.045, MSE = 2.34), *post hoc* analysis revealed no significant improvement in either the rTMS group (F = 2.36, p = 0.134) or sham group (F = 1.82, p = 0.186). No significant group effect (F = 0.00–2.49, p = 0.119–0.984, MSE = 0.00–3.37), time effect (F = 0.00–2.50, p = 0.119–1.000, MSE = 0.00–1.63), or group × time effect (F = 0.00–3.09, p = 0.083–1.000, MSE = 0.00–0.18) was found on other subscale scores.

TABLE 2 | Scores (means ± SD) of MMSE, CDR, and PVLT at baseline and after rTMS/sham treatment in the rTMS group (n = 35) and sham group (n = 34).

	rTMS group			Sham group			95% CI (SA vs. rA)
	Baseline	After treatment (SA)	95% CI	Baseline	After treatment (rA)	95% CI	
MMSE	15.71 ± 5.60	17.17 ± 6.06**	−2.32 to −0.59	15.62 ± 6.49	16.18 ± 6.95	−1.50 to 0.38	−2.14 to 4.13
Time orientation	1.20 ± 1.51	1.57 ± 1.46*	−0.70 to −0.05	1.47 ± 1.31	1.29 ± 1.45	−0.25 to 0.60	−0.42 to 0.98
Place orientation	3.20 ± 1.47	3.40 ± 1.63	−0.60 to 0.20	3.00 ± 1.63	3.24 ± 1.83	−0.63 to 0.16	−0.67 to 1.00
Registration	2.66 ± 0.48	2.83 ± 0.45	−0.35 to 0.01	2.50 ± 0.75	2.56 ± 0.82	−0.32 to 0.20	−0.05 to 0.59
Attention and calculation	2.11 ± 1.75	2.40 ± 1.85	−0.66 to 0.09	2.38 ± 1.76	2.62 ± 2.00	−0.59 to 0.12	−1.14 to 0.71
Recall	0.51 ± 0.89	0.91 ± 0.95*	−0.76 to −0.04	0.44 ± 0.75	0.62 ± 0.89	−0.41 to 0.06	−0.15 to 0.74
Language	6.03 ± 2.09	6.06 ± 2.25	−0.41 to 0.36	5.82 ± 2.53	5.85 ± 2.43	−0.49 to 0.43	−0.92 to 1.33
Naming	1.97 ± 0.17	1.94 ± 0.24	−0.03 to 0.09	1.82 ± 0.52	1.88 ± 0.41	−0.14 to 0.02	−0.10 to 0.22
Repetition	0.54 ± 0.51	0.60 ± 0.50	−0.22 to 0.11	0.62 ± 0.49	0.53 ± 0.51	−0.09 to 0.27	−0.17 to 0.31
Three−stage command	1.89 ± 1.02	1.86 ± 1.03	−0.30 to 0.36	1.50 ± 1.13	1.62 ± 1.23	−0.42 to 0.19	−0.31 to 0.79
Reading	0.74 ± 0.44	0.77 ± 0.43	−0.09 to 0.03	0.71 ± 0.46	0.68 ± 0.47	−0.08 to 0.13	−0.12 to 0.31
Writing	0.49 ± 0.51	0.49 ± 0.51	−0.08 to 0.08	0.62 ± 0.49	0.59 ± 0.50	−0.13 to 0.19	−0.34 to 0.14
Copying	0.40 ± 0.50	0.40 ± 0.50	−0.08 to 0.08	0.56 ± 0.50	0.56 ± 0.50	−0.17 to 0.17	−0.40 to 0.08
PVLT	18.74 ± 12.91	24.89 ± 14.08***#	−7.93 to −4.36	15.77 ± 12.73	17.77 ± 14.04*	−3.58 to −0.42	0.36 to 13.88
Immediate recall	13.94 ± 7.68	18.23 ± 8.01***#	−5.5 to −3.07	12.24 ± 8.65	13.24 ± 9.41	−2.28 to 0.28	0.80 to 9.19
Short delay recall	2.83 ± 3.21	4.17 ± 3.57**	−2.18 to −0.51	2.56 ± 3.39	2.97 ± 3.05	−1.37 to 0.55	−0.40 to 2.80
Long delay recall	1.97 ± 3.00	2.49 ± 3.81	−1.10 to 0.07	0.97 ± 1.99	1.56 ± 2.98	−1.20 to 0.02	−0.72 to 2.57
Distractor recall	2.03 ± 1.54	1.69 ± 1.02	−0.12 to 0.81	1.53 ± 1.38	1.53 ± 1.40	−0.33 to 0.33	−0.43 to 0.74
Intrusions	10.29 ± 11.02	12.11 ± 10.34	−4.62 to 0.96	8.21 ± 9.92	8.74 ± 10.57	−2.21 to 1.15	−1.65 to 8.40
CDR	6.10 ± 3.03	5.96 ± 2.92	−0.14 to 0.43	6.63 ± 3.36	6.56 ± 3.45	−0.21 to 0.35	−2.15 to 0.95
Memory	1.41 ± 0.50	1.34 ± 0.55	−0.04 to 0.19	1.40 ± 0.61	1.38 ± 0.63	−0.08 to 0.11	−0.33 to 0.24
Orientation	1.18 ± 0.66	1.09 ± 0.61	−0.01 to 0.19	1.24 ± 0.62	1.25 ± 0.65	−0.09 to 0.07	−0.47 to 0.14
Judgment and problem solving	1.07 ± 0.58	1.06 ± 0.57	−0.08 to 0.11	1.19 ± 0.77	1.18 ± 0.78	−0.02 to 0.04	−0.45 to 0.21
Community affairs	1.09 ± 0.61	1.10 ± 0.55	−0.11 to 0.08	1.06 ± 0.62	1.07 ± 0.57	−0.11 to 0.08	−0.24 to 0.30
Home and hobbies	1.06 ± 0.62	1.10 ± 0.60	−0.12 to 0.03	1.22 ± 0.71	1.24 ± 0.74	−0.14 to 0.11	−0.46 to 0.19
Personal care	0.29 ± 0.63	0.27 ± 0.62	−0.03 to 0.09	0.53 ± 0.71	0.44 ± 0.66	−0.04 to 0.22	−0.49 to 0.13

**p < 0.05; **p < 0.01; ***p < 0.001 vs. baseline; #p < 0.05 vs. sham group.*
CI, confidence interval; MMSE, Mini-Mental State Examination; PVLT, 12-Word Philadelphia Verbal Learning Test; CDR, Clinical Dementia Rating.

Adverse Effects

Two patients in the rTMS group and one patient in the sham group did not tolerate the rTMS/sham treatment due to adverse effects. One patient in the rTMS group reported local scalp discomfort persisting for longer than 15 min after the first treatment session. The other two patients (one in the rTMS group and one in the sham group) reported feeling transient fatigue, but they could not tolerate it and asked to withdraw. There were no serious adverse effects, i.e., seizures or manic episodes.

DISCUSSION

After the 2-week treatment, patients in the rTMS group performed better on MMSE and PVLT scales, and these improvements were significantly greater than those in the sham group, confirming most of our two hypotheses. This study is dedicated to selecting a precision target in the left parietal cortex with the highest functional connectivity to the hippocampus as the stimulation site and has demonstrated that this novel site is remarkably effective in improving the memory of AD patients. Given the situation that there is no effective way to cure AD, preliminary but promising findings of our study have brought hope to the clinical treatment in the future.

The result that some cognition improvements were accomplished after a 2-week rTMS treatment could be supported by the finding that a 2-week rTMS treatment applied over the left lateral parietal cortex could improve cognition and modulate the functional connectivity of the brain network in AD patients (Velioglu et al., 2021). AD patients' cognition decline might be related to disrupted integration and segregation in their large-scale brain networks (Dai and He, 2014), including the parietal memory network (Hu et al., 2019), inferring that connectivity between different brain regions was abnormally disturbed and that rTMS might strengthen residual brain tissue connectivity. Evidence showed that the functional connectivity value between the parietal cortex and hippocampus was positively correlated with associative memory improvement in healthy adults (Wang et al., 2014; Tambini et al., 2018). Our patients in the rTMS group scored significantly higher on the PVLT total score and its immediate recall subscale score. This is in line with findings that AD patients performed better on visual recognition memory after a 2-week 20 Hz rTMS treatment applied over the left lateral parietal cortex (Velioglu et al., 2021). In healthy people, transcranial direct current stimulation applied over the parietal cortex improves verbal episodic memory during the retrieval phase (Manenti et al., 2013). rTMS applied over the left lateral parietal cortex successfully increased the cortical–hippocampal connectivity and enhanced associative memory, inducing localized long-term potentiation of cortical–hippocampal networks (Wang et al., 2014). Long-term potentiation, the main form of synaptic plasticity, was considered an essential central cellular mechanism of memory and learning, and synaptic plasticity enhancement might explain rTMS efficacy in the cerebral cortex (Bliss and Collingridge, 1993; Esser et al., 2006). A study showing that synaptic plasticity induction was linked to rTMS aftereffect also supported this explanation (Hoogendam et al., 2010).

In the sham group, AD patients' PVLT total score improved significantly compared with their baseline, which was beyond our expectation. There were some possible reasons to explain this result. One was that patients continued to take medication, including cognitive enhancers, during rTMS sessions, enhancing patients' memory. Another could be explained by placebo response, an improvement of clinical symptoms caused by placebo treatment, or the environment in which patients received treatment. Patients' improvements might be linked to their optimistic attitudes, goal seeking, and expected treatment outcomes (Horing et al., 2014). Furthermore, the special attention of patients' caregivers and medical staff might also be a possible reason. Nonetheless, in the two groups, the proportions of patients who used medications were similar, reaching about 50%, and within the sham group, patients' immediate recall, short delay recall, and long delay recall were not statistically significant after the 2-week sham treatment. Meanwhile, improved patients' memory in the rTMS group was significantly better than that in the sham group. Therefore, we could exclude a medication effect and reasonably believe that the rTMS treatment is effective.

The rTMS treatment has the advantage of short treatment time and quick therapeutic response. Taking AD as an example, a systematic review showed that the duration of rTMS treatment varied from 1 to 18 weeks (Devi et al., 2014). After a single session of rTMS, action naming was improved immediately (Cotelli et al., 2006). And after 2–4 weeks of high-frequency rTMS, cognitive function was significantly strengthened, and this curative effect could be sustained for 2 months after treatment (Cotelli et al., 2011). Moreover, a 2-week rTMS treatment was as sufficient as longer-term treatment regarding the contribution on cognitive improvements in AD patients (Cotelli et al., 2011). The lasting time of rTMS efficacy in our study is not yet known and needs to be determined by follow-up studies.

However, there are several limitations in the current study. Firstly, there was no follow-up study on how long the effect of cognition and memory improvement could last. Secondly, we only used several neuropsychological scales to evaluate AD patients' memory and cognition, which might not provide a comprehensive understanding. Next, we would conduct follow-up studies using neuropsychological assessments and functional magnetic resonance imaging to determine rTMS efficacy duration. Thirdly, considering AD patients' benefits, more than half of them continued dementia-related medication at the same dosage, despite the fact that used medication presented no significant difference between the two groups.

CONCLUSION

This study is a pilot study to demonstrate the precision rTMS effect over the left parietal cortex on memory and cognition improvement in AD patients, presenting a novel and promising therapy for treating memory impairment in AD patients; provides an add-on treatment for AD patients who are taking medication; and lays the foundation for our future studies on functional connectivity of brain regions and efficacy lasting time. Moreover, efforts will also be made to identify the therapeutic

mechanism of AD, explore rTMS frequency and number of sessions, and further establish an optimal protocol.

DATA AVAILABILITY STATEMENT

The raw data supporting the conclusions of this article will be made available by the authors, without undue reservation.

ETHICS STATEMENT

The studies involving human participants were reviewed and approved by the Ethics Committee of Sir Run Run Shaw Hospital, School of Medicine, Zhejiang University (No: 20170228-1). The patients/participants provided their written informed consent to participate in this study.

AUTHOR CONTRIBUTIONS

WC, WH, MQ, and XLi conceived the study. YJ, LX, KY, YZhang, XLv, ZZ, ZC, YZhu, LW, YS, and WC conducted the tests and collected the data. YJ, LX, and KY analyzed the data. YJ, LX, KY, YS, and WC drafted the manuscript. All authors contributed to the article and approved the submitted version.

FUNDING

This research was supported by grants from the National Key Research & Development Program of China (no. 2017YFC1310502), National Natural Science Foundation of China (nos. 82071181 and 81661148045), Key Research & Development Program of Zhejiang Province (nos. 2020C03021 and 2018C03023), and Science and Technology Program of Hangzhou Municipality (no. 20190101A10).

ACKNOWLEDGMENTS

The authors would like to thank all patients for their kindness and willingness to be enrolled in this study.

REFERENCES

Alzheimer's Disease International (2019). *World Alzheimer report 2019: Attitudes to Dementia*. London: Alzheimer's Disease International.

American Psychiatric Association (2013). *Diagnostic and Statistical Manual of Mental Disorder*, 5th Edn. Washington, DC: American Psychiatric Publication.

Anand, A., Patience, A. A., Sharma, N., and Khurana, N. (2017). The present and future of pharmacotherapy of Alzheimer's disease: a comprehensive review. *Eur. J. Pharmacol.* 815, 364–375. doi: 10.1016/j.ejphar.2017.09.043

Bashir, S., Al-Hussain, F., Hamza, A., Shareefi, G. F., Abualait, T., and Yoo, W. K. (2020). Role of single low pulse intensity of transcranial magnetic stimulation over the frontal cortex for cognitive function. *Front. Hum. Neurosci.* 14:205. doi: 10.3389/fnhum.2020.00205

Battaglia, F. P., Benchenane, K., Sirota, A., Pennartz, C. M., and Wiener, S. I. (2011). The hippocampus: hub of brain network communication for memory. *Trends Cogn. Sci.* 15, 310–318. doi: 10.1016/j.tics.2011.05.008

Berryhill, M. E. (2012). Insights from neuropsychology: pinpointing the role of the posterior parietal cortex in episodic and working memory. *Front. Integr. Neurosci.* 6:31. doi: 10.3389/fnint.2012.00031

Bezdicek, O., Libon, D. J., Stepankova, H., Panenkova, E., Lukavsky, J., Garrett, K. D., et al. (2014). Development, validity, and normative data study for the 12-word Philadelphia Verbal Learning Test [czP(r)VLT-12] among older and very old Czech adults. *Clin. Neuropsychol.* 28, 1162–1181. doi: 10.1080/13854046.2014.952666

Birks, J. (2006). Cholinesterase inhibitors for Alzheimer's disease. *Cochrane Database Syst. Rev.* 1:CD005593. doi: 10.1002/14651858.CD005593

Bliss, T. V., and Collingridge, G. L. (1993). A synaptic model of memory: long-term potentiation in the hippocampus. *Nature* 361, 31–39. doi: 10.1038/361031a0

Cheng, C. P. W., Wong, C. S. M., Lee, K. K., Chan, A. P. K., Yeung, J. W. F., and Chan, W. C. (2018). Effects of repetitive transcranial magnetic stimulation on improvement of cognition in elderly patients with cognitive impairment: a systematic review and meta-analysis. *Int. J. Geriatr. Psychiatr.* 33, e1–e13. doi: 10.1002/gps.4726

Chu, C. S., Li, C. T., Brunoni, A. R., Yang, F. C., Tseng, P. T., and Tu, Y. K. (2021). Cognitive effects and acceptability of non-invasive brain stimulation on Alzheimer's disease and mild cognitive impairment: a component network meta-analysis. *J. Neurol. Neurosurg. Psychiatr.* 92, 195–203. doi: 10.1136/jnnp-2020-323870

Cotelli, M., Calabria, M., Manenti, R., Rosini, S., Zanetti, O., and Cappa, S. F. (2011). Improved language performance in Alzheimer disease following brain stimulation. *J. Neurol. Neurosurg. Psychiatr.* 82, 794–797. doi: 10.1136/jnnp.2009.197848

Cotelli, M., Manenti, R., Cappa, S. F., Geroldi, C., Zanetti, O., Rossini, P. M., et al. (2006). Effect of transcranial magnetic stimulation on action naming in patients with Alzheimer disease. *Arch. Neurol.* 63, 1602–1604. doi: 10.1001/archneur.63.11.1602

Cotelli, M., Manenti, R., Cappa, S. F., Zanetti, O., and Miniussi, C. (2008). Transcranial magnetic stimulation improves naming in Alzheimer disease patients at different stages of cognitive decline. *Eur. J. Neurol.* 15, 1286–1292. doi: 10.1111/j.1468-1331.2008.02202.x

Dai, Z., and He, Y. (2014). Disrupted structural and functional brain connectomes in mild cognitive impairment and Alzheimer's disease. *Neurosci. Bull.* 30, 217–232. doi: 10.1007/s12264-013-1421-0

Devi, G., Voss, H. U., Levine, D., Abrassart, D., Heier, L., Halper, J., et al. (2014). Open-label, short-term, repetitive transcranial magnetic stimulation in patients with Alzheimer's disease with functional imaging correlates and literature review. *Am. J. Alzheimers Dis. Other Dement.* 29, 248–255. doi: 10.1177/1533317513517047

Dong, X., Yan, L., Huang, L., Guan, X., Dong, C., Tao, H., et al. (2018). Repetitive transcranial magnetic stimulation for the treatment of Alzheimer's disease: a systematic review and meta-analysis of randomized controlled trials. *PLoS One* 13:e0205704. doi: 10.1371/journal.pone.0205704

Eliasova, I., Anderkova, L., Marecek, R., and Rektorova, I. (2014). Non-invasive brain stimulation of the right inferior frontal gyrus may improve attention in early Alzheimer's disease: a pilot study. *J. Neurol. Sci.* 346, 318–322. doi: 10.1016/j.jns.2014.08.036

Esser, S. K., Huber, R., Massimini, M., Peterson, M. J., Ferrarelli, F., and Tononi, G. (2006). A direct demonstration of cortical LTP in humans: a combined TMS/EEG study. *Brain Res. Bull.* 69, 86–94. doi: 10.1016/j.brainresbull.2005.11.003

Fargo, K. N., Aisen, P., Albert, M., Au, R., Corrada, M. M., DeKosky, S., et al. (2014). 2014 Report on the milestones for the US national plan to address Alzheimer's disease. *Alzheimers Dement.* 10, S430–S452. doi: 10.1016/j.jalz.2014.08.103

Folstein, M. F., Folstein, S. E., and McHugh, P. R. (1975). "Mini-mental state": a practical method for grading the cognitive state of patients for the clinician. *J. Psychiatr. Res.* 12, 189–198. doi: 10.1016/0022-3956(75)90026-6

Freedberg, M., Reeves, J. A., Toader, A. C., Hermiller, M. S., Voss, J. L., and Wassermann, E. M. (2019). Persistent enhancement of hippocampal network connectivity by parietal rTMS is reproducible. *Eneuro* 6:ENEURO.0129-19.2019. doi: 10.1523/ENEURO.0129-19.2019

Gangitano, M., Valero-Cabré, A., Tormos, J. M., Mottaghy, F. M., Romero, J. R., and Pascual-Leone, Á (2002). Modulation of input-output curves by low and high frequency repetitive transcranial magnetic stimulation of the motor cortex. *Clin. Neurophysiol.* 113, 1249–1257. doi: 10.1016/s1388-2457(02)00109-8

Greene, S. J., and Killiany, R. J. (2010). Subregions of the inferior parietal lobule are affected in the progression to Alzheimer's disease. *Neurobiol. Aging* 31, 1304–1311. doi: 10.1016/j.neurobiolaging.2010.04.026

Haffen, E., Chopard, G., Pretalli, J. B., Magnin, E., Nicolier, M., Monnin, J., et al. (2012). A case report of daily left prefrontal repetitive transcranial magnetic stimulation (rTMS) as an adjunctive treatment for Alzheimer disease. *Brain Stimul.* 5, 264–266. doi: 10.1016/j.brs.2011.03.003

Hoogendam, J. M., Ramakers, G. M., and Di Lazzaro, V. (2010). Physiology of repetitive transcranial magnetic stimulation of the human brain. *Brain Stimul.* 3, 95–118. doi: 10.1016/j.brs.2009.10.005

Horing, B., Weimer, K., Muth, E. R., and Enck, P. (2014). Prediction of placebo responses: a systematic review of the literature. *Front. Psychol.* 5:1079. doi: 10.3389/fpsyg.2014.01079

Hu, Y., Du, W., Zhang, Y., Li, N., Han, Y., and Yang, Z. (2019). Loss of parietal memory network integrity in Alzheimer's disease. *Front. Aging Neurosci.* 11:67. doi: 10.3389/fnagi.2019.00067

Hughes, C. P., Berg, L., Danziger, W., Coben, L. A., and Martin, R. L. (1982). A new clinical scale for the staging of dementia. *Br. J. Psychiatry* 140, 566–572. doi: 10.1192/bjp.140.6.566

Kim, K., Ekstrom, A. D., and Tandon, N. (2016). A network approach for modulating memory processes via direct and indirect brain stimulation: toward a causal approach for the neural basis of memory. *Neurobiol. Learn. Mem.* 134, 162–177. doi: 10.1016/j.nlm.2016.04.001

Koch, G., Bonnì, S., Pellicciari, M. C., Casula, E. P., Mancini, M., Esposito, R., et al. (2018). Transcranial magnetic stimulation of the precuneus enhances memory and neural activity in prodromal Alzheimer's disease. *Neuroimage* 169, 302–311. doi: 10.1016/j.neuroimage.2017.12.048

Lane, C. A., Hardy, J., and Schott, J. M. (2018). Alzheimer's disease. *Eur. J. Neurol.* 25, 59–70. doi: 10.1111/ene.13439

Liao, X., Li, G., Wang, A., Liu, T., Feng, S., Guo, Z., et al. (2015). Repetitive transcranial magnetic stimulation as an alternative therapy for cognitive impairment in Alzheimer's disease: a meta-analysis. *J. Alzheimers Dis.* 48, 463–472. doi: 10.3233/JAD-150346

Lin, Y., Jiang, W. J., Shan, P. Y., Lu, M., Wang, T., Li, R. H., et al. (2019). The role of repetitive transcranial magnetic stimulation (rTMS) in the treatment of cognitive impairment in patients with Alzheimer's disease: a systematic review and meta-analysis. *J. Neurol. Sci.* 398, 184–191. doi: 10.1016/j.jns.2019.01.038

Manenti, R., Brambilla, M., Petesi, M., Ferrari, C., and Cotelli, M. (2013). Enhancing verbal episodic memory in older and young subjects after non-invasive brain stimulation. *Front. Aging Neurosci.* 5:49. doi: 10.3389/fnagi.2013.00049

McShane, R., Westby, M. J., Roberts, E., Minakaran, N., Schneider, L., Farrimond, L. E., et al. (2019). Memantine for dementia. *Cochrane Database Syst. Rev.* 3:CD003154. doi: 10.1002/14651858.CD003154.pub6

Nichols, E., Szoeke, C. E., Vollset, S. E., Abbasi, N., Abd-Allah, F., Abdela, J., et al. (2019). Global, regional, and national burden of Alzheimer's disease and other dementias, 1990-2016: a systematic analysis for the Global Burden of Disease Study 2016. *Lancet Neurol.* 18, 88–106. doi: 10.1016/S1474-4422(18)30403-4

Ohn, S. H., Park, C. I., Lee, B. H., and Kim, Y. H. (2008). Effect of prefrontal repetitive transcranial magnetic stimulationon the enhancement of working memory. *J. Korean Acad. Rehabil. Med.* 32, 501–505.

Rossi, S., Hallett, M., Rossini, P. M., Pascual-Leone, A., and The Safety of Tms Consensus Group. (2009). Safety, ethical considerations, and application guidelines for the use of transcranial magnetic stimulation in clinical practice and research. *Clin. Neurophysiol.* 120, 2008–2039. doi: 10.1016/j.clinph.2009.08.016

Rossini, P. M., Burke, D., Chen, R., Cohen, L. G., Daskalakis, F., Di Iorio, R., et al. (2015). Non-invasive electrical and magnetic stimulation of the brain, spinal cord, roots and peripheral nerves: basic principles and procedures for routine clinical and research application. An updated report from an I.F.C.N. Committee. *Clin. Neurophysiol.* 126, 1071–1107. doi: 10.1016/j.clinph.2015.02.001

Sosa-Ortiz, A. L., Acosta-Castillo, I., and Prince, M. J. (2012). Epidemiology of dementias and Alzheimer's disease. *Arch. Med. Res.* 43, 600–608. doi: 10.1016/j.arcmed.2012.11.003

Spaniol, J., Davidson, P. S., Kim, A. S., Han, H., Moscovitch, M., and Grady, C. L. (2009). Event-related fMRI studies of episodic encoding and retrieval: meta-analyses using activation likelihood estimation. *Neuropsychologia* 47, 1765–1779. doi: 10.1016/j.neuropsychologia.2009.02.028

Tambini, A., Nee, D. E., and D'Esposito, M. (2018). Hippocampal-targeted theta-burst stimulation enhances associative memory formation. *J. Cogn. Neurosci.* 30, 1452–1472. doi: 10.1162/jocn_a_01300

Thielscher, A., and Kammer, T. (2004). Electric field properties of two commercial figure-8 coils in TMS: calculation of focality and efficiency. *Clin. Neurophysiol.* 115, 1697–1708. doi: 10.1016/j.clinph.2004.02.019

Valero-Cabré, A., Amengual, J. L., Stengel, C., Pascual-Leone, A., and Coubard, O. A. (2017). Transcranial magnetic stimulation in basic and clinical neuroscience: a comprehensive review of fundamental principles and novel insights. *Neurosci. Biobehav. Rev.* 83, 381–404. doi: 10.1016/j.neubiorev.2017.10.006

Velioglu, H. A., Hanoglu, L., Bayraktaroglu, Z., Toprak, G., Guler, E. M., Bektay, M., et al. (2021). Left lateral parietal rTMS improves cognition and modulates resting brain connectivity in patients with Alzheimer's disease: possible role of BDNF and oxidative stress. *Neurobiol. Learn. Mem.* 180, 107410. doi: 10.1016/j.nlm.2021.107410

Wagner, A. D., Shannon, B. J., Kahn, I., and Buckner, R. L. (2005). Parietal lobe contributions to episodic memory retrieval. *Trends Cogn. Sci.* 9, 445–453. doi: 10.1016/j.tics.2005.07.001

Wang, J. X., Rogers, L. M., Gross, E. Z., Ryals, A. J., Dokucu, M. E., Brandstatt, K. L., et al. (2014). Targeted enhancement of cortical-hippocampal brain networks and associative memory. *Science* 345, 1054–1057. doi: 10.1126/science.1252900

Winblad, B., Amouyel, P., Andrieu, S., Ballard, C., Brayne, C., Brodaty, H., et al. (2016). Defeating Alzheimer's disease and other dementias: a priority for European science and society. *Lancet Neurol.* 15, 455–532. doi: 10.1016/S1474-4422(16)00062-4

World Health Organization (WHO) (2017). *Global Action Plan on the Public Health Response to Dementia 2017-2025*. Geneva: WHO.

Zhao, J., Li, Z., Cong, Y., Zhang, J., Tan, M., Zhang, H., et al. (2017). Repetitive transcranial magnetic stimulation improves cognitive function of Alzheimer's disease patients. *Oncotarget* 8, 33864–33871. doi: 10.18632/oncotarget.13060

Zimerman, M., and Hummel, F. C. (2010). Non-invasive brain stimulation: enhancing motor and cognitive functions in healthy old subjects. *Front. Aging Neurosci.* 2:149. doi: 10.3389/fnagi.2010.00149

Conflict of Interest: The authors declare that the research was conducted in the absence of any commercial or financial relationships that could be construed as a potential conflict of interest.

The reviewer TC declared a shared affiliation, with no collaboration, with one of the authors XLi to the handling editor at the time of the review.

frontiers in Aging Neuroscience

ORIGINAL RESEARCH
published: 01 July 2021
doi: 10.3389/fnagi.2021.674688

Intermittent Hypoxia Training Prevents Deficient Learning-Memory Behavior in Mice Modeling Alzheimer's Disease: A Pilot Study

*Myoung-Gwi Ryou[1], Xiaoan Chen[2,3], Ming Cai[2,4], Hong Wang[2,4], Marianna E. Jung[2], Daniel B. Metzger[2], Robert T. Mallet[5] and Xiangrong Shi[2]**

[1] Department of Medical Laboratory Science and Public Health, Tarleton State University, Texas A&M University System, Stephenville, TX, United States, [2] Department of Pharmacology and Neuroscience, University of North Texas Health Science Center, Fort Worth, TX, United States, [3] College of Sports Science, Jishou University, Jishou, China, [4] College of Rehabilitation Sciences, Shanghai University of Medicine and Health Sciences, Shanghai, China, [5] Department of Physiology and Anatomy, University of North Texas Health Science Center, Fort Worth, TX, United States*

In mouse models of Alzheimer's disease (AD), normobaric intermittent hypoxia training (IHT) can preserve neurobehavioral function when applied before deficits develop, but IHT's effectiveness after onset of amyloid-β (Aβ) accumulation is unclear. This study tested the hypothesis that IHT improves learning-memory behavior, diminishes Aβ accumulation in cerebral cortex and hippocampus, and enhances cerebrocortical contents of the neuroprotective trophic factors erythropoietin and brain-derived neurotrophic factor (BDNF) in mice manifesting AD traits. Twelve-month-old female 3xTg-AD mice were assigned to untreated 3xTg-AD ($n = 6$), AD+IHT ($n = 6$), and AD+sham-IHT ($n = 6$) groups; 8 untreated wild-type (WT) mice also were studied. AD+IHT mice alternately breathed 10% O_2 for 6 min and room air for 4 min, 10 cycles/day for 21 days; AD+sham-IHT mice breathed room air. Spatial learning-memory was assessed by Morris water maze. Cerebrocortical and hippocampal $A\beta_{40}$ and $A\beta_{42}$ contents were determined by ELISA, and cerebrocortical erythropoietin and BDNF were analyzed by immunoblotting and ELISA. The significance of time (12 vs. 12 months + 21 days) and treatment (IHT vs. sham-IHT) was evaluated by two-factor ANOVA. The change in swimming distance to find the water maze platform after 21 d IHT (−1.6 ± 1.8 m) differed from that after sham-IHT (+5.8 ± 2.6 m). Cerebrocortical and hippocampal $A\beta_{42}$ contents were greater in 3xTg-AD than WT mice, but neither time nor treatment significantly affected $A\beta_{40}$ or $A\beta_{42}$ contents in the 3xTg-AD mice. Cerebrocortical erythropoietin and BDNF contents increased appreciably after IHT as compared to untreated 3xTg-AD and AD+sham-IHT mice. In conclusion, moderate, normobaric IHT prevented spatial learning-memory decline and restored cerebrocortical erythropoietin and BDNF contents despite ongoing Aβ accumulation in 3xTg-AD mice.

Keywords: Alzheimer's disease, beta-amyloid, BDNF, cerebral cortex, erythropoietin, intermittent hypoxia, memory-learning behavior

OPEN ACCESS

Edited by:
Hanting Zhang,
West Virginia University, United States

Reviewed by:
Scott Edward Counts,
Michigan State University, United States
Xavier Xifró,
University of Girona, Spain

****Correspondence:***
Xiangrong Shi
xiangrong.shi@unthsc.edu

Received: *03 March 2021*
Accepted: *27 May 2021*
Published: *01 July 2021*

Citation:
Ryou M-G, Chen X, Cai M, Wang H, Jung ME, Metzger DB, Mallet RT and Shi X (2021) Intermittent Hypoxia Training Prevents Deficient Learning-Memory Behavior in Mice Modeling Alzheimer's Disease: A Pilot Study. Front. Aging Neurosci. 13:674688. doi: 10.3389/fnagi.2021.674688

INTRODUCTION

Normobaric intermittent hypoxia (IH) exposures can harm or protect the central nervous system, depending on the cumulative dose, frequency, and intensity of the hypoxia (Navarrete-Opazo and Mitchell, 2014). Brief cyclic bouts of high-intensity IH are applied up to 8–12 h/day in rodents to model sleep apnea and its sequelae (Tahawi et al., 2001; Phillips et al., 2004; Gozal et al., 2010). Mounting evidence (Kuo et al., 2020) identifies sleep apnea as a potential risk factor for Alzheimer's disease (AD). Indeed, imposition of 10-min cycles alternating intense normobaric hypoxia (5% O_2) and 21% O_2 for 8 h/day over 4 weeks increased cerebrocortical amyloid-β (Aβ) accumulation in 6-month-old transgenic mice with Alzheimer's disease (AD) traits (Shiota et al., 2013). In contrast to intense IH modeling sleep apnea, exposure of rats to 5–8 daily cycles alternating 5–10 min moderate, normobaric hypoxia (9.5–10% O_2; ≤70 min hypoxia/session) and 4-min 21% O_2 for ≤3 weeks protected brain from ethanol withdrawal excitotoxicity (Jung et al., 2008; Ryou et al., 2017). A 20-day IH training (IHT) regimen protected the brain from ethanol-withdrawal stress by dampening cerebrocortical presenilin-1 induction and Aβ accumulation (Ryou et al., 2017). However, the question remains whether normobaric IHT can preserve neurobehavioral function and attenuate Aβ accumulation in transgenic AD mice.

Amyloid β is produced by proteolytic processing of a transmembrane protein, amyloid precursor protein, by β- and γ-secretases (Ashall and Goate, 1994). $Aβ_{42}$, admixed with smaller amounts of $Aβ_{40}$, is the predominant Aβ species in extracellular amyloid plaques, which are implicated in AD pathogenesis (Sisodia and Price, 1995). Furthermore, $Aβ_{42}$ is more fibrillogenic and neurotoxic than $Aβ_{40}$ (Klein et al., 1998; Fernandez et al., 2014). Brain $Aβ_{42}$ content is much higher in familial than sporadic AD, although neither $Aβ_{40}$ content nor the ratio of $Aβ_{42}/Aβ_{40}$ differed between these AD subtypes (Dinkel et al., 2020).

Intermittent hypoxia exposures stimulate expression and synthesis of the growth/trophic factors erythropoietin (EPO) (Bernaudin et al., 2002) and brain-derived neurotrophic factor (BDNF) (Hassan et al., 2018). A powerful neuroprotectant (Rabie and Marti, 2008; Mallet and Ryou, 2017; Rey et al., 2019), EPO is expressed in astrocytes (Bernaudin et al., 2000; Ruscher et al., 2002) and neurons (Bernaudin et al., 2000, 2002) in response to hypoxemia. BDNF protects neurons (Yang et al., 2014) and promotes neuronal differentiation and growth, synapse formation and plasticity, cognitive functions and learning-memory (Yamada and Nabeshima, 2003; Zhu et al., 2010; Park and Poo, 2013). Although continuous hypobaric IH exposures can promote BDNF expression and improve cognitive performance (Zhu et al., 2010), the ability of cyclic normobaric IHT to augment the brain's EPO and BDNF expression in the setting of nascent AD, and whether IHT-enhanced EPO and BDNF expression is associated with improved learning-memory function, is unknown.

Currently, there are no treatments for AD in patients with established pathology. Recent reports in cognitively impaired elderly patients have shown IHT to be a potentially powerful intervention to preserve cognitive function (Wang et al., 2020), but IHT's salutary mechanisms, and its effectiveness against symptomatic AD, are unknown. This study tested the hypothesis that a 21-day normobaric IHT regimen improves learning-memory behavior, diminishes $Aβ_{40}$ and $Aβ_{42}$ accumulation in cerebral cortex and hippocampus, and enhances cerebrocortical EPO and BDNF contents in transgenic AD mice. Since progressive Aβ accumulation is an AD hallmark (Jagust, 2018), the IHT intervention was initiated when the mice were 12 rather than 6 (Shiota et al., 2013) or 9 months old (Romberg et al., 2011) to assess the impact of IHT after Aβ accumulation already had begun in hippocampus and cerebral cortex (Belfiore et al., 2019), challenging IHT's ability to mitigate ongoing AD pathology.

METHODS AND MATERIALS

Animals

Female wild-type (WT) C57BL/B6 mice ($n = 8$) aged 11 months and female transgenic B6.Cg-PSEN1tm1Mpm with Tg-APPSwetauP301L AD mice ($n = 18$) aged 2 months were obtained from the Jackson Laboratory (JAX MMRRC Stock# 034830). The 3xTg-AD strain was selected because it is one of the most frequently studied transgenic AD models. Female 3xTg-AD mice were selected because it has been reported that "male transgenic mice may not exhibit the phenotypic traits" (descriptions: www.jax.org). By 12 months of age, Aβ plaques in these 3xTg-AD mice were significantly present in the brain (Belfiore et al., 2019). The mice were housed in the University of North Texas Health Science Center (UNTHSC) vivarium at 23 ± 1°C under a 24-h light (06:00–18:00) - dark (18:00–06:00) cycle. The animals were housed in groups of 4 or 5 in standard polycarbonate cages (28 × 17 × 12 cm) with corncob bedding and *ad libitum* access to food and water. AD mice were randomly assigned to one of three groups: 3xTg-AD pre-IHT control ($n = 6$), AD+IHT ($n = 6$; 21-day IHT program), or AD+sham-IHT ($n = 6$; 21-day sham IHT program). The study protocols were reviewed and approved by UNTHSC's Institutional Animal Care and Use Committee.

Behavior Testing

Morris water maze (MWM) tests of spatial learning-memory behavior were conducted as described by Joshi et al. (2020). The MWM protocol was designed to compare the difference in the changes of the MWM performances between the AD+IHT and AD+sham-IHT mice after the interventions, which would provide the effect of IHT on learning-memory behavior in 3xTg-AD mice following the intervention. The tests were conducted between 9:00 and 12:00, after 2 pre-test trials were conducted to habituate the mice to the water temperature (24 ± 1°C) and the route to the northwest (NW) quadrant, where a 5 × 5 cm Plexiglas escape platform was placed and submerged 1.5 cm below the water surface. Mice were allowed to stay on the platform for ∼10 s after reaching the platform during pre-test trials. The mouse was guided to the target site when the animal appeared to struggle to swim or when 3 min elapsed without finding the platform. The maze was divided into four equal quadrants, i.e., northeast (NE), southeast (SE), southwest

(SW), and NW quadrants. To facilitate learning of the platform location, visual cues including geometric shapes and a scene from nature were posted on the laboratory walls around the maze (Brody and Holtzman, 2006). The water was made opaque with non-toxic white Colorations Powder Tempera Paint. The test trials started ∼30 min after the animal completed pre-test trials. Animals started from the same point for pre-test trials and test trials, with the platform in the same location. All MWM test trials were continuously tracked using a computer-interfaced video system (Any-maze, Stoelting Co., Wood Dale, IL). Swimming duration, distance and speed were documented after releasing animals in the SE quadrant. The animals were dried with paper towels immediately after completing each test trial. Three test trials, separated by 5 min intervals, were conducted and the data averaged over the trials were reported. The test trials were completed within 20 min. All animals were able to independently locate the target site or platform after the pre-test trials.

Approximately 24 h after the MWM test, 8 WT and 6 AD mice (3xTg-AD control group) were weighed, anesthetized by ventilation with ∼5% isoflurane, decapitated, and the brains harvested. The mice in the AD+IHT and AD+sham-IHT groups underwent 21-day IHT or sham-IHT interventions. A post-intervention MWM session was conducted 24 h after the last IHT or sham-IHT session. The mice were anesthetized and the brains harvested 24 h after the post-intervention MWM testing.

Intermittent Hypoxia Training

Normobaric IHT was conducted after placing the home cages of the AD+IHT mice in a Plexiglas chamber (105 × 50 × 65 cm). Compressed 100% nitrogen gas was introduced into the chamber to lower O_2 to 10% for 6 min, and then the chamber was opened to reintroduce room air for 4 min. Ten hypoxia-normoxia cycles were administered per daily session for 21 consecutive days. This IHT protocol combining moderate hypoxia intensity (10% O_2) and duration (60 min cumulative hypoxia/session) was modified from a protocol that has proven to be cardio- (Zong et al., 2004; Mallet et al., 2006) and neuroprotective (Jung et al., 2008; Ryou et al., 2017) in animal models, and safe when applied to human subjects (Zhang et al., 2014; Wang et al., 2020). Fractions of O_2 and CO_2 in the chamber were continuously monitored throughout each IHT session (**Figure 1**) using a Perkin-Elmer (St. Louis, MO) model 1,100 mass spectrometer gas analyzer. The AD+sham-IHT mice were exposed to the room air adjacent to the IHT chamber. All IHT and sham-IHT sessions were carried out between 09:00 and 12:00.

Brain Protein Extraction

Cerebral cortex and both hippocampi were excised, placed separately in labeled vials, flash-frozen in liquid N_2, and stored at −80°C. Tissue proteins were extracted as described previously (Ju et al., 2012). Total protein concentrations in the extracts were measured by bicinchoninic acid assay (Thermo Fisher Scientific, Waltham, MA).

Analyses of Cerebrocortical and Hippocampal Proteins

Total $A\beta_{40}$ and $A\beta_{42}$ contents in the cerebrocortical and hippocampal tissues were measured by enzyme-linked immunosorbent assay (ELISA) kits ($A\beta_{40}$ Lot # KMB3481, $A\beta_{42}$ Lot # KMB3441, Fisher Scientific, Hanover Park, IL) according to the manufacturer's instructions. Tissue extracts and $A\beta_{40}$ and $A\beta_{42}$ standards were incubated with mouse Aβ antibody at room temperature for 1 h. After thorough washing, anti-rabbit IgG horseradish peroxidase solution was added and incubated for 30 min at room temperature. After another washing, stabilized chromogen was added, followed by 30 min incubation at room temperature in the dark. Stop solution then was applied and absorbance was measured at 450 nm in a Spectramax Plus spectrophotometer (Molecular Devices, San Jose, CA).

Cerebrocortical contents of BDNF and EPO also were determined by ELISA (BDNF Lot # AB212166, EPO Lot # AB119593, Abcam, Cambridge, MA). BDNF (0–2,000 pg/ml) and EPO (0–3,000 pg/ml) standards were prepared by serial dilution. Extracts and standards were incubated in antibody-coated 96 well plates for 1 h at room temperature, washed with wash buffer, and then incubated with 3,3′,5,5′-tetramethylbenzidine substrate to develop color. BDNF and EPO protein contents were determined by spectrophotometry. BDNF, EPO, $A\beta_{40}$, and $A\beta_{42}$ concentrations were normalized against corresponding total protein concentrations.

Erythropoietin, BDNF and β-actin were analyzed by immunoblotting of cerebrocortical protein extracts as described previously (Ryou et al., 2012). Proteins (40 μg/lane) were separated by 10% SDS gel electrophoresis, and then electrophoretically transferred to polyvinylidene fluoride membranes (Millipore, Danvers, MA). Immunoblotting was performed with rabbit anti-BDNF (Abcam, Cambridge, MA; catalog #ab1083189, lot #GR3227037-4), goat anti-EPO (R&D Systems, Minneapolis, MN; catalog #SF959, lot #FIW0618078), and mouse anti-β-actin (Santa Cruz Biotechnology, Dallas, TX; catalog #sc-47778, lot #J2816) primary antibodies, followed by horseradish peroxidase-conjugated goat anti-rabbit (ImmunoReagents, Raleigh, NC; part #GtxRb-003-DHRPX, lot #20-170-011217), goat anti-mouse (ImmunoReagents; part #GtxMu-003-FHRPX, lot #58-98-021618) and mouse anti-goat IgG (Santa Cruz Biotechnology; catalog #sc-2354, lot #10871). Band densities were quantified with Doc-It Image Acquisition Software (UPV, Upland, CA) and normalized to β-actin density.

Statistical Analysis

Single-factor analysis of variance (ANOVA) was applied to determine the group differences in body weight and MWM tests. Student's *t*-tests for two independent groups were applied to compare the baseline differences between the WT and 3xTg-AD groups and the post-intervention changes in the AD+IHT vs. AD+sham-IHT groups. Paired *t*-tests were applied to evaluate within-group changes in MWM performance post- vs. pre-intervention. Two-factor ANOVA was conducted to test the

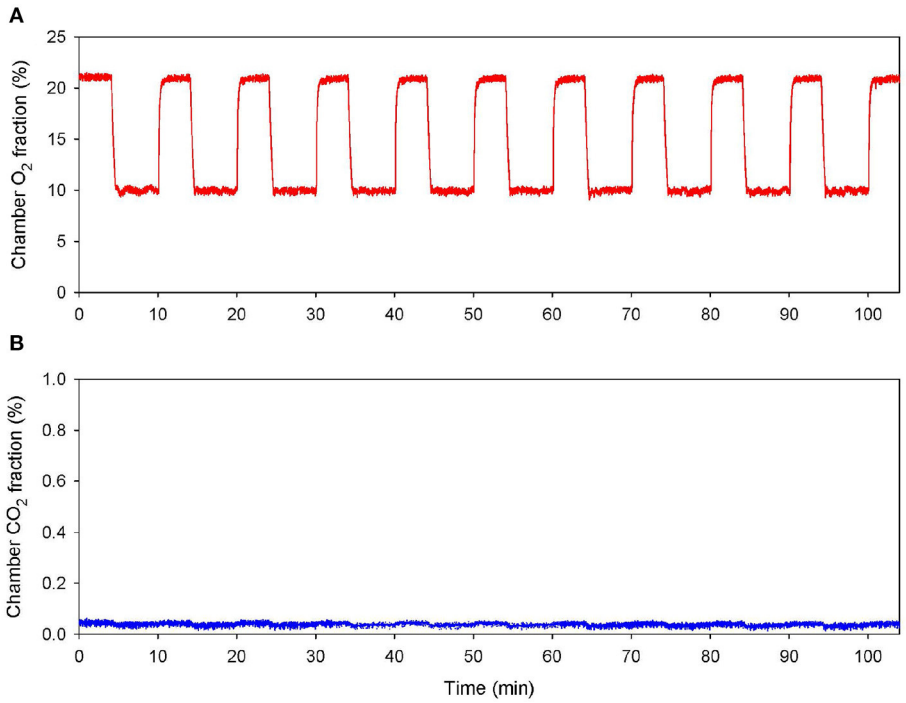

FIGURE 1 | Normobaric intermittent hypoxia training session. Continuous record of the fractional concentrations of O_2 **(A)** and CO_2 **(B)** within the chamber during an IHT session.

significance of time (12 months for untreated 3xTg-AD vs. 12 months plus 21 days for AD+IHT or AD+sham-IHT) and treatment (IHT vs. untreated 3xTg-AD and AD+sham-IHT) factors on the protein contents among the three 3xTg-AD groups. Duncan multiple range tests were applied *post*-hoc when ANOVA detected statistically significant effects of the major factor. Data are reported as group mean ± standard error of the mean. *P*-values < 0.05 were considered statistically significant, and *P*-values between 0.05 and 0.10 were taken to indicate trends. Statistical analyses were performed using Statistical Analysis System (SAS) software package version 9.4.

RESULTS

Morris Water Maze Tests

Baseline MWM performance and body weight did not differ between the WT and 3xTg-AD mice (**Table 1**). The overall swimming duration to find the submerged platform placed in the NW quadrant did not decline significantly in the AD+IHT (-7.95 ± 10.49 s) or AD+Sham-IHT mice (-3.78 ± 9.82 s), and the changes in swimming duration did not differ between those two groups (**Figure 2A**). Furthermore, there were no significant group differences in the durations swum in any of the four quadrants (**Figures 2B–E**). However, the swimming distance to find the platform (**Figure 2F**) increased by 5.8 ± 2.6 m during the 21 d sham-IHT program ($P = 0.077$), and the change in swimming distance was greater ($P < 0.05$) than that of the IHT program (-1.6 ± 1.8 m). The two protocols also produced divergent effects ($P < 0.05$) on the distances swum in the opposite (SE) quadrant (AD+IHT: -0.9 ± 0.5 m vs. AD+sham-IHT: $+1.0 \pm 0.6$ m) and the SW quadrant (AD+IHT: -1.12 ± 0.66 m vs. AD+sham-IHT: $+1.87 \pm 0.94$ m).

Overall swimming speed (**Figure 2K**) was not altered by 21 d IHT (-0.03 ± 0.02 m/s) and tended to increase over 21 d sham-IHT ($+0.06 \pm 0.03$ m/s, $P = 0.08$). The change of overall swimming speed in the IHT group differed from that of the sham-IHT group ($P < 0.05$). The changes in swimming speed in the target (NW) quadrant (**Figure 2L**) tended to decrease in the IHT group (-0.06 ± 0.03 m/s, $P = 0.06$), which was significantly slower ($P < 0.05$) than that in the sham-IHT group (0.03 ± 0.02 m/s), indicating that 21 d IHT intervention likely made the AD+IHT mice do more "thinking" than swimming during the MWM test, especially in the target quadrant. However, in the other three quadrants, the changes in swimming speed of the AD-IHT group were all above the zero line. In addition, the changes in swimming speed in the SW quadrant (**Figure 2O**) differed ($P < 0.05$) between the IHT group (0.02 ± 0.01 m/s) vs. the sham-IHT group (0.06 ± 0.01 m/s, $P = 0.02$). This increased swimming speed in the AD+sham-IHT group was associated with a greater swimming distance (**Figure 2F**) with no difference in swimming duration (**Figure 2A**) as compared to the AD+IHT group, suggesting spatial learning-memory decline, not physical impairment, occurred in the 3xTg-AD mice following 21 d sham-IHT.

Neither 21 d IHT nor sham-IHT produced significant changes in total mobile time during MWM tests (IHT: -13.3 ± 9.1 s vs.

TABLE 1 | Results of Morris Water Maze test.

Groups		WT	3xTg-AD			ANOVA *P-value*
			Pre	IHT	Sham	
Weight (g)		36.0 ± 1.9	39.2 ± 2.8	40.3 ± 3.4	43.0 ± 6.1	0.224
Overall swimming	Duration (s)	55.7 ± 9.2	48.6 ± 9.7	47.2 ± 10.3	60.6 ± 5.3	0.712
	Distance (m)	9.28 ± 1.69	9.39 ± 1.75	8.64 ± 1.75	6.63 ± 1.39	0.561
	Speed (m/s)	0.16 ± 0.01	0.19 ± 0.01	0.19 ± 0.01	0.14 ± 0.02	0.208
	Mobile-time (s)	50.6 ± 9.2	45.6 ± 9.8	47.0 ± 10.2	55.1 ± 4.9	0.886
Swimming in NW (target) quadrant	Duration (s)	14.8 ± 2.4	14.6 ± 3.1	10.6 ± 2.4	11.2 ± 2.6	0.363
	Distance (m)	2.24 ± 0.47	2.51 ± 0.49	2.08 ± 0.42	1.71 ± 0.34	0.766
	Speed (m/s)	0.15 ± 0.02	0.17 ± 0.02	0.19 ± 0.01	0.16 ± 0.02	0.149
Swimming in NE quadrant	Duration (s)	11.9 ± 2.4	10.6 ± 2.0	12.9 ± 4.6	24.2 ± 5.4	0.381
	Distance (m)	2.17 ± 0.42	2.16 ± 0.39	1.91 ± 0.42	1.63 ± 0.37	0.536
	Speed (m/s)	0.18 ± 0.01	0.21 ± 0.01	0.15 ± 0.04	0.10 ± 0.03	0.717
Swimming in SE quadrant	Duration (s)	17.2 ± 3.2	14.1 ± 2.7	14.5 ± 3.1	11.0 ± 3.5	0.252
	Distance (m)	2.88 ± 0.56	2.88 ± 0.54	2.91 ± 0.56	1.73 ± 0.42	0.530
	Speed (m/s)	0.16 ± 0.01	0.20 ± 0.01	0.20 ± 0.01	0.17 ± 0.42	0.370
Swimming in SW quadrant	Duration (s)	11.9 ± 2.0	9.4 ± 2.5	9.2 ± 2.4	14.2 ± 3.6	0.741
	Distance (m)	1.99 ± 0.35	1.84 ± 0.45	1.74 ± 0.38	1.57 ± 0.34	0.507
	Speed (m/s)	0.16 ± 0.01	0.20 ± 0.01	0.19 ± 0.01	0.15 ± 0.03	0.276
Mean distance from the target site (m)		0.47 ± 0.03	0.44 ± 0.03	0.49 ± 0.01	0.52 ± 0.04	0.687

Single-factor analysis of variance (ANOVA) revealed no group differences in body weight and MWM performance between wild type (WT) mice and the 3xTg-AD groups. Values are group means ± standard error of the mean from 8 WT, 6 pre-treatment 3xTg-AD mice (designated "Pre"), 6 3xTg-AD mice completing IHT ("IHT"), and 6 3xTg-AD completing the sham-IHT program ("Sham"). NE, NW, SE, and SW denote northeast, northwest, southeast, and southwest MWM quadrants, respectively. The target platform was placed in the NW quadrant.

sham-IHT: +1.3 ± 7.4 s), and the respective changes did not differ ($P = 0.24$). Mean distance swimming around the MWM platform during the testing decreased (−0.15 ± 0.02 m, $P = 0.01$) following IHT, which was unchanged after sham-IHT (−0.06 ± 0.05 m, $P = 0.23$), suggesting that IHT intervention made the AD-IHT mice better oriented to and more concentrated on the target quarter during the MWM test. The difference between these responses was marginally significant ($P = 0.10$). Although body weight fell in the AD+IHT mice (−2.3 ± 0.8 g, $P = 0.03$) but not in the AD+sham-IHT group (−1.1 ± 1.0 g, $P = 0.33$), the weight changes over the course of IHT *vs*. sham-IHT did not differ ($P = 0.39$). None of the animals showed any physical impairment after 21-day IHT or sham-IHT.

$A\beta_{40}$ and $A\beta_{42}$ Contents

Baseline cerebrocortical $A\beta_{40}$ contents (**Figure 3A**) were similar in the WT (28.1 ± 3.8 pg/ml) and 3xTg-AD mice (29.6 ± 5.3 pg/ml). Cerebrocortical $A\beta_{40}$ contents in the 3xTg-AD groups were not affected by time ($P = 0.127$) or treatment factors ($P = 0.165$). However, cerebrocortical $A\beta_{42}$ contents (**Figure 3B**) were nearly 8-fold greater ($P < 0.01$) in the 3xTg-AD (107.4 ± 20.7 pg/ml) than WT mice (13.7 ± 0.3 pg/ml). Cerebrocortical $A\beta_{42}$ contents increased further (time factor $P = 0.087$) in the 22-day-older AD+IHT (163 ± 27 pg/ml) and AD+sham-IHT mice (325 ± 100 pg/ml) vs. the untreated 3xTg-AD mice, and IHT tended to dampen $A\beta_{42}$ accumulation (treatment factor $P = 0.081$) vs. sham-IHT.

Hippocampal $A\beta_{40}$ content (**Figure 3D**) was 5-fold greater ($P = 0.057$) in the 3xTg-AD (263 ± 85 pg/ml) vs. WT mice (55 ± 12 pg/ml), while $A\beta_{42}$ content (**Figure 3E**) was almost 18-fold greater ($P < 0.01$) in the 3xTg-AD (799 ± 144 pg/ml) than WT mice (45 ± 5 pg/ml). Neither hippocampal $A\beta_{40}$ nor $A\beta_{42}$ contents in the three 3xTg-AD groups were affected by the time or treatment factors. Cerebrocortical (**Figure 3C**) and hippocampal (**Figure 3F**) $A\beta_{42}$:$A\beta_{40}$ content ratios mirrored $A\beta_{42}$ contents.

Erythropoietin and BDNF Contents

Immunoblotting (**Figure 4**) revealed sharply lower β-actin-normalized cerebrocortical EPO (**Figure 4B**: $P = 0.083$) and BDNF (**Figure 4D**: $P = 0.084$) contents in the untreated 3xTg-AD mice (EPO: 0.15 ± 0.06; BDNF: 0.28 ± 0.15) vs. WT mice (EPO: 1.49 ± 0.64; BDNF: 1.70 ± 0.67). In the post-treatment groups, β-actin-normalized EPO contents (**Figure 4B**: AD+IHT: 0.90 ±0.49; AD+sham-IHT: 0.27 ± 0.18) were not significantly affected by time factor ($P = 0.217$) or treatment factor ($P = 0.257$). However, BDNF contents (**Figure 4D**) were significantly influenced by both

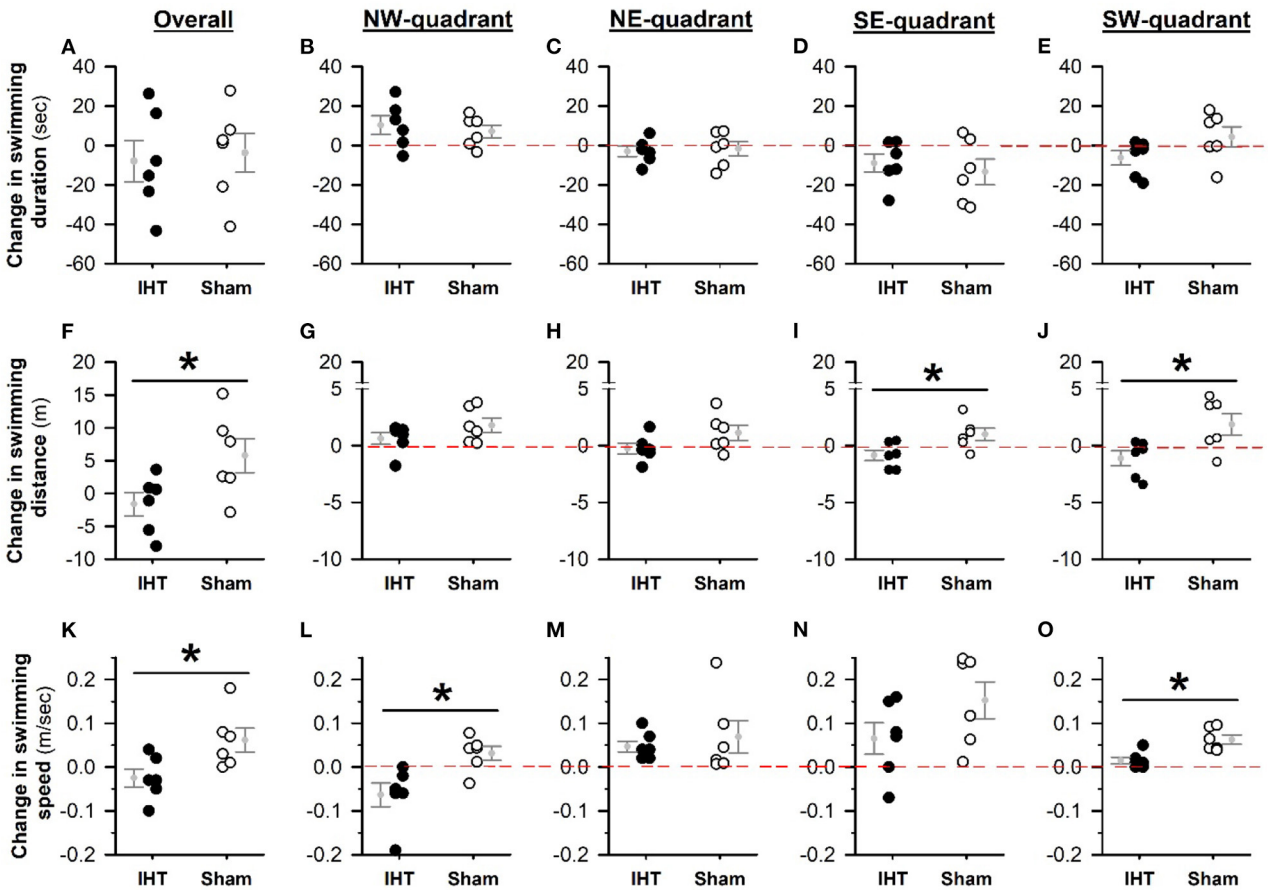

FIGURE 2 | Changes in MWM tests from pre-treatment baseline. The changes in MWM performance variables (i.e., the differences between post- and pre-intervention values) are plotted for the IHT and sham-IHT interventions. A value below the zero line (the horizontal dashed line in each quadrant-specific graph) indicates a decrease in the variable after vs. before intervention, and a value above the zero line indicates an increase. Although changes in swimming duration after IHT vs. sham-IHT did not differ **(A)**, the change in swimming distance to find the submerged platform in the sham-IHT mice exceeded that of the IHT mice **(F)**. These between-group differences are significant in the SE **(I)** and SW **(J)** quadrants, but not in the target NW **(G)** and NE **(H)** quadrants. Swimming distance in the target (NW) quadrant increased in both the IHT and sham-IHT groups **(G)**. However, in the IHT group the changes in swimming distance in the other three quadrants are all below zero, but in the sham-IHT group are above zero **(H–J)**. The overall swimming speed **(K)** tended to increase after sham-IHT but not IHT, and this treatment effect was statistically significant in the target **(L)** and SW **(O)** quadrants. Individual data points and group mean ± standard error of the mean are plotted. *$P < 0.05$ for the indicated comparison.

time ($P = 0.004$) and treatment factors ($P = 0.003$). β-actin-normalized BDNF contents (**Figure 4D**) in the AD+IHT mice (1.52 ± 0.14) were doubled vs. AD+sham-IHT mice (0.75 ± 0.62) and increased over 5-fold vs. pre-treated 3xTg-AD (0.28 ± 0.15).

Figure 5 presents cerebrocortical EPO (panel A) and BDNF (panel B) contents (ng/g tissue) measured by ELISA. Although the difference in EPO contents (**Figure 5A**) in WT (35.1 ± 9.0) vs. 3xTg-AD mice (18.1 ± 2.9) did not attain statistical significance ($P = 0.123$), BDNF content (**Figure 5B**) was greater ($P < 0.05$) in the WT (13.5 ± 0.7) vs. 3xTg-AD mice (8.2 ± 1.6). Both EPO and BDNF contents were affected by the time (EPO: $P = 0.047$; BDNF: $P = 0.002$) and treatment factors (EPO: $P = 0.008$; BDNF: $P = 0.001$). *Post-hoc* analysis confirmed that 21-day IHT increased cerebrocortical EPO and BDNF contents. Thus, EPO and BDNF contents (ng/g tissue) in the AD+IHT group (EPO: 43.1 ± 8.7; BDNF: 22.4 ± 4.8) exceeded those in the pre-treatment 3xTg-AD mice (EPO: 18.1 ± 2.9; BDNF: 8.2 ± 1.6). EPO content (**Figure 5A**) in the AD+IHT mice also exceeded that of the AD+sham-IHT mice (19.3 ± 3.3), and a trend toward higher BDNF content in the AD+IHT vs. AD+sham-IHT mice (12.9 ± 1.4) was noted (**Figure 5B**).

DISCUSSION

This study demonstrated that a 21-day normobaric IHT intervention, initiated after the onset of cerebrocortical and hippocampal $A\beta_{42}$ accumulation, prevented declination of spatial learning-memory function in transgenic mice predisposed to develop AD-like neurobehavioral impairments. Specifically,

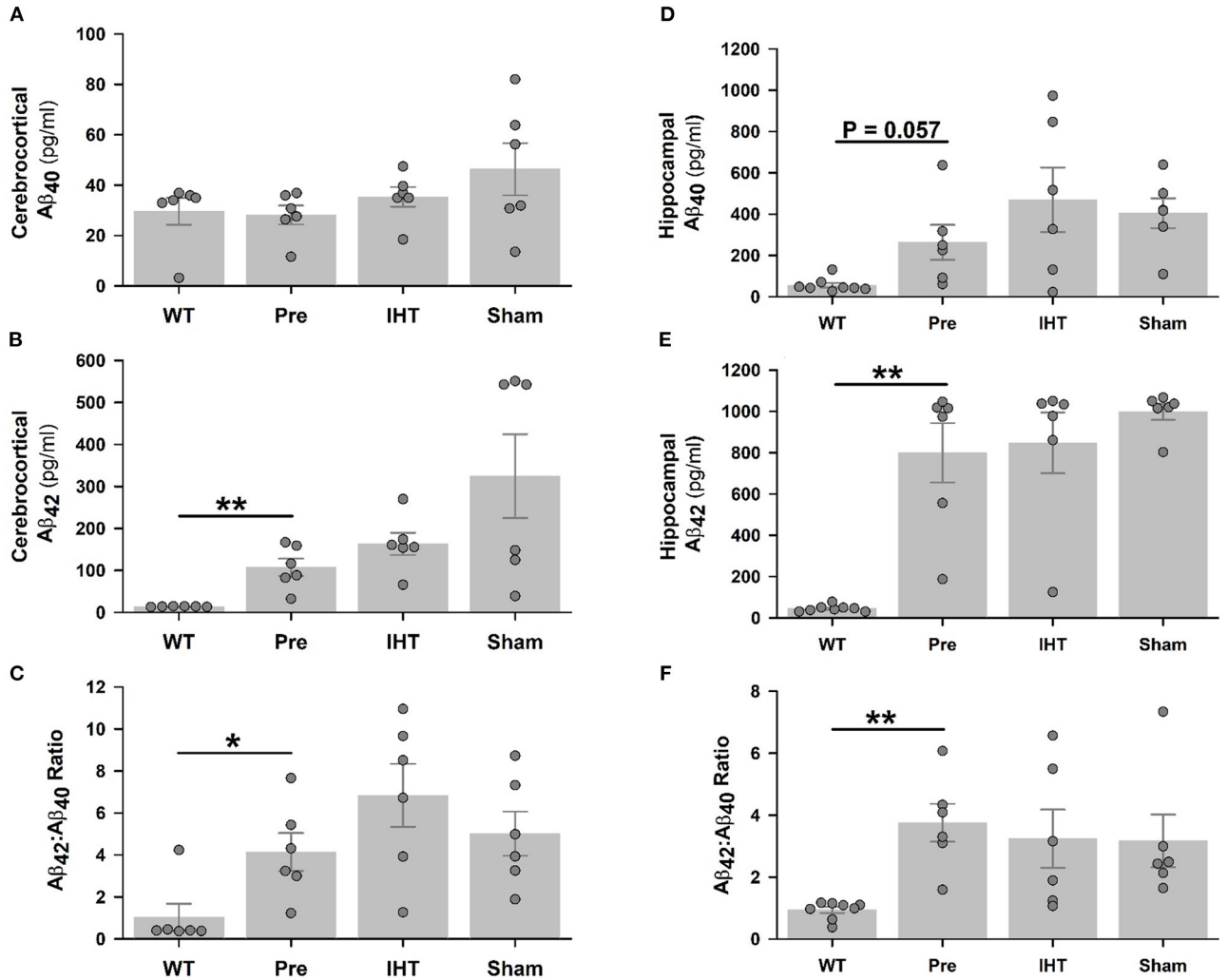

FIGURE 3 | Total $A\beta_{40}$ and $A\beta_{42}$ contents determined by ELISA. Although cerebrocortical $A\beta_{40}$ contents **(A)** were similar in the WT, 3xTg-AD, AD+IHT and AD+sham-IHT mice, cerebrocortical $A\beta_{42}$ **(B)**, and the $A\beta_{42}/A\beta_{40}$ ratio **(C)** were greater in the 3xTg-AD than WT mice. Hippocampal $A\beta_{40}$ content was marginally increased ($P = 0.057$) in the 3xTg-AD vs. WT mice **(D)**, and hippocampal $A\beta_{42}$ **(E)** and the $A\beta_{42}/A\beta_{40}$ ratio **(F)** were greater in the 3xTg-AD than WT mice. Both the time factor ($P = 0.087$) and the treatment factor ($P = 0.081$) tended to significantly influence the cerebrocortical $A\beta_{42}$ according to two-factor ANOVA. However, neither these factor altered the hippocampal $A\beta_{42}$ vs. the pre-intervention 3xTg-AD group. $A\beta_{40}$ contents or $A\beta_{42}/A\beta_{40}$ ratios in the cerebral cortex or hippocampus were not affected by the time or treatment factors. Individual data points and group mean ± standard error of the mean are plotted. $^*P < 0.05$, $^{**}P < 0.01$ for comparisons indicated by horizontal lines.

in the MWM test the overall swimming distance to find a submerged platform was significantly shorter in the AD+IHT than the AD+sham-IHT mice, and the IHT intervention made the AD+IHT mice better oriented to the target quarter. Notably, IHT effected this improvement without significantly dampening $A\beta_{40}$ accumulation in the cerebral cortex and hippocampus, although the cerebrocortical $A\beta_{42}$ content tended to be diminished (treatment factor $P = 0.081$) in the AD+IHT as compared to the AD+sham-IHT mice following 21-day interventions. Instead, the functional improvement may be ascribable, at least in part, to IHT-induction of the neuroprotective trophic/growth factors EPO and BDNF.

Learning-Memory vs. Amyloid-β in 3xTg-AD Mice

Previously, we reported that a 20-day normobaric IHT program protected the brain from ethanol-withdrawal stress by dampening cerebrocortical presenilin-1 overexpression and $A\beta_{40}$ and $A\beta_{42}$ accumulation in 4 month-old, non-AD rats (Ryou et al., 2017). Here, however, cerebrocortical and hippocampal Aβ contents were not affected significantly by the IHT intervention. Although the two studies were conducted in different species, the fact that the mice already were 12 months old at the start of the IHT program may account for the lack of an IHT effect on Aβ content. The older brain may have a reduced plasticity or adaptability, dampening its responsiveness to IHT.

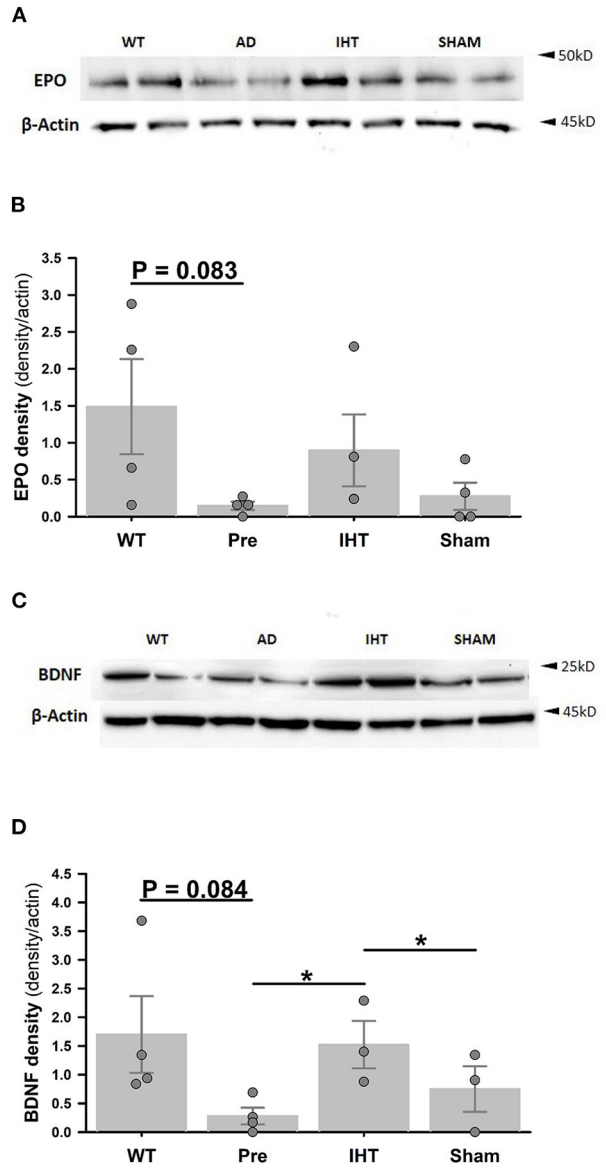

FIGURE 4 | Cerebrocortical erythropoietin and BDNF immunoblots. **(A)** Cerebrocortical erythropoietin (EPO) and β-actin immunoblots. **(B)** EPO band densities normalized to β-actin band densities. **(C)** Cerebrocortical BDNF and β-actin immunoblots. **(D)** BDNF densities normalized to β-actin band densities. Analyses of the band densities indicated that cerebrocortical EPO and BDNF contents were lower in the 3xTg-AD vs. WT mice. IHT, but not sham-IHT, tended to restore EPO and BDNF contents in the 3xTg-AD mice. For EPO and BDNF contents, treatment factors are $P = 0.257$ and $P = 0.003$, respectively, and time factors are $P = 0.217$ and $P = 0.004$, respectively. $^*P < 0.05$ for comparisons indicated by horizontal lines. Individual data points and group mean ± standard error of the mean are shown.

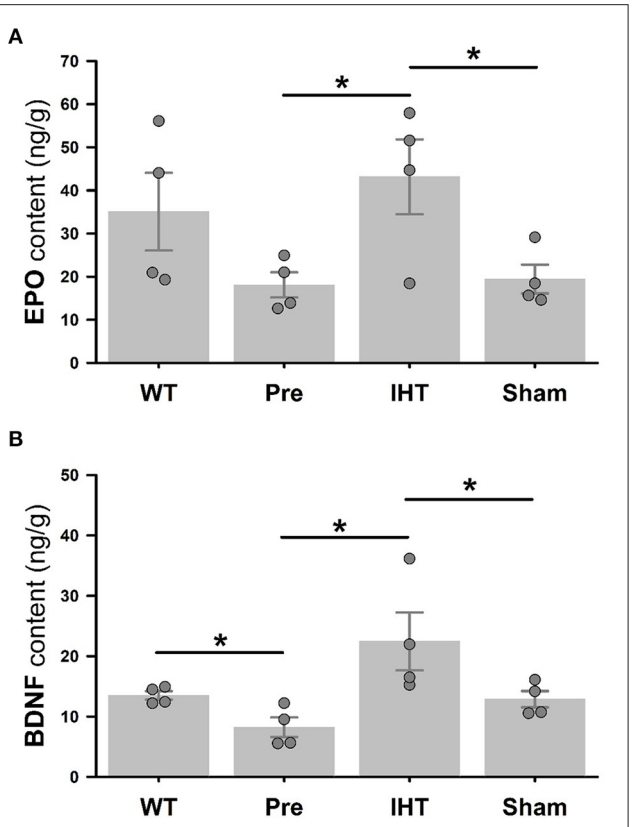

FIGURE 5 | ELISA analyses of cerebrocortical EPO and BDNF. Cerebrocortical EPO **(A)** and BDNF **(B)** contents are significantly greater in the AD+IHT than pre-intervention 3xTg-AD mice. For EPO and BDNF contents, treatment factors are $P = 0.008$ and $P = 0.001$, respectively, and time factors are $P = 0.047$ and $P = 0.002$, respectively. $^*P < 0.05$ for comparisons indicated by horizontal lines. Individual data points and group mean ± standard error of the mean are shown.

Also, unlike the rats, the mice were predisposed genetically to develop hallmarks of AD. The accumulated $A\beta_{42}$ in the 3xTg-AD mice may be innately more difficult to eradicate than the Aβ accumulation in rats experiencing ethanol withdrawal (Ryou et al., 2017).

Despite similar cerebrocortical and hippocampal Aβ contents (**Figure 3**), the spatial learning-memory behavior of AD mice appeared to be improved by IHT vs. sham-IHT (**Figure 2**). This finding is concordant with a recent longitudinal study showing no correlation of amyloidosis with cognitive outcome in transgenic AD mice (Focke et al., 2019). Arguably, Aβ content might not be a quantitatively sensitive predictor of the changes in learning-memory function in transgenic AD mice (Foley et al., 2015). Although cerebrocortical $A\beta_{42}$ contents tended to be lower ($P = 0.081$) in the AD+IHT than AD+sham-IHT mice, there was no intervention effect on hippocampal $A\beta_{42}$ contents between these two groups. Therefore, IHT induction of the neuroprotective trophic/growth factors EPO and BDNF could constitute a mechanism improving learning-memory function in the AD+IHT mice.

Trophic Factors and Neuroprotection

The specific mechanism of IHT-induced brain protection or recovery is not fully understood, but the hypoxia-responsive transcription factor, hypoxia-inducible factor (HIF) appears to play a key role in the transition from the acute to second

phases of cellular adaptation to various neuropathological conditions (Semenza, 2009; Lukyanova et al., 2013; Dengler et al., 2014; Rybnikova and Samoilov, 2015). In the acute phase, cytoprotection is effected by regulating ion channel permeability, protein phosphorylation, and post-translational modification (Li et al., 2017). HIF activation, specifically stabilization of the O_2-regulated HIF-1α subunit, promotes expression of key elements of the second phase of adaptation, including EPO, BDNF, antioxidant enzymes, and anti-apoptotic proteins (Rybnikova and Samoilov, 2015; Vetrovoy et al., 2017).

Erythropoietin has been shown to protect neurons from ischemic damage (Sakanaka et al., 1998; Malhotra et al., 2006; Ratilal et al., 2014), suppress neuronal apoptosis and necroptosis (Rabie and Marti, 2008; Mallet and Ryou, 2017) by attenuating cytokine production and inflammation (Villa et al., 2003), reduce astrocyte edema in stroke (Gunnarson et al., 2009), and promote brain angiogenesis after focal ischemia (Li et al., 2007). EPO-loaded lipid nanoparticles restored memory and cognitive functions of AD mice (Dara et al., 2019). The present study demonstrated that moderate, normobaric IHT increased endogenous EPO content in the cerebral cortex of 3xTg-AD mice. The increased EPO content after 21-day normobaric IHT was associated with improved MWM performance in the IHT-treated vs. sham-IHT AD mice.

Brain content of the neurotrophin BDNF is decreased in AD, Huntington disease and Parkinson's disease (Hock et al., 2000; Zuccato et al., 2008; Miranda et al., 2019). In AD, the greatest declines in BDNF are in the hippocampus and the parietal, entorhinal, and frontal cortices (Hock et al., 2000). In the present study, cerebrocortical BDNF content was indeed lower in the 3xTg-AD than wild-type mice. Nonetheless, this AD-related difference could be reversed by 21-day normobaric IHT, which markedly increased cerebrocortical BDNF and EPO contents vs. those of untreated and sham-IHT-treated 3xTg-AD mice. Collectively, augmented expression of these neuroprotective trophic/growth factors could contribute to improved learning-memory behavior in the 3xTg-AD mice.

Relationship Between EPO and BDNF Expression

The molecular signaling mechanisms mediating the parallel increases in cerebrocortical erythropoietin and BDNF contents in the IHT-treated 3xTg-AD mice are not yet known. In particular, evidence is equivocal regarding the hierarchy between EPO and BDNF expression. Exogenous BDNF increased EPO expression and signaling in rat cortical neurons (Wu et al., 2010), and pharmacological induction of BDNF expression activated EPO formation and suppressed inflammation in a murine microglial cell line (Lai et al., 2018). On the other hand, EPO increased BDNF content in rat brain following embolic stroke (Wang et al., 2004) and in neurotoxin-challenged rat hippocampal neurons (Viviani et al., 2005), increased BDNF content and anti-apoptotic signaling in brains of haloperidol-challenged rats (Pillai et al., 2008), and augmented hippocampal BDNF content and preserved spatial and fear memory in aged rats (Jia et al., 2016). EPO mobilization of intracellular Ca^{2+} sequentially activates calcium-calmodulin dependent protein kinase and CREB-1, the principal promoter of BDNF gene transcription (Viviani et al., 2005; Song et al., 2015), yet BDNF-activated kinases also mobilize CREB-1 in mouse cortical neurons, potentially intensifying BDNF formation (Kim et al., 2017). Further research is essential to decipher the potentially reciprocal inductions of EPO and BDNF, and their contributions to IHT-induced cognitive improvements in animal models of AD.

Importance of IH Dose

Hypoxia intensity or inspired fraction of O_2 (F_IO_2) and cumulative exposure duration are the major factors that determine if IH exposures are potentially detrimental or beneficial. Previously, Shiota et al. reported a significant increase in $A\beta_{42}$ content (with no changes in $A\beta_{40}$ content and MWM performance) in 6-month-old male 3xTg-AD mice following the intervention of 10-min exposure to intense (5% O_2) normobaric hypoxia interspersed with 10-min 21% O_2 for 8 h/day over 4 weeks (Shiota et al., 2013). Recently, Arias-Cavieres et al. (2020) reported diminished synaptic long-term potentiation (LTP) in mouse hippocampus and impaired Barnes maze performance after IH exposures of 1-min ∼4.5% O_2 and 5-min 21% O_2 for 8 h/day over 10 days. This adverse outcome was ascribed to over-accumulation of reactive oxygen species (ROS) mediated by excessive HIF-1α mobilization. In contrast, Jung et al. found 5–8 daily cycles of 5–10 min hypoxia (F_IO_2 9.5–10%) and 4-min normoxia over 20 days mitigated oxidative stress and behavior deficits in rats during abrupt ethanol-withdrawal following 35-day ethanol intoxication (Jung et al., 2008). Ryou et al. reported a similar IH protocol in ethanol-withdrawn rats prevented cerebrocortical $A\beta_{40}$ and $A\beta_{42}$ accumulation, probably by moderating ethanol withdrawal-induced γ-secretase overactivation and oxidative damage (Ryou et al., 2017). In the IH studies of Jung et al. (2008) and Ryou et al. (2017), cumulative hypoxia (F_IO_2 9.5–10%) durations were 25–70 min per daily session and 483 min or ∼8 h over the 20-day IHT program, well below the dose and intensity of IH exposures modeling sleep apnea (Shiota et al., 2013; Arias-Cavieres et al., 2020).

In dogs, moderate IH exposures eliciting cardioprotective adaptations lowered the partial pressure of arterial O_2 (PaO_2) to 45–50 mmHg (Mallet et al., 2006). In humans, similar PaO_2 values lower arterial O_2 saturation from 97 to 70–75% (Zhang et al., 2014) and cerebral tissue O_2 saturation from 70–75 to 50–55% (Liu et al., 2017). During such IH exposures, moderate hypoxemia-induced cerebral vasodilation maintains adequate O_2 delivery to meet the brain's metabolic demands (Liu et al., 2017). However, intense IH exposures to simulate sleep apnea may induce more severe hypoxemia, e.g., PaO_2 *c.* 35 mmHg (Wall et al., 2014). Although such intense IH elicits robust HIF-1α activation and EPO expression (Wall et al., 2014), it likely imposes tissue hypoxia so severe that O_2 supply falls below neuronal metabolic demand, injuring the central nervous system.

Study Limitations and Perspectives

Because the hippocampus is a center of learning and memory, the lack of EPO and BDNF data in that region precludes

definitive conclusions regarding the mechanisms of IHT-improved learning-memory behavior in the 3xTg-AD mice. Hyperphosphorylated tau, which like Aβ accumulates in brains of AD patients, was not measured in this study. Tau hyperphosphorylation, although possibly not fully manifest at 12 months in the 3xTg-AD mice (Belfiore et al., 2019), could be strongly associated with learning-memory impairment. However, it should be noted that amyloid β accumulation precedes tau hyperphosphorylation in 3xTg-AD mice (Belfiore et al., 2019); indeed, amyloid β creates the inflammatory milieu that activates the tau-phosphorylating protein kinases (Ontiveros-Torres et al., 2016; Huber et al., 2018). Since IHT did not significantly lower amyloid β content in the cerebral cortex or hippocampus, it could be postulated that IHT may not have altered tau phosphorylation in the present study. Nonetheless, evaluation of tau phosphorylation and hippocampal EPO and BDNF contents in IHT- vs. sham-IHT-treated 3xTg-AD mice, and analysis of IHT's impact on neuronal injury and death in the 3xTg-AD mice, are appropriate extensions of this work. Furthermore, additional cognitive behavioral assessments such as the Barnes maze test, the Y-maze test, and the Novel object-recognition test should be applied to support the favorable effects of IHT on the MWM assessment of spatial learning behavior. Neuroimaging studies of cerebral cortex and hippocampus could determine if IHT-augmentation of EPO and BDNF is associated with structural adaptations, e.g., *de novo* neurogenesis (Shingo et al., 2001; Zhu et al., 2010).

Although the persistence of the IHT-induced benefits in 3xTg-AD mice is not yet known, IHT-related improvements in learning-memory behavior and augmented expression of neuroprotective growth/trophic factors may persist well beyond completion of the IHT intervention. In a rat model of ethanol intoxication-withdrawal, an IHT regimen similar to the present one sharply attenuated neurobehavioral deficits during acute ethanol withdrawal, and this protection remained effective against a second ethanol withdrawal 5 weeks after completing IHT (Ju et al., 2012). Long-term assessments of spatial learning-memory and brain Aβ, EPO and BDNF contents beyond 24 h post-IHT are appropriate goals of future studies.

CONCLUSIONS

A 3-week moderate, normobaric IHT regimen stabilized neurobehavioral function and induced expression of the neuroprotective trophic factors EPO and BDNF, without lowering already-accumulated amyloid-β, in transgenic mice modeling AD. The IHT regimen augmented cerebrocortical EPO and BDNF contents, thereby reversing the depletion of these neuroprotective trophic/growth factors in 3xTg-AD mice, in the face of ongoing Aβ accumulation. Thus, IHT can activate cerebrocortical EPO and BDNF formation even after the onset of AD pathogenesis. The enhanced EPO and BDNF contents were associated with improved spatial learning-memory function in the 3xTg-AD mice vs. age-matched controls without IHT intervention. This study in transgenic mice displaying the AD phenotype provides the first empirical evidence that IHT initiated after AD onset can prevent cognitive decline, identifies potential molecular underpinnings of this cognitive improvement, and supports the possibility that moderate, normobaric IHT regimens could be effectively applied for treating AD after the onset of $A\beta_{42}$ accumulation.

DATA AVAILABILITY STATEMENT

The raw data supporting the conclusions of this article will be made available by the corresponding author upon request.

ETHICS STATEMENT

The animal study was reviewed and approved by Institutional Animal Care and Use Committee at UNTHSC.

AUTHOR CONTRIBUTIONS

M-GR, XC, MC, HW, MJ, RM, and XS: conceived and planned experiments. M-GR, XC, and XS: analyzed data. M-GR, MJ, RM, and XS: interpreted results of experiments, prepared figures and drafted manuscript, and edited the manuscript. All authors: performed experiments and approved final version of manuscript.

FUNDING

This work was supported by Texas Alzheimer's Research and Care Consortium Investigator Grant Program; UNTHSC Center for Healthy Aging Faculty Development Fund (to XS), National Institute of Aging AG053974 (to MJ), China National Social Science Project 15BTY088 (to XC), and UNTHSC Division of Research Development and Commercialization Basic Research Program (to RM).

ACKNOWLEDGMENTS

We sincerely thank Dr. Michael Forster for his support and Dr. Nathalie Sumien for making the MWM system available for this study.

REFERENCES

Arias-Cavieres, A., Khuu, M. A., Nwakudu, C. U., Barnard, J. E., Dalgin, G., and Garcia, A. J., III. (2020). A HIF1a-dependent pro-oxidant state disrupts synaptic plasticity and impairs spatial memory in response to intermittent hypoxia. *eNeuro* 7:ENEURO.0024-20.2020. doi: 10.1523/ENEURO.0024-20.2020

Ashall, F., and Goate, A. M. (1994). Role of the beta-amyloid precursor protein in Alzheimer's disease. *Trends Biochem. Sci.* 19, 42–46. doi: 10.1016/0968-0004(94)90173-2

Belfiore, R., Rodin, A., Ferreira, E., Velazquez, R., Branca, C., Caccamo, A., et al. (2019). Temporal and regional progression of Alzheimer's disease-like pathology in 3xTg-AD mice. *Aging Cell* 18:e12873. doi: 10.1111/acel.12873

Bernaudin, M., Bellail, A., Marti, H. H., Yvon, A., Vivien, D., Duchatelle, I., et al. (2000). Neurons and astrocytes express EPO mRNA: oxygen-sensing mechanisms that involve the redox-state of the brain. *Glia* 30, 271–278. doi: 10.1002/(SICI)1098-1136(200005)30:3<271::AID-GLIA6>3.0.CO;2-H

Bernaudin, M., Nedelec, A. S., Divoux, D., MacKenzie, E. T., Petit, E., and Schumann-Bard, P. (2002). Normobaric hypoxia induces tolerance to focal permanent cerebral ischemia in association with an increased expression of hypoxia-inducible factor-1 and its target genes, erythropoietin and VEGF in the adult mouse brain. *J. Cereb. Blood Flow Metab*. 22, 393–403. doi: 10.1097/00004647-200204000-00003

Brody, D. L., and Holtzman, D. M. (2006). Morris water maze search strategy analysis in PDAPP mice before and after experimental traumatic brain injury. *Exp. Neurol*. 197, 330–340. doi: 10.1016/j.expneurol.2005.10.020

Dara, T., Vatanara, A., Sharifzadeh, M., Khani, S., Vakilinezhad, M. A., Vakhshiteh, F., et al. (2019). Improvement of memory deficits in the rat model of Alzheimer's disease by erythropoietin-loaded solid lipid nanoparticles. *Neurobiol. Learn. Mem*. 166:107082. doi: 10.1016/j.nlm.2019.107082

Dengler, V. L., Galbraith, M., and Espinosa, J. M. (2014). Transcriptional regulation by hypoxia inducible factors. *Crit. Rev. Biochem. Mol. Biol*. 49, 1–15. doi: 10.3109/10409238.2013.838205

Dinkel, F., Trujillo-Rodriguez, D., Villegas, A., Streffer, J., Mercken, M., Lopera, F., et al. (2020). Decreased deposition of beta-amyloid 1-38 and increased deposition of beta-amyloid 1-42 in brain tissue of presenilin-1 e280a familial Alzheimer's disease patients. *Front. Aging Neurosci*. 12:220. doi: 10.3389/fnagi.2020.00220

Fernandez, M. A., Klutkowski, J. A., Freret, T., and Wolfe, M. S. (2014). Alzheimer presenilin-1 mutations dramatically reduce trimming of long amyloid β-peptides (Aβ) by γ-secretase to increase 42-to-40-residue Aβ. *J. Biol. Chem*. 289, 31043–31052. doi: 10.1074/jbc.M114.581165

Focke, C., Blume, T., Zott, B., Shi, Y., Deussing, M., Peters, F., et al. (2019). Early and longitudinal microglial activation but not amyloid accumulation predicts cognitive outcome in PS2APP mice. *J. Nucl. Med*. 60, 548–554. doi: 10.2967/jnumed.118.217703

Foley, A. M., Ammar, Z. M., Lee, R. H., and Mitchell, C. S. (2015). Systematic review of the relationship between amyloid-β levels and measures of transgenic mouse cognitive deficit in Alzheimer's disease. *J. Alzheimers Dis*. 44, 787–795. doi: 10.3233/JAD-142208

Gozal, D., Nair, D., and Goldbart, A. D. (2010). Physical activity attenuates intermittent hypoxia-induced spatial learning deficits and oxidative stress. *Am. J. Respir. Crit. Care Med*. 182, 104–112. doi: 10.1164/rccm.201001-0108OC

Gunnarson, E., Song, Y., Kowalewski, J. M., Brismar, H., Brines, M., Cerami, A., et al. (2009). Erythropoietin modulation of astrocyte water permeability as a component of neuroprotection. *Proc. Natl. Acad. Sci. U. S. A*. 106, 1602–1607. doi: 10.1073/pnas.0812708106

Hassan, A., Arnold, B. M., Caine, S., Toosi, B. M., Verge, V. M. K., and Muir, G. D. (2018). Acute intermittent hypoxia and rehabilitative training following cervical spinal injury alters neuronal hypoxia- and plasticity-associated protein expression. *PLoS ONE* 13:e0197486. doi: 10.1371/journal.pone.0197486

Hock, C., Heese, K., Hulette, C., Rosenberg, C., and Otten, U. (2000). Region-specific neurotrophin imbalances in Alzheimer disease: decreased levels of brain-derived neurotrophic factor and increased levels of nerve growth factor in hippocampus and cortical areas. *Arch. Neurol*. 57, 846–851. doi: 10.1001/archneur.57.6.846

Huber, C. M., Yee, C., May, T., Dhanala, A., and Mitchell, C. S. (2018). Cognitive decline in preclinical Alzheimer's disease: amyloid-beta versus tauopathy. *J. Alzheimers Dis*. 61, 265–281. doi: 10.3233/JAD-170490

Jagust, W. (2018). Imaging the evolution and pathophysiology of Alzheimer disease. *Nat. Rev. Neurosci*. 19, 687–700. doi: 10.1038/s41583-018-0067-3

Jia, Z., Xue, R., Ma, S., Xu, J., Guo, S., Li, S., et al. (2016). Erythropoietin attenuates the memory deficits in aging rats by rescuing the oxidative stress and inflammation and promoting BDNF releasing. *Mol. Neurobiol*. 53, 5664–5670. doi: 10.1007/s12035-015-9438-1

Joshi, C. R., Stacy, S., Sumien, N., Ghorpade, A., and Borgmann, K. (2020). Astrocyte HIV-1 tat differentially modulates behavior and brain MMP/TIMP balance during short and prolonged induction in transgenic mice. *Front. Neurol*. 11:593188. doi: 10.3389/fneur.2020.593188

Ju, X., Mallet, R. T., Downey, H. F., Metzger, D. B., and Jung, M. E. (2012). Intermittent hypoxia conditioning protects mitochondrial cytochrome c oxidase of rat cerebellum from ethanol withdrawal stress. *J. Appl. Physiol*. 112, 1706–1714. doi: 10.1152/japplphysiol.01428.2011

Jung, M. E., Simpkins, J. W., Wilson, A. M., Downey, H. F., and Mallet, R. T. (2008). Intermittent hypoxia conditioning prevents behavioral deficit and brain oxidative stress in ethanol-withdrawn rats. *J. Appl. Physiol*. 105, 510–517. doi: 10.1152/japplphysiol.90317.2008

Kim, J., Lee, S., Choi, B. R., Yang, H., Hwang, Y., Park, J. H., et al. (2017). Sulforaphane epigenetically enhances neuronal BDNF expression and TrkB signaling pathways. *Mol. Nutr. Food Res*. 61:194. doi: 10.1002/mnfr.201600194

Klein, A., Kowall, N., and Ferrante, R. (1998). Neurotoxicity and oxidative damage of beta amyloid 1-42 versus beta amyloid 1-40 in the mouse cerebral cortex. *Ann. N. Y. Acad. Sci*. 893, 314–320. doi: 10.1111/j.1749-6632.1999.tb07845.x

Kuo, C. Y., Hsiao, H. T., Lo, I. H., and Nikolai, T. (2020). Association between obstructive sleep apnea, its treatment, and alzheimer's disease: systematic mini-review. *Front. Aging Neurosci*. 12:591737. doi: 10.3389/fnagi.2020.591737

Lai, S. W., Chen, J. H., Lin, H. Y., Liu, Y. S., Tsai, C. F., Chang, P. C., et al. (2018). Regulatory effects of neuroinflammatory responses through brain-derived neurotrophic factor signaling in microglial cells. *Mol. Neurobiol*. 55, 7487–7499. doi: 10.1007/s12035-018-0933-z

Li, S., Hafeez, A., Noorulla, F., Geng, X., Shao, G., Ren, C., et al. (2017). Preconditioning in neuroprotection: from hypoxia to ischemia. *Prog. Neurobiol*. 157, 79–91. doi: 10.1016/j.pneurobio.2017.01.001

Li, Y., Lu, Z., Keogh, C. L., Yu, S. P., and Wei, L. (2007). Erythropoietin-induced neurovascular protection, angiogenesis, and cerebral blood flow restoration after focal ischemia in mice. *J. Cereb. Blood Flow Metab*. 27, 1043–1054. doi: 10.1038/sj.jcbfm.9600417

Liu, X., Xu, D., Hall, J. R., Ross, S., Chen, S., Liu, H., et al. (2017). Enhanced cerebral perfusion during brief exposures to cyclic intermittent hypoxemia. *J. Appl. Physiol*. 123, 1689–1697. doi: 10.1152/japplphysiol.00647.2017

Lukyanova, L. D., Sukoyan, G. V., and Kirova, Y. I. (2013). Role of proinflammatory factors, nitric oxide, and some parameters of lipid metabolism in the development of immediate adaptation to hypoxia and HIF-1α accumulation. *Bull. Exp. Biol. Med*. 154, 597–601. doi: 10.1007/s10517-013-2008-5

Malhotra, S., Savitz, S. I., Ocava, L., and Rosenbaum, D. M. (2006). Ischemic preconditioning is mediated by erythropoietin through PI-3 kinase signaling in an animal model of transient ischemic attack. *J. Neurosci. Res*. 83, 19–27. doi: 10.1002/jnr.20705

Mallet, R. T., and Ryou, M. G. (2017). Erythropoietin: endogenous protection of ischemic brain. *Vitam. Horm*. 105, 197–232. doi: 10.1016/bs.vh.2017.01.002

Mallet, R. T., Ryou, M. G., Williams, A. G., Jr., Howard, L., and Downey, H. F. (2006). Beta1-Adrenergic receptor antagonism abrogates cardioprotective effects of intermittent hypoxia. *Basic Res. Cardiol*. 101, 436–446. doi: 10.1007/s00395-006-0599-y

Miranda, M., Morici, J. F., Zanoni, M. B., and Bekinschtein, P. (2019). Brain-derived neurotrophic factor: a key molecule for memory in the healthy and the pathological brain. *Front. Cell Neurosci*. 13:363. doi: 10.3389/fncel.2019.00363

Navarrete-Opazo, A., and Mitchell, S. G. (2014). Therapeutic potential of intermittent hypoxia: a matter of dose. *Am. J. Physiol. Regul. Integr. Comp. Physiol*. 307, R1181–1197. doi: 10.1152/ajpregu.00208.2014

Ontiveros-Torres, M., Labra-Barrios, M. L., Díaz-Cintra, S., Aguilar-Vázquez, A. R., Moreno-Campuzano, S., Flores-Rodríguez, P., et al. (2016). Fibrillar amyloid-β accumulation triggers an inflammatory mechanism leading to hyperphosphorylation of the carboxyl-terminal end of tau polypeptide in the hippocampal formation of the 3×Tg-AD transgenic mouse. *J. Alzheimers Dis*. 52, 243–269. doi: 10.3233/JAD-150837

Park, H., and Poo, M. M. (2013). Neurotrophin regulation of neural circuit development and function. *Nat. Rev. Neurosci*. 14, 7–23. doi: 10.1038/nrn3379

Phillips, S. A., Olson, E. B., Morgan, B. J., and Lombard, J. H. (2004). Chronic intermittent hypoxia impairs endothelium-dependent dilation in rat cerebral and skeletal muscle resistance arteries. *Am. J. Physiol. Heart Circ. Physiol*. 286, H388–393. doi: 10.1152/ajpheart.00683.2003

Pillai, A., Dhandapani, K. M., Pillai, B. A., Terry, A. V., Jr, and Mahadik, P. S. (2008). Erythropoietin prevents haloperidol treatment-induced neuronal apoptosis through regulation of BDNF. *Neuropsychopharmacology* 33, 1942–1951. doi: 10.1038/sj.npp.1301566

Rabie, T., and Marti, H. H. (2008). Brain protection by erythropoietin: a manifold task. *Physiology* 23, 263–274. doi: 10.1152/physiol.00016.2008

Ratilal, B. O., Arroja, M. M., Rocha, J. P., Fernandes, A. M., Barateiro, A. P., Brites, D. M., et al. (2014). Neuroprotective effects of erythropoietin pretreatment in a rodent model of transient middle cerebral artery occlusion. *J. Neurosurg.* 121, 55–62. doi: 10.3171/2014.2.JNS132197

Rey, F., Balsari, A., Giallongo, T., Ottolenghi, S., Di Giulio, A. M., Samaja, M., et al. (2019). Erythropoietin as a neuroprotective molecule: an overview of its therapeutic potential in neurodegenerative diseases. *ASN Neuro* 11:1759091419871420. doi: 10.1177/1759091419871420

Romberg, C., Mattson, M. P., Mughal, M. R., Bussey, T. J., and Saksida, L. M. (2011). Impaired attention in the 3xTgAD mouse model of Alzheimer's disease: rescue by donepezil (Aricept). *J. Neurosci.* 31, 3500–3507. doi: 10.1523/JNEUROSCI.5242-10.2011

Ruscher, K., Freyer, D., Karsch, M., Isaev, N., Megow, D., Sawitzki, B., et al. (2002). Erythropoietin is a paracrine mediator of ischemic tolerance in the brain: evidence from an *in vitro* model. *J. Neurosci.* 22, 10291–10301. doi: 10.1523/JNEUROSCI.22-23-10291.2002

Rybnikova, E., and Samoilov, M. (2015). Current insights into the molecular mechanisms of hypoxic pre- and postconditioning using hypobaric hypoxia. *Front. Neurosci.* 9:388. doi: 10.3389/fnins.2015.00388

Ryou, M. G., Liu, R., Ren, M., Sun, J., Mallet, R. T., and Yang, S. H. (2012). Pyruvate protects the brain against ischemia-reperfusion injury by activating the erythropoietin signaling pathway. *Stroke* 43, 1101–1107. doi: 10.1161/STROKEAHA.111.620088

Ryou, M. G., Mallet, R. T., Metzger, D. B., and Jung, M. E. (2017). Intermittent hypoxia training blunts cerebrocortical presenilin 1 overexpression and amyloid-beta accumulation in ethanol-withdrawn rats. *Am. J. Physiol. Regul. Integr. Comp. Physiol.* 313, R10–R18. doi: 10.1152/ajpregu.00050.2017

Sakanaka, M., Wen, T. C., Matsuda, S., Masuda, S., Morishita, E., Nagao, M., et al. (1998). *In vivo* evidence that erythropoietin protects neurons from ischemic damage. *Proc. Natl. Acad. Sci. U. S. A.* 95, 4635–4640. doi: 10.1073/pnas.95.8.4635

Semenza, G. L. (2009). Regulation of oxygen homeostasis by hypoxia-inducible factor 1. *Physiology* 24, 97–106. doi: 10.1152/physiol.00045.2008

Shingo, T., Sorokan, S. T., Shimazaki, T., and Weiss, S. (2001). Erythropoietin regulates the *in vitro* and *in vivo* production of neuronal progenitors by mammalian forebrain neural stem cells. *J. Neurosci.* 21, 9733–9743. doi: 10.1523/JNEUROSCI.21-24-09733.2001

Shiota, S., Takekawa, H., Matsumoto, S. E., Takeda, K., Nurwidya, F., Yoshioka, Y., et al. (2013). Chronic intermittent hypoxia/reoxygenation facilitate amyloid-beta generation in mice. *J. Alzheimers Dis.* 37, 325–333. doi: 10.3233/JAD-130419

Sisodia, S. S., and Price, L. D. (1995). Role of the beta-amyloid protein in Alzheimer's disease. *Faseb J.* 9, 366–370. doi: 10.1096/fasebj.9.5.7896005

Song, J. H., Yu, J. T., and Tan, L. (2015). Brain-derived neurotrophic factor in Alzheimer's disease: risk, mechanisms, and therapy. *Mol. Neurobiol.* 52, 1477–1493. doi: 10.1007/s12035-014-8958-4

Tahawi, Z., Orolinova, N., Joshua, I. G., Bader, M., and Fletcher, E. C. (2001). Altered vascular reactivity in arterioles of chronic intermittent hypoxic rats. *J. Appl. Physiol.* 90, 2007–2013; discussion 2000. doi: 10.1152/jappl.2001.90.5.2007

Vetrovoy, O. V., Rybnikova, E. A., and Samoilov, M. O. (2017). Cerebral mechanisms of hypoxic/ischemic postconditioning. *Biochemistry* 82, 392–400. doi: 10.1134/S000629791703018X

Villa, P., Bigini, P., Mennini, T., Agnello, D., Laragione, T., Cagnotto, A., et al. (2003). Erythropoietin selectively attenuates cytokine production and inflammation in cerebral ischemia by targeting neuronal apoptosis. *J. Exp. Med.* 198, 971–975. doi: 10.1084/jem.20021067

Viviani, B., Bartesaghi, S., Corsini, E., Villa, P., Ghezzi, P., Garau, A., et al. (2005). Erythropoietin protects primary hippocampal neurons increasing the expression of brain-derived neurotrophic factor. *J. Neurochem.* 93, 412–421. doi: 10.1111/j.1471-4159.2005.03033.x

Wall, A. M., Corcoran, A. E., O'Halloran, K. D., and O'Connor, J. J. (2014). Effects of prolyl-hydroxylase inhibition and chronic intermittent hypoxia on synaptic transmission and plasticity in the rat CA1 and dentate gyrus. *Neurobiol. Dis.* 62, 8–17. doi: 10.1016/j.nbd.2013.08.016

Wang, H., Shi, X., Schenck, H., Hall, J. R., Ross, S. E., Kline, G. P., et al. (2020). Intermittent hypoxia training for treating mild cognitive impairment: a pilot study. *Am. J. Alzheimers Dis. Other Demen.* 35:1533317519896725. doi: 10.1177/1533317519896725

Wang, L., Zhang, Z., Wang, Y., Zhang, R., and Chopp, M. (2004). Treatment of stroke with erythropoietin enhances neurogenesis and angiogenesis and improves neurological function in rats. *Stroke* 35, 1732–1737. doi: 10.1161/01.STR.0000132196.49028.a4

Wu, C. L., Chen, S. D., Yin, J. H., Hwang, C. S., and Yang, I. D. (2010). Erythropoietin and sonic hedgehog mediate the neuroprotective effects of brain-derived neurotrophic factor against mitochondrial inhibition. *Neurobiol. Dis.* 40, 146–154. doi: 10.1016/j.nbd.2010.05.019

Yamada, K., and Nabeshima, T. (2003). Brain-derived neurotrophic factor/TrkB signaling in memory processes. *J. Pharmacol. Sci.* 91, 267–270. doi: 10.1254/jphs.91.267

Yang, J. L., Lin, Y. T., Chuang, P. C., Bohr, V. A., and Mattson, M. P. (2014). BDNF and exercise enhance neuronal DNA repair by stimulating CREB-mediated production of apurinic/apyrimidinic endonuclease 1. *Neuromolecular Med.* 16, 161–174. doi: 10.1007/s12017-013-8270-x

Zhang, P., Downey, H. F., Chen, S., and Shi, X. (2014). Two-week normobaric intermittent hypoxia exposures enhance oxyhemoglobin equilibrium and cardiac responses during hypoxemia. *Am. J. Physiol. Regul. Integr. Comp. Physiol.* 307, R721–730. doi: 10.1152/ajpregu.00191.2014

Zhu, X. H., Yan, H. C., Zhang, J., Qu, H. D., Qiu, X. S., Chen, L., et al. (2010). Intermittent hypoxia promotes hippocampal neurogenesis and produces antidepressant-like effects in adult rats. *J. Neurosci.* 30, 12653–12663. doi: 10.1523/JNEUROSCI.6414-09.2010

Zong, P., Setty, S., Sun, W., Martinez, R., Tune, J. D., Ehrenburg, I. V., et al. (2004). Intermittent hypoxic training protects canine myocardium from infarction. *Exp. Biol. Med.* 229, 806–812. doi: 10.1177/153537020422900813

Zuccato, C., Marullo, M., Conforti, P., MacDonald, M. E., Tartari, M., and Cattaneo, E. (2008). Systematic assessment of BDNF and its receptor levels in human cortices affected by Huntington's disease. *Brain Pathol.* 18, 225–238. doi: 10.1111/j.1750-3639.2007.00111.x

Conflict of Interest: The authors declare that the research was conducted in the absence of any commercial or financial relationships that could be construed as a potential conflict of interest.

frontiers in Aging Neuroscience

ORIGINAL RESEARCH
published: 03 September 2021
doi: 10.3389/fnagi.2021.722580

Phosphodiesterase-4D Knockdown in the Prefrontal Cortex Alleviates Memory Deficits and Synaptic Failure in Mouse Model of Alzheimer's Disease

Yongchuan Shi[1†], Jinpeng Lv[2†], Ling Chen[3†], Guojun Luo[1], Mengjia Tao[4], Jianchun Pan[4], Xiaoxiong Hu[5], Jianwen Sheng[5], Shanjin Zhang[5], Min Zhou[1] and Huizhen Fan[5]**

[1] Department of Medicine, Jinshan Branch of the Sixth People's Hospital of Shanghai, Shanghai Jiao Tong University, Shanghai, China, [2] School of Pharmaceutical Engineering, Changzhou University, Changzhou, China, [3] Key Laboratory of Clinical Cancer Pharmacology and Toxicology Research of Zhejiang Province, Department of Clinical Pharmacy, Affiliated Hangzhou First People's Hospital, Zhejiang University School of Medicine, Hangzhou, China, [4] School of Pharmacy, Brain Institute, Wenzhou Medical University, Wenzhou, China, [5] Department of Gastroenterology, The People's Hospital of Yichun City, Yi Chun University, Yichun, China

OPEN ACCESS

Edited by:
Ying Xu,
University at Buffalo, United States

Reviewed by:
Fushun Wang,
Nanjing University of Chinese Medicine, China
Zengliang Jin,
Capital Medical University, China

***Correspondence:**
Min Zhou
zhoumin-1209@163.com
Huizhen Fan
fanfanyc@163.com

[†] *These authors have contributed equally to this work*

Received: *09 June 2021*
Accepted: *30 June 2021*
Published: *03 September 2021*

Citation:
Shi Y, Lv J, Chen L, Luo G, Tao M, Pan J, Hu X, Sheng J, Zhang S, Zhou M and Fan H (2021) Phosphodiesterase-4D Knockdown in the Prefrontal Cortex Alleviates Memory Deficits and Synaptic Failure in Mouse Model of Alzheimer's Disease. Front. Aging Neurosci. 13:722580. doi: 10.3389/fnagi.2021.722580

Phosphodiesterase 4 (PDE4)-dependent cAMP signaling plays a crucial role in cognitive impairment associated with Alzheimer's disease (AD). However, whether inhibition of PDE4 subtypes or their splice variants in the prefrontal cortex positively regulates synaptic plasticity and antioxidative stress, and reverses β-amyloid 1–42 (Aβ1–42, Aβ42)-induced cognitive impairment still need to be clarified. The present study determined whether and how PDE4D knockdown by microinjection of lenti-PDE4D-miRNA into the prefrontal cortex reversed Aβ1–42-induced cognitive impairment in behavioral, neurochemical, and molecular biology assays. The results suggested that PDE4D knockdown increased time to explore the novel object and decreased latency to leave the platform in novel object recognition and step-down passive avoidance tests. Further study suggested that PDE4D knockdown decreased the number of working memory errors in the eight-arm maze test. These effects were prevented by PKA inhibitor H89. The subsequent experiment suggested that inhibition of PDE4D in the prefrontal cortex rescued the long-term potentiation (LTP) and synaptic proteins' expression; it also increased antioxidant response by increasing superoxide dismutase (SOD) and decreasing malondialdehyde (MDA) levels. PDE4D knockdown also increased phosphorylated cAMP response element-binding protein (pCREB), brain-derived neurotrophic factor (BNDF), and anti-apoptotic proteins' expression, i.e., the ratio of Bcl-2/Bax, and decreased caspase-3 level in the prefrontal cortex. These findings extend the previous findings and support the hypothesis that RNA interference-mediated PDE4D knockdown in the prefrontal cortex ameliorated memory loss associated with synaptic failure in an AD mouse model by its antioxidant, anti-apoptotic, and neuroprotective properties.

Keywords: PDE4D knockdown, cognitive deficits, synaptic failure, antioxidant-and antiapoptotic response, neuroprotection

INTRODUCTION

Alzheimer's disease (AD), the most common degenerative and irreversible brain disease causing dementia in the elderly, is characterized by progressive cognitive deterioration and memory loss (Selkoe, 2001). Clinically, pathological features of AD are extracellular senile plaques composed of fibrillar amyloid-β (Aβ) peptides and intracellular neurofibrillary tangles containing hyperphosphorylated tau, accompanied by synaptic dysfunction and neuronal death (Mangialasche et al., 2010). Although many studies are trying to find the targets for the treatment of AD, the key targets and how to control the progression of AD and related dementia are still unknown.

Phosphodiesterase-4 (PDE4), an enzyme catalyzing cAMP hydrolysis, plays a crucial role in memory consolidation and retention. Previous studies showed that PDE4 negatively regulated memory performance by decreasing hippocampal neurogenesis (Bruel-Jungerman et al., 2005; Epp et al., 2007). While inhibition of PDE4 by rolipram significantly improves hippocampal long-term potentiation (LTP) (Titus et al., 2013). Moreover, rolipram increases the levels of cAMP and phosphorylation of CREB (pCREB) (Schneider, 1984; Li, 2009), and improves learning and memory (Romano et al., 1996; Otmakhov et al., 2004) by increasing the survival and proliferation of newborn neurons in the dentate gyrus (Nakagawa et al., 2002; Fujioka et al., 2004; Sasaki et al., 2007). Indeed, PDE4 has four subtypes (PDE4A-D) that are expressed as at least 25 distinct splice variants (Houslay, 2001; Conti et al., 2003; Cheung et al., 2007; Chandrasekaran et al., 2008; Zhang, 2009). Their differential distributions in brain regions show different roles of individual PDE4 subtypes in central neuron system (CNS) disorders (Cherry and Davis, 1999; Pérez-Torres et al., 2000). For example, PDE4B is involved in depression (Millar et al., 2005) and anxiety (Zhang et al., 2008), whereas PDE4D plays an important role in memory and cognitive dysfunction (Zhang et al., 2002). Unfortunately, development of non-selective PDE4 inhibitors for therapeutic purposes has been hindered by side effects such as nausea and vomiting (Robichaud et al., 2001), which appear to be PDE4 subtype-specific (Robichaud et al., 2002). Therefore, targeting specific PDE4 isoforms, i.e., PDE4A, B, or D, could overcome this issue (Zhang et al., 2018).

The present study investigated whether inhibition of PDE4D by microinjection of lenti-PDE4D-miRNA into the prefrontal cortex of mice would rescue Aβ1–42-induced memory loss and cognitive deterioration. We found that PDE4D knockdown in the prefrontal cortex ameliorated long-term potentiation (LTP) in Aβ1–42-treated mice. The expression of Bcl-2, Bax, caspase-3, protein kinase A (PKA), phosphorylation of CREB (pCREB), and BDNF in the prefrontal cortex were also examined to decipher how PDE4D deficiency could ameliorate memory by regulation of the anti-apoptotic and neuroprotective pathway.

MATERIALS AND METHODS

Animals

Adult male ICR mice, weighing 23–28 g, were provided by Beijing Weitong Lihua Animal Center, Chinese Academy of Sciences. The mice were raised in a temperature-controlled room with a humidity of 50–60%, natural light, circadian rhythm, and free access to food and water. The behavioral tests were carried out between 9:00 a.m. and 4:00 p.m. All procedures were carried out in a quiet room according to the "NIH Guide for the Care and Use of Laboratory Animals" (NIH Publications No. 80-23, revised 1996) and were approved by the Wenzhou Medical University Committee on Animal Care and Use and Jinshan Branch of the Sixth People's Hospital of Shanghai, Jiao Tong University.

Surgery

All surgery was conducted under aseptic conditions, including autoclaves of all surgery supplies before surgery and the use of a hot bead sterilizer for contaminated supplies during surgery. Mice were anesthetized with ketamine and Xylazine (100 and 10 mg/kg, i.p.) (Zhang et al., 2014). In order to relieve pain, mice were given carprofen (5 mg/kg, s.c.) before and after surgery. The fur on the top of the head was then shaved off, and the mouse was placed in a stereotaxic apparatus followed by asepsis with iodine and 70% alcohol. A 3-cm incision was made at the top of the head along the sagittal seam to expose the skull and a hole was drilled in the skull over the injection site following the coordinates (Nagai et al., 2007): Anterior-posterior (AP, from Bregma), +1.5 mm, medial-lateral (ML, from midline), ± 0.5 mm and dorsal-ventral (DV, from dura) −1.2 mm. A guide cannula (30-gauge) was implanted at the drilling site and fixed with dental tray powder. To permit diffusion after microinjection, the infusion cannula was left in place for an extra 5 min. The mice were allowed to recover for 3 days before receiving Aβ1–42 peptide (0.4 μg/μl, 1 μl/side) treatment. The lenti-PDE4D-miRNA (4DmiRNA) (5×10^6 TU/μl, 1 μl/side) was microinjected 1 day after Aβ1–42 treatment. The behavioral tests were conducted 14 days after lenti-PDE4D-miRNA treatment. To determine the role of cAMP signaling in PDE4D knockdown-induced memory enhancement, PKA inhibitor H89 (2.5 μM/side) was administered for 14 days (from days 8 to 23).

Drugs and Treatment

Aβ1–42 (rPeptide, Aβ42, United States) was dissolved in 0.9% sterile saline, at a final concentration of 0.4 μg/μl and incubated at 37°C for 4 days to obtain aggregated Aβ before micro-infusion into prefrontal cortex. H89 (Sigma-Aldrich, United States) were dissolved in artificial cerebrospinal fluid (ACSF) for prefrontal cortex microinjection from day 8 to day 22 (once a day). A total of 60 mice were randomly divided into 5 groups (12 mice in each group) for behavioral tests. The groups were normal control + vehicle, Aβ1–42 + vehicle, Aβ1–42 + 4DmiRNA, Aβ1–42 + 4DmiRNA + H89, and Aβ1–42 + H89. After behavioral tests, mice were sacrificed for LTP recording (half brain) and an immunoblot assay (the other half brain).

The primary antibodies of anti-PSD95, anti-BDNF, and anti-SYN were purchased from Abcam Biotechnology Company (Abcam, Cambridge, MA). Anti-pCREB and anti-CREB were purchased from Merck Millipore (Millipore, Billerica, MA, United States). All the secondary antibodies (anti-rabbit lgG) were purchased from MultiSciences Biotech Co., Ltd. (MultiSciences, Hangzhou, China). The Cu-Zn/MnSOD and SOD ELISA kit was purchased from Shanghai Beyotime Biological Technology Co., Ltd. (Beyotime Sciences, United Kingdom).

Construction of Long-Form Lenti-PDE4D-miRNA

The construction of long-form PDE4D-miRNA was performed as described previously (Li et al., 2011). The sequence for the PDE4D miRNA (miRNA-mir hairpin structure) was 5-AATGGAGTCACAATCAAGTCAGTTTTGGCCACTGACTGACTGACTTGAGTGACTCCATT-3. The first 21-nts stretch is the antisense target sequence. The final sequence represents nts 1–8 and 11–21 of the sense target sequences. This miRNA sequence targets nucleotides 642–662 of the rat PDE4D4 coding sequence (GenBank accession no. AF031373), which corresponds to amino acids 214–221 within the UCR1 domain of long-form PDE4D isoforms such as PDE4D4/5; the NC sequence from Invitrogen (Carlsbad, CA, United States) was 5 -GAAATGTACTGCGCGTGGAGACGTTTTGGCCACTGACTGACGTCTCCACGCAGTACATTT-3. In both 4DmiRNA and NC sequences, the middle 19 nts (overstriking) were constant and came from the miR-155 hairpin loop. The lentiviral particles were produced by transiently transfecting HEK293T cells with a transfer plasmid containing EGFP and 4DmiRNA or NC.

Behavioral Experiments

Open Field Test

The experiment was measured by an automatic activity monitoring system recording the interruption of an infrared beam (16 × 16). Each mouse was placed in the center of an autonomous activity test chamber (30 cm × 30 cm × 30 cm, with a built-in camera to record mouse activity) for accommodation for 5 min. In the test session, mouse activity was recorded within 10 min. The spontaneous activity chamber was wiped with alcohol after each test and feces were removed to avoid affecting the spontaneous activity of the next mouse (Xu et al., 2005).

Novel Object Recognition Test

In the acclimation session, mice were placed in a well-lighted test box (60 × 60 × 15 cm) facing the lateral wall and allowed to move freely for 5 min. The next day was a familiarization session, in which mice were placed back to the open field box, 6 cm from the side wall, and allowed to move for 5 min. There were two identical objects in this session, A1 and A2, both of which were hard weights to prevent mice from pushing and damaging them. The cumulative exploration time (A1, A2) of each object was measured, with the total time recorded as E0 and the process recorded as T0. The test session was conducted 1 h and 24 h after the familiarization session. In this session, the original object A was replaced with object B. The mice were allowed to move inside for 5 min and the cumulative exploration time (A1, B) of each object was measured. The total time was recorded as E2, and the process was recorded as T2. After each experiment, objects were wiped with 75% alcohol to avoid odor interference. The experiment was a blind test because the experimenter did not know the treatment status of the mice.

Criteria considered as exploratory behavior: (1) Mice were within 5 cm from the object; (2) mice gazed, smelt, or touched objects (head); (3) no account was taken of lying on or walking near an object. The results were expressed as discrimination index (DI), and the calculation formula was as follows: DI = B-A/E1or DI = B-A/E2 or DI = A2′-A1/E1 or DI = A2′-A1/E2 (Xu et al., 2015).

Step-Down Passive Avoidance Test

The test was carried out utilizing a square chamber within a wooden platform on one side of the grid floor. The grid floor of the chamber could receive an electric shock from an isolated pulse stimulator when the mice stepped down. The test included three sessions: Habituation, training, and retention. A mouse was first habituated to the apparatus for 5 min and then the training session was conducted 1 h later. In this training session, a mouse was placed on the wooden platform and was subjected to a foot shock (0.4–0.8 mA, 40 V, 0.5 s, 50 Hz, 20 sec intertribal interval) to see if it jumped off the platform with its feet fully exposed to the grid floor. The mouse was considered to have taken the task when it stayed on the platform over 60 s in the training session. Retention tests were conducted 3 h and 24 h after the training session, respectively. During the retention session, the electric shock of the grid was removed, a mouse was individually placed on the platform and the time when it first jumped off the platform was recorded as step-down latency, with an upper cutoff time of 300 s (Wang et al., 2020).

Eight-Arm Radial Maze (8-RAM)

The 8-RAM maze was placed 40 cm above the ground. The central area of the maze had a diameter of 30 cm and eight arms (50 cm × 12 cm, surrounded by a wall 4.5-cm high) extending at equal angles and equal lengths to all sides (Pu et al., 2007). After 1 week of acclimation, the mice were weighed and fasted for 24 h before each test. On days 8–11 of the acclimation session, food was placed in the middle and on each arm every day before animals were placed in the maze. In this session, 3–4 mice were simultaneously placed in the maze and allowed to move freely and ingest food for 10 min. Days 12–18 were the training and test session. Only four of the eight arms (arms 3, 5, 6, and 8, respectively) were fed during each exercise, which were maintained throughout the experiment. The mice were placed in the central area of the maze each day, and the doors were closed around the central area for 30 s before opening. The mice could choose to enter any arm for food intake. When the mouse entered the arm with food and received food, it was recorded as a one-time correct choice; otherwise, it was a wrong choice. Re-entering the arm with food was called a working memory error, and re-entering the arm without food was called a reference memory error. Total memory error = reference memory error + working

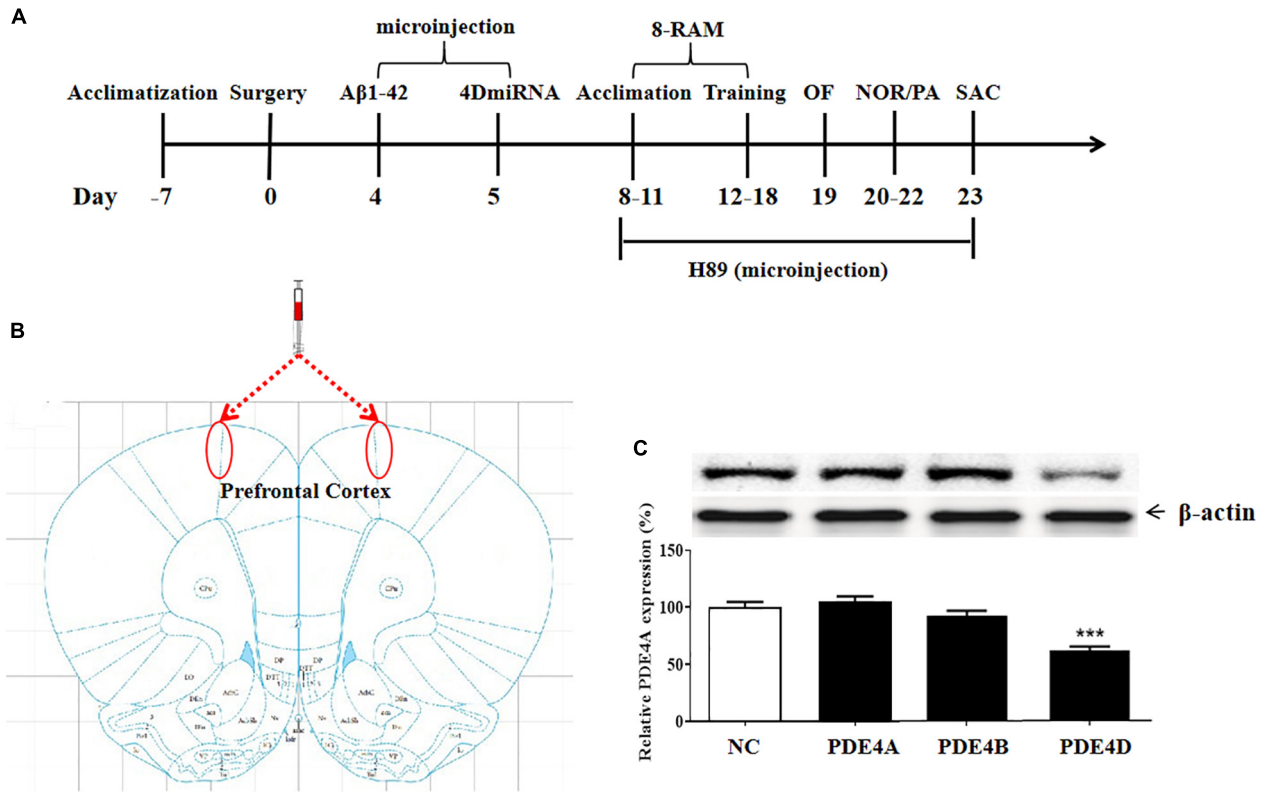

FIGURE 1 | (A) Experimental design and the test order. Aβ 42 was microinfused into bilateral prefrontal cortices of mice on day 4 after surgery. Lentiviral vectors containing negative control sequence (NC) or 4DmiRNA were microinfused into bilateral prefrontal cortices of mice on day 5 after surgery. H89 or artificial cerebrospinal fluid were microinjected once daily starting from days 8 to 22. Behavioral experiments were performed from days 19 to 22, 30 min after H89 treatment. Animals were sacrificed for biochemical assays after behavioral tests (day 23). OF, open field test; NOR, novel object recognition test; PA, passive avoidance test; 8-RAM, eight-arm radial maze; SAC, sacrifice. **(B)** Photomicrographs of representative cannula placements in the brain region of microinjection are indicated by the red ellipse corresponding to the region. **(C)** PDE4 subtypes expression in the prefrontal cortex. PDE4D expression, but not PDE4A and PDE4B, was decreased after microinjection of lenti-PDE4D-miRNA into the prefrontal cortex for 2 weeks. Values were the means ± SEM with 12 mice in each group. ***$P < 0.001$ vs. vehicle-treated control group (NC).

memory error. After each experiment, the object was wiped with 75% alcohol to avoid odor interference.

Electrophysiological Recording

After behavioral tests, the half brain of mice was used for all field potential experiments, i.e., long-term potentiation (LTP). Slices were prepared as described previously (Misner and Sullivan, 1999). Briefly, brains were removed and coronal slices (350 mm) were cut using a vibratome (Precisionary Instruments, Greenville, NC, United States) in ice-cold solution (120 mM NaCl, 3.5 mM KCl, 0.7 mM $CaCl_2$, 4 mM $MgCl_2$, 1.25 mM NaH_2PO_4, 26 mM $NaHCO_3$, 10 mM glucose) bubbled with 95% O_2/5% CO_2 for the electrophysiological recording. LTP of the prefrontal cortex was induced by high-frequency stimulation consisting of a single train of 100 pulses delivered at 100 Hz. This high-frequency stimulation paradigm was used to induce a short-lasting form of LTP in the control slices, so that the potentiation of LTP in other groups could be recorded (Zhang et al., 2018). Experiments and subsequent analyses were performed by investigators who were blinded to the genotype of the mice.

Determination of SOD Activity in the Prefrontal Cortex

The activity of superoxide dismutase (SOD, EC 1.15.1.1) was measured by monitoring its ability to inhibit the photochemical reduction of nitroblue tetrazolium (NBT). A total of 100 mM of TRIS/HCl (pH 7.8), 75 mM of NBT, 2 μM of riboflavin, 6 mM of EDTA, and 200 μL of supernatant were contained in each 1.5-mL reaction mixture. The OD value was determined in the absorbance at 560 nm (the production of blue formazan). One unit of SOD was defined as the amount which was needed to suppress the rate of NBT reduction by 50%, as previously described by Winterbourn et al. (1975). The enzyme activity was expressed as units/mg protein.

Determination of Malondialdehyde (MDA) Level in the Prefrontal Cortex

Malondialdehyde, an indicator of lipid peroxidation, is determined spectrophotometrically using the thiobarbituric acid analysis method according to Ohkawa et al. (1979) description. Briefly, 200 μL of supernatant was added and briefly mixed with 1 mL of 50% trichloroacetic acid in 0.1 M of HCl

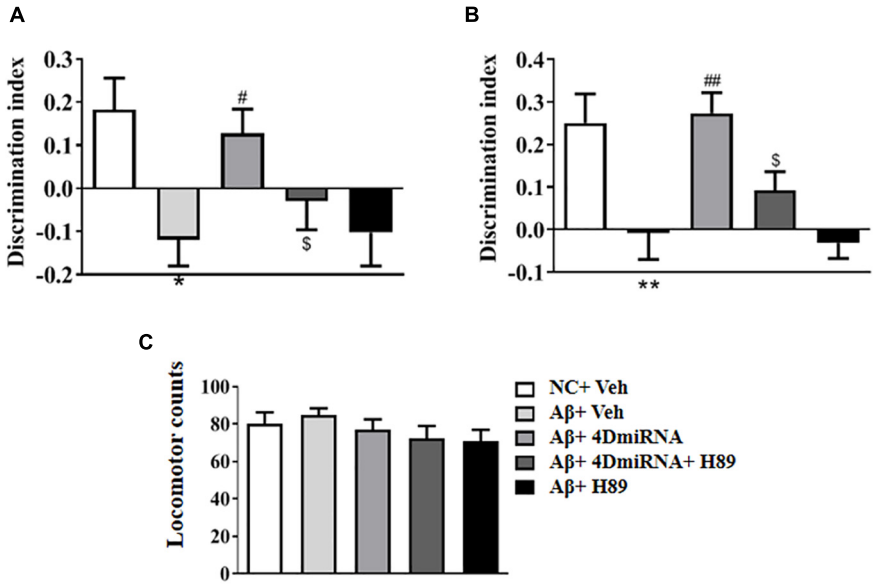

FIGURE 2 | PDE4D deficiency improved cognition and memory in the novel object recognition test in Aβ1–42-treated mice. The discrimination index 3 h **(A)** and 24 h **(B)** after the training session was recorded after microinjection of lenti-PDE4D-miRNA into the prefrontal cortex for 2 weeks. In the open field test, the total distance traveled did not shown a change after PDE4D deficiency. **(C)** Values were the means ± SEM with 12 mice in each group. $^{*}P < 0.05$, $^{**}P < 0.01$ vs. control group (NC); $^{\#}P < 0.05$, $^{\#\#}P < 0.01$ vs. Aβ+Veh group; $^{\$}P < 0.05$ vs. Aβ+4DmiRNA group.

and 1 mL of 26 mM thiobarbituric acid. After vortex-mixing, samples were kept at 95℃ for 20 min. Then, the sample was centrifuged at 960 × g for 10 min, and the supernatant was read in the absorbance at 532 nm. A calibration curve was drawn using MDA as the standard curve and the results were expressed in nmol/mg protein.

Western Blot Analysis

The prefrontal cortex tissues were homogenized in lysis buffer containing protease and phosphatase inhibitors and centrifuged at 12,000 rpm for 30 min at 4°C. The supernatant was mixed with loading buffer and heated to 95°C to denature the proteins. Protein concentrations were determined using the bicinchoninic acid (BCA) protein assay. The 10% sodium dodecyl sulfate polyacrylamide gel electrophoresis (SDS-PAGE) was applied to separate the protein samples (30 μg of protein/sample), and then the proteins were transferred onto a nitrocellulose filter (NC) membrane by making use of an electrophoretic transfer system (Bio-Rad, United States). Subsequently, the membranes were blocked with blocking buffer which contained 2.5% bovine serum albumin (BSA) in Tris-buffered saline and 0.1% Tween 20 (TBST) for 1.5 h at 25℃ and incubated with the corresponding primary antibodies overnight at 4℃. And then the blots were incubated with peroxidase-conjugated secondary antibodies for 1 h at 25℃, followed with visualizing which used enhanced chemiluminescence.

Statistical Analysis

All the experiments were performed in triplicate and the results were calculated by the mean ± standard error of the mean (SEM). Statistical analysis was performed according to *t*-test using GraphPad Prism 5.0 software and the value of $p < 0.05$ was considered statistically significant.

RESULTS

Downregulation of PDE4D Expression by Microinjection of Lenti-PDE4D-miRNA Into the Prefrontal Cortex of Mice

The experimental procedure is illustrated as **Figure 1A**. To determine the role of long-form PDE4D variants in memory, lentiviral vectors harboring either 4DmiRs (miRNAs designed to target long-form PDE4Ds such as PDE4D4/5) or the normal control sequence were microinfused into the prefrontal cortex of mice as shown in **Figure 1B**. On day 23, the prefrontal cortex tissues of the mice were taken from the mouse brain for immunoblot assay. The results showed that microinjection of lenti-PDE4D-miRNA into the prefrontal cortex decreased the expression of PDE4D in the prefrontal cortex ($P < 0.001$), but did not affect PDE4A and PDE4B expression as shown in **Figure 1C**.

PDE4D Knockdown Reversed Aβ1–42-Induced Memory Impairment in the Novel Object Recognition (NOR) Test

To evaluate the therapeutic effects of PDE4D deficiency on the cognitive and memory impairment in Aβ1–42-treated mice, behavioral tests such as novel object recognition (NOR) were conducted. Mice were exposed to a pair of identical objects for 5 min, the discrimination ability was observed 3 and 24 h later, respectively. As shown in **Figures 2A,B**, PDE4D knockdown

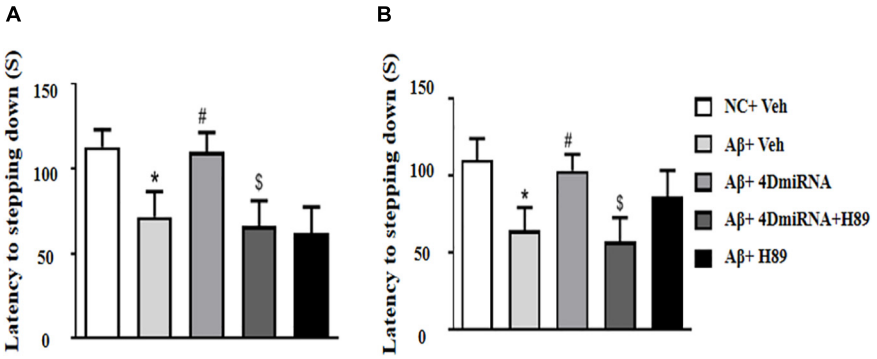

FIGURE 3 | PDE4D deficiency improved memory in the step-down passive avoidance test in Aβ1–42-treated mice. The latency to jump down to the floor 3 h **(A)** and 24 h **(B)** after the training session was recorded after microinjection of lenti-PDE4D-miRNA into the prefrontal cortex. Values were the means ± SEM with 12 mice in each group. $^{*}P < 0.05$ vs. control group (NC); $^{\#}P < 0.05$ vs. Aβ+Veh group; $^{\$}P < 0.05$ vs. Aβ+4DmiRNA group.

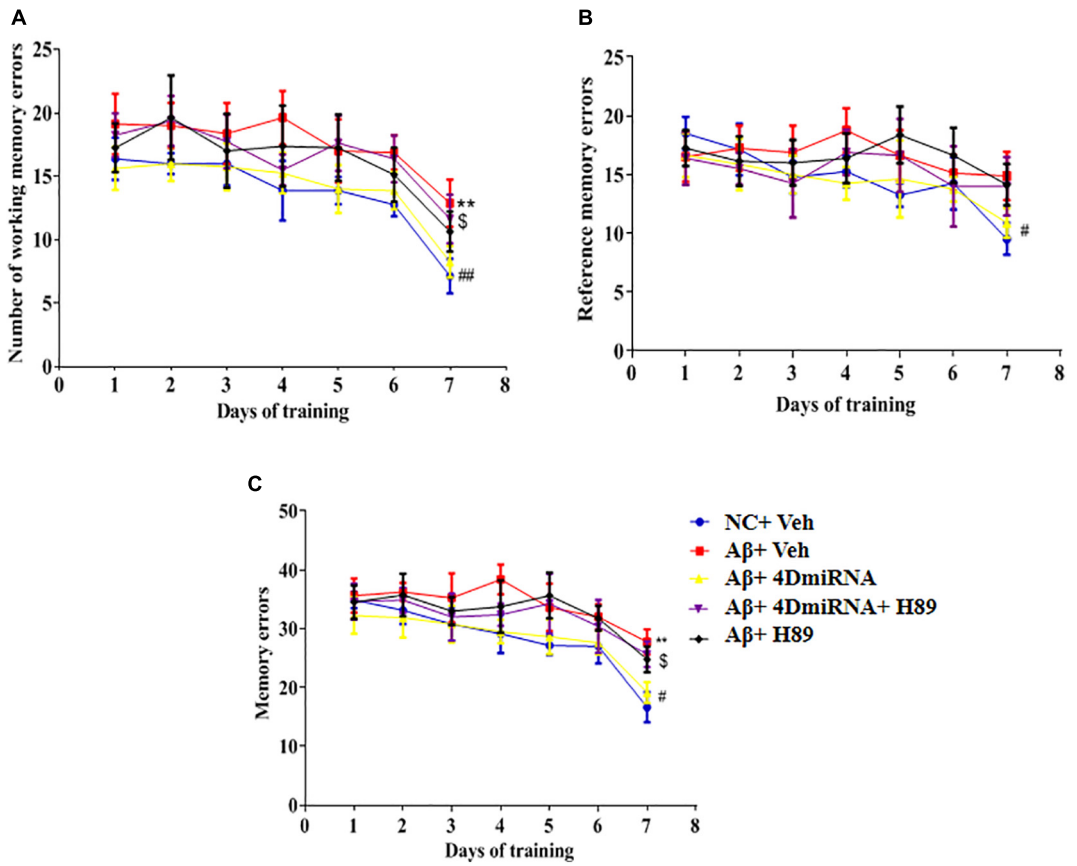

FIGURE 4 | PDE4D deficiency improved memory in the eight-arm maze test in Aβ1–42-treated mice. The working memory errors, **(A)** reference memory errors, **(B)** and the total memory errors **(C)** were recorded after microinjection of lenti-PDE4D-miRNA into the prefrontal cortex. Values were the means ± SEM with 12 mice in each group. $^{**}P < 0.01$ vs. control group (NC); $^{\#}P < 0.05$, $^{\#\#}P < 0.01$ vs. Aβ+Veh group; $^{\$}P < 0.05$ vs. Aβ+4DmiRNA group.

in the prefrontal cortex improved discrimination in the Aβ1–42-treated mice, both in 3- ($P < 0.05$; $P < 0.05$) and 24-h ($P < 0.01$; $P < 0.01$) test sessions. However, these results of PDE4D deficiency on memory enhancement were suppressed by treatment with PKA inhibitor H89 ($P < 0.05$; $P < 0.05$); while H89 treatment alone did not change the discrimination index. Importantly, the total distance animals traveled in the open field test were not found to change (**Figure 2C**), suggesting similar exploration and motor functioning. These findings suggest that this effect is dependent on PDE4D-PKA signaling.

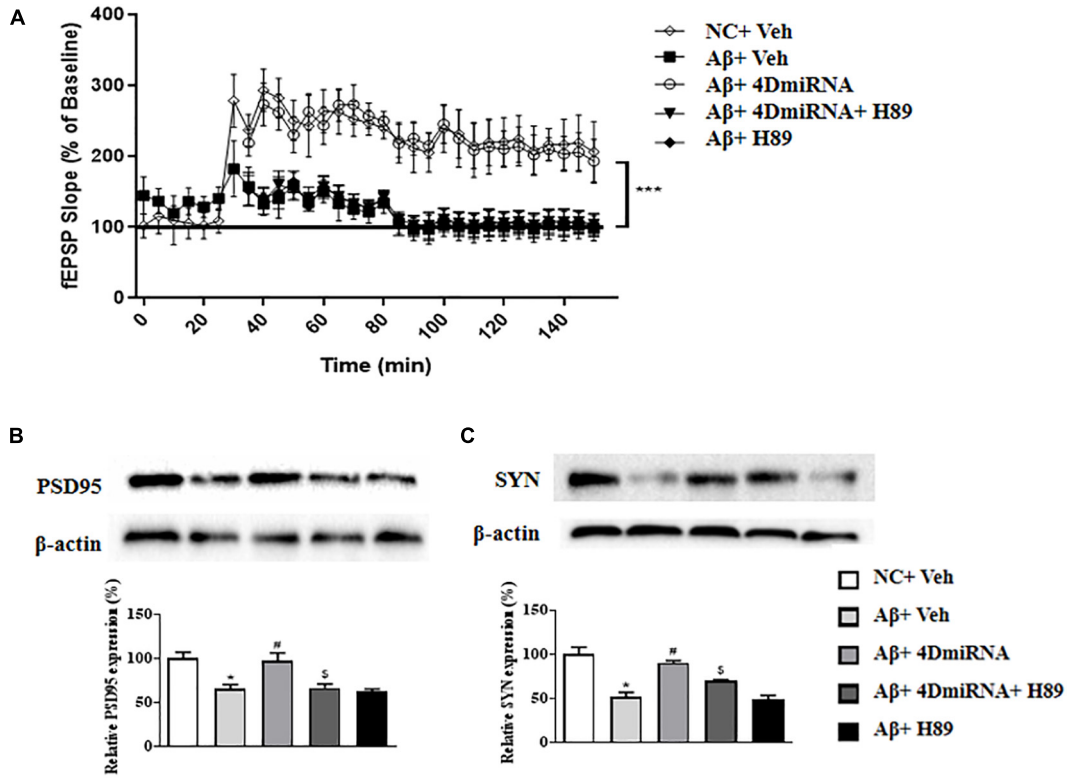

FIGURE 5 | PDE4D deficiency improved LTP **(A)** and increased PSD95 and synaptophysin expression **(B,C)** in the prefrontal cortex of Aβ1–42-treated mice. Data are presented as mean ± SEM (n = 12); values are the means ± SEM, $^{*}P < 0.05$, $^{***}p < 0.001$ vs. control group (NC); $^{\#}P < 0.05$ vs. Aβ+Veh group; $^{\$}P < 0.05$ vs. Aβ+4DmiRNA group.

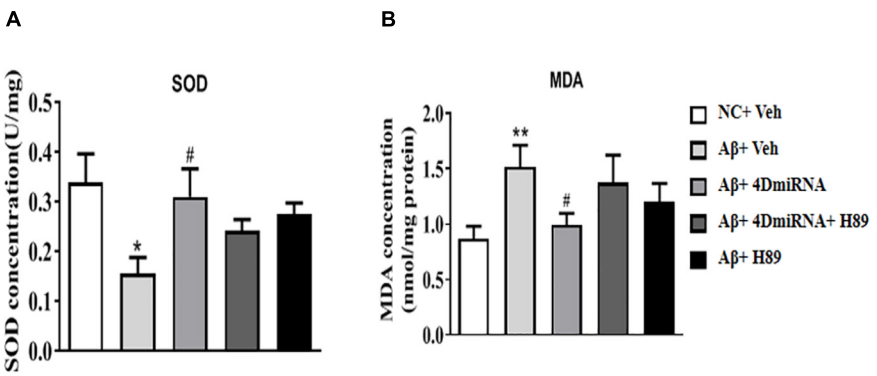

FIGURE 6 | PDE4D deficiency increased SOD activity **(A)** and decreased MDA **(B)** level in Aβ1–42-treated mice. Data are presented as mean ± SEM (n = 12); values are the means ± SEM, $^{*}P < 0.05$, $^{**}P < 0.01$ vs. control group (NC); $^{\#}P < 0.05$ vs. Aβ+Veh group.

PDE4D Knockdown Reversed Aβ1–42-Induced Memory Impairment in the Step-Down Passive Avoidance (PA) Test

The memory-enhancing effect of PDE4D knockdown was determined by measurement of emotional memory performance in the PA test both in 3- and 24-h test sessions. As shown in **Figures 3A,B**, Aβ1–42 affected memory retention, as evidenced by the fact that the average latency to jump down from the platform was noticeably shorter, at both 3 and 24 h after training in the Aβ1–42-treated mice ($P < 0.05$; $P < 0.05$). However, the Aβ1–42-induced memory deficit was reversed in the groups treated with lenti-PDE4D-miRNA, which exhibited a greater tendency to avoid stepping onto the electrified floor as compared to the vehicle-treated Aβ1–42 group ($P < 0.05$; $P < 0.05$). This

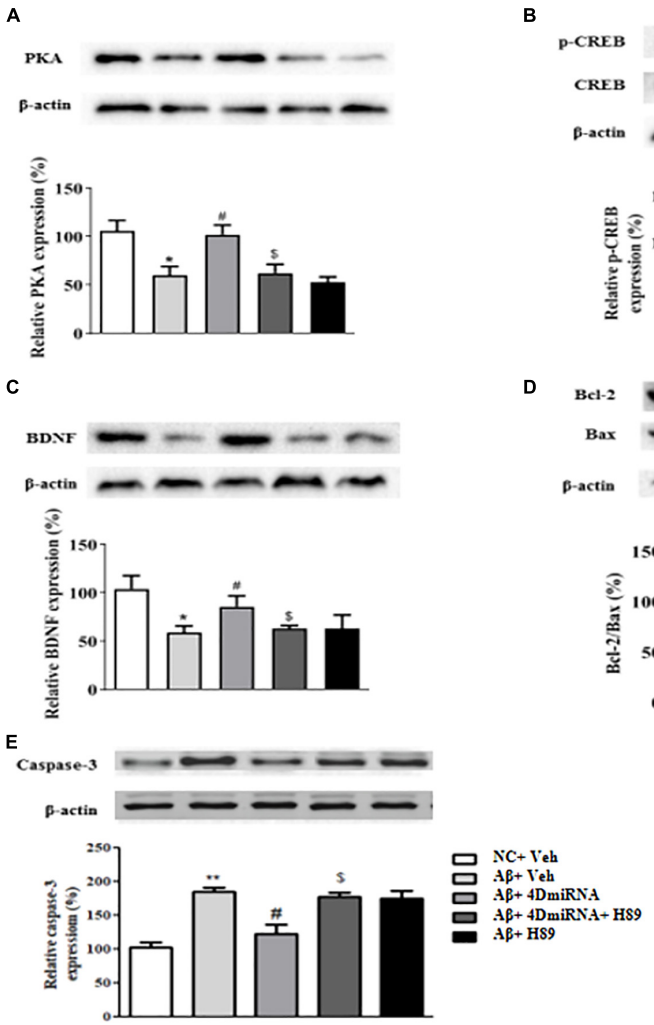

FIGURE 7 | PDE4D deficiency increased expression of PKA **(A)**, p-CREB **(B)**, BDNF **(C)**, Bcl-2/Bax **(D)**, and decreased caspase-3 **(E)** level in Aβ1–42-treated mice. Results are expressed as mean ± SEM (n = 12). $^{*}P < 0.05$, $^{**}P < 0.01$ vs. control group (NC); $^{\#}P < 0.05$ vs. Aβ+Veh group; $^{\$}P < 0.05$ vs. Aβ+4DmiRNA group.

effect was prevented by pretreatment with H89 in the lenti-PDE4D-miRNA-treated Aβ1–42 group ($P < 0.05$; $P < 0.05$).

PDE4D Knockdown Reversed Aβ1–42-Induced Memory Impairment in the Eight-Arm Maze Test

As shown in **Figure 4**, microinjection of Aβ1–42 into the prefrontal cortex induced a significant increase in working memory errors in mice ($P < 0.01$). These Aβ1–42-induced memory defects were prevented by intra-prefrontal cortex microinjection of lenti-PDE4D-miRNA, as evidenced by a reduced number of working memory errors compared to those of the vehicle-treated Aβ1-42 group ($P < 0.01$). This finding indicates enhanced long-term memory in these Aβ1–42-treated mice. The results were consistent with the previous study (Zhang et al., 2000), which suggested that Aβ1–42-induced memory retention impairment was reversed by PDE4D knockdown in the hippocampus. Although the changes in reference memory errors were not significant between the groups throughout the training and test sessions, the total memory errors were still ameliorated when PDE4D was knocked down in the prefrontal cortex ($P < 0.01$). However, this memory enhancement of PDE4D knockdown was prevented by treatment with PKA inhibitor H89 ($P < 0.05$). While H89 used alone did not affect the memory retention of mice.

PDE4D Knockdown Ameliorated Synaptic Plasticity and Increased Synaptic Proteins Expression in the Prefrontal Cortex of Aβ1–42-Treated Mice

Inhibition of PDE4 enzymes has previously been shown to enhance long-term potentiation in CA1 of the hippocampus (Barad et al., 1998; Navakkode et al., 2004). The present study

showed that intra-prefrontal cortex microinjection of lenti-PDE4D-miRNA for 2–3 weeks impaired the fEPSP slope in cortex slices in the Aβ1–42-treated mice as shown in **Figure 5A** ($P < 0.001$). However, these results of PDE4D deficiency on LTP enhancement were prevented by treatment with H89 ($P < 0.001$). However, H89 used alone did not induce any change on LTP expression in Aβ1–42-treated mice.

As shown in **Figures 5B,C**, two synapses-associated proteins, e.g., synaptophysin (SYN) and PSD-95, were significantly reduced when mice were treated with Aβ1–42 ($P < 0.05$; $P < 0.05$). Microinjection of lenti-PDE4D-miRNA into the prefrontal cortex of a mouse for 2–3 weeks significantly increased the levels of synaptophysin and PSD-95 ($P < 0.05$; $P < 0.05$). However, this increased synaptic protein expression of PDE4D knockdown was prevented by treatment with H89 ($P < 0.05$; $P < 0.05$).

PDE4D Knockdown Increased SOD Activities in the Prefrontal Cortex of Aβ1–42-Treated Mice

Aβ1–42-treated mice were found to decrease SOD level ($P < 0.05$); while PDE4D knockdown by microinjection of lenti-PDE4D-miRNA into the prefrontal cortex rescued this decreased SOD level ($P < 0.05$; **Figure 6A**). These effects of PDE4D knockdown on SOD activity was partially prevented by H89, but the difference was not significant. As shown in **Figure 6B**, PDE4D knockdown reversed the increase in MDA level in the prefrontal cortex of Aβ1–42-treated mice ($P < 0.05$). However, this PDE4D deficiency-induced decrease in MDA level was prevented by treatment of mice with H89 ($P < 0.05$). But H89 used alone seemed not to affect either SOD or MDA expression in these mice.

PDE4D Knockdown Increased the Levels of PKA, pCREB, BDNF, Bcl2/Bax, and Caspase-3 in the Prefrontal Cortex of Aβ1–42-Treated Mice

Given that CREB is an important downstream transcription factor of cAMP/protein kinase A (PKA) signaling and is critical for memory consolidation and synaptogenesis, we assessed PKA, CREB, pCREB, and BDNF levels in the prefrontal cortex after PDE4D deficiency in this brain region. As shown in **Figure 7A**, microinjection of lenti-PDE4D-miRNA into the prefrontal cortex recued the decreased expression of PKA in Aβ1–42-treated mice ($P < 0.05$). Although the total CREB levels in all groups were not significantly different, the relative pCREB expression, i.e., pCREB/CREB ratio, in the prefrontal cortex was significantly reduced in Aβ1–42-treated mice ($P < 0.05$). These effects were reversed by PDE4D deficiency in the prefrontal cortex ($P < 0.05$; **Figure 7B**). Moreover, the downstream BDNF expression was also decreased in Aβ1–42-treated mice ($P < 0.05$). This was also restored by microinjection of lenti-PDE4D-miRNA into the prefrontal cortex ($P < 0.05$; **Figure 7C**). This PDE4D deficiency-induced increased expression of PKA, pCREB, and BDNF was also prevented by H89 (P's < 0.05).

Bcl-2 is an anti-apoptotic protein that inhibits activation of the apoptotic cell death pathway (Belka and Budach, 2002); while Bax is a pro-apoptotic member of the Bcl-2 protein family (Oltvai et al., 1993; Lalier et al., 2007). Cleaved caspase-3, another protein related to cell death, plays a central role in the apoptotic signaling pathway (Salvesen, 2002). As shown in **Figure 7D**, PDE4D deficiency reversed Aβ1–42-induced increase in Bax and decrease in Bcl-2 levels as evidenced by the increased ratio of Bcl-2/Bax in the prefrontal cortex of these mice ($P < 0.05$). As shown in **Figure 7E**, PDE4D deficiency reversed Aβ1–42-induced increase in caspase-3 level in the prefrontal cortex of these mice ($P < 0.01$). However, these effects of PDE4D deficiency on the ratio of Bcl-2/Bax and expression of caspase-3 were prevented by H89 ($P < 0.05$), supporting the claim that cAMP-PKA signaling is involved in PDE4D knockdown-related anti-apoptotic effects.

DISCUSSION

The present study suggested that PDE4D knockdown by microinjection of lenti-PDE4D-miRNA into the prefrontal cortex protects Aβ1–42-induced cognitive and memory impairment in the novel object recognition, step-down passive avoidance, and eight-arm maze tests. The results showed that PDE4D knockdown prevented neurons against oligomeric Aβ1–42 neurotoxicity, as demonstrated by preservation of LTP expression and increased synapse-associated protein expression, e.g., synaptophysin and PSD95, in the prefrontal cortex. Furthermore, PDE4D deficiency increased SOD activity and decreased MDA level. These effects are related to the increased downstream protein expression, such as PKA, pCREB/CREB, BDNF, and Bcl-2/Bax, and the decreased caspase-3 level. The protective effect of PDE4D deficiency was reversed by treatment with the PKA inhibitor H89, indicating that the beneficial effects of PDE4D deficiency are mediated through PKA activation.

Aβ accumulation is known to interfere with the cAMP-activated pathway, which plays critical roles in memory retention. Thus, the development of cAMP-enhancing strategies by inhibition of PDE4 activity, particularly PDE4 subtypes, are potential for treatment of AD and dementia. Aβ1–42 is a pivotal pathogenic factor of AD that is more susceptible to aggregation and more toxic to neurons as compared with other fragments, such as Aβ25–35 (Cheng et al., 2010). Aβ1–42 deposition in the temporal and frontal cortex is considered as an early and critical event in AD pathogenesis. The prefrontal cortex is a brain region with high expression of PDE4D (Pérez-Torres et al., 2000; Lakics et al., 2010) and importantly involved in cognition (Romanski, 2004). In the pre-experiment, Aβ1–42 was microinjected into the prefrontal cortex of the mice first, and this verified the model of AD as successful, as evidenced by the fact that Aβ1–42-treated mice showed significant memory impairment in the novel object recognition test and step-down passive avoidance test. Here we investigated PDE4D splice variants' function using lentivirus-based RNA interference technology in the prefrontal

cortex of mice. Our results suggested that PDE4D knockdown by intra-prefrontal cortex microinjection of lenti-PDE4D-miRNA decreased PDE4D expression, but did not affect PDE4A and 4B levels in the prefrontal cortex. Previous studies indicated that rolipram, a non-selective PDE4 inhibitor, prevented exogenous Aβ1–42 peptide-induced memory impairment, which may result from inhibition of long-form PDE4 (Zhang et al., 2014). We extended the study and found that Aβ1–42 peptides induced sporadic (in the novel object recognition test), spatial (in the eight-arm maze task), and emotional memory (in the step-down passive avoidance test) impairment, which can be prevented by PDE4D4/5 knockdown in the prefrontal cortex. Further study suggested that PDE4D knockdown improved cell-based learning and memory function as evidenced by ameliorating the long-term potentiation in the cortex slices of Aβ1–42-treated mice. LTP is a persistent strengthening of synapses based on recent patterns of activity, which includes one pattern of synaptic activity that produces a long-lasting increase in signal transmission between neurons (Nicoll, 2017). As memories are thought to be encoded by modification of synaptic strength, LTP is widely considered as one of the major cellular mechanisms that underlies learning and memory. The prefrontal cortex has been recognized as playing a vital role in formation of declarative memory in particular, which describes the synthesis of episodic and semantic memory (Aujla and Beninger, 2001). Our study suggested that PDE4D knockdown in the brain including the prefrontal cortex results in enhancement of episodic, spatial, and emotional memory in the novel object recognition, eight-arm maze, and step-down passive avoidance tests, which may be related to improving neuronal structure and function in the prefrontal cortex. This hypothesis was supported by the fact that PDE4D deficiency reversed Aβ1–42-induced impairment of LTP expression in the prefrontal cortex of the Aβ1–42-treated mice. The fact that PDE4D deficiency-induced amelioration on LTP was blocked by H89 suggests that the memory-enhancing effects of PDE4D inhibition may be involved in the cAMP/PKA-related downstream signaling pathway.

Increasing studies indicated that synaptic loss in the cortex is one of the crucial factors involving cognitive dysfunction (Scheff and Price, 2003; Scheff et al., 2006). The therapeutic treatments that promote synaptic plasticity may have potential benefit for patients with early or prodromal AD. Synaptophysin and PSD-95 are two synapse-associated proteins that are important for the formation of long-lasting, latent memories (Bessieres et al., 2020). Our study suggested that the levels of these two proteins were significantly decreased in Aβ1–42-treated mice, but PDE4D deficiency in the prefrontal cortex increased the expression of synaptophysin and PSD-95, indicating the role of PDE4D inhibition in amelioration of synaptic plasticity and neuronal atrophy in the progression of AD.

Recent evidence suggests that oxidative stress is involved in the mechanism of Aβ-induced neurotoxicity and AD pathogenesis (Jhoo et al., 2004). Neuronal cell exposure to Aβ was found to increase reactive oxygen species (ROS) production, which includes lipid peroxidation, protein oxidation, and the formation of hydrogen peroxide (Behl et al., 1994). In clinical investigation, researchers also found the increases of lipid peroxidation, protein carbonyl, and oxidation of mitochondrial DNA in the brain of AD patients (Lyras et al., 1997). Malondialdehyde is the most abundant individual aldehyde resulting from lipid peroxidation and can be considered as a marker of lipid peroxidation. Superoxide dismutase catalyzes the conversion of the toxic superoxide radical to less reactive hydrogen peroxide, contributing to protection from Aβ-induced neurotoxicity. In the present study, PDE4D knockdown in the prefrontal cortex increased SOD activity and decreased MDA level, suggesting that inhibition of PDE4D restored the antioxidant status of brain that may confer neuroprotection due to alleviation of oxidative damage induced by Aβ1–42. BDNF is one of the most important neuroprotective factors that plays a crucial role in repairing and maintaining neurons. The BDNF gene contains a cAMP response element (CRE) that phosphorylated CREB (pCREB) binds to enhance transcription (Yadang et al., 2020). Previous study suggested that Aβ1–42 decreased both pCREB and BDNF expression in the brain of AD mouse models (Lv et al., 2021). In our present study, PDE4D knockdown rescued Aβ1–42-induced reduction of BDNF and pCREB/CREB levels in the prefrontal cortex, which were consistent with previous studies that suggested that some PDE4 inhibitors, such as rolipram, increase pCREB/CREB ratio and BDNF levels in the frontal cortex and hippocampus of AD mice (Wimmer et al., 2020). Considering that some PDE inhibitors, such as PDE2 and PDE5 inhibitors, exhibit neuroprotective effects by regulating the balance of pro-apoptotic and anti-apoptotic processes, we also determined the role of PDE4D in regulation of imbalance of pro-apoptotic and anti-apoptotic dynamics. We examined the ratio of Bcl-2 to Bax and caspase-3 expression in the presence or absence of PDE4D inhibition in Aβ1–42-treated mice. We found that inhibition of PDE4D in the prefrontal cortex reduced apoptotic protein expression, as evidenced by an increased Bcl2/Bax ratio and decreased caspase-3 level. Further studies are ongoing in our laboratory that would decipher the detailed mechanism related to the role of PDE4D-cAMP signaling in the progression of AD.

In summary, the present study demonstrated that the memory-enhancing effects of lenti-PDE4D-miRNA may be mediated primarily via activated cAMP/CREB signaling, which may modulate several parameters of synaptic proteins, antioxidant factors, and anti-apoptotic and neuroprotective proteins. Targeting long-form PDE4D variants may be a potential target for treating memory loss associated with AD.

DATA AVAILABILITY STATEMENT

The original contributions presented in the study are included in the article/supplementary material, further inquiries can be directed to the corresponding author/s.

ETHICS STATEMENT

The animal study was reviewed and approved by the Wenzhou Medical University Committee on Animal Care and Use and Jinshan Branch of the Sixth People's Hospital of Shanghai, Jiao Tong University.

AUTHOR CONTRIBUTIONS

YS and JL: investigation, writing, and original draft. LC: writing, funding acquisition. GL: investigation and resources. MT: data curation. JP: funding acquisition. MZ: conceptualization, methodology and funding acquisition. HF: conceptualization and project administration. All authors contributed to the article and approved the submitted version.

FUNDING

This project was supported by the Shanghai Jinshan District Medical Key Specialty Construction Project (No. JSZK2019A04) to MZ, the Zhejiang Provincial Public Welfare Research Project (No. 2018C37082) to LC, and the Natural Science Foundation of Zhejiang Province (No. LY21H310004) to JP.

REFERENCES

Aujla, H., and Beninger, R. J. (2001). Hippocampal-prefrontocortical circuits: PKA inhibition in the prefrontal cortex impairs delayed nonmatching in the radial maze in rats. *Behav. Neurosci.* 115, 1204–1211. doi: 10.1037/0735-7044.115.6.1204

Barad, M., Bourtchouladze, R., Winder, D. G., Golan, H., and Kandel, E. (1998). Rolipram, a type IV-specific phosphodiesterase inhibitor, facilitates the establishment of long-lasting long-term potentiation and improves memory. *Proc. Natl. Acad. Sci. U.S.A.* 95, 15020–15025. doi: 10.1073/pnas.95.25.15020

Behl, C., Davis, J. B., Lesley, R., and Schubert, D. (1994). Hydrogen peroxide mediates amyloid beta protein toxicity. *Cell* 77, 817–827. doi: 10.1016/0092-8674(94)90131-7

Belka, C., and Budach, W. (2002). Anti-apoptotic Bcl-2 proteins: structure, function and relevance for radiation biology. *Int. J. Radiat. Biol.* 78, 643–658. doi: 10.1080/09553000210137680

Bessieres, B., Travaglia, A., Mowery, T. M., Zhang, X., and Alberini, C. M. (2020). Early life experiences selectively mature learning and memory abilities. *Nat. Commun.* 11:628.

Bruel-Jungerman, E., Laroche, S., and Rampon, C. (2005). New neurons in the dentate gyrus are involved in the expression of enhanced long-term memory following environmental enrichment. *Eur. J. Neurosci.* 21, 513–521. doi: 10.1111/j.1460-9568.2005.03875.x

Chandrasekaran, A., Toh, K. Y., Low, S. H., Tay, S. K., Brenner, S., and Goh, D. L. (2008). Identification and characterization of novel mouse PDE4D isoforms: molecular cloning, subcellular distribution and detection of isoform-specific intracellular localization signals. *Cell Signal.* 20, 139–153. doi: 10.1016/j.cellsig.2007.10.003

Cheng, Y. F., Wang, C., Lin, H. B., Li, Y. F., Huang, Y., Xu, J. P., et al. (2010). Inhibition of phosphodiesterase-4 reverses memory deficits produced by Aβ25-35 or Aβ1-40 peptide in rats. *Psychopharmacology (Berl)* 212, 181–191. doi: 10.1007/s00213-010-1943-3

Cherry, J. A., and Davis, R. L. (1999). Cyclic AMP phosphodiesterases are localized in regions of the mouse brain associated with reinforcement, movement, and affect. *J. Comp. Neurol.* 407, 287–301. doi: 10.1002/(sici)1096-9861(19990503)407:2<287::aid-cne9>3.0.co;2-r

Cheung, Y. F., Kan, Z., Garrett-Engele, P., Gall, I., Murdoch, H., Baillie, G. S., et al. (2007). PDE4B5, a novel, super-short, brain-specific cAMP phosphodiesterase-4 variant whose isoform-specifying N-terminal region is identical to that of cAMP phosphodiesterase-4D6 (PDE4D6). *J. Pharmacol. Exp. Ther.* 322, 600–609. doi: 10.1124/jpet.107.122218

Conti, M., Richter, W., Mehats, C., Livera, G., Park, J. Y., and Jin, C. (2003). Cyclic AMP-specific PDE4 phosphodiesterases as critical components of cyclic AMP signaling. *J. Biol. Chem.* 278, 5493–5496. doi: 10.1074/jbc.r200029200

Epp, J. R., Spritzer, M. D., and Galea, L. A. (2007). Hippocampus-dependent learning promotes survival of new neurons in the dentate gyrus at a specific time during cell maturation. *Neuroscience* 149, 273–285. doi: 10.1016/j.neuroscience.2007.07.046

Fujioka, T., Fujioka, A., and Duman, R. S. (2004). Activation of cAMP signaling facilitates the morphological maturation of newborn neurons in adult hippocampus. *J. Neurosci.* 24, 319–328. doi: 10.1523/jneurosci.1065.03.2004

Houslay, M. D. (2001). PDE4 cAMP-specific phosphodiesterases. *Prog. Nucleic Acid Res. Mol. Biol.* 69, 249–315. doi: 10.1016/s0079-6603(01)69049-4

Jhoo, J. H., Kim, H. C., Nabeshima, T., Yamada, K., Shin, E. J., Jhoo, W. K., et al. (2004). Beta-amyloid (1-42)-induced learning and memory deficits in mice: involvement of oxidative burdens in the hippocampus and cerebral cortex. *Behav. Brain Res.* 155, 185–196. doi: 10.1016/j.bbr.2004.04.012

Lakics, V., Karran, E. H., and Boess, F. G. (2010). Quantitative comparison of phosphodiesterase mRNA distribution in human brain and peripheral tissues. *Neuropharmacology* 59, 367–374. doi: 10.1016/j.neuropharm.2010.05.004

Lalier, L., Cartron, P. F., Juin, P., Nedelkina, S., Manon, S., Bechinger, B., et al. (2007). Bax activation and mitochondrial insertion during apoptosis. *Apoptosis* 12, 887–896. doi: 10.1007/s10495-007-0749-1

Li, C. (2009). A new syndrome of ankyloglossia and ulnar ray defects in a Newfoundland kindred. *Clin. Dysmorphol.* 18, 158–159. doi: 10.1097/mcd.0b013e328324440d

Li, Y. F., Cheng, Y. F., Huang, Y., Conti, M., Wilson, S. P., O'Donnell, J. M., et al. (2011). Phosphodiesterase-4D knock-out and RNA interference-mediated knock-down enhance memory and increase hippocampal neurogenesis via increased cAMP signaling. *J. Neurosci.* 31, 172–183. doi: 10.1523/jneurosci.5236-10.2011

Lv, J., Lu, C., Jiang, N., Wang, H., Huang, H., Chen, Y., et al. (2021). Protective effect of ginsenoside Rh2 on scopolamine-induced memory deficits through regulation of cholinergic transmission, oxidative stress and the ERK-CREB-BDNF signaling pathway. *Phytother. Res.* 35, 337–345. doi: 10.1002/ptr.6804

Lyras, L., Cairns, N. J., Jenner, A., Jenner, P., and Halliwell, B. (1997). An assessment of oxidative damage to proteins, lipids, and DNA in brain from patients with Alzheimer's disease. *J. Neurochem.* 68, 2061–2069. doi: 10.1046/j.1471-4159.1997.68052061.x

Mangialasche, F., Solomon, A., Winblad, B., Mecocci, P., and Kivipelto, M. (2010). Alzheimer's disease: clinical trials and drug development. *Lancet Neurol.* 9, 702–716.

Millar, J. K., Pickard, B. S., Mackie, S., James, R., Christie, S., Buchanan, S. R., et al. (2005). DISC1 and PDE4B are interacting genetic factors in schizophrenia that regulate cAMP signaling. *Science* 310, 1187–1191. doi: 10.1126/science.1112915

Misner, D. L., and Sullivan, J. M. (1999). Mechanism of cannabinoid effects on long-term potentiation and depression in hippocampal CA1 neurons. *J. Neurosci.* 19, 6795–6805. doi: 10.1523/jneurosci.19-16-06795.1999

Nagai, T., Takuma, K., Kamei, H., Ito, Y., Nakamichi, N., Ibi, D., et al. (2007). Dopamine D1 receptors regulate protein synthesis-dependent long-term recognition memory via extracellular signal-regulated kinase 1/2 in the prefrontal cortex. *Learn. Mem.* 14, 117–125. doi: 10.1101/lm.461407

Nakagawa, S., Kim, J. E., Lee, R., Malberg, J. E., Chen, J., Steffen, C., et al. (2002). Regulation of neurogenesis in adult mouse hippocampus by cAMP and the cAMP response element-binding protein. *J. Neurosci.* 22, 3673–3682. doi: 10.1523/jneurosci.22-09-03673.2002

Navakkode, S., Sajikumar, S., and Frey, J. U. (2004). The type IV-specific phosphodiesterase inhibitor rolipram and its effect on hippocampal long-term potentiation and synaptic tagging. *J. Neurosci.* 24, 7740–7744. doi: 10.1523/jneurosci.1796-04.2004

Nicoll, R. A. (2017). A brief history of long-term potentiation. *Neuron* 93, 281–290. doi: 10.1016/j.neuron.2016.12.015

Ohkawa, H., Ohishi, N., and Yagi, K. (1979). Assay for lipid peroxides in animal tissues by thiobarbituric acid reaction. *Anal. Biochem.* 95, 351–358. doi: 10.1016/0003-2697(79)90738-3

Oltvai, Z. N., Milliman, C. L., and Korsmeyer, S. J. (1993). Bcl-2 heterodimerizes in vivo with a conserved homolog, Bax, that accelerates programmed cell death. *Cell* 74, 609–619. doi: 10.1016/0092-8674(93)90509-o

Otmakhov, N., Khibnik, L., Otmakhova, N., Carpenter, S., Riahi, S., Asrican, B., et al. (2004). Forskolin-induced LTP in the CA1 hippocampal region is NMDA receptor dependent. *J. Neurophysiol.* 91, 1955–1962. doi: 10.1152/jn.00941.2003

Pérez-Torres, S., Miró, X., Palacios, J. M., Cortés, R., Puigdoménech, P., and Mengod, G. (2000). Phosphodiesterase type 4 isozymes expression in human brain examined by in situ hybridization histochemistry and[3H]rolipram binding autoradiography. Comparison with monkey and rat brain. *J. Chem. Neuroanat.* 20, 349–374. doi: 10.1016/s0891-0618(00)00097-1

Pu, F. L., Mishima, K., Irie, K., Motohashi, K., Tanaka, Y., Orito, K., et al. (2007). Neuroprotective effects of quercetin and rutin on spatial memory impairment in an 8-arm radial maze task and neuronal death induced by repeated cerebral ischemia in rats. *J. Pharmacol. Sci.* 104, 329–334. doi: 10.1254/jphs.fp0070247

Robichaud, A., Savoie, C., Stamatiou, P. B., Lachance, N., Jolicoeur, P., Rasori, R., et al. (2002). Assessing the emetic potential of PDE4 inhibitors in rats. *Br. J. Pharmacol.* 135, 113–118. doi: 10.1038/sj.bjp.0704457

Robichaud, A., Savoie, C., Stamatiou, P. B., Tattersall, F. D., and Chan, C. C. (2001). PDE4 inhibitors induce emesis in ferrets via a noradrenergic pathway. *Neuropharmacology.* 40, 262–269. doi: 10.1016/s0028-3908(00)00142-8

Romano, A., Delorenzi, A., Pedreira, M. E., Tomsic, D., and Maldonado, H. (1996). Acute administration of a permeant analog of cAMP and a phosphodiesterase inhibitor improve long-term habituation in the crab *Chasmagnathus*. *Behav. Brain Res.* 75, 119–125. doi: 10.1016/0166-4328(96)00179-9

Romanski, L. M. (2004). Domain specificity in the primate prefrontal cortex. *Cogn. Affect. Behav. Neurosci.* 4, 421–429. doi: 10.3758/cabn.4.4.42

Salvesen, G. S. (2002). Caspases: opening the boxes and interpreting the arrows. *Cell Death Differ.* 9, 3–5. doi: 10.1038/sj.cdd.4400963

Sasaki, T., Kitagawa, K., Omura-Matsuoka, E., Todo, K., Terasaki, Y., Sugiura, S., et al. (2007). The phosphodiesterase inhibitor rolipram promotes survival of newborn hippocampal neurons after ischemia. *Stroke* 38, 1597–1605. doi: 10.1161/strokeaha.106.476754

Scheff, S. W., and Price, D. A. (2003). Synaptic pathology in Alzheimer's disease: a review of ultrastructural studies. *Neurobiol. Aging* 24, 1029–1046. doi: 10.1016/j.neurobiolaging.2003.08.002

Scheff, S. W., Price, D. A., Schmitt, F. A., and Mufson, E. J. (2006). Hippocampal synaptic loss in early Alzheimer's disease and mild cognitive impairment. *Neurobiol. Aging* 27, 1372–1384. doi: 10.1016/j.neurobiolaging.2005.09.012

Schneider, H. H. (1984). Brain cAMP response to phosphodiesterase inhibitors in rats killed by microwave irradiation or decapitation. *Biochem. Pharmacol.* 33, 1690–1693. doi: 10.1016/0006-2952(84)90295-8

Selkoe, D. J. (2001). Alzheimer's disease: genes, proteins, and therapy. *Physiol. Rev.* 81, 741–766.

Titus, D. J., Sakurai, A., Kang, Y., Furones, C., Jergova, S., Santos, R., et al. (2013). Phosphodiesterase inhibition rescues chronic cognitive deficits induced by traumatic brain injury. *J. Neurosci.* 33, 5216–5226. doi: 10.1523/jneurosci.5133-12.2013

Wang, Y., Gao, S., Zheng, V., Chen, L., Ma, M., Shen, S., et al. (2020). A novel PDE4D inhibitor BPN14770 reverses scopolamine-induced cognitive deficits via cAMP/SIRT1/Akt /Bcl-2 Pathway. *Front. Cell Dev. Biol.* 8:599389. doi: 10.3389/fcell.2020.599389

Wimmer, M. E., Blackwell, J. M., and Abel, T. (2020). Rolipram treatment during consolidation ameliorates long-term object location memory in aged male mice. *Neurobiol. Learn. Mem.* 169:107168. doi: 10.1016/j.nlm.2020.107168

Winterbourn, C. C., Hawkins, R. E., Brian, M., and Carrell, R. W. (1975). The estimation of red cell superoxide dismutase activity. *J. Lab. Clin. Med.* 85, 337–341.

Xu, Y., Ku, B. S., Yao, H. Y., Lin, Y. H., Ma, X., Zhang, Y. H., et al. (2005). The effects of curcumin on depressive-like behaviors in mice. *Eur. J. Pharmacol.* 518, 40–46. doi: 10.1016/j.ejphar.2005.06.002

Xu, Y., Pan, J., Sun, J., Ding, L., Ruan, L., Reed, M., et al. (2015). Inhibition of phosphodiesterase 2 reverses impaired cognition and neuronal remodeling caused by chronic stress. *Neurobiol. Aging* 36, 955–970. doi: 10.1016/j.neurobiolaging.2014.08.028

Yadang, F. S. A., Nguezeye, Y., Kom, C. W., Betote, P. H. D., Mamat, A., Tchokouaha, L. R. Y., et al. (2020). Scopolamine-induced memory impairment in mice: neuroprotective effects of *Carissa edulis* (Forssk.) Valh (Apocynaceae) aqueous extract. *Int. J. Alzheimers Dis.* 2020:6372059.

Zhang, C., Cheng, Y., Wang, H., Wang, C., Wilson, S. P., Xu, J., et al. (2014). RNA interference-mediated knockdown of long-form phosphodiesterase-4D (PDE4D) enzyme reverses amyloid-beta42-induced memory deficits in mice. *J. Alzheimers Dis.* 38, 269–280. doi: 10.3233/jad-122236

Zhang, C., Xu, Y., Chowdhary, A., Fox, D. I. I. I., Gurney, M. E., Zhang, H. T., et al. (2018). Memory enhancing effects of BPN14770, an allosteric inhibitor of phosphodiesterase-4D, in wild-type and humanized mice. *Neuropsychopharmacology* 43, 2299–2309. doi: 10.1038/s41386-018-0178-6

Zhang, H. T. (2009). Cyclic AMP-specific phosphodiesterase-4 as a target for the development of antidepressant drugs. *Curr. Pharm. Des.* 15, 1688–1698. doi: 10.2174/138161209788168092

Zhang, H. T., Crissman, A. M., Dorairaj, N. R., Chandler, L. J., and O'Donnell, J. M. (2000). Inhibition of cyclic AMP phosphodiesterase (PDE4) reverses memory deficits associated with NMDA receptor antagonism. *Neuropsychopharmacology.* 23, 198–204. doi: 10.1016/s0893-133x(00)00108-1

Zhang, H. T., Huang, Y., Jin, S. L., Frith, S. A., Suvarna, N., Conti, M., et al. (2002). Antidepressant-like profile and reduced sensitivity to rolipram in mice deficient in the PDE4D phosphodiesterase enzyme. *Neuropsychopharmacology* 27, 587–595.

Zhang, H. T., Huang, Y., Masood, A., Stolinski, L. R., Li, Y., Zhang, L., et al. (2008). Anxiogenic-like behavioral phenotype of mice deficient in phosphodiesterase 4B (PDE4B). *Neuropsychopharmacology* 33, 1611–1623. doi: 10.1038/sj.npp.1301537

Conflict of Interest: The authors declare that the research was conducted in the absence of any commercial or financial relationships that could be construed as a potential conflict of interest.

Publisher's Note: All claims expressed in this article are solely those of the authors and do not necessarily represent those of their affiliated organizations, or those of the publisher, the editors and the reviewers. Any product that may be evaluated in this article, or claim that may be made by its manufacturer, is not guaranteed or endorsed by the publisher.

frontiers in Aging Neuroscience

ORIGINAL RESEARCH
published: 02 February 2022
doi: 10.3389/fnagi.2021.813923

Predicted Cognitive Conversion in Guiding Early Decision-Tailoring on Patients With Cognitive Impairment

Yu Zheng[1†], Yin Liu[2,3†], Jiawen Wu[2,3], Yi Xie[4], Siyu Yang[2,3], Wanting Li[2,3], Huaiqing Sun[2,3], Qing He[5,6] and Ting Wu[2,3*]*

[1] Department of Rehabilitation Medicine, The First Affiliated Hospital of Nanjing Medical University, Nanjing, China, [2] Division of Brain Rehabilitation, Department of Neurology, The First Affiliated Hospital of Nanjing Medical University, Nanjing, China, [3] Department of Neurology, The First Affiliated Hospital of Nanjing Medical University, Nanjing, China, [4] Intensive Care Unit, Wuxi No.2 People's Hospital, Wuxi, China, [5] Department of Neurology, Xuzhou First People's Hospital, Xuzhou, China, [6] Department of Neurology, The Affiliated Hospital of China University of Mining and Technology, Xuzhou, China

Background: Cognitive decline is the most dominant and patient-oriented symptom during the development of Alzheimer's disease (AD) and mild cognitive impairment (MCI). This study was designed to test the feasibility of hybrid convolutional neural networks and long-short-term memory (CNN-LSTM) modeling driven early decision-tailoring with the predicted long-term cognitive conversion in AD and MCI.

Methods: Characteristics of patients with AD or MCI covering demographic features, clinical features, and time-dependent neuropsychological-related features were fused into the hybrid CNN-LSTM modeling to predict cognitive conversion based on a 4-point change in the AD assessment scale-cognition score. Treatment reassignment rates were estimated based on the actual and predicted cognitive conversion at 3 and 6 months according to the prespecified principle; that is if the ADAS-cog score of the patient declines less than 4 points or increases at either follow-up time point, the medical treatment recommended upon their diagnosis would be considered insufficient. Therefore, it is recommended to upgrade the medical treatment upon diagnosis. Actual and predicted treatment reassignment rates were compared in the general population and subpopulations categorized by age, gender, symptom severity, and the intervention subtypes.

Results: A total of 224 patients were included in the analysis. The hybrid CNN-LSTM model achieved the mean AUC of 0.735 (95% CI: 0.701–0.769) at 3 months and 0.853 (95% CI: 0.814–0.892) at 6 months in predicting cognitive conversion status. The AUC at 6 months was significantly impacted when data collected at 3 months were withdrawn. The predicted cognitive conversion suggested a revision of medical treatment in 46.43% (104/224) of patients at 3 months and 54.02% (121/224) at 6 months as compared with 62.05% (139/224) at 3 months (p = 0.001) and 62.50% (140/224) at 6 months (p = 0.069) according to their actual cognitive conversion. No significant differences were detected between treatment reassignment rates estimated based on actual and predicted cognitive conversion in all directions at 6 months.

Conclusion: Using the synergistic advances of deep learning modeling and featured longitudinal information, our hypothesis was preliminarily verified with the comparable

OPEN ACCESS

Edited by:
Fushun Wang,
Nanjing University of Chinese Medicine, China

Reviewed by:
Chunming Xie,
Southeast University, China
Feng Bai,
Nanjing Drum Tower Hospital, China

***Correspondence:**
Ting Wu
wuting80000@126.com
Qing He
heqing80000@sina.com

† These authors have contributed equally to this work

Specialty section:
This article was submitted to Alzheimer's Disease and Related Dementias, a section of the journal Frontiers in Aging Neuroscience

Received: *12 November 2021*
Accepted: *06 December 2021*
Published: *02 February 2022*

Citation:
Zheng Y, Liu Y, Wu J, Xie Y, Yang S, Li W, Sun H, He Q and Wu T (2022) Predicted Cognitive Conversion in Guiding Early Decision-Tailoring on Patients With Cognitive Impairment. Front. Aging Neurosci. 13:813923. doi: 10.3389/fnagi.2021.813923

predictive performance in cognitive conversion. Results provided the possibility of reassigned recommended treatment for those who may suffer from cognitive decline in the future. Considering the limited diversity of treatment strategies applied in this study, the real-world medical situation should be further simulated.

Keywords: Alzheimer's disease, mild cognitive impairment, decision-tailoring, deep learning, Alzheimer's disease assessment scale, cognitive conversion, medical treatment reassignment

BACKGROUND

According to the Alzheimer's Disease International, the estimated prevalence of dementia is about 50 million people worldwide in 2018 and will be projected to triple in 2050 (Koszewicz et al., 2021). Alzheimer's disease (AD) and mild cognitive impairment (MCI) are two major types of dementia, which have launched significant economic load and medical burden for the families and healthcare systems (Hill et al., 2017).

With the increasing efforts in predicting the occurrence and development of AD and MCI, age and gender have often been identified as the most important risk factors. Previous studies have shown that for elders aged 65 years or more, there were significantly more women who have developed AD compared with a high proportion of men who have developed MCI with an OR of 1.54 (95%CI: 1.2–2.0) (Petersen et al., 2010; Wu et al., 2017). Moreover, studies on biomarkers have formed an important basis for the early diagnosis of dementia (Hort et al., 2010). The β amyloid deposition, pathologic tau, and neurodegeneration (A-T-N) framework proposed by Jack et al. (2018) is intended to define the diagnosis of AD by the presence of amyloid-β and phosphorylated tau that measured either in plasma, cerebrospinal fluid (CSF), or neuroimaging. While in the search for prognostic biomarkers of dementia, the field still focused heavily on neuroimaging and CSF markers. For instance, several studies have reported that the progression of AD or MCI could be predicted by advanced neuroimaging techniques, including MRI findings, FDG-PET, or CSF examination (Jack et al., 1999; Killiany et al., 2000; Shaw et al., 2009; Zhang et al., 2012). In fact, professionals have advocated that at least one neuroimaging examination and several CSF/plasma examinations are needed for monitoring the progression of dementia (Langa and Levine, 2014). However, the major barrier leading to this destination is the poor compliance to these examinations and the difficulties in the collection of the corresponding information in real clinical practice. In addition, even these difficulties can be conquered, their specificity and accuracy in the prediction of prognosis of dementia have not been guaranteed in the current context (Carrillo et al., 2013; Hepp et al., 2016).

For the majority of patients diagnosed with AD and MCI, cognitive impairment is recognized as the most dominant and patient-oriented symptom. Progression of cognitive impairment is normally monitored through longitudinal neuropsychological assessments using cognitive scales such as the Alzheimer's Disease Assessment Scale-Cognition (ADAS-Cog) or the Mini-Mental State Examination (MMSE). This longitudinal information can be scheduled and collected sequentially through face-to-face interviews in the hospital, community, or at home. According to Xue et al. (2018) neuropsychological assessments were proved to be more practical compared with neuroimaging and CSF/plasma examinations and more accurate in the reflection of cognitive function than baseline information alone. This inspired us to ask whether sequential neuropsychological-related information along with other clinical data can be used to predict cognitive trajectory. Upon this thought, the long-term cognitive decline can be foreseen with which medical treatment for AD or MCI could be redirected at the early stage. Considering the high heterogeneity in the individual progression of dementia and huge difficulties in the prediction of its trajectory, traditional statistical models may not be powerful enough to provide accurate predictive outcomes. In particular, the cognitive trajectory that was impacted by the sequential time features would probably not be captured by traditional regression algorithms (Verbeke et al., 2014). Upon this data signature, we were, therefore, promoted to construct a novel deep learning model comprised of convolutional neural networks (CNN) and long-short-term memory (LSTM) networks. This hybrid CNN-LSTM network is capable to handle longitudinal data with varying lengths of follow-ups, help capture temporal dynamics, and, therefore, make accurate predictions based on the sequential data (Hochreiter and Schmidhuber, 1997; Cho et al., 2014; Chung et al., 2014; Ioannou et al., 2020).

In this study, we used the subset data from three ongoing, longitudinal, cohort studies conducted by our research team. The aim of this study was (1) to explore the predictive potential of longitudinal neuropsychological information on cognitive conversion reflected by ADAS-Cog upon the diagnosis of AD and MCI and (2) to compare the reassignment rates estimated by the deep learning modeling according to the actual status. If the long-term cognitive status can be successfully predicted with our hybrid CNN-LSTM modeling, then recommendations on treatment redirection can be provided at the early stage of AD or MCI.

Abbreviations: AD, Alzheimer's disease; MCI, mild cognitive impairment; CSF, cerebrospinal fluid; MRI, magnetic resonance imaging; FDG-PET, fluorodeoxyglucose positron emission tomography; ADAS-Cog, Alzheimer's Disease Assessment Scale-Cognition; MMSE, Mini-Mental State Examination; GBE, ginkgo biloba extract; CNN, convolutional neural networks; LSTM: long-short-term memory; NINCDS-ADRDA, National Institute of Neurological and Communicative Disorders and Stroke and the Alzheimer's Disease and Related Disorders Association; IADL, instrumental activity of daily living; GDS, geriatric depression scale; QOL-AD, quality of life-Alzheimer's disease; NPI, neuropsychiatric inventory; CI, cognition improved; CNI, cognition not improved; HIS, Hachinski ischemic score; CDR, clinical dementia rating; DSST, digit symbol substitute test; TMT A, trail making test A; TMT B, trail making test B; ALT, alanine aminotransferase; TC, total cholesterol; TG, triglyceride; LDL, low density lipoprotein; ERP, event-related potentials; ROC, receiver operating curve; AUC, area under curve; CI, confidence interval; AUPRC, area under precision-recall curve; AI, artificial intelligence; P-tau, phosphor-tau; Aβ, beta-amyloid.

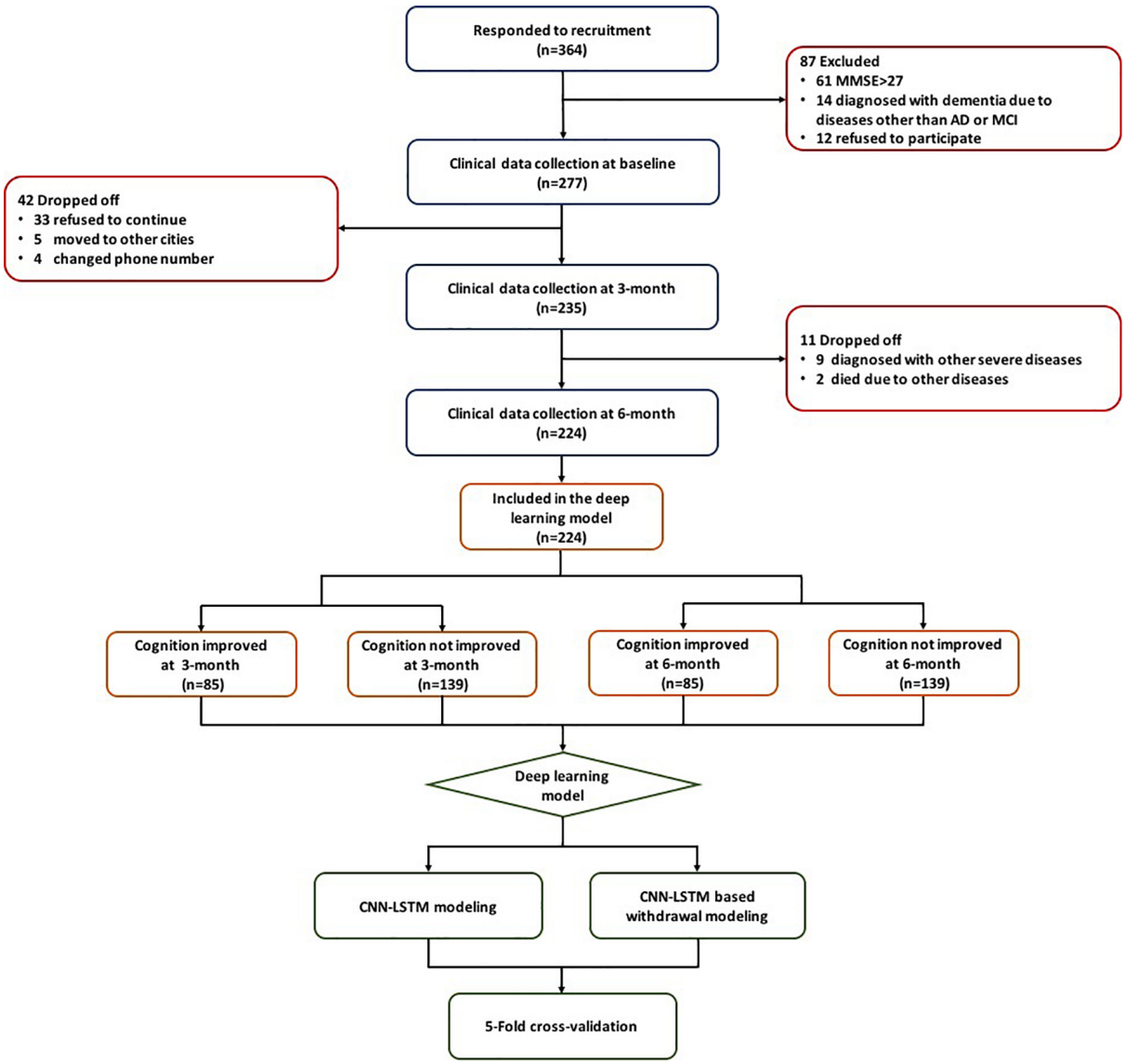

FIGURE 1 | Flowchart of this study.

MATERIALS AND METHODS

Patient Data

This study utilized three cohorts including 364 patients from the First Affiliated Hospital of Nanjing Medical University (ClinicalTrials.gov ID: NCT03090516 and Chinese Clinical Trial Registry ID: ChiCTR-INR-15007420) and 111 patients from communities in Nanjing, China. Patients from the above three cohorts were treated with either observation, exercise, monotherapy (donepezil or ginkgo biloba extract [GBE]), or donepezil and GBE combination. All of these patients met the following inclusion criteria: (1) diagnosed with AD or MCI according to the NINCDS/ADRDA guidelines; (2) MMSE score of 27 or less; (3) able to follow medical instruction or assessment requirement; (4) complete available baseline and longitudinal data, such as age, course of the disease, comorbidities, blood biochemical examination, clinical scales assessed during three visits (e.g., baseline, 3 months, and 6 months); and (5) signed informed consent (Cummings, 1993; Dubois et al., 2007). The flowchart of this study is shown in **Figure 1**.

Predictive Variables and Target Outcomes

As data from these cohorts were presented with a varying treatment plan, disease duration, visiting frequency, and inclusion criteria, all patients have no data beyond 6 months at this moment. We chose a 3-month spacing between time points based on the visit frequency of follow-up patients to ensure most patients had efficient data for model building (baseline, 3 months, and 6 months).

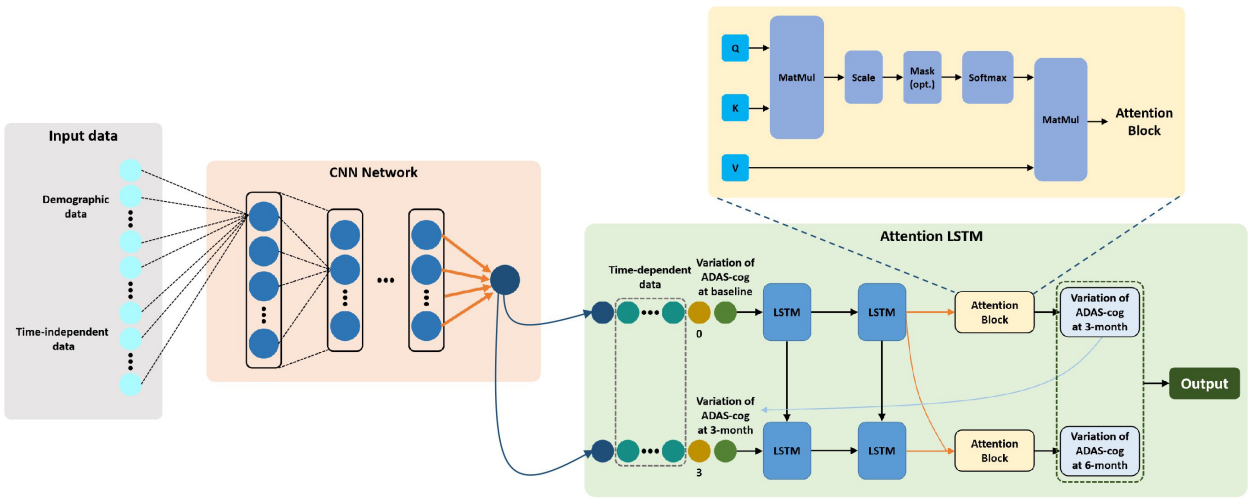

FIGURE 2 | Workflow of CNN-LSTM modeling and architecture of proposed network composition. *The architecture of the hybrid CNN-LSTM model combines two modules. The CNN module (light pink) is composed of five fully connected layers and a rectified linear unit (ReLU) activation unit and then followed by a sigmoid activation function to generate a score representative of non-time dependent features. Next, the LSTM module (light green) was trained to extract both non- and time-dependent features to generate outputs for estimating cognitive conversion status in multiple time points. The attention block (light yellow) denoted an attention mechanism proposed by Vaswani et al. (2017) which was used to perform feature-weighted fusion across time steps to make an accurate prediction. *The yellow block used here refers to "scaled dot-product attention," explicitly explained by Vaswani et al. (2017) Given a task-related query vector Q, it can calculate the attention value by calculating the attention distribution associated with the key (K) and assigning it to the value (V). This attention block is applied to find the "resonance" between hidden vectors from each time step, namely, find the most relevant embedding features for high-level representations recognition.

Data in the merged database were stored in EXCEL format. The predictors used in our deep learning model of cognitive conversion prediction that were originated from tables in the database but not limited to demographics, medical history, intervention subtype, neuropsychological outcomes, and laboratory and neuroelectrophysiological results are listed in **Supplementary Table 1**. Time-dependent variables such as ADAS-cog (Rosen et al., 1984), MMSE (Folstein et al., 1975), the instrumental activity of daily living (IADL) (Thomas et al., 1998), geriatric depression scale (GDS) (Defrancesco et al., 2018), quality of life-Alzheimer's disease (QOL-AD) (Lawton, 1997), and neuropsychiatric inventory (NPI) (Cummings et al., 1994) for the evaluation of neurobehavioral status were recorded at 3 month intervals (Cummings, 1993; Logsdon et al., 2002; LaPlante, 2010; Benedetti et al., 2018; Jiang et al., 2020; Vik-Mo et al., 2020).

According to the guidelines published by the American College of Physicians and the American Academy of Family Physicians, a decline of 4 points or more in the ADAS-cog score is used to define a clinically important improvement (Qaseem et al., 2008). Based on this, we used ADAS-cog as the target outcome and adopted 4 points as the threshold so that patients with different cognitive conversion during follow-ups were further classified (Qaseem et al., 2008; Raina et al., 2008). Specifically, patients whose ADAS-cog score had a decline of 4 points or more were grouped as cognition improved (CI), and patients whose ADAS-cog score remained stable or increased were grouped as cognition not improved (CNI) (Sabbagh et al., 2020).

The Hybrid Convolutional Neural Networks and Long-Short-Term Memory Modeling

Data Preprocessing

We first excluded patients with missing feature variables covering more than 50% of the whole record number, as higher proportions of missing data limit the prediction ability of the proposed model. We then imputed missing data of remaining features with the mean or the mode of existing data in the same feature for continuous or categorical variables, respectively (Kang, 2013). Normalization was subsequently applied; therefore, all data are normalized to have zero mean and unit variance.

Model Development and Training Details

A hybrid model comprised of cascaded classical CNN and state-of-art LSTM was constructed to forecast 3-month interval cognitive conversion status (CI vs. CNI at 3 months and 6 months) in individual patients (**Figure 2**). Briefly, CNN with stacked multiple full connection layers was used to aggregate and extract features of all non-sequential state information. We then applied the sigmoid activation function to generate the score of the non-sequential state (time-independent data) information. The detailed architecture of CNN was explained in **Supplementary Figure 1**. Afterward, the generated score was combined with all other time-dependent data, the corresponding time-sequential information (baseline or 3-month) as well as the cognitive conversion status (improved or not) to fuse into the LSTM network. This specialized LSTM model was trained to use the encoded latent representation from the previous time point

TABLE 1 | Demographics and cognitive conversion distribution at 3 and 6 months.

Patient characteristics	Total (n = 224)	3-month		6-month	
		Cognition not improved (n = 139)	Cognition improved (n = 85)	Cognition not improved (n = 140)	Cognition improved (n = 84)
Age in year, mean (SD)	69.75 (8.52)	69.24 (9.17)	70.58 (7.32)	69.13 (9.07)	70.79 (7.45)
Gender, n (%)					
Male	87 (38.84)	51 (36.69)	36 (42.35)	52 (37.14)	35 (47.67)
Female	137 (61.16)	88 (63.31)	49 (57.65)	88 (62.86)	49 (58.33)
Education in year, mean (SD)	13.00 (4.32)	13.22 (4.72)	12.66 (3.55)	13.31 (4.79)	12.49 (3.35)
Height in centimeter	162.70 (3.69)	162.71 (4.29)	162.67 (2.44)	162.61 (3.92)	162.84 (3.30)
Weight in kilogram	63.09 (4.98)	62.72 (4.41)	63.71 (5.77)	62.58 (4.19)	63.95 (6.00)
Comorbidities, n (%)					
Hypertension	44 (19.64)	27 (19.42)	17 (20.00)	28 (20.00)	16 (19.05)
Diabetes mellitus	16 (7.14)	10 (7.19)	6 (7.06)	8 (5.71)	8 (9.52)
Thyropathy	6 (2.68)	5 (3.60)	1 (1.18)	6 (4.29)	0 (0.00)
Cardiovascular disorders	13 (5.80)	7 (5.04)	6 (7.06)	9 (6.43)	4 (4.76)
Asthma	3 (1.34)	1 (0.72)	2 (2.35)	1 (0.71)	2 (2.38)
Cerebrovascular disorders	17 (7.59)	14 (10.07)	3 (3.53)	13 (9.29)	4 (4.76)
Hyperlithuria	1 (0.45)	1 (0.72)	0 (0.00)	0 (0.00)	1 (1.19)
Hyperlipidemia	7 (3.12)	5 (3.60)	2 (2.35)	5 (3.57)	2 (2.38)
Interventions, n (%)					
Observation	62 (27.68)	53 (38.13)	9 (10.59)	56 (40.00)	6 (7.14)
Exercise	22 (9.82)	15 (10.79)	7 (8.24)	17 (12.14)	5 (5.95)
Donepezil	55 (24.55)	30 (21.58)	25 (29.41)	26 (18.57)	29 (34.52)
GBE	38 (16.96)	16 (11.51)	22 (25.88)	17 (12.14)	21 (25.00)
Donepezil and GBE	47 (20.98)	25 (17.99)	22 (25.88)	24 (17.14)	23 (27.38)
HIS, mean (SD)	0.97 (0.81)	1.01 (0.81)	0.91 (0.81)	0.99 (0.80)	0.95 (0.83)
Family medical history, n (%)					
Yes	45 (20.09)	26 (18.71)	19 (22.35)	24 (17.14)	21 (25.00)
No	179 (79.91)	113 (81.29)	66 (77.65)	116 (82.86)	63 (75.00)
MMSE, mean (SD)	23.46 (3.83)	23.96 (3.86)	22.64 (3.64)	23.94 (3.95)	22.65 (3.49)
ADAS-Cog, mean (SD)	16.62 (9.55)	13.79 (8.88)	21.25 (8.82)	13.97 (9.26)	21.04 (8.35)
IADL, mean (SD)	15.63 (2.47)	15.55 (2.38)	15.75 (2.62)	15.60 (2.34)	15.68 (2.69)
NPI, mean (SD)	3.47 (9.55)	3.17 (7.44)	3.97 (12.28)	4.11 (11.49)	2.41 (4.73)
QOL-AD, mean (SD)	31.91 (6.26)	32.53 (6.21)	30.89 (6.23)	32.33 (6.22)	31.21 (6.30)
GDS, mean (SD)	6.72 (6.44)	6.66 (6.33)	6.81 (6.65)	6.64 (6.07)	6.84 (7.04)
Anxiety, mean (SD)	1.25 (1.94)	0.79 (1.64)	2.01 (2.16)	0.84 (1.61)	1.95 (2.24)
CDR, mean (SD)	1.07 (0.27)	1.07 (0.29)	1.07 (0.26)	1.06 (0.26)	1.10 (0.30)
DSST, mean (SD)	31.86 (8.02)	32.27 (9.58)	31.18 (4.39)	31.99 (9.72)	31.63 (3.82)
TMT A, mean (SD)	82.88 (21.63)	82.08 (24.95)	84.18 (14.72)	83.08 (26.00)	82.53 (11.16)
TMT B, mean (SD)	218.28 (56.84)	217.75 (65.81)	219.14 (38.24)	217.94 (66.13)	218.84 (36.84)

as well as the multivariate relations of the current time point (Gers and Schmidhuber, 2001). Using this process, the underlying temporal characteristics in the given time-dependent ADAS-cog score were captured. Notably, the attention mechanism was applied to perform feature-weighted fusion across time steps to improve the prediction accuracy (Vaswani et al., 2017). This procedure was made to empower the model to find significant useful information related to the current output in the input data and eventually improve the quality of the output.

We implemented the above model building on the publicly available library sklearn and open framework PyTorch on Python 3.6 using a computer with one NVidia GTX 1080Ti GPU. The batch size was set to 3,600 when training the CNN-LSTM model, with the optimizer used as the Adam algorithm (Kingma and Ba, 2014). The learning rate was reduced from 0.01, and the number of iterations of training is 1,000 epochs. The output model was selected based on the epoch, resulting in the highest AUC in the validation cohorts. For training the specialized LSTM model, the teacher forcing strategy is used to improve the learning efficiency of the model.

Model Withdrawal Procedure

To explore the impact of the cognitive conversion status at each time step during the evaluation of the patient, we used the trained hybrid model to test and evaluate the robustness of a single time point on the ADAS-cog score; that is, by changing the

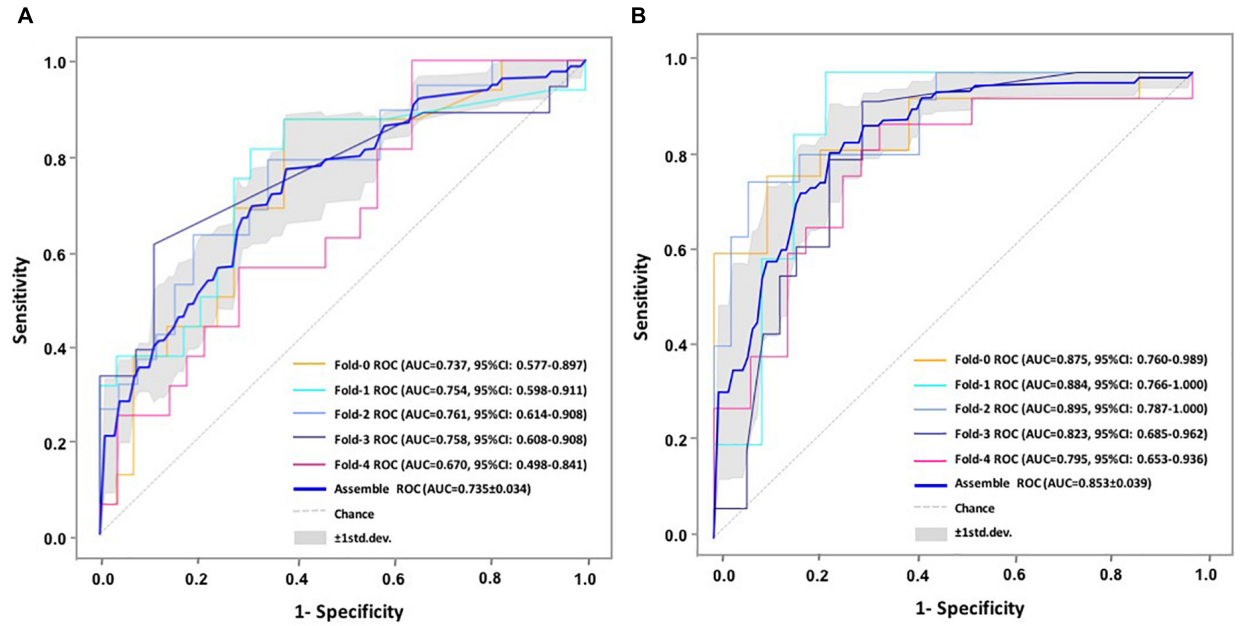

FIGURE 3 | ROC comparisons of cognitive conversion at 3 and 6 months with CNN-LSTM modeling. **(A)** ROC comparisons of cognitive conversion at 3 months; **(B)** ROC comparisons of cognitive conversion at 6 months.

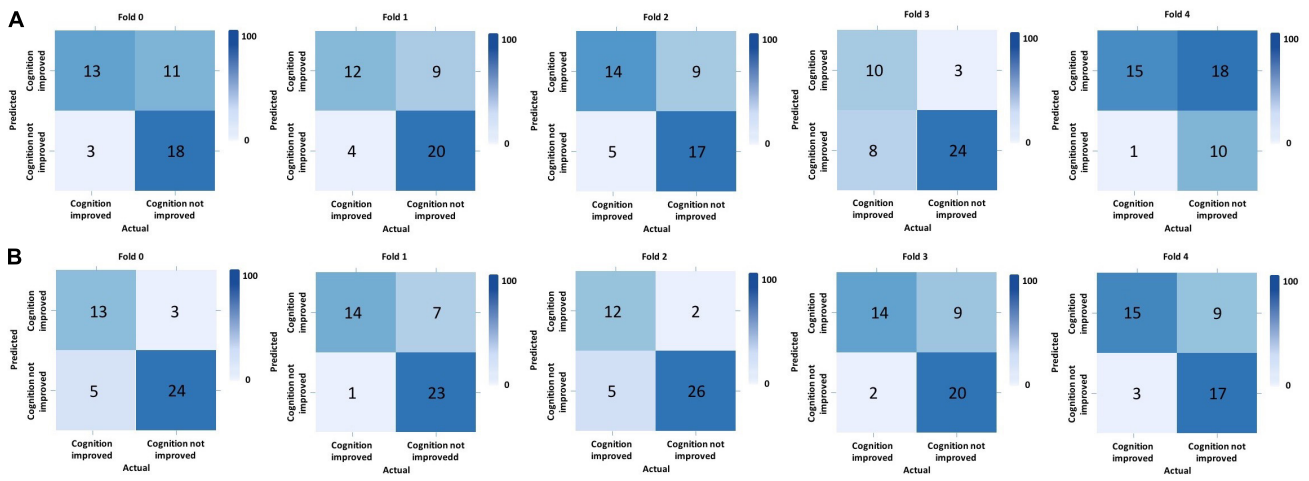

FIGURE 4 | Predictive performance evaluation of CNN-LSTM modeling with confusion matrix at 3 and 6 months. *Computed classification confusion matrix using our hybrid CNN-LSTM modeling in five-fold cross-validation. **(A)** Confusion matrix at 3 months; **(B)** Confusion matrix at 6 months.

model input through withdrawing the mid-point information (simulating situations of follow-up absence), the degree of impact of ADAS-cog at 3 months can be evaluated.

Model Performance Measurements and Statistical Analysis

Descriptive statistics (mean, standard deviation counts, and proportions) were provided to demonstrate the sample characteristics with respect to statistical quantitative and qualitative features.

For hybrid CNN-LSTM model evaluation, five-fold cross-validation was applied, and assembled ROC curves with AUCs were used to assess model performance at 3 and 6 months. Performance measurements including AUC, sensitivity, and specificity with 95% confidence interval (95% CI) were assessed using the optimal cut-off value (Youden index = sensitivity + specificity − 1).

We expected that the implementation of deep learning modeling could potentially guide the recommended treatment plan, especially on patients who may suffer from continuous cognitive decline during follow-ups. According

TABLE 2 | Predictive performance evaluation of CNN-LSTM modeling at 3 and 6 months.

		Accuracy (95%CI)	Sensitivity (95%CI)	Specificity (95%CI)	Positive predictive value (95%CI)	Negative predictive value (95%CI)	F-score	AUC (95%CI)	AUPRC
Fold 0	3-month	0.711 (0.557–0.836)	0.875 (0.617–0.984)	0.621 (0.423–0.793)	0.560 (0.349–0.756)	0.900 (0.683–0.988)	0.683	0.737 (0.577–0.897)	0.522
	6-month	0.844 (0.705–0.935)	0.778 (0.524–0.936)	0.889 (0.708–0.976)	0.824 (0.566–0.962)	0.857 (0.673–0.96)	0.800	0.875 (0.760–0.989)	0.818
Fold 1	3-month	0.733 (0.581–0.854)	0.813 (0.544–0.960)	0.690 (0.492–0.847)	0.591 (0.364–0.793)	0.870 (0.664–0.972)	0.684	0.754 (0.598–0.911)	0.631
	6-month	0.844 (0.705–0.935)	1.000 (0.782–1.000)	0.767 (0.577–0.901)	0.682 (0.451–0.861)	1.000 (0.852–1.000)	0.811	0.884 (0.766–1.000)	0.666
Fold 2	3-month	0.711 (0.557–0.836)	0.790 (0.544–0.939)	0.654 (0.443–0.828)	0.625 (0.406–0.812)	0.810 (0.581–0.946)	0.698	0.761 (0.614–0.908)	0.680
	6-month	0.867 (0.732–0.949)	0.765 (0.501–0.932)	0.929 (0.765–0.991)	0.867 (0.595–0.983)	0.867 (0.693–0.962)	0.813	0.895 (0.787–1.000)	0.806
Fold 3	3-month	0.778 (0.629–0.888)	0.611 (0.357–0.827)	0.889 (0.708–0.976)	0.786 (0.492–0.953)	0.774 (0.589–0.904)	0.688	0.758 (0.608–0.908)	0.705
	6-month	0.778 (0.629–0.888)	0.938 (0.698–0.998)	0.690 (0.492–0.847)	0.625 (0.406–0.812)	0.952 (0.762–0.999)	0.750	0.823 (0.685–0.962)	0.571
Fold 4	3-month	0.591 (0.432–0.737)	1.00 (0.794–1.000)	0.357 (0.186–0.559)	0.471 (0.298–0.649)	1.000 (0.692–1.000)	0.640	0.670 (0.498–0.841)	0.479
	6-month	0.750 (0.597–0.868)	0.889 (0.653–0.986)	0.654 (0.443–0.828)	0.640 (0.425–0.820)	0.895 (0.669,0.987)	0.744	0.795 (0.653–0.936)	0.693

to recommendations by multiple guidelines, it is assumed that if patient's ADAS-cog score declines less than 4 points or increases at either follow-up time point (every 3 months), the medical treatment recommended upon their diagnosis would be considered insufficient for avoiding the cognitive decline in the future (Farlow and Cummings, 2007; Cummings et al., 2015; Grossberg et al., 2019). Therefore, it is recommended to redirect or upgrade the medical treatment. Upon the above rationales, it was hypothesized that if our deep learning modeling could successfully predict the long-term cognitive conversion, it could be used to guide the early decision-making redirection. Therefore, we first estimated the treatment reassignment rates based on the actual and predicted cognitive conversion (namely, the target outcome) at 3 and 6 months according to the above principle. The actual and predicted treatment reassignment rates were then compared with chi-square testing (adjusted if necessary) in the general population and according to age, gender, and symptom severity as well as intervention subtypes within all directions. STATA 16.0 (StataCorp LLC, TX, United States) was utilized to perform the above analysis, and the statistical significance was determined with $p < 0.05$.

RESULTS

Demographics and Cognitive Conversion Distribution

Patient demographics and distribution according to cognitive conversion (e.g., improved or not improved) at 3 and 6 months are demonstrated in **Table 1**. A number of 224 patients were included, of whom 85 at 3 months and 84 at 6 months were identified as CI population, while 139 at 3 months and 140 at 6 months were identified as CNI. There were more men (137 accounted for 61.16%) than women (87 accounted for 38.84%) enrolled with an average age of 69.75 ± 8.52 years. Hypertension was the predominant comorbidity in 44 (19.64%) patients. Patients were referred for different treatments mainly based on the severity of cognitive impairment and the interests of the original cohorts in which they were enrolled, including 62 (27.68%) for observation, 22 (9.82%) for exercise, 55 (24.55%) for donepezil monotherapy, 38 (16.96%) of GBE monotherapy, and 47 (20.98%) for GBE and donepezil combination.

Predictive Performance of Hybrid Convolutional Neural Networks and Long-Short-Term Memory Modeling

We performed five-fold cross-validation to test the model stability and to obtain the predicted outcomes of all patients. Our hybrid CNN-LSTM modeling showed a considerable good predictive capacity in identifying cognitive conversion status at sequential time points. As shown in **Figure 3**, the hybrid model achieved a mean AUC of 0.735 (95% CI: 0.701–0.769) at 3 months and 0.853 (95% CI: 0.814–0.892) at 6 months. The predictive performance achieved by the proposed model was considered good at 3 and 6 months, with the detailed information provided in **Figure 4** and **Table 2**.

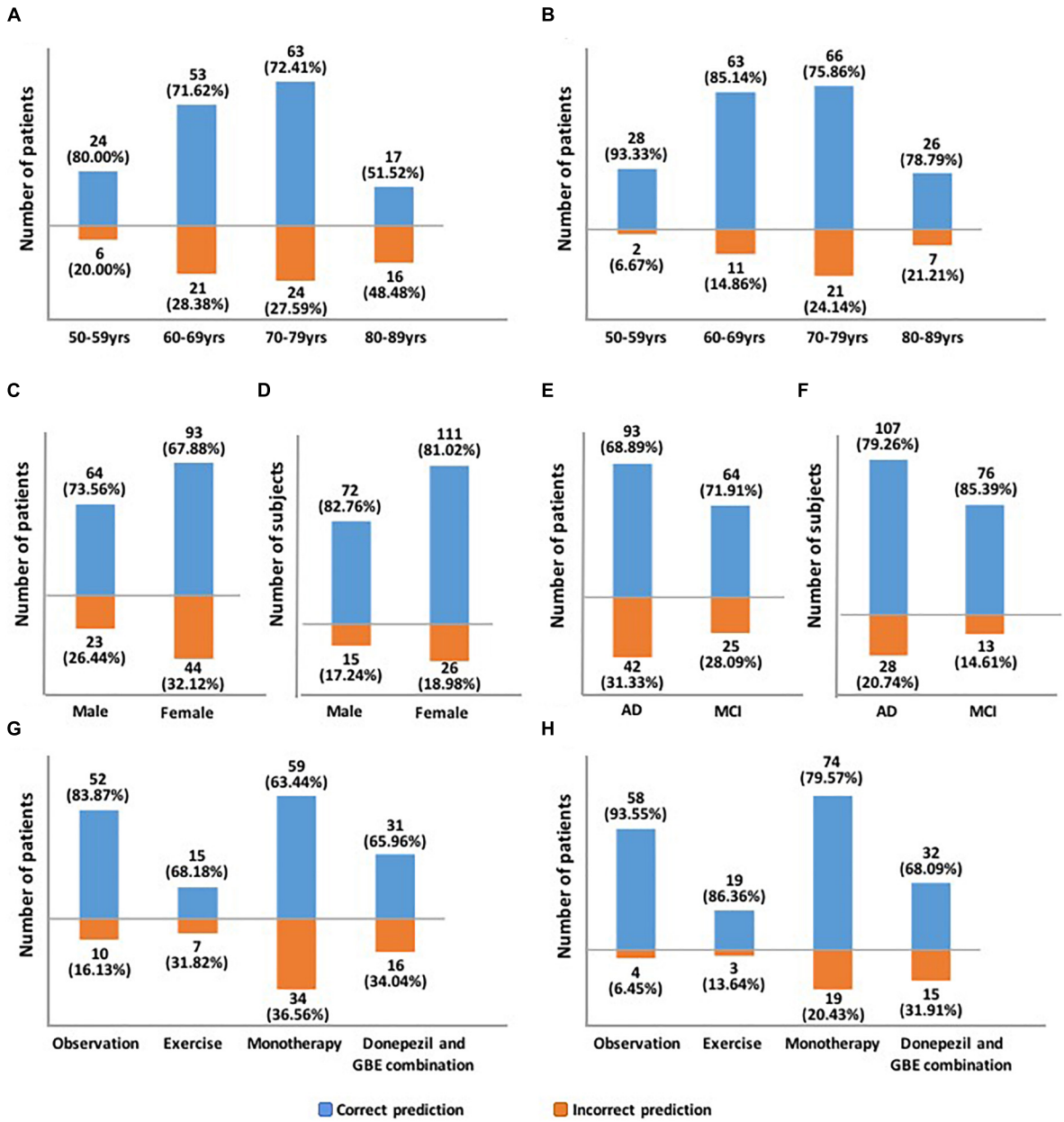

FIGURE 5 | Demonstration of predictive accuracy stratified by age, gender, symptom severity, and intervention subtypes. **(A)** Predictive accuracy stratified by age at 3 months; **(B)** Predictive accuracy stratified by age at 6 months; **(C)** Predictive accuracy stratified by gender at 3 months; **(D)** Predictive accuracy stratified by gender at 6 months; **(E)** Predictive accuracy stratified by symptom severity at 3 months; **(F)** Predictive accuracy stratified by symptom severity at 6 months; **(G)** Predictive accuracy stratified by intervention subtypes at 3 months; **(H)** Predictive accuracy stratified by intervention subtypes at 6 months.

TABLE 3 | Predictive performance evaluation of CNN-LSTM-based withdrawal modeling at 6 months.

	Accuracy (95%CI)	Sensitivity (95%CI)	Specificity (95%CI)	Positive predictive value (95%CI)	Negative predictive value (95%CI)	F-score	AUC (95%CI)	AUPRC
Fold 0	0.778 (0.629–0.888)	0.556 (0.308–0.785)	0.926 (0.757–0.991)	0.833 (0.516–0.979)	0.757 (0.577–0.889)	0.667	0.796 (0.656–0.937)	0.725
Fold 1	0.756 (0.605–0.871)	0.800 (0.519–0.957)	0.733 (0.541–0.877)	0.600 (0.361–0.809)	0.880 (0.688–0.975)	0.686	0.721 (0.554–0.888)	0.499
Fold 2	0.756 (0.605–0.871)	0.941 (0.713–0.999)	0.643 (0.441–0.814)	0.615 (0.406–0.798)	0.947 (0.740–0.999)	0.744	0.803 (0.661–0.944)	0.669
Fold 3	0.689 (0.534–0.818)	0.500 (0.247–0.753)	0.793 (0.603–0.920)	0.571 (0.289–0.823)	0.742 (0.554–0.881)	0.533	0.663 (0.491–0.834)	0.517
Fold 4	0.682 (0.524–0.814)	0.556 (0.308,0.785)	0.769 (0.564–0.910)	0.625 (0.354–0.848)	0.714 (0.513–0.868)	0.588	0.692 (0.529–0.855)	0.575

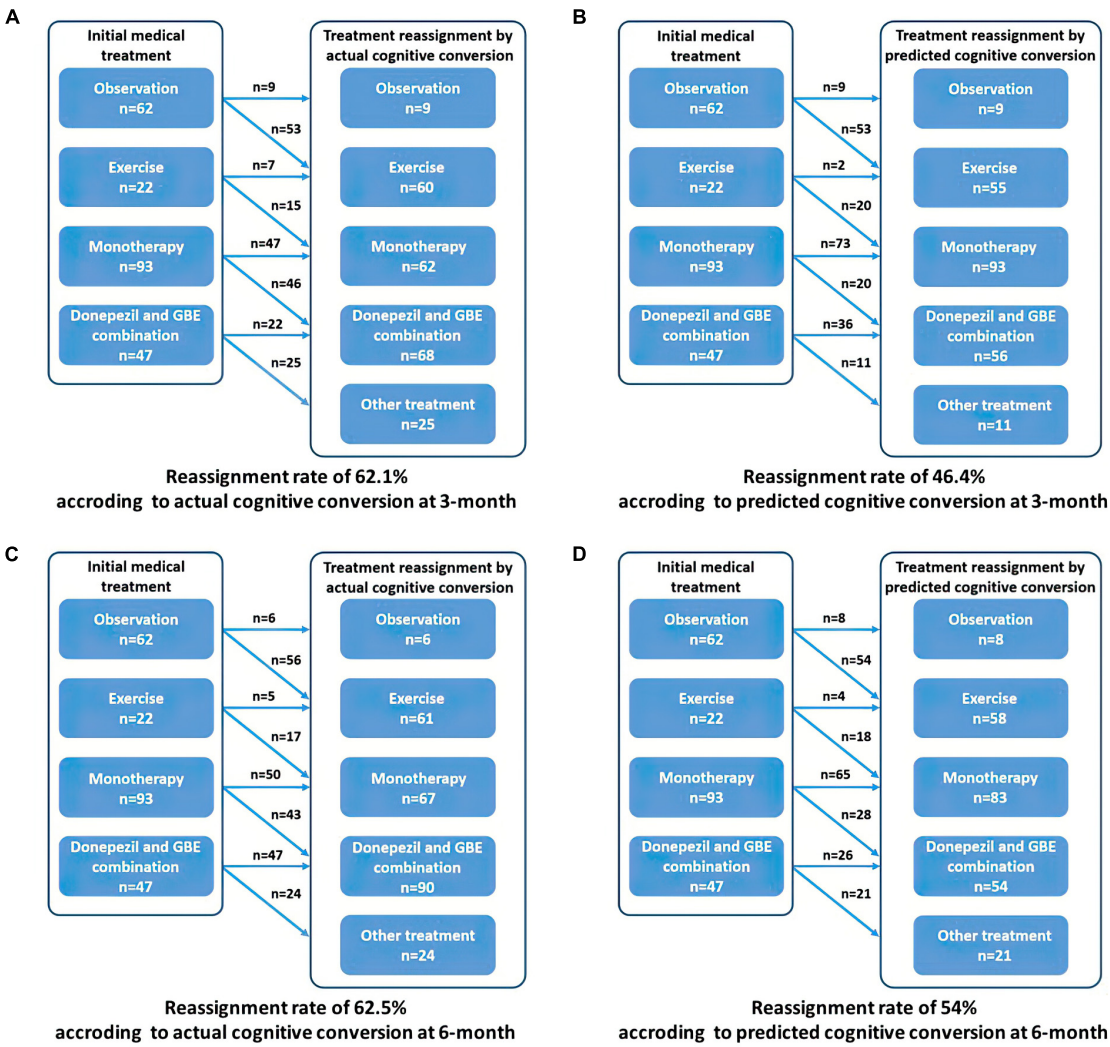

FIGURE 6 | Recommended treatment reassignment following actual and predictive cognitive conversion at 3 and 6 months. **(A)** Treatment reassignment according to actual cognitive conversion at 3 months; **(B)** Treatment reassignment according to predicted cognitive conversion at 3 months; **(C)** Treatment reassignment according to actual cognitive conversion at 6 months; **(D)** Treatment reassignment according to predicted cognitive conversion at 6 months. *Another treatment indicates additional memantine, psychological interventions combined with pharmacological therapy or novel pharmacological approaches involving strategies to reduce amyloid and/or tau deposition.

The proposed hybrid model generally provided accurately predicted outcomes in 70.09% of patients at 3 months and 81.70% at 6 months. To validate the generalizability of the proposed model, **Figure 5** and **Supplementary Table 2** provide the representative subgroup results according to age, gender, symptom severity, and intervention subtype between actual and predicted cognitive conversion at 3 and 6 months. Predictive performance was superior in male patients who were under observation at 3 months and exercise at 6 months.

In addition, we constructed the withdrawal model to further explore the importance of time-sequential data on the stability of our previously built CNN-LSTM modeling. As shown in **Figure 3** and **Supplementary Figure 2**, without the incorporation of data collected at 3 months, the AUC at 6 months decreased from 0.853 (95% CI: 0.814–0.892) to 0.734 (95% CI: 0.678–0.790), indicating that the AUC was moderately impacted by the withdrawal of data collected at 3 months. Another evaluation matrix of CNN-LSTM based withdrawal modeling at 6 months is demonstrated in **Supplementary Figure 3** and **Table 3**.

Recommended Treatment Reassignment Following Actual and Predicted Cognitive Conversion at 3 and 6 Months

Based on the prespecified principle, over half of the patients need reclassified treatment with a fraction of 62.05% (139/224) at 3 months and 62.50% (140/224) at 6 months as determined by their actual cognitive conversion. According to our hybrid CNN-LSTM algorithms, the predicted conversion could potentially guide the treatment reassignment in 46.43% (104/224) of patients

TABLE 4 | Comparison between actual results and AI-predicted results after 3 and 6 months.

	3-month				6-month			
	Actual reassignment status	**Predicted reassignment status**	X^2	***p* value**	**Actual reassignment status**	**Predicted reassignment status**	X^2	***p* value**
Overall, n (%)	139/224 (62.05)	104/224 (46.43)	11.017	0.001	140/224 (62.50)	121/224 (54.02)	3.314	0.069
Observation	53/62 (85.48)	53/62 (85.48)	0.000	1.000	56/62 (90.32)	54/62 (87.10)	0.322	0.570
Exercise	15/22 (68.18)	20/22 (90.91)	–	0.132	17/22 (77.27)	18/22 (81.82)	–	1.000
Monotherapy	46/93 (49.46)	20/93 (21.51)	15.876	0.000	43/93 (46.24)	28/93 (30.11)	5.126	0.024
Donepezil and GBE combination	25/47 (53.19)	11/47 (23.40)	8.824	0.003	24/47 (51.06)	21/47 (44.68)	0.384	0.536
Age, n (%)								
50–59y, n (%)	25/30 (83.33)	23/30 (76.67)	0.147	0.519	24/30 (80.00)	24/30 (80.00)	0.000	1.000
Observation	15/17 (10.79)	16/17 (15.38)	–	1.000	15/17 (10.71)	15/17 (12.40)	–	1.000
Exercise	–	–	–	–	–	–	–	–
Monotherapy	7/10 (5.04)	5/10 (4.82)	–	0.650	7/10 (5.00)	6/10 (4.96)	–	1.000
Donepezil and GBE combination	3/3 (2.16)	2/3 (1.92)	–	1.000	2/3 (1.43)	3/3 (2.47)	–	1.000
60–69yr, n (%)	42/74 (56.76)	35/74 (47.30)	1.327	0.249	44/74 (59.50)	37/74 (50.00)	1.336	0.248
Observation	15/18 (83.33)	16/18 (88.89)	–	1.000	17/18 (94.44)	15/18 (83.33)	–	0.603
Exercise	6/8 (75.00)	8/8 (100.00)	–	0.467	6/8 (75.00)	7/8 (87.50)	–	1.000
Monotherapy	12/30 (40.00)	7/30 (23.33)	1.926	0.165	10/30 (33.33)	8/30 (26.67)	0.317	0.573
Donepezil and GBE combination	9/18 (50.00)	4/18 (22.22)	3.010	0.083	11/18 (61.11)	7/18 (38.89)	1.778	0.182
70–79yr, n (%)	49/87 (56.32)	33/87 (37.93)	5.905	0.015	51/87 (58.62)	42/87 (48.28)	1.871	0.171
Observation	16/19 (84.21)	15/19 (78.95)	–	1.000	17/19 (89.47)	17/19 (89.47)	–	1.000
Exercise	6/9 (66.67)	8/9 (88.89)	–	0.576	7/9 (77.78)	7/9 (77.78)	–	1.000
Monotherapy	19/39 (66.67)	7/39 (17.95)	8.308	0.004	18/39 (46.15)	10/39 (25.64)	3.566	0.059
Donepezil and GBE combination	8/20 (40.00)	3/20 (15.00)	–	0.155	9/20 (45.00)	8/20 (40.00)	0.102	0.749
80–89yr, n (%)	23/33 (69.79)	13/33 (39.39)	6.111	0.013	21/33 (63.64)	18/33 (54.55)	0.564	0.453
Observation	7/8 (87.50)	6/8 (75.00)	–	1.000	7/8 (87.50)	7/8 (87.50)	–	1.000
Exercise	3/5 (60.00)	4/5 (80.00)	–	1.000	4/5 (80.00)	4/5 (80.00)	–	1.000
Monotherapy	8/14 (57.14)	1/14 (7.14)	–	0.013	8/14 (57.14)	4/14 (28.57)	–	0.252
Donepezil and GBE combination	5/6 (83.33)	2/6 (33.33)	–	0.242	2/6 (33.33)	3/6 (50.00)	–	1.000
Gender								
Male, n (%)	51/87 (58.62)	40/87 (45.98)	2.778	0.095	52/87 (59.77)	45/87 (51.72)	1.142	0.285
Observation	21/25 (84.00)	22/25 (88.00)	–	1.000	23/25 (92.00)	21/25 (84.00)	–	0.667
Exercise	8/10 (80.00)	9/10 (90.00)	–	1.000	9/10 (90.00)	9/10 (90.00)	–	1.000
Monotherapy	14/35 (40.00)	6/35 (17.14)	4.480	0.034	15/35 (42.86)	8/35 (22.86)	3.173	0.075
Donepezil and GBE combination	8/17 (47.06)	3/17 (17.65)	–	0.141	5/17 (29.41)	7/17 (41.18)	0.515	0.473
Female, n (%)	88/137 (64.23)	64/137 (46.72)	8.511	0.004	88/137 (64.23)	76/137 (55.47)	2.187	0.139
Observation	32/37 (86.49)	31/37 (83.78)	0.107	0.744	33/37 (89.19)	33/37 (89.19)	–	1.000
Exercise	7/12 (58.33)	11/12 (91.67)	–	0.155	8/12 (66.67)	9/12 (75.00)	–	1.000
Monotherapy	32/58 (55.17)	14/58 (24.14)	11.672	0.001	28/58 (48.28)	20/58 (34.48)	2.275	0.132
Donepezil and GBE combination	17/30 (55.17)	8/30 (26.67)	5.554	0.018	19/30 (63.33)	14/30 (46.67)	1.684	0.194
AD, n (%)	76/135 (56.30)	56/135 (41.48)	5.929	0.015	78/135 (57.78)	66/135 (48.89)	2.143	0.143
Symptom severity								
Observation	24/31 (77.42)	23/31 (74.19)	0.088	0.767	27/31 (87.10)	25/31 (80.65)	–	0.731
Exercise	15/22 (68.18)	20/22 (90.91)	–	0.132	17/22 (77.27)	18/22 (81.82)	–	1.000
Monotherapy	21/52 (40.38)	9/52 (17.31)	6.746	0.009	20/52 (38.46)	11/52 (21.54)	3.722	0.054
Donepezil and GBE combination	16/30 (53.33)	4/30 (13.33)	–	0.002	14/30 (46.67)	12/30 (40.00)	0.271	0.602
MCI, n (%)	63/89 (70.79)	48/89 (53.93)	5.385	0.020	62/135 (45.93)	55/135 (40.74)	1.222	0.269
Observation	29/31 (93.55)	30/31 (96.77)	–	1.000	29/31 (93.55)	29/31 (93.55)	–	1.000
Exercise	–	–	–	–	–	–	–	–
Monotherapy	25/41 (60.98)	11/41 (26.83)	9.705	0.002	23/41 (56.10)	17/41 (41.46)	1.757	0.185
Donepezil and GBE combination	9/17 (52.94)	7/17 (41.18)	0.472	0.492	10/17 (58.82)	9/17 (52.94)	0.119	0.730

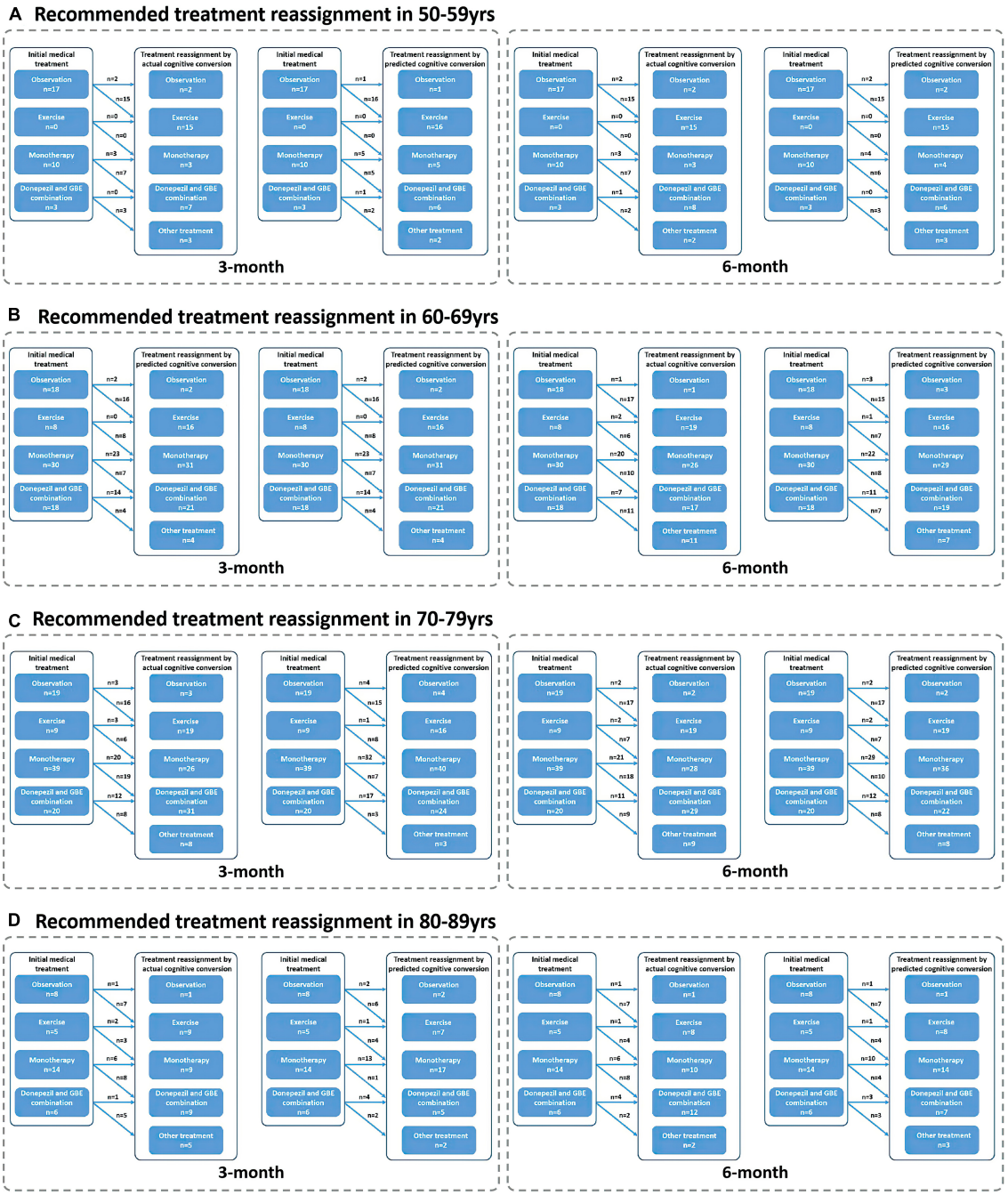

FIGURE 7 | Recommended treatment reassignment following actual and predictive cognitive conversion according to age at 3 and 6 months. **(A)** Treatment reassignment according to actual and predicted cognitive conversion at 3 and 6 months in 50–59 years; **(B)** Treatment reassignment according to actual and predicted cognitive conversion at 3 and 6 months in 60–69 years; **(C)** Treatment reassignment according to actual and predicted cognitive conversion at 3 and 6 months in 70–79 years; **(D)** Treatment reassignment according to actual and predicted cognitive conversion at 3 and 6 months in 80–89 years. *Another treatment indicates additional memantine, psychological interventions combined with pharmacological therapy or novel pharmacological approaches involving strategies to reduce amyloid and/or tau deposition.

at 3 months and 54.02% (121/224) at 6 months (**Figure 6**). No significant difference (p = 0.069) was noted in actual and predicted treatment reassignment at 6 months. We also estimated the treatment reassignment rate in subgroups categorized by age, gender, symptom severity, and intervention subtypes within all directions. Generally, no significant differences in treatment reassignment rates were detected between actual and predicted cognitive conversion in all directions at 6 months. Detailed

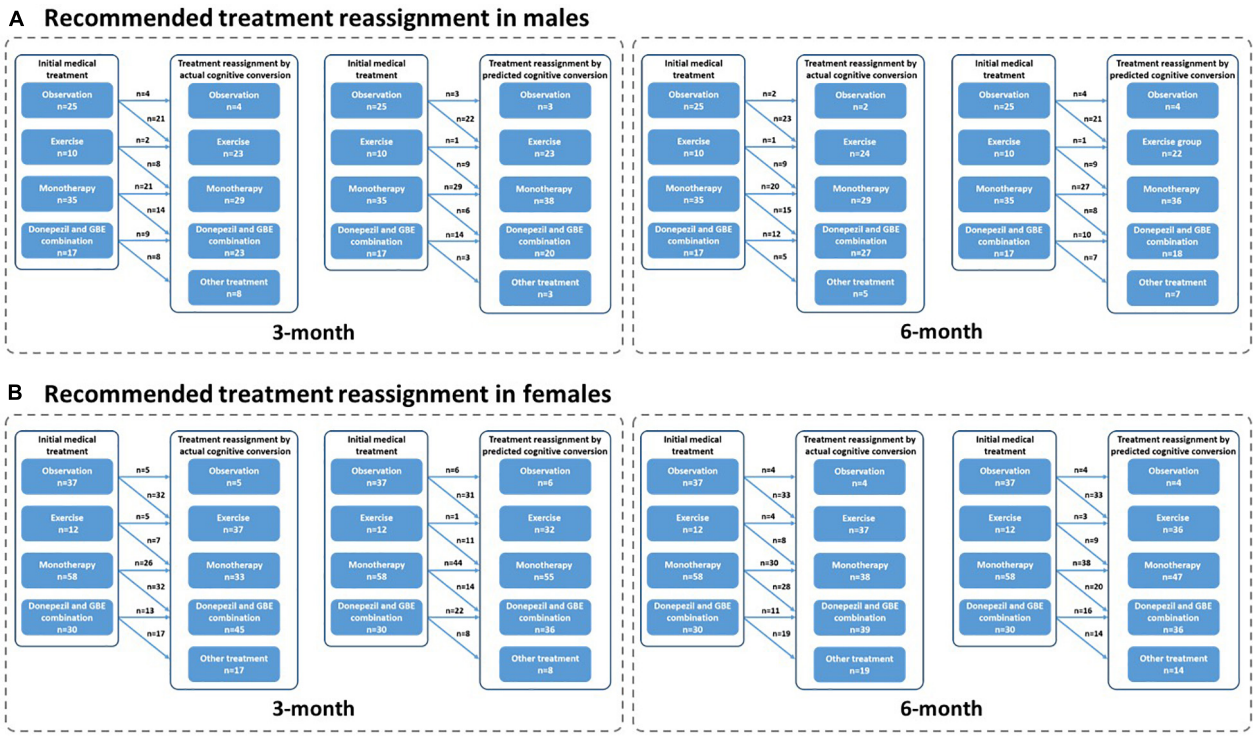

FIGURE 8 | Recommended treatment reassignment following actual and predictive cognitive conversion according to gender at 3 and 6 months. **(A)** Treatment reassignment according to actual and predicted cognitive conversion at 3 and 6 months in men; **(B)** Treatment reassignment according to actual and predicted cognitive conversion at 3 and 6 months in women. *Another treatment indicates additional memantine, psychological interventions combined with pharmacological therapy or novel pharmacological approaches involving strategies to reduce amyloid and/or tau deposition.

statistics regarding subgroup analysis of treatment reassignment are provided in **Table 4**.

DISCUSSION

Progressive cognitive impairment is currently considered as the major symptom in patients with AD or MCI. Studies and reviews have suggested improved clinical outcomes (e.g., suspended or postponed cognitive decline) in patients who were managed upon early diagnosis (Livingston et al., 2017; Regan et al., 2017; Bachurin et al., 2018; Green et al., 2019; Mintun et al., 2021). Advanced diagnostic strategies (e.g., genetic or plasma screening) have been proposed, therefore early intervention could be delivered directly (Nakamura et al., 2018; Giau et al., 2019; Palmqvist et al., 2019; Karikari et al., 2020). However, there remain concerns regarding a fairly high proportion of the quick decline in cognitive function in a short period due to distinctions in terms of the progressive variation of dementia. In the view of medical professionals, this situation would be attributed to, to some extent, the lack of strategies available to guide treatment decision-making even the diagnosis of AD or MCI at the early stage.

The concept of artificial intelligence (AI) has recently permeated almost every sector of the healthcare system. Its recent expansion of plasma phosphor-tau (P-tau) and other biomarkers in the prediction regarding the risk of developing AD is an ideal example (Palmqvist et al., 2021). Nonetheless, there is an ongoing demand for the continual process of integrating and optimizing these synergistic advances in guiding medical decision-making in the real clinical context.

In this study, we first estimated the reassignment rates according to our prespecified principle (as mentioned earlier) using the datasets from three ongoing cohorts. Using AI techniques would allow us to compare the reassignment rates estimated by the deep learning modeling according to the actual status. Upon this perspective, our findings based on the predicted cognitive conversion at 3 and 6 months verified our hypothesis and provided preliminary recommendations on treatment reassignment at the early stage of AD or MCI.

Generally, predicted cognitive conversion according to our hybrid CNN-LSTM algorithms led to a recommendation of treatment reassignment in 46.43% (104/224) of patients at 3 months and 54.02% (121/224) at 6 months as compared with 62.05% (139/224) at 3 months (X^2 = 11.017, p = 0.001) and 62.50% (140/224) at 6 months (X^2 = 3.314, p = 0.069) according to their actual cognitive conversion (**Figures 6–9** and **Table 4**). This indicated that a proportion of 74.7% of patients at 3 months and 86.4% at 6 months would be potentially benefited from deep learning modeling-guided treatment reassignment.

Interestingly, patients referred for observation and treated with monotherapy (GBE/donepezil) were more likely to be

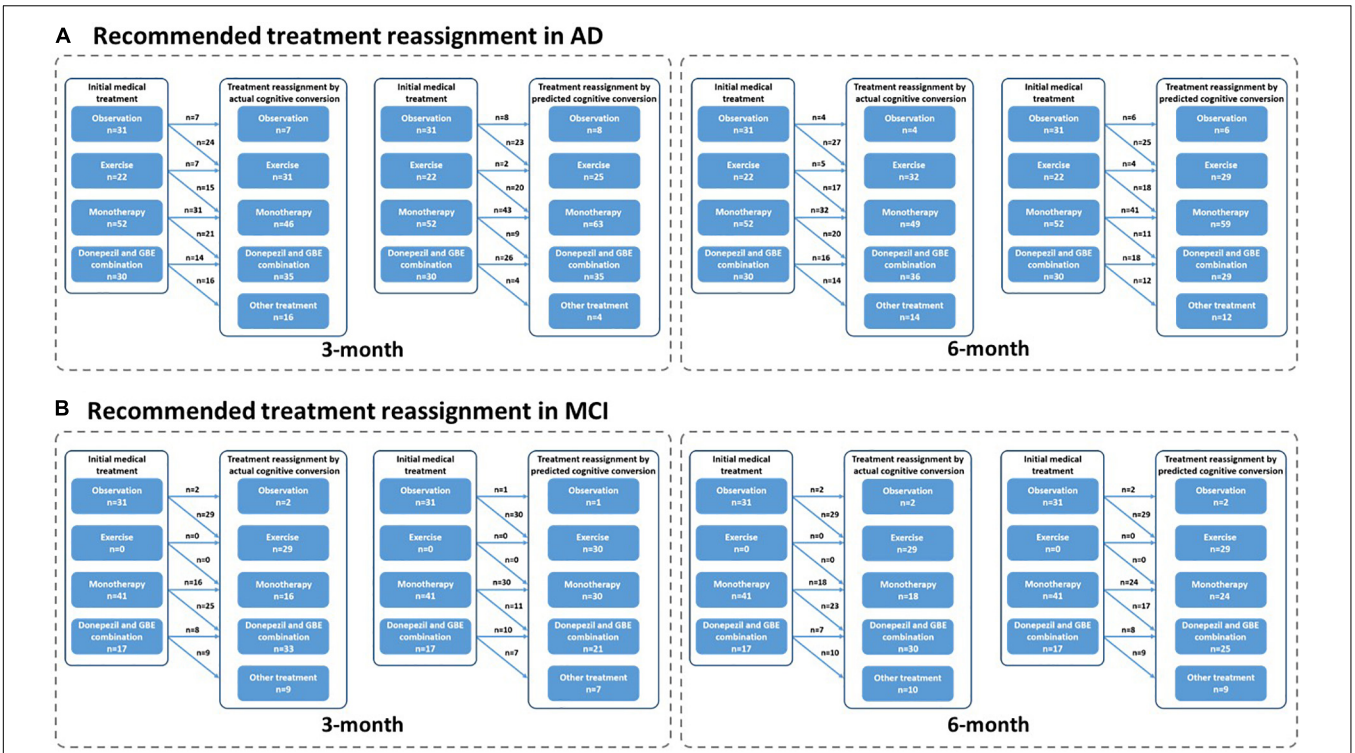

FIGURE 9 | Recommended treatment reassignment following actual and predictive cognitive conversion according to symptom severity at 3 and 6 months. **(A)** Treatment reassignment according to actual and predicted cognitive conversion at 3 and 6 months in AD; **(B)** Treatment reassignment according to actual and predicted cognitive conversion at 3 and 6 months in MCI. *Another treatment indicates additional memantine, psychological interventions combined with pharmacological therapy or novel pharmacological approaches involving strategies to reduce amyloid and/or tau deposition.

reclassified according to their actual cognitive conversion. However, a discrepancy that occurred between the actual and predicted reassignment status, with 44.4% (20/43) of patients at 3 months and 65.1% (28/46) at 6 months in this subgroup to be benefited, would be mainly attributed to the declined predictive accuracy in patients treated with monotherapy (GBE/donepezil). Considering the advantages of the hybrid CNN-LSTM algorithms in handling temporal data and capturing long-term dependencies, it was not surprising that the predictive performance was superior at 6 months than 3 months (Lara-Benítez et al., 2021). This was mainly benefited from its automatic feature learning ability with multiple temporal data (e.g., data at baseline and 3 months), which further enriched the predictive performance at 6 months. However, the predictive algorithm is different at 3 months, especially without the application of CNN featured algorithms. This highlighted the importance of adding time-sequential data to compensate for the above limitation in improving reassignment accuracy, while the increased costs and workload due to additional follow-ups would be further considered and balanced. It is important to emphasize that our follow-up is limited to 6 months at present, and long-term follow-up would be valuable to assess whether predictive performance can be further improved when the cognitive decline slows down with less heterogeneity and variation (Cortes et al., 2007; Vellas et al., 2007; Rockwood et al., 2008; De Rui et al., 2014). In contrast, the debated effectiveness of monotherapy (e.g., GBE and donepezil) may also increase the predictive uncertainty at both 3 and 6 months (Schneider et al., 2005; Mazza et al., 2006; Yuan et al., 2017; Birks and Harvey, 2018). Nonetheless, our results provided opportunities when neurological clinicians recommended medical treatment upon the diagnosis of AD or MCI, our model redirected management in averagely 80% of cases according to the actual cognitive conversion at 3 and 6 months, offering the potential to avoid a cognitive decline in the future. Unfortunately, a proportion of up to 26.3% of patients was not followed by our deep learning modeling, despite the dramatic efforts to optimize predictive performance and improve reassignment accuracy. Perhaps, this reflected nuanced medical management regarding factors such as age, gender, symptom severity, individual sensitivity, and variations in response to medical treatment, compliance to medical treatment, or other factors, which were not included in this study. Results of our subgroup analysis in reassignment rates also supported the above assumption.

Importantly, our findings could be placed into the context of guidelines highlighting the evidence-based classification criteria according to symptomatology and physiopathology to enable real-world testing of the value of our proposed strategy in a fashion that may assist the decision-making upon the diagnosis of AD or MCI. Since the diversity of medical treatment was limited due to the utilization of datasets from three registered cohorts, it cannot completely represent the real-world situation. However,

our study may serve as a template and has preliminarily verified by the application of deep learning modeling-guided decision-making in the treatment of dementia among AD or MCI. In fact, the currently proposed deep learning modeling successfully simulated the actual reassignment status, and several concerns are pending for investigation. For instance, the prognosis following the deep learning modeling-guided reassignment of medical treatment needs to be verified with well-designed studies before its application in real clinical circumstances. We used the increase in ADAS-cog score for more than 4 points as the cut-off to define cognitive decline. Similar to all neuropsychological assessments, the actual cognitive function may not be completely followed due to the sensitivity and specificity of ADAS-cog (Chu et al., 2000; Monllau et al., 2007; Rockwood et al., 2007; Balsis et al., 2012; Skinner et al., 2012; Verma et al., 2015). Although we reported the actual and predicted reassignment rates according to our prespecified principles, it was not totally evidence-based, indicating that some elements of referral bias cannot be excluded in this study. Our deep learning modeling was featured with handling time-sequential data especially for longitudinal cognitive scores extracted from multiple neuropsychological assessments, and the lack of data in terms of Aβ, tau, and other neurodegenerative biomarkers would consequently be assumed to impact the predictive performance of our deep learning modeling (Choi and Jin, 2018; Lee et al., 2019; Janelidze et al., 2020). In fact, plasma and CSF samples were not planned in the three registered cohort studies, highlighting that future studies must take these elements into account.

CONCLUSION

To sum up, we provided an example of hybrid CNN-LSTM modeling-driven early decision-tailoring in AD or MCI. Using deep learning modeling and featured longitudinal information, our hypothesis was preliminarily verified so that it may provide those suffering from cognitive decline in the future with chances to redirect treatment at the early stage. Considering the limited diversity of treatment strategies applied in this study, the real-world medical situation was not comprehensively simulated. Enlarged sample and diverse treatment datasets need to be further tested when considering the integration of this novel AI strategy into routine clinical practice of AD and MCI.

DATA AVAILABILITY STATEMENT

The original contributions presented in the study are included in the article/**Supplementary Material**, further inquiries can be directed to the corresponding authors.

ETHICS STATEMENT

The studies involving human participants were reviewed and approved by the First Affiliated Hospital of Nanjing Medical University (Reference numbers: 2013-SRFA-089 and 2016-SR-134). The patients/participants provided their written informed consent to participate in this study.

AUTHOR CONTRIBUTIONS

TW and YZ conceived the design of the study and prepared the original draft. TW and QH contributed to data curation, funding acquisition, supervision, and critical revision of the manuscript. YZ and YL were responsible for designing the statistical strategy. JW, YX, SY, WL, and HS were responsible for data acquisition. All authors read and contributed intellectually important content and approved the final manuscript.

FUNDING

This study was funded by the National Natural Science Foundation of China (Grant Nos. 81772454 and 81971237), the Jiangsu Municipal Science and Technology Bureau (Grant No. BE2017734), and the Nanjing Municipal Science and Technology Bureau (Grant No. 2019060002 [2021KF21]). The funding bodies had no role in the study design, data collection, analysis, and interpretation of data.

ACKNOWLEDGMENTS

The authors are grateful for the support of the medical and research staff of this study Xintong Zhang and Shenrui Wang, from the Department of Rehabilitation Medicine of the First Affiliated Hospital of Nanjing Medical University, are appreciated especially for their contribution to data processing and integration. Finally, the authors particularly appreciate the patients and families for their participation in this study.

SUPPLEMENTARY MATERIAL

The Supplementary Material for this article can be found online at: https://www.frontiersin.org/articles/10.3389/fnagi.2021.813923/full#supplementary-material

REFERENCES

Bachurin, S. O., Gavrilova, S. I., Samsonova, A., Barreto, G. E., and Aliev, G. (2018). Mild cognitive impairment due to Alzheimer disease: contemporary approaches to diagnostics and pharmacological intervention. *Pharmacol. Res.* 129, 216–226. doi: 10.1016/j.phrs.2017.11.021

Balsis, S., Unger, A. A., Benge, J. F., Geraci, L., and Doody, R. S. (2012). Gaining precision on the Alzheimer's disease assessment scale-cognitive: a comparison of item response theory-based scores and total scores. *Alzheimers Dement.* 8, 288–294. doi: 10.1016/j.jalz.2011.05.2409

Benedetti, A., Wu, Y., Levis, B., Wilchesky, M., Boruff, J., Ioannidis, J. P. A., et al. (2018). Diagnostic accuracy of the geriatric depression scale-30, geriatric depression scale-15, geriatric depression Scale-5 and Geriatric Depression

Scale-4 for detecting major depression: protocol for a systematic review and individual participant data meta-analysis. *BMJ Open* 8:e026598. doi: 10.1136/bmjopen-2018-026598

Birks, J. S., and Harvey, R. J. (2018). Donepezil for dementia due to Alzheimer's disease. *Cochrane Database Syst. Rev.* 6:Cd001190. doi: 10.1002/14651858.CD001190.pub3

Carrillo, M. C., Blennow, K., Soares, H., Lewczuk, P., Mattsson, N., Oberoi, P., et al. (2013). Global standardization measurement of cerebral spinal fluid for Alzheimer's disease: an update from the Alzheimer's association global biomarkers consortium. *Alzheimers Dement.* 9, 137–140. doi: 10.1016/j.jalz.2012.11.003

Cho, K., Merrienboer, B. V., Bahdanau, D., and Bengio, Y. (2014). On the properties of neural machine translation: encoder-decoder approaches. *arXiv* [Preprint] arXiv:1409.1259,

Choi, H., and Jin, K. H. (2018). Predicting cognitive decline with deep learning of brain metabolism and amyloid imaging. *Behav. Brain Res.* 344, 103–109. doi: 10.1016/j.bbr.2018.02.017

Chu, L. W., Chiu, K. C., Hui, S. L., Yu, G. K., Tsui, W. J., and Lee, P. W. (2000). The reliability and validity of the Alzheimer's disease assessment scale cognitive subscale (ADAS-Cog) among the elderly Chinese in Hong Kong. *Ann. Acad. Med. Singap.* 29, 474–485.

Chung, J., Gulcehre, C., Cho, K. H., and Bengio, Y. (2014). Empirical evaluation of gated recurrent neural networks on sequence modeling. *arXiv* [Preprint] arXiv:1412.3555,

Cortes, F., Portet, F., Touchon, J., and Vellas, B. (2007). Six and 18-month changes in mild to moderate Alzheimer's patients treated with acetylcholinesterase inhibitors: what can we learn for clinical outcomes of therapeutic trials? *J. Nutr. Health Aging* 11, 330–337.

Cummings, J. L. (1993). Mini-mental state examination. norms, normals, and numbers. *JAMA* 269, 2420–2421.

Cummings, J. L., Isaacson, R. S., Schmitt, F. A., and Velting, D. M. (2015). A practical algorithm for managing Alzheimer's disease: what, when, and why? *Ann. Clin. Transl. Neurol.* 2, 307–323. doi: 10.1002/acn3.166

Cummings, J. L., Mega, M., Gray, K., Rosenberg-Thompson, S., Carusi, D. A., and Gornbein, J. (1994). the neuropsychiatric inventory: comprehensive assessment of psychopathology in dementia. *Neurology* 44, 2308–2314. doi: 10.1212/wnl.44.12.2308

De Rui, M., Coin, A., Granziera, S., Girardi, A., Catanzaro, S., Manzato, E., et al. (2014). Short- and long-term efficacy of cholinesterase inhibitors in older adults with alzheimer's disease and mixed dementia: results of a 21-month observational study. *Panminerva Med.* 16.

Defrancesco, M., Pechlaner, R., Kiechl, S., Willeit, J., Deisenhammer, E. A., Hinterhuber, H., et al. (2018). What characterizes depression in old age? Results from the bruneck study. *Pharmacopsychiatry* 51, 153–160. doi: 10.1055/s-0043-119417

Dubois, B., Feldman, H. H., Jacova, C., Dekosky, S. T., Barberger-Gateau, P., Cummings, J., et al. (2007). Research criteria for the diagnosis of Alzheimer's disease: revising the NINCDS-ADRDA criteria. *Lancet Neurol.* 6, 734–746. doi: 10.1016/s1474-4422(07)70178-3

Farlow, M. R., and Cummings, J. L. (2007). Effective pharmacologic management of Alzheimer's disease. *Am. J. Med.* 120, 388–397. doi: 10.1016/j.amjmed.2006.08.036

Folstein, M. F., Folstein, S. E., and McHugh, P. R. (1975). Mini-mental state. A practical method for grading the cognitive state of patients for the clinician. *J. Psychiatr. Res.* 12, 189–198. doi: 10.1016/0022-3956(75)90026-6

Gers, F. A., and Schmidhuber, E. (2001). LSTM recurrent networks learn simple context-free and context-sensitive languages. *IEEE Trans. Neural. Netw.* 12, 1333–1340. doi: 10.1109/72.963769

Giau, V. V., Bagyinszky, E., Yang, Y. S., Youn, Y. C., An, S. S. A., and Kim, S. Y. (2019). Genetic analyses of early-onset Alzheimer's disease using next generation sequencing. *Sci. Rep.* 9:8368. doi: 10.1038/s41598-019-44848-2

Green, C., Handels, R., Gustavsson, A., Wimo, A., Winblad, B., Sköldunger, A., et al. (2019). Assessing cost-effectiveness of early intervention in Alzheimer's disease: an open-source modeling framework. *Alzheimers Dement.* 15, 1309–1321. doi: 10.1016/j.jalz.2019.05.004

Grossberg, G. T., Tong, G., Burke, A. D., and Tariot, P. N. (2019). Present algorithms and future treatments for Alzheimer's disease. *J. Alzheimers Dis.* 67, 1157–1171. doi: 10.3233/jad-180903

Hepp, D. H., Vergoossen, D. L., Huisman, E., Lemstra, A. W., Berendse, H. W., Rozemuller, A. J., et al. (2016). Distribution and load of amyloid-β pathology in parkinson disease and dementia with lewy bodies. *J. Neuropathol. Exp. Neurol.* 75, 936–945. doi: 10.1093/jnen/nlw070

Hill, N. T., Mowszowski, L., Naismith, S. L., Chadwick, V. L., Valenzuela, M., and Lampit, A. (2017). Computerized cognitive training in older adults with mild cognitive impairment or dementia: a systematic review and meta-analysis. *Am. J. Psychiatry* 174, 329–340. doi: 10.1176/appi.ajp.2016.16030360

Hochreiter, S., and Schmidhuber, J. (1997). Long short-term memory. *Neural Computation* 9, 1735–1780.

Hort, J., O'Brien, J. T., Gainotti, G., Pirttila, T., Popescu, B. O., Rektorova, I., et al. (2010). EFNS guidelines for the diagnosis and management of Alzheimer's disease. *Eur. J. Neurol.* 17, 1236–1248. doi: 10.1111/j.1468-1331.2010.03040.x

Ioannou, G. N., Tang, W., Beste, L. A., Tincopa, M. A., Su, G. L., Van, T., et al. (2020). Assessment of a deep learning model to predict hepatocellular carcinoma in patients with hepatitis C cirrhosis. *JAMA Netw. Open* 3:e2015626. doi: 10.1001/jamanetworkopen.2020.15626

Jack, C. R. Jr., Bennett, D. A., Blennow, K., Carrillo, M. C., Dunn, B., Haeberlein, S. B., et al. (2018). NIA-AA research framework: toward a biological definition of Alzheimer's disease. *Alzheimers Dement.* 14, 535–562. doi: 10.1016/j.jalz.2018.02.018

Jack, C. R. Jr., Petersen, R. C., Xu, Y. C., O'Brien, P. C., Smith, G. E., Ivnik, R. J., et al. (1999). Prediction of AD with MRI-based hippocampal volume in mild cognitive impairment. *Neurology* 52, 1397–1403. doi: 10.1212/wnl.52.7.1397

Janelidze, S., Mattsson, N., Palmqvist, S., Smith, R., Beach, T. G., Serrano, G. E., et al. (2020). Plasma P-tau181 in Alzheimer's disease: relationship to other biomarkers, differential diagnosis, neuropathology and longitudinal progression to Alzheimer's dementia. *Nat. Med.* 26, 379–386. doi: 10.1038/s41591-020-0755-1

Jiang, Y., Yang, H., Zhao, J., Wu, Y., Zhou, X., and Cheng, Z. (2020). Reliability and concurrent validity of Alzheimer's disease assessment scale - cognitive subscale, Chinese version (ADAS-Cog-C) among Chinese community-dwelling older people population. *Clin. Neuropsychol.* 34(sup1), 43–53. doi: 10.1080/13854046.2020.1750704

Kang, H. (2013). The prevention and handling of the missing data. *Korean J. Anesthesiol.* 64, 402–406. doi: 10.4097/kjae.2013.64.5.402

Karikari, T. K., Pascoal, T. A., Ashton, N. J., Janelidze, S., Benedet, A. L., Rodriguez, J. L., et al. (2020). Blood phosphorylated tau 181 as a biomarker for Alzheimer's disease: a diagnostic performance and prediction modelling study using data from four prospective cohorts. *Lancet Neurol.* 19, 422–433. doi: 10.1016/s1474-4422(20)30071-5

Killiany, R. J., Gomez-Isla, T., Moss, M., Kikinis, R., Sandor, T., Jolesz, F., et al. (2000). Use of structural magnetic resonance imaging to predict who will get Alzheimer's disease. *Ann. Neurol.* 47, 430–439.

Kingma, D. P., and Ba, J. J. A. P. A. (2014). Adam: a method for stochastic optimization. *arXiv* [Preprint] arXiv:1412.6980,

Koszewicz, M., Jaroch, J., Brzecka, A., Ejma, M., Budrewicz, S., Mikhaleva, L. M., et al. (2021). Dysbiosis is one of the risk factor for stroke and cognitive impairment and potential target for treatment. *Pharmacol. Res.* 164:105277. doi: 10.1016/j.phrs.2020.105277

Langa, K. M., and Levine, D. A. (2014). The diagnosis and management of mild cognitive impairment: a clinical review. *JAMA* 312, 2551–2561. doi: 10.1001/jama.2014.13806

LaPlante, M. P. (2010). The classic measure of disability in activities of daily living is biased by age but an expanded IADL/ADL measure is not. *J. Gerontol. B Psychol. Sci. Soc. Sci.* 65, 720–732. doi: 10.1093/geronb/gbp129

Lara-Benítez, P., Carranza-García, M., and Riquelme, J. C. (2021). An experimental review on deep learning architectures for time series forecasting. *Int. J. Neural. Syst.* 31:2130001. doi: 10.1142/s0129065721300011

Lawton, M. P. (1997). Assessing quality of life in Alzheimer disease research. *Alzheimer Dis. Assoc. Disord.* 11(Suppl. 6), 91–99.

Lee, G., Nho, K., Kang, B., Sohn, K. A., and Kim, D. (2019). Predicting Alzheimer's disease progression using multi-modal deep learning approach. *Sci. Rep.* 9:1952. doi: 10.1038/s41598-018-37769-z

Livingston, G., Sommerlad, A., Orgeta, V., Costafreda, S. G., Huntley, J., Ames, D., et al. (2017). Dementia prevention, intervention, and care. *Lancet* 390, 2673–2734. doi: 10.1016/s0140-6736(17)31363-6

Logsdon, R. G., Gibbons, L. E., McCurry, S. M., and Teri, L. (2002). Assessing quality of life in older adults with cognitive impairment. *Psychosom. Med.* 64, 510–519. doi: 10.1097/00006842-200205000-00016

Mazza, M., Capuano, A., Bria, P., and Mazza, S. (2006). Ginkgo biloba and donepezil: a comparison in the treatment of Alzheimer's dementia in a randomized placebo-controlled double-blind study. *Eur. J. Neurol.* 13, 981–985. doi: 10.1111/j.1468-1331.2006.01409.x

Mintun, M. A., Lo, A. C., Duggan Evans, C., Wessels, A. M., Ardayfio, P. A., Andersen, S. W., et al. (2021). Donanemab in early Alzheimer's disease. *N. Engl. J. Med.* 384, 1691–1704. doi: 10.1056/NEJMoa2100708

Monllau, A., Pena-Casanova, J., Blesa, R., Aguilar, M., Bohm, P., Sol, J. M., et al. (2007). [Diagnostic value and functional correlations of the ADAS-Cog scale in Alzheimer's disease: data on NORMACODEM project]. *Neurologia* 22, 493–501.

Nakamura, A., Kaneko, N., Villemagne, V. L., Kato, T., Doecke, J., Doré, V., et al. (2018). High performance plasma amyloid-β biomarkers for Alzheimer's disease. *Nature* 554, 249–254. doi: 10.1038/nature25456

Palmqvist, S., Janelidze, S., Stomrud, E., Zetterberg, H., Karl, J., Zink, K., et al. (2019). Performance of fully automated plasma assays as screening tests for alzheimer disease-related β-amyloid status. *JAMA Neurol.* 76, 1060–1069. doi: 10.1001/jamaneurol.2019.1632

Palmqvist, S., Tideman, P., Cullen, N., Zetterberg, H., Blennow, K., Dage, J. L., et al. (2021). Prediction of future Alzheimer's disease dementia using plasma phospho-tau combined with other accessible measures. *Nat. Med.* 27, 1034–1042. doi: 10.1038/s41591-021-01348-z

Petersen, R. C., Roberts, R. O., Knopman, D. S., Geda, Y. E., Cha, R. H., Pankratz, V. S., et al. (2010). Prevalence of mild cognitive impairment is higher in men, The Mayo Clinic Study of Aging. *Neurology* 75, 889–897. doi: 10.1212/WNL.0b013e3181f11d85

Qaseem, A., Snow, V., Cross, J. T. Jr., Forciea, M. A., Hopkins, R. Jr., Shekelle, P., et al. (2008). Current pharmacologic treatment of dementia: a clinical practice guideline from the American College of physicians and the American Academy of family physicians. *Ann. Intern. Med.* 148, 370–378. doi: 10.7326/0003-4819-148-5-200803040-00008

Raina, P., Santaguida, P., Ismaila, A., Patterson, C., Cowan, D., Levine, M., et al. (2008). Effectiveness of cholinesterase inhibitors and memantine for treating dementia: evidence review for a clinical practice guideline. *Ann. Intern. Med.* 148, 379–397. doi: 10.7326/0003-4819-148-5-200803040-00009

Regan, B., Wells, Y., Farrow, M., O'Halloran, P., and Workman, B. (2017). MAXCOG-maximizing cognition: a randomized controlled trial of the efficacy of goal-oriented cognitive rehabilitation for people with mild cognitive impairment and early alzheimer disease. *Am. J. Geriatr. Psychiatry* 25, 258–269. doi: 10.1016/j.jagp.2016.11.008

Rockwood, K., Dai, D., and Mitnitski, A. (2008). Patterns of decline and evidence of subgroups in patients with Alzheimer's disease taking galantamine for up to 48 months. *Int. J. Geriatr. Psychiatry* 23, 207–214. doi: 10.1002/gps.1864

Rockwood, K., Fay, S., Gorman, M., Carver, D., and Graham, J. E. (2007). The clinical meaningfulness of ADAS-Cog changes in Alzheimer's disease patients treated with donepezil in an open-label trial. *BMC Neurol.* 7:26. doi: 10.1186/1471-2377-7-26

Rosen, W. G., Mohs, R. C., and Davis, K. L. (1984). A new rating scale for Alzheimer's disease. *Am. J. Psychiatry* 141, 1356–1364. doi: 10.1176/ajp.141.11.1356

Sabbagh, M., Sadowsky, C., Tousi, B., Agronin, M. E., Alva, G., Armon, C., et al. (2020). Effects of a combined transcranial magnetic stimulation (TMS) and cognitive training intervention in patients with Alzheimer's disease. *Alzheimers Dement.* 16, 641–650. doi: 10.1016/j.jalz.2019.08.197

Schneider, L. S., DeKosky, S. T., Farlow, M. R., Tariot, P. N., Hoerr, R., and Kieser, M. (2005). A randomized, double-blind, placebo-controlled trial of two doses of Ginkgo biloba extract in dementia of the Alzheimer's type. *Curr. Alzheimer Res.* 2, 541–551. doi: 10.2174/156720505774932287

Shaw, L. M., Vanderstichele, H., Knapik-Czajka, M., Clark, C. M., Aisen, P. S., Petersen, R. C., et al. (2009). Cerebrospinal fluid biomarker signature in Alzheimer's disease neuroimaging initiative subjects. *Ann. Neurol.* 65, 403–413. doi: 10.1002/ana.21610

Skinner, J., Carvalho, J. O., Potter, G. G., Thames, A., Zelinski, E., Crane, P. K., et al. (2012). The Alzheimer's disease assessment scale-cognitive-plus (ADAS-Cog-Plus): an expansion of the ADAS-Cog to improve responsiveness in MCI. *Brain Imaging Behav.* 6, 489–501. doi: 10.1007/s11682-012-9166-3

Thomas, V. S., Rockwood, K., and McDowell, I. (1998). Multidimensionality in instrumental and basic activities of daily living. *J. Clin. Epidemiol.* 51, 315–321. doi: 10.1016/s0895-4356(97)00292-8

Vaswani, A., Shazeer, N., Parmar, N., Uszkoreit, J., Jones, L., Gomez, A. N., et al. (2017). Attention is all you need. *arXiv* [Preprint] arXiv:1706.03762,

Vellas, B., Andrieu, S., Cantet, C., Dartigues, J. F., and Gauthier, S. (2007). Long-term changes in ADAS-cog: what is clinically relevant for disease modifying trials in Alzheimer? *J. Nutr. Health Aging* 11, 338–341.

Verbeke, G., Fieuws, S., Molenberghs, G., and Davidian, M. (2014). The analysis of multivariate longitudinal data: a review. *Stat. Methods Med. Res.* 23, 42–59. doi: 10.1177/0962280212445834

Verma, N., Beretvas, S. N., Pascual, B., Masdeu, J. C., and Markey, M. K. (2015). New scoring methodology improves the sensitivity of the Alzheimer's disease assessment scale-cognitive subscale (ADAS-Cog) in clinical trials. *Alzheimers Res. Ther.* 7:64. doi: 10.1186/s13195-015-0151-0

Vik-Mo, A. O., Giil, L. M., Borda, M. G., Ballard, C., and Aarsland, D. (2020). The individual course of neuropsychiatric symptoms in people with Alzheimer's and Lewy body dementia: 12-year longitudinal cohort study. *Br. J. Psychiatry* 216, 43–48. doi: 10.1192/bjp.2019.195

Wu, Y. T., Beiser, A. S., Breteler, M. M. B., Fratiglioni, L., Helmer, C., Hendrie, H. C., et al. (2017). The changing prevalence and incidence of dementia over time - current evidence. *Nat. Rev. Neurol.* 13, 327–339. doi: 10.1038/nrneurol.2017.63

Xue, H., Zhai, J., He, R., Zhou, L., Liang, R., and Yu, H. (2018). Moderating role of positive aspects of caregiving in the relationship between depression in persons with Alzheimer's disease and caregiver burden. *Psychiatry Res.* 261, 400–405. doi: 10.1016/j.psychres.2017.12.088

Yuan, Q., Wang, C. W., Shi, J., and Lin, Z. X. (2017). Effects of Ginkgo biloba on dementia: an overview of systematic reviews. *J. Ethnopharmacol.* 195, 1–9. doi: 10.1016/j.jep.2016.12.005

Zhang, S., Han, D., Tan, X., Feng, J., Guo, Y., and Ding, Y. (2012). Diagnostic accuracy of 18 F-FDG and 11 C-PIB-PET for prediction of short-term conversion to Alzheimer's disease in subjects with mild cognitive impairment. *Int. J. Clin. Pract.* 66, 185–198. doi: 10.1111/j.1742-1241.2011.02845.x

Conflict of Interest: The authors declare that the research was conducted in the absence of any commercial or financial relationships that could be construed as a potential conflict of interest.

frontiers in Aging Neuroscience

ORIGINAL RESEARCH
published: 30 March 2022
doi: 10.3389/fnagi.2022.854031

Chronic PPARγ Stimulation Shifts Amyloidosis to Higher Fibrillarity but Improves Cognition

Tanja Blume[1†], Maximilian Deussing[2†], Gloria Biechele[3], Finn Peters[1], Benedikt Zott[4,5], Claudio Schmidt[2], Nicolai Franzmeier[6], Karin Wind[1,2], Florian Eckenweber[2], Christian Sacher[2], Yuan Shi[1], Katharina Ochs[1], Gernot Kleinberger[7,8], Xianyuan Xiang[7], Carola Focke[2], Simon Lindner[2], Franz-Josef Gildehaus[2], Leonie Beyer[2], Barbara von Ungern-Sternberg[2], Peter Bartenstein[2], Karlheinz Baumann[9], Helmuth Adelsberger[3], Axel Rominger[10,11], Paul Cumming[2,12], Michael Willem[7], Mario M. Dorostkar[1,13], Jochen Herms[1,10,13†] and Matthias Brendel[1,2,10†]*

[1] DZNE – German Center for Neurodegenerative Diseases, Munich, Germany, [2] Department of Nuclear Medicine, University Hospital of Munich, Ludwig Maximilian University of Munich, Munich, Germany, [3] Department of Radiology, University Hospital of Munich, Ludwig Maximilian University of Munich, Munich, Germany, [4] Institute of Neuroscience, Technical University of Munich, Munich, Germany, [5] Department of Diagnostic and Interventional Neuroradiology, Klinikum Rechts der Isar, Technical University of Munich, Munich, Germany, [6] Institute for Stroke and Dementia Research, University Hospital of Munich, Ludwig Maximilian University of Munich, Munich, Germany, [7] Metabolic Biochemistry, Faculty of Medicine, Biomedical Center (BMC), Ludwig Maximilian University of Munich, Munich, Germany, [8] ISAR Bioscience GmbH, Planegg, Germany, [9] Roche Pharma Research and Early Development, Neuroscience Discovery, Roche Innovation Center Basel, F. Hoffmann-La Roche Ltd., Basel, Switzerland, [10] SyNergy, Ludwig Maximilian University of Munich, Munich, Germany, [11] Department of Nuclear Medicine, Inselspital Bern, Bern, Switzerland, [12] School of Psychology and Counselling, Queensland University of Technology, Brisbane, QLD, Australia, [13] Center for Neuropathology and Prion Research, Ludwig Maximilian University of Munich, Munich, Germany

We undertook longitudinal β-amyloid positron emission tomography (Aβ-PET) imaging as a translational tool for monitoring of chronic treatment with the peroxisome proliferator-activated receptor gamma (PPARγ) agonist pioglitazone in Aβ model mice. We thus tested the hypothesis this treatment would rescue from increases of the Aβ-PET signal while promoting spatial learning and preservation of synaptic density. Here, we investigated longitudinally for 5 months PS2APP mice (N = 23; baseline age: 8 months) and App^{NL-G-F} mice (N = 37; baseline age: 5 months) using Aβ-PET. Groups of mice were treated with pioglitazone or vehicle during the follow-up interval. We tested spatial memory performance and confirmed terminal PET findings by immunohistochemical and biochemistry analyses. Surprisingly, Aβ-PET and immunohistochemistry revealed a shift toward higher fibrillary composition of Aβ-plaques during upon chronic pioglitazone treatment. Nonetheless, synaptic density and spatial learning were improved in transgenic mice with pioglitazone treatment, in association with the increased plaque fibrillarity. These translational data suggest that a shift toward higher plaque fibrillarity protects cognitive function and brain integrity. Increases in the Aβ-PET signal upon immunomodulatory treatments targeting Aβ aggregation can thus be protective.

Keywords: pioglitazone, Aβ-PET, App^{NL-G-F} mice, PS2APP mice, microglia, Aβ-plaque composition

OPEN ACCESS

Edited by:
Rodrigo Morales, University of Texas Health Science Center at Houston, United States

Reviewed by:
Jaqueline Generoso, Universidade do Extremo Sul Catarinense, Brazil
Raquel Sanchez-Varo, Universidad de Málaga, Spain

****Correspondence:***
Matthias Brendel
matthias.brendel@med.uni-muenchen.de

† These authors have contributed equally to this work

Specialty section:
This article was submitted to Alzheimer's Disease and Related Dementias, a section of the journal Frontiers in Aging Neuroscience

Received: *13 January 2022*
Accepted: *25 February 2022*
Published: *30 March 2022*

Citation:
Blume T, Deussing M, Biechele G, Peters F, Zott B, Schmidt C, Franzmeier N, Wind K, Eckenweber F, Sacher C, Shi Y, Ochs K, Kleinberger G, Xiang X, Focke C, Lindner S, Gildehaus F-J, Beyer L, von Ungern-Sternberg B, Bartenstein P, Baumann K, Adelsberger H, Rominger A, Cumming P, Willem M, Dorostkar MM, Herms J and Brendel M (2022) Chronic PPARγ Stimulation Shifts Amyloidosis to Higher Fibrillarity but Improves Cognition. Front. Aging Neurosci. 14:854031. doi: 10.3389/fnagi.2022.854031

INTRODUCTION

Alzheimer's disease (AD) has become the most common cause of dementia, and is imposing a significant burden on health care systems of societies with aging populations (Ziegler-Graham et al., 2008). During the past few decades, research on AD pathogenesis led to the formulation of a model that accumulation of amyloid beta (Aβ)-plaques and neurofibrillary tangles, the histologically characterizing hallmarks of AD (Braak and Braak, 1991), triggers a cascade of neurodegenerative events, leading to disease progression (Sasaguri et al., 2017). Additionally, novel emerging evidence indicates that neuroinflammation plays an important role in pathogenesis and progression of AD and many other neurodegenerative diseases (Zimmer et al., 2014; Heneka et al., 2015). In AD, activated microglial cells are able to bind and phagocytize soluble Aβ, and to some degree also the fibrillary Aβ aggregates, as part of the increased inflammatory response (Heneka et al., 2015). However, others report that Aβ-recognition receptors on microglia downregulate during the progression of AD, such that microglial cells eventually undergo senescence, characterized by reduced phagocytosis of Aβ-aggregates (Hickman et al., 2008). With time, the decreased microglial activity is permissive to expansion of fibrillar amyloidosis (Heppner et al., 2015; Blume et al., 2018) and a high proportion of dystrophic microglia were observed in human AD brain *post mortem* (Streit et al., 2014). These observations have led some to speculate that the microglial response is overwhelmed by the massive Aβ-deposition occurring in advanced AD, such that their chronic activation has a detrimental impact on disease progression (Hickman et al., 2008; Lee and Landreth, 2010).

It might follow that treatment with anti-inflammatory drugs should alleviate AD progression. Pioglitazone is an anti-inflammatory insulin sensitizer widely used to treat hyperglycemia in type 2 diabetes *via* activation of peroxisome proliferator-activated receptor gamma (PPAR-γ). Treatment with pioglitazone enables microglial cells to undergo a phenotypic conversion from a pro-inflammatory toward an anti-inflammatory and neuroprotective phenotype (Mandrekar-Colucci et al., 2012; Yamanaka et al., 2012). Furthermore, activation of PPAR-γ in the brains of AD mice initiate a coupled metabolic cycle with the Liver X Receptor to increase brain apolipoprotein E levels, which promotes the ability of microglial cells to phagocyte and degrade both soluble and fibrillary Aβ (Mandrekar-Colucci et al., 2012; Yamanaka et al., 2012). However, another study showed that only low-dose PPAR-γ agonist treatment, but not the conventional doses, promotes an Aβ-clearing effect by increasing (LDL Receptor Related Protein 1 (LRP1) in human brain microvascular endothelial cells (HBMECs) (Moon et al., 2012). Despite this compelling preclinical evidence, a meta-analysis encompassing nine clinical studies did not compelling support a beneficial effect of PPAR-γ agonist treatment on cognition and memory in in patients with mild-to-moderate AD (Cheng et al., 2016). Furthermore, a phase III trial of pioglitazone in patients with mild AD was discontinued due to lacking efficacy (Geldmacher et al., 2011). It remains a conundrum why the translation of PPARγ stimulation into human AD failed, which calls for further investigation to uncover the basis of the seemingly false lead. Conceivably, the efficacy of pioglitazone may be confined to a specific stage of AD, or in cases distinguished by a particular biomarker.

Given this background, we hypothesized that Aβ-load and composition would determine the individual efficacy of PPARγ stimulation effect in the progression of AD mouse models. Therefore, we undertook serial small animal positron emission tomography (μPET) with the Aβ-tracer [^{18}F]florbetaben (Manook et al., 2012; Rominger et al., 2013; Brendel et al., 2015a,b) in two AD mouse models with distinct Aβ-plaque composition. The transgenic PS2APP-line develops dense fibrillary Aβ-plaques with late debit whereas the knock-In mouse model App^{NL-G-F} develops more diffuse oligomeric Aβ-plaques with early debut. Both strains of mice were treated with pioglitazone or vehicle for 5 months during the phase of main Aβ accumulation. We conducted behavioral assessments of spatial learning and confirmed longitudinal PET findings by immunohistochemical analysis and biochemical analysis, thus aiming to test the hypothesis that response to pioglitazone would depend on the type of Aβ-plaques formed in transgenic mice.

MATERIALS AND METHODS

Study Design

Groups of PS2APP and App^{NL-G-F} mice were randomized to either treatment (PS2APP-PIO N = 13, all female; App^{NL-G-F}-PIO N = 14, N = 10 male, N = 4 female) or vehicle (PS2APP-VEH N = 10, all female; App^{NL-G-F}-VEH N = 23 N = 9 male, N = 14 female) groups at the age of 8 (PS2APP) and 5 (App^{NL-G-F}) months. In PS2APP mice, the baseline [^{18}F]florbetaben-PET scan (Aβ-PET) was performed at the age of 8 months, followed by initiation of pioglitazone treatment or vehicle for a period of 5 months and a follow-up Aβ-PET scan at 13 months. In App^{NL-G-F} mice, the baseline Aβ-PET scan was performed at the age of 5 month, followed by initiation of pioglitazone treatment or vehicle, for a period of 5 months. Follow-up Aβ-PET scans were acquired at 7.5 and 10 months of age, which was the study termination in App^{NL-G-F} mice. Mice were fed *ad libitum* with food pellets formulated with pioglitazone at a dose of 350 mg/kg or unaltered control pellets. The food was available to the mice without restriction.

For all mice, behavioral testing after the terminal PET scan was followed by immunohistochemical and biochemical analyses of randomized hemispheres. The TSPO-PET arm of the study and detailed analyses of neuroinflammation imaging are reported in a separate manuscript focusing on the predictive value of TSPO-PET for outcome of PPARγ-related immunomodulation (Biechele et al., 2022). The sample size estimation of the *in vivo* PET study was based on previous experience and calculated by G*power (V3.1.9.2, Kiel, Germany), assuming a type I error $\alpha = 0.05$ and a power of 0.8 for group comparisons, a 10% drop-out rate per time-point (including TSPO-PET), and a treatment effect of 5% change in the PET signal. Shared datapoints between the study arms are indicated.

Animals

PS2APP transgenic (Ozmen et al., 2008), App^{NL-G-F} APP knock-in (Saito et al., 2014) and wild-type C57Bl/6 mice were used in this investigation (for details see **Supplementary Material**). All experiments were performed in compliance with the National Guidelines for Animal Protection, Germany, with approval of the local animal care committee of the Government of Oberbayern (Regierung Oberbayern) and overseen by a veterinarian. The experiments complied with the ARRIVE guidelines and were carried out in accordance with the U.K. Animals (Scientific Procedures) Act, 1986 and associated guidelines, EU Directive 2010/63/EU for animal experiments. Animals were housed in a temperature and humidity-controlled environment with a 12-h light–dark cycle, with free access to food (Ssniff) and water.

Aβ-PET Acquisition and Reconstruction

[^{18}F]florbetaben radiosynthesis was performed as previously described (Rominger et al., 2013). This procedure yielded a radiochemical purity exceeding 98% and a specific activity of 80 ± 20 GBq/μmol at the end of synthesis. Mice were anesthetized with isoflurane (1.5%, delivered *via* a mask at 3.5 L/min in oxygen) and received a bolus injection [^{18}F]florbetaben 12 ± 2 MBq in 150 μL of saline to a tail vein. Following placement in the tomograph (Siemens Inveon DPET), a single frame emission recording for the interval 30–60 min p.i., which was preceded by a 15-min transmission scan obtained using a rotating [^{57}Co] point source. The image reconstruction procedure consisted of three-dimensional ordered subset expectation maximization (OSEM) with four iterations and twelve subsets followed by a maximum *a posteriori* (MAP) algorithm with 32 iterations. Scatter and attenuation correction were performed and a decay correction for [^{18}F] was applied. With a zoom factor of 1.0 and a 128 × 128 × 159 matrix, a final voxel dimension of 0.78 × 0.78 × 0.80 mm was obtained.

Small-Animal PET Data Analyses

Volumes of interest (VOIs) were defined on the MRI mouse atlas (Dorr et al., 2007). A forebrain target VOI (15 mm^3) was used for group comparisons and an additional hippocampal target VOI (8 mm^3) served for correlation analysis with spatial learning. We calculated [^{18}F]florbetaben standard-uptake-value ratios (SUVRs) using the established white matter (PS2APP; 67 mm^3; pons, midbrain, hindbrain and parts of the subcortical white matter) and periaqueductal gray (App^{NL-G-F}; 20 mm^3) reference regions (Brendel et al., 2016; Overhoff et al., 2016; Sacher et al., 2019).

Water Maze

Two different water maze tasks were applied due to changing facilities between the investigations of PS2APP and App^{NL-G-F} cohorts. We used a principal component analysis of the common read outs of each water maze task to generate a robust index for correlation analyses in individual mice (Biechele et al., 2020). The principal component of the water maze test was extracted from three spatial learning read-outs (PS2APP: escape latency, distance, platform choice; App^{NL-G-F}: escape latency, frequency to platform, time spent in platform quadrant). Thus, one quantitative index of water maze performance per mouse was generated for correlation with PET imaging readouts. The experimenter was blind to the phenotype of the animals.

Water Maze in PS2APP Mice

PS2APP and age-matched wild-type mice were subjected to a modified Morris water maze task as described previously (Sauvage et al., 2000; Busche et al., 2015; Keskin et al., 2017; Focke et al., 2019) yielding escape latency, distance to the correct platform and correct choice of the platform as read-outs.

Water Maze in App^{NL-G-F} Mice

App^{NL-G-F} mice (treated and vehicle) and 14 age- and sex-matched wild-type mice (vehicle) underwent a classical Morris water maze test, which was performed according to a standard protocol with small adjustments (Bromley-Brits et al., 2011) as previously described (Sacher et al., 2019). Details are provided in the **Supplementary Material**.

Immunohistochemistry

Immunohistochemistry in brain regions corresponding to PET analyses was performed for fibrillary as well as pre-fibrillary Aβ, microglia and synaptic density as previously published (Dorostkar et al., 2010; Brendel et al., 2017a,b). We obtained immunofluorescence labeling of pre-fibrillary Aβ using NAB228 (Thermo Fisher Scientific, Waltham, Massachusetts, United States) with a dilution of 1:500 (Monasor et al., 2020). For histological staining against fibrillar Aβ, we used methoxy-X04 (TOCRIS, Bristol, United Kingdom) at a dilution of 0.01 mg/ml in the same slice as for NAB228 staining. We obtained immunofluorescence labeling of microglia using an Iba-1 antibody (Wako, Richmond, United States) with a dilution of 1:200 co-stained with CD68 (BioRad, Hercules, CA, United States) with a dilution of 1:100. The synaptic density was measured using an anti-vesicular glutamate transporter 1 (VGLUT1) primary antibody (1:500, MerckMillipore, Billerica, Massachusetts, United States). Quantification was calculated as area-%. Details are provided in the **Supplementary Material**.

Biochemical Characterization of Brain Tissue

DEA (0.2% Diethylamine in 50 mM NaCl, pH 10) and RIPA lysates (20 mM Tris-HCl (pH 7.5), 150 mM NaCl, 1 mM Na2EDTA, 1% NP-40, 1% sodium deoxycholate, 2.5 mM sodium pyrophosphate) were prepared from brain hemispheres. The later was centrifuged at 14,000 g (60 min at 4°C) and the remaining pellet was homogenized in 70% formic acid (FA fraction). The FA fraction was neutralized with 20 × 1 M Tris-HCl buffer at pH 9.5 and used further diluted for Aβ analysis. Aβ contained in FA fractions was quantified by a sandwich immunoassay using the Meso Scale Aβ Triplex plates and Discovery SECTOR Imager 2400 as described previously (Page et al., 2008). Samples were measured in triplicates.

Statistics

The principal component of the water maze test was extracted using SPSS 26 statistics (IBM Deutschland GmbH, Ehningen,

Germany). Prior to the PCA, the linear relationship of the data was tested by a correlation matrix and items with a correlation coefficient < 0.3 were discarded. The Kaiser-Meyer-Olkin (KMO) measure and Bartlett's test of sphericity were used to test for sampling adequacy and suitability for data reduction. Components with an Eigenvalue >1.0 were extracted and a varimax rotation was selected. Water maze results were also used as an endpoint in the dedicated manuscript on serial TSPO-PET in both cohorts (Biechele et al., 2022). For immunohistochemistry quantifications GraphPad Prism (GraphPad Software, San Diego, California, United States) was used. All analyses were performed by an operator blinded to the experimental conditions. Data were normally distributed according to Shapiro−Wilk or D'Agostino-Pearson test. One-way analysis of variance (ANOVA) including Bonferroni *post-hoc* correction was used for group comparisons >2 subgroups. For assessment of inter-group differences at single time points, Student's *t*-test (unpaired, two-sided) was applied. All results are presented as mean ± SEM. *P*-values <0.05 are defined as statistically significant.

RESULTS

Long-Term Pioglitazone Treatment Provokes a Significant Increase of the Aβ-PET Signal in PS2APP Mice

First, we analyzed serial changes of fibrillar amyloidosis under chronic pioglitazone treatment by [^{18}F]florbetaben Aβ-PET in PS2APP mice and wild-type controls. Vehicle treated PS2APP mice showed an elevated Aβ-PET SUVR when compared to vehicle treated wild-type at 8 (+20.4%, $p < 0.0001$) and 13 months of age (+37.9%, $p < 0.0001$). As expected, the Aβ-PET SUVR of wild-type mice did not change between 8 and 13 months of age (0.831 ± 0.003 vs. 0.827 ± 0.008: $p = 0.645$). Surprisingly, pioglitazone treatment provoked a stronger longitudinal increase in the Aβ-PET signal of PS2APP mice (+21.4%) when compared to vehicle treated PS2APP mice (+14.1%, $p = 0.002$). At the follow-up time point, the Aβ-PET SUVR was significantly elevated when compared to untreated PS2APP mice (**Figure 1**; 1.140 ± 0.014 vs. 1.187 ± 0.011; $p = 0.0017$). Pioglitazone treatment in wild-type mice provoked no changes of Aβ-PET SUVR compared to vehicle-treated wild-type mice at the follow-up time-point (0.827 ± 0.008 vs. 0.823 ± 0.005: $p = 0.496$; for images of wild-type mice see **Supplementary Figure 1**). Taken together, we found a significant increase in the Aβ-PET signal, which implied an increase in fibrillary Aβ-levels under pioglitazone treatment in PS2APP mice.

Aβ-PET Detects a Strong Increase of the Fibrillar Aβ-Load in *App*$^{NL-G-F}$ Mice During Chronic PPARγ Stimulation

Next, we sought to validate our unexpected findings in PS2APP mice a mouse model with differing Aβ plaque composition, namely the *App*$^{NL-G-F}$ mouse, which has limited fibrillarity due to endogenous expression of APP with three FAD mutations (Saito et al., 2014). Strikingly, the effect of pioglitazone treatment on the Aβ-PET signal was even stronger in *App*$^{NL-G-F}$ mice than in PS2APP mice. There was a pronounced increase of the Aβ-PET signal during chronic pioglitazone treatment (+17.2%) compared to vehicle (+5.3%, $p < 0.0001$). *App*$^{NL-G-F}$ mice with pioglitazone treatment had a higher Aβ-PET SUVR at 7.5 (+4.6%, $p = 0.0071$) and 10 (+7.7%, $p < 0.0001$) months of age when compared to vehicle-treated *App*$^{NL-G-F}$ mice (**Figure 2**). The baseline level of Aβ-PET SUVR was non-significantly lower in treated compared to untreated *App*$^{NL-G-F}$ mice (0.878 ± 0.010 vs. 0.906 ± 0.006, $p = 0.1350$). In both mouse models, the Aβ-signal increase after pioglitazone-treatment compared to baseline scans was pronounced in the frontotemporal cortex and hippocampal area (**Figures 1A**, **2A**). In summary, the pioglitazone treatment augmented the Aβ-PET signal increase in both mouse models; this unexpected result was more pronounced in the *App*$^{NL-G-F}$ model, which expresses less fibrillary Aβ plaques.

Pioglitazone Triggers A Shift Toward Increased Aβ-Plaque Fibrillarity in Two Distinct Mouse Models of Amyloidosis

Given the unexpected *in vivo* findings, we set about to evaluate the molecular correlates of the potentiation of Aβ-PET signal during pioglitazone treatment in AD model mice. The (immuno)histochemical analysis showed that the observed increase of the Aβ-PET signal was predominantly explicable by a change in plaque composition rather than by a change in plaque density (**Figure 3**). In both mouse models, the proportion of fibrillary Aβ stained with methoxy-X04 increased significantly under pioglitazone treatment compared to vehicle treated animals (PS2APP: 29.6 ± 3.5% vs. 15.2 ± 0.7%, $p = 0.0056$, **Figure 3C**; *App*$^{NL-G-F}$: 9.1 ± 1.6% vs. 4.4 ± 0.4%, $p = 0.0001$, **Figure 3D**). Pioglitazone treatment had no significant effect on the proportion of pre-fibrillary Aβ stained with NAB228 in PS2APP mice (PS2APP: 65.4 ± 6.1% vs. 67.0 ± 6.9%, $p = 0.865$, **Figure 3C**). In *App*$^{NL-G-F}$ mice, however, the proportion of pre-fibrillary Aβ decreased significantly in treated animals (*App*$^{NL-G-F}$: 26.7 ± 1.7% vs. 34.5 ± 1.7%, $p = 0.0138$, **Figure 3E**). The effect size of pioglitazone treatment on plaque morphology was larger in *App*$^{NL-G-F}$ mice than in PS2APP mice, which was reflected by a significantly increased overlay of methoxy-X04 and NAB228 positive plaques proportions in relation to untreated mice (PS2APP: 40.4 ± 3.6% vs. 25.1 ± 2.1%, $p = 0.0075$, **Figure 3C**; *App*$^{NL-G-F}$: 35.0 ± 3.4% vs. 12.9 ± 1.3%, $p = 0.0005$, **Figure 3E**). We attribute this effect to the generally diffuse nature of the plaque composition of *App*$^{NL-G-F}$ mice, which predominantly contain high oligomeric and low fibrillary fractions of Aβ (Monasor et al., 2020) (compare **Figures 3A,B**).

The number of methoxy positive Aβ-plaques were similar between vehicle and pioglitazone treated groups for PS2APP (1,016 ± 107 vs. 1,118 ± 121, $p = 0.547$, **Figure 3D**) and *App*$^{NL-G-F}$ mice (242 ± 56 vs. 266 ± 33, $p = 0.722$, **Figure 3F**). Notably there was no significant effect of chronic pioglitazone treatment on the different insoluble Aβ species (Aβ40, Aβ42) as well as on the level of the soluble Aβ42-isoform observed in

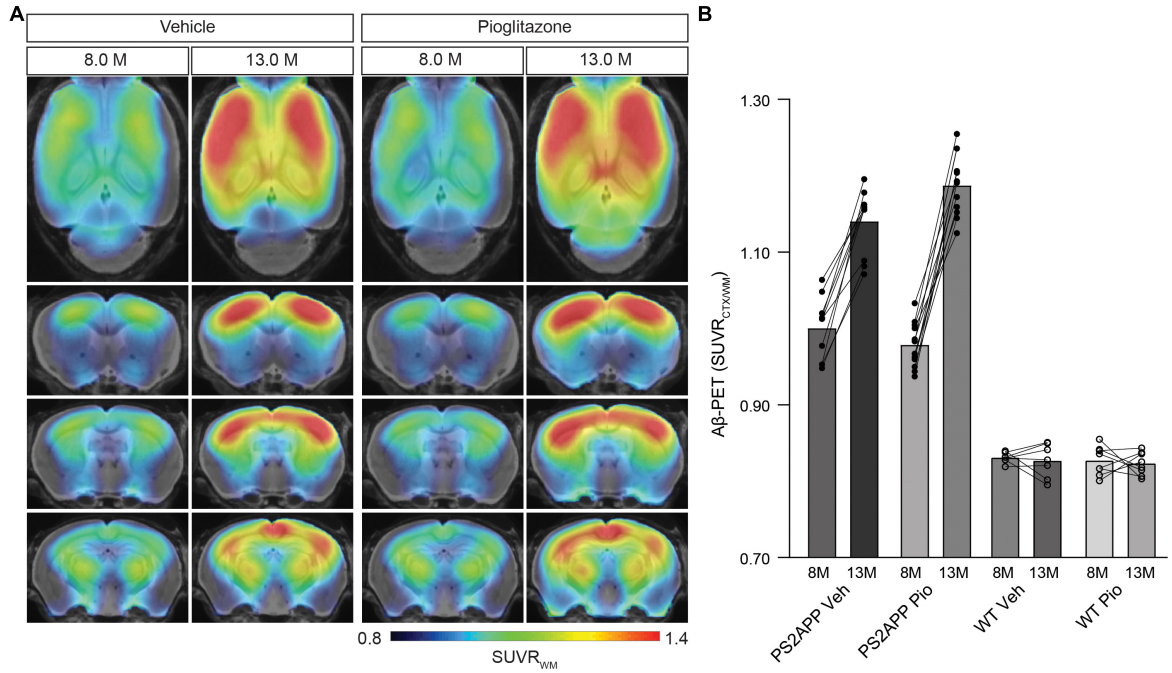

FIGURE 1 | PPARγ stimulation in PS2APP mice provokes an increase in the Aβ-PET signal. **(A)** Regional analysis of group-averaged standardized uptake value ratio (SUVR) images of the Aβ-PET radiotracer [^{18}F]florbetaben in untreated and in pioglitazone-treated PS2APP mice aged 8 and 13 months. Coronal and axial slices are projected upon a standard MRI template. **(B)** Plots show cortical SUVR values of [^{18}F]florbetaben in PS2APP and wild-type (WT) mice between 8 and 13 months of age under vehicle (Veh) or pioglitazone (Pio) treatment. The Aβ-PET signal increased in PS2APP mice during aging, but the increase was more pronounced in pioglitazone treated mice [$F_{(1,\ 12)}$ = 12.9; p = 0.0017]. In wild-type animals, no difference was observed between untreated and treated animals during aging [$F_{(1,\ 13)}$ = 0.490; p = 0.496]. Data are presented as mean ± SEM. P values of Bonferroni *post-hoc* test result from two-way ANOVA. N = 10–13 PS2APP; N = 7–8 WT. PET images of wild-type mice are provided in **Supplementary Figure 1**.

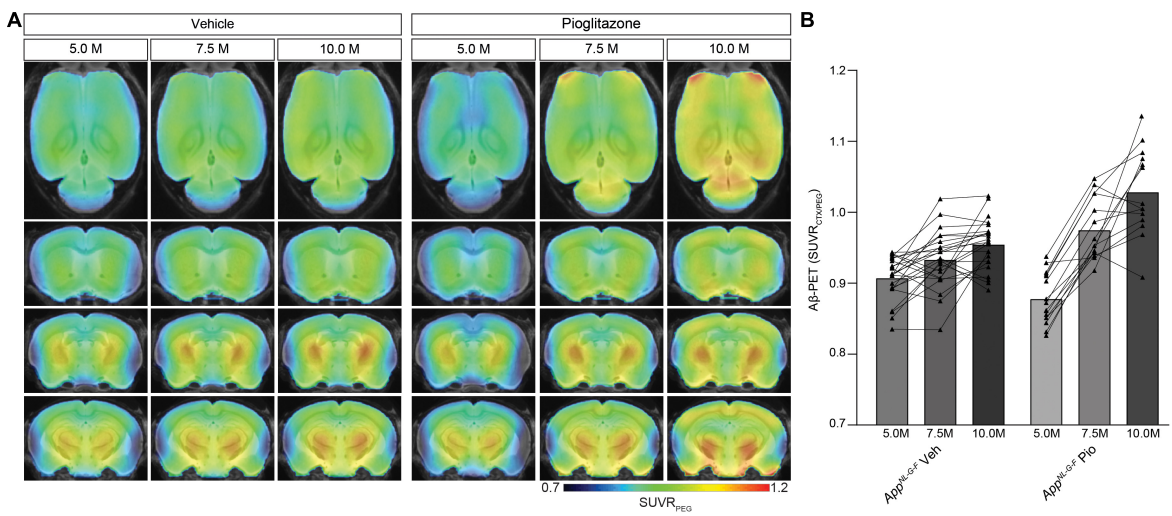

FIGURE 2 | Distinct Aβ-PET signal increase upon PPARγ stimulation in *App*$^{NL-G-F}$ mice with limited plaque fibrillarity and without overexpression of APP. **(A)** Regional analysis of group-averaged standardized uptake value ratios (SUVR) of the Aβ-PET radiotracer [^{18}F]florbetaben in untreated and in pioglitazone treated *App*$^{NL-G-F}$ animals at the age of 5, 7.5, and 10 months. Coronal and axial slices are projected upon a standard MRI template. **(B)** Plots show cortical SUVR of [^{18}F]florbetaben in *App*$^{NL-G-F}$ mice between the age of 5 and 10 months under vehicle or pioglitazone treatment. Aβ-PET signal increased in untreated mice during age but the increase was more pronounced in pioglitazone treated *App*$^{NL-G-F}$ mice [$F_{(2,\ 70)}$ = 20.12; p < 0.0001]. Data are presented as mean ± SEM. P-values of Bonferroni *post-hoc* test result from two-way ANOVA. N = 14–23.

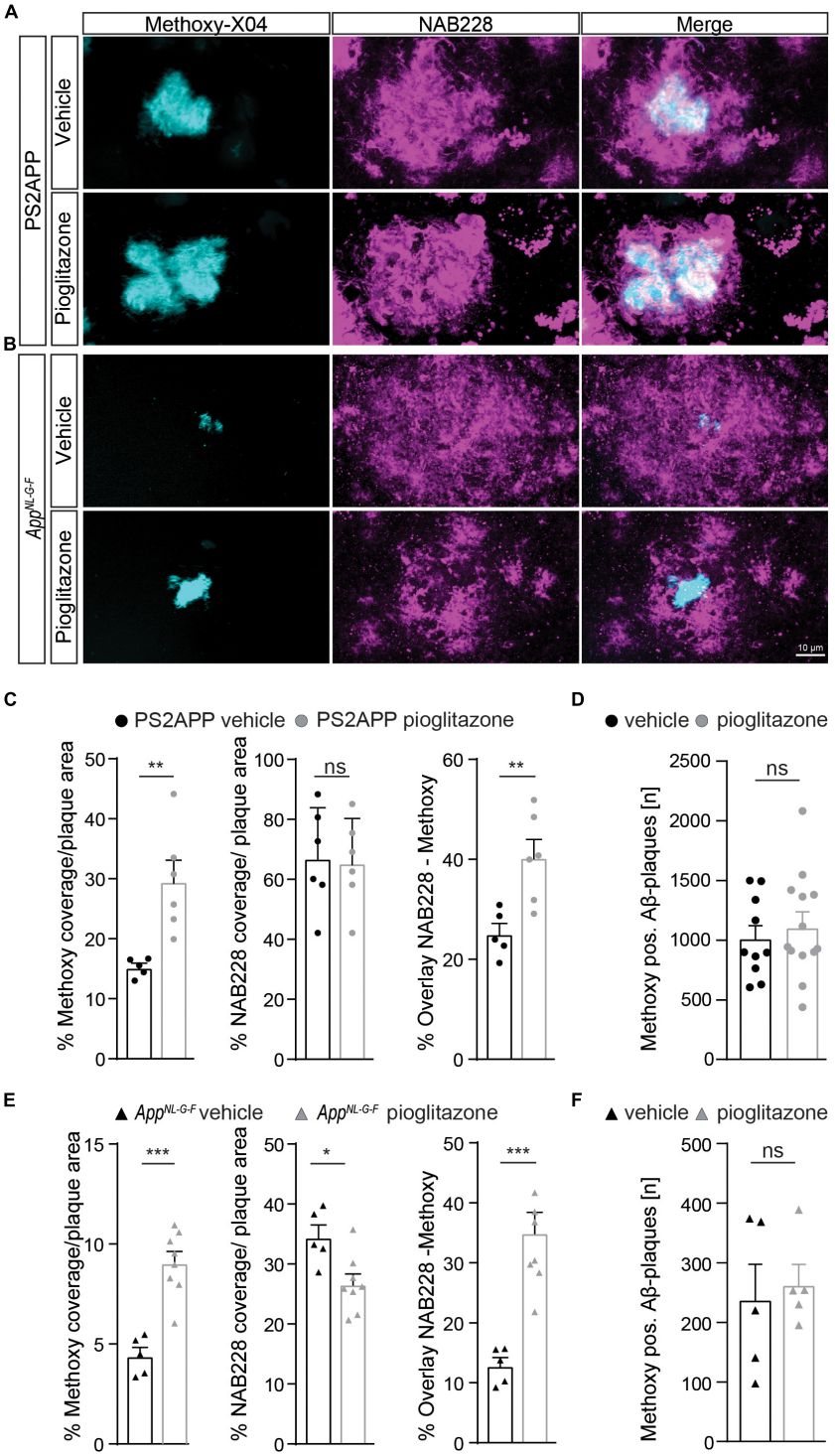

FIGURE 3 | Pioglitazone treatment triggers a change in plaque composition in two different mouse models of amyloidosis. Staining of fibrillary Aβ (methoxy-X04, cyan) and pre-fibrillary Aβ (NAB228, magenta) in vehicle and pioglitazone treated PS2APP mice **(A)** and App^{NL-G-F} mice **(B)**. **(C)** The plaque area covered by methoxy-X04 staining was significantly higher [$t_{(9)} = 3.612$; $p = 0.0056$], whereas the plaque area covered by NAB228 staining remained equal [$t_{(10)} = 0.175$; $p = 0.865$] in pioglitazone treated PS2APP mice. The overlay of NAB228 and methoxy staining increased under pioglitazone treatment [$t_{(9)} = 3.432$; $p = 0.0075$]. **(D)** The number of methoxy positive Aβ-plaques did not change under pioglitazone treatment in PS2APP-mice. **(E)** In App^{NL-G-F} mice, methoxy coverage [$t_{(11)} = 5.802$; $p = 0.0001$], NAB228 coverage [$t_{(11)} = 5.80$; $p = 0.0001$], as well as the overlay of both staining [$t_{(11)} = 2.93$; $p = 0.0138$], increased under pioglitazone treatment. **(F)** In App^{NL-G-F} mice, the number of methoxy positive Aβ-plaques did not change under pioglitazone. Data are presented as mean ± SEM; $n = 5$–13 mice. Two-sample student's *t*-test results: $^{*}p < 0.05$; $^{**}p < 0.01$; $^{***}p < 0.001$.

either mouse model (**Supplementary Figure 2**). Taken together, our results indicate that the potentiated increase of the Aβ-PET signal upon pioglitazone treatment reflected a change in plaque composition from less dense pre-fibrillar amyloid aggregates to fibrillary Aβ-fractions.

Microglial Activation Is Reduced Upon PPARγ Stimulation in Both Alzheimer's Disease Mouse Models

To confirm changes in the activation state of microglial cells, we performed Iba1 as well as CD68 immunohistochemical staining of activated microglia in both mouse models. We observed that pioglitazone treatment significantly decreased microglial activation in both mouse models (**Figure 4**). In PS2APP mice, PPARγ stimulation provoked a one-third reduction of area coverage of Iba1-positive microglial cells (area: 9.1 ± 0.6%) compared to untreated mice (14.0 ± 0.5%, p = 0.0003), and also a significant reduction of CD68-positive microglial cells area (7.6 ± 0.4% vs. 9.9 ± 0.3%, p = 0.0018). In pioglitazone treated App^{NL-G-F} mice, the area reduction was less pronounced, but still significant for Iba1-positive microglial cells (9.4 ± 0.2% vs. 10.6 ± 0.2%, p = 0.0015) and CD68-positive microglial cells (2.7 ± 0.1% vs. 3.0 ± 0.1%, p = 0.0141) compared to untreated mice. Thus, we observed a consistent net reduction of activated microglial coverage in both models; the lesser effect in App^{NL-G-F} mice might indicate partial compensation by triggering of microglial activation due to increased fibrillary Aβ levels (Sebastian et al., 2020).

Cognitive Function Is Improved by Chronic Pioglitazone Treatment in Association With an Increasing Aβ-PET Rate of Change

Finally, we aimed to elucidate whether the observed longitudinal changes in the composition of Aβ-plaques affected synaptic density and hippocampus related cognitive performance.

In PS2APP mice, treatment with pioglitazone resulted in a significant reduction of the water maze performance index compared to untreated mice during the probe trial (**Figure 5A**; p = 0.0155), whereas in wild-type animals there was no difference between treated and untreated animals ($p > 0.999$). The water maze performance index of pioglitazone treated PS2APP mice correlated strongly with the rate of increase in Aβ-PET signal (**Figure 5C**; R = 0.686; p = 0.0097). In App^{NL-G-F} mice, pioglitazone treatment did not result in a significant change of spatial learning performance (**Figure 5B**; $p > 0.999$). Accordingly, the water maze performance index and the rate of change in the Aβ-PET signal of pioglitazone treated App^{NL-G-F} mice did not correlate significantly (**Figure 5D**; R = 0.341; p = 0.254). There was no significant association between the water maze performance index and the Aβ-PET rate of change in vehicle treated PS2APP or App^{NL-G-F} mice.

To explore the basis of water maze results in PS2APP mice at the molecular level, we performed staining of synaptic density in the hippocampus. Aβ-oligomers are the primary neurotoxic forms of Aβ, while Aβ-fibrils have less neurotoxicity (Hardy and Selkoe, 2002; Haass and Selkoe, 2007; Zott et al., 2019). Thus, we hypothesized that pre-synaptic density in the hippocampal CA1-Area would be rescued upon pioglitazone-treatment. In wild-type mice we did not observe altered changed VGLUT1 density under pioglitazone treatment (**Figure 5E**, F; 0.519 ± 0.007 1/μm vs. 0.502 ± 0.008 1/μm, p = 0.810). In PS2APP mice, however, we found that pioglitazone treatment significantly rescued spine density in the CA1-region of the hippocampus compared to untreated animals (**Figures 5E,F**; 0.497 ± 0.006 1/μm vs. 0.459 ± 0.007 1/μm, p = 0.0012), supporting the hippocampal-dependent water maze results.

DISCUSSION

To our knowledge, this is the first large-scale longitudinal PET study of cerebral Aβ-deposition in two distinct AD mouse models treated with the PPARγ agonist pioglitazone. We combined *in vivo* PET monitoring with behavioral testing and detailed immunohistochemical analysis. Our main finding was an unexpected potentiation in both mouse models of the increasing Aβ-PET signal during 5 months of pioglitazone treatment. This increase occurred despite an improvement of spatial learning and prevention of synaptic loss in the PS2APP mice. Immunohistochemistry revealed a shift toward plaque composition of higher fibrillarity as the molecular correlate of the Aβ-PET signal in both mouse models. In PS2APP mice this increase was directly associated with improved cognitive performance, whereas in App^{NL-G-F} mice such an effect was not observed.

Aβ-PET enables longitudinal *in vivo* detection of Aβ-plaques, which plays an important role in AD diagnosis, monitoring disease progression, and as an endpoint for therapeutic treatment effects (Valotassiou et al., 2018). In our preceding observational and interventional studies, we validated in AD model mice the clinically established Aβ-PET tracer [^{18}F]florbetaben relative to histologically defined indices Aβ deposition (Brendel et al., 2015a,b). So far, an enhanced or increasing [^{18}F]florbetaben-PET signal has been interpreted as an indicator of disease progression or treatment failure (Laforce et al., 2018). Unexpectedly, we found that pioglitazone potentiated the increasing Aβ-PET signal in two mouse models compared to vehicle controls; in both cases, this increase was due to a shift of the plaque composition toward higher fibrillarity, and away from the more neurotoxic oligomeric form. However, ELISA measurements of plaque associated fibrillary Aβ extracted with formic acid did not indicate a change in the Aβ species composition in brain. This suggests that Aβ-PET imaging and immunohistochemical analysis detect treatment effects on Aβ-plaque composition that do not arise from a shift in the levels of Aβ species, and which may thus evade detection in studies of CSF or plasma content (Hansson et al., 2018).

Furthermore, our study provides evidence that rescued spatial learning deficits and prevented hippocampal synaptic loss can occur despite an increasing Aβ-PET signal upon immunomodulation. The combined results might sound contradictory, but according to the amyloid cascade hypothesis,

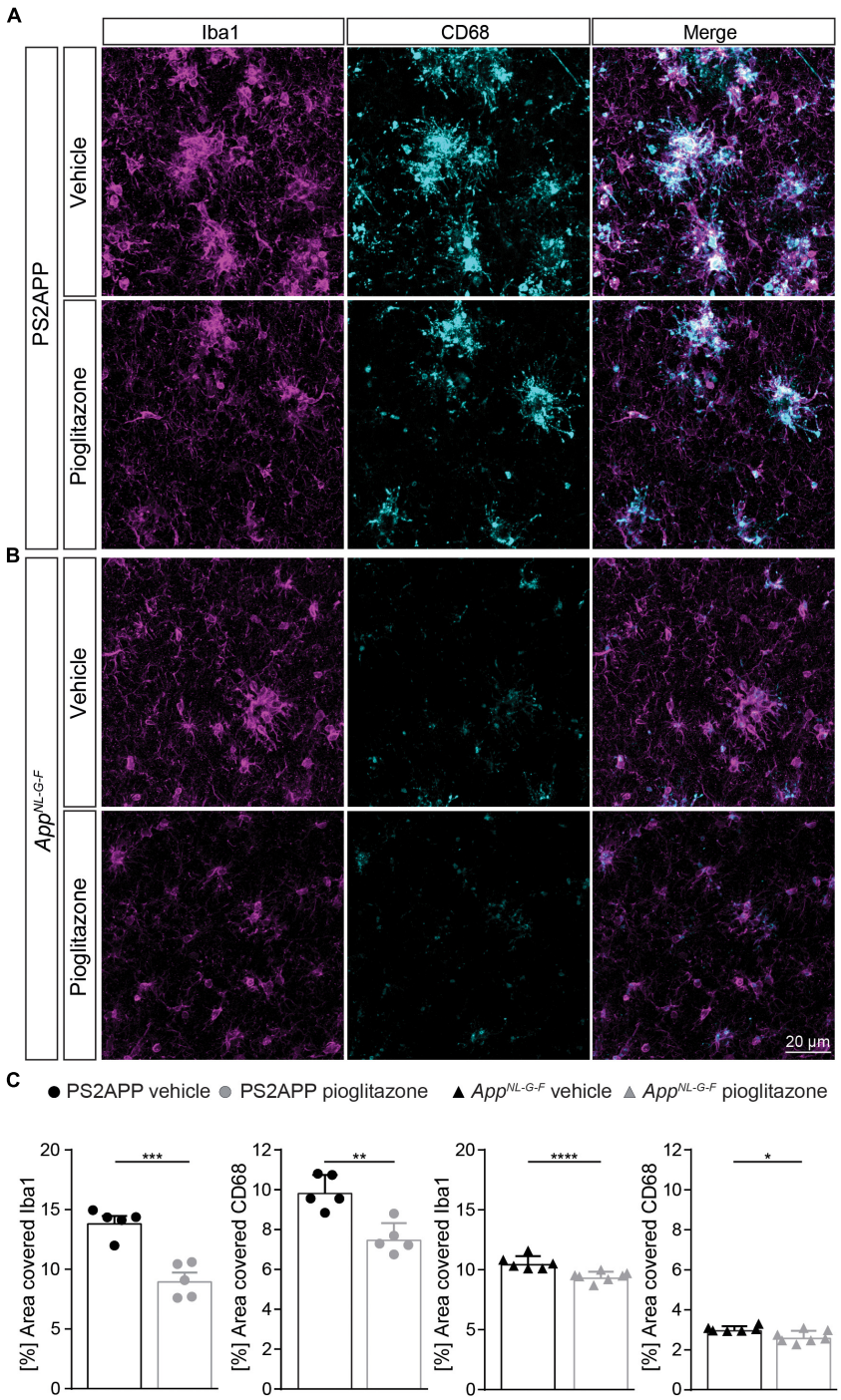

FIGURE 4 | Pioglitazone treatment reduces microglial activation in both AD mouse models. Iba1- (magenta) as well as CD68-(cyan) positive microglial cells in PS2APP **(A)** and App^{NL-G-F} mice **(B)**. **(C)** The area of Iba1 positive microglial cells [$t_{(8)} = 5.95$; $p = 0.0003$] as well as CD68 positive microglial cells [$t_{(8)} = 4.58$; $p = 0.0018$] decreased in treated PS2APP mice. The same effect was observed in App^{NL-G-F} mice were the area covered by Iba1 positive [$t_{(11)} = 4.21$; $p = 0.0015$] as well as CD68 positive microglial cells [$t_{(11)} = 2.91$; $p = 0.014$] were significantly reduced in treated compared to untreated mice. Data are presented as mean ± SEM; $n = 5–7$ mice. Two-sample student's t-test results: $^{*}p < 0.05$; $^{**}p < 0.01$; $^{****}p < 0.0001$.

Aβ-oligomers rather than Aβ-fibrils are the neurotoxic Aβ-forms (Haass and Selkoe, 2007; Selkoe and Hardy, 2016). Indeed, high concentrations of Aβ-oligomers isolated from brain of AD patients correlated significantly with the degree of cognitive impairment prior to death (Lue et al., 1999; McLean et al., 1999; Wang et al., 1999). Furthermore, Aβ-oligomers have been shown

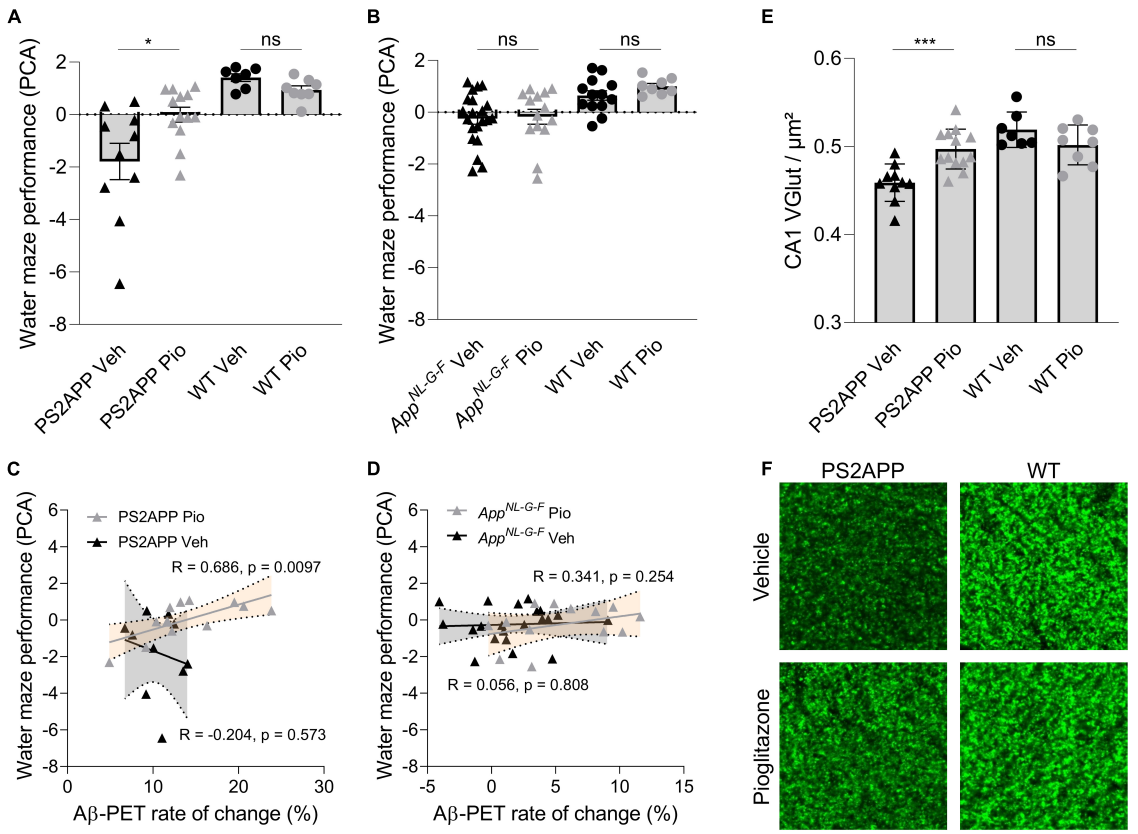

FIGURE 5 | Improved spatial learning correlates with an increased Aβ-PET rate of change in PS2APP mice. **(A)** One-way ANOVA revealed a significant difference of the water maze performance index between pioglitazone treated and untreated PS2APP and wild-type groups [$F_{(3,\ 34)} = 10.37$; $p < 0.0001$; $N = 7$–13]. Group-wise comparisons revealed that pioglitazone treated PS2APP mice achieved a higher performance index in the water maze test compared to untreated PS2APP mice ($p = 0.016$), whereas wild-type animals showed no significant difference between treatment groups ($p > 0.999$). **(B)** One-way ANOVA revealed a significant difference of the water maze performance index between pioglitazone treated and untreated $App^{NL\text{-}G\text{-}F}$ and WT groups [$F_{(3,\ 34)} = 5.825$; $p = 0.0016$]. However, pioglitazone treated $App^{NL\text{-}G\text{-}F}$ mice showed no difference in the water maze performance index when compared to untreated $App^{NL\text{-}G\text{-}F}$ mice ($p > 0.999$) and wild-type animals again showed no significant difference between treatment groups ($p > 0.999$). Scatter plots show correlations between the Aβ-PET rate of change ([^{18}F]florbetaben; ΔSUVR) during the treatment period and individual cognitive testing scores in **(C)** PS2APP mice and in **(D)** $App^{NL\text{-}G\text{-}F}$ mice (R indicates Pearson's coefficient of correlation) **(E)** The decrease in synaptic density in the hippocampal CA1-region as assessed by VGLUT1 staining was ameliorated in treated PS2APP mice when compared to untreated mice ($p = 0.0012$), whereas no such treatment effect was seen in wild-type animals [$p = 0.810$; group effect: $F_{(3,\ 34)} = 12.03$; $p < 0.0001$; $N = 7$–13]. **(F)** VGLUT1 staining in the hippocampal CA1-region of representative untreated and treated PS2APP mice (left column) as well as of representative untreated and treated wild-type (WT) mice (right column). Statistics of group wise comparisons derive from one-way ANOVA with Bonferroni *post-hoc* correction: $^{*}p < 0.05$; $^{***}p < 0.005$. Data are presented as mean ± SEM.

to disrupt long-term potentiation at synapses and provoke long-term depression (Cullen et al., 1997; Hu et al., 2008; Klyubin et al., 2014). Thus, improved spatial learning and rescued synaptic density could reflect a therapeutically induced shift of Aβ to hypercondensed plaques, in keeping with observations of greater neuritic damage in association with more diffuse plaques (Ulrich et al., 2014; Wang et al., 2016). Furthermore, strongly in line with our present data, a recent study argued that microglia promoted formation of dense-core plaques may play a protective role in AD (Huang et al., 2021).

The shift in plaque composition was more pronounced in App^{NL-G-F} mice than in the PS2APP model. Due to the expression of the Arctic mutation (Saito et al., 2014), the Aβ-deposits of the App^{NL-G-F} line consist predominantly of Aβ-oligomers (Sacher et al., 2019; Monasor et al., 2020). However, we observed no improvement in cognition in the APP knock-in mouse line after pioglitazone treatment. We attribute the lacking improvement of spatial learning to the minor deterioration of this model in water maze assessment at 10 months of age (Masuda et al., 2016; Sacher et al., 2019). Our present observation stand in contrast with previous studies showing that PPAR-γ agonists reduced Aβ-plaque formation by increasing Aβ-clearance (Camacho et al., 2004; Mandrekar-Colucci et al., 2012; Yamanaka et al., 2012). However, those studies only performed endpoint analyses, in part after short-term treatment of 9 days (Mandrekar-Colucci et al., 2012); the current work is the first to perform longitudinal *in vivo* monitoring of Aβ-deposition over a 5-month chronic PPAR-γ treatment period. We note that the divergent results could also reflect the different markers used for immunohistochemistry

compared to our present differentiated analysis of fibrillar and less dense pre-fibrillar Aβ components. As such, the decreased NAB228-positive plaque fraction in our treated App^{NL-G-F} mice fits to the earlier reported decrease of the 6E10-positive area in APPPS1 mice (Mandrekar-Colucci et al., 2012). We note that the biochemical source of the Aβ-PET signal is still a matter of controversy, since some studies found no impact of non-fibrillar plaque components (Catafau et al., 2016) whereas others postulated a significant contribution of non-fibrillar Aβ to the Aβ-PET signal (Ikonomovic et al., 2016, 2018, 2020). Recently, we were able to show that non-fibrillar components of Aβ plaques indeed contribute to the net Aβ-PET signal (Biechele et al., 2022). Therefore, increases in the [^{18}F]florbetaben-PET signal must be precisely differentiated and interpreted with caution. Development of new PET tracers that selectively target oligomeric Aβ may realize a more precise discrimination of neurotoxic Aβ plaque manifestation (Sehlin et al., 2016; Fang et al., 2019) and its impact on disease severity.

In line with previous pioglitazone studies (Mandrekar-Colucci et al., 2012; Yamanaka et al., 2012), we observed a decrease in microglial activity (Biechele et al., 2021), thus confirming the immunomodulatory effect of the drug. Since earlier studies have shown that fibrillary Aβ-deposits activate microglial cells (Sebastian et al., 2020) which then migrate toward the fibrillar deposits (Füger et al., 2017), resulting in an increased number of activated microglial cells surrounding Aβ-plaques (Blume et al., 2018), the inactivation and migration effects could cancel each other out. Based on our findings in both AD models, we conclude that, by increasing plaque fibrillarity, the immunomodulatory effect of pioglitazone overweighs the potential triggering of activated microglia. Modulating microglial phenotype to restore their salutogenic effects may prove crucial in new therapeutic trials (Lewcock et al., 2020). In several preclinical and clinical trials, pioglitazone proved to be a promising immunomodulatory approach for treatment of AD, especially in patients with comorbid diabetes (Liu et al., 2015; Cao et al., 2018). However, a large phase III trial of pioglitazone in patients with mild AD was discontinued due to lacking efficacy (Geldmacher et al., 2011). Our data calls for monitoring of the effects of PPARγ agonists by Aβ-PET, which may help to stratify treatment responders based on their individual rates of Aβ plaque accumulation. Based on our results, we submit that personalized PPARγ agonist treatment might be effective when the patient has capacity to successfully shift toxic pre-fibrillar Aβ toward fibrillar parts of the plaque.

We note as a limitation that PPARγ receptor agonists represent a rather unspecific class of drugs since PPARγ is involved in various pathways in addition to peroxisome activation, notably including glucose metabolism and insulin sensitization [48]. Future studies should address if the observed effects on Aβ plaque composition are also present for more selective immunomodulation strategies such as NLRP3 regulators [49]. Two different water maze examinations were performed in the present study due a switch of the laboratory. Hence, although we calculated a similar water maze performance index by a PCA of the main read-outs of each examination, the obtained results and the sensitivity to detect spatial learning deficits are not comparable between both Aβ mouse models.

CONCLUSION

In conclusion, chronic pioglitazone treatment provoked a longitudinal Aβ-PET signal increase in transgenic and knock-in mice due to a shift toward hypercondensed fibrillar Aβ plaques. The increasing rate of Aβ-PET signal increase with time was accompanied by ameliorated cognitive performance and attenuated synaptic loss after pioglitazone treatment. It follows that increasing Aβ-PET signal need not always indicate a treatment failure, since it is the composition of Aβ plaques that determines their neurotoxiticy. In summary, our preclinical data indicate that a shift toward increasing fibrillar amyloidosis can be beneficial for the preservation of cognitive function and synaptic integrity.

DATA AVAILABILITY STATEMENT

The raw data supporting the conclusions of this article will be made available by the authors, without undue reservation.

ETHICS STATEMENT

The animal study was reviewed and approved by the Regierung von Oberbayern. Written informed consent was obtained from the owners for the participation of their animals in this study.

AUTHOR CONTRIBUTIONS

KB, HA, AR, PC, MW, MMD, JH, and MB conceived the study and analyzed the results. TB, MD, and MB wrote the manuscript with further input from all co-authors. MD, GB, CSc, KW, FE, CSa, and CF performed the small animal, PET experiments, and small animal PET data analyses. TB, FP, YS, KO, GK, XX, MMD, and JH performed immunohistochemistry experiments, analyses, and interpretation. F-JG and SL performed PET tracer synthesis and analyses. NF analyzed and interpreted serial PET data and contributed to their analysis. GB, BZ, KW, and HA performed spatial learning tests and interpretation. BU-S, KB, and MW supplied the study with animal models and interpreted the dedicated results. All authors contributed with intellectual content.

FUNDING

This study was supported by the FöFoLe Program of the Faculty of Medicine of the Ludwig Maximilian University, Munich (grant to MB). This work was funded by the Deutsche Forschungsgemeinschaft (DFG, German Research Foundation) to AR and MB—project numbers BR4580/1-1/RO5194/1-1. The work was supported by the Deutsche Forschungsgemeinschaft (DFG, German Research Foundation)

under Germany's Excellence Strategy within the framework of the Munich Cluster for Systems Neurology (EXC 2145 SyNergy—ID 390857198). MB was supported by the Alzheimer Forschung Initiative e.V (Grant No. 19063p).

ACKNOWLEDGMENTS

We thank Karin Bormann-Giglmaier and Rosel Oos for excellent technical assistance. Florbetaben precursor was provided by Piramal Imaging. We thank Takashi Saito and Takaomi C. Saido for providing the App^{NL-G-F} mice.

SUPPLEMENTARY MATERIAL

The Supplementary Material for this article can be found online at: https://www.frontiersin.org/articles/10.3389/fnagi.2022.854031/full#supplementary-material

REFERENCES

Biechele, G., Blume, T., Deussing, M., Zott, B., Shi, Y., Xiang, X., et al. (2021). Chronic PPARγ Stimulation Shifts Amyloidosis to Higher Fibrillarity but Improves Cognition. *bioRxiv* [Preprint]. doi: 10.1101/2021.05.30.446348

Biechele, G., Monasor, L. S., Wind, K., Blume, T., Parhizkar, S., Arzberger, T., et al. (2022). Glitter in the Darkness? Non-fibrillar β-Amyloid Plaque Components Significantly Impact the β-Amyloid PET Signal in Mouse Models of Alzheimer Disease. *J. Nucl. Med.* 63, 117–124. doi: 10.2967/jnumed.120.261858

Biechele, G., Wind, K., Blume, T., Sacher, C., Beyer, L., Eckenweber, F., et al. (2020). Microglial Activation in the Right Amygdala-Entorhinal-Hippocampal Complex is Associated with Preserved Spatial Learning in AppNL-G-F mice. *NeuroImage* 230:117707. doi: 10.1016/j.neuroimage.2020.117707

Blume, T., Focke, C., Peters, F., Deussing, M., Albert, N. L., Lindner, S., et al. (2018). Microglial response to increasing amyloid load saturates with aging: a longitudinal dual tracer *in vivo* μPET-study. *J. Neuroinflammation* 15:307. doi: 10.1186/s12974-018-1347-6

Braak, H., and Braak, E. (1991). Neuropathological stageing of Alzheimer-related changes. *Acta Neuropathol.* 82, 239–259. doi: 10.1007/BF00308809

Brendel, M., Kleinberger, G., Probst, F., Jaworska, A., Overhoff, F., Blume, T., et al. (2017b). Increase of TREM2 during Aging of an Alzheimer's Disease Mouse Model Is Paralleled by Microglial Activation and Amyloidosis. *Front. Aging Neurosci.* 9:8. doi: 10.3389/fnagi.2017.00008

Brendel, M., Focke, C., Blume, T., Peters, F., Deussing, M., Probst, F., et al. (2017a). Time Courses of Cortical Glucose Metabolism and Microglial Activity Across the Life Span of Wild-Type Mice: a PET Study. *J. Nucl. Med.* 58, 1984–1990. doi: 10.2967/jnumed.117.195107

Brendel, M., Jaworska, A., Grießinger, E., Rötzer, C., Burgold, S., Gildehaus, F. J., et al. (2015a). Cross-sectional comparison of small animal [18F]-florbetaben amyloid-PET between transgenic AD mouse models. *PLoS One* 10:e0116678. doi: 10.1371/journal.pone.0116678

Brendel, M., Jaworska, A., Herms, J., Trambauer, J., Rötzer, C., Gildehaus, F.-J., et al. (2015b). Amyloid-PET predicts inhibition of de novo plaque formation upon chronic γ-secretase modulator treatment. *Mol. Psychiatry* 20, 1179–1187. doi: 10.1038/mp.2015.74

Brendel, M., Probst, F., Jaworska, A., Overhoff, F., Korzhova, V., Albert, N. L., et al. (2016). Glial Activation and Glucose Metabolism in a Transgenic Amyloid Mouse Model: a Triple-Tracer PET Study. *J. Nucl. Med.* 57, 954–960. doi: 10.2967/jnumed.115.167858

Bromley-Brits, K., Deng, Y., and Song, W. (2011). Morris water maze test for learning and memory deficits in Alzheimer's disease model mice. *J. Vis. Exp.* 53:2920. doi: 10.3791/2920

Busche, M. A., Kekuš, M., Adelsberger, H., Noda, T., Förstl, H., Nelken, I., et al. (2015). Rescue of long-range circuit dysfunction in Alzheimer's disease models. *Nat. Neurosci.* 18, 1623–1630. doi: 10.1038/nn.4137

Camacho, I. E., Serneels, L., Spittaels, K., Merchiers, P., Dominguez, D., and De, S. B. (2004). Peroxisome-proliferator-activated receptor gamma induces a clearance mechanism for the amyloid-beta peptide. *J. Neurosci.* 24, 10908–10917. doi: 10.1523/JNEUROSCI.3987-04.2004

Cao, B., Rosenblat, J. D., Brietzke, E., Park, C., Lee, Y., Musial, N., et al. (2018). Comparative efficacy and acceptability of antidiabetic agents for Alzheimer's disease and mild cognitive impairment: a systematic review and network meta-analysis. *Diabetes Obes. Metab.* 20, 2467–2471. doi: 10.1111/dom.13373

Catafau, A. M., Bullich, S., Seibyl, J. P., Barthel, H., Ghetti, B., Leverenz, J., et al. (2016). Cerebellar Amyloid-β Plaques: how Frequent Are They, and Do They Influence 18F-Florbetaben SUV Ratios? *J. Nucl. Med.* 57, 1740–1745. doi: 10.2967/jnumed.115.171652

Cheng, H., Shang, Y., Jiang, L., Shi, T., and Wang, L. (2016). The peroxisome proliferators activated receptor-gamma agonists as therapeutics for the treatment of Alzheimer's disease and mild-to-moderate Alzheimer's disease: a meta-analysis. *Int. J. Neurosci.* 126, 299–307. doi: 10.3109/00207454.2015.1015722

Cullen, W. K., Suh, Y. H., Anwyl, R., and Rowan, M. J. (1997). Block of LTP in rat hippocampus *in vivo* by beta-amyloid precursor protein fragments. *Neuroreport* 8, 3213–3217. doi: 10.1097/00001756-199710200-00006

Dorostkar, M. M., Dreosti, E., Odermatt, B., and Lagnado, L. (2010). Computational processing of optical measurements of neuronal and synaptic activity in networks. *J. Neurosci. Methods* 188, 141–150. doi: 10.1016/j.jneumeth.2010.01.033

Dorr, A., Sled, J. G., and Kabani, N. (2007). Three-dimensional cerebral vasculature of the CBA mouse brain: a magnetic resonance imaging and micro computed tomography study. *NeuroImage* 35, 1409–1423. doi: 10.1016/j.neuroimage.2006.12.040

Fang, X. T., Hultqvist, G., Meier, S. R., Antoni, G., Sehlin, D., and Syvänen, S. (2019). High detection sensitivity with antibody-based PET radioligand for amyloid beta in brain. *NeuroImage* 184, 881–888. doi: 10.1016/j.neuroimage.2018.10.011

Focke, C., Blume, T., Zott, B., Shi, Y., Deussing, M., Peters, F., et al. (2019). Early and Longitudinal Microglial Activation but Not Amyloid Accumulation Predicts Cognitive Outcome in PS2APP Mice. *J. Nucl. Med.* 60, 548–554. doi: 10.2967/jnumed.118.217703

Füger, P., Hefendehl, J. K., Veeraraghavalu, K., Wendeln, A. C., Schlosser, C., Obermüller, U., et al. (2017). Microglia turnover with aging and in an Alzheimer's model *via* long-term *in vivo* single-cell imaging. *Nat. Neurosci.* 20, 1371–1376. doi: 10.1038/nn.4631

Geldmacher, D. S., Fritsch, T., McClendon, M. J., and Landreth, G. (2011). A randomized pilot clinical trial of the safety of pioglitazone in treatment of patients with Alzheimer disease. *Arch. Neurol.* 68, 45–50. doi: 10.1001/archneurol.2010.229

Haass, C., and Selkoe, D. J. (2007). Soluble protein oligomers in neurodegeneration: lessons from the Alzheimer's amyloid β-peptide. *Nat. Rev. Mol. Cell Biol.* 8, 101–112. doi: 10.1038/nrm2101

Hansson, O., Seibyl, J., Stomrud, E., Zetterberg, H., Trojanowski, J. Q., Bittner, T., et al. (2018). CSF biomarkers of Alzheimer's disease concord with amyloid-β PET and predict clinical progression: a study of fully automated immunoassays in BioFINDER and ADNI cohorts. *Alzheimers Dement.* 14, 1470–1481. doi: 10.1016/j.jalz.2018.01.010

Hardy, J., and Selkoe, D. J. (2002). The amyloid hypothesis of Alzheimer's disease: progress and problems on the road to therapeutics. *Science* 297, 353–356. doi: 10.1126/science.1072994

Heneka, M. T., Carson, M. J., Khoury, J. E., Landreth, G. E., Brosseron, F., Feinstein, D. L., et al. (2015). Neuroinflammation in Alzheimer's disease. *Lancet Neurol.* 14, 388–405. doi: 10.1016/S1474-4422(15)70016-5

Heppner, F. L., Ransohoff, R. M., and Becher, B. (2015). Immune attack: the role of inflammation in Alzheimer disease. Nature reviews. *Neuroscience* 16, 358–372. doi: 10.1038/nrn3880

Hickman, S. E., Allison, E. K., and El Khoury, J. (2008). Microglial Dysfunction and Defective -Amyloid Clearance Pathways in Aging Alzheimer's Disease Mice. *J. Neurosci.* 28, 8354–8360. doi: 10.1523/JNEUROSCI.0616-08.2008

Hu, N. W., Smith, I. M., Walsh, D. M., and Rowan, M. J. (2008). Soluble amyloid-beta peptides potently disrupt hippocampal synaptic plasticity in the absence of cerebrovascular dysfunction *in vivo*. *Brain* 131, 2414–2424. doi: 10.1093/brain/awn174

Huang, Y., Happonen, K. E., Burrola, P. G., O'Connor, C., Hah, N., Huang, L., et al. (2021). Microglia use TAM receptors to detect and engulf amyloid β plaques. *Nat. Immunol.* 22, 586–594. doi: 10.1038/s41590-021-00913-5

Ikonomovic, M. D., Buckley, C. J., Abrahamson, E. E., Kofler, J. K., Mathis, C. A., Klunk, W. E., et al. (2020). Post-mortem analyses of PiB and flutemetamol in diffuse and cored amyloid-β plaques in Alzheimer's disease. *Acta Neuropathol.* 140, 463–476. doi: 10.1007/s00401-020-02175-1

Ikonomovic, M. D., Buckley, C. J., Heurling, K., Sherwin, P., Jones, P. A., Zanette, M., et al. (2016). Post-mortem histopathology underlying β-amyloid PET imaging following flutemetamol F 18 injection. *Acta Neuropathol. Commun.* 4:130. doi: 10.1186/s40478-016-0399-z

Ikonomovic, M. D., Fantoni, E. R., Farrar, G., and Salloway, S. (2018). Infrequent false positive [18 F]flutemetamol PET signal is resolved by combined histological assessment of neuritic and diffuse plaques. *Alzheimers Res. Ther.* 10, 1–4. doi: 10.1186/s13195-018-0387-6

Keskin, A. D., Kekuš, M., Adelsberger, H., Neumann, U., Shimshek, D. R., Song, B., et al. (2017). BACE inhibition-dependent repair of Alzheimer's pathophysiology. *Proc. Natl. Acad. Sci. U. S. A.* 114, 8631–8636. doi: 10.1073/pnas.1708106114

Klyubin, I., Ondrejcak, T., Hayes, J., Cullen, W. K., Mably, A. J., Walsh, D. M., et al. (2014). Neurotransmitter receptor and time dependence of the synaptic plasticity disrupting actions of Alzheimer's disease Aβ *in vivo*. *Philos. Trans. R. Soc. Lond. B Biol. Sci.* 369:20130147. doi: 10.1098/rstb.2013.0147

Laforce, R., Soucy, J.-P., Sellami, L., Dallaire-Théroux, C., Brunet, F., Bergeron, D., et al. (2018). Molecular imaging in dementia: past, present, and future. *Alzheimers Dement.* 14, 1522–1552. doi: 10.1016/j.jalz.2018.06.2855

Lee, C. Y., and Landreth, G. E. (2010). The role of microglia in amyloid clearance from the AD brain. *J. Neural Transm.* 117, 949–960. doi: 10.1007/s00702-010-0433-4

Lewcock, J. W., Schlepckow, K., Di Paolo, G., Tahirovic, S., Monroe, K. M., and Haass, C. (2020). Emerging Microglia Biology Defines Novel Therapeutic Approaches for Alzheimer's Disease. *Neuron* 108, 801–821. doi: 10.1016/j.neuron.2020.09.029

Liu, J., Wang, L. N., and Jia, J. P. (2015). Peroxisome proliferator-activated receptor-gamma agonists for Alzheimer's disease and amnestic mild cognitive impairment: a systematic review and meta-analysis. *Drugs Aging* 32, 57–65. doi: 10.1007/s40266-014-0228-7

Lue, L.-F., Kuo, Y.-M., Roher, A. E., Brachova, L., Shen, Y., Sue, L., et al. (1999). Soluble Amyloid β Peptide Concentration as a Predictor of Synaptic Change in Alzheimer's Disease. *Am. J. Pathol.* 155, 853–862. doi: 10.1016/s0002-9440(10)65184-x

Mandrekar-Colucci, S., Karlo, J. C., and Landreth, G. E. (2012). Mechanisms Underlying the Rapid Peroxisome Proliferator-Activated Receptor- -Mediated Amyloid Clearance and Reversal of Cognitive Deficits in a Murine Model of Alzheimer's Disease. *J. Neurosci.* 32, 10117–10128. doi: 10.1523/JNEUROSCI.5268-11.2012

Manook, A., Yousefi, B. H., Willuweit, A., Platzer, S., Reder, S., Voss, A., et al. (2012). Small-Animal PET Imaging of Amyloid-Beta Plaques with [11C]PiB and Its Multi-Modal Validation in an APP/PS1 Mouse Model of Alzheimer's Disease. *PLoS One* 7:e31310. doi: 10.1371/journal.pone.0031310

Masuda, A., Kobayashi, Y., Kogo, N., Saito, T., Saido, T. C., and Itohara, S. (2016). Cognitive deficits in single App knock-in mouse models. *Neurobiol. Learn. Mem.* 135, 73–82. doi: 10.1016/j.nlm.2016.07.001

McLean, C. A., Cherny, R. A., Fraser, F. W., Fuller, S. J., Smith, M. J., Beyreuther, K., et al. (1999). Soluble pool of Abeta amyloid as a determinant of severity of neurodegeneration in Alzheimer's disease. *Ann. Neurol.* 46, 860–866. < 860:aid-ana8 > 3.0.co;2-m doi: 10.1002/1531-8249(199912)46:6

Monasor, L. S., Müller, S. A., Colombo, A. V., Tanrioever, G., König, J., Roth, S., et al. (2020). Fibrillar Aβ triggers microglial proteome alterations and dysfunction in Alzheimer mouse models. *eLife* 9:e54083 doi: 10.7554/eLife.54083

Moon, J. H., Kim, H. J., Yang, A. H., Kim, H. M., Lee, B.-W., Kang, E. S., et al. (2012). The effect of rosiglitazone on LRP1 expression and amyloid β uptake in human brain microvascular endothelial cells: a possible role of a low-dose thiazolidinedione for dementia treatment. *Int. J. Neuropsychopharmacol.* 15, 135–142. doi: 10.1017/S1461145711001611

Overhoff, F., Brendel, M., Jaworska, A., Korzhova, V., Delker, A., Probst, F., et al. (2016). Automated Spatial Brain Normalization and Hindbrain White Matter Reference Tissue Give Improved [18F]-Florbetaben PET Quantitation in Alzheimer's Model Mice. *Front. Neurosci.* 10:45. doi: 10.3389/fnins.2016.00045

Ozmen, L., Albientz, A., Czech, C., and Jacobsen, H. (2008). Expression of Transgenic APP mRNA Is the Key Determinant for Beta-Amyloid Deposition in PS2APP Transgenic Mice. *Neurodegener. Dis.* 6, 29–36. doi: 10.1159/000170884

Page, R. M., Baumann, K., Tomioka, M., Pérez-Revuelta, B. I., Fukumori, A., Jacobsen, H., et al. (2008). Generation of Abeta38 and Abeta42 is independently and differentially affected by familial Alzheimer disease-associated presenilin mutations and gamma-secretase modulation. *J. Biol. Chem.* 283, 677–683. doi: 10.1074/jbc.M708754200

Rominger, A., Brendel, M., Burgold, S., Keppler, K., Baumann, K., Xiong, G., et al. (2013). Longitudinal Assessment of Cerebral -Amyloid Deposition in Mice Overexpressing Swedish Mutant -Amyloid Precursor Protein Using 18F-Florbetaben PET. *J. Nucl. Med.* 54, 1127–1134. doi: 10.2967/jnumed.112.114660

Sacher, C., Blume, T., Beyer, L., Peters, F., Eckenweber, F., Sgobio, C., et al. (2019). Longitudinal PET Monitoring of Amyloidosis and Microglial Activation in a Second-Generation Amyloid-β Mouse Model. *J. Nucl. Med.* 60, 1787–1793. doi: 10.2967/jnumed.119.227322

Saito, T., Matsuba, Y., Mihira, N., Takano, J., Nilsson, P., Itohara, S., et al. (2014). Single App knock-in mouse models of Alzheimer's disease. *Nat. Neurosci.* 17, 661–663. doi: 10.1038/nn.3697

Sasaguri, H., Nilsson, P., Hashimoto, S., Nagata, K., Saito, T., Strooper, B., et al. (2017). APP mouse models for Alzheimer's disease preclinical studies. *EMBO J.* 36, 2473–2487. doi: 10.15252/embj.201797397

Sauvage, M., Brabet, P., Holsboer, F., Bockaert, J., and Steckler, T. (2000). Mild deficits in mice lacking pituitary adenylate cyclase-activating polypeptide receptor type 1 (PAC1) performing on memory tasks. *Mol. Brain Res.* 84, 79–89. doi: 10.1016/S0169-328X(00)00219-9

Sebastian, M. L., Müller, S. A., Colombo, A. V., Tanrioever, G., König, J., Roth, S., et al. (2020). Fibrillar Aβ triggers microglial proteome alterations and dysfunction in Alzheimer mouse models. *eLife* 9:e54083.

Sehlin, D., Fang, X. T., Cato, L., Antoni, G., Lannfelt, L., and Syvänen, S. (2016). Antibody-based PET imaging of amyloid beta in mouse models of Alzheimer's disease. *Nat. Commun.* 7:306. doi: 10.1038/ncomms10759

Selkoe, D. J., and Hardy, J. (2016). The amyloid hypothesis of Alzheimer's disease at 25 years. *EMBO Mol. Med.* 8, 595–608. doi: 10.15252/emmm.201606210

Streit, W. J., Xue, Q. S., Tischer, J., and Bechmann, I. (2014). Microglial pathology. *Acta Neuropathol. Commun.* 2, 1–17. doi: 10.1186/s40478-014-0142-6

Ulrich, J. D., Finn, M. B., Wang, Y., Shen, A., Mahan, T. E., Jiang, H., et al. (2014). Altered microglial response to Aβ plaques in APPPS1-21 mice heterozygous for TREM2. *Mol. Neurodegener.* 9, 1–9. doi: 10.1186/1750-1326-9-20

Valotassiou, V., Malamitsi, J., Papatriantafyllou, J., Dardiotis, E., Tsougos, I., Psimadas, D., et al. (2018). SPECT and PET imaging in Alzheimer's disease. *Ann. Nucl. Med.* 32, 583–593. doi: 10.1007/s12149-018-1292-6

Wang, J., Dickson, D. W., Trojanowski, J. Q., and Lee, V. M. (1999). The levels of soluble versus insoluble brain Abeta distinguish Alzheimer's disease from normal and pathologic aging. *Exp. Neurol.* 158, 328–337. doi: 10.1006/exnr.1999.7085

Wang, Y., Ulland, T. K., Ulrich, J. D., Song, W., Tzaferis, J. A., Hole, J. T., et al. (2016). TREM2-mediated early microglial response limits diffusion and toxicity of amyloid plaques. *J. Exp. Med.* 213, 667–675. doi: 10.1084/jem.20151948

Yamanaka, M., Ishikawa, T., Griep, A., Axt, D., Kummer, M. P., and Heneka, M. T. (2012). PPAR/RXR -Induced and CD36-Mediated Microglial Amyloid-Phagocytosis Results in Cognitive Improvement in Amyloid Precursor Protein/Presenilin 1 Mice. *J. Neurosci.* 32, 17321–17331. doi: 10.1523/JNEUROSCI.1569-12.2012

Ziegler-Graham, K., Brookmeyer, R., Johnson, E., and Arrighi, H. M. (2008). Worldwide variation in the doubling time of Alzheimer's disease incidence rates. *Alzheimers Dement.* 4, 316–323. doi: 10.1016/j.jalz.2008.05.2479

Zimmer, E., Leuzy, A., Benedet, A., Breitner, J., Gauthier, S., and Rosa-Neto, P. (2014). Tracking neuroinflammation in Alzheimer's disease: the role of positron

emission tomography imaging. *J. Neuroinflammation* 11:120. doi: 10.1186/1742-2094-11-120

Zott, B., Simon, M. M., Hong, W., Unger, F., Chen-Engerer, H.-J., Frosch, M. P., et al. (2019). A vicious cycle of β amyloid-dependent neuronal hyperactivation. *Science* 365, 559–565. doi: 10.1126/science.aay0198

Conflict of Interest: GK is an employee of ISAR bioscience. KB is an employee of Roche. AR has received research support and speaker honoraria from Siemens. MB received speaker honoraria from GE healthcare, Roche, and LMI and is an advisor of LMI.

The remaining authors declare that the research was conducted in the absence of any commercial or financial relationships that could be construed as a potential conflict of interest.

Publisher's Note: All claims expressed in this article are solely those of the authors and do not necessarily represent those of their affiliated organizations, or those of the publisher, the editors and the reviewers. Any product that may be evaluated in this article, or claim that may be made by its manufacturer, is not guaranteed or endorsed by the publisher.

frontiers | Frontiers in Aging Neuroscience

ORIGINAL RESEARCH
published: 01 April 2022
doi: 10.3389/fnagi.2022.873929

Dihuang-Yinzi Alleviates Cognition Deficits *via* Targeting Energy-Related Metabolism in an Alzheimer Mouse Model as Demonstrated by Integration of Metabolomics and Network Pharmacology

Guanghui Han[1†], Weizhe Zhen[1†], Yuan Dai[2†], Hongni Yu[1], Dongyue Li[3] and Tao Ma[1]*

[1] Dongfang Hospital, Beijing University of Chinese Medicine, Beijing, China, [2] School of Health Preservation and Rehabilitation, Chengdu University of Traditional Chinese Medicine, Chengdu, China, [3] College of Traditional Chinese Medicine, Beijing University of Chinese Medicine, Beijing, China

OPEN ACCESS

Edited by:
Fushun Wang,
Nanjing University of Chinese Medicine, China

Reviewed by:
Zijuan Liu,
Oakland University, United States
Shijun Yan,
Indiana University Bloomington, United States
Jinhai Huo,
University of Florida, United States

***Correspondence:**
Tao Ma
matao327@126.com

[†] These authors have contributed equally to this work

Specialty section:
This article was submitted to Alzheimer's Disease and Related Dementias, a section of the journal Frontiers in Aging Neuroscience

Received: 11 February 2022
Accepted: 23 February 2022
Published: 01 April 2022

Citation:
Han G, Zhen W, Dai Y, Yu H, Li D and Ma T (2022) Dihuang-Yinzi Alleviates Cognition Deficits via Targeting Energy-Related Metabolism in an Alzheimer Mouse Model as Demonstrated by Integration of Metabolomics and Network Pharmacology. Front. Aging Neurosci. 14:873929. doi: 10.3389/fnagi.2022.873929

Energy metabolism disturbance and the consequent reactive oxygen species (ROS) overproduction play a key and pathogenic role in the onset and progression of Alzheimer's disease (AD). Dihuang-Yinzi (DHYZ) is a traditional Chinese herbal prescription clinically applied to treat AD and other neurodegenerative diseases for a long time. However, the systematical metabolic mechanism of DHYZ against AD remains largely unclear. Here we aimed to explore the mechanism of DHYZ in the treatment of AD comprehensively in an *in vivo* metabolic context by performing metabolomics analysis coupled with network pharmacology study and experimental validation. The network pharmacology was applied to dig out the potential target of DHYZ against AD. The metabolomics analysis based on UPLC-HRMS was carried out to profile the urine of 2× Tg-AD mice treated with DHYZ. By integrating network pharmacology and metabolomics, we found DHYZ could ameliorate 4 key energy-related metabolic pathways, including glycerophospholipid metabolism, nicotinate/nicotinamide metabolism, glycolysis, and tricarboxylic acid cycle. Besides, we identified 5 potential anti-AD targets of DHYZ, including DAO, HIF1A, PARP1, ALDH3B2, and ACHE, and 14 key differential metabolites involved in the 4 key energy-related metabolic pathways. Furthermore, DHYZ depressed the mitochondrial dysfunction and the resultant ROS overproduction through ameliorating glycerophospholipid metabolism disturbance. Thereby DHYZ increased nicotinamide adenine dinucleotide (NAD^+) content and promoted glycolysis and tricarboxylic acid (TCA) cycle, and consequently improved oxidative phosphorylation and energy metabolism. In the present study, we provided a novel, comprehensive and systematic insight into investigating the therapeutic efficacy of DHYZ against AD *via* ameliorating energy-related metabolism.

Keywords: Alzheimer's disease, Dihuang-Yinzi, metabolomics, network pharmacology, energy metabolism, mitochondria, reactive oxygen species

INTRODUCTION

Alzheimer's disease (AD) is complex neurodegenerative dementia in aging people and places a substantial burden on the economy and psychology on society (Grubman et al., 2019). With the in-depth study of AD, the abnormality of energy metabolism has attracted a lot of attention in recent years (Minhas et al., 2021). As an organ with the highest energy requirements, the brain is vulnerable to energy metabolism impairments. The energy metabolism is composed of several important metabolic pathways, including glycolysis, tricarboxylic acid (TCA) cycle, the pentose phosphate pathway (PPP), oxidative phosphorylation (OxPhos), etc. It has shown that the astrocyte glycolysis is disturbed resulting in a decrease in glucose utilization, and deficits in synaptic plasticity and memory of AD patients and mouse models (Le Douce et al., 2020). The abnormalities in the TCA cycle and OxPhos are also closely related to AD pathology (Shaerzadeh et al., 2014; Pawlosky et al., 2017; Puchowicz and Seyfried, 2017). β-amyloid (Aβ), one of the most important hallmarks of AD, can cause the chronic reprogramming of energy-related metabolisms, including OxPhos and glycolysis (Baik et al., 2019).

Metabolomics is a powerful phenotyping technique that identifies and quantifies small molecular metabolites and their complements in cells, tissues, and biological fluids, and provides a highly sensitive and specific method for measurement of multi-parameters of disease phenotypes at a systematic level (van der Velpen et al., 2019). The applications of metabolomics in AD help us to identify the changes of metabolites in the brain, serum, and urine, which may play an important role in the pathogenesis of AD at preclinical and clinical stages (Woo et al., 2010; Liu et al., 2013; Mapstone et al., 2014; Shao et al., 2020). Given the fact that the metabolic variation is reversible in the early stage of AD, profiling the metabolomic characteristics of the pathological progression of AD is of particular relevance for the treatment or impeding disease progression (Oresic et al., 2011; Mapstone et al., 2014). In the recent decade, many metabolomics studies had been performed to discover and identify differential metabolites or biomarkers to facilitate understanding of the pathogenesis, diagnosis, and prognosis of AD, and evaluating of the therapeutic efficacy of drugs against AD by using plasma, serum, cerebrospinal fluid, saliva, and urine samples (Oresic et al., 2011; Tsuruoka et al., 2013; Mapstone et al., 2014). Since urinary metabolomics analysis has many advantages, such as non-invasive, sensitive, convenient, rapid, etc., it has received great attention in AD treatment, diagnosis, and drug evaluation (Liu et al., 2019; Wei et al., 2019; Wang et al., 2021).

Network pharmacology is a comprehensive technique integrating traditional pharmacology, bioinformatics, chemoinformatics, and systems biology. The application of network pharmacology provides us with the objective evidence of the herbal prescription intervention in AD and sheds light on developing novel drugs for AD treatment (Zeng et al., 2019; Gu et al., 2020). Given network pharmacology is an effective way to predict the complex mechanisms of traditional Chinese herbal prescriptions, it has widely been used in clarifying their multi-target effect on neurodegenerative diseases, including in AD, combing with metabolomics, or other omics (Yuan et al., 2017; Yun et al., 2021).

Dihuang-Yinzi (DHYZ) is a traditional Chinese herbal prescription, mainly composed of 15 herbs, such as Rehmannia, Cistanche, Dogwood, Morinda, etc. (**Table 1**). Clinically, DHYZ has been used in the treatment of neurodegenerative diseases, including AD, for a long time (Lee et al., 2021). In recent years, many studies demonstrated that DHYZ exhibits neuroprotective functions in a variety of neurological diseases (Hu et al., 2009; Qiu et al., 2016). DHYZ can inhibit neuronal apoptosis through mitochondria- and endoplasmic reticulum-dependent pathways, induce expression of glial-derived neurotrophic factor (GDNF), and maintain the ultrastructure of the blood-brain barrier (BBB) (Zhang et al., 2017; Zhang J. et al., 2018). Furthermore, DHYZ improved the cognition of ischemic mice by depressing the expression of extracellular signal-regulated protein kinase (ERK) and synaptophysin (SYP) (Hu et al., 2009). A study based on a meta-analysis shows that DHYZ can significantly improve the cognitive function and daily activities of AD patients (Lee et al., 2021). Our previous studies have shown that DHYZ can ameliorate the learning and memory impairments of rat and mouse model of AD by depressing mitochondrial impairments and improving energy production (Ma et al., 2012; Huang et al., 2018; Yan et al., 2018). However, the comprehensive mechanism of therapeutic effects of DHYZ against AD especially at holistic metabolic level remains elusive so far.

In the present study, we performed metabolomics analysis coupled with a network pharmacology study to explore the key metabolites and their related metabolic pathways in treatment with DHYZ, and key targets of DHYZ against AD (**Figure 1**). Our result provided a novel multi-dimensional perspective of the therapeutic efficacy of DHYZ against AD and a scientific basis for its further clinical precision medication.

MATERIALS AND METHODS

Herbal Materials

The herbal materials, namely Cistanches Herba (*Cistanche deserticola* Y.C.Ma), Morindae Officinalis Radix (*Morinda officinalis* How), Rehmanniae Radix Praeparata (*Rehmannia glutinosa* Libosch), Corni Fructus (*Cornus officinalis* Sieb. et Zucc), Aconiti Lateralis Radix Praeparata (*Aconitum carmichaelii* Debx.), Cinnamomi Cortex (*Cinnamomum cassia* Presl), Ophiopogonis Radix (*Ophiopogon japonicus* (L.f) Ker-Gawl.), Dendrobii Caulis (*Dendrobium nobile* Lindl.), Schisandrae Chinensis Fructus (*Schisandra chinensis* (Turcz.) Baill.), Polygalae Radix (*Polygala tenuifolia* Willd.), Acori Tatarinowii Rhizoma (*Acorus tatarinowii* Schott), Poria (*Poria cocos* (Schw.) Wolf), Menthae Haplocalycis Herba (*Mentha haplocalyx* Briq.), Zingiberis Rhizoma Recens (*Zingiber officinale* Rosc.), and Jujubae Fructus (*Ziziphus jujuba* Mill.) used for the preparation of DHYZ were obtained from Dongfang Hospital, Beijing University of Chinese Medicine. All the above-mentioned herbal medicines used to prepare DHYZ have been kindly authenticated

TABLE 1 | Component herbs of DHYZ.

Pharmaceutical name	Botanical plant name	Family and plant parts used	English name	Chinese name	Amount in preparation (g)
Cistanches Herba	*Cistanche deserticola* Y.C.Ma	Orobanchaceae; Fleshy stem	cistanche	Rou Cong Rong	15
Morindae Officinalis Radix	*Morinda officinalis* How	Rubiaceae; Root	morinda	Ba Ji Tian	15
Rehmanniae Radix Praeparata	*Rehmannia glutinosa* Libosch	Scrophulariaceae; Root tuber	rehmannia	Shu Di Hang	15
Corni Fructus	*Cornus officinalis* Sieb. et Zucc	Cornaceae; fruit	dogwood	Shan Zhu Yu	15
Aconiti Lateralis Radix Praeparata	*Aconitum carmichaelii* Debx.	Ranunculaceae; Subroot	aconite	Zhi Fu Zi	15
Cinnamomi Cortex	*Cinnamomum cassia* Presl	Lauraceae; bark	cinnamon	Rou Gui	15
Ophiopogonis Radix	*Ophiopogon japonicus* (L.f) Ker-Gawl.	Liliaceae; Root tuber	ophiopogon	Mai Dong	15
Dendrobii Caulis	*Dendrobium nobile* Lindl.	Orchidaceae; stem	dendrobium	Shi Hu	15
Schisandrae Chinensis Fructus	*Schisandra chinensis* (Turcz.) Baill	Magnoliaceae; fruit	schisandrae	Wu Wei Zi	15
Polygalae Radix	*Polygala tenuifolia* Willd.	Polygalaceae; Root	polygala	Yuan Zhi	15
Acori Tatarinowii Rhizoma	*Acorus tatarinowii* Schott	Araceae; tuber	calamus	Shi Chang Pu	15
Poria	*Poria cocos* (Schw.) Wolf	Polypores; sclerotium	poria	Fu Ling	15
Menthae Haplocalycis Herba	*Mentha haplocalyx* Briq.	Labiatae; Aerial part	mint	Bo He	15
Zingiberis Rhizoma Recens	*Zingiber officinale* Rosc.	Zingiberaceae; rhizome	ginger	Sheng Jiang	10
Jujubae Fructus	*Ziziphus jujuba* Mill.	Jujubae; fruit	jujube	Da Zao	5

by Dr. Yuan Dai (Associate professor, Chengdu University of Traditional Chinese Medicine).

Preparation of Dihuang-Yinzi Extract

The formula of DHYZ (one dose) is presented in **Table 1** as described previously (Huang et al., 2018). All the herbs in DHYZ (10 doses) were added in distilled water (1:4 w/v), soaked for 2 h, and extracted at 100°C for 2 times, 2 h each time. The decoctions were mixed, filtered, and dried by decompressing at 60°C to the drying extract (5.53 g of herbal mixtures generated 1 g drying extract). Then the drying powder was mixed thoroughly, stored at 4°C, and dissolved in normal saline at the desired concentrations before use.

Reagents and Materials

Standards of loganin (Lot No. 36483), echinacoside (Lot No. 07538), Verbascoside (Lot No. V4015), Erianin (Lot No. PHL83499), Cinnamic Acid (Lot No. C80857), Tenuifolin (Lot No. PHL83546), Quercetin (Lot No. PHR1488), Ruscogenin (Lot No. SMB00295), Kaempferol (Lot No. 60010), Beta-sitosterol (Lot No. S1270), and Schisandrin (Lot No. SML0054) were purchased from Sigma-Aldrich Co. LLC (St. Louis, MO, United States). Formic acid, methanol, ammonium acetate, ammonium hydroxide, and acetonitrile used in UPLC were provided by Fisher Scientific Co. LLC (Fair Lawn, NJ, United States). The ultrapure water (18.2 MΩ·cm) used in the experiment was prepared with Milli-Q IQ 7003 purified water system (Merck Millipore, Darmstadt, Germany).

Fingerprint Spectrum Analysis

The fingerprint spectrum of multi-components of the DHYZ was characterized by ultrahigh-pressure liquid chromatography (UPLC). The analyses were performed with Waters ACQUITY UPLC system (Waters Corp., Milford, MA, United States) equipped with a photo-diode array (PDA), a quaternary pump, an autosampler, and empower software. Chromatographic separation was performed on the Waters BEH C_{18} column (50 mm × 2.1 mm, 1.7 μm) at 40°C with the detector of wavelength 220 nm. The mobile phase was a mixture of water containing 0.1% formic acid (A) and acetonitrile containing 0.1% formic acid (B). A linear gradient elution was conducted as follows: 0–3 min, 5–10%B; 3–10 min, 10–85%B; 10–15 min, 95%B; 15–20 min, 5%B. The flow rate was 0.4 mL/min and the total injection volume was 2 μL.

Animals and Grouping

Three-month-old male APPswe/PS1dE9 (2× Tg-AD) mice which harbor human APPswe (Swedish mutations K594N/M595L) and presenilin-1 with exon 9 deleted (PS1dE9) under the control of the constitutively active PrP gene promoter (Jankowsky et al., 2004) and non-transgenic (Non-Tg) littermates of the same month were provided by the Nanjing Biomedical Research Institute of Nanjing University (Nanjing, China). All mice were adaptively reared for 30 days in the SPF animal laboratory in Dongfang Hospital, Beijing University of Chinese Medicine, China. After adaptive breeding, 4-month-old Non-Tg mice (n = 20) were designed as the

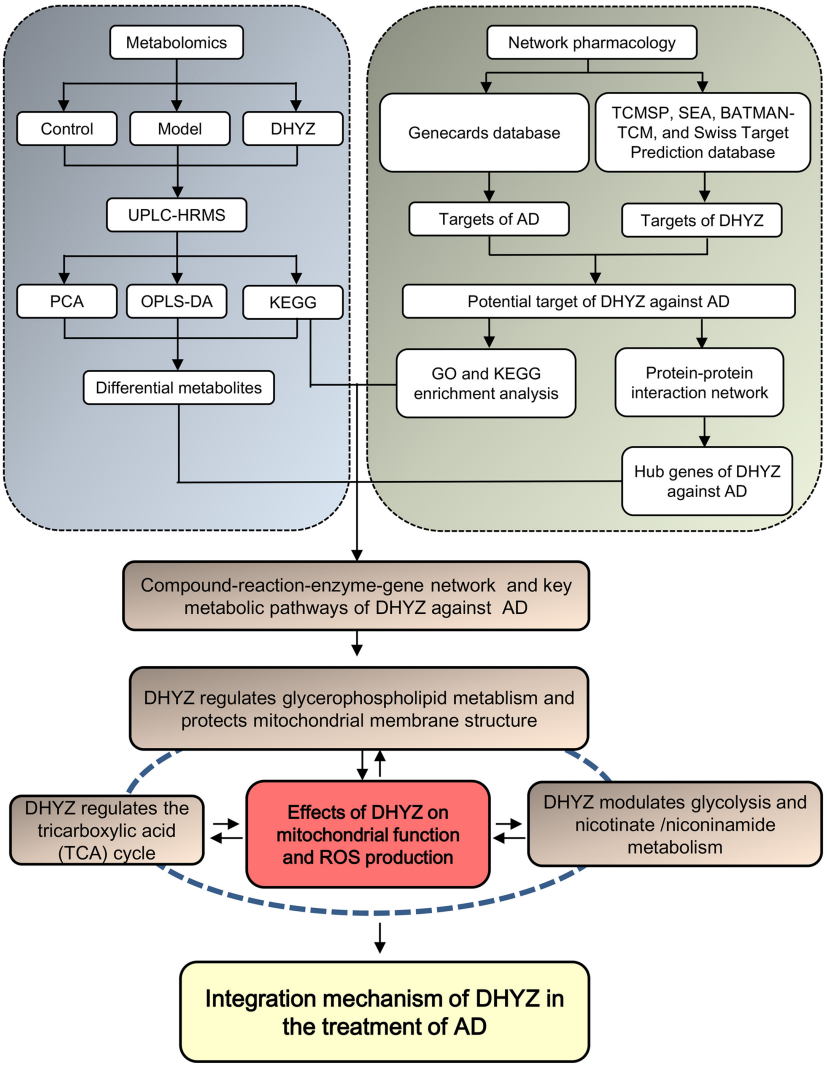

FIGURE 1 | Schematic diagram of the integrated study of DHYZ against AD combining urine metabonomics and network pharmacology.

control group, and 2× Tg-AD mice were randomly divided into model group and DHYZ group, with 20 mice in each group. All the mice are housed individually in cages, the ambient temperature is 23 ± 1°C, and relative humidity is 55 ± 5% under. All mice were raised in an environment with a cycle of 12h:12h light/dark, with the intake of food and water *ad libitum*. All the animals were handled according to the NIH Guide for the Care and Use of Laboratory Animals (NIH Publications No. 80-23, revised 1996). All animal studies were approved by the Animal Care and Welfare Committee of Dongfang Hospital, Beijing University of Chinese Medicine, China.

Administration of Dihuang-Yinzi

Estimate the dosage of DHYZ in mice based on the dosage for adults (crude drug: 3.5 g/kg BW•day). All 4-month old mice were intragastrically administered DHYZ at a dose of 35 g crude drug/kg BW•day (6.3 g drying extract/kg BW•day) for 180 days, once a day. The mice in the control group and the model group were intragastrically given the same volume of sterilized saline for 180 days, once a day.

Morris Water Maze

patial learning and memory were analyzed using the Morris water maze (MWM) tests which were performed as described previously (Dai et al., 2020). Briefly, the place navigation test included 5 days of training, 2 pieces of training a day, and the interval between the 2 pieces of training was more than 1 h. 24 h after the end of the place navigation test, that is, the 6th day of the experiment, the spatial probe test was performed. From the 7th to the 9th day of the experiment, the visible-platform test was performed to evaluate the impact of mouse vision on the ability to search the platform.

Network Pharmacology Analysis

The composite ingredients of Cinnamon, Dendrobium, Ophiopogon, and Polygala were searched in Bioinformatics Analysis Tool for Molecular Mechanism of Traditional Chinese Medicine (BATMAN-TCM[1]), and screened with the high gastrointestinal absorption (GI absorption) and drug-like properties (DL) in SwissADME[2]. The composite ingredients of other herbs in DHYZ were obtained by searching in the Traditional Chinese Medicine Systems Pharmacology Database and Analysis Platform (TCMSP[3]). The composite ingredients were filtered with oral bioavailability (OB) $\geq$30%, and drug-like property (DL) $\geq$0.18. The chemical structure and SMILES number of all composite ingredients were obtained with the PubChem[4]. The molecular targets of these composite ingredients were screened by importing the chemical structure formula into the SwissTargetPrediction[5] database and the SMILES number into the SEA[6] database. The candidate therapeutic targets of AD were collected by searching the keywords of "Alzheimer" in the genecards[7] database. The intersection of molecular targets of DHYZ and candidate therapeutic targets for AD treatment is considered to be the predicted targets for DHYZ against AD. All the predicted targets were imported into UniProtKB[8] to standardize the gene and protein names. The predicted targets were imported into the Metascape[9] for GO and Kyoto Encyclopedia of Genes and Genomes (KEGG) enrichment analysis, with the KEGG pathway analysis was set as $P < 0.05$. The herbs-composite ingredients-potential targets network was established by utilizing the Cytoscape 3.8.2 (National Institute of General Medical Science, United States). The predicted targets of DHYZ for AD treatment were imported into STRING 11.0[10] to construct the PPI network, and the hub genes were screened by CytoHubba in Cytoscape 3.8.2.

Metabolomics Analysis

Sample Preparation

After intragastrically administrated for 180 days, the mice were put in 3600M021 Mice Metabolic Cages (TECNIPLAST S.p. A, BUGUGGIATE, VA, Italy), and the urine samples were collected and centrifuged. All urine samples were stored at −80°C before UPLC-HRMS Analysis.

Untargeted Ultra-High-Performance Liquid Chromatography-High-Resolution Mass Spectrometer Analysis

Separation conditions by UPLC Untargeted metabolomics analysis were conducted by using 3 different analytical methods on an Ultimate 3000 ultra-high-performance liquid chromatography coupled with Q Exactive^{TM} quadrupole-Orbitrap high-resolution mass spectrometer UPLC-HRMS system (Thermo Fisher Scientific, United States). For methods 1 and 2 (M1, 2), the polar metabolome extracts were profiled on reverse-phase chromatographic separation with positive and negative ionization detection, respectively. Metabolites were separated by using an Acquity^{TM} HSS C18 column (Waters Co., United States, 2.1 mm × 100 mm) for M1. Furthermore, other mobile phases were employed to eluted metabolites separated on an Acquity^{TM} BEH C18 column (Waters Co., United States, 1.7 μm, 2.1 mm × 100 mm). As for Method 3, HILIC separation was utilized by using an Acquity^{TM} BEH amide column (Waters Co., United States, 1.7 μm, 2.1 mm × 100 mm) after 5 μL aliquots of metabolites extract injected, and 5% water in acetonitrile as weak eluent and 40% acetonitrile in water as strong eluent which was both added ammonium acetate to as buffer salt to improve separation.

Data Processing and Analysis

The full scan and data-dependent MS2 metabolic profiles data were further processed with Compound Discoverer (CD version 3.0 Thermo Fisher Scientific) for comprehensive component extraction. The polar metabolites were structurally annotated through searching acquired MS2 against a local proprietary iPhenome^{TM} SMOL high-resolution MS/MS spectrum library created using authentic standards, NIST 17 Tandem MS/MS library (National Institute of Standards and Technology), local version MoNA (MassBank of North America), as well as mzCloud library (Thermo Fisher Scientific, United States). Besides, the exact m/z of MS1 spectra was searched against a local KEGG, HMDB metabolite chemical database. For metabolite identification or structural annotation, mass accuracy of precursor within ±5ppm was a prerequisite, meanwhile, isotopic information including at least 1 isotopes within 10 ppm and a fit score of relative isotopic abundance pattern 70% were introduced to confirm the chemical formula in addition to exact mass. Furthermore, retention time information as well as high-resolution MS/MS spectra similarity was employed to strictly confirm the structural annotation of metabolites. The area under curve values as extracted as quantitative information of metabolites with XCalibur Quan Browser information, all peak areas data for the annotated metabolites were exported into Excel software for trim and organization before statistics (Microsoft, United States).

The metabolome data deriving from different measurements were merged and those detected with multiple methods were excluded to guarantee uniqueness of metabolite and lipid, and then Log2 was transformed for final statistical analysis. The principal component analysis (PCA), as well as the orthogonal partial least square-discriminant analysis (OPLS-DA), was conducted with SIMCA-P software (Umetrics, Sweden), and another univariate analysis including independent sample *t*-test and *p*-value FDR adjust, as well as metabolic pathway analysis was conduct on the MetaboAnalyst website.

[1]http://bionet.ncpsb.org/batman-tcm
[2]http://www.swissadme.ch
[3]https://old.tcmsp-e.com/tcmsp.php
[4]https://pubchem.ncbi.nlm.nih.gov/
[5]http://www.Swisstargetprediction.ch/
[6]https://sea.bkslab.org/
[7]https://www.genecards.org/
[8]http://www.uniprot.org/
[9]https://metascape.org/gp/index.html#/main/step1
[10]https://string-db.org

Kyoto Encyclopedia of Genes and Genomes Enrichment Analysis of Differential Metabolites

The intersection of the differential metabolites of the model group *vs.* the control group and the DHYZ group *vs.* model group are considered to be the main differential metabolites involved in the AD treatment by DHYZ. All these metabolites were inputted in MetaboAnalyst 5.0[11] for KEGG enrichment and pathway analysis.

Compound-Reaction-Enzyme-Gene Network Construction

The differential metabolites and hub genes closely related to DHYZ treatment of AD were imported into MetScape in Cytoscape 3.8.2 to construct a visual network including the interactions among metabolites, hub genes, pathways, and enzymes.

Antibodies and Western Blot Analysis

Primary antibodies used in Western blot analysis were as follows: polyclonal anti D-amino-acid oxidase (DAO) antibody (1:1000, ab187525, abcam, Cambridge, United Kingdom), polyclonal anti- aldehyde dehydrogenase 3 family member B2 (ALDH3B2) antibody (1:1000, SAB1410380, Sigma-Aldrich, Merck KGaA Co, Darmstadt, Germany), monoclonal anti-hypoxia-inducible factor 1-alpha (HIF1A) antibody (1:1000, #36169, Cell Signaling Technology, MA, United States), monoclonal anti-Poly [ADP-ribose] polymerase 1 (PARP-1) antibody (1:1000, #9532S, Cell Signaling Technology, MA, United States), monoclonal anti-acetylcholinesterase (AChE) antibody (1:500, sc-373901, Santa Cruz Biotech., Inc., TX, United States), monoclonal anti-pyruvate dehydrogenase kinase 1 (PDHK1) antibody (1:1000, #3820, Cell Signaling Technology, MA, United States), monoclonal anti-pyruvate dehydrogenase (PDH) antibody (1:1000, #3205, Cell Signaling Technology, MA, United States), polyclonal anti-phospho-pyruvate dehydrogenase (phospho-PDH) antibody (1:1000, #31866, Cell Signaling Technology, MA, United States), monoclonal anti-β actin antibody (C4) (1:2000, sc-47778, Santa Cruz Biotech., Inc., TX, United States), monoclonal anti-GAPDH antibody (1:2000, sc-47724, Santa Cruz Biotech., Inc., TX, United States). Goat anti-rabbit IgG-HRP (1:5000, sc-2004) and goat anti-mouse IgG-HRP (1:5000, sc-2302) secondary antibody were provided by Santa Cruz Biotech., Inc. (TX, United States).

After being dissected, the mouse brains were homogenized in ice-cold RIPA lysis buffer (Applygen Technologies, Beijing, China) supplemented with cOmplete protease inhibitor cocktail (Roche Diagnostic GmbH, Mannheim, Germany) with Dounce homogenizer. The brain homogenates were centrifuged at 12,000 *g* and 4°C for 10 min, and the supernatant was transferred to a new EP tube for later assay. After protein quantification using the Pierce BCA protein assay kit (Thermo Fisher Scientific, IL, United States), 50 μg of total protein lysate was subjected to SDS-PAGE and electrophoretically transferred to polyvinylidene fluoride (PVDF) membranes (Millipore, MA, United States). Primary antibodies were used to detect the corresponding protein level in the mouse brain. GAPDH and β-actin served as loading control of total protein. Immunoreactive bands were detected with species-specific HRP-conjugated secondary antibodies, developed with Pierce ECL Western Blotting Substrate (Thermo Fisher Scientific, IL, United States), and images were captured with GeneGnome XRQ bio imaging system (Syngene Inc., Cambridge, United Kingdom). The images were analyzed and quantified with the Image J 1.46r (NIH, United States).

Energy Charge Measurement

After being deeply anesthetized by using sodium pentobarbital, mouse brains were excised. 5 mouse brains from each group were homogenized with cold saline solution, added to 4% perchloric acid to precipitate the protein, and centrifuged at 3000 rpm for 10 min at 4°C. The supernatant was neutralized with potassium hydroxide and subjected to reverse-phase HPLC (Microsorb C18; Rainin Instruments Co. Swiss). The column eluate was monitored at an absorbance of 254 nm, and the adenosine triphosphate (ATP), adenosine diphosphate (ADP), and adenosine monophosphate (AMP) concentrations were calculated from the peak area using ChromatoPack CR-4A (Shimadzu Seiki Inc., Japan). The energy charge (EC) was calculated as follows: $EC = ATP + 0.5ADP/(ATP + ADP + AMP)$.

Transmission Electron Microscopy

After anesthetized, 3 mouse brains were fixed with 4% paraformaldehyde perfusion, and then taken and fixed overnight at 4°C with the same fixative. The hippocampuses of the mouse brains were cut into a small block of 1 mm^3 and put into 1% osmium tetroxide. Then the blocks were drowned into graded series of ethanol and then in acetone. Brain tissue slices were embedded with Poly/Bed 812 embedding kit (Polysciences, Warrington, PA, United States), sliced on Ultracut E ultramicrotome (Reichert, Buffalo, NY, United States), and then stained with uranyl acetate and lead citrate. The tissue sections were observed with a Hitachi H7650 transmission electron microscope (Hitachi High-Tech, Fukuoka, Japan), and images were collected with an AMT Camera System at an acceleration voltage of 80.0 kV.

Isolation of Brain Mitochondria

Mouse cerebral mitochondria were isolated according to the method of Lai and Clark (1979). Mouse brains were homogenized in isolation buffer (225 mM mannitol, 75 mM sucrose, 1 mM EGTA, 5 mM HEPES, 2 mg/mL fat-free BSA) using a motorized Dounce homogenizer with eight up-and-down strokes. The homogenate was centrifuged at 1,500 *g* for 5 min, and the resulting supernatant was adjusted to 14% Percoll and centrifuged at 12,000 *g* for 10 min. The mitochondrial pellet was resuspended in isolation buffer and recentrifuged at 8000 *g* for 10 min. Mitochondria were finally washed and resuspended in an isolation buffer. Protein concentrations were determined by the bicinchoninic acid (BCA) protein assay kit (Pierce Chemical Co., United States) with BSA as a standard protein.

[11] https://www.metaboanalyst.ca/

Isolation of Phospholipids From Mitochondria of Mouse Brain

Phospholipids were isolated according to the modified methods of Bligh and Dyer (1959) and Sparagna et al. (2005). For each sample, 0.08 nmol of 1,1′,2,2′-tetramyristoyl cardiolipin (M_4CL) was added as internal standard per 120 μg mitochondrial protein. Then methanol, chloroform, and HCl were added to mitochondrial extraction, and the mixture was vortexed for 1 min and centrifuged at 3,000 *g*. The lower organic layer was transferred to a clean glass tube and dried under a stream of nitrogen. The phospholipids extracts were resuspended in 100 μL of hexane-isopropanol (30:40, v/v).

Tetralinoleoyl-Cardiolipin Quantitation

Tetralinoleoyl-cardiolipin (L_4-CL) quantification was performed according to the methods of Bowron et al. (2013) with some modifications. Briefly, 10 μL of phospholipid extract was injected onto an Ultimate 3000 ultra-high-performance liquid chromatography (UPLC) (Thermo Fisher Scientific, United States). Chromatographic separation was performed on the Waters BEH C_8 column (50 mm × 2.1 mm, 1.7 μm) at 35°C. The mobile phase A and B were 0.1% ammonium hydroxide in water and methanol, respectively, with the following gradient: 0–1.7 min, 10–90% B; 1.7–3.7 min, 90–99% B; 3.7–4.7 min, 99% B; 4.7–5.0 min, 10% B. Flow rate was 0.2 mL/min. L_4-CL was eluted between 3.0 and 3.4 min.

A Q Exactive™ quadrupole-Orbitrap high-resolution mass spectrometer (HRMS) (Thermo Fisher Scientific, United States) was used in electrospray negative ion mode. L_4-CL was detected by HRMS using transition with m/z 725.5 > 291.1. Collision energy for L_4-CL was 36 eV. The L_4-CL concentration of each sample was calculated with a calibration standard and corrected for the volume of the assay sample and its responding protein concentration.

Acetylcholine Assay

After being anesthetized with sodium pentobarbital, the mice were killed by decapitation, and the brain was stripped on ice. After rinsing with frozen physiological saline, the brain was added with methanol and denounced in a glass homogenizer in an ice bath. The homogenate was vortexed for 30 min and centrifuged at 10000 *g* for 30 min. Discarded the supernatant, and place it in a nitrogen blower to heat and blow-dry.

The level of acetylcholine in the mouse brain was detected by using Acetylcholine Assay Kit (A105-1, Nanjing Jiancheng Bioengineering Institute, Nanjing, China) according to the manufacturer's instructions. The entire mixture was mixed thoroughly and preserved at RT for 10 min before reading on a BioTek ELX800 Reader (BioTek, Winooski, VT, United States) at absorbance 550 nm.

NAD^+ Measurement

The level of nicotinamide adenine dinucleotide (NAD^+) in the mouse brain was measured with NAD^+/NADH Assay Kit (S0175, Beyotime Biotechnology, Shanghai, China) according to the manufacturer's instructions. The mixture was performed to read on BioTek ELX800 Reader at absorbance 450 nm.

Immunofluorescence and Confocal Microscopy

For immunofluorescence staining, the frozen sections were permeabilized with 0.3% Triton X-100 and blocked with 5% (vol/vol) bovine serum albumin (BSA) in PBS. Then the sections were incubated with primary antibodies, including anti-S100B antibody (1:500, AMAb91038, Atlas Antibodies AB, Stockholm, Sweden), anti-ALDH3B2 antibody (1:50, HPA045132, Atlas Antibodies AB, Stockholm, Sweden), Anti-8-Oxoguanine (8-OxoG) Antibody (1:100, MAB3560, Millipore, Sigma-Aldrich Co. LLC., CA, United States) at 4°C overnight. Secondary antibodies were either FITC- -conjugated goat anti-mouse IgG antibody (1:100, 115-095-003, Jackson ImmunoResearch Laboratories, Inc., PA, United States), Alexa Fluor® 594-conjugated goat anti-rabbit IgG antibody (1:50, 111-585-003, Jackson ImmunoResearch Laboratories, Inc., PA, United States) or Alexa Fluor® 594-conjugated goat anti-mouse IgG antibody (1:50, 115-585-003, Jackson ImmunoResearch Laboratories, Inc., PA, United States), and incubated for 2 h in dark at RT. After washing in PBS, the sections were mounted with DAPI-containing mounting media (C1211, APPLYGEN, Beijing, China). Immunofluorescence reactivity or DAPI was detected by Olympus IX71 microscope and Olympus FV500 confocal laser-scanning microscope (Olympus, Japan), and analyzed with Image J 1.46r.

Measurements of Mitochondrial Membrane Potential

Isolated mitochondrial membrane potential (MMP) ($\Delta\psi m$) was measured with JC1-Mitochondrial Membrane Potential Assay Kit (ab113850, abcam, Cambridge, United Kingdom) according to the manufacturer's instruction. Briefly, isolated mitochondria were mixed with a working JC-1 solution diluted with dilution buffer. Then the mixture was loaded in a read plate and detected by Synergy H1 Hybrid Multi-Mode Microplate Reader at the excitation wavelength of 535 or 475 nm and emission wavelength at 590 or 530 nm. MMP was determined by the ratio of fluorescence intensity between 590 and 530 nm.

Mitochondrial Swelling Assay

Mitochondrial swelling was evaluated as described by Zangeneh et al. (2018). The mitochondrial swelling was determined by measuring decreased absorbance at 540 nm *via* BioTek Synergy H1 Hybrid Multi-Mode Microplate Reader. The cerebral mitochondria of mice were suspended in swelling buffer (70 mmol/L of sucrose, 230 mmol/L of mannitol, 3 mmol/L of HEPES, 2 mmol/L of Tris-phosphate, 5 mmol/L of succinate, and 1 μmol/L of rotenone). The mixture was incubated at 30°C for 1 h. The absorbance was measured at 5 and 45 min.

Mitochondrial Respiratory Chain Complex I, II, III, and IV Enzyme Activity Assay

Mitochondrial respiratory chain complex I II, III, and IV were measured by Complex I Enzyme Activity Microplate Assay Kit (ab109721, abcam, Cambridge, United Kingdom), Complex II Enzyme Activity Microplate Assay Kit (ab109908,

abcam, Cambridge, United Kingdom), MitoTox Complex II + III OxPhos Activity Assay Kit (ab109905, abcam, Cambridge, United Kingdom), and Complex IV Rodent Enzyme Activity Microplate Assay Kit (ab109911, abcam, Cambridge, United Kingdom) respectively according to the manufacturer's recommendation. Briefly 80 μg mitochondrial proteins were loaded in a 96-well plate, and the enzyme activity was determined colorimetrically with BioTek Synergy H1 Hybrid Multi-Mode Microplate Reader (BioTek, Winooski, VT, United States) by detecting the light absorption value of the sample at 450 nm (complex I), 600 nm (complex II), and 550 nm (complex III and complex IV) respectively.

Reactive Oxygen Species Assay

Cerebral reactive oxygen species (ROS) was assessed as described by Ali et al. (2015, 2018) previously with some modification. ROS assay was based on the oxidation of 2′7′-dichlorodihydrofluorescin diacetate (DCFH-DA) to 2′7′-dichlorofluorescein (DCF). Briefly, brain homogenate was diluted with ice-cold Lock's buffer (pH 7.4) to a final concentration of 5 mg tissue/mL. Then the Lock's buffer, diluted brain homogenate, and DCFH-DA (final concentration of 5 mmol/L) were mixed and incubated at RT for 15 min. The conversion of DCFH-DA to the DCF was determined by BioTek Synergy H1 Hybrid Multi-Mode Microplate Reader with excitation at 484 nm and emission at 530 nm. The ROS level was quantified from the DCF-standard curve and expressed as relative DCF pmol/mg protein.

Lipid Peroxidation Assay

The LPO levels in the mouse brain were determined by analyzing the malondialdehyde (MDA) level. MDA was examined by using the commercial lipid peroxidation assay kit (ab118970, abcam) according to the manufacturer's instructions. The samples were analyzed with BioTek Synergy H1 Hybrid Multi-Mode Microplate Reader with excitation at 532 nm and emission at 553 nm.

Statistical Analysis

Statistical analysis was carried out using the SPSS program (version 20.0 for windows) (IBM, Armonk, NY, United States). Values were expressed as mean ± SEM. 18 mice were used for the MWM test, and 5 mice were used for metabolomics analysis. The escape latencies and average swimming speed in the MWM test were analyzed with two-way repeated-measures ANOVA followed by Fisher's protected least significant difference (LSD) test for *post hoc* comparisons. Other data from behavioral assay were analyzed using one-way ANOVA followed by the LSD test for *post hoc* comparisons. The metabolomic data were transformed with Log2 for final statistical analysis. The PCA and the OPLS-DA were conducted with SIMCA-P software (Umetrics, Sweden), and another univariate analysis including independent sample *t*-test and *p*-value FDR adjust. $P \leq 0.05$ and $P \leq 0.01$ were considered to be statistically significant and highly significant, respectively.

RESULTS

Ultra-High-Performance Liquid Chromatography Profile of Dihuang-Yinzi

The chromatographic fingerprint of multi-components of the DHYZ was characterized by UPLC. As shown in **Figure 2**, 11 ingredients in DHYZ were identified and determined by comparing them with the standard reference compounds. The names of the 11 composite ingredients and their source herbs are listed in **Table 2**.

Effects of Dihuang-Yinzi on Learning and Memory Deficits in 2× Tg-AD Mice

To evaluate the effects of DHYZ on spatial learning and memory ability in 2× Tg-AD mice, the MWM test was employed to assess learning capacity *via* escape latency (i.e., time spent to reach the hidden platform). As shown in **Figure 3A**, during the 5-day training session of the place navigation test, the average escape latency of all the three groups of mice gradually declined, and two-way ANOVA with repeated measuring revealed that there were significant differences among the three groups: day, $F(4, 68) = 150.60$, $P < 0.0001$; treatment, $F(2, 34) = 98.79$, $P < 0.0001$; day by treatment interaction, $F(8, 136) = 9.515$, $P < 0.0001$. During the training session from the 2nd to the 5th day, Non-Tg mice exhibited a shorter escape latency than 2× Tg-AD mice (day1, $P > 0.9999$; day2∼day5, $P < 0.0001$). At the same time, on the 3rd to 5th day, DHYZ treatment could significantly diminish the escape latency of 2× Tg-AD mice as compared to the mice of model group (day1, $P = 0.4755$; day2, $P = 0.1278$; day3, $P = 0.0012$; day4 and day5, $P < 0.0001$). The escape latency may also be determined by the mouse's physical fitness. To explore whether DHYZ decreased the escape latency of mice due to the impact on their physical fitness, we measured the average swimming speed of the mice. As shown in **Figure 3B**, there was no significant difference in the average swimming speed among all three groups: day, $F(4, 68) = 27.600$, $P = 0.472$; treatment, $F(2, 34) = 5.375$, $P = 0.596$; day by treatment interaction, $F(8, 136) = 3.413$, $P = 0.219$. This indicates that DHYZ reduced the escape latency of 2× Tg-AD mice not by affecting their physical fitness.

In spatial probe test performed on the 6th day of the MWM test, there was a significant difference in the number of times each group of mice crossed the platform area where the platform was originally located [$F(2,51) = 21.89$, $P < 0.0001$] based on one-way ANOVA (**Figure 3C**). Meanwhile, DHYZ increased the number of times crossing the platform area remarkably ($P = 0.0208$). The quadrant where the platform was originally located was defined as the target quadrant (that is quadrant IV); the diagonal position of the target quadrant was defined as the opposite quadrant (that is quadrant II). As shown in **Figure 3D**, there were significant differences in the quadrant occupancy of the 3 groups of mice in the target quadrant [$F(2,51) = 25.12$, $P < 0.0001$] and the opposite quadrant [$F(2,51) = 9.76$, $P < 0.0001$] based on one-way *ANOVA*. Furthermore, 2× Tg-AD mice showed shorter residence time in the target quadrant ($P < 0.0001$) and longer residence time in the opposite quadrant ($P = 0.0084$) compared to Non-Tg mice. Compared with the model group, DHYZ administration

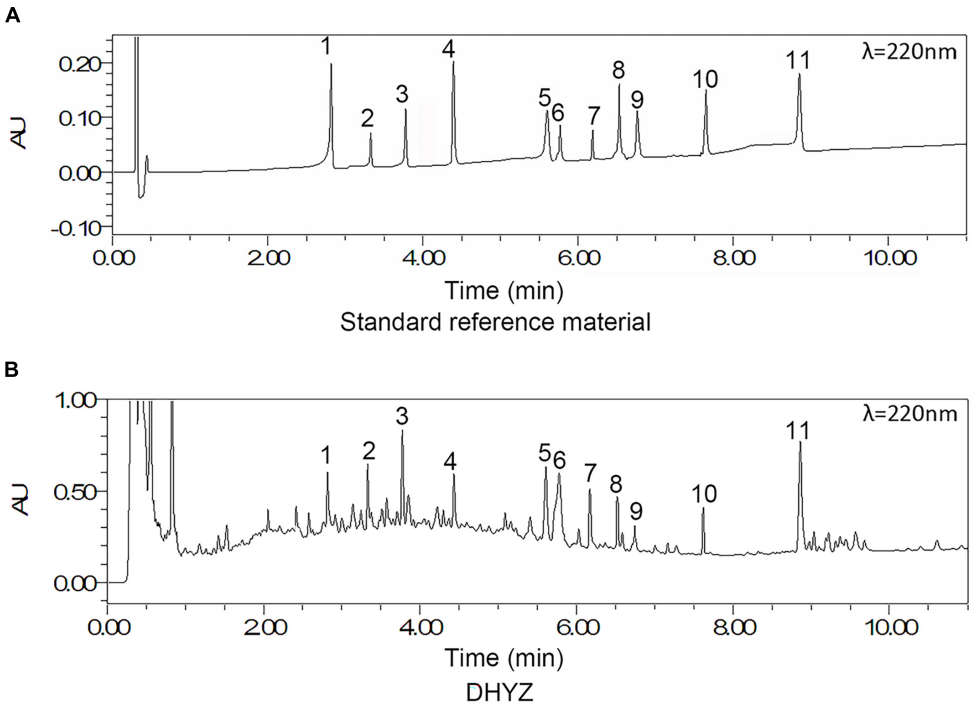

FIGURE 2 | UPLC-UV chromatograms of DHYZ at 220 nm. Representative chromatograms of standard reference compound **(A)** and DHYZ **(B)** were shown respectively. Peak no.: 1. loganin, 2. echinacoside, 3. verbascoside, 4. erianin, 5. cinnamic acid, 6. tenuifolin, 7. quercetin, 8. ruscogenin, 9. kaempferol, 10. beta-sitosterol, and 11. schisandrin A.

dramatically increased the residence time of 2× Tg-AD mice in the target quadrant ($P = 0.0042$) and reduced the residence time in the opposite quadrant ($P = 0.0074$). The swimming trajectories of three groups of mice in the spatial probe test were shown in **Figure 3E**.

The escape latency of mice searching for the hidden platform in the MWM depended not only on their spatial cognition ability and physical fitness, but also on their visual ability. To determine whether there was a difference in the eyesight of each group of mice and whether this difference would affect the ability of mice to search for the platform, the visible-platform test was performed. As shown in **Figures 3F,G**, under the premise that the platform was visible, there was no significant difference in the escape latency among the three groups of mice: treatment, $F(2, 34) = 0.7231$, $P = 0.4926$; day by treatment interaction, $F(4, 68) = 0.7010$, $P = 0.5939$, and at the same time, there was no significant difference in their swimming speed: day, $F(2, 34) = 0.6492$, $P = 0.5228$; treatment, $F(2, 34) = 0.9291$, $P = 0.4047$; day by treatment interaction, $F(4, 68) = 1.8190$, $P = 0.1352$. These results indicated that the difference in the escape latency of the three groups of mice searching platforms in the MWM test has nothing to do with their visual acuity and physical strength.

TABLE 2 | Composite ingredients and their source herbs.

Active ingredient	Chromatographic retention time (min)	Source herb
loganin	2.813	dogwood
echinacoside	3.331	cistanche, jujube
verbascoside	3.774	rehmannia, dogwood, jujube, ginger
erianin	4.433	dendrobium
cinnamic acid	5.629	cinnamon
tenuifolin	5.778	polygala
quercetin	6.272	cistanche, jujube
ruscogenin	6.515	ophiopogon
kaempferol	6.733	calamus
beta-sitosterol	7.648	morinda
schisandrin A	8.881	schisandrae

Network Pharmacology Analysis of Dihuang-Yinzi

To explore the active ingredients and potential molecular targets of DHYZ which have therapeutic effects on AD, we performed network pharmacological analysis. First, 123 composite compounds in DHYZ were retrieved from the database (**Supplementary Table 1**). Moreover, based on the obtained composite compounds, we identified 829 predicted targets of DHYZ. After searching the keywords of "Alzheimer" in the genecards, 1119 AD-related targets were collected. 192 common targets as potential therapeutic targets of DHYZ against AD were obtained *via* matching the predicted targets of DHYZ and AD (**Figure 4A** and **Supplementary Table 2**). All the 192 targets were normalized to their official symbols and then were

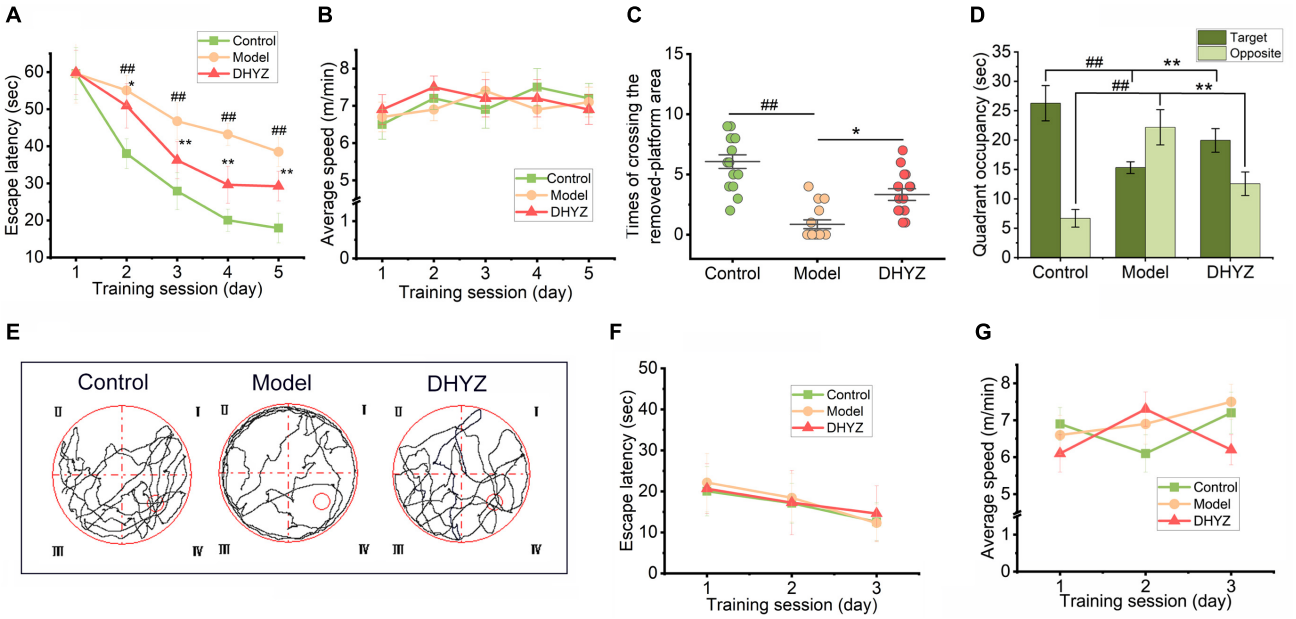

FIGURE 3 | DHYZ treatment improves spatial memory of 2× Tg-AD mice in the Morris water maze (MWM) test. In the place navigation test, the escape latency **(A)** and average swimming speed **(B)** of each group were recorded. In the spatial probe test, the times of crossing the removed platform area **(C)**, the residence time of the 3 groups of mice in the target quadrant, and the opposite quadrant **(D)** were assayed, and representative images of the route of travel **(E)** were recorded. The escape latency **(F)** and average swimming speed **(G)** in the visible-platform test were measured. All data are presented as the mean ± SEM (n = 18 mice per group). $^{\#\#}P < 0.01$, model *vs.* control; $^{*}P < 0.05$ and $^{**}P < 0.01$, DHYZ *vs.* model. AD, Alzheimer; DHYZ, Dihuang-Yinzi.

input into STRING 11.0 to construct a PPI network which gave a whole view of the relationship within the targets (**Figure 4B**). By using the CytoHubba to calculate the hub genes, we combined the scores of 15 computational methods, then choosed the top 15 genes as the hub genes, including *NDUFA12*, *NDUFS1*, *GAPDH*, *IL10*, *AKT1*, *SIRT1*, *HIF1A*, *NOS3*, *HSPA1A*, *PARP1*, *ARG1*, *LDHA*, *ACHE*, *ALDH3B2*, and *DAO* (**Supplementary Table 3**). All hub genes were presented as the faint yellow nodes in the PPI network (**Figure 4B**), suggesting that these hub genes might be the key target genes for DHYZ to improve cognitive dysfunction in AD.

We then constructed the herbs-composite ingredients-potential targets network by Cytoscape 3.8.2 for a global view, which was constituted by 15 herbs that make up DHYZ, 123 composite ingredients, and 192 potential targets for DHYZ to treat AD (**Figure 4C**). We next performed GO and KEGG pathways enrichment analyses. The top-twenty enriched GO terms ranked by p-value in biological processes, cell components, and molecular functions are presented in **Figure 4D** and **Supplementary Table 4**. The top-five terms in GO biological processes were the generation of precursor metabolites and energy (GO:0006091), response to oxidative stress (GO:0006979), cellular response to chemical stress (GO:0062197), energy derivation by oxidation of organic compounds (GO:0015980), cellular response to oxidative stress (GO:0034599). This indicated that restoring energy metabolism and inhibiting oxidative stress are major aspects of DHYZ's anti-AD effect. In terms of GO cellular components, the top-five enriched items were mitochondrial respiratory chain complex I (GO:0005747), NADH dehydrogenase complex (GO:0030964), respiratory chain complex I (GO:0045271), oxidoreductase complex (GO:1990204), respiratory chain complex (GO:0098803). Regarding GO molecular functions, the top-five terms were oxidoreductase activity (GO:0016491), oxidoreductase activity, acting on NAD(P)H, quinone or similar compound as acceptor (GO:0016655), electron transfer activity (GO:0009055), NAD(P)H dehydrogenase (quinone) activity (GO:0003955), oxidoreductase activity, acting on NAD(P)H (GO:0016651). This shows that DHYZ's efficacy in treating AD involves the protection of mitochondrial function, oxidative phosphorylation, oxidoreductase system, etc. According to the KEGG enrichment analysis, the pathways affected significantly were Non-alcoholic fatty liver disease (NAFLD), AD, signaling, and other neurodegenerative diseases, such as Parkinson's disease (PD), Huntington's disease (HD), etc. In particular, KEGG enrichment analysis revealed that the DHYZ's efficacy involves AD and other neurodegenerative diseases related pathways, oxidative phosphorylation, HIF-1 signaling pathway, etc. (**Figure 4E** and **Supplementary Table 5**).

Untargeted Metabonomics Profiling of Alzheimer's Disease Treatment by Dihuang-Yinzi

To identify the significantly changed metabolites of 2× Tg-AD mice with DHYZ treatment, we performed a untargeted metabolomics analysis. Principal component analysis (PCA) and OPLS-DA in multivariate analysis were performed to

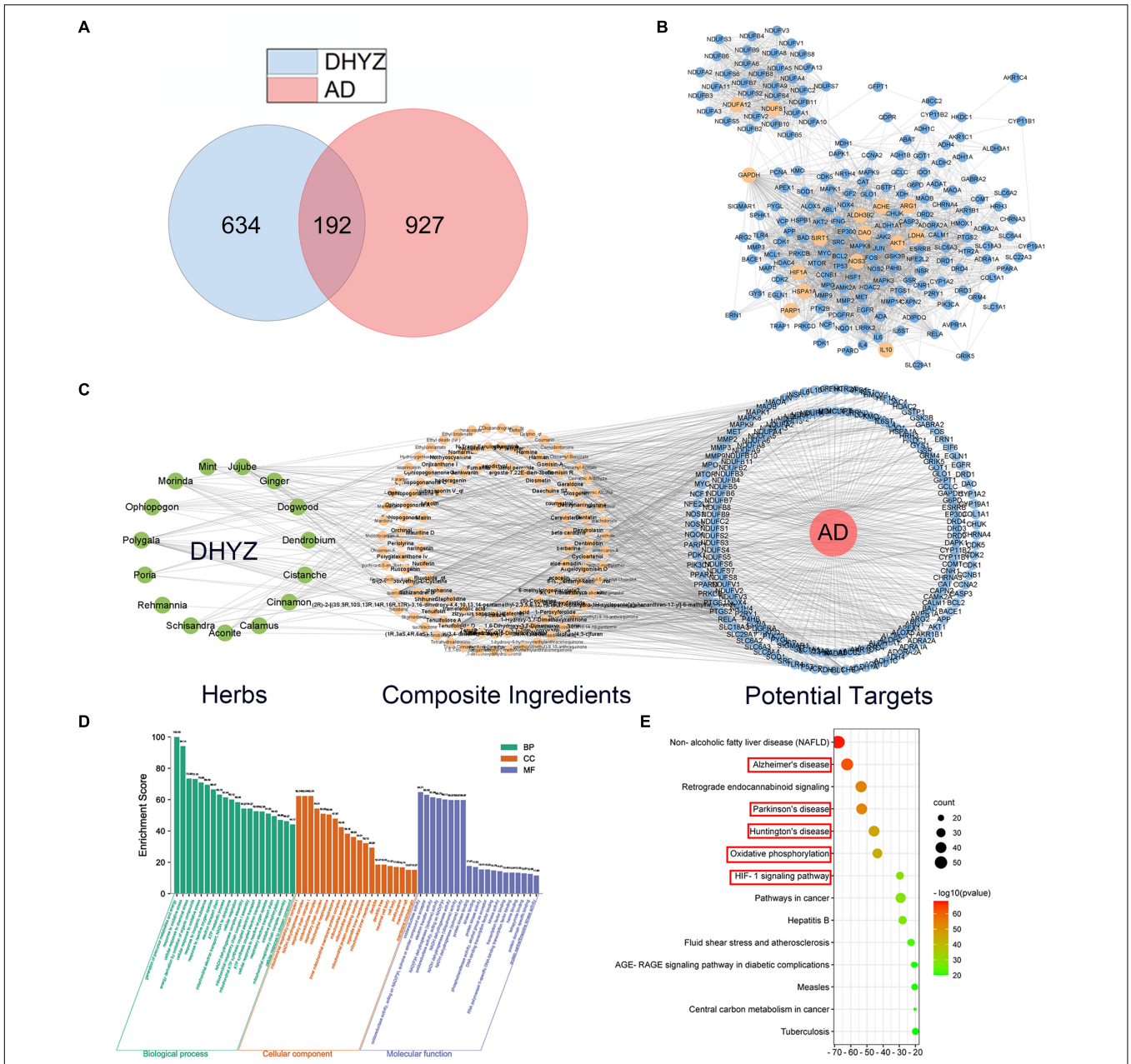

FIGURE 4 | Network pharmacology analysis of DHYZ against AD. **(A)** Venn diagrams of the targets of DHYZ and AD, and common-targets of DHYZ against AD. **(B)** The protein-protein interaction network of targets of DHYZ against AD. The nodes with faint yellow color represent the hub genes. **(C)** The herbs-composite ingredients-potential targets network of DHYZ in the treatment of AD. The green, faint yellow, and blue nodes represent herbs that makeup DHYZ, composite ingredients, and the potential target genes, respectively. GO enrichment **(D)** and KEGG pathway enrichment analyses **(E)** were performed to probe the biological function and potential mechanisms of 192 potential target genes of DHYZ in treating AD. GO, gene ontology; KEGG, Kyoto Encyclopedia of Genes and Genomes; BP, biological processes; CC, cell components; MF, molecular functions; AD, Alzheimer's disease; DHYZ, Dihuang-Yinzi.

evaluate and determine the endogenous substances that changed significantly in rodent urine, and are also used to screen the metabolites that varied remarkably in 2× Tg-AD mice after DHYZ treatment. As shown in **Figure 5A**, OPLS-DA revealed that the five samples in each group are clustered together, and there was a significant distinction among samples from different groups.

The R^2Y (cum) and Q^2 (cum) in OPLS-DA were 0.877 and 0.542, respectively, using the data from the model *vs.* control group and 0.853 and 0.596, using the data from the DHYZ *vs.* model group, respectively. 999 times permutation tests were performed to test the robustness of OPLS-DA modeling and verify the validity of the data multivariate analysis model (**Figure 5B**). The permutation test showed the models were

non-overfitting and reliable. These results indicated that the samples from the control group, model group, and DHYZ group could be distinguished well, and DHYZ treatment resulted in obvious metabolic variations in 2× Tg-AD mice. As shown in **Figure 5C**, S-plot was employed to identify altered metabolites that markedly contributed to the differences between the model and control groups and the differences between DHYZ and model groups, respectively. Moreover, volcano plots revealed that the up-regulated (red plots) and down-regulated (blue plots) metabolites were significantly different between the model and control group and between the DHYZ and model group with $P < 0.05$ and fold change (FC) >2 (**Figure 5D**).

Based on $P < 0.05$ and FC > 2, 64 differential metabolites were identified in the urine between the model and the control group; 44 differential metabolites were identified between the DHYZ and model groups. Finally, 22 common metabolites were identified as differential metabolites that DHYZ affected 2× Tg-AD mice in urine (**Figure 5E** and **Table 3**). To further visualize the variation in metabolites among the control, model, and DHYZ group, we plotted the heat map to show the 22 differential metabolites changed among the 3 groups (**Figure 5F**). Notably, compared with the control group, most of the differential metabolites that changed in the model group were reversed after DHYZ intervention, indicating that DHYZ could ameliorate metabolic perturbation in 2× Tg-AD mice.

To further reveal the key metabolic pathways involved in process of the AD treatment by DHYZ, we performed KEGG pathway enrichment by using the MetaboAnalyst 5.0. Based on pathway impact >0.1, 6 signaling pathways were enriched: TCA cycle, pyruvate metabolism, glycolysis/gluconeogenesis, arginine biosynthesis, nicotinate, nicotinamide metabolism, and glycerophospholipid metabolism (**Figures 5G,H**). The key differential metabolites involved in these pathways were pyruvate, succinate, fumarate, citrate, phosphoenolpyruvate, cis-aconitate, (s)-lactate, L-citrulline, nicotinate, nicotinamide, choline, and sn-glycerol-3-phosphate. All pathways with $P < 0.05$ or pathway impact >0.1 were listed in **Table 4**.

Integrated Analysis of Metabolomics and Network Pharmacology in the Treatment of Alzheimer's Disease by Dihuang-Yinzi

As it is aimed to obtain a systematic and comprehensive view of mechanisms of DHYZ against AD, we constructed an interaction network based on metabolomics and network pharmacology (**Figure 6**). Differential metabolites were imported into the MetScape plugin in Cytoscape to construct the compound-reaction-enzyme-gene networks. By matching the hub genes screened in network pharmacology analysis with the differential metabolites in MetScape analysis, we identified 5 key target genes, including *DAO*, *HIF1A*, *ALDH3B2*, *PARP1*, and *ACHE*. 14 related key metabolites were identified as follows: cis-aconitic acid, citric acid, phosphoenolpyruvic acid, pyruvic acid, fumaric acid, succinic acid, L-lactic acid, malonic acid, nicotinamide, guanine, hypoxanthine, nicotinic acid, glycerol-3-phosphate, and choline. The 4 key pathways were the TCA cycle, glycolysis, nicotinate and nicotinamide metabolism, and glycerophospholipid metabolism (**Table 5**). These data revealed that all the 5 key target genes, 14 metabolites, and 4 key metabolic pathways may play essential roles in the therapeutic effect of DHYZ against AD.

Effects of Dihuang-Yinzi on Glycerophospholipid Metabolism and the Structure and Function of Mitochondria

As confirmed by metabolomics analysis, DHYZ could elevate the relative abundance of phosphatidate ($P < 0.01$) and choline ($P < 0.01$) in the urine of 2× Tg-AD mice (**Figure 7A**). Since phosphatidate is an important precursor for the synthesis of cardiolipin (CL) which is the signature phospholipid of mitochondrial membranes, we determined the content of Tetralinoleoyl-cardiolipin (L_4-CL), the major CL species, in the mouse brains. The cerebral L_4-CL level in 2× Tg-AD mice decreased significantly ($P < 0.01$), and DHYZ could reverse this trend remarkedly ($P < 0.01$) (**Figure 7B**). Acetylcholine (Ach), a precursor of choline, is the cerebral neurotransmitter most closely related to learning and memory. As shown in **Figure 7C**, the Ach level in the brain of mice in model group decreased remarkably compared to the control group ($P < 0.01$), and DHYZ treatment increased the cerebral Ach level in 2× Tg-AD mice dramatically ($P < 0.01$). Acetylcholinesterase (AchE) is a clinically proven therapeutic target for AD treatment. Using Western blotting assay, we confirmed that DHYZ could down-regulate AchE expression ($P < 0.01$) in 2× Tg-AD mice (**Figure 7D**). These results were consistent with the effect of DHYZ on improving the learning and memory of AD mice as confirmed in behavioral tests.

As the signature phospholipid of mitochondrial membranes, CL is closely related to the function and structure integrity of mitochondria, and a decrease in the CL level would results in serious destruction to the mitochondrial membrane disruption (Kameoka et al., 2018). As shown in **Figure 7E**, we observed the obvious swelling, membrane structure destruction, cristae breakage in mitochondria in 2× Tg-AD mice. On the contrary, DHYZ could protect the mitochondria from those ultrastructure destructions. In line with this, DHYZ increased MMP and depressed mitochondrial swelling in 2× Tg-AD mice (**Figures 7F,G**).

The OxPhos system consists of 5 enzymatic complexes (Complexes I to V) which form the mitochondrial respiratory chain are embedded in the inner mitochondrial membrane. The OxPhos is strongly associated with mitochondrial membrane integrity. To study the impact of DHYZ on OxPhos, we measured the activities of Complex I ∼ IV. Consistent with the protecting role of DHYZ in mitochondrial membrane integrity, DHYZ treatment markedly improved the activities of the Complex I, III, and IV respectively ($P < 0.01$), but had no significant effect on the activity of the Complex II (**Figure 7H**).

Mitochondria are the major source and producer of intracellular ROS. Overproduction of ROS and the resultant oxidative stress are the indicators of mitochondrial dysfunction. To investigate whether DHYZ could inhibit oxidative stress, we assessed oxidative damage by quantifying 8-Oxoguanine (8-OxoG) adducts and the conversion of DCFH-DA to the DCF

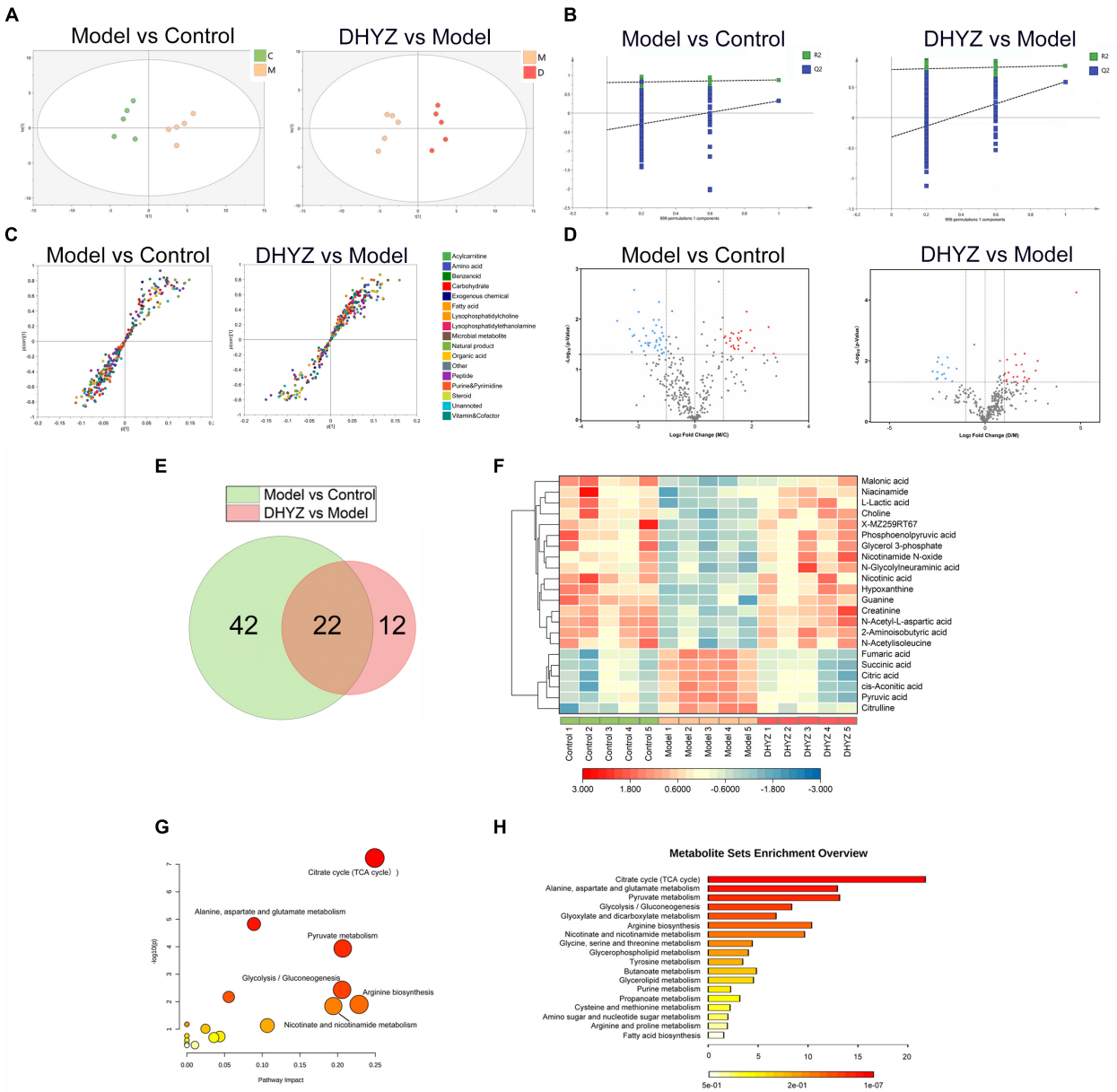

FIGURE 5 | Untargeted metabonomics profiling of AD treatment by DHYZ. **(A)**Score plot of PCA modeling to maximize inter-group differentiation of metabolomics data between the model and control group and between DHYZ and model group. **(B)** 999 times permutation to test the robustness of OPLS-DA modeling between model and control group and between DHYZ and model group. **(C)** S-plot of OPLS-DA model differentiating the model *vs.* control group and the DHYZ *vs.* mode group. **(D)** Volcano plot to visualize differential metabolites of significance between the model and control group and between the DHYZ and model group. **(E)** Venn diagrams of potential metabolites between the model and control group, and between the DHYZ and model group. **(F)** The heat map of potential metabolites involved in 2× Tg-AD mice treated by DHYZ. MetaboAnalyst analysis and visualization of metabolism pathway involved in treating AD with DHYZ. **(G)** Summary of pathway analysis visualized by the dot chart. The dots represent the pathways that were matched pathway impact values from pathway topology analysis and *p*-values from pathway enrichment analysis. **(H)** KEGG enrichment analysis of metabolism pathway for associated urinary metabolites in 2× Tg-AD mice treated with DHYZ. Metabolites with $P < 0.05$ and fold change (FC) >2 were highlighted with red (up-regulated) and blue (down-regulated), respectively. C, control group; M, model group; D, DHYZ group. KEGG, Kyoto Encyclopedia of Genes and Genomes; AD, Alzheimer's disease; DHYZ, Dihuang-Yinzi.

in the brain of AD mice. As shown in **Figures 7I,J**, 2× Tg-AD mice exhibited excessive ROS production, especially in the hippocampus, as compared with the control mice ($P < 0.01$), and DHYZ dramatically eliminate ROS overload in the brain of AD mice ($P < 0.01$). Excessive production of ROS results in lipid peroxidation (LPO) and malondialdehyde (MDA) generation, the latter is the hallmark of oxidative damage on the cellular membrane system, including the mitochondrial membrane. As

TABLE 3 | Differential metabolites in the urine of 2× Tg-AD mice treated by DHYZ.

No	Class	Metabolite	HMDB	m/z	Model *vs.* Control		DHYZ *vs.* Model	
					P	Log_2FC	*P*	Log_2FC
1	Amino acid	Citrulline	HMDB0000904	176.10	0.0018	1.5410	0.0029	−1.0654
2	Amino acid	N-Acetylisoleucine	HMDB0061684	174.11	0.0187	−1.1439	0.0294	1.1873
3	Amino acid	N-Acetyl-L-aspartic acid	HMDB0000812	174.04	0.0326	−1.2431	0.0244	1.2255
4	Amino acid	Creatinine	HMDB0000562	114.06	0.0311	−1.2653	0.0456	1.7897
5	Amino acid	Choline	HMDB0000097	104.10	0.0311	−1.2834	0.0257	1.0508
6	Carbohydrate	N-Glycolylneuraminic acid	HMDB0000833	324.09	0.0231	−1.5321	0.0312	2.0584
7	Carbohydrate	L-Lactic acid	HMDB0000190	89.02	0.0166	−1.5633	0.0376	1.5230
8	Carbohydrate	Phosphatidate	HMDB00636	171.00	0.0217	−1.6789	0.0313	1.4140
9	Organic acid	Pyruvic acid	HMDB0000243	87.01	0.0234	1.6462	0.0101	−1.6273
10	Organic acid	cis-Aconitic acid	HMDB0000072	173.01	0.0264	1.8495	0.0183	−1.6000
11	Organic acid	Phosphoenolpyruvic acid	HMDB0000263	166.96-166.98	0.0364	−2.1785	0.0313	1.8467
12	Organic acid	Citric acid	HMDB0000094	191.02	0.0353	2.2725	0.0257	−2.1395
13	Organic acid	Fumaric acid	HMDB0000134	115.00	0.0376	2.6311	0.0470	−1.7610
14	Organic acid	2-Aminoisobutyric acid	HMDB0001906	102.05	0.0218	−1.1071	0.0260	1.0385
15	Organic acid	Succinic acid	HMDB0000254	117.02	0.0187	2.5398	0.0333	−2.3221
16	Organic acid	Methylmalonate	HMDB00202	103.00	0.0045	−1.2553	0.0100	1.1760
17	Purine and Pyrimidine	Guanine	HMDB0000132	152.06	0.0072	−1.9736	0.0061	1.5794
18	Purine and Pyrimidine	Hypoxanthine	HMDB0000157	137.05	0.0132	−1.3563	0.0425	1.1240
19	Unannotated	X-MZ259RT67		259.10	0.0103	−1.2613	0.0488	1.0559
20	Vitamin and Cofactor	Nicotinamide N-oxide	HMDB0002730	139.05	0.0305	−1.3816	0.0155	1.8438
21	Vitamin and Cofactor	Nicotinic acid	HMDB0001488	124.04	0.0280	−1.1512	0.0396	1.0409
22	Vitamin and Cofactor	Niacinamide	HMDB0001406	123.06	0.0335	−1.2190	0.0382	1.0404

TABLE 4 | Pathways were affected significantly after DHYZ intervention with $P < 0.05$ or pathway impact >0.1.

Pathway Name	Match Status	*p*	−log(p)	Holm p	FDR	Impact	Details
tricarboxylic acid cycle (TCA cycle)	6/20	5.9036E-8	7.2289	4.959E-6	4.959E-6	0.24929	KEGG
Alanine, aspartate and glutamate metabolism	5/28	1.4882E-5	4.8273	0.0012352	6.2506E-4	0.08894	KEGG SMP
Pyruvate metabolism	4/22	1.1493E-4	3.9396	0.009424	0.0032179	0.20684	KEGG SMP
Glycolysis/Gluconeogenesis	3/26	0.0036879	2.4332	0.29872	0.077447	0.20594	KEGG SMP
Glyoxylate and dicarboxylate metabolism	3/32	0.0067053	2.1736	0.53643	0.11265	0.05556	KEGG
Arginine biosynthesis	2/14	0.012543	1.9016	0.99086	0.17237	0.22843	KEGG
Nicotinate and nicotinamide metabolism	2/15	0.014364	1.8427	1.0	0.17237	0.1943	KEGG SMP
Glycerophospholipid metabolism	2/36	0.073657	1.1328	1.0	0.68747	0.10675	KEGG

expected, we observed that the MDA level was significantly elevated compared to the control group ($P < 0.01$) due to oxidative injury, and DHYZ treatment remarkably decreased the MDA level ($P < 0.01$) (**Figure 7K**).

Taken together, DHYZ improved glycerophospholipid metabolism and increased CL levels, thereby protecting mitochondrial membrane integrity and mitochondrial function, and reducing ROS overproduction and oxidative damage. At the same time, DHYZ restored Ach levels and improved cognitive performance by inhibiting AchE activity (**Figure 7L**).

Dihuang-Yinzi Adjusted Nicotinate and Nicotinamide Metabolism and Promoted Glycolysis

As previously demonstrated by metabolomic analysis, the nicotinate and nicotinamide metabolism is one of the key metabolism pathways for DHYZ against AD. As shown in **Figure 8A**, the relative abundance of nicotinic acid ($P < 0.05$) and nicotinamide ($P < 0.01$) decreased in the urine of 2× Tg-AD mice. In line with this, there was a significant decrease in the level of nicotinamide adenine dinucleotide (NAD^+) in the brain of 2× Tg-AD mice ($P < 0.01$) (**Figure 8B**). Postintervention, DHYZ markedly increased the levels of urinal nicotinic acid ($P < 0.01$) and nicotinamide ($P < 0.01$), and cerebral NAD^+ content ($P < 0.01$) in 2× Tg-AD mice. Besides, the depletion of intracellular NAD^+ might also result from the upregulation of Poly [ADP-ribose] polymerase 1 (PARP-1), we determined PARP-1 expression in the brain of 2× Tg-AD mice by Western blotting. As shown in **Figure 8C**, PARP-1 level elevated dramatically in 2× Tg-AD mice as compared to the control mice ($P < 0.01$), and DHYZ markedly depressed the level of PARP-1 in 2× Tg-AD mice ($P < 0.01$).

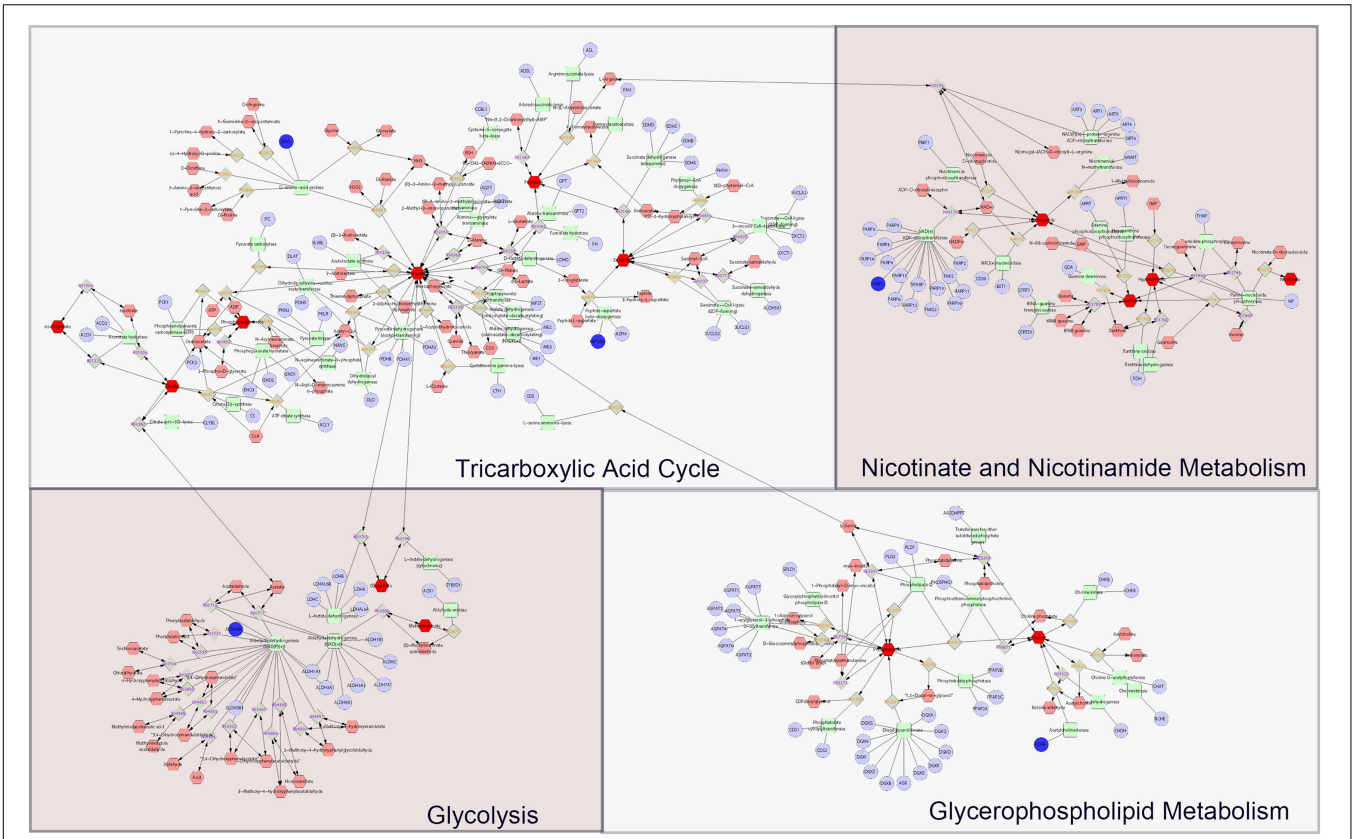

FIGURE 6 | The compound-reaction-enzyme-gene networks based on the key metabolites and targets of DHYZ against AD. The faint red hexagons, gray diamonds, green round rectangle, and purple circles represent the compounds, reactions, proteins, and genes, respectively. The scarlet hexagons and dark blue circles represent the key metabolites and target genes of DHYZ against AD. AD, Alzheimer's disease; DHYZ, Dihuang-Yinzi.

In glycolysis, NAD^+ is served as an essential coenzyme for glyceraldehyde-3-phosphate dehydrogenase which catalyzes the conversion of glyceraldehyde-3-phosphate to 1,3-diphosphoglycerate (Ju et al., 2017). The levels of L-lactic acid, an important end product of glycolysis, in the urine of 2× Tg-AD mice were significantly reduced as shown by metabolomic analysis ($P < 0.01$), which might be partly due to NAD^+ depletion. DHYZ remarkably elevated the level of L-lactic acid ($P < 0.01$), and thus promote glycolysis in 2× Tg-AD mice (**Figure 8D**). As one of the critical targets of DHYZ against AD, ALDH3B2 expression decreased significantly in the brain of 2× Tg-AD mice as compared to the control mice ($P < 0.01$), which was detected with fluorescence immunoassay and Western blotting (**Figures 8E,F**). In contrast, DHYZ could upregulate the cerebral ALDH3B2 expression in 2× Tg-AD mice ($P < 0.01$), and this was consistent with the predominantly glycolysis-promoting role of DHYZ (**Figures 8E,F**). Furthermore, as shown in **Figure 8E**, ALDH3B2 colocalized to S100B, a marker of astrocytes, in control mice. This implies that ALDH3B2 was mainly expressed in astrocytes that are the main sites of glycolysis.

Taken together, we conclude that there was an obvious disturbance in nicotinate/nicotinamide metabolism and glycolysis in 2× Tg-AD mice. DHYZ could ameliorate this chaos by elevating the abundance of nicotinic acid and nicotinamide and restoring the level of NAD^+ by depressing the PAPR-1. Furthermore, DHYZ promoted glycolysis by upregulating ALDH3B2, improving glyceraldehyde-3-phosphate conversion, and elevating the level of L-lactic acid which is an important energy substance produced by glycolysis and delivered by astrocytes to neurons *via* astrocyte-neuron lactate shuttle (ANLS) (**Figure 8G**).

Dihuang-Yinzi Improved Tricarboxylic Acid Cycle and Promoted Energy Production

Given that DHYZ ameliorated the structural and functional impairments of the mitochondria, we next investigated whether DHYZ could also modulate and preserve the TCA cycle, oxidative phosphorylation pathways, and related energy generation process that occurs in the mitochondria. Metabolomics analysis demonstrated that the contents of 4 intermediate metabolites in the TCA cycle in the urine of 2× Tg-AD mice increased remarkably, including pyruvic acid ($P < 0.05$), citric acid ($P < 0.01$), succinic acid ($P < 0.05$), and fumaric acid ($P < 0.01$) (**Figure 9A**). The obvious accumulation of the 4 intermediate metabolites indicated that the pronounced disturbance occurred

TABLE 5 | The information of key targets, metabolites, and metabolic pathways.

Related pathway	Target gene	Key metabolite
TCA cycle	*DAO*, *HIF1A*	cis-Aconitic acid, Citric acid, Phosphoenolpyruvic acid, Pyruvic acid, Fumaric acid, Succinic acid
Glycolysis	*ALDH3B2*	L-Lactic acid, Methylmalonic acid
Nicotinate and Nicotinamide Metabolism	*PARP1*	Nicotinamide, Guanine, Hypoxanthine, Nicotinic acid
Glycerophospholipid Metabolism	*ACHE*	Phosphatidate, Choline

in TCA cycle of 2× Tg-AD mice. On the contrary, DHYZ could decrease the level of urine pyruvic acid ($P < 0.05$), citric acid ($P < 0.05$), succinic acid ($P < 0.05$), and fumaric acid ($P < 0.01$) in 2× Tg-AD mice dramatically (**Figure 9A**).

D-amino-acid oxidase (DAO) is one of the potential targets of DHYZ against AD as the bioinformatics analysis revealed. We further confirmed the expression of DAO in the brain of 2× Tg-AD mice by using Western blotting. As shown in **Figure 9B**, the DAO level in the brain of 2× Tg-AD mice dramatically decreased compared to the control mice ($P < 0.01$). In contrast, DHYZ significantly upregulated DAO expression in 2× Tg-AD mice ($P < 0.01$). The upregulation of hypoxia-inducible factor 1-alpha (HIF1A) results in increased expression of pyruvate dehydrogenase kinase 1 (PDHK1), which leads to phosphorylation of pyruvate dehydrogenase (PDH) and depresses the entry of pyruvate into the TCA cycle (Lai et al., 2013). DHYZ markedly reduced the levels of HIF1A ($P < 0.01$) and PDHK1 ($P < 0.05$), and depressed the phosphorylation of PDH ($P < 0.01$), consistent with the decrease of pyruvic acid level which means more pyruvic acid was utilized and entered the TCA cycle in 2× Tg-AD mice.

The TCA cycle is the core pathway of OxPhos which is the main way to meet the high energy demand of the central nervous system (CNS). To determine whether the beneficial effects of DHYZ on the TCA cycle could result in improved energy supplement in the brain of 2× Tg-AD mice, we measured the level of the cerebral adenosine triphosphate (ATP), adenosine diphosphate (ADP), and adenosine monophosphate (AMP). As can be seen in **Figure 9C**, DHYZ treatment significantly increased the levels of ATP ($P < 0.01$) and EC ($P < 0.01$). Consistent with this result, the AMP level decreased remarkably in DHYZ-treated 2× Tg-AD mice ($P < 0.01$). Interestingly, despite the marked increase in the ADP level ($P < 0.01$) in 2× Tg-AD mice compared to the control mice, there was no significant change in ADP level ($P > 0.05$) in 2× Tg-AD mice upon DHYZ treatment.

Collectively, DHYZ increased the L-lactic acid level to enhance the supplement of the energy substrate of the TCA cycle. DHYZ down-regulates HIF1A and PDHK1, thereby inhibiting the phosphorylation of PDH and promoting the entry of pyruvate into the TCA cycle. Besides, DHYZ elevated the expression of DAO which converted D-alanine to pyruvic acid, and promoted the potential supplementary pyruvic acid into the TCA cycle. At the same time, the levels of pyruvic acid, citric acid, succinic acid, and fumaric acid decreased, and the level of ATP increased dramatically in 2× Tg-AD mice upon DHYZ treatment, indicating its facilitating role in the TCA cycle and related energy metabolism (**Figure 9D**).

DISCUSSION

As the most common form of severe dementia, AD has complex and confusing pathogenesis. In the present study, we integrated the metabolomics and network pharmacology analysis to investigate the comprehensive relationship of the herbal ingredients, their crucial targets, differential metabolites, and related metabolic pathways. Our data presented here exhibited a systematical mechanism of DHYZ against AD, by which DHYZ could improve the cognition in 2× Tg-AD mice by ameliorating the disturbance of the 4 key energy-related metabolism pathways. The 4 key energy-related metabolic pathways targeted by DHYZ were linked by mitochondrial damage and the resultant ROS overload, forming an interconnected and complete network system (**Figure 10**). The results of the present study showed that DHYZ exhibited therapeutic efficacy against AD *via* the synergistic effect of multiple targets and multiple pathways. First, DHYZ improved the glycerophospholipid metabolism and depressed the resultant mitochondrial membrane disruption which contributes to OxPhos decline and the excess production of ROS. ROS overproduction might in turn cause further mitochondrial damage and DHYZ blocked the vicious circle of ROS overload and mitochondrial dysfunction. Secondly, overproduced ROS led to DNA damage which subsequently upregulated PARP-1 expression. DHYZ depressed PARP-1 and the resulting NAD^+ depletion which contributed to the disturbance of nicotinate/nicotinamide metabolism and glycolysis. The third, DHYZ promoted the glycolysis and inhibited ROS-induced mitochondrial dysfunction, in turn, improved TCA cycle and energy supplement.

Dihuang-Yinzi is a well-accepted traditional Chinese herbal prescription which is widely used for the treatment of various aging-related diseases and neurological deficits, such as AD, Parkinson's disease, amyotrophic lateral sclerosis, arteriosclerosis, aging-related stroke, etc. (Hu et al., 2009; Qiu et al., 2016; Lee et al., 2021). The effectiveness of DHYZ has been proven *via* clinical verification for a long time (Lee et al., 2021). In the present study, we investigated and evaluated the effects of DHYZ on spatial memory and cognition of 2× Tg-AD mice by MWM. DHYZ ameliorated cognitive impairment and memory dysfunction in 2× Tg-AD mice. Taking into account the interference of physical and visual capacity of 2× Tg-AD mice on cognitive function assessment, we confirmed that DHYZ has no significant effect on the physical fitness and visual acuity of 2× Tg-AD mice through visible-platform tests and measuring the swimming speed of each mouse.

Alzheimer's disease is a progressive, irreversible, complex, and multifactorial neurodegenerative disease that lacks a curative

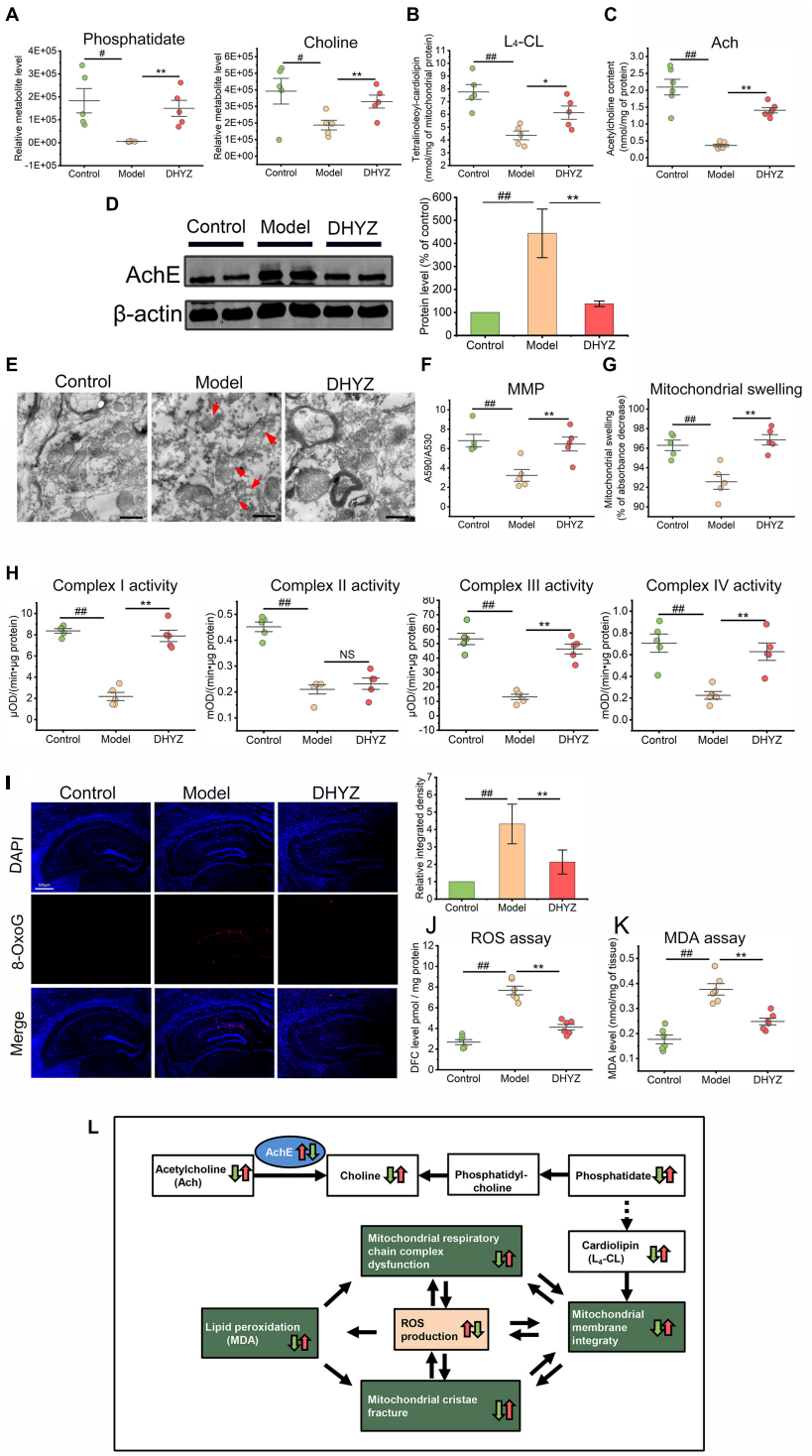

FIGURE 7 | The preservation effects of DHYZ on the glycerophospholipid metabolism and the structure and function of mitochondria. **(A)** Metabolomics analysis illustrating the relative levels of urine phosphatidate and choline. The level of L_4-CL (n = 5) **(B)** and Ach (n = 6) **(C)** in the brain of 2× Tg-AD mice were determined with LC-MS and fluorescence chemistry assay, respectively. **(D)** The AchE expression was detected by Western blotting (n = 3). **(E)** Representative electron micrographs of hippocampal tissues of mice of the control, model, and DHYZ group. Red arrows denote the lesions of mitochondrial ultramicrostructure (magnification ×40 000, scale bar = 500 nm). MMP **(F)** and mitochondrial swelling **(G)** were measured to assess the integrity of the mitochondrial membrane. **(H)** The activities of respiratory chain complexes I, II, III, and IV were assessed to evaluate the mitochondrial function. **(I)** Representative images of immunofluorescence staining of 8-OxoG (red, Alexa Fluor® 594; blue, DAPI) and the corresponding histogram of 8-OxoG relative intensity in hippocampus regions

(Continued)

FIGURE 7 | of mice of the control, model, and DHYZ group (n = 5 mice per group; magnification ×40, scale bar = 500 μm). **(J)** The scatter dot plot diagram of ROS level is expressed as DFC level. **(K)** The LPO was determined by measuring the MDA level. **(L)** Diagram depicting alteration in glycerophospholipid metabolism and the structure and function of mitochondria in AD mouse in response to DHYZ treatment. White squares represent metabolites, green squares represent mitochondrion function, blue ellipses represent target proteins or key enzymes. Red up-arrows and green down-arrows indicate up-regulation and down-regulation, respectively. Left arrows represent model *vs.* control; right arrows represent DHYZ *vs.* model. All data are presented as the mean ± SEM. $^{\#}P < 0.05$ and $^{\#\#}P < 0.01$, model *vs.* control; $^{*}P < 0.05$ and $^{**}P < 0.01$, DHYZ *vs.* model. AD, Alzheimer's disease; DHYZ, Dihuang-Yinzi; L_4-CL, tetralinoleoyl-cardiolipin; Ach, acetylcholine; AchE, acetylcholinesterase; MMP, mitochondrial membrane potential; 8-OxoG, 8-Oxoguanine; ROS, reactive oxygen species; LPO, lipid peroxidation; MDA, malondialdehyde.

treatment. The complexity of AD is a key impediment in the search for effective drug targets to treat or reverse AD-associated cognitive decline. As a consequence, the exploration of the biomarker for early diagnosis and the overall assessment of drug efficacy would be extremely advantageous to controlling AD progression and improving therapeutic outcomes. Metabolomics provides us with a powerful tool to detect perturbation in metabolites that reflect the variation of the downstream biological process of genomics, transcriptomics, and proteomics, and thus it can more accurately reflect the distinction of biological profiles between the "diseased" state as compared with the "healthy" one. For these reasons, several studies focusing on metabolome in AD have been performed over the last 5 years (Toledo et al., 2017; Varma et al., 2018; Arnold et al., 2020; Huo et al., 2020). For clinical purposes, the urinary metabolomic analysis has many advantages compared with other metabolomics analysis, such as non-invasiveness, sensitivity, convenience, and speed, etc., so it has unique predominant in AD diagnosis, drug treatment evaluation, and pathogenesis research, etc. (Khamis et al., 2017; Tynkkynen et al., 2019). Given that the pattern of single target drug treatment almost hardly to meet the requirement of the treatment for complex disease, traditional Chinese herbal prescription has become a new trend in the treatment of AD for its advantages of multi-component and multi-target with the little side effect (Yang et al., 2017; Pei et al., 2020). Metabolomics coupled with network pharmacology provides us with a systematic and novel insight of revealing the treatment of complex diseases like AD by herbal formula and provides new prospects of the potential purposeful drugs to treat AD. In the present study, we performed the urinary metabolomics coupled with network pharmacology analysis to investigate the systematical mechanism of DHYZ acting on AD through multimolecule, multitarget, and multipathway. Our results present here represented a research paradigm of AD treatment by multicomponent drugs, such as traditional Chinese herbal prescription.

As an important lipid component of mammalian cell membranes, glycerophospholipid is the most abundant type of phospholipids *in vivo* (van Meer and de Kroon, 2011). In view of this, glycerophospholipid metabolism plays a crucial role in maintaining the normal ultrastructure and function of organelles, including mitochondria. Besides, glycerophospholipids also play an important role in material transport, signal transduction, and protein function (van Meer and de Kroon, 2011; Bohdanowicz and Grinstein, 2013). CL is a specific phospholipid that composes the inner mitochondrial membrane, which is required for maintaining mitochondrial function and the optimal activity of many mitochondrial enzymes in cellular energy metabolism (Pointer and Klegeris, 2017; Chao et al., 2019). In the CNS, CL exists in neurons and glial cells, and participates in regulating its metabolic process, supporting mitochondrial function and promoting the vitality of brain cells (Pointer and Klegeris, 2017). Studies have found that the CL level significantly decreased in the brains of elderly people and AD patients (Petrosillo et al., 2008; Pointer and Klegeris, 2017). The content of mitochondrial CL in brain of senescent rats was significantly reduced by 26% compared to young rats (Ruggiero et al., 1992). In line with these results, our metabolomics analysis confirmed that the levels of CL and phosphatidate, the key substance for the CL synthesis, decreased dramatically in 2× Tg-AD mice. Furthermore, our data presented here revealed the significant reduction in the content of the cerebral L_4-CL, a major CL species in the brain. Notably, DHYZ administration promoted glycerophospholipid metabolism by increasing the levels of phosphatidate, CL, and L_4-CL in 2× Tg-AD mice. In previous studies, we found DHYZ could improve cognition in transgenetic AD mice and AD rats with the intracerebroventricular injection of amyloid-β peptide by ameliorating mitochondrion disturbance (Ma et al., 2012; Huang et al., 2018; Yan et al., 2018). Consistent with these findings, DHYZ could preserve the structure and function of the mitochondria *via* ameliorating the mitochondrial membrane destruction and maintaining mitochondrial integrity.

A large fraction of the total intracellular ROS is generated during the process of OxPhos in the inner mitochondrial membrane (Fontana et al., 2020). The destruction and dysfunction of mitochondria weaken enzymatic activities of the respiratory chain complex I, II, III, and IV, which are crucial for the OxPhos, and result in the abundant release of ROS in the AD brain (Tonnies and Trushina, 2017). ROS-induced mitochondrial oxidative stress promotes further destruction and dysfunction of mitochondria, thus forming a vicious cycle in the AD brain (Singh et al., 2019). DHYZ is composed of 15 kinds of herbs, which contain a variety of active ingredients including loganin, echinacoside, verbascoside, etc., which have antioxidant capacity and can inhibit the generation of ROS (Wang et al., 2015; Cheng et al., 2020; Vasincu et al., 2020). Our previous study showed that echinacoside could inhibit the accumulation of misfolded protein, including Aβ through improving endoplasmic reticulum stress (Dai et al., 2020). Consistent with those findings, our data in the present study revealed that ROS release increased and the activities of the respiratory chain complex I, II, III, and IV decreased dramatically in the brain of 2× Tg-AD mice. In light of the protective role against mitochondrial membrane destruction, DHYZ could depress the ROS overproduction and ameliorate the

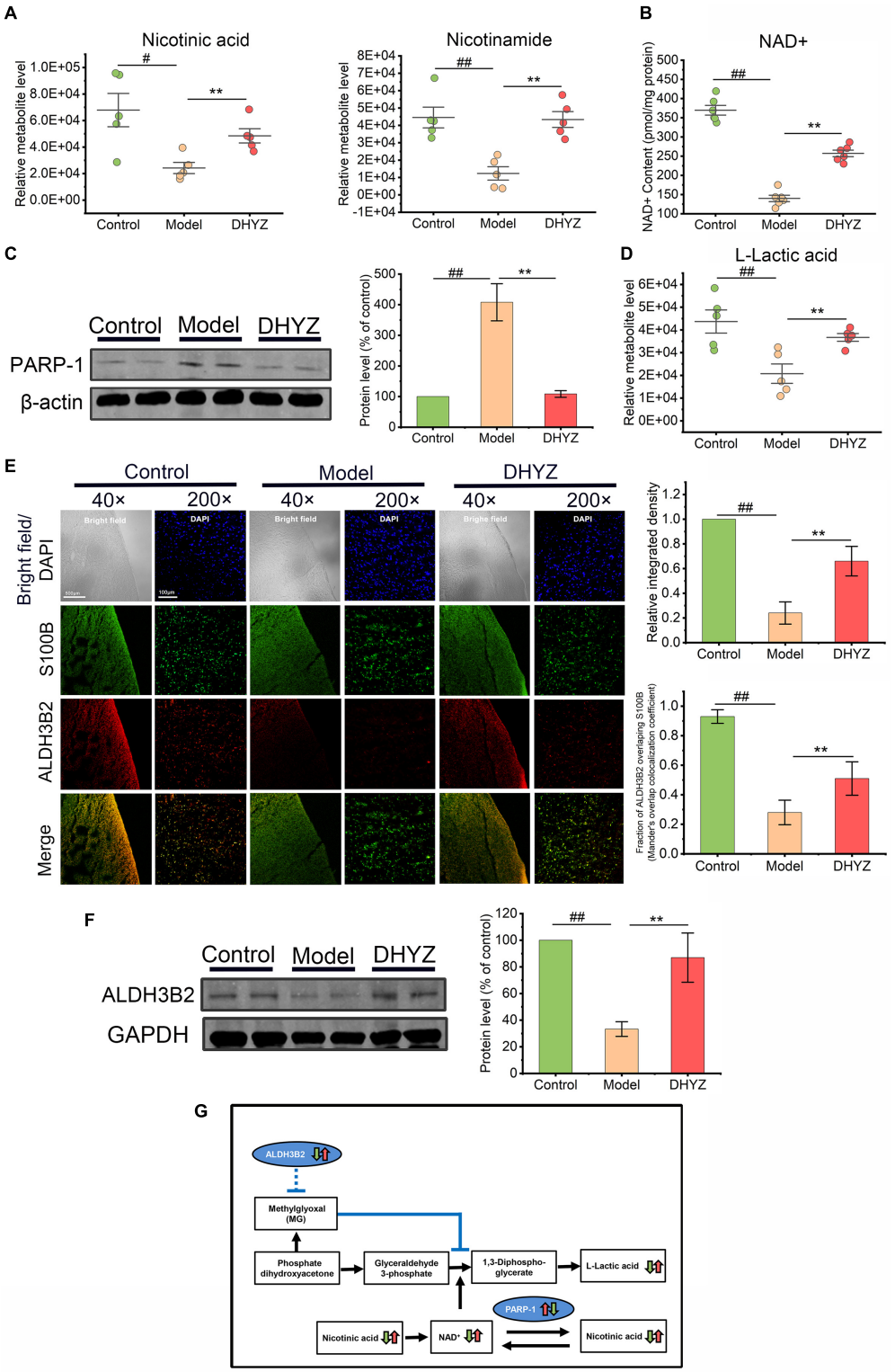

FIGURE 8 | The preservation effects of DHYZ on nicotinate and nicotinamide Metabolism and glycolysis. **(A)** Metabolomics analysis illustrating the relative levels of urine nicotinic acid and nicotinamide (n = 5). **(B)** The scatter dot plot diagram of the level of NAD^+ in the brain of mice in three groups was determined by photochemical assay (n = 6). **(C)** The protein level of PARP-1 was measured by western blot analysis (n = 3). **(D)** The relative level of urine L-lactic acid as illustrated in metabolomics analysis (n = 5). **(E)** Representative images of immunofluorescence staining of ALDH3B2 (Red, Alexa Fluor® 594) and S100B (Green, FITC) (n = 5 mice per group; magnification ×40, scale bar = 500 μm; ×200, scale bar = 100 μm); the corresponding histogram of ALDH3B2 relative intensity in mouse cerebral

(Continued)

FIGURE 8 | cortex, and Mander's overlap colocalization coefficient of ALDH3B2 and S100B ($n = 5$). **(F)** The protein level of ALDH3B2 was measured by western blot analysis ($n = 3$). **(G)** Diagram depicting preservation effects of DHYZ on nicotinate/nicotinamide Metabolism and glycolysis in 2× Tg-AD mice. All data are presented as the mean ± SEM. $^{\#}P < 0.05$ and $^{\#\#}P < 0.01$, model *vs.* control; $^{*}P < 0.05$ and $^{**}P < 0.01$, DHYZ *vs.* model. AD, Alzheimer's disease; DHYZ, Dihuang-Yinzi; NAD+, nicotinamide adenine dinucleotide; PARP-1, Poly [ADP-ribose] polymerase 1; ALDH3B2, aldehyde dehydrogenase 3 family member B2.

activity of the respiratory chain in mitochondria, thus blocking the vicious cycle of ROS release and mitochondrial dysfunction.

Choline is the precursor of acetylcholine which can activate acetylcholine receptors and further participate in the immune response of the CNS, and the imbalance of choline can lead to the occurrence of AD (Velazquez et al., 2019). The cholinergic hypothesis proposed that the pathogenesis of AD is closely related to the reduction of acetylcholine synthesis (Bartus et al., 1982). Wang et al. (2019) found that the levels of choline and acetylcholine in the hippocampus and cerebral cortex of APP/PS1 transgenic mice were significantly decreased. Ladner and Lee (1998) reported that the increase of acetylcholinesterase AChE in the brain tissue of AD patients can rapidly degrade acetylcholine ACh, thereby worsening the pathological state of AD patients. AChE is one of the key target enzymes in AD, which still represent the main pharmacotherapeutic approach in AD treatment. As metabolomics analysis confirmed in the present study, the content of phosphatidate was reduced in 2× Tg-AD mice. Phosphatidate is an important substrate for the synthesis of choline which can be converted into phosphatidylcholine which is the precursor of choline and acetylcholine (Lee and Ridgway, 2020). Our data presented here revealed that the levels of choline and acetylcholine in 2× Tg-AD mice were reduced, and these changes were reversed by DHYZ treatment *via* depressing the expression of AChE.

Niacin is the amide form of vitamin B3, including two forms of nicotinic acid and niacinamide which are closely related to neuronal development, survival, and death, and exhibits neuroprotective effects on neurodegenerative diseases, including AD, Parkinson's disease, and Huntington's diseases (Gasperi et al., 2019). As the precursors of NAD^+, nicotinic acid and nicotinamide are more intimately involved in the salvage synthesis process of NAD^+ (Martens et al., 2018). There is an obvious disturbance in nicotinate and nicotinamide metabolism in the mouse model and patients who suffered from AD (Spector, 1979; Fu et al., 2014; Rawji et al., 2020; Mousa and Mousa, 2021). PARP-1 plays a key role in AD pathogenesis and participates in multiple stress processes including DNA damage repair, inflammation, autophagy dysregulation, genomic stability maintenance, differentiation (Mao and Zhang, 2021). In the brains of AD patients, ROS overproduction leads to mitochondrial damage and the double-strand DNA breaks, resulting in the activation of PARP-1. It has been shown that PARP1 activity is increased in AD, and may exacerbate inflammatory response *via* NF-κB (Chiarugi and Moskowitz, 2003; Salech et al., 2017). The activated PARP-1 catalyzes the poly (ADP-ribosylation), which cleaves the NAD + and transfers the ADP-ribose moieties to the enzyme itself or to an acceptor protein to form branched polymers of ADP-ribose (Martire et al., 2016; Ryu et al., 2018). Previous studies have found that the reduction of nicotinic acid and niacinamide is closely related to the pathogenesis of AD (Mousa and Mousa, 2021). Yu et al. (2021) found that metabolites related to the metabolism of nicotinic acid and niacinamide decreased in drosophila overexpressing Aβ through the metabolomics analysis. After being given nicotinamide as a supplement, the mitochondrial defects and the behavioral disorders were rescued (Yu et al., 2021). NAD^+ is a cofactor of the dehydrogenation of glyceraldehyde 3-phosphate in the glycolysis process (Baker et al., 2014). In 2× Tg-AD mice, the level of NAD^+ decreases, which hinders the glycolysis process, and results in obstacles to the production of L-lactic acid which is transferred from astrocytes to neuron as fuel for the TCA cycle, a process known as the astrocyte-neuron lactate shuttle (ANLS) (**Figure 10**). In our experiment, DHYZ could depress the upregulation of PARP-1 in 2× Tg-AD mice, which was the potential target of DHYZ against AD. Furthermore, the content of urine nicotinic acid, niacinamide, and cerebral NAD^+ decreased in 2× Tg-AD mice. This data is consistent with the upregulation of PARP-1 in the brain of 2× Tg-AD mice. Administration of DHYZ dramatically increased the content of nicotinic acid, nicotinamide, and NAD^+ in 2× Tg-AD mice. Notably, as an inhibitor of PARP-1, nicotinamide may provide therapeutic benefits in AD by diminishing neuroinflammation, microglial activation, oxidative stress, and apoptosis (Turunc Bayrakdar et al., 2014; Salech et al., 2020). Our results presented here showed therapeutic potential for DHYZ against AD targeting PARP-1 and nicotinamide metabolism.

Glycolysis disturbance is another crucial event in AD pathogenesis (Fu and Jhamandas, 2014). With aging, the main risk factors for AD, have intensified, the utilization of glucose by the brain through glycolysis has also been significantly reduced (Yao et al., 2011; Ding et al., 2013). Lactic acid, the main product of glycolysis, is generated in astrocytes and transferred into neurons as substrate convert to pyruvic acid for energy production with the TCA cycle (Fu and Jhamandas, 2014; Sun et al., 2020). Reduced lactate content in the neurons of the hippocampus and cortex was observed in the APP/PS1 mouse model, which in turn was associated with an energy crisis, downregulated expression of long-term memory-related proteins, and resulted in memory deficits (Schousboe et al., 2003; Zhou et al., 2018). Increasing the content of lactic acid through drug intervention can reverse the cognitive impairment of AD mice (Lu et al., 2019). Our results are in line with a number of previous studies (Zhang M. et al., 2018; El Hayek et al., 2019), suggesting lactic acid levels are significantly reduced in 2× Tg-AD mice, implying that glycolysis is disrupted, which may interfere with neuronal energy metabolism. After the intervention of DHYZ, the content of lactic acid in 2× Tg-AD mice increased, which means that glycolysis disorders were ameliorated. Methylmalonic acid (MMA) is a dicarboxylic acid

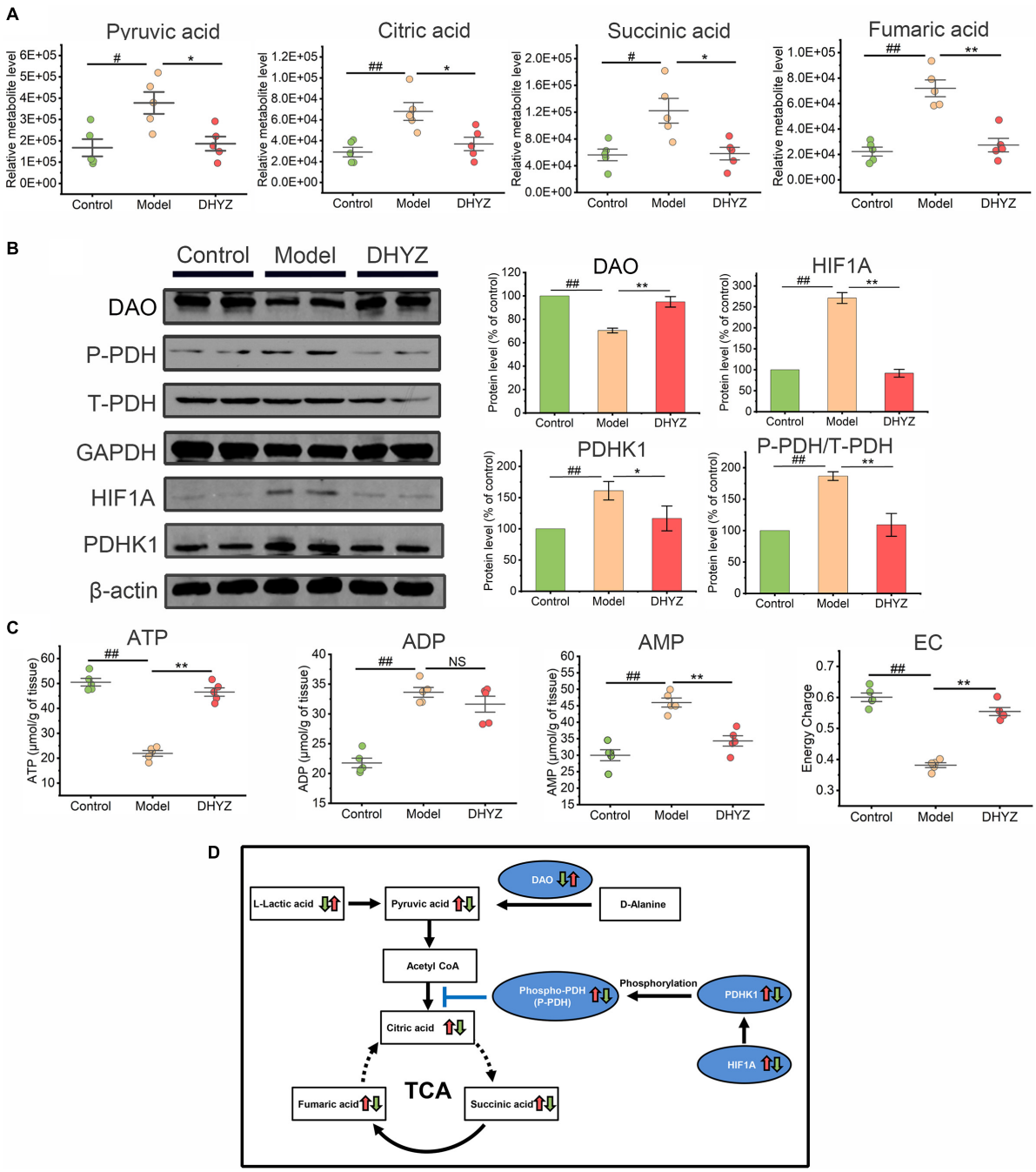

FIGURE 9 | The preservation effects of DHYZ on the tricarboxylic acid (TCA) cycle. **(A)** Metabolomics analysis illustrating the relative levels of urine pyruvic acid, citric acid, succinic acid, and fumaric acid (n = 5). **(B)** The protein levels of DAO, phosphorylation of PDH, total PDH, HIF1A, and PDHK1 were measured by western blot analysis (n = 3). **(C)** The levels of ATP, ADP, and AMP in the brain of mice in 3 groups was determined by reverse-phase HPLC assay (n = 5). The energy charge (EC) was calculated as EC = ATP + 0.5ADP/(ATP + ADP + AMP). **(D)** Diagram depicting of protective effects of DHYZ on the TCA cycle in 2× Tg-AD mice. All data are presented as the mean ± SEM. $^{\#}P < 0.05$ and $^{\#\#}P < 0.01$, model *vs.* control; $^{*}P < 0.05$ and $^{**}P < 0.01$, DHYZ *vs.* model. AD, Alzheimer's disease; DHYZ, Dihuang-Yinzi; DAO, d-amino-acid oxidase; HIF1A, hypoxia-inducible factor 1-alpha; PDHK1, pyruvate dehydrogenase kinase 1; T-, P-PDH, total, or phosphorylated pyruvate dehydrogenase; ATP, adenosine triphosphate; ADP, adenosine diphosphate; AMP, adenosine monophosphate; EC, energy charge.

related to the metabolism of several amino acids and generated with ALDH3B2 in glycolysis (Kolker et al., 2003). Serot, et al. revealed that CSR MMA was significantly lower in aging subjects *vs.* younger ones, however, MMA showed a higher level in CSF of AD subjects as compared to healthy control (Joosten et al., 1997; Serot et al., 2005). Interestingly, our data showed

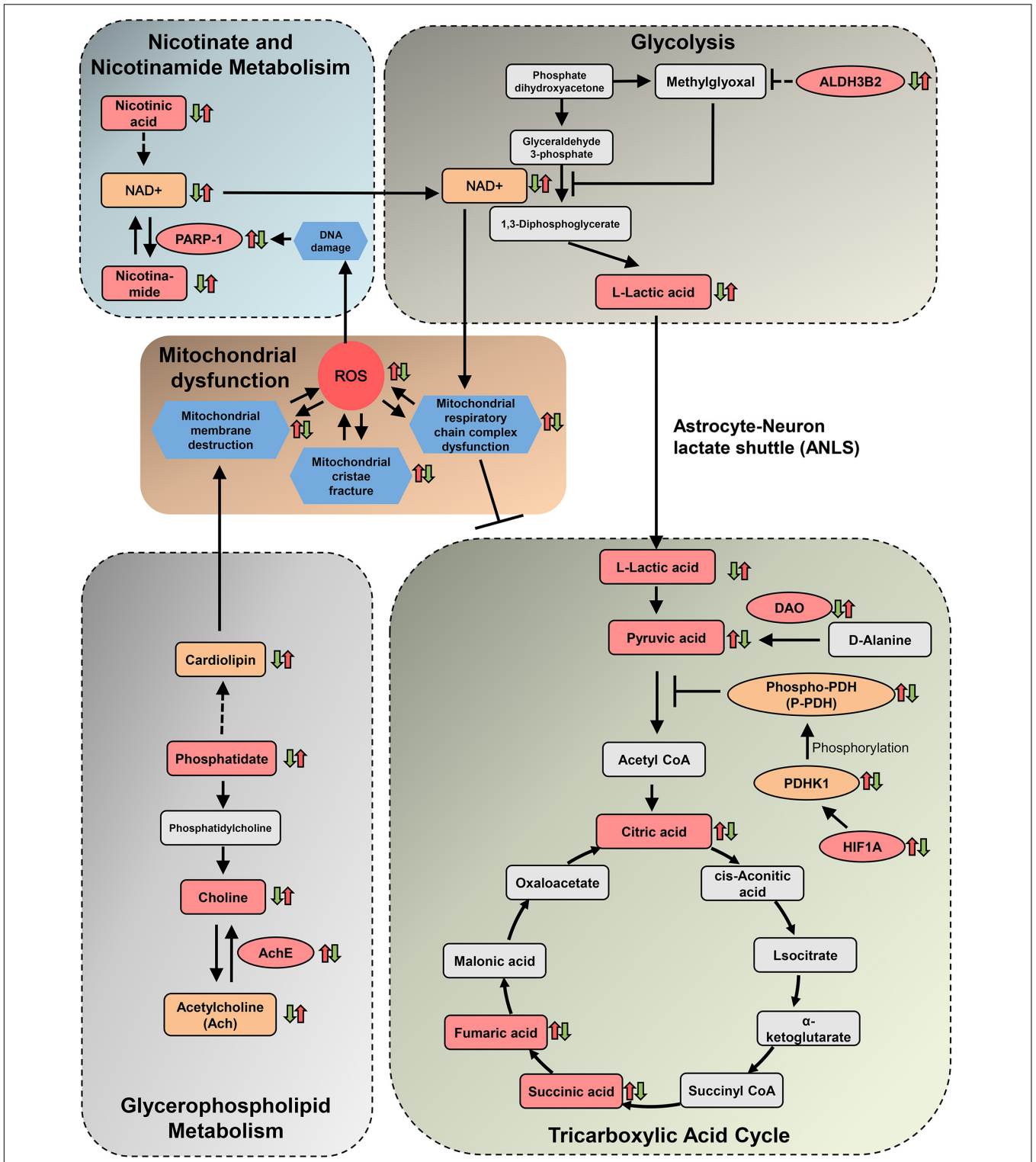

FIGURE 10 | Diagram depicting protective effects of DHYZ on oxidative stress and related metabolism. The squares represent metabolites, the dark pink squares represent urine differential metabolites revealed by metabolomics analysis, the orange squares represent cerebral metabolites confirmed by other experimental verification. The dark pink ellipses represent target proteins of DHYZ against AD, the orange ellipses represent key enzymes regulated by DHYZ. Red up-arrows and green down-arrows indicate up-regulation and down-regulation, respectively. Left arrows represent model *vs.* control; right arrows represent DHYZ *vs.* model. NAD^+, nicotinamide adenine dinucleotide; PARP-1, Poly [ADP-ribose] polymerase 1; ALDH3B2, aldehyde dehydrogenase 3 family member B2. AchE, acetylcholinesterase; DAO, d-amino-acid oxidase; HIF1A, hypoxia-inducible factor 1-alpha; PDHK1, pyruvate dehydrogenase kinase 1; T-, P-PDH, total, or phosphorylated pyruvate dehydrogenase; ROS, reactive oxygen species.

a decreased urine MMA level in 2× Tg-AD mice which partly may be attributed to the effect of separation of the blood-brain barrier. Furthermore, our results showed that ALDH3B2, another potential target of DHYZ against AD, was specifically expressed in astrocytes, implying that ALDH3B2 may play a key role in aerobic glycolysis.

The brain is the organ with the highest metabolism and energy demand, which is up to 20% of whole-body energy in humans, and proper brain function produces large dynamic variations in energy metabolism through the TCA cycle coupled with OxPhos (Arnold et al., 2018). Due to this, energy metabolism impairment has been considered as both an early marker of AD pathology and a risk factor for AD, and the disruption of energy metabolism is regarded as a prominent feature, a fundamental component, and even a novel biomarker of AD pathogenesis (Weise et al., 2018; Butterfield and Halliwell, 2019; Perez Ortiz and Swerdlow, 2019). One of the main characteristics of AD is the severe region-specific decline of the cerebral metabolic rate for glucose (CMRglc). Furthermore, the decrease of CMRglc correlates with dementia severity in AD as the disease progression. Besides, the enzymes involved in the TCA cycle and OxPhos downregulate in the AD brain. By studying the cerebrospinal fluid (CSF) and plasma metabolism of AD patients, Van der Velpen et al. found that they exhibited disrupted core energy metabolism based on the TCA cycle, and the main intermediate metabolites involved, including cis-aconitic acid, citric acid, pyruvic acid, and phosphoenolpyruvic acid, were significantly increased (van der Velpen et al., 2019; Yan et al., 2020). Arnold et al. (2020) confirmed there were significant differences in the level of metabolites related to energy metabolism and mitochondrial function in the serum of AD and MCI patients by investigating serum metabolomics of females with APOE ε4 genotype. In the neuronal energy metabolism in CNS, the ANLS between astrocytes and neurons connects the glycolysis occurring in astrocytes with the TCA cycle in neurons. Then, the L-lactic acid is converted to pyruvic acid in the neuron. DAO level was significantly associated with the severity of the cognitive deficits in AD patients (Lin et al., 2017). DAO and amino acids can regulate the N-methyl-D-aspartate (NMDA) receptor function and DAO can catalyze the conversion of D-alanine to pyruvate in the peroxisome, which in turn enters the TCA cycle (Lin et al., 2017). At the same time, PDH oxidized pyruvic acid to form acetyl-CoA entering the TCA cycle. PDH may be inactivated through phosphorylation by PDHK1 which is upregulated by HIF1A. Our previous studies revealed that DHYZ could significantly ameliorate cerebral energy metabolism deficits (Ma et al., 2012; Huang et al., 2018). In our present study, ATP production and EC were declined in the brain tissue of 2× Tg-AD mice, and DHYZ could markedly ameliorate the disturbance of energy production. By increasing L-lactate levels, DHYZ promotes ANLS, which in turn increases neuronal energy metabolism. Furthermore, our data revealed that the levels of 4 key metabolites, including pyruvic acid, citric acid, succinic acid, and fumaric acid, were significantly recovered after DHYZ treatment, which means that DHYZ can ameliorate TCA cycle disorders. As a potential target of DHYZ against AD, DAO was upregulated in the brain of 2× Tg-AD mice after DHYZ treatment, which promoted the pyruvic acid supplement to enter TCA cycle. Furthermore, DHYZ could promote the TCA cycle by depressing HIF1A and PDHK1, and the phosphorylation of PDH to improve pyruvic acid entry into the TCA cycle.

Kyoto Encyclopedia of Genes and Genomes enrichment revealed that DHYZ had multiple protective efficacies upon the neurodegenerative diseases, including AD, Parkinson's disease (PD), and Huntington's disease (HD). In line with clinical applications of DHYZ for a long time, we found that therapeutic drug targets mostly concentrated in neurodegenerative diseases, such as AD, PD, and PD, and the majority of the targets were closely related to energy metabolism. KEGG and GO enrichment analysis of our current study revealed that DHYZ affected OxPhos with high $-\log_{10}$ (p-value). At the same time, NAFLD was also a key disease with KEGG enrichment of DHYZ targets. A reasonable explanation for this might be that AD and NAFLD share some common pathogenesis and mechanism related to abnormal lipid metabolism as demonstrated by many studies (de la Monte, 2017; Wang et al., 2020).

CONCLUSION

Our study demonstrated that DHYZ improves cognitive performance in AD mice by targeting 4 key energy-related metabolic pathways. The regulation of the above metabolic pathways by DHYZ involves 5 key target genes and 14 differential metabolites. The central key to the regulation of 4 energy-related metabolic pathways by DHYZ is the protection of mitochondrial structure and function. Our data have implications for exploring the comprehensive mechanism of traditional Chinese herbal prescription in the treatment of AD.

DATA AVAILABILITY STATEMENT

The original contributions presented in the study are included in the article/**Supplementary Material**, further inquiries can be directed to the corresponding author/s.

ETHICS STATEMENT

The animal study was reviewed and approved by Animal Care and Welfare Committee of Dongfang Hospital, Beijing University of Chinese Medicine, China.

AUTHOR CONTRIBUTIONS

TM designed the research and projected the experimental approach. GH, WZ, YD, HY, and DL performed the research and analyzed the data. GH, WZ, HY, DL, and TM wrote the manuscript. All authors contributed to the article and approved the final manuscript.

FUNDING

This research was funded by grants from the National Natural Science Foundation of China (Nos. 81973786 and 81673929).

SUPPLEMENTARY MATERIAL

The Supplementary Material for this article can be found online at: https://www.frontiersin.org/articles/10.3389/fnagi.2022.873929/full#supplementary-material

REFERENCES

Ali, T., Badshah, H., Kim, T. H., and Kim, M. O. (2015). Melatonin attenuates D-galactose-induced memory impairment, neuroinflammation and neurodegeneration *via* RAGE/NF-K B/JNK signaling pathway in aging mouse model. *J. Pineal Res.* 58, 71–85. doi: 10.1111/jpi.12194

Ali, T., Kim, T., Rehman, S. U., Khan, M. S., Amin, F. U., Khan, M., et al. (2018). Natural dietary supplementation of anthocyanins *via* PI3K/Akt/Nrf2/HO-1 pathways mitigate oxidative stress, neurodegeneration, and memory impairment in a mouse model of Alzheimer's disease. *Mol. Neurobiol.* 55, 6076–6093. doi: 10.1007/s12035-017-0798-6

Arnold, M., Nho, K., Kueider-Paisley, A., Massaro, T., Huynh, K., Brauner, B., et al. (2020). Sex and APOE epsilon4 genotype modify the Alzheimer's disease serum metabolome. *Nat. Commun.* 11:1148. doi: 10.1038/s41467-020-14959-w

Arnold, S. E., Arvanitakis, Z., Macauley-Rambach, S. L., Koenig, A. M., Wang, H. Y., Ahima, R. S., et al. (2018). Brain insulin resistance in type 2 diabetes and Alzheimer disease: concepts and conundrums. *Nat. Rev. Neurol.* 14, 168–181. doi: 10.1038/nrneurol.2017.185

Baik, S. H., Kang, S., Lee, W., Choi, H., Chung, S., Kim, J. I., et al. (2019). A breakdown in metabolic reprogramming causes microglia dysfunction in Alzheimer's disease. *Cell Metab.* 30, 493.e6–507.e6. doi: 10.1016/j.cmet.2019.06.005

Baker, B. Y., Shi, W., Wang, B., and Palczewski, K. (2014). High-resolution crystal structures of the photoreceptor glyceraldehyde 3-phosphate dehydrogenase (GAPDH) with three and four-bound NAD molecules. *Protein Sci.* 23, 1629–1639. doi: 10.1002/pro.2543

Bartus, R. T., Dean, R. L. III, Beer, B., and Lippa, A. S. (1982). The cholinergic hypothesis of geriatric memory dysfunction. *Science* 217, 408–414.

Bligh, E. G., and Dyer, W. J. (1959). A rapid method of total lipid extraction and purification. *Can. J. Biochem. Physiol.* 37, 911–917. doi: 10.1139/o59-099

Bohdanowicz, M., and Grinstein, S. (2013). Role of phospholipids in endocytosis, phagocytosis, and macropinocytosis. *Physiol. Rev.* 93, 69–106. doi: 10.1152/physrev.00002.2012

Bowron, A., Frost, R., Powers, V. E., Thomas, P. H., Heales, S. J., and Steward, C. G. (2013). Diagnosis of Barth syndrome using a novel LC-MS/MS method for leukocyte cardiolipin analysis. *J. Inherit. Metab. Dis.* 36, 741–746. doi: 10.1007/s10545-012-9552-4

Butterfield, D. A., and Halliwell, B. (2019). Oxidative stress, dysfunctional glucose metabolism and Alzheimer disease. *Nat. Rev. Neurosci.* 20, 148–160. doi: 10.1038/s41583-019-0132-6

Chao, H., Lin, C., Zuo, Q., Liu, Y., Xiao, M., Xu, X., et al. (2019). Cardiolipin-dependent mitophagy guides outcome after traumatic brain injury. *J. Neurosci.* 39, 1930–1943. doi: 10.1523/JNEUROSCI.3415-17.2018

Cheng, Y. C., Chu, L. W., Chen, J. Y., Hsieh, S. L., Chang, Y. C., Dai, Z. K., et al. (2020). Loganin attenuates high glucose-induced schwann cells pyroptosis by inhibiting ROS generation and NLRP3 inflammasome activation. *Cells* 9:1948. doi: 10.3390/cells9091948

Chiarugi, A., and Moskowitz, M. A. (2003). Poly(ADP-ribose) polymerase-1 activity promotes NF-kappaB-driven transcription and microglial activation: implication for neurodegenerative disorders. *J. Neurochem.* 85, 306–317. doi: 10.1046/j.1471-4159.2003.01684.x

Dai, Y., Han, G., Xu, S., Yuan, Y., Zhao, C., and Ma, T. (2020). Echinacoside suppresses amyloidogenesis and modulates F-actin remodeling by targeting the ER stress sensor PERK in a mouse model of Alzheimer's disease. *Front. Cell Dev. Biol.* 8:593659. doi: 10.3389/fcell.2020.593659

de la Monte, S. M. (2017). Insulin resistance and neurodegeneration: progress towards the development of new therapeutics for Alzheimer's disease. *Drugs* 77, 47–65. doi: 10.1007/s40265-016-0674-0

Ding, F., Yao, J., Rettberg, J. R., Chen, S., and Brinton, R. D. (2013). Early decline in glucose transport and metabolism precedes shift to ketogenic system in female aging and Alzheimer's mouse brain: implication for bioenergetic intervention. *PLoS One* 8:e79977. doi: 10.1371/journal.pone.0079977

El Hayek, L., Khalifeh, M., Zibara, V., Abi Assaad, R., Emmanuel, N., Karnib, N., et al. (2019). Lactate mediates the effects of exercise on learning and memory through sirt1-dependent activation of hippocampal brain-derived neurotrophic factor (BDNF). *J. Neurosci.* 39, 2369–2382. doi: 10.1523/JNEUROSCI.1661-18.2019

Fontana, D., Mauri, M., Renso, R., Docci, M., Crespiatico, I., Rost, L. M., et al. (2020). ETNK1 mutations induce a mutator phenotype that can be reverted with phosphoethanolamine. *Nat. Commun.* 11:5938. doi: 10.1038/s41467-020-19721-w

Fu, L., Doreswamy, V., and Prakash, R. (2014). The biochemical pathways of central nervous system neural degeneration in niacin deficiency. *Neural Regen. Res.* 9, 1509–1513. doi: 10.4103/1673-5374.139475

Fu, W., and Jhamandas, J. H. (2014). Role of astrocytic glycolytic metabolism in Alzheimer's disease pathogenesis. *Biogerontology* 15, 579–586. doi: 10.1007/s10522-014-9525-0

Gasperi, V., Sibilano, M., Savini, I., and Catani, M. V. (2019). Niacin in the central nervous system: an update of biological aspects and clinical applications. *Int. J. Mol. Sci.* 20:974. doi: 10.3390/ijms20040974

Grubman, A., Chew, G., Ouyang, J. F., Sun, G., Choo, X. Y., Mclean, C., et al. (2019). A single-cell atlas of entorhinal cortex from individuals with Alzheimer's disease reveals cell-type-specific gene expression regulation. *Nat. Neurosci.* 22, 2087–2097. doi: 10.1038/s41593-019-0539-4

Gu, L., Lu, J., Li, Q., Wu, N., Zhang, L., Li, H., et al. (2020). A network-based analysis of key pharmacological pathways of Andrographis paniculata acting on Alzheimer's disease and experimental validation. *J. Ethnopharmacol.* 251:112488. doi: 10.1016/j.jep.2019.112488

Hu, R., Yin, C. L., Wu, N., Cui, G. Y., Meng, H., Wu, X. G., et al. (2009). Traditional Chinese herb Dihuang Yinzi (DY) plays neuroprotective and anti-dementia role in rats of ischemic brain injury. *J. Ethnopharmacol.* 121, 444–450. doi: 10.1016/j.jep.2008.09.035

Huang, Q., Zhao, Y. L., Gao, J. F., Jing, Z. W., Zhang, N., and Ma, T. (2018). Effect of Dihuang Yinzi on mitochondrial structure and function in central nerve of Alzheimer's disease rats. *Chinese J. Exp. Trad. Med. Form.* 24, 99–104.

Huo, Z., Yu, L., Yang, J., Zhu, Y., Bennett, D. A., and Zhao, J. (2020). Brain and blood metabolome for Alzheimer's dementia: findings from a targeted metabolomics analysis. *Neurobiol. Aging* 86, 123–133. doi: 10.1016/j.neurobiolaging.2019.10.014

Jankowsky, J. L., Fadale, D. J., Anderson, J., Xu, G. M., Gonzales, V., Jenkins, N. A., et al. (2004). Mutant presenilins specifically elevate the levels of the 42 residue beta-amyloid peptide *in vivo*: evidence for augmentation of a 42-specific gamma secretase. *Hum. Mol. Genet.* 13, 159–170. doi: 10.1093/hmg/ddh019

Joosten, E., Lesaffre, E., Riezler, R., Ghekiere, V., Dereymaeker, L., Pelemans, W., et al. (1997). Is metabolic evidence for vitamin B-12 and folate deficiency more frequent in elderly patients with Alzheimer's disease? *J. Gerontol. A Biol. Sci. Med. Sci.* 52, M76–M79. doi: 10.1093/gerona/52a.2.m76

Ju, H. Q., Ying, H., Tian, T., Ling, J., Fu, J., Lu, Y., et al. (2017). Mutant Kras- and p16-regulated NOX4 activation overcomes metabolic checkpoints in development of pancreatic ductal adenocarcinoma. *Nat. Commun.* 8:14437. doi: 10.1038/ncomms14437

Kameoka, S., Adachi, Y., Okamoto, K., Iijima, M., and Sesaki, H. (2018). Phosphatidic acid and cardiolipin coordinate mitochondrial dynamics. *Trends Cell Biol.* 28, 67–76. doi: 10.1016/j.tcb.2017.08.011

Khamis, M. M., Adamko, D. J., and El-Aneed, A. (2017). Mass spectrometric based approaches in urine metabolomics and biomarker discovery. *Mass Spectrom. Rev.* 36, 115–134. doi: 10.1002/mas.21455

Kolker, S., Schwab, M., Horster, F., Sauer, S., Hinz, A., Wolf, N. I., et al. (2003). Methylmalonic acid, a biochemical hallmark of methylmalonic acidurias but no

inhibitor of mitochondrial respiratory chain. *J. Biol. Chem.* 278, 47388–47393. doi: 10.1074/jbc.M308861200

Ladner, C. J., and Lee, J. M. (1998). Pharmacological drug treatment of Alzheimer disease: the cholinergic hypothesis revisited. *J. Neuropathol. Exp. Neurol.* 57, 719–731. doi: 10.1097/00005072-199808000-00001

Lai, J. C., and Clark, J. B. (1979). Preparation of synaptic and nonsynaptic mitochondria from mammalian brain. *Methods Enzymol.* 55, 51–60. doi: 10.1016/0076-6879(79)55008-3

Lai, J. H., Jan, H. J., Liu, L. W., Lee, C. C., Wang, S. G., Hueng, D. Y., et al. (2013). Nodal regulates energy metabolism in glioma cells by inducing expression of hypoxia-inducible factor 1alpha. *Neuro Oncol.* 15, 1330–1341. doi: 10.1093/neuonc/not086

Le Douce, J., Maugard, M., Veran, J., Matos, M., Jego, P., Vigneron, P. A., et al. (2020). Impairment of glycolysis-derived l-serine production in astrocytes contributes to cognitive deficits in Alzheimer's disease. *Cell Metab.* 31, 503.e8–517.e8. doi: 10.1016/j.cmet.2020.02.004

Lee, J., and Ridgway, N. D. (2020). Substrate channeling in the glycerol-3-phosphate pathway regulates the synthesis, storage and secretion of glycerolipids. *Biochim. Biophys. Acta Mol. Cell Biol. Lipids* 1865:158438. doi: 10.1016/j.bbalip.2019.03.010

Lee, J. Y., Kim, J. Y., Lee, J. Y., Jung, J. H., and Jung, I. C. (2021). Efficacy of Jihwangeumja (Dihuang Yinzi) on cognitive function and activities of daily living in patients with Alzheimer disease: a protocol for a systematic review and meta-analysis. *Medicine* 100:e25592. doi: 10.1097/MD.0000000000025592

Lin, C. H., Yang, H. T., Chiu, C. C., and Lane, H. Y. (2017). Blood levels of D-amino acid oxidase vs. D-amino acids in reflecting cognitive aging. *Sci. Rep.* 7:14849. doi: 10.1038/s41598-017-13951-7

Liu, S., Wu, H., Xue, G., Ma, X., Wu, J., Qin, Y., et al. (2013). Metabolic alteration of neuroactive steroids and protective effect of progesterone in Alzheimer's disease-like rats. *Neural Regen. Res.* 8, 2800–2810. doi: 10.3969/j.issn.1673-5374.2013.30.002

Liu, Y., Liu, Z., Wei, M., Hu, M., Yue, K., Bi, R., et al. (2019). Pharmacodynamic and urinary metabolomics studies on the mechanism of *Schisandra polysaccharide* in the treatment of Alzheimer's disease. *Food Funct.* 10, 432–447. doi: 10.1039/c8fo02067a

Lu, W. T., Sun, S. Q., Li, Y., Xu, S. Y., Gan, S. W., Xu, J., et al. (2019). Curcumin ameliorates memory deficits by enhancing lactate content and MCT2 expression in APP/PS1 transgenic mouse model of Alzheimer's disease. *Anat. Rec.* 302, 332–338. doi: 10.1002/ar.23969

Ma, T., Wang, X., Zhang, Y., Zheng, H., and Zhang, W. (2012). Dihuang-Yinzi decotion improves cognition and energy metabolism of Alzheimer mice. *Int. J. Trad. Chinese Med.* 36, 539–543.

Mao, K., and Zhang, G. (2021). The role of PARP1 in neurodegenerative diseases and aging. *FEBS J.* [Epub ahead of print]. doi: 10.1111/febs.15716

Mapstone, M., Cheema, A. K., Fiandaca, M. S., Zhong, X., Mhyre, T. R., Macarthur, L. H., et al. (2014). Plasma phospholipids identify antecedent memory impairment in older adults. *Nat. Med.* 20, 415–418. doi: 10.1038/nm.3466

Martens, C. R., Denman, B. A., Mazzo, M. R., Armstrong, M. L., Reisdorph, N., Mcqueen, M. B., et al. (2018). Chronic nicotinamide riboside supplementation is well-tolerated and elevates NAD(+) in healthy middle-aged and older adults. *Nat. Commun.* 9:1286.

Martire, S., Fuso, A., Mosca, L., Forte, E., Correani, V., Fontana, M., et al. (2016). Bioenergetic Impairment In Animal And Cellular Models of Alzheimer's disease: PARP-1 inhibition rescues metabolic dysfunctions. *J. Alzheimers Dis.* 54, 307–324. doi: 10.3233/JAD-151040

Minhas, P. S., Latif-Hernandez, A., Mcreynolds, M. R., Durairaj, A. S., Wang, Q., Rubin, A., et al. (2021). Restoring metabolism of myeloid cells reverses cognitive decline in ageing. *Nature* 590, 122–128.

Mousa, T. Y., and Mousa, O. Y. (2021). *Nicotinic Acid Deficiency*. Treasure Island, FL: StatPearls.

Oresic, M., Hyotylainen, T., Herukka, S. K., Sysi-Aho, M., Mattila, I., Seppanan-Laakso, T., et al. (2011). Metabolome in progression to Alzheimer's disease. *Transl. Psychiatry* 1:e57. doi: 10.1038/tp.2011.55

Pawlosky, R. J., Kemper, M. F., Kashiwaya, Y., King, M. T., Mattson, M. P., and Veech, R. L. (2017). Effects of a dietary ketone ester on hippocampal glycolytic and tricarboxylic acid cycle intermediates and amino acids in a 3xTgAD mouse model of Alzheimer's disease. *J. Neurochem.* 141, 195–207.

Pei, H., Ma, L., Cao, Y., Wang, F., Li, Z., Liu, N., et al. (2020). Traditional chinese medicine for Alzheimer's disease and other cognitive impairment: a review. *Am. J. Chin. Med.* 48, 487–511. doi: 10.1142/S0192415X20500251

Perez Ortiz, J. M., and Swerdlow, R. H. (2019). Mitochondrial dysfunction in Alzheimer's disease: role in pathogenesis and novel therapeutic opportunities. *Br. J. Pharmacol.* 176, 3489–3507. doi: 10.1111/bph.14585

Petrosillo, G., Matera, M., Casanova, G., Ruggiero, F. M., and Paradies, G. (2008). Mitochondrial dysfunction in rat brain with aging Involvement of complex I, reactive oxygen species and cardiolipin. *Neurochem. Int.* 53, 126–131. doi: 10.1016/j.neuint.2008.07.001

Pointer, C. B., and Klegeris, A. (2017). Cardiolipin in central nervous system physiology and pathology. *Cell Mol. Neurobiol.* 37, 1161–1172. doi: 10.1007/s10571-016-0458-9

Puchowicz, M. A., and Seyfried, T. N. (2017). Novel ketone body therapy for managing Alzheimer's disease: an Editorial Highlight for Effects of a dietary ketone ester on hippocampal glycolytic and tricarboxylic acid cycle intermediates and amino acids in a 3xTgAD mouse model of Alzheimer's disease. *J. Neurochem.* 141, 162–164. doi: 10.1111/jnc.13979

Qiu, H., Li, J. H., Yin, S. B., Ke, J. Q., Qiu, C. L., and Zheng, G. Q. (2016). Dihuang yinzi, a classical chinese herbal prescription, for amyotrophic lateral sclerosis: a 12-year follow-up case report. *Medicine* 95:e3324. doi: 10.1097/MD.0000000000003324

Rawji, K. S., Young, A. M. H., Ghosh, T., Michaels, N. J., Mirzaei, R., Kappen, J., et al. (2020). Niacin-mediated rejuvenation of macrophage/microglia enhances remyelination of the aging central nervous system. *Acta Neuropathol.* 139, 893–909.

Ruggiero, F. M., Cafagna, F., Petruzzella, V., Gadaleta, M. N., and Quagliariello, E. (1992). Lipid composition in synaptic and nonsynaptic mitochondria from rat brains and effect of aging. *J. Neurochem.* 59, 487–491. doi: 10.1111/j.1471-4159.1992.tb09396.x

Ryu, K. W., Nandu, T., Kim, J., Challa, S., Deberardinis, R. J., and Kraus, W. L. (2018). Metabolic regulation of transcription through compartmentalized NAD(+) biosynthesis. *Science* 360:eaan5780. doi: 10.1126/science.aan5780

Salech, F., Ponce, D. P., Paula-Lima, A. C., Sanmartin, C. D., and Behrens, M. I. (2020). Nicotinamide, a Poly [ADP-Ribose] polymerase 1 (PARP-1) inhibitor, as an adjunctive therapy for the treatment of Alzheimer's disease. *Front. Aging Neurosci.* 12:255. doi: 10.3389/fnagi.2020.00255

Salech, F., Ponce, D. P., Sanmartin, C. D., Rogers, N. K., Chacon, C., Henriquez, M., et al. (2017). PARP-1 and p53 regulate the increased susceptibility to oxidative death of lymphocytes from MCI and AD patients. *Front. Aging Neurosci.* 9:310. doi: 10.3389/fnagi.2017.00310

Schousboe, A., Sonnewald, U., and Waagepetersen, H. S. (2003). Differential roles of alanine in GABAergic and glutamatergic neurons. *Neurochem. Int.* 43, 311–315. doi: 10.1016/s0197-0186(03)00017-2

Serot, J. M., Barbe, F., Arning, E., Bottiglieri, T., Franck, P., Montagne, P., et al. (2005). Homocysteine and methylmalonic acid concentrations in cerebrospinal fluid: relation with age and Alzheimer's disease. *J. Neurol. Neurosurg. Psychiatry* 76, 1585–1587. doi: 10.1136/jnnp.2004.056119

Shaerzadeh, F., Motamedi, F., and Khodagholi, F. (2014). Inhibition of akt phosphorylation diminishes mitochondrial biogenesis regulators, tricarboxylic acid cycle activity and exacerbates recognition memory deficit in rat model of Alzheimer's disease. *Cell Mol. Neurobiol.* 34, 1223–1233.

Shao, Y., Ouyang, Y., Li, T., Liu, X., Xu, X., Li, S., et al. (2020). Alteration of metabolic profile and potential biomarkers in the plasma of Alzheimer's disease. *Aging Dis.* 11, 1459–1470. doi: 10.14336/AD.2020.0217

Singh, A., Kukreti, R., Saso, L., and Kukreti, S. (2019). Oxidative stress: a key modulator in neurodegenerative diseases. *Molecules* 24:1583. doi: 10.3390/molecules24081583

Sparagna, G. C., Johnson, C. A., Mccune, S. A., Moore, R. L., and Murphy, R. C. (2005). Quantitation of cardiolipin molecular species in spontaneously hypertensive heart failure rats using electrospray ionization mass spectrometry. *J. Lipid Res.* 46, 1196–1204. doi: 10.1194/jlr.M500031-JLR200

Spector, R. (1979). Niacin and niacinamide transport in the central nervous system. *In vivo* studies. *J. Neurochem.* 33, 895–904. doi: 10.1111/j.1471-4159.1979.tb09919.x

Sun, Y., Wang, Y., Chen, S. T., Chen, Y. J., Shen, J., Yao, W. B., et al. (2020). Modulation of the astrocyte-neuron lactate shuttle system contributes to

neuroprotective action of fibroblast growth factor 21. *Theranostics* 10, 8430–8445. doi: 10.7150/thno.44370

Toledo, J. B., Arnold, M., Kastenmuller, G., Chang, R., Baillie, R. A., Han, X., et al. (2017). Metabolic network failures in Alzheimer's disease: a biochemical road map. *Alzheimers Dement.* 13, 965–984. doi: 10.1016/j.jalz.2017.01.020

Tonnies, E., and Trushina, E. (2017). Oxidative stress, synaptic dysfunction, and Alzheimer's disease. *J. Alzheimers Dis.* 57, 1105–1121.

Tsuruoka, M., Hara, J., Hirayama, A., Sugimoto, M., Soga, T., Shankle, W. R., et al. (2013). Capillary electrophoresis-mass spectrometry-based metabolome analysis of serum and saliva from neurodegenerative dementia patients. *Electrophoresis* 34, 2865–2872. doi: 10.1002/elps.201300019

Turunc Bayrakdar, E., Uyanikgil, Y., Kanit, L., Koylu, E., and Yalcin, A. (2014). Nicotinamide treatment reduces the levels of oxidative stress, apoptosis, and PARP-1 activity in Abeta(1-42)-induced rat model of Alzheimer's disease. *Free Radic. Res.* 48, 146–158. doi: 10.3109/10715762.2013.857018

Tynkkynen, T., Wang, Q., Ekholm, J., Anufrieva, O., Ohukainen, P., Vepsalainen, J., et al. (2019). Proof of concept for quantitative urine NMR metabolomics pipeline for large-scale epidemiology and genetics. *Int. J. Epidemiol.* 48, 978–993. doi: 10.1093/ije/dyy287

van der Velpen, V., Teav, T., Gallart-Ayala, H., Mehl, F., Konz, I., Clark, C., et al. (2019). Systemic and central nervous system metabolic alterations in Alzheimer's disease. *Alzheimers Res. Ther.* 11:93. doi: 10.1186/s13195-019-0551-7

van Meer, G., and de Kroon, A. I. (2011). Lipid map of the mammalian cell. *J. Cell Sci.* 124, 5–8. doi: 10.1242/jcs.071233

Varma, V. R., Oommen, A. M., Varma, S., Casanova, R., An, Y., Andrews, R. M., et al. (2018). Brain and blood metabolite signatures of pathology and progression in Alzheimer disease: a targeted metabolomics study. *PLoS Med.* 15:e1002482. doi: 10.1371/journal.pmed.1002482

Vasincu, A., Neophytou, C. M., Luca, S. V., Skalicka-Wozniak, K., Miron, A., and Constantinou, A. I. (2020). 6-O-(3", 4"-di-O-trans-cinnamoyl)-alpha-l-rhamnopyranosylcatalpol and verbascoside: cytotoxicity, cell cycle kinetics, apoptosis, and ROS production evaluation in tumor cells. *J. Biochem. Mol. Toxicol.* 34:e22443. doi: 10.1002/jbt.22443

Velazquez, R., Ferreira, E., Knowles, S., Fux, C., Rodin, A., Winslow, W., et al. (2019). Lifelong choline supplementation ameliorates Alzheimer's disease pathology and associated cognitive deficits by attenuating microglia activation. *Aging Cell* 18:e13037. doi: 10.1111/acel.13037

Wang, A., Pi, Z., Liu, S., Zheng, Z., Liu, Z., and Song, F. (2021). Mass spectrometry-based urinary metabolomics for exploring the treatment effects of Radix ginseng-Schisandra chinensis herb pair on Alzheimer's disease in rats. *J. Sep. Sci.* 44, 3158–3166. doi: 10.1002/jssc.202100061

Wang, W., Zhu, N., Yan, T., Shi, Y. N., Chen, J., Zhang, C. J., et al. (2020). The crosstalk: exosomes and lipid metabolism. *Cell Commun. Signal.* 18:119. doi: 10.1186/s12964-020-00581-2

Wang, Y., Guan, X., Chen, X., Cai, Y., Ma, Y., Ma, J., et al. (2019). Choline supplementation ameliorates behavioral deficits and Alzheimer's disease-like pathology in transgenic APP/PS1 mice. *Mol. Nutr. Food Res.* 63:e1801407. doi: 10.1002/mnfr.201801407

Wang, Y. H., Xuan, Z. H., Tian, S., and Du, G. H. (2015). Echinacoside protects against 6-hydroxydopamine-induced mitochondrial dysfunction and inflammatory responses in PC12 cells *via* reducing ROS production. *Evid. Based Complement. Alternat. Med.* 2015:189239. doi: 10.1155/2015/189239

Wei, M., Liu, Z., Liu, Y., Li, S., Hu, M., Yue, K., et al. (2019). Urinary and plasmatic metabolomics strategy to explore the holistic mechanism of lignans in *S. chinensis* in treating Alzheimer's disease using UPLC-Q-TOF-MS. *Food Funct.* 10, 5656–5668. doi: 10.1039/c9fo00677j

Weise, C. M., Chen, K., Chen, Y., Kuang, X., Savage, C. R., Reiman, E. M., et al. (2018). Left lateralized cerebral glucose metabolism declines in amyloid-beta positive persons with mild cognitive impairment. *Neuroimage Clin.* 20, 286–296. doi: 10.1016/j.nicl.2018.07.016

Woo, D. C., Lee, S. H., Lee, D. W., Kim, S. Y., Kim, G. Y., Rhim, H. S., et al. (2010). Regional metabolic alteration of Alzheimer's disease in mouse brain expressing mutant human APP-PS1 by 1H HR-MAS. *Behav. Brain Res.* 211, 125–131. doi: 10.1016/j.bbr.2010.03.026

Yan, X., Hu, Y., Wang, B., Wang, S., and Zhang, X. (2020). Metabolic dysregulation contributes to the progression of Alzheimer's disease. *Front. Neurosci.* 14:530219. doi: 10.3389/fnins.2020.530219

Yan, Y., Han, R., Gao, J. F., Tang, X., Zhang, N., Tao, M. A., et al. (2018). Effect of Dihuang Yinzi on mitochondrial biosynthesis and oxidative damage in ad rats. *Chinese J. Exp. Tradit. Med. Formul.* 24, 105–110.

Yang, W. T., Zheng, X. W., Chen, S., Shan, C. S., Xu, Q. Q., Zhu, J. Z., et al. (2017). Chinese herbal medicine for Alzheimer's disease: Clinical evidence and possible mechanism of neurogenesis. *Biochem. Pharmacol.* 141, 143–155. doi: 10.1016/j.bcp.2017.07.002

Yao, J., Rettberg, J. R., Klosinski, L. P., Cadenas, E., and Brinton, R. D. (2011). Shift in brain metabolism in late onset Alzheimer's disease: implications for biomarkers and therapeutic interventions. *Mol. Aspects Med.* 32, 247–257. doi: 10.1016/j.mam.2011.10.005

Yu, Y., Fedele, G., Celardo, I., Loh, S. H. Y., and Martins, L. M. (2021). Parp mutations protect from mitochondrial toxicity in Alzheimer's disease. *Cell Death Dis.* 12:651.

Yuan, H., Ma, Q., Cui, H., Liu, G., Zhao, X., Li, W., et al. (2017). How can synergism of traditional medicines benefit from network pharmacology? *Molecules* 22:1135. doi: 10.3390/molecules22071135

Yun, W., Dan, W., Liu, J., Guo, X., Li, M., and He, Q. (2021). Investigation of the mechanism of traditional chinese medicines in angiogenesis through network pharmacology and data mining. *Evid. Based Complement. Alternat. Med.* 2021:5539970. doi: 10.1155/2021/5539970

Zangeneh, F., Vazirizadeh, A., Mirshamsi, M. R., Fakhri, A., Faizi, M., and Pourahmad, J. (2018). Induction of apoptosis by an extract of persian gulf marine mollusc, turbo coronatus through the production of reactive oxygen species in mouse melanoma cells. *Asian Pac. J. Cancer Prev.* 19, 3479–3488. doi: 10.31557/APJCP.2018.19.12.3479

Zeng, Q., Li, L., Siu, W., Jin, Y., Cao, M., Li, W., et al. (2019). A combined molecular biology and network pharmacology approach to investigate the multi-target mechanisms of Chaihu Shugan San on Alzheimer's disease. *Biomed. Pharmacother.* 120:109370. doi: 10.1016/j.biopha.2019.109370

Zhang, J., Zhang, Z., Bao, J., Yu, Z., Cai, M., Li, X., et al. (2017). Jia-Jian-Di-Huang-Yin-Zi decoction reduces apoptosis induced by both mitochondrial and endoplasmic reticulum caspase12 pathways in the mouse model of Parkinson's disease. *J. Ethnopharmacol.* 203, 69–79. doi: 10.1016/j.jep.2016.12.053

Zhang, J., Zhang, Z., Zhang, W., Li, X., Wu, T., Li, T., et al. (2018). Jia-Jian-Di-Huang-Yin-Zi decoction exerts neuroprotective effects on dopaminergic neurons and their microenvironment. *Sci. Rep.* 8:9886. doi: 10.1038/s41598-018-27852-w

Zhang, M., Cheng, X., Dang, R., Zhang, W., Zhang, J., and Yao, Z. (2018). Lactate deficit in an Alzheimer disease mouse model: the relationship with neuronal damage. *J. Neuropathol. Exp. Neurol.* 77, 1163–1176. doi: 10.1093/jnen/nly102

Zhou, Q., Zheng, H., Chen, J., Li, C., Du, Y., Xia, H., et al. (2018). Metabolic fate of glucose in the brain of APP/PS1 transgenic mice at 10 months of age: a (13)C NMR metabolomic study. *Metab. Brain Dis.* 33, 1661–1668. doi: 10.1007/s11011-018-0274-7

Conflict of Interest: The authors declare that the research was conducted in the absence of any commercial or financial relationships that could be construed as a potential conflict of interest.

Publisher's Note: All claims expressed in this article are solely those of the authors and do not necessarily represent those of their affiliated organizations, or those of the publisher, the editors and the reviewers. Any product that may be evaluated in this article, or claim that may be made by its manufacturer, is not guaranteed or endorsed by the publisher.

frontiers | Frontiers in Aging Neuroscience

ORIGINAL RESEARCH
published: 05 April 2022
doi: 10.3389/fnagi.2022.810206

Long-Term Effect of Acetylcholinesterase Inhibitors on the Dorsal Attention Network of Alzheimer's Disease Patients: A Pilot Study Using Resting-State Functional Magnetic Resonance Imaging

Ken-ichiro Yamashita[1,2], Taira Uehara[3], Yoshihide Taniwaki[4], Shozo Tobimatsu[5] and Jun-ichi Kira[1,2]*

[1] Translational Neuroscience Center, Graduate School of Medicine, International University of Health and Welfare, Otawara, Japan, [2] Department of Neurology, Brain and Nerve Center, Fukuoka Central Hospital, Fukuoka, Japan, [3] Department of Neurology, International University of Health and Welfare Narita Hospital, Chiba, Japan, [4] Department of Neurology, Fukuoka Sanno Hospital, Fukuoka, Japan, [5] Department of Orthoptics, Faculty of Medicine, Fukuoka International University of Health and Welfare, Fukuoka, Japan

OPEN ACCESS

Edited by:
Fushun Wang,
Nanjing University of Chinese Medicine, China

Reviewed by:
Ilhami Gulcin,
Atatürk University, Turkey
Rosaleena Mohanty,
Karolinska Institutet, Sweden

***Correspondence:**
Ken-ichiro Yamashita
kyamashita@kouhoukai.or.jp

Specialty section:
This article was submitted to Alzheimer's Disease and Related Dementias, a section of the journal Frontiers in Aging Neuroscience

Received: *06 November 2021*
Accepted: *11 March 2022*
Published: *05 April 2022*

Citation:
Yamashita K-i, Uehara T, Taniwaki Y, Tobimatsu S and Kira J-i (2022) Long-Term Effect of Acetylcholinesterase Inhibitors on the Dorsal Attention Network of Alzheimer's Disease Patients: A Pilot Study Using Resting-State Functional Magnetic Resonance Imaging. Front. Aging Neurosci. 14:810206. doi: 10.3389/fnagi.2022.810206

Background: Alzheimer's disease (AD) is the most common condition of all neurodegenerative diseases and is characterized by various cognitive dysfunctions. Recent resting-state functional magnetic resonance imaging (rs-fMRI) studies have revealed the physiological dynamics of functionally connected brain networks, which are called resting-state networks (RSNs). Associations between impairments of RSNs and various neuropsychiatric diseases, such as AD, have been reported. Acetylcholinesterase inhibitors (AChEIs) have been used as a pharmacological treatment for mild-to-moderate moderate AD, and short-term improvements in cognitive functions and RSNs in restricted areas have been reported.

Objective: We aimed to characterize AChEI-related RSN changes by acquiring two sets of rs-fMRI data separated by approximately 3 to 6 months.

Methods: Seventeen patients with AD and nine healthy subjects participated in this study. Independent component analysis was performed on the rs-fMRI data of AChEI-responsive and non-responsive AD patients, stratified according to change in Mini-Mental State Examination (MMSE) scores after 3 to 6 months of AChEI therapy. In addition, a region of interest-based analysis of the rs-fMRI data before therapy was performed to explore the functional connectivity (FC) changes associated with AchEI therapy.

Results: Responders showed a significantly greater increase in MMSE scores, especially for orientation for time, than that of non-responders following AChEI therapy.

A subtraction map of MMSE score differences (responders minus non-responders) in the independent component analysis revealed higher FC of the dorsal attention network in responders compared with that in non-responders. Moreover, in the region of interest analysis of untreated status data, the dorsal attention network showed significant negative FC with the right planum temporale, which belongs to the ventral attention network, proportional to MMSE score change.

Conclusion: The negative correlation of the FC of the dorsal attention network and right planum temporale before AChEI therapy and MMSE score change may be a biomarker of the therapeutic effect of AChEIs for AD.

Keywords: Alzheimer's disease, resting-state fMRI, acetylcholinesterase inhibitors, dorsal attention network, resting-state networks

INTRODUCTION

Alzheimer's disease (AD) is the most common cause of dementia and presents with a variety of cognitive dysfunctions. In addition to brain atrophy, particularly in the hippocampus and parietal lobe as shown using structural magnetic resonance imaging (MRI) (Frisoni et al., 2010), AD patients exhibit hypoperfusion in the temporal lobe and the medial and lateral parts of the parietal lobe even in the early stage of AD as shown using functional neuroimaging techniques, such as positron emission tomography and single-photon emission computed tomography (Neary et al., 1987; Burns et al., 1989).

Although functional MRI (fMRI) techniques have revealed increased deoxy-hemoglobin during the performance of cognitive tasks in brain regions related to higher brain function (Ojemann et al., 1998), resting-state fMRI (rs-fMRI) studies have demonstrated hyperactivation in the anterior cingulate (AC) gyrus and the medial and lateral areas of the parietal lobe, where amyloid β preferentially deposits when the brain is not engaged in cognitive tasks (Sperling et al., 2009). These regions show synchronized patterns of activation, termed the default mode network (DMN), which is highly active during mind-wandering conditions. Thus, this hyperactivation is assumed to be related to the pathological changes in AD (Busche et al., 2008). Furthermore, rs-fMRI studies have detected several other functionally connected large-scale networks, which are now known as resting-state networks (RSNs) (Yeo et al., 2011; Lee et al., 2012).

Acetylcholinesterase inhibitors (AChEIs) and N-methyl-D-aspartate receptor antagonists (memantine) were developed according to the amyloid cascade hypothesis and are currently used as a therapeutic approach for AD (Özbey et al., 2016; Özgeriş et al., 2016). These drugs are effective in improving the cognitive functions and psychological symptoms of patients with AD (Rogers et al., 1998; Reisberg et al., 2003). A double-blind placebo-controlled study of AD patients revealed a significantly greater improvement in the cognitive component score of the Alzheimer's Disease Assessment Scale Japanese version (ADAS-J cog) for 24 weeks in the donepezil-treated group compared with that in the placebo group (Homma et al., 2000). Furthermore, a randomized comparison study of donepezil and galantamine in AD patients indicated that the long-term efficacy of AChEIs on Mini-Mental State Examination (MMSE) score lasted at least 26 weeks; moreover, in patients who received galantamine, MMSE scores at 52 weeks were not significantly different from those at baseline (Wilcock et al., 2003).

An rs-fMRI study that evaluated the association between AChEI effects and functional connectivity (FC) changes in AD patients reported increased FC in the orbitofrontal network, which correlated with cognitive improvement after 12 weeks of treatment (Griffanti et al., 2016). Although the increased FC of the orbitofrontal network with AChEI treatment based on independent component analysis (ICA) reflects the improvement in cognitive function in AD patients, FC differences in RSNs between responders and non-responders before AChEI therapy has not yet been explored.

Therefore, in this study, we aimed to examine FC changes associated with AChEI therapy for AD by acquiring rs-fMRI data at two time points: before and after AChEI treatment. We performed a correlation analysis between cognitive scale scores (MMSE and its subscale scores) and FC among the RSNs of the rs-fMRI data acquired before AChEI therapy.

MATERIALS AND METHODS

Subjects

Seventeen AD patients (six males and 11 females; mean age ± standard deviation [SD], 77.3 ± 8.2 years) participated in the study from 2015 to 2019 at Fukuoka Sanno Hospital, and nine age-matched healthy controls (three males and six females; aged 71.5 ± 11.5 years) were enrolled in the study. Diagnosis of AD was made by two neurologists (KY and YT), based on National Institute on Aging and Alzheimer's Association criteria (McKhann et al., 2011). Brain MRIs of all subjects showed no abnormalities except brain atrophy. Subjects were all right-handed and had no history of neurological disorders. None of the subjects were taking psychiatric medications, including memantine.

Procedure

All subjects except normal subjects participated in two sessions, each of which comprised the MMSE (Folstein et al., 1975)

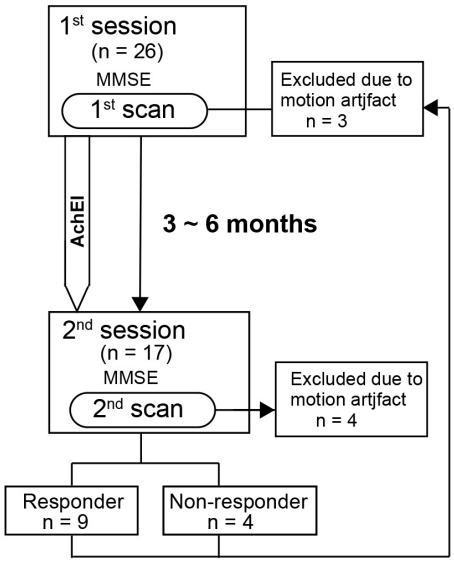

FIGURE 1 | Time schedule for the detection of resting-state network changes following acetylcholinesterase inhibitor therapy in patients with Alzheimer's disease.

and an rs-fMRI scan. The first and second sessions were separated by approximately 3 to 6 months, which corresponds to the duration of AChEI effectiveness as shown in previous studies (**Figure 1**). AChEIs indicate the effect of acetylcholine (ACH) increment by inhibiting acetylcholinesterase (AchE). AChE activity was measured using a spectrophotometer, which estimates colorimetric product (412 nm) formed from a reaction between 5,5′-dithgiobis (2-nitrobenzoic acid) and AChE-derived thiocholine (Özgeriş et al., 2016). During the first session, the MMSE was administered to all participants, and the main subscale scores of orientation for time (OT, scale 0–5), orientation for place (scale 0–5), delayed recall (DR, scale 0–3), and calculation (scale 0–5) were used for subsequent analyses. After the first rs-fMRI scan, AChEI therapy was initiated for AD patients (eight received donepezil, seven received rivastigmine, and two received galantamine). Although various criteria of increased MMSE score have been used previously (Miranda et al., 2015; Gallucci et al., 2016), we classified patients into responders and non-responders during the second session according to criteria based on the Mendiondo model-estimated curve of MMSE decline using a cubic or logarithmic function of MMSE score (Mendiondo et al., 2000). Briefly, the responder group consisted of subjects with second session MMSE scores that were higher than estimated MMSE scores based on the Mendiondo model, and the non-responder group consisted of subjects with MMSE scores that were lower than those estimated by the model. A Mann-Whitney test was used to compare the demographic features and cognitive performance between the two groups.

Image Acquisition

A 3 Tesla MRI scanner (Achieva TX, Philips Medical Systems, Netherlands) was used to acquire MRI data during both study sessions. Scout images were first collected to center the field of view on the subject's brain. Three dimensional T1-weighted turbo field echo images were obtained for anatomical reference (repetition time = 8.1 ms; echo time = 3.8 ms; field of view = 240 mm; matrix size = 240 × 240; slice thickness = 1.0 mm). For functional imaging, a gradient-echo echo-planar sequence was used (repetition time = 2,800 ms; echo time = 30 ms; flip angle = 90 degrees; 40 × 3 mm slices; in-plane resolution of 3 × 3 mm). One functional run was acquired, and the total scanning time was 7 min.

Image Analysis

Preprocessing of imaging data was performed using the SPM8 software[1]. Functional images were slice timing corrected, realigned, normalized to echo-planar imaging template based on Montreal Neurological Institute coordinates, and spatially smoothed (full width at half maximum = 8 mm). The first five functional volumes were excluded from the analysis to take into account the equilibrium of longitudinal magnetization.

To reduce motion-related effects during rs-fMRI scanning, we calculated framewise displacement, which represents a six-dimensional time series across frames for each subject (Power et al., 2012). Subjects who had more than 90% of time points with a framewise displacement below 0.5 mm were included for analysis (Power et al., 2014). This criterion was applied to both the first and second scans.

In the first step, we performed ICA on the second scan data using the CONN software[2] (Whitfield-Gabrieli and Nieto-Castanon, 2012). The gray matter signal was filtered using a bandpass filter (0.01–0.1 Hz) to reduce the effect of low-frequency physiologic noise. White matter and cerebrospinal fluid signals were regressed out during the denoising step. The group ICA analysis using the fast ICA algorithm involved concatenating the blood-oxygen-level-dependent signal across subjects to identify independent spatial components and back-projecting these components onto individual subjects, which resulted in regression coefficients maps that represented the FC between the independent components (Calhoun et al., 2001). We set 20 independent components to be identified, which included the DMN and the sensorimotor, frontoparietal, dorsal attention (DAN), salience (SN), language, and visual networks. We then generated a subtraction map of the drug efficacy differences between the responder and non-responder groups in each session to identify FC changes due to AChEI treatment.

After performing ICA of the second scan data, we conducted a region of interest (ROI) analysis, whereby ROIs were anatomically defined using the FSL Harvard-Oxford maximum probability cortical atlas, with bilateral regions divided into left and right hemispheres (168 ROIs) in the first scan data. The anatomical regions and RSNs that were significantly different between responders' and non-responders' second scan data were plotted as seeds for the ROI-to-ROI analysis of the first scan data. Using the same data for seed selection and ROI analysis results in distorted descriptive statistics and invalid statistical

[1]http://www.fil.ion.ucl.ac.uk/spm/

[2]https://www.nitrc.org/projects/conn/

inferences (Kriegeskorte et al., 2009). Moreover, several studies have performed ICA in one group with no *a priori* assumptions for deciding the seed for a subsequent ROI analysis of another group (Brier et al., 2012; Tsvetanov et al., 2016). Therefore, we performed ICA on the second scan data to establish the seed and subsequently performed ROI-to-ROI analysis using the first scan data. Pearson linear correlation coefficients between the time course of the signal of each ROI and the average signal of the seed were calculated using CONN. ROI-to-ROI one-sample *t*-tests were used to determine significant connectivity between the seed and ROI in each group. Connectivity estimated by the ICA was considered significant when the corrected *p*-value for the cluster-level false-discovery rate (*p*-FDR) was less than 0.05 (Bueno et al., 2018). Seed-level *p*-FDR as implemented in CONN was used for the statistical analysis of the ROI analysis. The threshold used for the seed-level *p*-FDR was set at 0.05.

Spearman's rank-order correlation analysis was performed in the AD patients to verify the association between MMSE subscale score change from the first to the second session and z-transformed *r*-values of the seed to significant ROI for the responders versus non-responders contrast.

RESULTS

Behavior Data

All patients completed at least 3 months of AChEI therapy (mean doses of donepezil, galantamine, and rivastigmine were 6, 16, and 10.5 mg/day, respectively). Second scan data of four subjects (three responders and one non-responder) and first scan data of three subjects (three responders) were excluded because of excessive FD criteria. The ratio of time points with FD below 0.5 mm in the rs-fMRI scan of the responder, non-responder, and healthy control groups were 92.8 ± 5.9%, 97.8 ± 2.8%, and 97.4 ± 3.4% in the first session, respectively. The FD values of the responders and non-responders were 95.9 ± 2.1% and 96.7 ± 2.5% in the second session, respectively. Finally, the second scan data of 13 subjects (nine responders and four non-responders) and the first scan data of 19 subjects (six responders, four non-responders, and nine healthy subjects) were included in the final analyses. There were no significant differences in age at examination among the three groups. In addition, the interval between the first and second scans did not differ significantly between the responder group (mean ± SD: 144.9 ± 43.5 days) and non-responder groups (mean ± SD: 132.5 ± 46.8 days; i.e., the therapeutic duration did not significantly differ between the two groups).

The MMSE scores of the responders, non-responders, and healthy control groups were 18.4 ± 2.6, 19.0 ± 1.2, and 28.7 ± 1.6 for the first session, respectively, and 22.1 ± 2.5 and 17.5 ± 2.4 for the second session (healthy controls completed the MMSE during the first session only), respectively. In the responder group, three received donepezil, four received rivastigmine, and two received galantamine. In the non-responder group, two received donepezil and two received rivastigmine. All main MMSE subscale scores of the first session were not significantly different between responders and non-responders; however, both MMSE ($p < 0.01$) and main MMSE subscale scores (OT, orientation for place, delayed recall, and calculation) were significantly lower in patients than in healthy controls. Compared with responders, non-responders had significantly lower MMSE ($p < 0.05$) and OT ($p < 0.05$) scores in the second session (**Table 1**).

Imaging Data

Among the RSNs related to cognitive function changes, the ICA of the second session revealed significant differences in drug efficacy between responders and non-responders in the DAN and visual network. In the DAN, the right inferior temporal gyrus ($t = 11.2$, p-FDR < 0.05) and left angular gyrus ($t = 6.9$, p-FDR < 0.05) showed significantly higher FC in responders rather than non-responders (**Figure 2**). In the visual network, the left cerebellum ($t = 7.6$, p-FDR < 0.05) had significantly higher FC in the responders than in the non-responders.

In the next step, we used the DAN, which is related to higher cognitive functions, as seeds (containing 3,137 voxels) for the ROI-to-ROI analysis of the first scan dataset before AChEI therapy. In healthy subjects, the DAN was significantly connected to the bilateral superior parietal lobules, bilateral pre- and postcentral gyri, bilateral supramarginal gyri, right inferior temporal gyrus, and right lateral occipital cortex (**Figure 3A**). Although responders showed significant FC between the DAN and right planum temporale (PT) and the primary sensory and motor areas, similarly to healthy subjects (**Figure 3B**), only the FC between the DAN and right PT was significant in non-responders (**Figure 3C** and **Table 2**).

The subtraction z-score map of responders versus healthy control subjects revealed significant positive FC between the DAN and the right superior frontal gyrus (SFG) ($t[13] = 5.5$,

TABLE 1 | Demographic features of healthy controls, responders, and non-responders.

	AD		Normal
	Responder	Non-responder	
N	9	4	9
Age	76.2 ± 10.6	74.8 ± 3.0	71.5 ± 11.3
M:F	3:6	2:2	3:6
Days (Scan 1 – Scan 2)	144.9 ± 43.5	132.5 ± 46.8	
MMSE (1st)	18.4 ± 2.6††	19.0 ± 1.2††	28.7 ± 1.6
OT (0–5)	2.4 ± 0.9††	1.8 ± 0.5††	4.6 ± 0.4
OP (0–5)	3.3 ± 1.0††	3.0 ± 1.2††	5.0 ± 0.0
DR (0–3)	1.0 ± 0.9†	0.8 ± 1.0†	2.4 ± 0.7
Calculation (0–5)	1.7 ± 1.3††	2.8 ± 1.5†	4.6 ± 0.7
MMSE (2nd)	22.1 ± 2.5	17.5 ± 2.4*	
OT (0–5)	3.2 ± 1.2	1.3 ± 1.3*	
OP (0–5)	4.3 ± 0.7	2.8 ± 1.7	
DR (0–3)	0.9 ± 0.8	0.5 ± 1.0	
Calculation (0–5)	2.9 ± 1.4	2.8 ± 1.5	

*Data are shown as means ± standard deviations. The first MMSE test was performed on six responders and four non-responders. †$p < 0.05$ compared with healthy subjects. ††$p < 0.01$ compared with healthy subjects. *$p < 0.05$ compared with responders. MMSE, Mini-Mental State Examination; OP, orientation for place; OT, orientation for time; DR, delayed recall.*

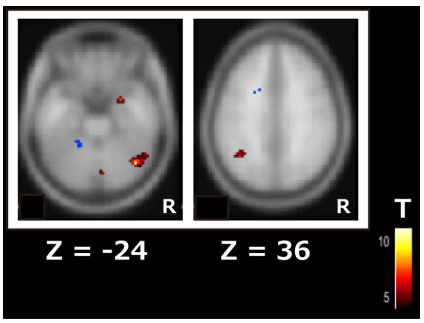

FIGURE 2 | Subtraction map of responders minus non-responders for the dorsal attention network using independent component analysis of the second scan data. The color bar indicates the *t*-value.

$p < 0.05$, FDR corrected; **Figure 4A**), whereas the subtraction z-score map of non-responders versus healthy controls showed significant positive FC between the DAN and AC ($t[11] = 5.2$, $p < 0.05$, FDR corrected; **Figure 4B**). Responders showed significant negative FC between the DAN and right PT ($t[8] = -6.2$, $p < 0.05$, FDR corrected; **Figure 4C**), which was not observed in the non-responders.

For elucidating the differences among three AChEIs, we conducted the ROI analysis using the first scan data of the five AD patients (three responders and two non-responders) who used donepezil. As a result, no significant regions detected in the contrast of responders versus non-responders were related to donepezil. ROI analysis of patients treated with rivastigmine or galantamine was not performed because of the small sample size (only three patients were treated with rivastigmine, and two patients were treated with galantamine).

To examine the relationship between AchEI treatment on cognitive function and FC before therapy, we performed Spearman's correlation analysis between change in MMSE score (ΔMMSE; second session MMSE score minus first session MMSE score)/first session MMSE score and z-transformed *r*-values from the DAN to the right SFG, AC, and right PT ROIs that were

TABLE 2 | Regions significantly connected with the dorsal attention network in the region of interest analysis.

	Region	T	p-FDR
Normal	Rt. Superior Parietal Lobule	17.75	0.0001
	Rt. Postcentral Gyrus	13.80	0.0001
	Rt. Supramarginal Gyrus	9.46	0.0007
	Lt. Postcentral Gyrus	6.57	0.0048
	Rt. Precentral Gyrus	6.32	0.0053
	Lt. Supramarginal Gyrus	6.09	0.0053
	Lt. Superior Parietal Lobule	6.02	0.0053
	Rt. Frontal Pole	−5.56	0.0053
	Lt. Precentral Gyrus	5.10	0.0119
	Rt. Inferior Temporal Gyrus	4.87	0.0147
	Rt. Lateral Occipital Cortex	3.90	0.0450
Responder	Lt. Superior Parietal Lobule	12.22	0.0070
	Rt. Supramarginal Gyrus	10.88	0.0070
	Rt. Superior Parietal Lobule	9.23	0.0076
	Rt. Superior Frontal Gyrus	9.07	0.0076
	Rt. Lateral Occipital Cortex	8.22	0.0091
	Rt. Occipital Pole	6.24	0.0225
	Rt. Precentral Gyrus	5.99	0.0225
	Rt. Postcentral Gyrus	5.96	0.0225
	Rt. Planum Temporale	5.93	0.0225
	Rt. Cerebellum	−5.88	0.0225
	Lt. Supramarginal Gyrus	5.07	0.0405
	Lt. Postcentral Gyrus	4.81	0.0475
Non-responder	Rt. Planum Temporale	24.02	0.0264
Responder > Non-responder	Rt. Planum Temporale	−6.18	0.0441

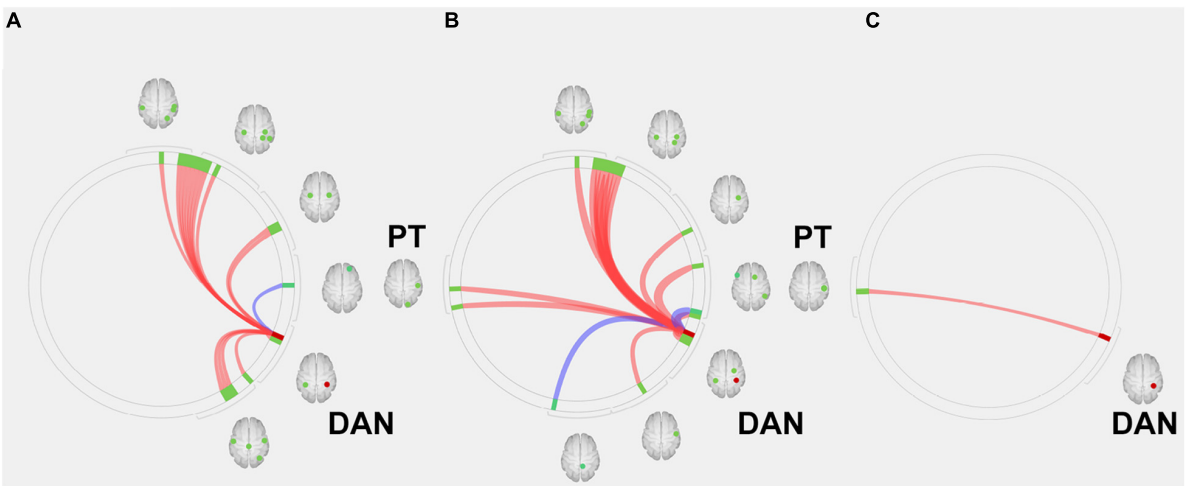

FIGURE 3 | Region of interest (ROI)-to-ROI connectivity values for regions significantly ($p < 0.05$ false-discovery rate corrected) connected with the dorsal attention network in **(A)** healthy subjects, **(B)** responders, and **(C)** and non-responders. Red and blue lines indicate positive and negative connectivity, respectively. Red circles indicate the seed (DAN), and green circles indicate significant ROIs. DAN, dorsal attention network; PT, planum temporale.

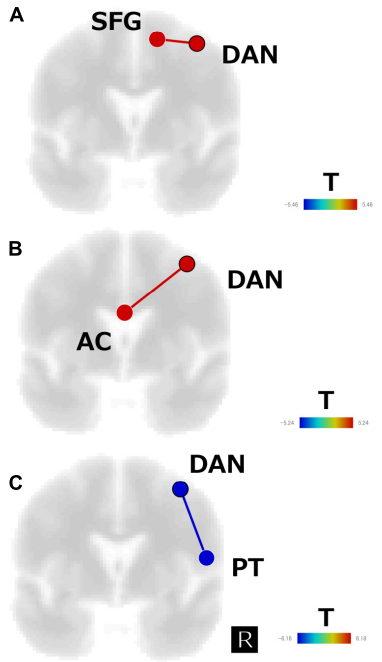

FIGURE 4 | Subtraction map of **(A)** responders minus healthy subjects, **(B)** non-responders minus healthy subjects, and **(C)** responders minus non-responders for the regions of interest analysis of the first scan data. The connectivity map is displayed in the coronal view and overlaid on a template image. The color bar indicates the *t*-value. SFG, superior frontal gyrus; AC, anterior cingulate; DAN, dorsal attention network; PT, planum temporale.

significantly connected to the DAN as a therapeutic index. Similarly Spearman's correlation analysis between change in OT score (ΔOT; second session OT score minus first session OT score)/first session OT score and z-transformed *r*-values from the DAN to the right SFG, AC, and right PT was executed.

Results revealed no significant correlation between ΔOT/first session OT, ΔMMSE/first session MMSE scores, and z-transformed *r*-values from the DAN to the right SFG. Although the FC between the DAN and right PT was significantly negatively correlated with ΔMMSE/first session MMSE score ($r = -0.59$, $p < 0.05$), there was no significant correlation between the DAN and right PT FC and ΔOT/first session OT score (**Figure 5A**). The FC between the DAN and AC was negatively correlated with ΔOT/first session OT score ($r = -0.68$, $p < 0.05$). There was no significant correlation between ΔMMSE/first session MMSE score and FC between the DAN and AC (**Figure 5B**).

DISCUSSION

In the present study, we revealed that compared with AD patients who did not respond to AChEIs, those who did respond exhibited lower FC between the DAN and right PT (part of the ventral attention network [VAN]) before therapy. This suggested that the FC between the DAN and VAN is associated with the decline in MMSE scores in AchEI-resistant AD patients. Moreover, AD patients who did not respond to AChEIs showed significantly greater positive FC between the DAN and AC than that of normal subjects; moreover, a significant OT-related decrement in *r*-values was revealed in these areas.

Anatomically, the PT is part of the superior temporal gyrus, and the left PT is associated with verbal processing (Hickock, 2009). The significantly higher FC between the DAN and right PT pre-AchEI therapy differentiated non-responders from responders (Corbetta and Shulman, 2002; Hirnstein et al., 2013). However, AchEI-responsive AD patients maintained significant FC from the DAN to the primary sensory and motor areas, similar to that of healthy subjects, except for the FC to the right PT.

A previous single-photon emission computed tomography study of AD patients who were non-responsive to donepezil showed a significantly greater reduction in regional cerebral blood flow of the lateral and medial frontal lobes compared with that of responders (Hanyu et al., 2003). Moreover, several rs-fMRI studies in Apolipoprotein E ε4-positive AD patients reported higher FC of the bilateral dorsolateral prefrontal cortex (part of the DAN) following donepezil therapy (Zaidel et al., 2012) and higher FC of the DAN, the control network, and SN after AchEI treatment than that of untreated AD patients (Wang et al., 2014). These AchEI-related FC increases in the attentional network are consistent with our ICA results following AchEI treatment and suggest that improvement in attentional function may ameliorate the OT score.

Although several rs-fMRI studies have investigated the effects of AChEIs, few studies have focused on the FC between RSNs before therapy. One rs-fMRI study directly compared imaging data before and after AchEI therapy using the middle and posterior cingulate cortices as seeds and found significant increases in the FC of the parahippocampal, temporal, parietal, and prefrontal cortices, which largely overlap the DMN (Li et al., 2012). Another rs-fMRI study that directly compared FC between before and 12 weeks after donepezil treatment reported increased FC in the orbitofrontal network with improvement in cognitive function (Griffanti et al., 2016). In contrast, our ICA on rs-fMRI data did not reveal any significant differences in FC, other than in the DAN, between responders and non-responders after long-term AchEI therapy.

Both AD patients who were responsive and non-responsive to AchEI treatment showed higher FC between the PT and the DAN. Moreover, the ROI analysis showed that compared with healthy control subjects, patients showed higher FC between the SFG and AC and the DAN. Previous studies on the inter-RSN FC in AD patients reported higher FC between the frontoparietal network and the DMN in AD patients than in cognitively normal subjects (Contreras et al., 2019). Furthermore, increases in the FC between the DMN and the DAN similar to those observed in our study have been demonstrated in studies comparing AD patients and individuals with mild cognitive impairment (Wang et al., 2019). In contrast to the findings on inter-RSN FC, AD patients have been found to have lower intra-RSN FC than that of MCI and healthy subjects (Zhang et al., 2015). More specifically, AD patients have shown lower intrinsic FC in the memory-related subsystems of the DMN (Qi et al., 2018). Therefore, the functional separation of RSNs from the DAN following AchEI treatment may underlie the improvement in MMSE scores, especially OT scores.

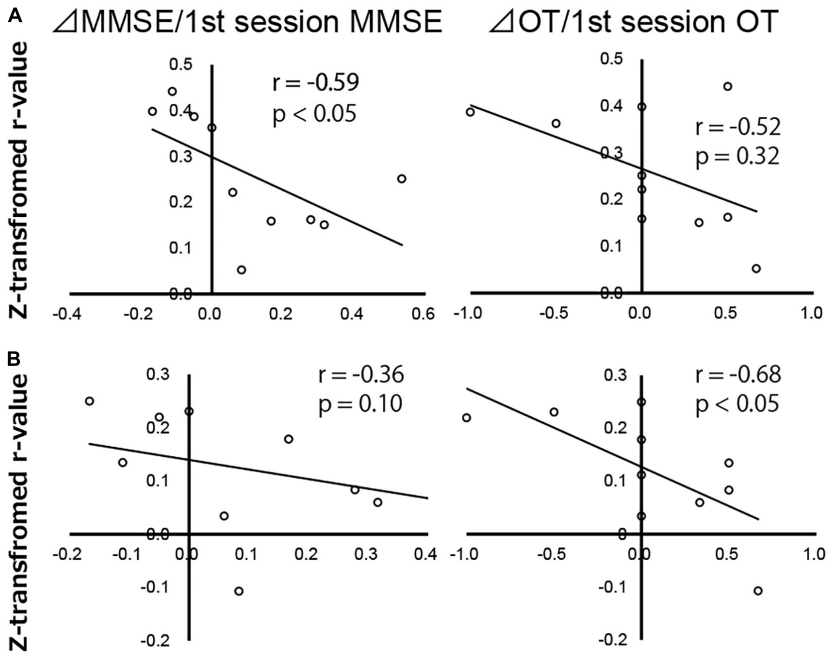

FIGURE 5 | Correlation map of Alzheimer's disease patients between change in Mini-Mental State Examination score (ΔMMSE)/first session MMSE score, change in orientation for time score (ΔOT)/first session OT score, and z-transformed *r*-values of the dorsal attention network to the **(A)** right planum temporale and **(B)** anterior cingulate gyrus, analyzed using Spearman's rank correlation test. Each circle represents data from one subject.

In addition to AD patients, an rs-fMRI study using ICA reported higher FC between the DMN and the central executive network in patients with schizophrenia than in healthy controls, and the severity of hallucinations was positively correlated with the DMN–CEN FC (Manoliu et al., 2014a). Furthermore, patients with major depressive disorder show higher inter-RSN FC between the SN and DMN, coupled with lower intra-FC within the anterior insula, which belongs to the SN, than do healthy controls (Manoliu et al., 2014b). Thus, the variability in FC, especially the hyperconnectivity between RSNs, may underlie the pathophysiology of various neuropsychiatric diseases.

A previous rs-fMRI study revealed that OT score positively correlates with FC between the VAN and posterior cingulate cortex, which belongs to the DMN (Yamashita et al., 2019). Responders in our study showed higher OT scores alongside lower FC between the DAN and PT, which is near the VAN, compared with non-responders, whereas non-responders exhibited higher FC between the DAN and AC gyrus, which belongs to the DMN. Therefore, lower FC between the DAN and VAN-DMN combination may induce future improvements in the OT score. Thus, an rs-fMRI scan in AD patients before therapy may predict the therapeutic effect of AChEIs.

A limitation of this study is the relatively small sample size due to the exclusion of patients because of motion artifacts. Therefore, our results should be considered preliminary and require confirmation in a larger sample size study. The effect of white matter burden and APOE4 as representative confounders of the fMRI studies especially in AD patients were not estimated in this study. It should be expected removing these potential confounders in the future studies. Although we presumed there was no significant difference of brain atrophy between responders and non-responders based on visual inspection of structural MR images, measurement of brain atrophy should be performed like former confounders.

In addition, several prospective studies with pre-therapeutic rs-fMRI scans are necessary to confirm the effects of AChEIs on the DAN. Because the increase in intra-network FC of the DMN was reported after 12 months of galantamine use (Blautzik et al., 2016), intra-network FC analyses of the DAN, VAN, and DMN before and after therapy should be performed in addition to inter-network FC analyses. Nevertheless, despite these limitations, the functional dysconnection between the DAN and VAN observed in this study may be a potential therapeutic biomarker for AD.

CONCLUSION

Improvement in MMSE scores, particularly OT subscale scores, in AChEI-responsive AD patients was associated with increased FC of the DAN. ROI analysis using a DAN seed of rs-fMRI data before therapy revealed that FC changes between the right PT and AC were negatively correlated with MMSE and OT score changes. These results suggested that the increased FC between RSNs may be involved in the cognitive dysfunctions observed in patients with AD.

DATA AVAILABILITY STATEMENT

The raw data supporting the conclusions of this article will be made available by the authors, without undue reservation.

ETHICS STATEMENT

The studies involving human participants were reviewed and approved by the Fukuoka Sanno Hospital. The patients/participants provided their written informed consent to participate in this study.

AUTHOR CONTRIBUTIONS

K-IY: conceptualization and data analysis. TU: data analysis. YT: data collection. ST and J-IK: supervise the research. All authors contributed to the article and approved the submitted version.

FUNDING

This work was supported in part by a Grant-in-Aid for Scientific Research (C) to K-IY (JSPS KAKENHI Grant Number JP20K07888) from the Japan Society for the Promotion of Science, Japan.

ACKNOWLEDGMENTS

We would like to thank our reviewers for their thoughtful comments on the manuscript. We are also grateful to all the research participants.

REFERENCES

Blautzik, J., Keeser, D., Paolini, M., Kirsch, V., Berman, A., Coates, U., et al. (2016). Functional connectivity increase in the default-mode network of patients with alzheimer's disease after long-term treatment with galantamine. *Eur. Neuropsychopharmacol.* 26, 602–613. doi: 10.1016/j.euroneuro.2015.12.006

Brier, M. R., Thomas, J. B., Snyder, A. Z., Benzinger, T. L., Zhang, D., Raichle, M. E., et al. (2012). Loss of intranetwork and internetwork resting state functional connections with alzheimer's disease progression. *J. Neurosci.* 32, 8890–8899. doi: 10.1523/JNEUROSCI.5698-11.2

Bueno, A. P. A., Pinaya, W. H. L., Moura, L. M., Bertoux, M., Radakovic, R., Kiernan, M. C., et al. (2018). Structural and functional papez circuit integrity in amyotrophic lateral sclerosis. *Brain Imaging Behav.* 12, 1622–1630. doi: 10.1007/s11682-018-9825-0

Burns, A., Philpot, M. P., Costa, D. C., Ell, P. J., and Levy, R. (1989). The investigation of alzheimer's disease with single photon emission tomography. *J. Neurol. Neurosurg. Psychiatry.* 52, 248–253. doi: 10.1136/jnnp.52.2.248

Busche, M. A., Eichhoff, G., Adelsberger, H., Abramowski, D., Wiederhold, K. H., Haass, C., et al. (2008). Clusters of hyperactive neurons near amyloid plaques in a mouse model of alzheimer's disease. *Science* 321, 1686–1689. doi: 10.1126/science.1162844

Calhoun, V. D., Adali, T., Pearlson, G. D., and Pekar, J. J. (2001). A method for making group inferences from functional mri data using independent component analysis. *Hum. Brain. Mapp.* 14, 140–151. doi: 10.1002/hbm.1048

Contreras, J. A., Avena-Koenigsberger, A., Risacher, S. L., West, J. D., Tallman, E., McDonald, B. C., et al. (2019). Resting state network modularity along the prodromal late onset alzheimer's disease continuum. *Neuroimage Clin.* 22:101687. doi: 10.1016/j.nicl.2019.101687

Corbetta, M., and Shulman, G. L. (2002). Control of goal-directed and stimulus-driven attention in the brain. *Nat. Rev. Neurosci.* 3, 201–215. doi: 10.1038/nrn755

Folstein, M. F., Folstein, S. E., and McHugh, P. R. (1975). Mini-mental state: a practical method for grading the cognitive state of patients for the clinician. *J. Psychiatr. Res.* 12, 189–198. doi: 10.1016/0022-3956(75)90026-6

Frisoni, G. B., Fox, N. C., Jack, C. R. Jr., Scheltens, P., and Thompson, P. M. (2010). The clinical use of structural MRI in alzheimer disease. *Nat. Rev. Neurol.* 6, 67–77. doi: 10.1038/nrneurol.2009.215

Gallucci, M., Spagnolo, P., Aricò, M., and Grossi, E. (2016). Predictors of response to cholinesterase inhibitors treatment of alzheimer's disease: date mining from the TREDEM registry. *J. Alzheimers Dis.* 50, 969–979. doi: 10.3233/JAD-150747

Griffanti, L., Wilcock, G. K., Voets, N., Bonifacio, G., Mackay, C. E., Jenkinson, M., et al. (2016). Donepezil enhances frontal functional connectivity in alzheimer's disease: a pilot study. *Dement. Geriatr. Cogn. Dis. Extra.* 6, 518–528. doi: 10.1159/000450546

Hanyu, H., Shimizu, T., Tanaka, Y., Takasaki, M., Koizumi, K., and Abe, K. (2003). Regional cerebral blood flow patterns and response to donepezil treatment in patients with alzheimer's disease. *Dement. Geriatr. Cogn. Disord.* 15, 177–182. doi: 10.1159/000068785

Hickock, G. (2009). The functional neuroanatomy of language. *Phys. Life Rev.* 3, 121–143. doi: 10.1016/j.plrev.2009.06.001

Hirnstein, M., Westerhausen, R., and Hugdahl, K. (2013). The right planum temporale is involved in stimulus-driven. Auditory attention–evidence from transcranial magnetic stimulation. *PLoS One* 8:e57316. doi: 10.1371/journal.pone.0057316

Homma, A., Takeda, M., Imai, Y., Udaka, F., Hasegawa, K., Kameyama, M., et al. (2000). Clinical efficacy and safety of donepezil on cognitive and global function in patients with alzheimer's disease. a 24-week, multicenter, double-blind, placebo-controlled study in japan. e2020 study group. dement. *Geriatr. Cogn. Disord.* 11, 299–313. doi: 10.1159/000017259

Kriegeskorte, N., Simmons, W. K., Bellgowan, P. S. F., and Baker, C. I. (2009). Circular analysis in systems neuroscience: the dangers of double dipping. *Nat. Neurosci.* 12, 535–540. doi: 10.1038/nn.2303

Lee, M. H., Hacker, C. D., Snyder, A. Z., Corbetta, M., Zhang, D., Leuthardt, E. C., et al. (2012). Clustering of resting state networks. *PLoS One* 7:e40370. doi: 10.1371/journal.pone.0040370

Li, W., Antuono, P. G., Xie, C., Chen, G., Jones, J. L., Ward, B. D., et al. (2012). Changes in regional cerebral blood flow and functional connectivity in the cholinergic pathway associated with cognitive performance in subjects with mild alzheimer's disease after 12-week donepezil treatment. *Neuroimage* 60, 1083–1091. doi: 10.1016/j.neuroimage.2011.12.077

Manoliu, A., Riedl, V., Zherdin, A., Mühlau, M., Schwerthöffer, D., Scherr, M., et al. (2014a). Aberrant dependence of default mode/central executive network interactions on anterior insular salience network activity in schizophrenia. *Schizophr. Bull.* 40, 428–437. doi: 10.1093/schbul/sbt037

Manoliu, A., Meng, C., Brandl, F., Doll, A., Tahmasian, M., Scherr, M., et al. (2014b). Insular dysfunction within the salience network is associated with severity of symptoms and aberrant inter-network connectivity in major depressive disorder. *Front. Hum. Neurosci.* 7:930. doi: 10.3389/fnhum.2013.00930

McKhann, G. M., Knopman, D. S., Chertkow, H., Hyman, B. T., Jack, C. R. Jr., Kawas, C. H., et al. (2011). The diagnosis of dementia due to alzheimer's disease: recommendations from the national institute on aging-alzheimer's association workgroups on diagnostic guidelines for alzheimer's disease. *Alzheimers Dement.* 7, 263–269. doi: 10.1016/j.jalz.2011.03.005

Mendiondo, M. S., Ashford, J. W., Kryscio, R. J., and Schmitte, F. A. (2000). Modelling mini mental state examination changes in alzheimer's disease. *Stat. Med.* 19, 1607–1616. doi: 10.1002/(sici)1097-0258(20000615/30)19:11/12<1607::aid-sim449<3.0.co;2-o

Miranda, L. F., Gomes, K. B., Silveira, J. N., Pianetti, G. A., Byrro, R. M., Peles, P. R., et al. (2015). Predictive factors of clinical response to cholinesterase inhibitors in mild and moderate alzheimer's disease and mixed dementia: a one-year naturalistic study. *J. Alzheimers Dis.* 45, 609–620. doi: 10.3233/JAD-142148

Neary, D., Snowden, J. S., Shields, R. A., Burjan, A. W., Northen, B., MacDermott, N., et al. (1987). Single photon emission tomography using 99m Tc-HM-PAO in the investigation of dementia. *J. Neurol. Neurosurg. Psychiatry* 50, 1101–1109. doi: 10.1136/jnnp.50.9.1101

Ojemann, J. G., Buckner, R. L., Akbudak, E., Snyder, A. Z., Ollinger, J. M., McKinstry, R. C., et al. (1998). Functional MRI studies of word-stem completion: reliability across laboratories and comparison to blood flow

imaging with PET. *Hum. Brain Mapp.* 6, 203–215. doi: 10.1002/(sici)1097-019319986:4<203::aid-hbm2<3.0.co;2-7

Özbey, F., Taslimi, P., Gülçin, Ý, Maraş, A., Göksu, S., and Supuran, C. T. (2016). Synthesis of diaryl ethers with acetylcholinesterase, butyrylcholinesterase and carbonic anhydrase inhibitory actions. *J. Enzyme Inhib. Med. Chem.* 31, 79–85. doi: 10.1080/14756366.2016.1189422

Özgeriş, B., Göksu, S., Köse, L. P., Gülçin, Ý, Salmas, R. E., Durdagi, S., et al. (2016). Acetylcholinesterase and carbonic anhydrase inhibitory properties of novel urea and sulfamide derivatives incorporating dopaminergic 2-aminotetralin scaffolds. *Bioorg. Med. Chem.* 24, 2318–2329. doi: 10.1016/j.bmc.2016.04.002

Power, J. D., Barnes, K. A., Snyder, A. Z., Schlaggar, B. L., and Petersen, S. E. (2012). Spurious but systemic correlation in functional connectivity MRI networks arise from subject motion. *Neuroimage* 59, 2142–2154. doi: 10.1016/j.neuroimage.2011.10.018

Power, J. D., Mitra, A., Laumann, T. O., Snyder, A. Z., Schlaggar, B. L., and Petersen, S. E. (2014). Methods to detect, characterize, and remove motion artifact in resting state FMRI. *Neuroimage* 84, 320–341. doi: 10.1016/j.neuroimage.2013.08.048

Qi, H., Liu, H., Hu, H., He, H., and Zhao, X. (2018). Primary disruption of the memory-related subsystems of the default mode network in alzheimer's disease: resting-state functional connectivity MRI study. *Front. Aging Neurosci.* 10:344. doi: 10.3389/fnagi.2018.00344

Reisberg, B., Doody, R., Stöffler, A., Schmitt, F., Ferris, S., Möbius, H. J., et al. (2003). Memantine in moderate-to-severe alzheimer's disease. *N. Engl. J. Med.* 348, 1333–1341. doi: 10.1056/NEJMoa013128

Rogers, S. L., Farlow, M. R., Doody, R. S., Mohs, R., and Friedhoff, L. T. (1998). A 24-week, double-blind, placebo-controlled trial of donepezil in patients with alzheimer's disease. Donepezil study group. *Neurology* 50, 136–145. doi: 10.1212/wnl.50.1.136

Sperling, R. A., Laviolette, P. S., O'Keefe, K., O'Brien, J., Rentz, D. M., Pihlajamaki, M., et al. (2009). Amyloid deposition is associated with impaired default network function in older persons without dementia. *Neuron* 63, 178–188. doi: 10.1016/j.neuron.2009.07.003

Tsvetanov, K. A., Henson, R. N. A., Tyler, L. K., Razi, A., Geerligs, L., Ham, T. E., et al. (2016). Extrinsic and intrinsic brain network connectivity maintains cognition across the lifespan despite accelerated decay of regional brain activation. *J. Neurosci.* 36, 3115–3126. doi: 10.1523/JNEUROSCI.2733-15.2016

Wang, J., Liu, J., Wang, Z., Sun, P., Li, K., and Liang, P. (2019). Dysfunctional interactions between the default mode network and the dorsal attention network in subtypes of amnestic mild cognitive impairment. *Aging* 11, 9147–9166. doi: 10.18632/aging.102380

Wang, L., Day, J., Roe, C. M., Brier, M. R., Thomas, J. B., Benzinger, T. L., et al. (2014). The effect of APOE ε4 allele on cholinesterase inhibitors in patients with alzheimer disease: evaluation of the feasibility of resting state functional connectivity magnetic resonance imaging. *Alzheimer Dis. Assoc. Disord.* 28, ,122–127. doi: 10.1097/WAD.0b013e318299d096

Whitfield-Gabrieli, S., and Nieto-Castanon, A. (2012). Conn: a functional connectivity toolbox for correlated and anticorrelated brain networks. *Brain Connect.* 2, 125–141. doi: 10.1089/brain.2012.0073

Wilcock, G., Howe, I., Coles, H., Lilienfeld, S., Truyen, L., Zhy, Y., et al. (2003). A long-term comparison of galantamine and donepezil in the treatment of alzheimer's disease. *Drugs Aging.* 20, 777–789. doi: 10.2165/00002512-200320100-00006

Yamashita, K., Uehara, T., Prawiroharjo, P., Yamashita, K., Togao, O., Hiwatashi, A., et al. (2019). Functional connectivity change between posterior cingulate cortex and ventral attention network relates to the impairment of orientation for time in Alzheimer's disease patients. *Brain Imaging Behav.* 13, 154–161. doi: 10.1007/s11682-018-9860-x

Yeo, B. T., Krienen, F. M., Sepulcre, J., Sabuncu, M. R., Lashkari, D., Hollinshead, M., et al. (2011). The organization of the human cerebral cortex estimated by intrinsic functional connectivity. *J. Neurophysiol.* 106, 1125–1165. doi: 10.1152/jn.00338.2011

Zaidel, L., Allen, G., Cullum, C. M., Briggs, R. W., Hynan, L. S., Weiner, M. F., et al. (2012). Donepezil effects on hippocampal and prefrontal functional connectivity in alzheimer's disease: preliminary report. *J. Alzheimers Dis.* 31(Suppl. 3), S221–S226. doi: 10.3233/JAD-2012-120709

Zhang, Z., Zheng, H., Liang, K., Wang, H., Kong, S., Hu, J., et al. (2015). Functional degeneration in dorsal and ventral attention systems in amnestic mild cognitive impairment and alzheimer's disease: an FMRI study. *Neurosci. Lett.* 585, 160–165. doi: 10.1016/j.neulet.2014.11.050

Conflict of Interest: The authors declare that the research was conducted in the absence of any commercial or financial relationships that could be construed as a potential conflict of interest.

frontiers | Frontiers in Aging Neuroscience

ORIGINAL RESEARCH
published: 24 June 2022
doi: 10.3389/fnagi.2022.891773

Effects of Tempeh Probiotics on Elderly With Cognitive Impairment

Yvonne Suzy Handajani[1†], Yuda Turana[2†], Yogiara Yogiara[3], Sagita Pratiwi Sugiyono[4], Vincent Lamadong[4], Nelly Tina Widjaja[1], Geovannie Audrey Moniqe Christianto[3] and Antonius Suwanto[3,5]*

[1] Center of Health Research, Atma Jaya Catholic University of Indonesia, Jakarta, Indonesia, [2] Department of Neurology, School of Medicine and Health Sciences, Atma Jaya Catholic University of Indonesia, Jakarta, Indonesia, [3] Faculty of Biotechnology, Atma Jaya Catholic University of Indonesia, Jakarta, Indonesia, [4] School of Medicine and Health Sciences, Atma Jaya Catholic University of Indonesia, Jakarta, Indonesia, [5] Department of Biology, Faculty of Mathematics and Natural Science, IPB University, Bogor, Indonesia

OPEN ACCESS

Edited by:
Shijun Xu,
Chengdu University of Traditional Chinese Medicine, China

Reviewed by:
Talitha Best,
Central Queensland University, Australia
Laura Bianchi,
University of Siena, Italy

***Correspondence:**
Yuda Turana
yuda.turana@atmajaya.ac.id

[†]These authors have contributed equally to this work

Specialty section:
This article was submitted to Alzheimer's Disease and Related Dementias, a section of the journal Frontiers in Aging Neuroscience

Received: *08 March 2022*
Accepted: *01 June 2022*
Published: *24 June 2022*

Citation:
Handajani YS, Turana Y, Yogiara Y, Sugiyono SP, Lamadong V, Widjaja NT, Christianto GAM and Suwanto A (2022) Effects of Tempeh Probiotics on Elderly With Cognitive Impairment. Front. Aging Neurosci. 14:891773. doi: 10.3389/fnagi.2022.891773

Introduction: Oral consumption of probiotics can alter Gut Microbiota by causing changes in the production of probiotic derivatives. Therefore, by utilizing Gut-Brain-Axis (GBA), probiotics could provide an opportunity for central nervous system (CNS) modulation, including cognitive function. Tempeh is a traditional Indonesian food rich in probiotics and beneficial for cognitive function. However, the type of probiotics that play a role in cognitive improvement and the number of probiotics needed for the benefits of increasing cognitive function was unknown.

Method: This experimental study involved a total of 93 subjects, divided into 3 groups: A, B and C/control (n: 33, 32, and 28), who were provided with probiotic supplementation isolated from tempeh for 12 weeks intervention. Inclusion criteria were age > 60 years, and memory impairment with the third repetition value of Word List Memory Immediate Recall (WLMIR) < 7. Subjects with diabetes were excluded. Cognitive function examinations were carried out before and after treatment. The tempeh-derived probiotics were prepared trough several processes. Genomic isolation, detection of GABA-encoding genes, and species identification using the 16S-rRNA gene encoding were performed.

Results: The probiotics isolate used in the intervention was identified as *Limosilactobacillus fermentum*. We assigned this isolate as *L. fermentum* A2.8. The presence of the gene encoding GABA was found on this isolate. There was an increase in the cognitive domains of memory, learning process, and verbal fluency ($p < 0.05$) in group A (probiotics at concentration of 10^8 CFU/mL). Memory function, visuospatial, and verbal fluency improved ($p < 0.05$) in group B (probiotics at concentration of 10^7 CFU/mL). Only an increase in the memory domain was observed in the control group. Improvement of the learning process occurred only in group A ($p = 0.006$).

Conclusion: Administration of probiotics derived from *L. fermentum A2.8* increased the cognitive domains of memory, language and visuospatial function. However, probiotic supplementation at a concentration of 10^8 CFU/mL was better in improving the learning process. This study succeeded in detecting Lactic Acid Bacterial isolates *L. fermentum A2.8*

that enclosed gene encoding glutamate decarboxylase (gad) which is involved in the synthesis of -aminobutyric acid (GABA), a neurotransmitter vital for cognitive function.

Keywords: cognitive, elderly, *Limosilactobacillus fermentum*, probiotic, tempeh

INTRODUCTION

With the increase in life expectancy, health issues associated with aging must be addressed. Currently, cognitive impairment is a common health problem found among the elderly. It is estimated that people with dementia will continue to increase in the future, especially in Asia (Nichols et al., 2022).

Studies have demonstrated that microbiota performs a variety of roles in brain health, with the Gut-Brain Axis (GBA) showing a close relationship between the digestive system and the brain (Carabotti et al., 2015). Various studies have demonstrated the mechanisms underlying the GBA. The presence and diversity of microbiota in the gut greatly influences the GBA mechanism, ultimately affecting cognitive function and signifying that cognitive function does not merely rely on an internal relationship through neuronal mechanisms. The gut microbiota (GM) influences both brain structure and cognition (Carabotti et al., 2015; Fernandez-Real et al., 2015; Chen et al., 2021; Feng et al., 2022). Modifying gut probiotic composition by probiotic supplementation might contribute to a prevention and therapy methods of Alzheimer's Disease (AD) (Kowalski and Mulak, 2019).

Oral consumption of probiotics can alter GM by increasing the diversity and number of beneficial microbes, causing changes in the production of probiotic derivatives, reducing inflammation, changing HPA axis function, and altering gut barrier integrity (Plaza-Diaz et al., 2019). Therefore, by utilizing GBA, probiotics could provide an opportunity for central nervous system (CNS) modulation and serve as a possible therapeutic adjunct for some CNS-related conditions (Genedi et al., 2019). Wang et al. (2020) and Yang et al. (2020) also stated that probiotics could change gut dysbiosis and microbiota, improve cognitive function decline, decrease Aβ levels in the hippocampus (associated with the pathophysiology of AD), maintain neuronal structural integrity and plasticity, and reduce trimethylamine-n-oxide (TMAO) synthesis and neuroinflammation. Park et al. (2020) showed that *L. fermentum* exerts a beneficial effect on the regulation of immune response and can provide health improvements, including cognition. Other study has stated that *L.* fermentum produce neuromodulator which contributes to improve cognitive function by inhibiting acetylcholinesterase (AChE) activity (Musa et al., 2017).

Tempeh is a traditional Indonesian food rich in probiotics and beneficial for cognitive function (Stéphanie et al., 2017; Stephanie et al., 2018). A study by Handajani et al. (2020) found that the intervention of giving 100 grams of tempeh improved cognitive function in the elderly compared to controls. However, in these studies, the type of probiotics that play a role in cognitive improvement and the number of probiotics needed for the benefits of increasing cognitive function was unknown.

This study aimed to determine how beneficial the administration of probiotics derived from tempeh is for the elderly with cognitive impairment. The study was done in two stages: first, by isolating the type of bacteria that is safe and beneficial, then by providing those probiotics in two different concentrations to the elderly with cognitive impairment.

MATERIALS AND METHODS

This study was an experimental study, which included two phases: the preparation of isolates, and provision of the intervention isolates.

Intervention Isolate Preparation

Bacterial Isolation

Lactic acid bacteria (LAB) used in this study were isolated from tempeh A, which were previously studied to have the ability to improve cognitive functions among the elderly (Handajani et al., 2020). The LABs were grown and maintained on de Mann Rogosa and Sharpe Agar media. (MRSA) (Oxoid, Oxoid, Ltd., Hampshire, UK) supplemented with 0.3% $CaCO_3$ (Chen et al., 2010). They were then incubated under anaerobic conditions, with an incubation temperature of 35°C for 24–48 h. Gram assays and catalase tests confirmed the grown colonies. Hemolysis tests were also carried out for the initial safety screening of the bacterial isolates. The hemolysis tests were performed on Blood Agar Base media (Oxoid, Oxoid, Ltd., Hampshire, UK). We routinely culture the isolate in MRS media which is the standard medium to grow LAB (Onda et al., 2002; Chen et al., 2010; Hwanhlem et al., 2011).

Genomic Isolation, Detection of GABA-Encoding Genes, and Identification Using the 16S-rRNA Encoding Gene

Genomic DNA was extracted using the Wizard® Genomic DNA Purification Kit (Promega, Corp., Madison, United States). The isolation procedure followed the protocol described in the manual kit. The glutamate decarboxylase gene (*gad*) were detected through the PCR amplification technique (Lin et al., 2017; Wu et al., 2017). Glutamate decarboxylase is the enzyme involved in gamma-aminobutyric acid (GABA) synthesis. The primers used to amplify the *gad* gene (**Table 1**) is a modification of the primers listed by Wu et al. (2017) by eliminating the restriction enzyme recognition sequence present in the primary sequence. The positive isolates for the *gad* gene were then identified using DNA sequencing of the *pheS* encoding gene (Archer and Halami, 2015). The pheS coding gene was amplified using the pheS-F primer (5′-CGCCAGACATCTTCAAGACG-3′) and pheS-R (5′-GAGCGGCTGGAAGAATTACG-3′) (Archer and Halami, 2015). The isolates used for the intervention were reconfirmed by their species using DNA sequencing

TABLE 1 | Primary sequences for *gad* gene detection.

Primary	Nucleotide sequence primer (5′ – 3′)	References
Lb-gadA-F	ATGAATAAAAACGATCAGGAAAC	Wu et al., 2017
Lb-gadA-R	TTAACTTCGAACGGTGGTC	
Lb-gadB-F	ATGGCTATGTTGTATGG	
Lb-gadB-R	TTAGTGCGTGAACCCGTATT	
Lp-gadB-F	ATGGCAATGTTATACGGTAAACAC	
Lp-gadB-R	TCAGTGTGTGAATCCGTATTTC	
gadBFerm-1	ATGTCACTTTACGGAAAGTACGACCAAG	Lin et al., 2017
gadBFerm-2	TTAGTGGGTAAAGCCGTACTTTTTCAGG	

of the gene encoding 16S-rRNA. For identification, primers 63F (5′-CAGGCCTAACACATGCAAGTC-3′) and 1387R (5′-GGGCGGWGTGTACAAGGC-3′) were used (Marchesi et al., 1998). The PCR conditions followed the steps described by Marchesi et al. (1998) DNA Sequencing was carried out at Apical Scientific Sdn. Bhd, Malaysia.

Bacterial Microencapsulation Using Maltodextrin

Isolates used for the microencapsulation process were randomly selected and based on the detection of the *gad* gene. For the microencapsulation of bacteria, *L. fermentum* A2.8 was used with two concentrations of bacterial cells, 10^8 and 10^7 CFU/mL, respectively. The microencapsulation process used maltodextrin DE 10–12 (Qinhuangdao Lihuastarch Co. Ltd., China) as filler. The cell suspension was mixed with 10% Maltodextrin DE 10–12. As a control in the intervention experiment, 10% Maltodextrin without cell suspension was used. Microencapsulation was done by spray-drying (Mini Spray Dryer B-290, BÜCHI Labortechnik AG, Flawil, Switzerland). The microencapsulation process followed the procedure described by Bhagwat et al. (2020) with modifications to the spray-dry conditions, which were as follows; inlet temperature 120°C, aspirator 95%, pump 18%, flow 45 ml/min, and outlet temperature 68°C. All microbiological processes, including bacteria culture and microencapsulation, was performed in the laboratory at the Faculty of Biotechnology Atma Jaya Catholic University of Indonesia, Indonesia.

Preparation of Subjects for Intervention

The participants were recruited in the elderly community which was part of the elderly target area of School of Medicine and Health Sciences, Atma Jaya Catholic University of Indonesia. The inclusion criteria were elderly with memory disorders with the value of the third repetition of Word List Memory Immediate Recall (WLMIR) < 7 (Fillenbaum et al., 2008; Turana et al., 2014). The exclusion criteria were a diagnosis of diabetes or blood glucose of > 200 mg/dL, to avoid an increase in blood glucose level, since the extract given were mixed with artificial flavoring, severe vision and hearing impairments that inhibited the interview process. Participants who were conducted in this study were not living alone and accompanied with family members as their caregiver during consent and interview.

A total of 200 subjects were eligible and examined for physical health and cognitive function as well as other health variables,

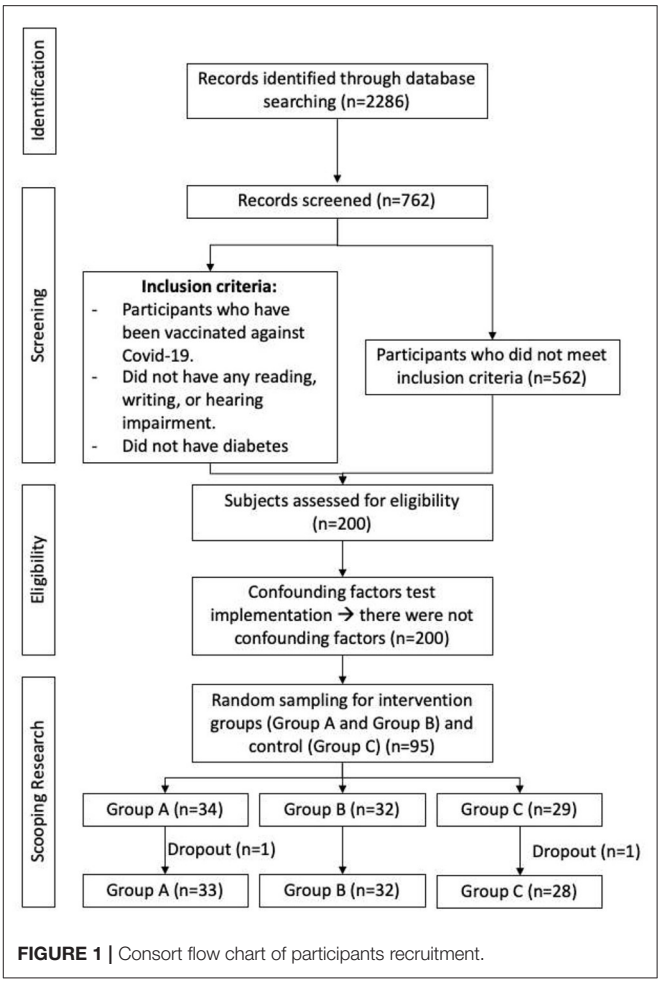

FIGURE 1 | Consort flow chart of participants recruitment.

such as diabetes, hypertension, dyslipidemia, heart disease, lung disease, joint disorders, depression, eye, and ear disorder. With random sampling without blinding, the intervention phase was conducted on three groups of elderly: group A, B, and Control, each with 33, 32, 28 subjects, respectively, with a total of 93 participants (**Figure 1**). Cognitive function assessments were carried out on subjects who met the criteria before and after the intervention. The cognitive function domains assessed were memory (WLMIR) and language function (verbal fluency) using tools from the Consortium to Establish a Registry for Alzheimer's Disease (CERAD), and visuospatial function using the Clock Drawing Test (CDT) assessment (Fillenbaum et al., 2008; Kim et al., 2018). Cognitive tests were performed by doctors (SPS, VL) who have received training and were supervised by a neurologist (YT).

The interventions provided to the three subject groups were: intervention A probiotic powder with a cell density equivalent to OD1, intervention B probiotic powder with 10 times more dilute *Lactobacillus* bacteria, and maltodextrin powder for the control subjects. The probiotic intervention was given as a pre-packaged solution in bottles with 100 ml water solvent and orange-flavoring. This research was conducted for 12 weeks. Participants

were urged to stop consuming any fermented-derived foods (such as tofu, soy milk, yogurt, and cassava tape). Control group was not given any probiotics. Trained workers who have been briefed, distributed probiotics to participants as well as monitoring and evaluating daily compliance of consumption using a card. This card functions like both a calendar and reminder to the participants and trained workers.

Univariate analysis was conducted to see the demographic characteristics of the respondents. Then a bivariate analysis was performed using the Wilcoxon matched-pairs test to compare the pre and post-intervention values on cognitive variables. BM SPSS software version 22 (IBM, New York, USA) was used for statistical analyses, with statistical significance set at $p < 0.05$. This research was approved by the ethics committee of Atma Jaya Catholic University of Indonesia FKIK NO: 10/07/KEP/-FKUAJ/2019 and received approval from each subject.

RESULTS

Lactic Acid Bacteria Isolate

There were bacteria colonies identified as lactic acid bacteria during the bacteria separation process, which generated a distinct, clear zone surrounding the colonies. This clear zone appears due to the acid produced by bacteria dissolving the $CaCO_3$ in the media. After identifying the lactic acid bacteria, 24 isolates were randomly picked from Tempeh A. The selection of these isolates was made subjectively based on the morphology of the growing colonies.

The isolates that did not produce a clear zone were confirmed as Gram-positive bacteria and catalase-negative. All bacterial isolates did not have hemolytic activity. Meanwhile, three isolates, namely isolate A2.7, A2.8, and A4.9 were detected to have the *gadB* gene after amplification using gadBFerm-1 and gadBFerm-2 primer pair. Detection using other primer pairs did not show positive results. Identification using the *pheS* gene on the three isolates showed similarities to the bacterium *Limosilactobacillus fermentum (L. fermentum)*. Among the three isolates, isolate A2.8 was randomly selected to be microencapsulated into probiotic powder for intervention purposes. To assure its identity, isolate A2.8 was re-identified using the 16S-rRNA gene, and the results consistently showed similarities (99.7%) to *L. fermentum*. Hence, we assigned isolate A2.8 as *L. fermentum* A2.8. The microencapsulation process produced three types of probiotic powder: group A probiotic powder containing 10^8 CFU/mL probiotic, group B containing 10^7 CFU/mL probiotic, and group C containing only maltodextrin powder. To determine the presence or absence of contamination, a check was carried out on Eosine Methylene Blue Agar media to detect Enterobacteriaceae group and the results were zero (not detected).

We made the orange-flavored probiotics drink by mixing the microencapsulated powder with 100 ml of orange-flavored solution, and no food preservation was added to this solution. Each subject received seven bottles of this solutions. These drinks were distributed to the subjects every week and suggested to be stored in the refrigerator before use. However, the viability test of probiotics after solubilization in this solution has not been conducted and might become a limitation of this study because bacterial viability during storage could not be assured.

Intervention on Subjects

During the study, 1 subject dropped out from group A and 1 subject from the Control group- ultimately, the number of subjects who completed research in each group was not significantly different. Most of the study participants were aged 65 years and over (77.4%), female (64.5%), and had an educational background below 9 years (84.9%) (**Table 3**). **Table 2** also shows no significant difference between the three study groups in sociodemographic aspects, with an exception in group B where the percentage of women is higher than the other groups. The reasons for dropping out of the study were tedium in taking daily supplements and changing places of residence. There were not any confounding factors such as diet and medications.

Baseline cognitive score for each group were listed in **Table 2**. After 12 weeks of intervention, this study found an improvement in the cognitive domains of memory, verbal fluency, and learning process in group A, and an improvement in visuospatial, memory, and verbal fluency cognitive domains in group B. Only improvement of memory function was found in the Control group. Improvement of the learning process only occurred in group A (see **Table 4**). It can be concluded that probiotic intervention can increase cognitive functions of memory, visuospatial, and verbal fluency ($p < 0.05$), with improvements in learning processes being more noticeable in intervention group A.

DISCUSSION

Probiotics and Cognitive Function

Most of the subjects were aged 65 years and over (77.4%), female (64.5%), and had an educational background of below 9 years (84.9%). The sociodemographic distribution of participants in this study is similar to previous studies (Handajani et al., 2020; Suriastini et al., 2020) that enrolled subjects from communities in Indonesia. The participation of subjects in these studies, and likewise in ours, is influenced by employment status (resulting in a higher involvement of women than men), and by the majority of Indonesia's elderly population having a poor level of education (63%) (Handajani et al., 2020; Suriastini et al., 2020; Statistik Penduduk Lanjut Usia, 2021). Results from this study reaffirm that the improvement in cognitive function when consuming tempeh is due to the content of microbiota and probiotics in tempeh. In a previous study, consumption of tempeh for 6 months was found to significantly increase cognitive function in the elderly population group with mild cognitive impairment (MCI) (Handajani et al., 2020). Animal studies found that the extract from tempeh can affect brain function through its role in the gastrointestinal system (Hamad et al., 2016; Kridawati et al., 2020). In a study comparing the administration of tempeh and soy milk for 28 days, Stephanie et al. (2018) found that tempeh

TABLE 2 | Baseline cognitive scores of group A, B, and Control.

Variable	N total (%) = 93	Group A ($n = 33$)		Group B ($n = 32$)		Control ($n = 28$)		*p* value
		Mean	Min-Max (Median)	Mean	Min-Max (Median)	Mean	Min-Max (Median)	
CDT	93 (100%)	0.61	0–2 (0)	0.69	0–2 (0)	0.86	0–2 (0)	0.589
WLMIR 1	93 (100%)	2.21	0–5 (2)	2.31	0–6 (2)	2.64	0–5 (3)	0.543
WLMIR 3	93 (100%)	3.88	0–8 (4)	4.63	0–8 (5)	5.18	3–9 (5)	0.060
Learning process	93 (100%)	1.67	−2–4 (2)	2.31	−3–6 (2)	2.54	0–5 (3)	0.141
Verbal fluency	93 (100%)	9.97	5–18 (10)	11.47	4–24 (11)	11.71	3–20 (12)	0.309

TABLE 3 | Demographic characteristics of group A, B, and Control.

Variable		N total (%) = 93	Group A	Group B	Control	*p* value
Demographic characteristics						
Age	≥65	72 (77.4)	26 (36.1)	25 (34.7)	21 (29.2)	0.934
	60–65	21 (22.6)	7 (33.3)	7 (33.3)	7 (33.3)	
Gender	Female	60 (64.5)	23 (38.3)	18 (30)	19 (31.7)	0.026
	Male	33 (35.5)	10 (30.3)	14 (42.4)	9 (27.3)	
Education	<9 years	79 (84.9)	29 (36.7)	23 (29.1)	27 (34.2)	0.481
	≥9 years	14 (15.1)	4 (28.6)	9 (64.3)	1 (7.1)	

TABLE 4 | Cognitive score differences between group A, B, and Control.

Cognitive domain	Variable	Group A ($n = 33$)			Group B ($n = 32$)			Control group ($n = 28$)		
		n	Median (Min–Max)	*p*-value	n	Median (Min–Max)	*p*-value	*n*	Median (Min–Max)	*p*-value
Executive function and visuospatial	CDT pre	33	0.00 (0–2)	0.083	32	0.00 (0–2)	0.008*	28	0.00 (0–2)	0.257
	CDT post	33	0.00 (0–2)		32	2.00 (0–2)		28	2.00 (0–2)	
Memory	WLMIR 1 pre	33	2.00 (0–5)	0.099	32	2.00 (0–6)	0.002*	28	3.00 (0–5)	0.003*
	WLMIR 1 post	33	3.00 (0–6)		32	3.50 (0–6)		28	4.00 (1–7)	
	WLMIR 3 pre	33	4.00 (0–8)	0.000*	32	5.00 (0–8)	0.017*	28	5.00 (3–9)	0.017*
	WLMIR 3 post	33	6.00 (2–9)		32	6.00 (0–10)		28	6.00 (3–10)	
	Learning process pre	33	2.00 (-2–4)	0.006*	32	2.00 (-3–6)	0.641	28	3.00 (0–5)	0.946
	Learning process post	33	3.00 (-2–7)		32	2.50 (0–6)		28	3.00 (0–5)	
Language	Verbal fluency pre	33	10.00 (5–18)	0.034	32	11.00 (4–24)	0.000*	28	12.00 (3–20)	0.436
	Verbal fluency post	33	12.00 (4–18)		32	14.50 (6–25)		28	11.50 (0–25)	

CDT, Clock Drawing Test; WLMIR, Word List Memory Immediate Recall.
**p < 0.05 using Wilcoxon Test.*

consumption modulated gut microbiota, increasing amounts of *Bifidobacterium* and *A. muciniphila*.

Although tempeh comes from the fermentation of *Rhizopus oligosporus*, many other types of bacteria found in tempeh can be beneficial. In this study, the isolated and identified bacteria was *L. fermentum*. This is in accordance with the study done by Radita et al. (2017) where the dominant bacteria in tempeh was found to be *Lactobacillus* from the phylum *Firmicutes*, formed from the tempeh soaking process.

Several mechanisms explain the influence of the microbiota on cognitive function, occurring through the GBA, including neurological and endocrine pathways. Probiotics that enter the digestive system will affect neurological pathways such as the vagus nerve and neurotransmitter activities in the gastrointestinal tract, including GABA, serotonin, melatonin,

and acetylcholine, among others, activating catecholamines. The endocrine pathway affects GBA through the activation of enteroendocrine cells. Probiotics consumed produce metabolites such as short-chain fatty acids (SCFA) for the synthesis of serotonin, which contributes to metabolic pathways in the brain. A disturbance in the environment of the gut microbiota can induce cognitive impairment (Appleton, 2018).

In addition, probiotics also contain peptidoglycans, a unique component that helps regulate the immune system among its many roles and also found in brain tissue due to systemic translocation. Through interactions with specific receptors, such as peptidoglycan recognition protein (PGRP) and Nod-like receptors, peptidoglycans affect motor, socio-emotional, and cognitive development processes (Tosoni et al., 2019). *L. fermentum*, itself, can reduce neuroinflammation and memory impairment caused by LPS. In addition to the production of neuromodulators, memory enhancement is also caused by the administration of *L. fermentum*-containing milk which inhibits AChE activity (Musa et al., 2017).

Kobayashi et al. (2019a,b) showed a significant increase in cognitive function of delayed recall memory in the subgroup with cognitive deficits, where the intervention had a greater impact on subjects with cognitive deficits. Research by Beltagy et al. (2021) also demonstrated increased concentrations of acetylcholine, dopamine, serotonin, and anti-oxidants in Alzheimer's disease, as well as increased ATP1A1 activity in the hippocampus, from probiotic supplementation. Another study assessed changes in the composite z score of three measures of memory and attention during 12 weeks of administration of *Lactobacillus plantarum* mixed with fermented soybean powder and found significant improvements in memory and attention scores (Hwang et al., 2019).

Athari Nik Azm et al. (2018) conducted a study by giving probiotic powder to Wistar rats every day for 8 weeks, then rats were induced to develop Alzheimer's with amyloid (Aβ1-42). Learning and memory behavior were tested using the Morris Water Maze Test. The rats' drinking water was mixed with probiotic powder *Lactobacillus acidophilus*, *L. fermentum*, *Bifidobacterium lactis*, and *Bifidobacterium longum*. The time and distance required for the Alzheimer's-probiotic (AP) group in the test decreased significantly compared to the Alzheimer's (Aβ) group. Administration of probiotics in the AP group could prevent learning and memory decline due to an increase in brain-derived neurotrophic factor (BDNF) expression and GABA production (Athari Nik Azm et al., 2018).

One study also reported significant improvements in attention and memory domains in the probiotic group, with significantly greater attention scores than the placebo group after the intervention. However, some improvements were also seen in the learning and recall subtests in the placebo group, which the authors acknowledge can represent a learning effect across the test (Ohsawa et al., 2018).

Improvements in cognitive assessment results may be associated with improvements in other aspects, such as physical performance, which is a known predictor of cognitive impairment (Kamo et al., 2018; Ogawa et al., 2018).

Our study found that probiotic intervention in group A, which had lower overall memory scores before the intervention (WLMIR 3 score pre-test), had a more significant effect on improving the learning process. Learning process (assessment of recurring memory, which was the substraction between WLMIR 3 and WLMIR 1, comparing post and pre-test) is a better assessment to evaluate improvement of learning and new memory, compared to single assessment (WLMIR 1).

Mechanism of Action

This study succeeded in detecting three LAB isolates that had gene encoding glutamate decarboxylase (*gad*), an enzyme involved in synthesizing GABA. The study conducted by Gao et al. proved that GABA concentrations decreased with age after reaching adulthood. GABA concentrations in the frontal cortex are estimated to decrease by as much as 5% per decade with age. Decreased concentrations of GABA in the frontal cortex may cause cognitive decline because the frontal cortex plays an essential role in cognitive function (Gao et al., 2013).

Spatial and temporal memory is associated with neuronal oscillatory activity in the hippocampus, where the N-methyl-D-aspartate (NMDA)-type glutamate receptors on neurons play a role in modulating memory. In addition to NMDA receptors, 5-GABAA receptors at the base of dendrites receive excitatory input. Both receptors are complemented in controlling signal transduction in hippocampal cells (Möhler, 2009).

In several studies, LAB has been shown to increase elderly cognitive function by producing neurotransmitters and neuromodulators, reducing neuroinflammation, inhibiting acetylcholinesterase (AChE), and increasing BDNF expression (Akbari et al., 2016; Musa et al., 2017; Athari Nik Azm et al., 2018).

Bacterial species can produce large amounts of neurotransmitters, including GABA, dopamine, serotonin, and norepinephrine, as well as increase the availability of precursors such as tryptophan (Holzer and Farzi, 2014; Yano et al., 2015). Probiotics can also increase the availability of neuroactive compounds indirectly by stimulating metabolites through biosynthesis (Yano et al., 2015). Studies suggest that probiotic-induced changes in the gut were likely to cause functional changes in the brain, including behavioral shifts. However, the precise mechanism by which changes in gut metabolites mediate these neurochemical changes remains unclear. In addition to altered neurotransmitter production, it is thought that probiotics may influence the production of other bacterial-derived metabolites, particularly SCFA, which are thought to be involved in GBA communication (Dalile et al., 2019; Silva et al., 2020). *In vitro* models have shown an increase in SCFA (particularly acetate, butyrate and propionate) as a result of probiotic bacteria (Nagpal et al., 2018). Moreover, Wang et al. (2018) conducted a trial among young, adult, and older groups with *L. plantarum* and found that fecal acetate and propionate levels increased significantly in all three age groups, and slowly decreased to near baseline levels after

supplementation stopped. Probiotics can also increase the availability of neuroactive compounds indirectly by stimulating metabolites for biosynthesis.

Probiotics have been associated with increased gut barrier integrity and reduced permeability; this was thought to occur due to increased mucin expression and tight-junction stability that protects the epithelial barrier (Stoidis et al., 2011; Hemert et al., 2013). Consequently, probiotic interventions can reduce endotoxemia and inflammation levels.

In addition, probiotics can attenuate the deleterious effects of pro-inflammatory cytokines on the gut barrier by reducing pro-inflammatory and enhancing anti-inflammatory responses. Studies have shown that chronic supplementation with *L. salivarius* has been associated with significant reductions in serum concentrations of inflammatory markers such as high sensitivity C-reactive protein (hs-CRP), interleukin (IL)-6, IL-1b, and TNF-α (Rajkumar et al., 2015).

This study is the random sampling without blinding and the viability test of probiotics after solubilization in the solution has not been conducted and might become a limitation of this study. In the future, it is important to conduct study with subjects with severe cognitive conditions such as dementia with a longer intervention duration.

CONCLUSION

Administration of probiotics derived from *L. fermentum* at concentrations of 10^8 CFU/mL and 10^7 CFU/mL increased the cognitive domains of memory, language, and visuospatial function. However, probiotic supplementation with a 10^8 CFU/mL concentration was better at improving the learning process. This study succeeded in detecting Lactic Acid Bacterial isolates *L. fermentum* that had a gene encoding glutamate decarboxylase (gad) which is involved in the synthesis of GABA, known to play an essential role in cognitive function.

DATA AVAILABILITY STATEMENT

The original contributions presented in the study are included in the article/supplementary material, further inquiries can be directed to the corresponding author/s.

ETHICS STATEMENT

This research was approved by the Ethics Committee of Atma Jaya Unika FKIK NO: 10/07/KEP/-FKUAJ/2019. The patients/participants provided their written informed consent to participate in this study.

AUTHOR CONTRIBUTIONS

Study concept and design: YH, YT, and YY. Design of the studies and data acquisition: YH, YT, and NW. Analysis and interpretation of data: SPS and VL. Drafting the manuscript: YH, YT, YY, AS, GAMC, SPS, VL, and NW. Critical revision of the manuscript: YH, YT, YY, and AS. All authors contributed to the article and approved the submitted version.

FUNDING

This study was funded by the Kementerian Riset dan Pendidikan Tinggi Republik Indonesia Grant (ID 17/AKM/PNT/2019, March 27, 2019). The funders had no role in study design, data collection and analysis, decision to publish, or manuscript preparation.

ACKNOWLEDGMENTS

We would like to express our gratitude to the Nutrifood Research Center, PT. Nutrifood Indonesia, for providing food supplements during the study's intervention phase.

REFERENCES

Akbari, E., Asemi, Z., Daneshvar Kakhaki, R., Bahmani, F., Kouchaki, E., and Tamtaji, O. R. (2016). Effect of probiotic supplementation on cognitive function and metabolic status in Alzheimer's Disease: a randomized, double-blind and controlled trial. *Front. Aging Neurosci.* 8, 256. doi: 10.3389/fnagi.2016.00256

Appleton, J. (2018). The gut-brain axis: influence of microbiota on mood and mental health. *Integr Med (Encinitas)*. 17, 28–32.

Archer, A. C., and Halami, P. M. (2015). Probiotic attributes of Lactobacillus fermentum isolated from human feces and dairy products. *Appl. Microbiol. Biotechnol.* 99, 8113–8123. doi: 10.1007/s00253-015-6679-x

Athari Nik Azm, S., Djazayeri, A., Safa, M., Azami, K., Ahmadvand, B., and Sabbaghziarani, F. (2018). Lactobacilli and bifidobacteria ameliorate memory and learning deficits and oxidative stress in β-amyloid (1-42) injected rats. *Appl. Physiol. Nutr. Metab*. 43, 718–726. doi: 10.1139/apnm-2017-0648

Beltagy, D. M., Nawar, N. F., Mohamed, T. M., Tousson, E., and El-Keey, M. M. (2021). Beneficial consequences of probiotic on mitochondrial hippocampus in Alzheimer's disease. *J. Complement. Integr. Med*. 18, 761–767. doi: 10.1515/jcim-2020-0156

Bhagwat, A., Bhushette, P., and Annapure, U. S. (2020). Spray drying studies of probiotic Enterococcus strains encapsulated with whey protein and maltodextrin. *J. Basic Appl. Sci.* 9, 33. doi: 10.1186/s43088-020-00061-z

Carabotti, M., Scirocco, A., Maselli, M. A., and Severi, C. (2015). The gut-brain axis: interactions between enteric microbiota, central and enteric nervous systems. *Ann. Gastroenterol.* 28, 203–209.

Chen, Y., Xu, J., and Chen, Y. (2021). Regulation of neurotransmitters by the gut microbiota and effects on cognition in neurological disorders. *Nutrients*. 13, 2099. doi: 10.3390/nu13062099

Chen, Y. s., Wu, H. c., and Yanagida F. (2010). Isolation and characteristics of lactic acid bacteria isolated from ripe mulberries in Taiwan. *Braz. J. Microbiol.* 41, 916–921. doi: 10.1590/S1517-83822010000400010

Dalile, B., Van Oudenhove, L., Vervliet, B., and Verbeke, K. (2019). The role of short-chain fatty acids in microbiota-gut-brain communication. *Nat. Rev. Gastroenterol. Hepatol.* 16, 461–478. doi: 10.1038/s41575-019-0157-3

Feng, Y., Fu, S., Ma, C., Li, X., Wu, Y., Chen, F, et al. (2022). Interaction of gut, microbiota and brain function in patients with chronic insomnia: a regional homogeneity study. *Front. Neurosci*. 15. doi: 10.3389/fnins.2021.804843

Fernandez-Real, J. M., Serino, M., Blasco, G., Puig, J., Daunis-i-Estadella, J., Ricart, W., et al. (2015). Gut microbiota interacts with brain microstructure and function. *J. Clin. Endocrinol. Metab*. 100, 4505–4513. doi: 10.1210/jc.2015-3076

Fillenbaum, G. G., van Belle, G., Morris, J. C., Mohs, R. C., Mirra, S. S., and Davis, P. C. (2008). CERAD (Consortium to Establish a Registry for Alzheimer's Disease) the first 20 years. *Alzheimers Dement*. 4, 96–109. doi: 10.1016/j.jalz.2007.08.005

Gao, F., Edden, R. A. E., Li, M., Puts, N. A. J., Wang, G., Liu, C., et al. (2013). Edited magnetic resonance spectroscopy detects an age-related decline in brain GABA levels. *Neuroimage*. 78, 75–82. doi: 10.1016/j.neuroimage.2013.04.012

Genedi, M., Janmaat, I. E., Haarman, B. B. C. M., and Sommer, I. E. C. (2019). Dysregulation of the gut-brain axis in schizophrenia and bipolar disorder: probiotic supplementation as a supportive treatment in psychiatric disorders. *Curr. Opin. Psychiatry*. 32, 185–195. doi: 10.1097/YCO.0000000000000499

Hamad, A., Mani, V., Ramasamy, K., Lim, S., and Majeed, A. (2016). *Memory Enhancement in Rats by Soybean and Tempeh Extracts is Associated With Improved Cholinergic and Reduced Neuroinflammatory Activities*. Available online at: https://www.semanticscholar.org/paper/Memory-enhancement-in-rats-by-soybean-and-tempeh-is-Hamad-Mani/83446bc36d77191d43fe8691758d167572ea3d2a (accessed January 28, 2022).

Handajani, Y. S., Turana, Y., Yogiara, Y., Widjaja, N. T., Sani, T. P., and Christianto, G. A. M. (2020). Tempeh Consumption and Cognitive Improvement in Mild Cognitive Impairment. *Dement. Geriatr. Cogn. Disord.* 49, 497–502. doi: 10.1159/000510563

Hemert, S., van Verwe, J., and Schütz, B. (2013). Clinical studies evaluating effects of probiotics on parameters of intestinal barrier function. *Adv. Microbiol.* 3, 212–221. doi: 10.4236/aim.2013.32032

Holzer, P., and Farzi, A. (2014). Neuropeptides and the microbiota-gut-brain axis. *Adv. Exp. Med. Biol.* 817, 195–219. doi: 10.1007/978-1-4939-0897-4_9

Hwang, Y. H., Park, S., Paik, J. W., Chae, S. W., Kim, D. H., and Jeong, D. G. (2019). Efficacy and safety of lactobacillus plantarum C29-fermented soybean (DW2009) in individuals with mild cognitive impairment: a 12-week, multi-center, randomized, double-blind, placebo-controlled clinical trial. *Nutrients*. 11, E305. doi: 10.3390/nu11020305

Hwanhlem, N., Buradaleng, S., Wattanachant, S., Benjakul, S., Tani, A., and Maneerat, S. (2011). Isolation and screening of lactic acid bacteria from Thai traditional fermented fish (Plasom) and production of Plasom from selected strains. *Food Control*. 22, 401–407. doi: 10.1016/j.foodcont.2010.09.010

Kamo, T., Ishii, H., Suzuki, K., and Nishida, Y. (2018). Prevalence of sarcopenia and its association with activities of daily living among japanese nursing home residents. *Geriatr Nurs*. 39, 528–533. doi: 10.1016/j.gerinurse.2018.02.011

Kim, S., Jahng, S., Yu, K. H., Lee, B. C., and Kang, Y. (2018). Usefulness of the clock drawing test as a cognitive screening instrument for mild cognitive impairment and mild dementia: an evaluation using three scoring systems. *Dement Neurocogn. Disord*. 17, 100–109. doi: 10.12779/dnd.2018.17.3.100

Kobayashi, Y., Kinoshita, T., Matsumoto, A., Yoshino, K., Saito, I., and Xiao, J. Z. (2019b). Bifidobacterium Breve A1 supplementation improved cognitive decline in older adults with mild cognitive impairment: an open-label, single-arm study. *J. Prev. Alzheimers Dis*. 6, 70–75. doi: 10.14283/jpad.2018.32

Kobayashi, Y., Kuhara, T., Oki, M., and Xiao, J. Z. (2019a). Effects of Bifidobacterium breve A1 on the cognitive function of older adults with memory complaints: a randomised, double-blind, placebo-controlled trial. *Benef. Microbes*. 10, 511–20. doi: 10.3920/BM2018.0170

Kowalski, K., and Mulak, A. (2019). Brain-gut-microbiota axis in Alzheimer's disease. *J. Neurogastroenterol. Motil*. 25, 48–60. doi: 10.5056/jnm18087

Kridawati, A., Hardinsyah, H., Sulaeman, A., Rahardjo, T. B. W., and Hogervorst, E. (2020). Tempe, Tofu, and Amyloid-β 1-40 serum levels in ovariectomized rats. *J. Alzheimer's Dis*. 76, 159–163. doi: 10.3233/JAD-200220

Lin, Q., Li, D., and Qin, H. (2017). Molecular cloning, expression, and immobilization of glutamate decarboxylase from Lactobacillus fermentum YS2. *Electron. J. Biotechnol*. 27, 8–13. doi: 10.1016/j.ejbt.2017.03.002

Marchesi, J. R., Sato, T., Weightman, A. J., Martin, T. A., Fry, J. C., and Hiom, S. J. (1998). Design and evaluation of useful bacterium-specific PCR primers that amplify genes coding for bacterial 16S rRNA. *Appl Environ Microbiol*. 64, 795–799. doi: 10.1128/AEM.64.2.795-799.1998

Möhler, H. (2009). Role of GABAA receptors in cognition. *Biochem. Soc. Trans*. 37, 1328–1333. doi: 10.1042/BST0371328

Musa, N. H., Mani, V., Lim, S. M., Vidyadaran, S., Abdul Majeed, A. B., and Ramasamy, K. (2017). Lactobacilli-fermented cow's milk attenuated lipopolysaccharide-induced neuroinflammation and memory impairment in vitro and in vivo. *J. Dairy Res*. 84, 488–495. doi: 10.1017/S0022029917000620

Nagpal, R., Wang, S., Ahmadi, S., Hayes, J., Gagliano, J., and Subashchandrabose, S. (2018). Human-origin probiotic cocktail increases short-chain fatty acid production via modulation of mice and human gut microbiome. *Sci. Rep*. 8, 12649. doi: 10.1038/s41598-018-30114-4

Nichols, E., Steinmetz, J. D., Vollset, S. E., Fukutaki, K., Chalek, J., and Abd-Allah, F. (2022). Estimation of the global prevalence of dementia in 2019 and forecasted prevalence in 2050: an analysis for the Global Burden of Disease Study 2019. *Lancet Public Health*. 7, e105–e125. doi: 10.1016/S2468-2667(21)00249-8

Ogawa, Y., Kaneko, Y., Sato, T., Shimizu, S., Kanetaka, H., and Hanyu, H. (2018). Sarcopenia and muscle functions at various stages of Alzheimer disease. *Front. Neurol*. 9. doi: 10.3389/fneur.2018.00710

Ohsawa, K., Nakamura, F., Uchida, N., Mizuno, S., and Yokogoshi, H. (2018). Lactobacillus helveticus-fermented milk containing lactononadecapeptide (NIPPLTQTPVVVPPFLQPE) improves cognitive function in healthy middle-aged adults: a randomised, double-blind, placebo-controlled trial. *Int. J. Food Sci. Nutr*. 69, 369–376. doi: 10.1080/09637486.2017.1365824

Onda, T., Yanagida, F., Uchimura, T., Tsuji, M., Ogino, S., and Shinohara, T. (2002). Widespread distribution of the bacteriocin-producing lactic acid cocci in Miso-paste products. *J. Appl. Microbiol*. 92, 695–705. doi: 10.1046/j.1365-2672.2002.01573.x

Park, M. R., Shin, M., Mun, D., Jeong, S. Y., Jeong, D. Y., and Song, M. (2020). Probiotic Lactobacillus fermentum strain JDFM216 improves cognitive behavior and modulates immune response with gut microbiota. *Sci. Rep*. 10, 21701. doi: 10.1038/s41598-020-77587-w

Plaza-Diaz, J., Ruiz-Ojeda, F. J., Gil-Campos, M., and Gil, A. (2019). Mechanisms of action of probiotics. *Adv. Nutr*. 10. *S*49–66. doi: 10.1093/advances/nmy063

Radita, R., Suwanto, A., Kurosawa, N., Wahyudi, A., and Rusmana, I. (2017). Metagenome analysis of tempeh production: where did the bacterial community in tempeh come from? *Malays. J. Microbiol*. 13, 280–288. doi: 10.21161/mjm.101417

Rajkumar, H., Kumar, M., Das, N., Kumar, S. N., Challa, H. R., and Nagpal, R. (2015). Effect of probiotic Lactobacillus salivarius UBL S22 and prebiotic fructo-oligosaccharide on serum lipids, inflammatory markers, insulin sensitivity, and gut bacteria in healthy young volunteers: a randomized controlled single-blind pilot study. *J. Cardiovasc. Pharmacol. Ther*. 20, 289–298. doi: 10.1177/1074248414555004

Silva, Y. P., Bernardi, A., and Frozza, R. L. (2020). The role of short-chain fatty acids from gut microbiota in gut-brain communication. *Front. Endocrinol*. 11. doi: 10.3389/fendo.2020.00025

Statistik Penduduk Lanjut Usia (2021). *Badan Pusat Statistik*; *2021*. Jakarta: Badan Pusat Statistik.

Stephanie, K. F., Silo, W., Yogiara, Y., and Suwanto, A. (2018). Tempeh consumption enhanced beneficial bacteria in the human gut. *Food Res*. 3, 57–63. doi: 10.26656/fr.2017.3(1).230

Stéphanie, S., Ratih, N. K., Soka, S., and Suwanto, A. (2017). Effect of tempeh supplementation on the profiles of human intestinal immune system and gut *Microbiota*. 2017. doi: 10.5454/mi.11.1.2

Stoidis, C. N., Misiakos, E. P., Patapis, P., Fotiadis, C. I., and Spyropoulos, B. G. (2011). Potential benefits of pro- and prebiotics on intestinal mucosal immunity and intestinal barrier in short bowel syndrome. *Nutr. Res. Rev*. 24, 21–30. doi: 10.1017/S0954422410000260

Suriastini, N. W., Turana, Y., Supraptilah, B., Wicaksono, T. Y., and Mulyanto, E. D. (2020). Prevalence and risk factors of dementia and caregiver's knowledge of the early symptoms of Alzheimer's disease. *Aging Med. Healthcare*. 11, 60–66. doi: 10.33879/AMH.2020.065-1811.032

Tosoni, G., Conti, M., and Diaz Heijtz, R. (2019). Bacterial peptidoglycans as novel signaling molecules from microbiota to brain. *Curr. Opin. Pharmacol*. 48, 107–113. doi: 10.1016/j.coph.2019.08.003

Turana, Y., Ranakusuma, T. A. S., Purba, J. S., Amir, N., Ahmad, S. A., and Machfoed, M. H. (2014). Enhancing diagnostic accuracy of amci in the elderly: combination of olfactory test, pupillary response test, BDNF Plasma Level, and APOE Genotype. *Int. J. Alzheimers Dis*. 2014, e912586. doi: 10.1155/2014/912586

Wang, F., Xu, T., Zhang, Y., Zheng, T., He, Y., and He, F. (2020). Long-term combined administration of Bifidobacterium bifidum TMC3115 and Lactobacillus plantarum 45 alleviates spatial memory impairment and

gut dysbiosis in APP/PS1 mice. *FEMS Microbiol. Lett.* 367, fnaa048. doi: 10.1093/femsle/fnaa048

Wang, J., Wang, J., i,. H., Liu, S., Zhang, H., and Zhang, W. D., et al. (2018). Probiotic Lactobacillus plantarum promotes intestinal barrier function by strengthening the epithelium and modulating gut microbiota. *Front. Microbiol.* 9, 1953. doi: 10.3389/fmicb.2018.01953

Wu, Q., Tun, H. M., Law, Y. S., Khafipour, E., and Shah, N. P. (2017). Common distribution of gad operon in lactobacillus brevis and its GadA contributes to efficient GABA synthesis toward cytosolic near-neutral pH. *Front. Microbiol.* 8:206. doi: 10.3389/fmicb.2017.00206

Yang, X., Yu, D., Xue, L., Li H., and Du, J. (2020). Probiotics modulate the microbiota-gut-brain axis and improve memory deficits in aged SAMP8 mice. *Acta. Pharm. Sin B.* 10, 475–487. doi: 10.1016/j.apsb.2019.07.001

Yano, J. M., Donaldson, Y., u,. K., Shastri, G. P., Ann, G. G., and Ma, P. L., et al. (2015). Indigenous bacteria from the gut microbiota regulate host serotonin biosynthesis. *Cell.* 161, 264–276. doi: 10.1016/j.cell.2015.02.047

Author Disclaimer: The content is solely the responsibility of the authors and does not necessarily represent the funders.

Conflict of Interest: The authors declare that the research was conducted in the absence of any commercial or financial relationships that could be construed as a potential conflict of interest.

Publisher's Note: All claims expressed in this article are solely those of the authors and do not necessarily represent those of their affiliated organizations, or those of the publisher, the editors and the reviewers. Any product that may be evaluated in this article, or claim that may be made by its manufacturer, is not guaranteed or endorsed by the publisher.

frontiers | Frontiers in Aging Neuroscience

TYPE Original Research
PUBLISHED 22 July 2022
DOI 10.3389/fnagi.2022.914491

OPEN ACCESS

EDITED BY
Shijun Xu,
Chengdu University of Traditional Chinese Medicine, China

REVIEWED BY
Cecilia Beatriz Conde,
Medical Research Institute Mercedes and Martín Ferreyra (INIMEC), Argentina
Regina Dahlhaus,
Danube Private University, Austria

*CORRESPONDENCE
Changxi Zhou
zhouchangxi2002@aliyun.com
Tao Xin
xintao@sdfmu.edu.cn
Zhengping Jia
zhengping.jia@sickkids.ca

†These authors have contributed equally to this work

SPECIALTY SECTION
This article was submitted to Alzheimer's Disease and Related Dementias, a section of the journal Frontiers in Aging Neuroscience

RECEIVED 06 April 2022
ACCEPTED 27 June 2022
PUBLISHED 22 July 2022

CITATION
Zhang H, Ben Zablah Y, Zhang H, Liu A, Gugustea R, Lee D, Luo X, Meng Y, Li S, Zhou C, Xin T and Jia Z (2022) Inhibition of Rac1 in ventral hippocampal excitatory neurons improves social recognition memory and synaptic plasticity. *Front. Aging Neurosci.* 14:914491. doi: 10.3389/fnagi.2022.914491

Inhibition of Rac1 in ventral hippocampal excitatory neurons improves social recognition memory and synaptic plasticity

Haiwang Zhang[1,2,3†], Youssif Ben Zablah[2,3†], Haorui Zhang[2,3†], An Liu[4], Radu Gugustea[2,3], Dongju Lee[2,3], Xiao Luo[2,3], Yanghong Meng[2,3], Song Li[5], Changxi Zhou[6*], Tao Xin[1*] and Zhengping Jia[2,3*]

[1]Department of Neurosurgery, The First Affiliated Hospital of Shandong First Medical University & Shandong Provincial Qianfoshan Hospital, Shandong Medicine and Health Key Laboratory of Neurosurgery, Jinan, China, [2]Program in Neurosciences and Mental Health, The Hospital for Sick Children, Peter Gilgan Centre for Research and Learning, Toronto, ON, Canada, [3]Department of Physiology, Temerty Faculty of Medicine, University of Toronto, Toronto, ON, Canada, [4]The Key Laboratory of Developmental Genes and Human Disease, Ministry of Education, School of Life Sciences and Technology, Southeast University, Nanjing, China, [5]Department of Neurosurgery, Caoxian People's Hospital, Caoxian, China, [6]Department of Geriatrics, The Second Medical Center and National Clinical Research Center for Geriatric Diseases, Beijing, China

Rac1 is critically involved in the regulation of the actin cytoskeleton, neuronal structure, synaptic plasticity, and memory. Rac1 overactivation is reported in human patients and animal models of Alzheimer's disease (AD) and contributes to their spatial memory deficits, but whether Rac1 dysregulation is also important in other forms of memory deficits is unknown. In addition, the cell types and synaptic mechanisms involved remain unclear. In this study, we used local injections of AAV virus containing a dominant-negative (DN) Rac1 under the control of CaMKIIα promoter and found that the reduction of Rac1 hyperactivity in ventral hippocampal excitatory neurons improves social recognition memory in APP/PS1 mice. Expression of DN Rac1 also improves long-term potentiation, a key synaptic mechanism for memory formation. Our results suggest that overactivation of Rac1 in hippocampal excitatory neurons contributes to social memory deficits in APP/PS1 mice and that manipulating Rac1 activity may provide a potential therapeutic strategy to treat social deficits in AD.

KEYWORDS

social memory, APP/PS1 mouse model, ventral hippocampus, Rac1, LTP

Introduction

Social interaction and memory are essential for our health and success. Alzheimer's disease (AD), a leading cause of dementia, is a neurodegenerative disease characterized by progressive loss of various forms of memories, including social memory (Filali et al., 2011). Furthermore, impaired social memory in AD patients may lead to

patients developing apathy toward social engagement and can result in a preference for introversion. Due to the importance of social interaction for cognition and mental health (reviewed in: Berkman et al., 2000; Leser and Wagner, 2015), social isolation caused by AD could further worsen disease progression (Wilson et al., 2007; Ali et al., 2017). Currently, there is no cure or effective treatment available due to the limited understanding of the pathological mechanisms underlying AD. Numerous studies suggest that the excessive accumulation of amyloid-beta (Aβ) peptides and neurofibrillary tangles in the brain is the most common causative cause of AD (reviewed in: Hardy and Selkoe, 2002; Ballatore et al., 2007). However, other factors such as neuroinflammation, oxidative stress, and injury of cholinergic neurons, may also contribute to the pathogenic process of AD (reviewed in Serrano-Pozo et al., 2011; Spires-Jones and Hyman, 2014; Singh et al., 2016). How Aβ peptides lead to neuronal degeneration and memory loss remain unclear, but evidence has indicated that Aβ accumulation can impair long-term potentiation (LTP) (Walsh et al., 2002; Almeida et al., 2005; Snyder et al., 2005; Hsieh et al., 2006) and promote long-term depression (LTD) (Shankar et al., 2008; Li et al., 2009). LTP and LTD are the most extensively studied forms of synaptic plasticity widely considered to be key mechanisms underlying learning and memory (reviewed in: Bliss and Collingridge, 1993; Kandel et al., 2014). LTP deficits were widely observed in animal models of AD (reviewed in: Palop and Mucke, 2010; Mucke and Selkoe, 2012; Sheng et al., 2012), but further investigations are required to understand the molecular mechanisms by which LTP is affected by the disease and how they are related to memory deficits.

Rac1 is a member of the Rho family small GTPases known to be a central regulator of actin cytoskeleton dynamics, neuronal structures, synaptic plasticity, and memory maintenance (reviewed in: Lamprecht, 2014; Costa et al., 2020; Zhang et al., 2021b). In particular, overactivation of Rac1 has been shown to promote memory decay (Shuai et al., 2010; Gan et al., 2016; Jiang et al., 2016; Liu et al., 2016, 2018). Elevated Rac1 activity was observed in both human AD patients and animal AD models (Mendoza-Naranjo et al., 2007; Borin et al., 2018; Wu et al., 2019). In addition, reducing Rac1 activity improves spatial memory performance in AD (Wu et al., 2019), suggesting that Rac1 overactivation may contribute to spatial memory deficits in AD. However, whether Rac1 dysregulation is involved in other forms of memory impairments associated with AD is unknown. In addition, the brain regions, cell types and underlying mechanisms by which Rac1 leads to memory loss remain unclear. In this study, we suppressed Rac1 activity by viral expression of a dominant-negative (DN) mutant, Rac1-N17, specifically in the excitatory neurons of mouse ventral hippocampus. We showed that reducing Rac1 activity is sufficient to improve social recognition memory and rescue LTP impairment in APP/PS1 (APP) mice. Our results suggest that increased Rac1 activity contributes to social memory deficits in AD and therefore inhibiting Rac1 may provide a potential therapeutic strategy for ameliorating the social behavior deficit observed in AD patients.

Results

Impaired long-term potentiation in ventral hippocampus in APP/PS1 mice

To confirm synaptic deficits in APP mice, we carried out electrophysiological recordings at the Schaffer collateral-commissural pathway (CA3-CA1 synapse) in the ventral hippocampus, a brain region critically involved in social recognition memory (Okuyama et al., 2016). We first examined basal synaptic transmission using various stimulation intensities (1, 2, 3, 4, and 5 μA) but found no differences in input/output responses of field excitatory postsynaptic potentials (fEPSPs) between wild type (WT) and APP mice (**Figure 1A**). Presynaptic function as determined by paired-pulse facilitation (PPF) was also not altered in APP mice (**Figure 1B**). We compared LTP induced by theta-burst stimulation (TBS) and revealed that it was significantly lower in APP mice compared to WT (**Figures 1C,D**). These results suggest that, similar to dorsal hippocampus (Zhang et al., 2021a,b), LTP at CA1 synapse of ventral hippocampus is also impaired in three-month old APP mice.

Reduction of hippocampal Rac1 activity improves long-term potentiation in APP/PS1 mice

Previous studies have shown that Rac1 activity is upregulated in AD mice model (Borin et al., 2018; Wu et al., 2019). To investigate whether increased Rac1 activity in the hippocampus is responsible for the synaptic deficits in APP mice, we locally injected AAV virus which expressed a DN Rac1 mutant, Rac1-N17 (the amino acid Threonine at position 17 mutated to Asparagine) fused with EYFP or control EYFP under control of the excitatory neuronal promoter CaMKIIα, bilaterally into the hippocampus. We reasoned that overexpression of DN Rac1 mutant would reduce endogenous Rac1 activity. Immunostaining experiments following the viral injection showed that expression of Rac1-N17 was restricted to ventral hippocampus (**Figure 2A**). Colocalization of EYFP with neuronal marker, NeuN and the absence of colocalization with astrocytic marker, GFAP confirmed the neuronal and spine expression of Rac1-N17 (**Figures 2B–E**). Next, we analyzed Rac1 activity in protein lysates prepared from the hippocampus using a Rac1-activation assay. Consistent with the previous study (Wu et al., 2019), the level of active Rac1 was significantly increased in APP mice compared to WT mice (**Figure 3A**).

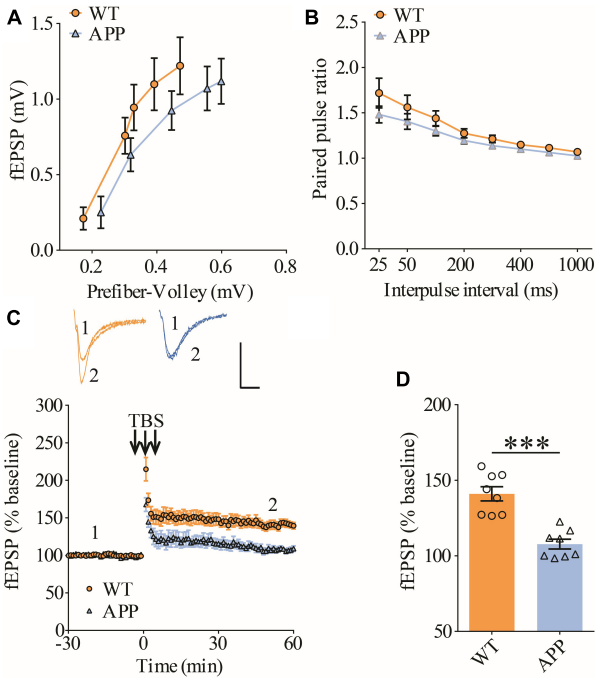

FIGURE 1
Impaired LTP in ventral hippocampus in APP mice. **(A)** Input output curves of fEPSP showing no differences between WT and APP mice (WT: n = 9 slices from 5 mice, APP: n = 5 slices from 5 mice; genotype: $F_{(1,12)}$ = 0.060, p = 0.811; prefiber volley: $F_{(4,48)}$ = 37.27, $p < 0.001$; repeated two-way ANOVA). **(B)** Paired pulse ratio showing no differences between WT and APP mice (WT: n = 8 slices from 5 mice, APP: n = 7 slices from 5 mice; genotype: $F_{(1,13)}$ = 1.658, p = 0.220; inter-pulse interval: $F_{(7,91)}$ = 33.74, $p < 0.001$; repeated two-way ANOVA). **(C)** TBS induced LTP at the CA1 synapse in WT and APP mice. Scale bars: 0.4 mV/10 ms. **(D)** Summary graph of last 10 min of recording showing impaired LTP in APP compared to WT mice (WT: n = 8 slices from 5 mice, APP: n = 8 slices from 5 mice, $p < 0.001$, two-tailed t-test). ***$P < 0.001$.

As expected, the level of active Rac1 was significantly reduced in APP mice expressing Rac1-N17 compared to EYFP control virus (Figures 3C–E). The level of phosphorylated active PAKs (P-Pak) was also reduced in APP mice expressing Rac1-N17 compared to EYFP control virus (Figures 3F,G). The levels of total or phosphorylated LIMK1 and cofilin were not affected in these mice. Electrophysiological recordings showed that expression of Rac1-EYFP had no effect on basal synaptic transmission, PPF, or TBS-LTP in WT mice (Figure 4), but significantly enhanced TBS-LTP without affecting basal synaptic strength or PPF (Figure 5) in APP mice. The expression of control EYFP had no effect on either basal synaptic transmission or LTP in both WT and APP/PS1 mice (Figures 4, 5). These results indicate that reducing Rac1 activity in excitatory hippocampal neurons was sufficient to improve the deficits in TBS-LTP impairment in APP mice.

Impaired social recognition memory in APP/PS1 mice

To evaluate social interaction and memory in APP mice, we used the three-chamber social interaction test and the five-trial social memory test. The three-chamber social interaction test (Figure 6A) consisted of three stages (stage 1: habituation; stage 2: sociability; and stage 3: social memory). Both APP and WT mice interacted more with stranger 1 (S1) than the empty cage, suggesting that sociability was intact in APP mice (Figure 6B). However, during the social memory stage, WT mice spent more time interacting with the novel stranger (S2) than S1, whereas APP mice interacted equally with S1 and S2, suggesting impaired social recognition memory in APP mice (Figures 6C,D). In the five-trial social memory test (Figure 6E), both WT and APP mice progressively spent less time interacting with the stranger mouse during the repeated exposures (trials 1–5), but showed a significant increase in interaction time when a novel stranger mouse was introduced on trial 6 (Figures 6F,G). However, APP mice spent significantly less time interacting with the novel stranger compared to WT mice on trial 6 (Figures 6F,G), suggesting impaired social recognition memory in APP mice. Collectively, these results suggest that APP mice are deficient in social recognition memory. In the open field test, there were no significant differences between WT and APP mice in travel distance/speed or the amount of time spent in center/periphery zone of the arena (Figures 6H–K). Similarly, there were no differences in total travel distance and the amount of time spent in the closed or open arms during the elevated plus maze test (Figures 6L–P). These results suggest that locomotor

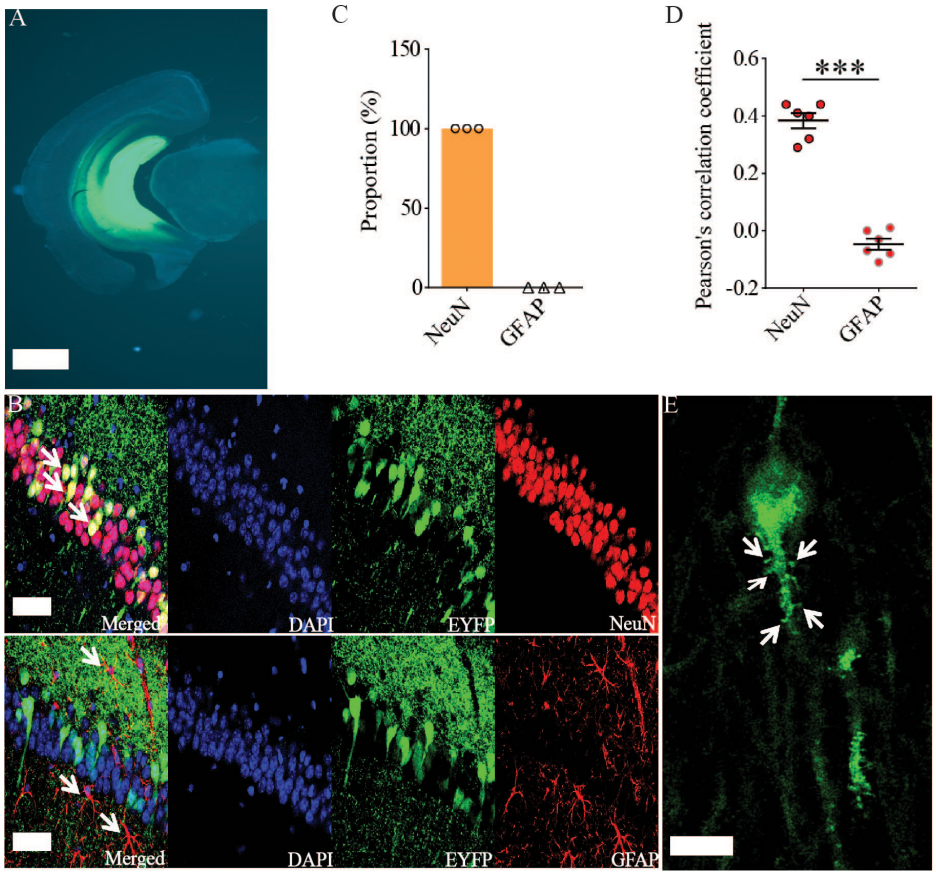

FIGURE 2
Viral expression of Rac1-N17 in the ventral hippocampus. **(A)** Brain section image showing the expression of Rac1-N17-EYFP in ventral hippocampus. Scale bar: 1 mm. Confocal images **(B)**, summary graph of colocalized cells **(C)**, and Pearson's correlation coefficient **(D)** showing the expression of Rac1-N17 (EYFP) colocalized with the neuronal marker NeuN, but not with the astrocytic marker GFAP. Arrows indicate neurons and astrocytes. Scale bar: 50 μm. **(E)** Higher magnification confocal image showing expression of Rac1-N17 in the dendrite and spines (arrows). Scale bar: 10 μm. ***$P < 0.001$.

activity and anxiety-like behavior were not significantly altered in three-month-old APP mice.

Reduction of hippocampal Rac1 activity improves social recognition memory in APP/PS1 mice

To investigate the functional consequence of reducing Rac1 activity in ventral excitatory hippocampal neurons, we examined social interaction and memory in both WT and APP mice expressing EYFP or Rac1-N17. Expression of Rac1-N17 in WT mice had no effect on social recognition memory in the three-chamber (**Figures 7A–C**) or the five-trial test (**Figures 7D,E**), or locomotor activity in the open field test (**Figures 7F–I**), but reduced anxiety-like behavior in the elevated plus maze in WT mice (**Figures 7J–N**). These results indicate that reducing Rac1 activity in hippocampal neurons had no effect on social behavior in WT mice. On the other hand, expression of Rac1-N17 in APP mice significantly improved social recognition memory in both three-chamber and five-trial repeated exposure tests (**Figures 8A–E**), without affecting locomotor activity or anxiety-like behavior (**Figures 8F–N**). These results suggest that overactivation of Rac1 activity in hippocampal neurons contributes to social memory deficits in APP mice.

Discussion

Rac1 is a crucial protein involved with learning and memory and its hyperactivity is associated with memory impairments through enhanced forgetting (Shuai et al., 2010; Jiang et al., 2016; Liu et al., 2016, 2018; Lv et al., 2019; Wu et al., 2019). In this study, we tested whether such Rac1-dependent forgetting mechanism would contribute to the social memory impairment observed in a mouse AD

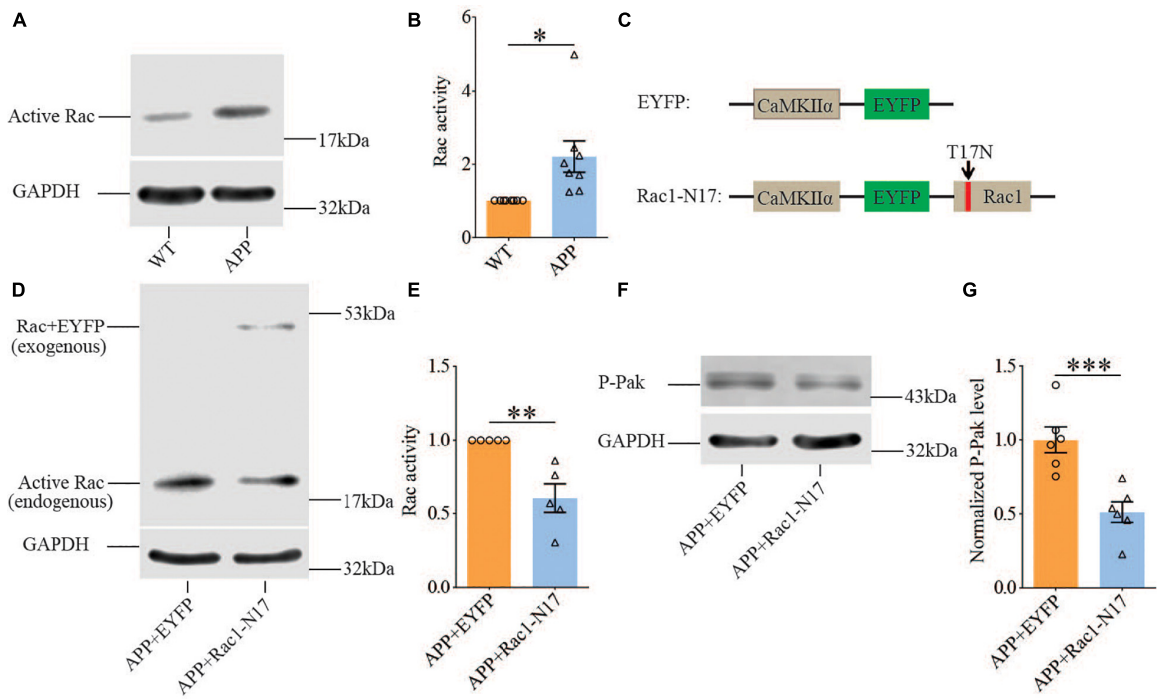

FIGURE 3
Increased Rac1 activity in APP mice and its reduction by expression of Rac1-N17. Western blots of active Rac1 assay **(A)** and summary graphs **(B)** showing increased level of active form of Rac1 in ventral hippocampus in APP compared to WT mice (WT: n = 8 independent experiments from 4 animals for each group, p = 0.0127, two-tailed paired t-test). AAV virus constructs of control EYFP and Rac1-N17 **(C)**, western blots **(D,F)**, and summary graph **(E,G)** showing decreased level of active Rac1 (n = 5 independent experiments from 3 animals for each group, p = 0.0335, two-tailed paired t-test) and phosphorylated active PAK1/2/3 (P-Pak) (n = 6 independent experiments from 3 animals for each group, $p < 0.001$, two-tailed paired t-test) in APP mice injected with Rac1-N17 virus (APP + Rac1-N17) compared to those injected with EYFP virus. Endogenous Rac1 refers to Rac1 protein expressed by the endogenous Rac1 gene, while exogenous Rac1 refers to EGFP-Rac1 fusion protein expressed by EYFP-Rac1-N17 viral infections. *$P < 0.05$, **$P < 0.01$, and $P < 0.001$.

model. We showed that Rac1 activity in the hippocampus of APP mice is significantly elevated (**Figures 3A,B**) in accordance with previous studies (Borin et al., 2018; Wu et al., 2019). This increased Rac1 activity is likely to contribute to the social memory deficit observed in APP mice since the expression of Rac1-N17 in the ventral hippocampus improves impaired social behavior in these mice (**Figures 8A–E**). The contribution of Rac1 on the social deficit in APP mice is also supported by the recording data showing that the reduced LTP in the ventral hippocampal CA3-CA1 synapse in APP mice is elevated by the expression of Rac1-N17 to reduce Rac1 activity (**Figures 5C,D**). Therefore, our results reveal that the Rac1-dependent mechanism is an important contributor to the social memory deficit in AD.

The role of Rac1 in learning and memory has been well studied and shown to be distinct in different brain regions. For example, in the amygdala, Rac1 is involved in the auditory fear memory during memory acquisition, consolidation, and reconsolidation (Wu et al., 2014; Gao et al., 2015; Das et al., 2017). Although early studies suggest that Rac1 participates in the acquisition and extinction of hippocampus-mediated memory (Martinez et al., 2007; Sananbenesi et al., 2007; Haditsch et al., 2009), more recent studies emphasize the role of Rac1 in memory forgetting but not in other processes in the hippocampus. The Rac1-dependent forgetting mechanism is initially demonstrated in *Drosophila*, in which the downregulation and upregulation of Rac1 activity is shown to delay and promote the aversive olfactory memory decay, respectively, without affecting its acquisition (Shuai et al., 2010). Such a Rac1-dependent forgetting mechanism has also been shown to affect various hippocampus-mediated memories in mice, including novel object recognition memory, contextual fear memory, spatial memory, and social memory (Jiang et al., 2016; Liu et al., 2016, 2018; Wu et al., 2019). In normal animals, Rac1 activity is elevated for a few days following induction of learning training, and this is accompanied by the extent of memory decay. Manipulating Rac1 activity within this time window by overactivation or inhibition hastens and slows down memory decay, respectively (Lv et al., 2019), suggesting that Rac1 activity is a key determinant of memory forgetting. Therefore, the activity of Rac1 is thought to

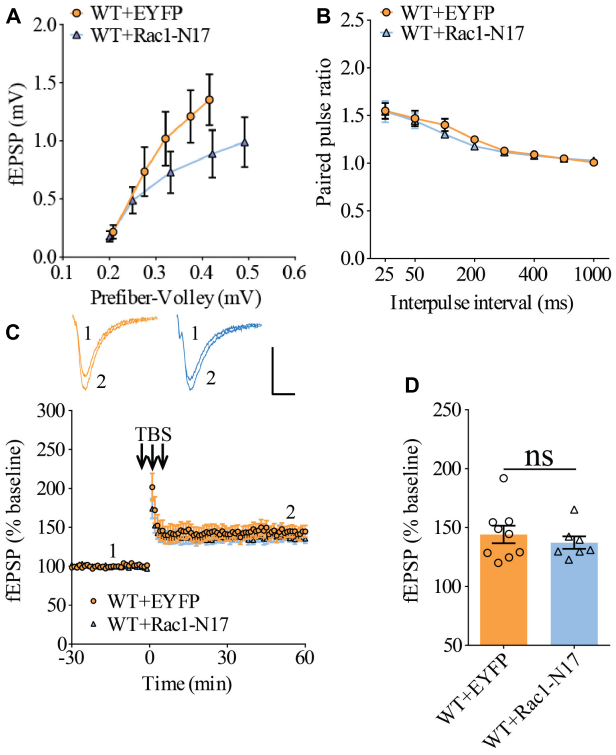

FIGURE 4
Normal LTP in WT mice overexpressing Rac1-N17 in ventral hippocampus. **(A)** Input–output curves of fEPSP showing no differences between WT mice expressing EYFP and Rac1-N17 (WT + EYFP n = 6 slices from 5 mice, WT + Rac1-N17 n = 6 slices from 4 mice; genotype: $F_{(1,10)}$ = 1.187, p = 0.301; prefiber volley: $F_{(4,40)}$ = 35.10, $p < 0.001$; repeated two-way ANOVA). **(B)** Paired pulse ratio showing no differences between WT mice expressing EYFP and Rac1-N17 (WT + EYFP: n = 8 slices from 5 mice, WT + Rac1-N17: n = 6 slices from 4 mice; genotype: $F_{(1,12)}$ = 0.223, p = 0.645; inter-pulse interval: $F_{(7,84)}$ = 57.35, $p < 0.001$; repeated two-way ANOVA). **(C)** TBS induced similar LTP at the CA1 synapse in WT mice expressing EYFP and Rac1-N17. Scale bars: 0.4 mV/10 ms. **(D)** Summary graph of last 10 min of recording showing similar levels of LTP in WT expressing EYFP or Rac1-N17 (WT + EYFP: n = 9 slices from 5 mice, WT + Rac1-N17: n = 7 slices from 4 mice, p = 0.486, two-tailed t-test).

be tightly regulated within a particular range to maintain animal's normal behavior. However, the activity of Rac1 can be altered under certain aversive conditions, such as during social isolation. For example, in mice that experience acute social isolation, there is significant elevation of Rac1 activity in the hippocampus, resulting in acceleration of social recognition memory decay without affecting its formation (Liu et al., 2018). Recently, it has been shown that there is a consistent increase in the level of active Rac1 in AD human patients and animal models (Wu et al., 2019). Such elevation of Rac1 in the hippocampus of AD mice is thought to underlie the spatial memory deficit assessed by the Morris water maze test, because specific inhibition of Rac1 activity in the dorsal hippocampus is sufficient to reverse this deficit. However, whether increased Rac1 activity is also responsible for other forms of memory deficits remain unclear, but the results from the present study provide an important step forward by showing that the increased Rac1 activity is also involved in social memory deficits in AD. In addition, the present study demonstrates that inhibiting Rac1 activity in ventral hippocampus is sufficient to improve social memory in APP mice, suggesting that Rac1 alterations in this brain region may be of particular importance. These results are consistent with a previous study showing that ventral hippocampal CA1 is required for social memory formation (Okuyama et al., 2016). It is important to note that other brain regions, such as dorsal CA2, are also involved in social memory (Hitti and Siegelbaum, 2014; reviewed in Tzakis and Holahan, 2019). Consistent with this, our previous study (Zhang et al., 2021a) shows that the manipulation of LIM-domain kinase (LIMK) activity in the dorsal hippocampus can also improve social memory deficit in APP mice. Therefore, both dorsal and ventral hippocampi contribute to social impairments in AD. It would be interesting to further study whether and how these two regions interact.

Despite that Rac1 plays a role in learning and memory, the underlying signaling pathway is not clear. Rac1, as a member of the Rho family of small GTPases, can potentially contribute to the regulation of memory through the modulation of the actin cytoskeleton and synaptic plasticity (**Figure 9**). Since the activation and translocation of Rac1 in the hippocampus during training can be blocked by the infusion of NMDA

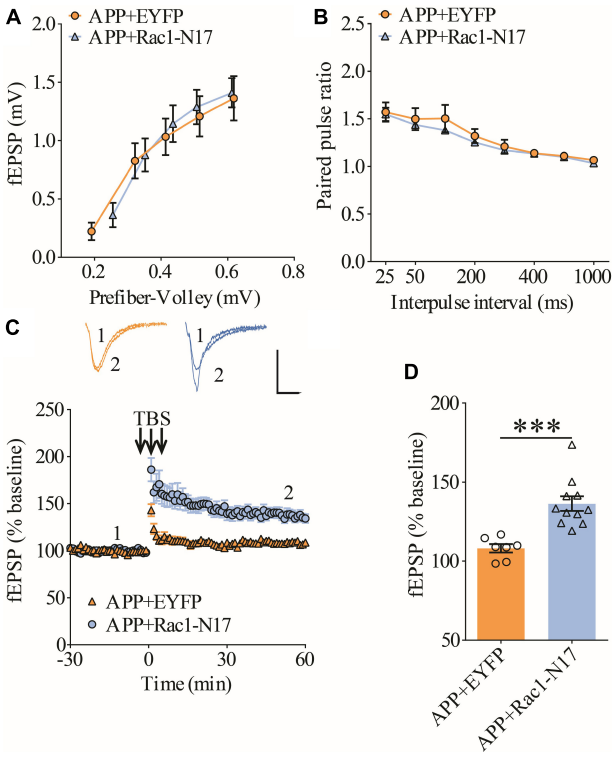

FIGURE 5
Improved LTP in APP mice expressing Rac1-N17 in ventral hippocampus. **(A)** Input–output curves of fEPSP showing no differences between APP mice expressing EYFP and Rac1-N17 (APP + EYFP: n = 8 slices from 4 mice, APP + Rac1-N17: n = 7 slices from 4 mice; genotype: $F_{(1,15)}$ = 0.216, p = 0.652; prefiber volley: $F_{(4,60)}$ = 81.90, $p < 0.001$; repeated two-way ANOVA). **(B)** Paired-pulse ratio analysis showing no differences between APP mice expressing EYFP and Rac1-N17 (APP + EYFP: n = 6 slices from 4 mice, APP + Rac1-N17: n = 8 slices from 4 mice; genotype: $F_{(1,12)}$ = 0.472, p = 0.505; inter-pulse interval: $F_{(7,84)}$ = 58.13, $p < 0.001$; repeated two-way ANOVA). **(C)** Enhanced LTP in APP/PS1 mice expressing Rac1-N17 compared to EYFP control. Scale bars: 0.4 mV/10 ms. **(D)** Summary graph of last 10 min of recording showing significantly higher LTP in APP mice expressing Rac1-N17 compared to APP mice expressing EYFP (APP + EYFP: n = 7 slices from 4 mice; APP + Rac1-N17: n = 11 slices from 4 mice; $p < 0.001$, two-tailed t-test). ***$P < 0.001$.

receptor inhibitors (Martinez et al., 2007), NMDAR receptors may be a crucial upstream mediator of Rac1 activation. Signals from NMDA receptors could be relayed by guanine nucleotide-exchange factors (GEFs) and GTPase-activating proteins (GAPs), upstream regulators of Rac1 that activate and inactivate Rac1, respectively (Rossman et al., 2005; reviewed in Bos et al., 2007; Cromm et al., 2015). Alterations of GEF and GAP activity are associated with impaired synaptic plasticity and cognitive deficits (Cahill et al., 2009; Kasri et al., 2009; Oh et al., 2010; Clement et al., 2012; Berryer et al., 2013; Zamboni et al., 2016). Rac1 can activate multiple downstream pathways to mediate cytoskeletal remodeling. One of these pathways involves the activation of P21-activated kinases (PAKs), which in turn activates LIMKs, leading to phosphorylation and inactivation of the actin regulator cofilin (**Figure 9**). Disruptions in PAK-LIMK-cofilin signaling are associated with impairments in synaptic function and memory (Meng et al., 2002, 2004, 2005; Asrar et al., 2009; Zhou et al., 2009; Huang et al., 2011). Other pathways include the WASP-family verprolin-homologous protein (WAVE) complex which can be recruited by active Rac1 to promote actin polymerization and branching *via* the activation of mDia and Arp2/3 complexes (Eden et al., 2002; reviewed in Faix and Grosse, 2006; Chen et al., 2017; Gao et al., 2019), both being reported to regulate memory forgetting (Gao et al., 2019). In addition to the actin cytoskeleton, Rac1 may also exert its effects on synaptic function *via* actin-independent pathways. For example, a recent study reported that Rac1 can affect PKCλ and PKMζ kinases (Cui et al., 2021). Both PKCλ and PKMζ are critically involved in AMPAR surface expression, and LTP induction and maintenance (reviewed in Sacktor, 2011; Ren et al., 2013). Furthermore, Rac1 may regulate LTP *via* gene transcription related processes. It has been reported that Rac1 is involved in the JNK signaling pathway (Kukekov et al., 2006), which is required for hippocampal LTP (Seo et al., 2012). In addition to cofilin, LIMK1 can directly phosphorylate and activate cAMP-responsive element-binding protein (CREB) to promote gene transcriptions and LTP maintenance (Yang et al., 2004; Todorovski et al., 2015). Because Aβ peptides can directly stimulate NMDA receptors

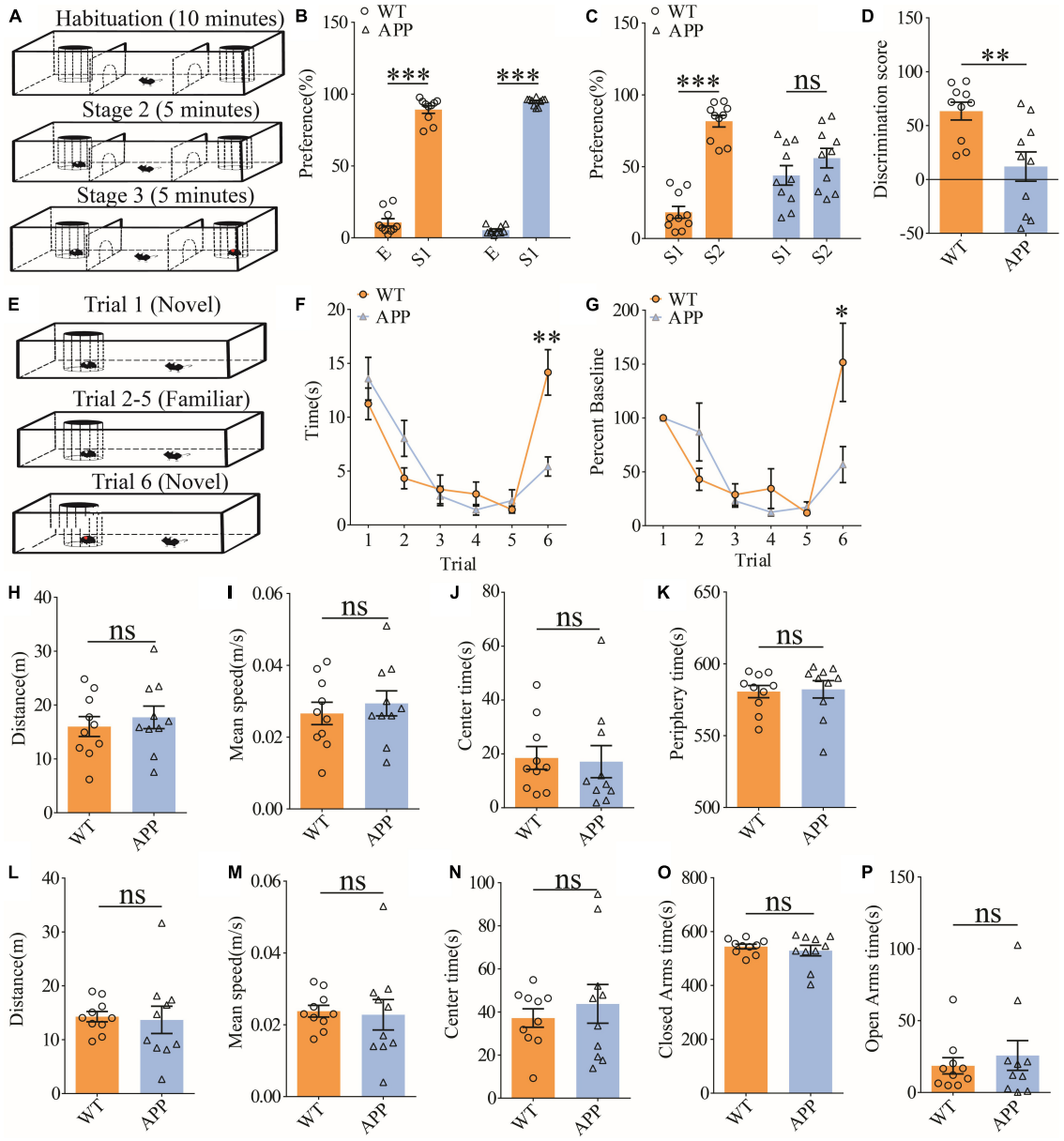

FIGURE 6

Impaired social recognition memory in APP mice. **(A)** Schematic of the three-chamber social interaction test: stage 1 (habituation), stage 2 (social interaction), and stage 3 (social recognition memory). **(B)** Normal sociability during stage 2 in APP mice (WT: $n = 10$, $p < 0.001$; APP: $n = 10$, $p < 0.001$; two-tailed paired t-test). **(C)** Impaired preference for S2 over S1 during stage 3 in APP mice (WT: $n = 10$, $p < 0.001$; APP: $n = 10$, $p = 0.227$; two-tailed paired t-test). **(D)** Discrimination scores during stage 3 showing impaired social memory in APP mice ($p = 0.005$, two-tailed t-test). **(E)** Schematic of the five-trial social memory test. **(F)** Both WT and APP mice showed gradual habituation for the first stranger during trials 1–5 (WT: $n = 10$, APP: $n = 10$; genotype group: $F_{(1,9)} = 0.016$, $p = 0.901$; trial: $F_{(4,36)} = 9.313$, $p < 0.001$; repeated two-way ANOVA). On trial 6, APP mice spent significantly less time interacting with the novel stranger compared to WT mice ($p = 0.002$, two-tailed t-test). **(G)** Normalized interaction time in the five-trial social test (WT: $n = 10$, APP: $n = 10$; genotype group: $F_{(1,9)} = 0.298$, $p = 0.598$; trial: $F_{(4,36)} = 8.517$, $p < 0.001$; repeated two-way ANOVA). On trial 6, APP mice showed significantly decreased time interacting with the novel stranger compared to WT mice ($p = 0.029$; two-tailed t-test). **(H)** Open field test showing similar travel distance in WT and APP mice (WT: $n = 10$, APP: $n = 10$, $p = 0.548$, two-tailed t-test). **(I)** Comparable travel speed between WT and APP mice during open field test (WT $n = 10$, APP $n = 10$, $p = 0.556$, two-tailed t-test). **(J)** Comparable time spent in center arena between WT and APP mice during open field test (WT: $n = 10$, APP: $n = 10$, $p = 0.849$, two-tailed t-test). **(K)** Comparable time spent in peripheral area between WT and APP mice during open field test (WT: $n = 10$, APP: $n = 10$, $p = 0.835$, two-tailed t-test). **(L)** Comparable travel distance between WT and APP mice during elevated plus maze test (WT: $n = 10$, APP: $n = 10$, $p = 0.830$, two-tailed t-test). **(M)** Comparable travel speed between WT and APP mice during elevated plus maze test (WT: $n = 10$, APP: $n = 10$, $p = 0.830$, two-tailed t-test). **(N)** Comparable time spent in center zone in elevated plus maze test between WT and APP mice during elevated plus maze test (WT: $n = 10$, APP: $n = 10$, $p = 0.518$, two-tailed t-test). **(O)** Comparable time spent in closed arms between WT and APP during elevated plus maze test (WT: $n = 10$, APP: $n = 10$, $p = 0.496$, two-tailed t-test). **(P)** Comparable time spent in open arms in between WT and APP mice during elevated plus maze test (WT: $n = 10$, APP: $n = 10$, $p = 0.549$, two-tailed t-test). $^*P < 0.05$, $^{**}P < 0.01$, and $^{***}P < 0.001$.

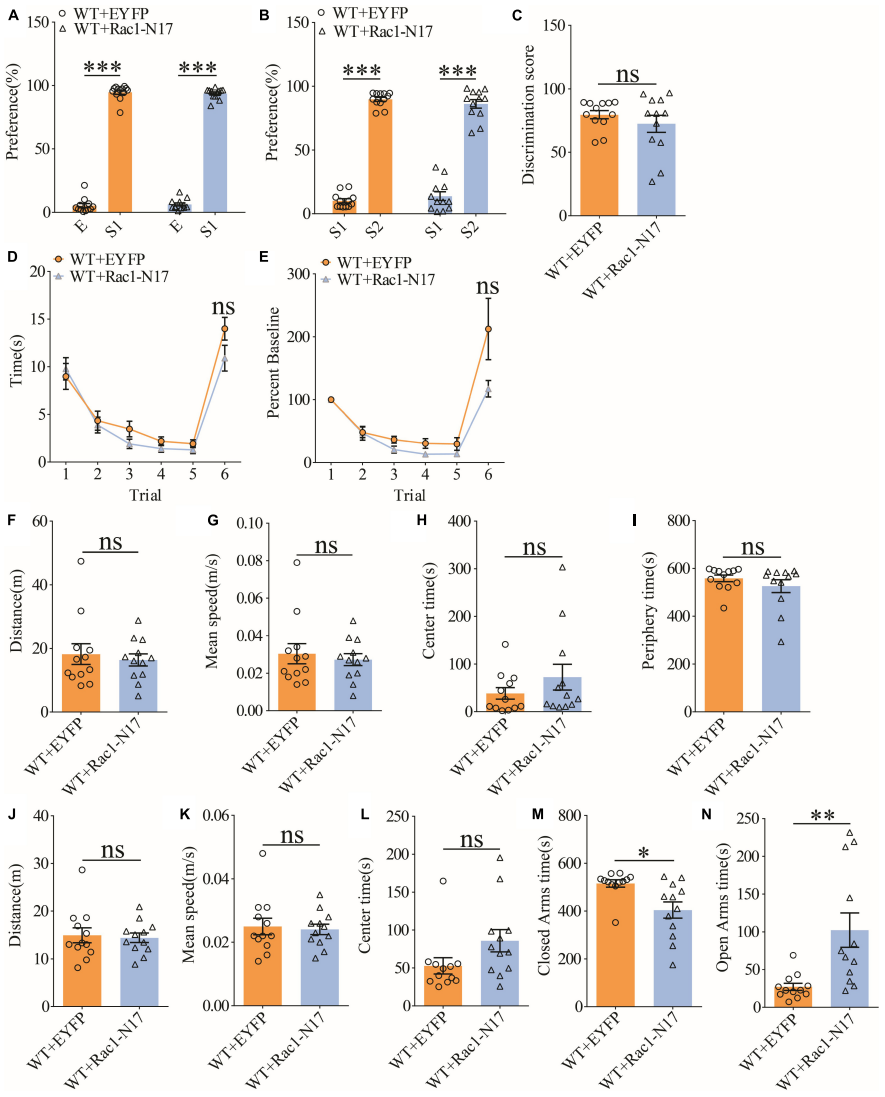

FIGURE 7

Normal social recognition memory in WT mice overexpressing Rac1-N17. **(A)** Normal sociability during stage 2 of the three-chamber social test in WT mice expressing EYFP or Rac1-N17 (WT + EYFP: $n = 12$, $p < 0.001$; WT + Rac1-N17: $n = 12$, $p < 0.001$; two-tailed paired t-test). **(B)** Preference for S2 over S1 during stage 3 of the three-chamber social test in WT mice expressing EYFP or Rac1-N17 (WT + EYFP: $n = 12$, $p < 0.001$; WT + Rac1-N17: $n = 12$, $p < 0.001$; two-tailed paired t-test). **(C)** Discrimination scores during stage 3 of three-chamber social test showing no difference in social memory between WT mice expressing EYFP and Rac1-N17 ($p = 0.345$, two-tailed t-test). **(D)** Similar performance in the five-trial social memory assay in WT mice expressing EYFP and Rac1-N17 during trials 1–5 (WT + EYFP: $n = 12$, WT + Rac1-N17: $n = 12$; genotype: $F_{(1,11)} = 0.010$, $p = 0.921$; trial: $F_{(4,44)} = 11.380$, $p < 0.001$; repeated two-way ANOVA) and on trial 6 ($p = 0.100$, two-tailed t-test). **(E)** Normalized interaction time showing similar performance in WT mice expressing EYFP and Rac1-N17 during trials 1–5 (WT + EYFP: $n = 12$, WT + Rac1-N17: $n = 12$; genotype: $F_{(1,11)} = 0.532$, $p = 0.485$; trial: $F_{(4,44)} = 29.120$, $p < 0.001$; repeated two-way ANOVA for trials 1–5) and on trial 6 of the five-trial social test ($p = 0.083$, two-tailed t-test). **(F)** Open field test showing comparable travel distance between WT mice expressing EYFP or Rac1-N17 (WT + EYFP: $n = 12$, WT + Rac1-N17: $n = 12$, $p = 0.635$, two-tailed t-test). **(G)** Comparable travel speed between WT mice expressing EYFP or Rac1-N17 during open field test (WT + EYFP: $n = 12$, WT + Rac1-N17: $n = 12$, $p = 0.619$, two-tailed t-test). **(H)** Comparable time spent in center arena between WT mice expressing EYFP or Rac1-N17 during open field test (WT + EYFP: $n = 12$, WT + Rac1-N17: $n = 12$, $p = 0.262$, two-tailed t-test). **(I)** Comparable time spent in peripheral arena WT mice expressing EYFP or Rac1-N17 during open field test (WT + EYFP: $n = 12$, WT + Rac1-N17: $n = 7$, $p = 0.292$, two-tailed t-test). **(J)** Comparable travel distance between WT mice expressing EYFP or Rac1-N17 during elevated plus maze test (WT + EYFP: $n = 12$, WT + Rac1-N17: $n = 12$, $p = 0.784$, two-tailed t-test). **(K)** Comparable travel speed between WT + EYFP and WT + Rac1-N17 mice during elevated plus maze test (WT + EYFP: $n = 12$, WT + Rac1-N17: $n = 12$, $p = 0.768$, two-tailed t-test). **(L)** Comparable time spent in center zone between WT mice expressing EYFP or Rac1-N17 during elevated plus maze test (WT + EYFP: $n = 12$, WT + Rac1-N17: $n = 12$, $p = 0.080$, two-tailed t-test). **(M)** Reduced time in closed arms in WT mice expressing Rac1-N17 compared to those expressing EYFP during elevated plus maze test (WT + EYFP: $n = 12$, WT + Rac1-N17: $n = 12$, $p = 0.010$, two-tailed t-test). **(N)** Increased time in open arms in WT mice expressing Rac1-N17 compared to those expressing EYFP during elevated plus maze test (WT + EYFP: $n = 12$, WT + Rac1-N17: $n = 12$, $p = 0.007$, two-tailed t-test). *$P < 0.05$, **$P < 0.01$, and $P < 0.001$.

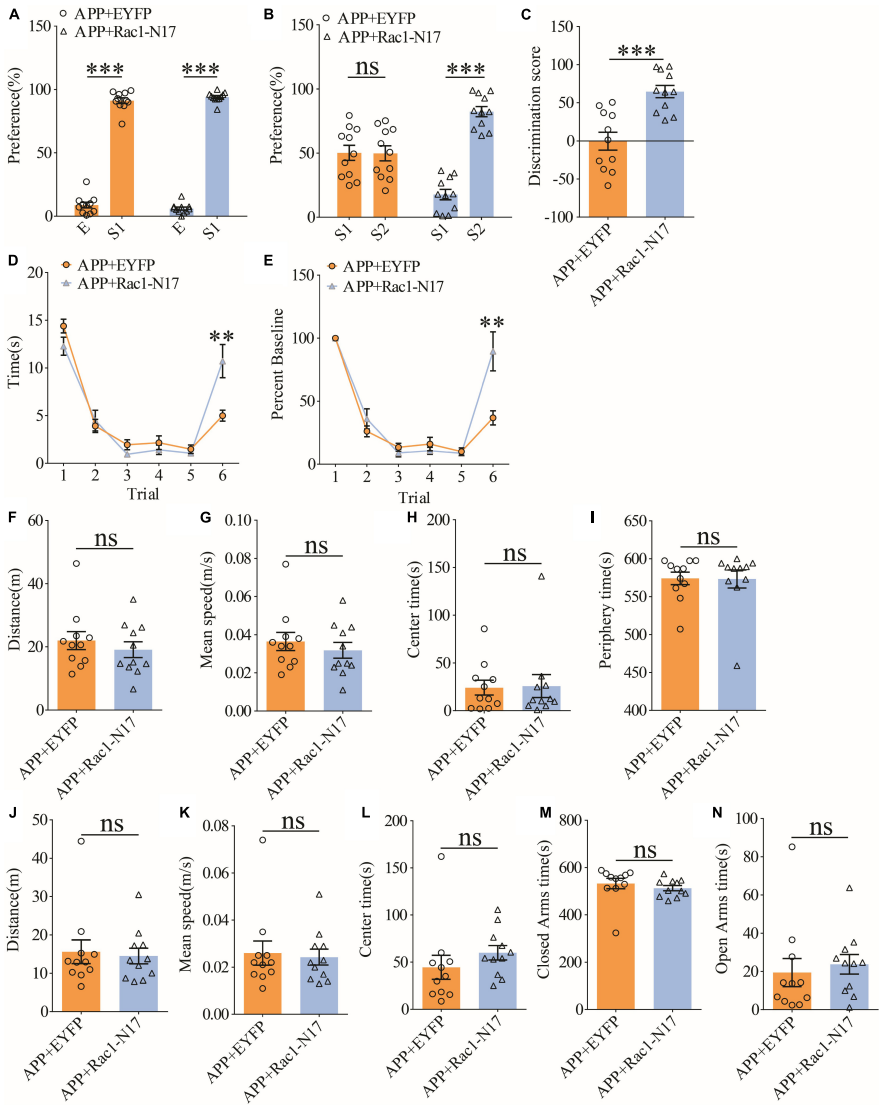

FIGURE 8

Improved social memory in APP mice expressing Rac1-N17. **(A)** Normal sociability during stage 2 of the three-chamber social test in APP mice expressing EYFP or Rac1-N17 (APP + EYFP: $n = 11$, $p < 0.001$; APP + Rac1-N17: $n = 11$, $p < 0.001$; two-tailed paired t-test). **(B)** Preference for S2 over S1 during stage 3 of three-chamber social test in APP mice expressing Rac1-N17 but not in APP mice expressing EYFP (APP + EYFP: $n = 11$, $p = 0.965$; APP + Rac1-N17: $n = 11$, $p < 0.001$; two-tailed paired t-test). **(C)** Discrimination scores during stage 3 of the three-chamber social test showing significantly improved social memory in APP mice expressing Rac1-N17 compared to APP mice expressing EYFP ($p < 0.001$, two-tailed t-test). **(D)** Similar performance in APP mice expressing EYFP and APP + Rac1-N17 during trials 1–5 of the five-trial social memory assay (APP + EYFP: $n = 11$, APP + Rac1-N17: $n = 11$; genotype: $F_{(1,10)} = 4.172$, $p = 0.068$; trial: $F_{(4,40)} = 45.451$, $p < 0.001$; repeated two-way ANOVA), but on trial 6, APP + Rac1-N17 mice spent significantly more time interacting with the novel stranger compared to APP + EYFP mice ($p = 0.009$, two-tailed t-test). **(E)** Normalized interaction time of the five-trial test during trials 1–5 (APP + EYFP: $n = 11$, APP + Rac1-N17: $n = 11$; genotype: $F_{(1,10)} = 0.628$, $p = 0.446$; trial: $F_{(4,40)} = 72.909$, $p < 0.001$; repeated two-way ANOVA), and on trial 6 ($p = 0.007$; two-tailed t-test). **(F)** Comparable travel distance between APP mice expressing EYFP or Rac1-N17 during open field test (APP + EYFP: $n = 11$, APP + Rac1-N17: $n = 11$, $p = 0.457$, two-tailed t-test). **(G)** Comparable travel speed between APP mice expressing EYFP or Rac1-N17 during open field test (APP + EYFP: $n = 11$, APP + Rac1-N17: $n = 11$, $p = 1.000$, two-tailed t-test). **(H)** Comparable time spent in center arena between APP mice expressing EYFP or Rac1-N17 during open field test (APP + EYFP: $n = 11$, APP + Rac1-N17: $n = 11$, $p = 0.910$, two-tailed t-test). **(I)** Comparable time spent in peripheral arena between APP mice expressing EYFP or Rac1-N17 during open field test (APP + EYFP: $n = 11$, APP + Rac1-N17: $n = 11$, $p = 0.960$, two-tailed t-test). **(J)** Comparable travel distance between APP mice expressing EYFP or Rac1-N17 during elevated plus maze test (APP + EYFP: $n = 11$, APP + Rac1-N17: $n = 11$, $p = 0.767$, two-tailed t-test). **(K)** Comparable travel speed between APP mice expressing EYFP or Rac1-N17 during elevated plus maze test (APP + EYFP: $n = 11$, APP + Rac1-N17: $n = 11$, $p = 0.782$, two-tailed t-test). **(L)** Comparable time spent in center zone between APP mice expressing EYFP or Rac1-N17 during elevated plus maze test (APP + EYFP: $n = 11$, APP + Rac1-N17: $n = 11$, $p = 0.311$, two-tailed t-test). **(M)** Comparable time spent in closed arms between APP mice expressing EYFP or Rac1-N17 during elevated plus maze test (APP + EYFP: $n = 11$, APP + Rac1-N17: $n = 11$, $p = 0.436$, two-tailed t-test). **(N)** Comparable time spent in open arms between APP mice expressing EYFP or Rac1-N17 during elevated plus maze test (APP + EYFP: $n = 11$, APP + Rac1-N17: $n = 11$, $p = 0.635$; two-tailed t-test). $^{**}P < 0.01$ and $^{***}P < 0.001$.

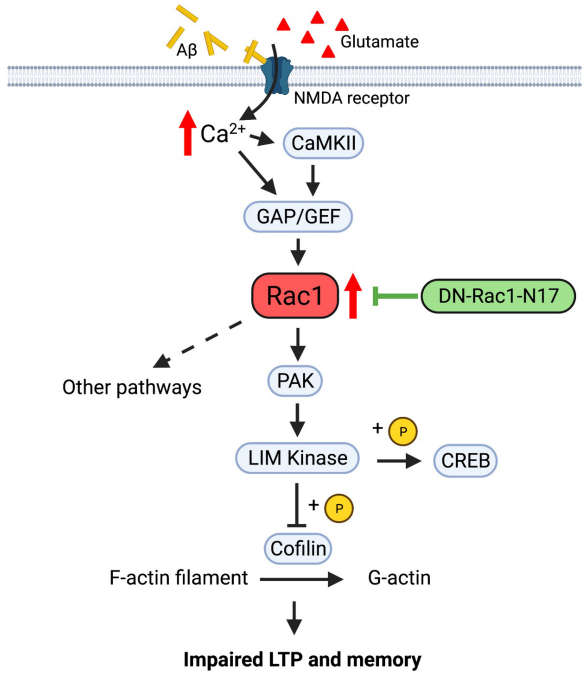

FIGURE 9
Regulation of LTP and memory by Rac1 in APP mice. In normal animals, Ca^{2+} influx from NMDA receptors activates Rac1 and multiple downstream signaling processes, including PAK-LIMK-cofilin pathway, to modulate actin reorganization, AMPA receptor trafficking and LTP expression. In APP mice, accumulation of Aβ peptides may lead to abnormal activation of NMDA receptors and hyperactive Rac1, which causes dysregulations of downstream proteins, including PAK, LIMK and cofilin, to impair LTP and memory. Expression of Rac1-N17 in hippocampal neurons reduces Rac1 activity and restores the function of some of its downstream proteins such as PAKs, thus improving LTP and memory in APP mice.

(Texidó et al., 2011), it is possible that abnormal activation of NMDA receptors by Aβ peptides leads to hyperactivation of Rac1, resulting in alterations in any of the aforementioned signaling processes to cause LTP and social memory deficits in APP mice. Our data that the level of P-PAKs (P-PAK1/2/3) is reduced in APP mice expressing Rac1-N17 suggest that changes in the PAK-LIMK-cofilin pathway may represent an important mechanism by which overactivation of Rac1 impairs LTP and memory in APP mice. These results are consistent with previous studies showing that manipulations of LIMK1 can improve social memory deficit in APP mice (Heredia et al., 2006; Henderson et al., 2016, 2019; Leung et al., 2018; Gory-Fauré et al., 2021; Zhang et al., 2021a). Although we found no differences in the protein level and activity of LIMK1 and cofilin in APP mice expressing Rac1-N17 using total hippocampal protein lysates, we cannot rule out the possibility that synaptic levels of these proteins are affected by the expression Rac1-N17.

In summary, this study shows that increased Rac1 activity contributes to impaired LTP in ventral hippocampus and social recognition memory. Future experiments would be to address how the Rac1 activity is enhanced by examining its upstream GEF and GAP in AD models and human patients. Defining the details of Rac1 signaling processes may provide potential new therapeutic strategies and molecular targets to treat AD and related brain disorders.

Materials and methods

Housing, maintenance, and use of mice

APP/PS1 transgenic mice (#34829-JAX) on mixed C57BL/6;C3H genetic background were obtained from the Jackson Laboratory. The mice were inbred and housed (2–5 mice per cage) on a 12/12 h light/dark cycle with food and water *ad libitum*. The following PCR primers were used for genotyping APP mice: oIMR 1644: AATAGAGAACGGCAGGAGCA; oIMR 1645: GCCATGAGGGCACTAATCAT. All experimental procedures were conducted according to the guidelines of the Canadian Council on Animal Care (CCAC) and approved by the Animal Care Committee at the Hospital for Sick Children, Canada. All experiments were performed blind to the genotype of the mice. Both male and female mice were used but no differences were noted between

sexes, therefore the data were pooled together for statistical analyses between genotypes. The age of the mice ranged from 3 to 4 months.

Surgical procedures

For viral injections, the AAV2/DJ-CaMKIIα-Rac1-N17 (Rac1 fused to EYFP, 7.6×10^{12}) and AAV2/DJ-CaMKIIα-EYFP (1.3×10^{13}) (produced through Canadian Neurophotonics Platform, Laval University, Canada) were injected bilaterally to the ventral hippocampus. Briefly, mice were anesthetized with isoflurane (2.0–2.5% in 1 L/min oxygen) and placed onto a stereotaxic frame. Body temperature was maintained at 37°C using a temperature controller. A midline scalp incision was made followed by craniotomies using a 0.6 mm drill bit. The virus was injected by a microsyringe pump with the injection speed of 0.3 μL/min. Six minutes after the injection, the needle was retrieved slowly. Injection site of ventral hippocampus (AP: −3.16 mm, DV: −4.00 mm, and ML: ±3.20 mm). At the end of the surgery, the skin was sutured sequentially, and the animals were given hydration and painkillers. The surgically operated mice were recovered for 3–4 weeks to allow for Rac1-N17 and EYFP expression before behavior tests were performed. The expression pattern of Rac1-N17 and EYFP as well as the injection sites were confirmed by immunohistochemical staining of fixed brain sections after behavior tests.

Slice electrophysiology

All electrophysiological recordings were done at the Schaffer collateral-commissural pathway in ventral hippocampus as previously described. In brief, the mouse brains were removed and 350 μm brain slices prepared in ice-cold artificial cerebrospinal fluid (ACSF) saturated with 95 O_2/5% CO_2. ACSF contained (in mM): 120.0 NaCl, 3.0 KCl, 1.2 $MgSO_4$, 1.0 NaH_2PO_4, 26.0 $NaHCO_3$, 2.0 $CaCl_2$, and 11.0 D-glucose. The slices were recovered at 28°C for at least 2 h before a single slice was transferred to a submersion chamber constantly perfused with 95% O_2/5% CO_2 saturated ACSF. Perfusion flow rate was maintained constant at 2 ml/min. Synaptic transmission was evoked by stimulation at 0.067 Hz and recorded with glass pipettes (3–4 MΩ) filed with ACSF. For input-output field potential experiments, the stimulus intensity was increased gradually (0, 1, 2, 3, 4, and 5 μA). PPFs were obtained at inter-pulse intervals of 25, 50, 100, 200, 300, 400, 500, or 1,000 ms, and calculated as the ratios of the second response peak values over the first response peak values. LTP was induced by three trains of theta burst stimulations (TBS, five pulses at 100 Hz every 200 ms) with an intertrain interval of 10 s. LTP was calculated and statistically evaluated by comparing the mean values of the last 10 min of the recording and the mean values of the entire baseline. All data acquisition and analysis were done using pCLAMP 10.7 (Axon Instruments, Foster City, CA, United States).

Active Rac1 assay

Mouse hippocampus was harvested and snap freeze in dry ice before being homogenized in cold lysis buffer which contains (in mM): 20 Tris–HCl (pH 7.5), 150 NaCl, 1 EDTA, 1 EGTA, 1% Triton X-100, 2.5 sodium pyrophosphate, 1 β-glycerophosphate, 1 Na3VO4, 20 NaF, and 1% protease inhibitor cocktail and phosphatase inhibitor. After shaking for one hour in 4°C, insoluble debris were removed *via* centrifugation at 10,000 rpm (for 15 min, at 4°C). The protein concentration was measured *via* BCA assay (Thermo-Fisher, #23225). One milliliter protein lysate with a concentration of 500 μg/ml was mixed with 10 μg GST-tagged PAK-PBD agarose beads (Cytoskeleton, PAK02) as instructed by the company protocol. After incubation in 4°C overnight, beads were washed for three times with cold lysis buffer before being separated on SDS-PAGE (15%) gels. Proteins were then transferred onto nitrocellulose membranes, blocked by 5% skim milk and incubated with primary antibody against total Rac1 (CST, #2465), P-PAK1 (CST, #2605S), and GAPDH (CST, #2118S) overnight at 4°C. The membrane was then incubated with HRP-conjugated goat anti-Rabbit IgG (CST, #7074S) for 1 h at room temperature. Then the blot was washed and developed using an enhanced chemiluminescence (Thermo-Fisher, #34579) method of detection and analyzed by Image Studio Lite software (Licor) as per manufacture's instruction.

Histology and immunohistochemistry

For immunohistochemistry staining, mice were anesthetized with injected ketamine (15 g/ml) followed by transcardial perfusion with 50 mL of pre-cooled 1X PBS sequentially and 4% paraformaldehyde 50 ml (4% PFA). The brain is taken and post-fixed in 4% PFA solution at 4°C overnight. The next day, after being thoroughly washed with 1X PBS, brain was embedded in 4% agarose gel. The brain was sliced to 40 μm coronal sections by a vibratome at room temperature. Sections were washed with PBS, incubated in blocking solution (0.3% Triton, 5% BSA in 1X PBS) for 1 h, with primary antibodies (for NeuN: 1:1000, CST, #12943; for GFAP: 1:500, CST, #3670) overnight at 4°C. The slides were then washed with PBS and incubated with secondary antibodies (dissolved in 0.05% Triton, 5% BSA in 1X PBS with dilution of 1:1,000; AlexaFluor 555, Thermo-Fisher, #A32794 and #A32773) at room temperature for 4 h. Following washing, the coverslips were mounted using Antifade mounting medium with DAPI (MJS Biolynx, #VECTH180010) for image

collection. Images were collected using a Leica epi-fluorescence microscope and a Nikon A1R or Leica SP8 lightning confocal microscope, under a 10× and 60× objective, respectively. The excitation used were 402 nm for DAPI, 488 nm for GFP, and 562 nm for Red. The emission used were 460 nm for DAPI, 509 nm for GFP, and 580 nm for Red. For colocalization analysis, Pearson's correlation coefficients were calculated for images using Coloc2 plugin from ImageJ. For each group, 4–6 images were analyzed from each of 6 mice. GFP was displayed as channel A and anti-NeuN or anti-GFAP were displayed as channel B. Channel thresholds were set as to include the full range of data as displayed in the colocalization tool 2D histogram. Average Pearson's coefficients for each mouse were plotted using Prism software and statistical analysis was done using Mann–Whitney test.

Behavioral tests

Animals were tested at the age of 3 ± 0.5 months. All behavioral tests were performed during the light cycle. The mice were tested in open field, elevated plus maze, three-chamber social interaction and five-trial repeated social test. At least 3-day intervals were given after each test. The open field apparatus was a rectangular Plexiglas box (40 cm long × 40 cm wide × 35 cm high) comprising four walls and an open roof. The illumination in the room was provided by centrally placed in-ceiling dim lights. All mice were individually tested in one 5 min session. Each subject was introduced to the apparatus in the same place of the arena near the center and allowed to explore the apparatus for 10 min. The apparatus was cleaned thoroughly with 75% ethanol before each subject was tested. The movement of the mouse was video tracked and analyzed off-line using ANY-maze software (Untied States). The box was divided into central (center 20 cm diameter) and peripheral fields for analysis. The elevated plus maze was composed of two open arms (35 cm long × 5 cm wide) and two closed arms of the same size with 10 cm high walls. The apparatus was placed 50 cm above the ground. The tested mice were individually placed in the center and allow for 10 min free exploration. The entries to and time spent in the open arms, center zone and closed arms were recorded. The maze was cleaned thoroughly with 75% ethanol before each mouse was tested. Traces of movement were tracked and analyzed off-line using ANY-maze software (United States). The movement distance, average speed, the entries to and time spent in the open arms, center zone, and closed arms were recorded. The maze was cleaned thoroughly with 75% ethanol between mice. The movement was tracked and analyzed using ANY-maze software (United States). Three chambers (60 cm long × 40 cm wide × 22 cm high) for social interaction connected by removable partitions in the plexiglass walls, which allowed animals to freely moving between the chambers. Mice were handled twice a day, 3 days before the test. Prior to the day of test, the handled mice were each habituated to the empty apparatus for 5 min. Stranger mice were contained in a cylindrical wired cage (8 cm diameter and 17 cm high) with bars spaced 1 cm apart placed in left and/or right chamber. The middle chamber was left empty all the time. Each test session consisted of three stages: stage 1: 10 min habituation stage with two empty cages; stage 2: 5 min sociability test with an unencountered stranger mouse (S1) and an empty cage; stage 3:5 min social memory test with the previously encountered stranger (S1) and a second novel stranger (S2). Each stage was separated by a 45 s^{-1} min interval. The amount of interaction (i.e., sniff time when the animal oriented its nose within 0.5 cm or physical contact of the mouse contained in the wired cage) was recorded. Data were analyzed as a percentage time spent investigating the target cage over the total time interacting with either cage using ANY-maze software (IL, United States). For five-trial social interaction test, the subject mouse was placed in a chamber (40 cm long × 20 cm wide × 22 cm high) and presented with a same sex juvenile, strange mouse in a cylindrical wired cage (8 cm diameter and 17 cm high) with bars spaced 1 cm apart. Six consecutive 1 min trials with a 30–45 s inter-trial interval was tested for each subject. On the last trial, a novel stranger juvenile mouse of the same sex was presented in the cage. The amount of interaction was recorded as the sniff time when the animal oriented its nose within 1 cm of the stranger mouse in the wired cage. The normalized baseline values were calculated by dividing the amount of interaction in each trial (2–6) to that of trial 1. Data were analyzed using ANY-maze software (IL, United States).

Statistical analyses

All the averaged data in the graphs were stated as mean ± SEM. and statistically evaluated by Student's *t*-test for comparisons of two groups or by ANOVA (one-, two-way or repeated measures, as appropriate) for comparisons of more than two groups followed by *post hoc* Fisher s LSD multiple comparison test using the SPSS program. For each set of data, values were first tested for their normal distribution using the Shapiro–Wilk test of normality. Data followed Gaussian normal distribution unless it is stated otherwise. $p < 0.05$ was considered significant and indicated with $^{*}p < 0.05$, $^{**}p < 0.01$, $^{***}p < 0.001$. The details of statistical data, including statistical methods, *p*-values and sample size, were provided in respective figure legends.

Data availability statement

The original contributions presented in this study are included in the article/supplementary material, further inquiries can be directed to the corresponding authors.

Ethics statement

All experimental procedures were conducted according to the guidelines of the Canadian Council on Animal Care (CCAC) and approved by the Animal Care Committee at the Hospital for Sick Children, Canada.

Author contributions

CZ, TX, and ZJ designed the study. HWZ, YB, HRZ, AL, RG, DL, and YM performed the experiments. HWZ, YB, HRZ, AL, DL, CZ, and SL analyzed and interpreted the data. HWZ, YB, HRZ, CZ, TX, and ZJ wrote the manuscript. All authors read and approved the final manuscript.

Funding

This work was supported by grants from the Canadian Institutes of Health Research (CIHR, MOP119421, PJT-155959, and PJT168922, ZJ), Canadian Natural Science and Engineering Research Council (NSERC RGPIN 341498 and RGPIN- 2017-06295, ZJ), Natural Science Foundation of China (81972340 and 82173140, TX), National Key R&D Program of China (2020YFC2008900, CZ), China Scholarship Council (CSC NO 201908520052, HWZ), and the Hospital for Sick Children Foundation.

Acknowledgments

We are grateful to all members of ZJ Labs for their technical assistance and comments on the manuscript.

Conflict of interest

The authors declare that the research was conducted in the absence of any commercial or financial relationships that could be construed as a potential conflict of interest.

Publisher's note

References

Ali, A. A., Khalil, M. G., Elariny, H. A., and karema, A. (2017). Study on social isolation as a risk factor in development of alzheimer's disease in rats. *Brain Disord. Ther.* 6:230. doi: 10.4172/2168-975x.1000230

Almeida, C. G., Tampellini, D., Takahashi, R. H., Greengard, P., Lin, M. T., Snyder, E. M., et al. (2005). Beta-amyloid accumulation in APP mutant neurons reduces PSD-95 and GluR1 in synapses. *Neurobiol. Dis.* 20, 187–198. doi: 10.1016/j.nbd.2005.02.008

Asrar, S., Meng, Y., Zhou, Z., Todorovski, Z., Huang, W. W., and Jia, Z. (2009). Regulation of hippocampal long-term potentiation by p21-activated protein kinase 1 (PAK1). *Neuropharmacology* 56, 73–80. doi: 10.1016/j.neuropharm.2008.06.055

Ballatore, C., Lee, V. M., and Trojanowski, J. Q. (2007). Tau-mediated neurodegeneration in Alzheimer's disease and related disorders. *Nat. Rev. Neurosci.* 8, 663–672. doi: 10.1038/nrn2194

Berkman, L. F., Glass, T., Brissette, I., and Seeman, T. E. (2000). From social integration to health: Durkheim in the new millennium. *Soc. Sci. Med.* 51, 843–857. doi: 10.1016/s0277-9536(00)00065-4

Berryer, M. H., Hamdan, F. F., Klitten, L. L., Møller, R. S., Carmant, L., Schwartzentruber, J., et al. (2013). Mutations in SYNGAP1 cause intellectual disability, autism, and a specific form of epilepsy by inducing haploinsufficiency. *Hum. Mutat.* 34, 385–394. doi: 10.1002/humu.22248

Bliss, T. V., and Collingridge, G. L. (1993). A synaptic model of memory: long-term potentiation in the hippocampus. *Nature* 361, 31–39. doi: 10.1038/361031a0

Borin, M., Saraceno, C., Catania, M., Lorenzetto, E., Pontelli, V., Paterlini, A., et al. (2018). Rac1 activation links tau hyperphosphorylation and Aβ dysmetabolism in Alzheimer's disease. *Acta Neuropathol. Commun.* 6:61. doi: 10.1186/s40478-018-0567-4

Bos, J. L., Rehmann, H., and Wittinghofer, A. (2007). GEFs and GAPs: critical elements in the control of small G proteins. *Cell* 129, 865–877. doi: 10.1016/j.cell.2007.05.018

Cahill, M. E., Xie, Z., Day, M., Photowala, H., Barbolina, M. V., Miller, C. A., et al. (2009). Kalirin regulates cortical spine morphogenesis and disease-related behavioral phenotypes. *Proc. Natl. Acad. Sci. U.S.A.* 106, 13058–13063. doi: 10.1073/pnas.0904636106

Chen, B., Chou, H. T., Brautigam, C. A., Xing, W., Yang, S., Henry, L., et al. (2017). Rac1 GTPase activates the WAVE regulatory complex through two distinct binding sites. *eLife* 6:e29795. doi: 10.7554/eLife.29795

Clement, J. P., Aceti, M., Creson, T. K., Ozkan, E. D., Shi, Y., Reish, N. J., et al. (2012). Pathogenic SYNGAP1 mutations impair cognitive development by disrupting maturation of dendritic spine synapses. *Cell* 151, 709–723. doi: 10.1016/j.cell.2012.08.045

Costa, J. F., Dines, M., and Lamprecht, R. (2020). The Role of Rac GTPase in Dendritic Spine Morphogenesis and Memory. *Front. Synap. Neurosci.* 12:12. doi: 10.3389/fnsyn.2020.00012

Cromm, P. M., Spiegel, J., Grossmann, T. N., and Waldmann, H. (2015). Direct Modulation of Small GTPase Activity and Function. *Angewandte Chemie* 54, 13516–13537. doi: 10.1002/anie.201504357

Cui, D., Jiang, X., Chen, M., Sheng, H., Shao, D., Yang, L., et al. (2021). Activation of Rac1 Has an Opposing Effect on Induction and Maintenance of Long-Term Potentiation in Hippocampus by Acting on Different Kinases. *Front. Mol. Neurosci.* 14:720371. doi: 10.3389/fnmol.2021.720371

Das, A., Dines, M., Alapin, J. M., and Lamprecht, R. (2017). Affecting long-term fear memory formation through optical control of Rac1 GTPase and PAK activity in lateral amygdala. *Sci. Rep.* 7:13930. doi: 10.1038/s41598-017-13674-9

Eden, S., Rohatgi, R., Podtelejnikov, A. V., Mann, M., and Kirschner, M. W. (2002). Mechanism of regulation of WAVE1-induced actin nucleation by Rac1 and Nck. *Nature* 418, 790–793. doi: 10.1038/nature00859

Faix, J., and Grosse, R. (2006). Staying in shape with formins. *Dev. cell* 10, 693–706. doi: 10.1016/j.devcel.2006.05.001

Filali, M., Lalonde, R., and Rivest, S. (2011). Anomalies in social behaviors and exploratory activities in an APPswe/PS1 mouse model of Alzheimer's disease. *Physiol. Behav.* 104, 880–885. doi: 10.1016/j.physbeh.2011.05.023

Gan, P., Ding, Z. Y., Gan, C., Mao, R. R., Zhou, H., Xu, L., et al. (2016). Corticosterone regulates fear memory via Rac1 activity in the hippocampus. *Psychoneuroendocrinology* 71, 86–93. doi: 10.1016/j.psyneuen.2016.05.011

Gao, Q., Yao, W., Wang, J., Yang, T., Liu, C., Tao, Y., et al. (2015). Post-training activation of Rac1 in the basolateral amygdala is required for the formation of both short-term and long-term auditory fear memory. *Front. Mol. Neurosci.* 8:65. doi: 10.3389/fnmol.2015.00065

Gao, Y., Shuai, Y., Zhang, X., Peng, Y., Wang, L., He, J., et al. (2019). Genetic dissection of active forgetting in labile and consolidated memories in Drosophila. *Proc. Natl. Acad. Sci. U.S.A.*116, 21191–21197. doi: 10.1073/pnas.1903763116

Gory-Fauré, S., Powell, R., Jonckheere, J., Lanté, F., Denarier, E., Peris, L., et al. (2021). Pyr1-Mediated Pharmacological Inhibition of LIM Kinase Restores Synaptic Plasticity and Normal Behavior in a Mouse Model of Schizophrenia. *Front. Pharmacol.* 12:627995. doi: 10.3389/fphar.2021.627995

Haditsch, U., Leone, D. P., Farinelli, M., Chrostek-Grashoff, A., Brakebusch, C., Mansuy, I. M., et al. (2009). A central role for the small GTPase Rac1 in hippocampal plasticity and spatial learning and memory. *Mol. Cell. Neurosci.* 41, 409–419. doi: 10.1016/j.mcn.2009.04.005

Hardy, J., and Selkoe, D. J. (2002). The amyloid hypothesis of Alzheimer's disease: progress and problems on the road to therapeutics. *Science* 297, 353–356. doi: 10.1126/science.1072994

Henderson, B. W., Gentry, E. G., Rush, T., Troncoso, J. C., Thambisetty, M., Montine, T. J., et al. (2016). Rho-associated protein kinase 1 (ROCK1) is increased in Alzheimer's disease and ROCK1 depletion reduces amyloid-β levels in brain. *J. Neurochem.* 138, 525–531. doi: 10.1111/jnc.13688

Henderson, B. W., Greathouse, K. M., Ramdas, R., Walker, C. K., Rao, T. C., Bach, S. V., et al. (2019). Pharmacologic inhibition of LIMK1 provides dendritic spine resilience against β-amyloid. *Sci. Signaling* 12:eaaw9318. doi: 10.1126/scisignal.aaw9318

Heredia, L., Helguera, P., de Olmos, S., Kedikian, G., Solá Vigo, F., LaFerla, F., et al. (2006). Phosphorylation of actin-depolymerizing factor/cofilin by LIM-kinase mediates amyloid beta-induced degeneration: a potential mechanism of neuronal dystrophy in Alzheimer's disease. *J. Neurosci.* 26, 6533–6542. doi: 10.1523/JNEUROSCI.5567-05.2006

Hitti, F. L., and Siegelbaum, S. A. (2014). The hippocampal CA2 region is essential for social memory. *Nature* 508, 88–92. doi: 10.1038/nature13028

Hsieh, H., Boehm, J., Sato, C., Iwatsubo, T., Tomita, T., Sisodia, S., et al. (2006). AMPAR removal underlies Abeta-induced synaptic depression and dendritic spine loss. *Neuron* 52, 831–843. doi: 10.1016/j.neuron.2006.10.035

Huang, W., Zhou, Z., Asrar, S., Henkelman, M., Xie, W., and Jia, Z. (2011). p21-Activated kinases 1 and 3 control brain size through coordinating neuronal complexity and synaptic properties. *Mol. Cell. Biol.* 31, 388–403. doi: 10.1128/MCB.00969-10

Jiang, L., Mao, R., Zhou, Q., Yang, Y., Cao, J., Ding, Y., et al. (2016). Inhibition of Rac1 Activity in the Hippocampus Impairs the Forgetting of Contextual Fear Memory. *Mol. Neurobiol.* 53, 1247–1253. doi: 10.1007/s12035-015-9093-6

Kandel, E. R., Dudai, Y., and Mayford, M. R. (2014). The molecular and systems biology of memory. *Cell* 157, 163–186. doi: 10.1016/j.cell.2014.03.001

Kukekov, N. V., Xu, Z., and Greene, L. A. (2006). Direct interaction of the molecular scaffolds POSH and JIP is required for apoptotic activation of JNKs. *J. Biol. Chem.* 281, 15517–15524. doi: 10.1074/jbc.M601056200

Lamprecht, R. (2014). The actin cytoskeleton in memory formation. *Progr. Neurobiol.* 117, 1–19. doi: 10.1016/j.pneurobio.2014.02.001

Leser, N., and Wagner, S. (2015). The effects of acute social isolation on long-term social recognition memory. *Neurobiol. Learn. Memory* 124, 97–103. doi: 10.1016/j.nlm.2015.07.002

Leung, C., Cao, F., Nguyen, R., Joshi, K., Aqrabawi, A. J., Xia, S., et al. (2018). Activation of Entorhinal Cortical Projections to the Dentate Gyrus Underlies Social Memory Retrieval. *Cell Rep.* 23, 2379–2391. doi: 10.1016/j.celrep.2018.04.073

Li, S., Hong, S., Shepardson, N. E., Walsh, D. M., Shankar, G. M., and Selkoe, D. (2009). Soluble oligomers of amyloid Beta protein facilitate hippocampal long-term depression by disrupting neuronal glutamate uptake. *Neuron* 62, 788–801. doi: 10.1016/j.neuron.2009.05.012

Liu, Y., Du, S., Lv, L., Lei, B., Shi, W., Tang, Y., et al. (2016). Hippocampal Activation of Rac1 Regulates the Forgetting of Object Recognition Memory. *Curr. Biol.* 26, 2351–2357. doi: 10.1016/j.cub.2016.06.056

Liu, Y., Lv, L., Wang, L., and Zhong, Y. (2018). Social Isolation Induces Rac1-Dependent Forgetting of Social Memory. *Cell Rep.* 25, 288.e–295.e. doi: 10.1016/j.celrep.2018.09.033

Lv, L., Liu, Y., Xie, J., Wu, Y., Zhao, J., Li, Q., et al. (2019). Interplay between α2-chimaerin and Rac1 activity determines dynamic maintenance of long-term memory. *Nat. Commun.* 10:5313. doi: 10.1038/s41467-019-13236-9

Martinez, L. A., Klann, E., and Tejada-Simon, M. V. (2007). Translocation and activation of Rac in the hippocampus during associative contextual fear learning. *Neurobiol. Learn. Memory* 88, 104–113. doi: 10.1016/j.nlm.2007.01.008

Mendoza-Naranjo, A., Gonzalez-Billault, C., and Maccioni, R. B. (2007). Abeta1-42 stimulates actin polymerization in hippocampal neurons through Rac1 and Cdc42 Rho GTPases. *J. Cell Sci.nce* 120, 279–288. doi: 10.1242/jcs.03323

Meng, J., Meng, Y., Hanna, A., Janus, C., and Jia, Z. (2005). Abnormal long-lasting synaptic plasticity and cognition in mice lacking the mental retardation gene Pak3. *J. Neurosci.* 25, 6641–6650. doi: 10.1523/JNEUROSCI.0028-05.2005

Meng, Y., Takahashi, H., Meng, J., Zhang, Y., Lu, G., Asrar, S., et al. (2004). Regulation of ADF/cofilin phosphorylation and synaptic function by LIM-kinase. *Neuropharmacology* 47, 746–754. doi: 10.1016/j.neuropharm.2004.06.030

Meng, Y., Zhang, Y., Tregoubov, V., Janus, C., Cruz, L., Jackson, M., et al. (2002). Abnormal spine morphology and enhanced LTP in LIMK-1 knockout mice. *Neuron* 35, 121–133. doi: 10.1016/s0896-6273(02)00758-4

Mucke, L., and Selkoe, D. J. (2012). Neurotoxicity of amyloid β-protein: synaptic and network dysfunction. *Cold Spring Harb. Perspect. Med.* 2:a006338. doi: 10.1101/cshperspect.a006338

Kasri, N., Nakano-Kobayashi, A., Malinow, R., Li, B., and Van Aelst, L. (2009). The Rho-linked mental retardation protein oligophrenin-1 controls synapse maturation and plasticity by stabilizing AMPA receptors. *Genes Dev.* 23, 1289–1302. doi: 10.1101/gad.1783809

Oh, D., Han, S., Seo, J., Lee, J. R., Choi, J., Groffen, J., et al. (2010). Regulation of synaptic Rac1 activity, long-term potentiation maintenance, and learning and memory by BCR and ABR Rac GTPase-activating proteins. *J. Neurosci.* 30, 14134–14144. doi: 10.1523/JNEUROSCI.1711-10.2010

Okuyama, T., Kitamura, T., Roy, D. S., Itohara, S., and Tonegawa, S. (2016). Ventral CA1 neurons store social memory. *Science* 353, 1536–1541. doi: 10.1126/science.aaf7003

Palop, J. J., and Mucke, L. (2010). Amyloid-beta-induced neuronal dysfunction in Alzheimer's disease: from synapses toward neural networks. *Nat. Neurosci.* 13, 812–818. doi: 10.1038/nn.2583

Ren, S. Q., Yan, J. Z., Zhang, X. Y., Bu, Y. F., Pan, W. W., Yao, W., et al. (2013). PKCλ is critical in AMPA receptor phosphorylation and synaptic incorporation during LTP. *EMBO J.* 32, 1365–1380. doi: 10.1038/emboj.2013.60

Rossman, K. L., Der, C. J., and Sondek, J. (2005). GEF means go: turning on RHO GTPases with guanine nucleotide-exchange factors. *Nat. Rev.* 6, 167–180. doi: 10.1038/nrm1587

Sacktor, T. C. (2011). How does PKMζ maintain long-term memory? *Nat. Rev. Neurosci.* 12, 9–15. doi: 10.1038/nrn2949

Sananbenesi, F., Fischer, A., Wang, X., Schrick, C., Neve, R., Radulovic, J., et al. (2007). A hippocampal Cdk5 pathway regulates extinction of contextual fear. *Nat. Neurosci.* 10, 1012–1019. doi: 10.1038/nn1943

Seo, J., Hong, J., Lee, S. J., and Choi, S. Y. (2012). c-Jun N-terminal phosphorylation is essential for hippocampal synaptic plasticity. *Neurosci. Lett.* 531, 14–19. doi: 10.1016/j.neulet.2012.09.048

Serrano-Pozo, A., Frosch, M. P., Masliah, E., and Hyman, B. T. (2011). Neuropathological alterations in Alzheimer disease. *Cold Spr. Harb. Perspect. Med.* 1:a006189. doi: 10.1101/cshperspect.a006189

Shankar, G. M., Li, S., Mehta, T. H., Garcia-Munoz, A., Shepardson, N. E., Smith, I., et al. (2008). Amyloid-beta protein dimers isolated directly from Alzheimer's brains impair synaptic plasticity and memory. *Nat. Med.* 14, 837–842. doi: 10.1038/nm1782

Sheng, M., Sabatini, B. L., and Sudhof, T. C. (2012). Synapses and alzheimer's disease. *Cold Spr. Harb. Perspect. Biol.* 4:a005777. doi: 10.1101/cshperspect.a005777

Shuai, Y., Lu, B., Hu, Y., Wang, L., Sun, K., and Zhong, Y. (2010). Forgetting Is Regulated through Rac Activity in Drosophila. *Cell* 140, 579–589. doi: 10.1016/j.cell.2009.12.044

Singh, S. K., Srivastav, S., Yadav, A. K., Srikrishna, S., and Perry, G. (2016). Overview of Alzheimer's Disease and Some Therapeutic Approaches Targeting Aβ by Using Several Synthetic and Herbal Compounds. *Oxid. Med. Cell. Longev.* 2016:7361613. doi: 10.1155/2016/7361613

Snyder, E. M., Nong, Y., Almeida, C. G., Paul, S., Moran, T., Choi, E. Y., et al. (2005). Regulation of NMDA receptor trafficking by amyloid-beta. *Nat. Neurosci.* 8, 1051–1058. doi: 10.1038/nn1503

Spires-Jones, T. L., and Hyman, B. T. (2014). The intersection of amyloid beta and tau at synapses in Alzheimer's disease. *Neuron* 82, 756–771. doi: 10.1016/j.neuron.2014.05.004

Texidó, L., Martín-Satué, M., Alberdi, E., Solsona, C., and Matute, C. (2011). Amyloid β peptide oligomers directly activate NMDA receptors. *Cell Calcium* 49, 184–190. doi: 10.1016/j.ceca.2011.02.001

Todorovski, Z., Asrar, S., Liu, J., Saw, N. M., Joshi, K., Cortez, M. A., et al. (2015). LIMK1 regulates long-term memory and synaptic plasticity via the transcriptional factor CREB. *Mol. Cell. Biol.* 35, 1316–1328. doi: 10.1128/MCB.01263-14

Tzakis, N., and Holahan, M. R. (2019). Social Memory and the Role of the Hippocampal CA2 Region. *Front. Behav. Neurosci.* 13:233. doi: 10.3389/fnbeh.2019.00233

Walsh, D. M., Klyubin, I., Fadeeva, J. V., Cullen, W. K., Anwyl, R., Wolfe, M. S., et al. (2002). Naturally secreted oligomers of amyloid beta protein potently inhibit hippocampal long-term potentiation in vivo. *Nature* 416, 535–539. doi: 10.1038/416535a

Wilson, R. S., Krueger, K. R., Arnold, S. E., Schneider, J. A., Kelly, J. F., Barnes, L. L., et al. (2007). Loneliness and risk of Alzheimer disease. *Arch. Gen. Psychiatry* 64, 234–240. doi: 10.1001/archpsyc.64.2.234

Wu, P., Ding, Z. B., Meng, S. Q., Shen, H. W., Sun, S. C., Luo, Y. X., et al. (2014). Differential role of Rac in the basolateral amygdala and cornu ammonis 1 in the reconsolidation of auditory and contextual Pavlovian fear memory in rats. *Psychopharmacology* 231, 2909–2919. doi: 10.1007/s00213-014-3462-0

Wu, W., Du, S., Shi, W., Liu, Y., Hu, Y., Xie, Z., et al. (2019). Inhibition of Rac1-dependent forgetting alleviates memory deficits in animal models of Alzheimer's disease. *Protein Cell* 10, 745–759. doi: 10.1007/s13238-019-0641-0

Yang, E. J., Yoon, J. H., Min, D. S., and Chung, K. C. (2004). LIM kinase 1 activates cAMP-responsive element-binding protein during the neuronal differentiation of immortalized hippocampal progenitor cells. *J. Biol. Chem.* 279, 8903–8910. doi: 10.1074/jbc.M311913200

Zamboni, V., Armentano, M., Sarò, G., Ciraolo, E., Ghigo, A., Germena, G., et al. (2016). Disruption of ArhGAP15 results in hyperactive Rac1, affects the architecture and function of hippocampal inhibitory neurons and causes cognitive deficits. *Sci. Rep.* 6:34877. doi: 10.1038/srep34877

Zhang, H., Ben Zablah, Y., Liu, A., Lee, D., Zhang, H., Meng, Y., et al. (2021a). Overexpression of LIMK1 in hippocampal excitatory neurons improves synaptic plasticity and social recognition memory in APP/PS1 mice. *Mol. Brain* 14:121. doi: 10.1186/s13041-021-00833-3

Zhang, H., Ben Zablah, Y., Zhang, H., and Jia, Z. (2021b). Rho Signaling in Synaptic Plasticity, Memory, and Brain Disorders. *Front. Cell Dev. Biol.* 9:729076. doi: 10.3389/fcell.2021.729076

Zhou, Z., Meng, Y., Asrar, S., Todorovski, Z., and Jia, Z. (2009). A critical role of Rho-kinase ROCK2 in the regulation of spine and synaptic function. *Neuropharmacology* 56, 81–89. doi: 10.1016/j.neuropharm.2008.07.031

frontiers | Frontiers in Aging Neuroscience

TYPE Original Research
PUBLISHED 29 July 2022
DOI 10.3389/fnagi.2022.916904

OPEN ACCESS

EDITED BY
Valentina Echeverria Moran,
United States Department of Veterans Affairs, United States

REVIEWED BY
Jose Felix Moruno-Manchon,
University of Texas Health Science Center at Houston, United States
Lisa Suzanne Robison,
Nova Southeastern University, United States

*CORRESPONDENCE
Ingrid Y. Liu
ycliu@gms.tcu.edu.tw

SPECIALTY SECTION
This article was submitted to Alzheimer's Disease and Related Dementias, a section of the journal Frontiers in Aging Neuroscience

RECEIVED 10 April 2022
ACCEPTED 11 July 2022
PUBLISHED 29 July 2022

CITATION
Suresh P, Jasmin S, Yen Y, Hsu H-J, Varinthra P, Pairojana T, Chen C-C and Liu IY (2022) Attenuation of HECT-E3 ligase expression rescued memory deficits in 3xTg-AD mice. *Front. Aging Neurosci.* 14:916904. doi: 10.3389/fnagi.2022.916904

Attenuation of HECT-E3 ligase expression rescued memory deficits in 3xTg-AD mice

Pavithra Suresh[1], Sureka Jasmin[2], Yun Yen[3,4,5,6,7], Hao-Jen Hsu[8], Peeraporn Varinthra[1], Tanita Pairojana[1], Chien-Chang Chen[9] and Ingrid Y. Liu[1]*

[1]Institute of Medical Sciences, Tzu Chi University, Hualien City, Taiwan, [2]Department of Molecular Biology and Human Genetics, Tzu Chi University, Hualien City, Taiwan, [3]Ph.D. Program for Cancer Molecular Biology and Drug Discovery, College of Medical Science and Technology, Taipei Medical University, Taipei City, Taiwan, [4]Graduate Institute of Cancer Biology and Drug Discovery, College of Medical Science and Technology, Taipei Medical University, Taipei City, Taiwan, [5]TMU Research Center of Cancer Translational Medicine, Taipei Medical University, Taipei City, Taiwan, [6]Cancer Center, Taipei Municipal WanFang Hospital, Taipei City, Taiwan, [7]Center for Cancer Translational Research, Tzu Chi University, Hualien City, Taiwan, [8]Department of Life Sciences, Tzu Chi University, Hualien City, Taiwan, [9]Institute of Biomedical Sciences, Academia Sinica, Taipei City, Taiwan

Alzheimer's disease (AD) is one of the most common progressive neurodegenerative disorders that cause deterioration of cognitive functions. Recent studies suggested that the accumulation of inflammatory molecules and impaired protein degradation mechanisms might both play a critical role in the progression of AD. Autophagy is a major protein degradation pathway that can be controlled by several HECT-E3 ligases, which then regulates the expression of inflammatory molecules. E3 ubiquitin ligases are known to be upregulated in several neurodegenerative diseases. Here, we studied the expressional change of HECT-E3 ligase using M01 on autophagy and inflammasome pathways in the context of AD pathogenesis. Our results demonstrated that the M01 treatment reversed the working memory deficits in 3xTg-AD mice when examined with the T-maze and reversal learning with the Morris water maze. Additionally, the electrophysiology recordings indicated that M01 treatment enhanced the long-term potentiation in the hippocampus of 3xTg-AD mice. Together with the improved memory performance, the expression levels of the NLRP3 inflammasome protein were decreased. On the other hand, autophagy-related molecules were increased in the hippocampus of 3xTg-AD mice. Furthermore, the protein docking analysis indicated that the binding affinity of M01 to the WWP1 and NEDD4 E3 ligases was the highest among the HECT family members. The western blot analysis also confirmed the decreased expression level of NEDD4 protein in the M01-treated 3xTg-AD mice. Overall, our results demonstrate that the modulation of HECT-E3 ligase expression level can be used as a strategy to treat early memory deficits in AD by decreasing NLRP3 inflammasome molecules and increasing the autophagy pathway.

KEYWORDS

Alzheimer's disease, 3xTg-AD, HECT-E3 ligase, learning and memory, autophagy, NLRP3 inflammasome

Introduction

Alzheimer's disease (AD) is characterized by excessive accumulation of β-amyloid protein, neurofibrillary tangles, and inflammatory molecules in various brain regions. Numerous studies have shown that neuroinflammation induced via inflammasome plays a critical role in the development of AD (Boland et al., 2008; Liu and Li, 2019; Zhang et al., 2021). The inflammasome is a protein complex consisting of three major proteins, including NLRP3 (NLR family pyrin domain containing 3), pro-caspase-1, and the adaptor protein apoptosis-associated Speck-like protein containing a CARD (caspase activation and recruitment domain) (ASC). In addition, the inflammasome regulates the release of cytokines by activating interleukin 1 beta (IL-1β). Notably, the upregulation of NLRP3 inflammasome-produced IL-1β in AD patients' brains (Kálmán et al., 1997; Benzing et al., 1999; Griffin et al., 2000) can lead to cognitive dysfunction. Thus, the NLRP3 inflammasome pathway could be a therapeutic target for AD.

Several inflammatory diseases such as Alzheimer's disease, Multiple sclerosis, and Traumatic brain injury are known to be associated with upregulation of NLRP3-inflammasome by the autophagy pathway (Moossavi et al., 2018; Holbrook et al., 2021; Zhao et al., 2021). Autophagy is a significant protein maintenance and degradation pathway that clears misfolded proteins and helps maintain homeostasis of synaptic transmission in the brain, which is tightly related to cognitive functions (Hylin et al., 2018; Hoffmann et al., 2019; Wang et al., 2019a). The autophagy process starts with the formation of the autophagosome. Beclin-1 acts as an initiator molecule for organizing the autophagosome, which is followed by vesicle elongation through lipidation of LC3 (microtubule-associated protein light chain 3B) by ATG (Autophagy related gene) complex (Chen et al., 2019). Ubiquitinated proteins and inclusion bodies are recruited into these autophagosomes by P62/SQSTM1 for degradation (Mizushima, 2007). A higher level of P62 could indicate autophagy dysfunction and protein accumulation. Beclin-1 is known to be decreased in the early stage of the AD patients' brains compared to the control group (Nixon et al., 2005; Pickford et al., 2008), suggesting a decline in autophagosome formation. In the animal model of cerebral ischemia, induction of autophagy by suppressing NLRP3 inflammasome is beneficial (Wang et al., 2019b). Besides, in the atg7 knockout mice, reduction of autophagy enhanced the activation of NLRP3 (Cho et al., 2014). Based on these studies, it is evident that maintaining homeostasis between autophagy-NLRP3 pathways could help prevent the pathogenesis of inflammatory-related diseases.

E3 ligases are classified into three subfamilies based on their substrates: RING (Really Interesting New Gene), HECT (Homologous to the E6-AP Carboxyl Terminus), and RBR (RING-Between RING-RING). Among these three families, only HECT possesses intrinsic catalytic activity. Specifically, HECT-E3 ligases can regulate autophagy by polyubiquitinating upstream molecules such as mTORC1 (mammalian target of rapamycin complex 1), ULK1 (Unc-51-like autophagy activating kinase), and beclin-1. Members of the HECT-E3 ligases family, such as NEDD4 (neuronal precursor cell-expressed developmentally downregulated 4) and WWP1 (WW domain containing E3 ubiquitin protein ligase 1), are known to directly target and degrade autophagy molecules to disrupt the autophagy process. These molecules also individually play a critical role in hippocampal-dependent learning and memory, such as fear and spatial memory (Pérez-Villegas et al., 2020). In addition, HECT-E3 ligases can regulate NLRP3 expression levels through post-translational modification. Thus, inducing the autophagy process and reducing inflammasome formation could be a new strategy to treat AD (Zhao et al., 2021).

Based on the relationship of E3 ligases with autophagy and inflammasomes in connection with the development of AD, we thus hypothesize that inhibiting E3 ligases expression can help induce the autophagy process as well as reduce the protein expression of inflammasome molecules, which in turn, enhances the memory performance in AD. A previous study has shown that the M01 compound can act as a potential HECT-E3 ligase inhibitor (Liu et al., 2017). Therefore, we decided to use M01 to modulate the HECT-E3 ligase expression with an attempt to investigate the changes in autophagy, inflammasome-related molecules, and memory performance in 3xTg-AD mice. Our results demonstrate that the administration of M01 effectively helped recover both working and reversal memory deficit in 3xTg-AD mice, accompanied by increased expression of autophagy molecules and decreased NLRP3 protein levels in the hippocampus. In addition, we detected a significant reduction in activated astrocyte levels in the M01-treated 3xTg-AD mice. Additionally, the Protein docking analysis indicates that among the HECT family members, the WWP1 and NEDD4 E3 ligases have the highest binding affinity to M01, which was later confirmed with the western blot analysis. These findings help give a better understanding of the homeostasis between autophagy and inflammation processes in the memory performance of AD. The overall result suggests that targeting modulation of E3 ligase expression could be a promising approach for treating early memory deficit in AD.

Materials and methods

Animals

Six-month-old 3xTg-AD (triple transgenic) and wild-type (WT) female mice were used in this study. 3xTg-AD mice were sourced from the Jackson Laboratory (Stock #34830

JAX) and maintained in the Laboratory Animal Center of Tzu Chi University for more than 10 generations. 3xTg-AD mice consist of mutations of APPSwe, PSEN1 M146, and Tau P301L. The animals were maintained under standardized conditions in a 12 h (light/dark) cycle with free access to food and water *ad libitum*. We executed all animal experiments according to the protocol approved by the Institutional Animal Care and Use Committee (IACUC). The approval number is #109047.

M01 preparation and treatment

M01 was synthesized as previously described (Liu et al., 2017). M01 was dissolved in saline: DMSO at a ratio of 9:1. The compound was orally delivered using gavage (ST-F172 0.9 mm x L 50 mm, 20G, Shineteh Instruments Co., Ltd.) 2 h before behavior tests.

Open field test (OFT)

To evaluate animals' exploratory behavior and locomotor activity, we performed an open field test (OFT) using the previously published protocol (Phasuk et al., 2021b). The open field chamber consists of a white base surrounded by four black walls measuring 50 cm (L) × 50 cm (W) × 50 cm (H). The speed and distance traveled in the chamber were recorded using a video camera and scored by automated software (EthoVision XT 15, Noldus Information Technology) for a 10 min session.

T-Maze—spontaneous alteration

Spontaneous alteration is a natural tendency of mice to alternate free choices in the T-maze through trials. To assess mice's spatial/working memory and alteration behavior, we performed T-maze-spontaneous alteration indicating mice's ability to differentiate between the novel and familiar arms. Mice with healthy cognition tend to spend more time in the novel arm (Rosenzweig et al., 2019). The T-maze consists of a white non-transparent board with three arms—a long tail measuring 30 cm and right and left arms (each 30 cm) connected to the tail at perfect right angles. In the trial session for 5 min, the animal was allowed to access only one arm (right familiar) by blocking the other (left novel) with a sliding door. In the test session (5 min) carried out after the trial session, the block was removed from the left arm, and the animal was allowed to access both arms freely. The time spent by the mice in both arms, latency to the novel arm, and alteration percentage to the novel arm [frequency to novel arm/(total frequency) multiplied by 100] were recorded and measured by automated software (EthoVision XT 15, Noldus Information Technology).

Morris water maze (MWM)

The Morris water maze procedure was adapted from the published protocol (Phasuk et al., 2021a). The Morris water maze test used a white, non-transparent tank 39 cm in height and 100 cm in diameter. The water-filled tank was maintained at 21 ± 1°C and made opaque by mixing non-toxic white paint (Cat. # 187203, Palmer paint products, USA). The pool was divided into four equal quadrants with a different cues. During visible training (day 1 and 2), a circular platform 5 cm in diameter was placed 1 cm above the water in a different quadrant in each trial, and the mice were placed on the platform for 20 s to allocate the cues. Then, the mice were allowed to explore the pool for 60 s. Mice were removed when they reached the platform or could not find the platform within 60 s. There were a total of five trials with inter-trial intervals of 30 min. During the hidden platform test, the platform was kept 1 cm below the water in the target quadrant, and the entrance point of mice was changed in each trial to avoid track memorization. The mice were given five trials a day to find the hidden platform with a trial period of 60 s for four consecutive days. The probe test was carried out on the 7th day, on which the platform was removed from the pool. The mice were placed through unfamiliar entrance points and allowed to swim freely for 60 s. On the following day of the probe test, a reversal-learning session was conducted with the platform opposite to the acclimatized target quadrant and five trials were performed (Arqué et al., 2008; Karabeg et al., 2013). A video tracking system (EthoVision XT 15, Noldus Information Technology) was used to measure the path length, swimming speed, escape latency, and percentage of time spent in each quadrant.

Immunoblotting analysis

The hippocampus was dissected from the whole brain for immunoblotting and lysed using 1X RIPA buffer (Millipore, USA) supplemented with protease and phosphatase inhibitors. The lysate was cleared by centrifugation at 13,500 rpm for 15 min at 4°C, and the supernatant was stored at −80°C for further experiments. The protein concentration was estimated by Bradford's method every time before gel electrophoresis. The protein samples were prepared in reducing agent (NuPAGE® Invitrogen) + LDS sample buffer (4X – NuPAGE® Invitrogen) and boiled at 95°C for 10 min. A 50 µg protein sample was separated by SDS–PAGE in an 8 or 12% polyacrylamide gel and transferred to a PVDF membrane (0.45 µm pore size) at 25 volts in a cold room overnight. The membrane was then blocked with 5% milk/1% BSA in tris buffered saline with

0.1% Tween 20 (TBST) for 1 h at room temperature. After blocking, primary antibodies against NLRP3 (1:1,000; Abcam, UK), Beclin-1 (1:1,000; Abcam, UK), P62 (1:1,000; Abcam, UK), Caspase 1 (1:1,000; Cell Signaling Technology, USA), LC3B (1:1,000; Abcam, UK), WWP1 (1:1000; Abnova), NEDD4 (1:1000; Merck millipore), and anti-β-actin (1:10,000; Sigma–Aldrich, USA) diluted in TBST with 0.1% BSA were added and incubated overnight in a shaker. The blots were transferred to appropriate secondary antibody conjugates diluted in 0.1% milk for 1 h, developed using ECL (Western lighting® Plus ECL, PerkinElmer Inc, MA, USA) and detected under a Bio-Rad ChemiDoc MP High-performance Cold Light Fluorescence Analysis system or High sensitivity biomedical imaging system chemstudio plus. The quantification of band intensities was performed using ImageJ version 1.52a (National Institutes of Health, USA).

Immunofluorescence staining and image analysis

The brains were collected from mice through cardiac perfusion using 4% paraformaldehyde (PFA) and 0.9% saline in PBS, kept in PFA for 48 h and then transferred to 30% sucrose. The brains were sliced into thin sections with 35 μm thickness using cryostat. The sections were permeabilized in permeating buffer (1% Triton + 2% Tween in PBS) for 30 min and blocked with 1% normal goat serum (NGS) + 0.3% Triton X-100 for 1 h at room temperature (RT). After blocking, primary antibodies against NLRP3 (1:100; Abcam, UK), Beclin-1 (1:100; Abcam, UK), P62 (1:100; Abcam, UK), and GFAP (1:200; Abcam, UK) were added and incubated overnight at 4°C. Respective secondary antibodies were added and incubated for 1 h at RT after washing the sections with 0.25% Triton+ PBS three times for 5 min each. DAPI (4'-6-Diamidino-2-phenylindole) was used to stain the DNA. The sections were mounted on 76 × 26 mm adhesive glass slides and covered with coverslips for imaging. Upright Conjugate Focus Microscope NIKON C2si+ confocal microscope was used to capture images with 10×, 20×, and 40× objective lenses under 405,488, and 561 nm wavelengths. All images were adjusted and cropped using ImageJ version 1.52a (National Institutes of Health, USA). The calculation was done using ImageJ software, 3–5 fields (200 × 200 μm) from 3 to 4 sections per mouse were used to calculate the positive area percentage of each antibody.

Electrophysiology

Extracellular recording of the CA1-CA3 Schaffer collateral synapse was performed as previously reported (Varinthra et al., 2021). The brains were removed with decapitation and immediately placed in ice-cold artificial cerebrospinal fluid (ACSF). Coronal sections of the hippocampus 350 μm thick were obtained in oxygenated ACSF using a vibrating microtome (Microslicer DTK-1000, Dosaka EM Co. Ltd., Kyoto, Japan). Slices were maintained in oxygenated ACSF with 95% O_2/5% CO_2 at 28–30°C for at least 2 h before transferring to the recording chamber. In the recording chamber, the brain slice was supplied with oxygen (O_2)-concentrated ACSF at a speed of 2–3 mL/min at 28°C. Field excitatory postsynaptic potentials (fEPSPs) were recorded from the CA1 stratum radiatum region of the hippocampus via glass micropipettes (PC-10 Needle Puller, Narishige, Japan) filled with ACSF. Stimulation was provided by stainless steel unipolar electrodes (Frederick Haer Company, Bowdoinham, ME, USA). Baseline stimulus intensity was set at the level that evoked 30–40% of the maximum fEPSPs response as determined from the input-output curve. Baseline fEPSPs were recorded for 20 min followed by high-frequency stimulation (HFS) with 3 trials of 100 pulses at 100 Hz for 60 s. The fEPSPs were stimulated every 20 s and recorded for 80 min. The signals were amplified by an Axon Multiclamp 700B amplifier, filtered at 1 kHz and digitized at 10 kHz by a CED MicroPower 1401 MKII interface (Cambridge Electronic Design, Cambridge, UK) using Signal software. The slope of fEPSPs is measured using Axon pCLAMP 11 electrophysiology data acquisition and analysis software.

Protein docking analysis

To predict the interaction between selected HECT-E3 ligases and M01, the DOCK module with "Induced fit" refinement in the MOE2020.09 software program (https://www.chemcomp.com) was used for molecular docking. M01 was manually built in the MOE software package to dock with different E3 ligases (PDB: 5C91, 3TUG, 1ND7, 3H1D, 5HPK with M01) for comparison. MOE software was used to eliminate the water molecules, and missing short loops were added. The binding free energy of the ligand to the receptor was estimated using GBVI/WSA ΔG, a force field-based scoring function. The scoring function was used to predict the binding affinity between M01 and selected E3 ligases. The lowest binding score represents better affinity.

Statistical analysis

All statistical analyses were performed using IBM SPSS 22 statistical software, and all values are presented as the mean ± SEM. One-way ANOVA was conducted to compare between groups. In addition, path length, speed, and latency during hidden platform trials and time spent during the probe test were analyzed using mixed-design repeated measure

ANOVA with trials and groups as within-subjects and between-subjects, respectively. For electrophysiological recording, one-way ANOVA followed by Tukey's *post hoc* test was applied for multiple comparisons. A $p < 0.05$ was considered statistically significant. ANOVA tables for western and IHC are shown in Supplementary Table 1. All graphs were plotted with GraphPad Prism 8.0 software.

Results

E3 ligase inhibitor, M01, rescued working memory deficits in 3xTg-AD mice

Carroll et al. (2010) found that female 3xTg mice exhibit higher Amyloid-beta and behavior deficits than age-matched controls (Carroll et al., 2010). (Stimmell and Baglietto-Vargas, 2019) found that 6-month-old female 3xTg mice showed spatial orientation deficit and higher pathology, specifically in the hippocampus, compared to male mice (Stimmell and Baglietto-Vargas, 2019). Therefore, we decided to use female 3xTg mice to study AD pathogenesis in our study. DMSO has been demonstrated to have an effect on animal behavior (Penazzi et al., 2017). However, the M01 dissolves better in DMSO; and therefore, we design a DMSO only group (the vehicle group) to evaluate the possible effect of DMSO on our study. We first performed an OFT to evaluate the effect of M01 on locomotor activity. Moving trace patterns were shown in the OFT paradigm (Figure 1A). No significant difference was found in moving distance (Figure 1B) between WT, 3xTg-untreated, and 3xTg-M01 but the 3xTg-vehicle group traveled less distance than other groups [$F_{(3, 30)} = 6.07$, $p < 0.05$]. Time spent in the outer zone shows a difference between 3xTg-untreated and vehicle groups [$F_{(3, 30)} = 3.765$, $p < 0.05$, Figure 1C) but shows no difference when compared with the WT and 3xTg-M01 groups.

To further determine the effect of M01 on working memory, we performed a T-maze test on all four groups. Normal mice usually spend a longer period of time exploring the novel arm or equal time in the novel and familiar arms. Here, 3xTg-untreated and vehicle groups show less alternation frequency toward the novel arm. However, the frequency of visiting the novel arm increased significantly in the M01-treated 3xTg group ($F_{(3,50)} = 9.940$, $p = 0.000$, Figure 1E), which is also evident from the tracing pattern (Figure 1D). We also found that both the 3xTg-untreated [$t_{(28)} = 3.651$, $p = 0.001$] and vehicle groups [$t_{(22)} = -2.433$, $p = 0.024$] spent a longer time in the familiar arm than the novel arm (Figure 1E). After the M01 treatment, 3xTg mice explored the familiar and novel arms equally [$t_{(20)} = -0.43$, $p = 0.966$] similar to WT [$t_{(30)} = 0.445$, $p = 0.659$] (Figure 1F). The 3xTg untreated and vehicle group spending more time in the familiar arm could be because of the anxiety and also working memory deficit. The 3xTg mice have been shown to exhibit anxiety-like behavior (Giménez-Llort et al., 2013; Pietropaolo et al., 2014).

E3 ligase inhibitor, M01, treatment rescued spatial reversal learning deficit in 3xTg-AD mice

Next, we investigated spatial memory using the Morris water maze (MWM). Throughout the training course, all the groups performed similarly. In the acquisition phase, by using mixed-design repeated ANOVA, we found that there was a significant difference observed between hidden platform days for swimming speed [$F_{(3, 99)} = 35.66$, $p = 0.000$, Figure 2A], path length [$F_{(3, 99)} = 33.35$, $p = 0.000$, Figure 2B] and latency to find the platform [$F_{(3, 99)} = 17.31$, $p = 0.000$, Figure 2C], while no interaction was observed between days and groups. These results indicated that all four groups can learn the task during the acquisition trials. During the reference memory test, all the groups spent longer time in the target quadrant than in other quadrants (Figure 2D). These data indicated that the spatial memory is still intact in 6-month-old 3xTg-AD mice.

During the reversal trial day, 3xTg-untreated and vehicle groups took longer to find the platform, while the WT and 3xTg-M01 groups performed significantly better. Throughout the reversal learning trials, the 3xTg-M01 group spent less time finding the newly positioned platform (latency) [$F_{(3, 33)} = 6.69$, $p < 0.05$, Figure 2F], and the path length for them to reach the platform was also decreased [$F_{(3, 33)} = 11.90$, $p < 0.05$, Figure 2G] compared with that of the 3xTg-Untreated and vehicle groups. In addition, the swimming trace patterns of the WT and the M01 treated groups were significantly different during MWM reversal trials (Figure 2E). All behavior experiments were performed 2 h after M01 treatment. For Morris water maze, the M01 was administered 2 h before the experiment every day. Therefore, the recorded behavioral impairment of the reversal trial should be the cumulative effect of the 8-day M01 treatment. These results demonstrated that M01 treatment effectively rescues early symptoms of working memory and reversal learning deficits in the 3xTg-AD mice.

E3 ligase inhibitor, M01, administration leads to increased protein levels of autophagy molecules and decreased NLRP3 inflammasome molecules in 3xTg-AD mice

We further investigated the changes in the protein levels of autophagy and inflammasome-related molecules after the M01 administration to 3xTg mice. As shown in Figure 3A, autophagy initiator molecule beclin-1 [$F_{(3,26)} = 5.763$, $p <$

10.3389/fnagi.2022.916904

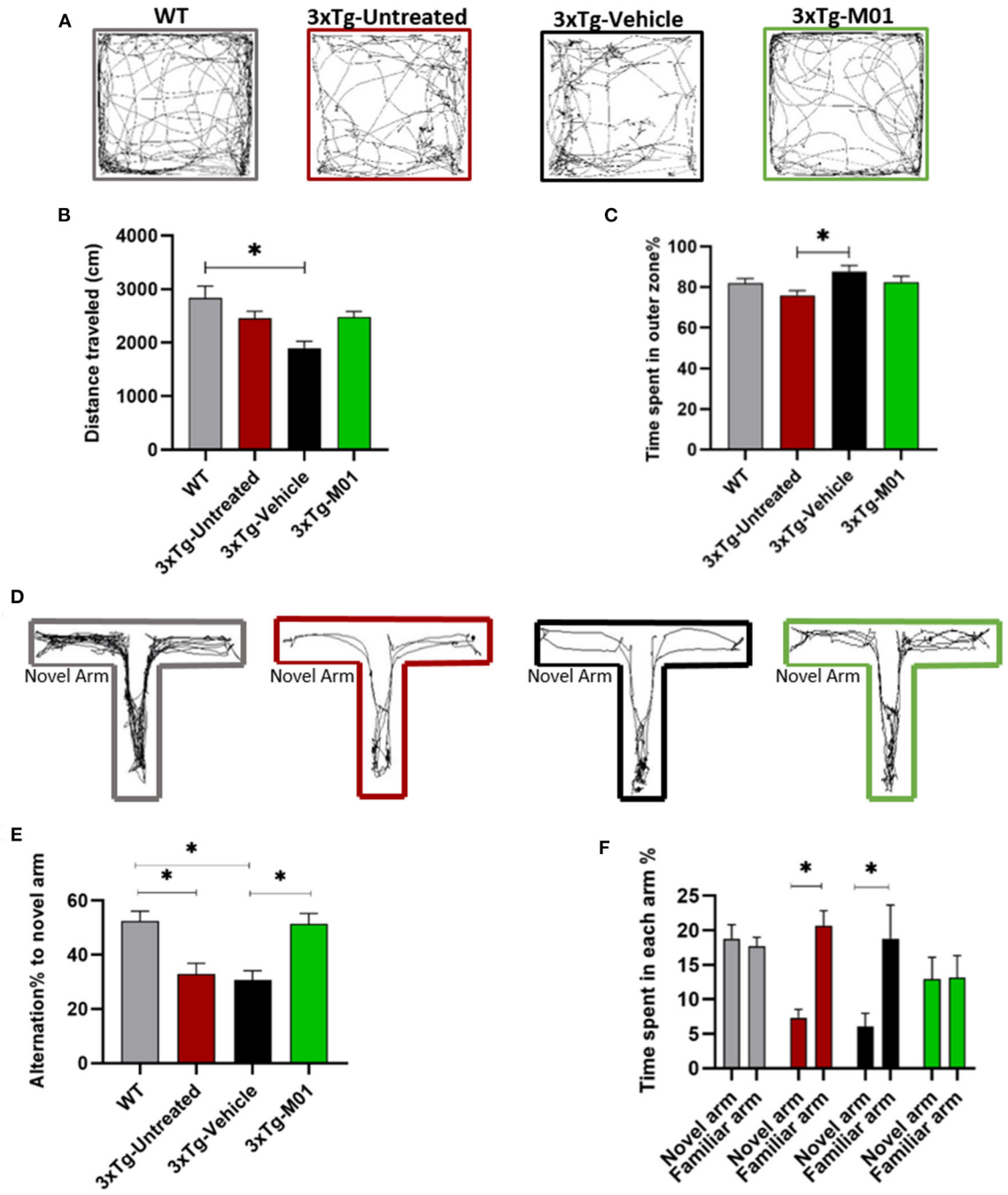

FIGURE 1
M01 rescued working memory deficits in 3xTg-AD mice. **(A)** Trace diagram of mice in the OFT. **(B)** distance traveled in the OFT shows difference between WT and 3xTg-vehicle group, and no statistical difference between 3xTg-M01 group. **(C)** Time spent in the outer zone by each group of mice shows significant difference between 3xTg- untreated and vehicle group but not with the other groups **(D)** Trace pattern of all the groups in the T-maze paradigm. **(E)** Quantification data represent the percentage of alternation frequency toward the novel arm. Statistical difference was observed between WT and 3xTg- untreated, vehicle groups. M01 treated 3xTg mice shows high alternation toward novel arm compared to 3xTg-Vehicle group. **(F)** Percentage of time spent in the novel and familiar arms. 3xTg-untreated and vehicle groups spent significantly more time in the familiar arm while WT and M01 groups explored both the arms equally. Data are expressed as the mean ± SEM. *$p < 0.05$, $n = 9–15$/group, and one-way ANOVA followed by Tukey's test were used to compare between groups.

10.3389/fnagi.2022.916904

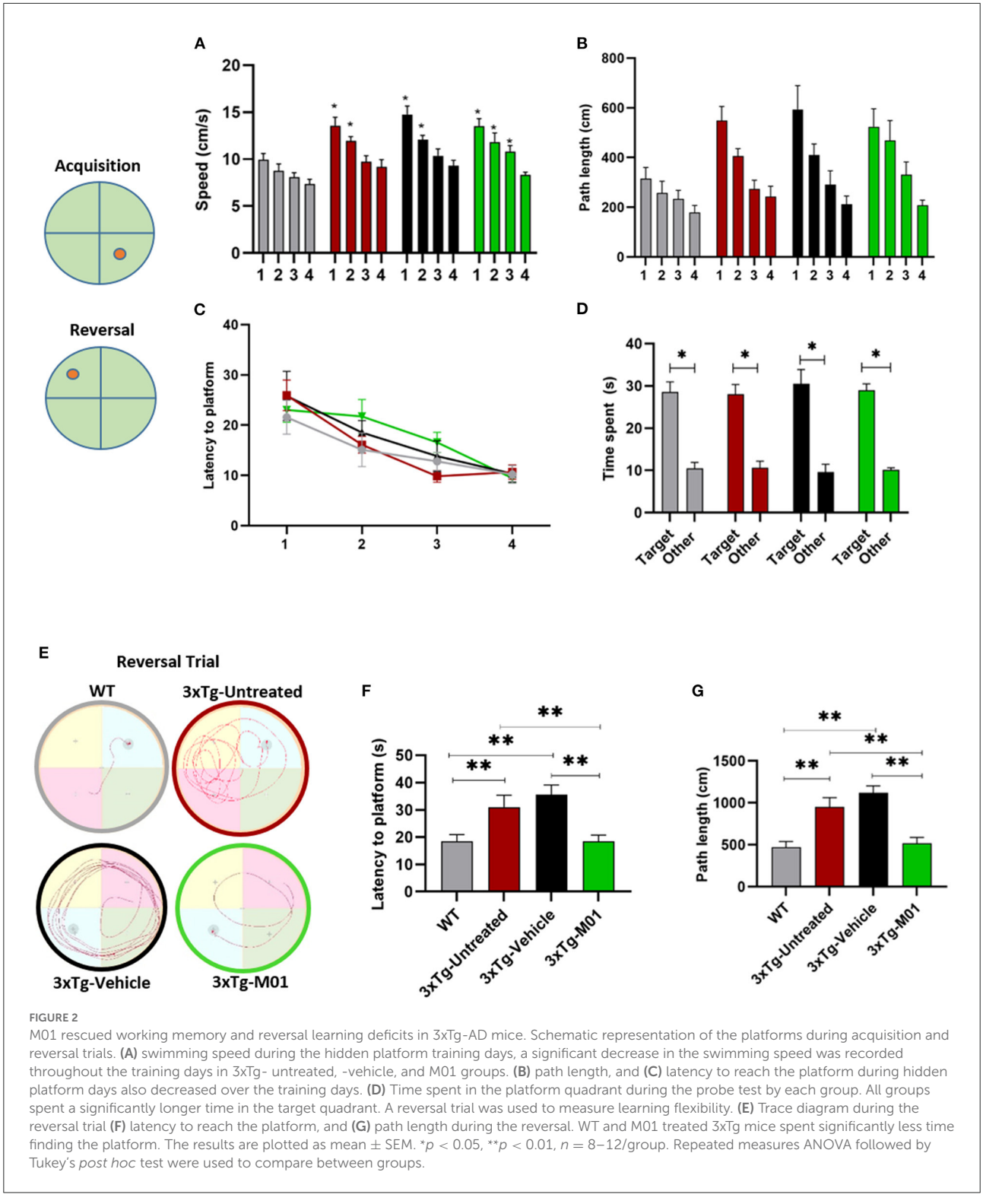

FIGURE 2
M01 rescued working memory and reversal learning deficits in 3xTg-AD mice. Schematic representation of the platforms during acquisition and reversal trials. **(A)** swimming speed during the hidden platform training days, a significant decrease in the swimming speed was recorded throughout the training days in 3xTg- untreated, -vehicle, and M01 groups. **(B)** path length, and **(C)** latency to reach the platform during hidden platform days also decreased over the training days. **(D)** Time spent in the platform quadrant during the probe test by each group. All groups spent a significantly longer time in the target quadrant. A reversal trial was used to measure learning flexibility. **(E)** Trace diagram during the reversal trial **(F)** latency to reach the platform, and **(G)** path length during the reversal. WT and M01 treated 3xTg mice spent significantly less time finding the platform. The results are plotted as mean ± SEM. $*p < 0.05$, $**p < 0.01$, $n = 8–12$/group. Repeated measures ANOVA followed by Tukey's *post hoc* test were used to compare between groups.

0.05] was downregulated in both the 3xTg-untreated ($p < 0.01$) and vehicle group ($p < 0.01$). After the administration of M01, we detected that beclin-1 protein levels were significantly increased in the hippocampus of the 3xTg-M01 group. We further confirmed the result using the immunofluorescent staining technique on the hippocampus and found that beclin-1

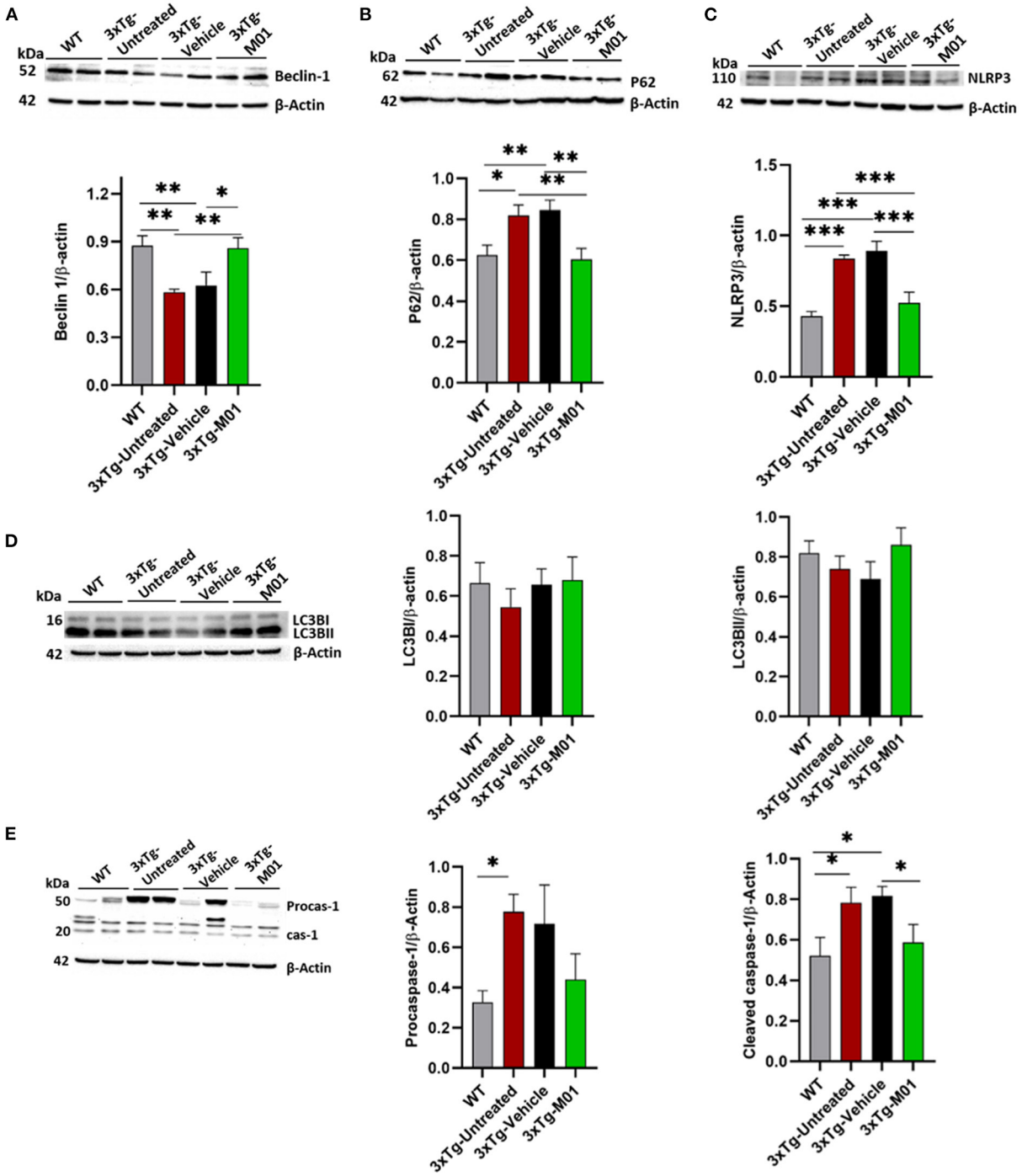

FIGURE 3
M01 administration increased the protein expression levels of autophagy-related molecules and decreased NLRP3 in the hippocampus. Immunoblots and quantification graphs of proteins **(A)** beclin-1expressed significantly less in 3xTg-untreated and vehicle groups compared to WT and M01 groups. **(B)** P62 expression is high in 3xTg-untreated and vehicle groups, and M01 decreased the P62 to WT level. **(C)** NLRP3 over-expressed in 3xTg-untreated and vehicle group, M01 administration significantly decreased NLRP3 level. **(D)** LC3BI&II shows no statistical difference between groups. **(E)** Pro-caspase-1 expressed significantly higher in 3xTg-untreated group compared to WT group. Cleaved caspase-1 expressed significantly higher in the 3xTg-untreated and -vehicle groups; M01 treatment significantly decreased the caspase-1 level in the hippocampus. The results are plotted as the mean ± SEM. $^{*}p \leq 0.05$, $^{**}p < 0.01$, $^{***}p < 0.001$, $n = 6–8$/group for western blot analysis.

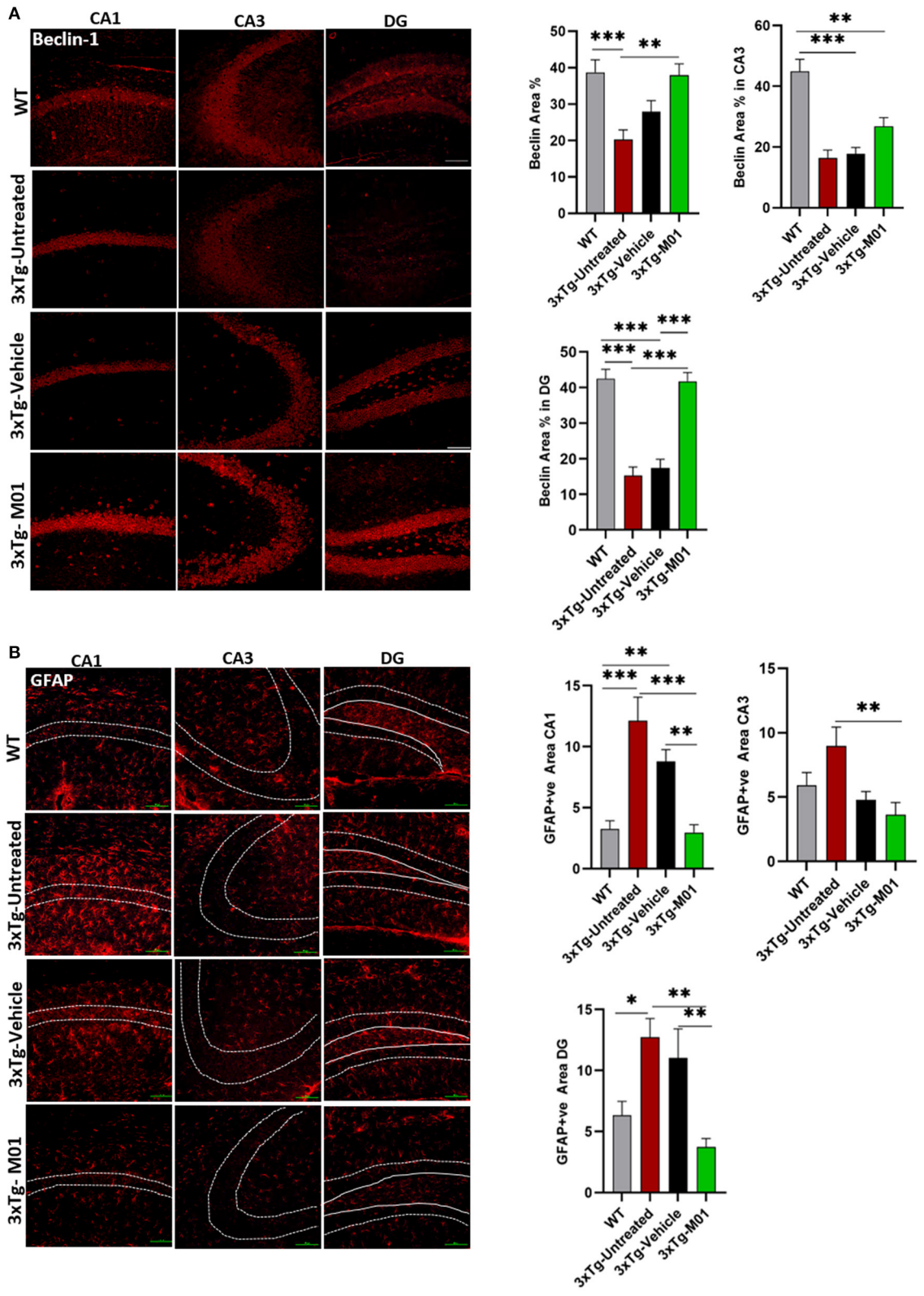

FIGURE 4
M01 administration increased beclin-1 and decreased GFAP expression levels in the hippocampus of 3xTg-AD mice. **(A)** The expression of Beclin-1 in CA1, DG, and CA3 significantly decreased in the 3xTg-untreated and -vehicle groups. M01 treatment increased the expression in CA1

(Continued)

FIGURE 4
and DG. The quantification graphs are demonstrated on the right panels. **(B)** The expression of GFAP in CA1, CA3, and DG of the hippocampus was significantly increased in 3xTg-untreated and -vehicle groups. M01 treatment significantly decreased the GFAP expression. The quantification graphs are demonstrated on the right side. Scale bar: 100 μm. The results are plotted as the mean ± SEM. *$p < 0.05$, **$p < 0.01$, ***$p < 0.001$ and $n = 3$–4 mice/group and 3 sections/mice for IF.

was upregulated in the M01 treated group in CA1 [$F_{(3, 57)} = 8.993$, $p = 0.000$], CA3 [$F_{(3, 76)} = 19.379$, $p = 0.000$] and DG [$F_{(3, 83)} = 33.390$, $p = 0.000$] when compared to the 3xTg-untreated and vehicle groups (Figure 4A). We also investigated the LC3 protein involved in the elongation and formation of autophagosomes, and found that the expression levels of LC3BI [$F_{(3, 24)} = 0.354$, $p = 0.787$] and LC3BII protein [$F_{(3, 24)} = 1.036$, $p = 0.392$] were not significantly different between the groups (Figure 3D). We then checked the autophagy substrate and reporter molecule P62 and noted that it was upregulated in the 3xTg-untreated and vehicle groups indicating that the attenuation of autophagy has occurred [$F_{(3, 24)} = 6.361$, $p < 0.01$, Figure 3B]. On the other hand, the M01 treatment reduced the P62 protein expression ($p = 0.785$) to the WT level which indicated that the autophagy functions at the normal level (Figure 3B).

The expression levels of NLRP3 [$F_{(3, 28)} = 13.892$, $p < 0.000$] and cleaved caspase-1 proteins [$F_{(3, 18)} = 3.698$, $p < 0.05$, Figure 3E], both of which are components of the inflammasome complex, was significantly upregulated in 3xTg-untreated and vehicle groups. M01 treatment decreased the NLRP3 inflammasome protein in the 3xTg mice (Figure 3C). We further performed immunofluorescent staining to confirm the differential expression levels and cell types of these molecules in the hippocampus and found that after treatment, 3xTg-M01 mice showed significant decrease of NLRP3 and P62 colocalization in the DG [$F_{(3, 59)} = 23.485$, $p = 0.000$, Figure 5A], CA3 [$F_{(3, 81)} = 19.515$, $p = 0.000$, Figure 5B], and CA1 [$F_{(3, 23)} = 8.545$, $p = 0.001$, Figure 5C] of the hippocampus. Thus, our results indicate that the administration of M01 can increase the surge of autophagic flux, which might have caused the decreased level of NLRP3 protein in the hippocampus of 3xTg-AD mice.

The over-activation of astrocytes can lead to the inhibition of proteasome pathways, which in turn causes the AD pathology development (Ozcelik et al., 2013), induction of autophagy reduced the astrogliosis in P301S Tau Transgenic mice. To determine whether the M01 treatment can decrease reactive astrocytes, we performed immunofluorescent staining in the hippocampus of 3xTg-AD mice. Interestingly, 3xTg-M01 group showed reduced expression of astrocytes marker, glial fibrillary acidic protein (GFAP), compared to the 3xTg-untreated and vehicle groups in CA1 [$F_{(3, 37)} = 12.827$ $p = 0.000$], CA3 [$F_{(3, 34)} = 4.037$ $p = 0.015$], and DG [$F_{(3, 33)} = 5.103$, $p = 0.005$] (Figure 4B).

M01-treated 3xTg-AD mice exhibited enhanced long-term potentiation in the hippocampal CA1 region

The dysregulation of inflammatory mediators has been known to disrupt neural plasticity (Di Filippo et al., 2008). Also, we found that M01 can decrease the inflammasome in 3xTg mice. Therefore, we performed extracellular recording in CA3-CA1 Schaffer collateral synapses in the hippocampus to see the effect of M01 on neural plasticity. No difference was observed in the baseline fEPSP recorded among the groups (Figures 6A,B). We observed that early long-term potentiation (E-LTPs) of 3xTg-untreated and 3xTg-vehicle mice recorded in the Schaffer collateral stimulation were impaired [$F_{(3, 36)} = 1438.64$, $p = 0.00$, Figure 6C] when compared to the WT and M01 groups. After the administration of M01, 3xTg-M01 mice showed improved induction of LTP, and the LTP lasted throughout the recording after HFS when compared to 3xTg-untreated and 3xTg-vehicle groups (Figures 6A–C). Interestingly, we observed that the vehicle (DMSO) group shows increased fEPSP. Based on a previous study, DMSO can influence the spine density in the APP_{SDL} AD mouse model (Penazzi et al., 2017). However, 3xTg-M01 group evoked higher fEPSP than the 3xTg-untreated and vehicle groups.

M01 has a high binding affinity with WWP1 and NEDD4 E3 ligase

To find the potential target of M01, we selected five E3 ligases involved in autophagy and AD for protein docking. A docking score was given to each E3 ligase (Supplementary Figure 1), which represents the binding affinity of M01 with the target. WWP1 (Figure 7A) and NEDD4 (Figure 7B) attained the lowest docking score among the other E3 ligases, indicating that both of these E3 ligases have preferable docking pose. We performed western blotting to confirm the docking results by checking the expression levels of WWP1 (Figure 7C), and NEDD4 protein (Figure 7D) in the hippocampus. We found a significant increase in the expression level of WWP1 protein [$F_{(3, 36)} = 3.487$, $p = 0.027$] in 3xTg-vehicle group compared to the WT group. The NEDD4 [$F_{(3, 35)} = 6.755$, $p = 0.001$) protein expression level was significantly higher in 3xTg-untreated and -vehicle groups compared to the WT group. After the M01 treatment, NEDD4 ($p < 0.05$) protein expression level was

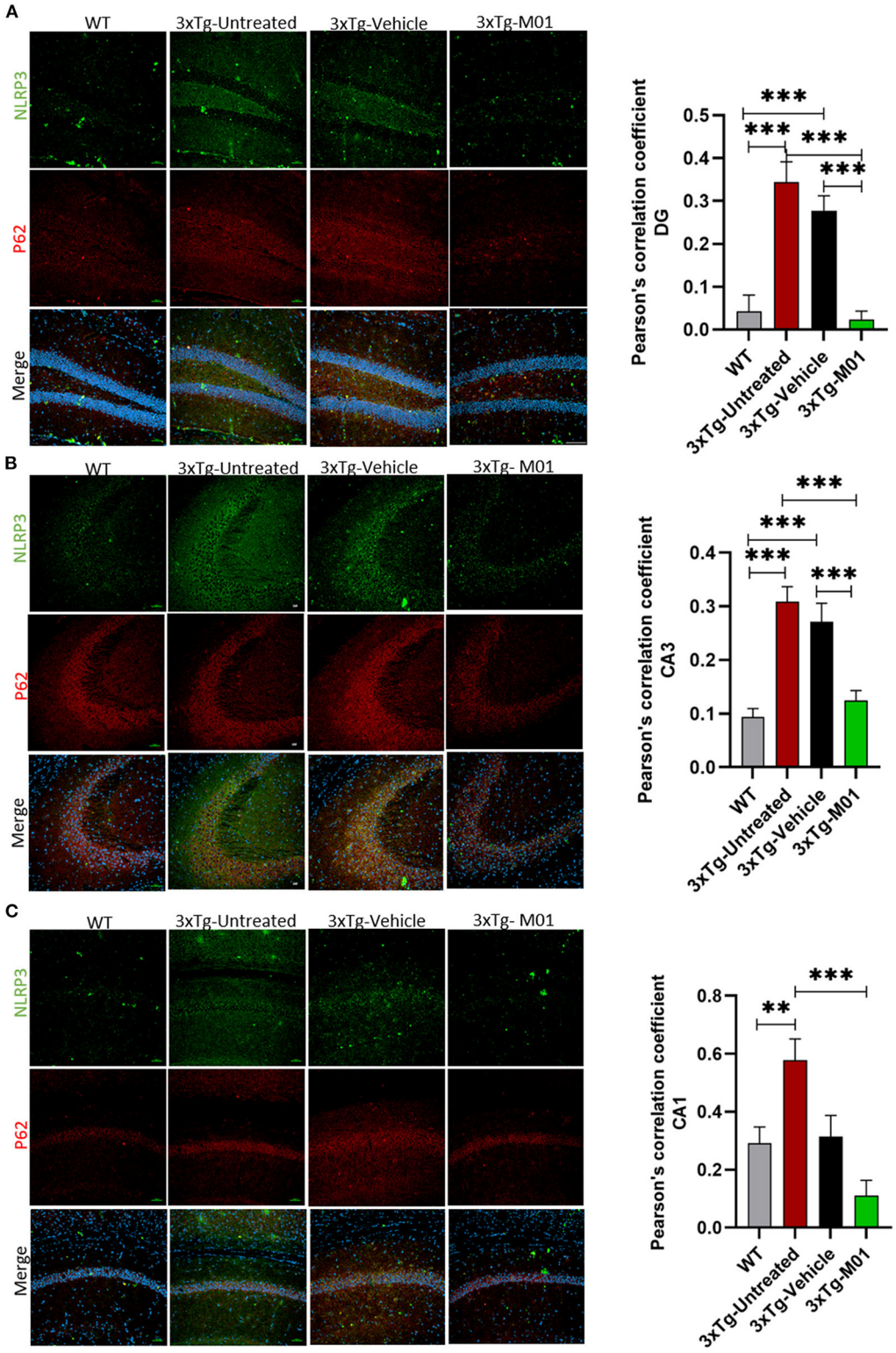

FIGURE 5
M01 administration decreased P62 and NLRP3 co-localization in the hippocampus of 3xTg-AD mice. The immunofluorescence staining NLRP3 (green), P62 (red), and merged (yellow) in **(A)** DG, **(B)** CA3, and **(C)** CA1. Co-localization of NLRP3 and P62 is significantly high in 3xTg-untreated and vehicle groups, M01 treatment decreased the co-localization of NLRP3 and p62 in the hippocampus of 3xTg mice. Pearson's correlation coefficient was applied to quantify the co-localization and graphs were plotted on the right panel. Scale bar: 100 μm. The results are presented as the mean ± SEM. $^{**}p < 0.01$, $^{***}p < 0.001$ and $n = 3$–4/group and 3 sections/mice for IF.

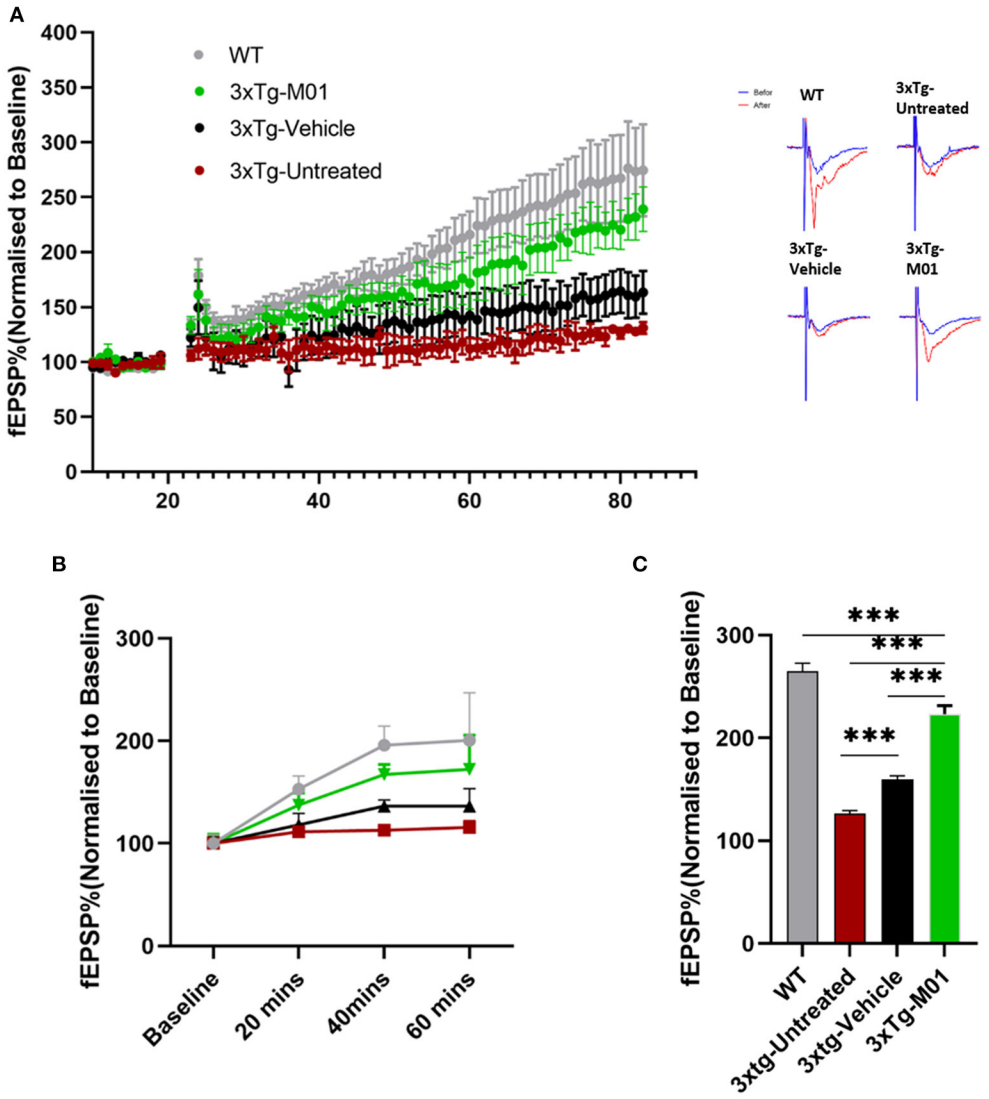

FIGURE 6
Enhanced CA1 long-term potentiation was recorded in M01-administered 3xTg-AD mice. **(A)** Average values of fEPSPs (normalized to baseline) were plotted for each group along with representative traces of LTP. **(B)** fEPSP slope plotted by different time points. **(C)** Quantitative graphs show a significant difference in LTP between WT, 3xTg-untreated, 3xTg-vehicle, and 3xTg-M01. ***$p \leq 0.000$. $n = 3–4$/group. The results are plotted as the mean ± SEM, and one-way ANOVA followed by Tukey's *post hoc* test was applied for multiple comparisons.

significantly decreased in 3xTg-M01 group compared to the 3xTg-vehicle group.

Discussion

The results of our study suggest that modulating HECT-E3 ligase expression level can effectively prevent memory decline in the early stage of AD, which seems to be associated with the enhancement of the autophagy process and reduced expression level of the NLRP3 inflammasome proteins. The AD drug development has recently been shifted to chronic inflammation reduction because limited success was achieved in clinical trials focusing on Aβ amyloid clearance (Morrison, 2016; Businaro et al., 2018). The accumulation of Aβ can release inflammatory cytokines (Wang et al., 2015), and impair synaptic transmission and memory performance (Karisetty et al., 2020). Here, we demonstrate that reducing the excessive inflammatory response by modulating HECT-E3 ligase to enhance the autophagy process is a promising therapeutic approach to preventing early memory decline in AD.

Autophagic dysregulation plays a critical role in the development of neurodegenerative diseases, especially AD. Studies have found that beclin-1 is downregulated in the cortex

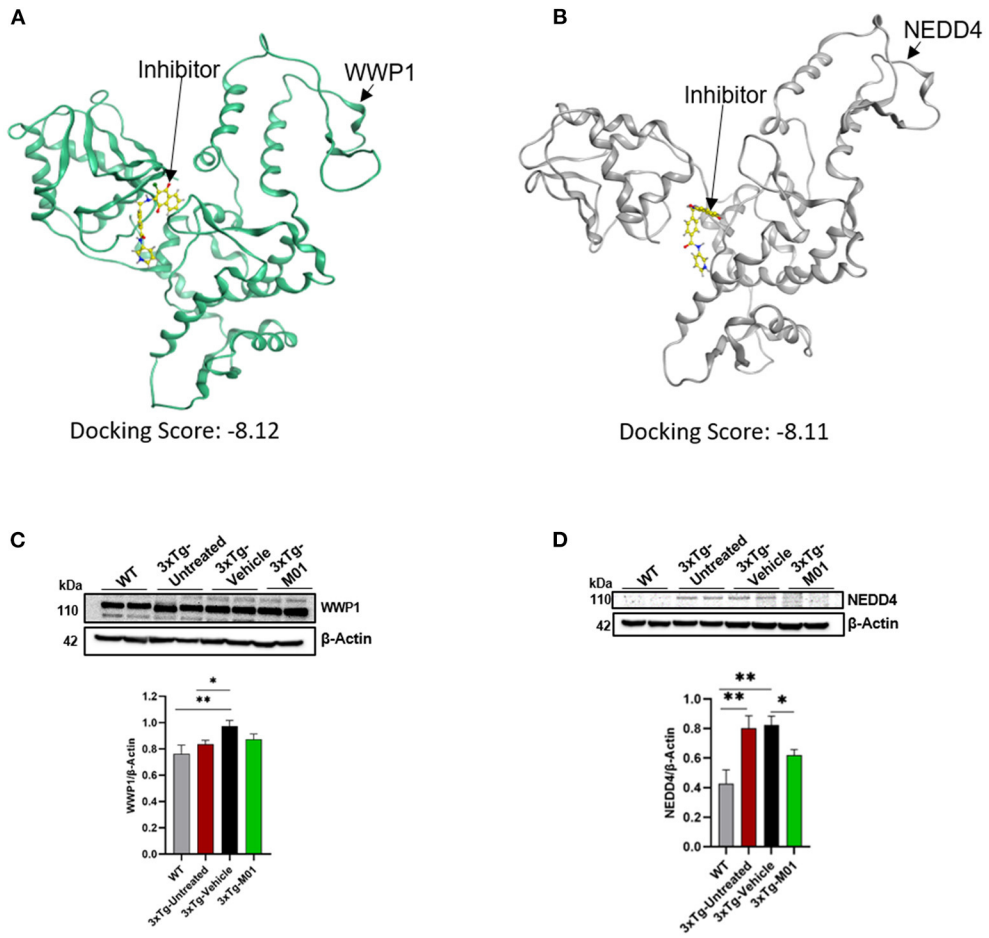

FIGURE 7
M01 has a high binding affinity with WWP1 and NEDD4 E3 ligase. Protein structure of **(A)** WWP1 (green) (PDB code: 1ND7), **(B)** NEDD4 (gray) (PDS code: 5C91) docked with M01 (yellow), **(C)** Images of western blotting of anti-WWP1, and **(D)** anti-NEDD4 antibodies against protein extraction from the hippocampus. M01 treatment significantly decreased the protein level of NEDD4 E3 ligase in 3xTg mice. The results are plotted as mean ± SEM. *$p < 0.05$, **$p < 0.01$. $n = 5–6$/ group for western blot analysis.

of AD patients (Pickford et al., 2008; Bieri et al., 2018). It is also reported that beclin-1 is cleaved during AD, which correlates with neuronal loss (Bieri et al., 2018), which supports the assumption that rescuing beclin-1 level to normal can decrease AD progression. In addition, a reduction in the autophagy process leads to the accumulation of inflammatory cytokines in the brain (Saitoh and Akira, 2016), while reversing autophagic function in the TgCRND8 AD mouse model improves learning and memory deficits (Yang et al., 2010). The autophagic adaptor protein P62 aids the degradation of the NLRP3 inflammasome through autophagosomes in human primary monocytes (Shi et al., 2012). Ising et al. found that NLRP3 inflammasome was activated in the cortex of frontotemporal dementia patients and Tau22 mice, a tau pathology mouse model (Ising et al., 2019). The autophagy pathway limits the NLRP3 inflammasome by eliminating inflammasome components and activating factors (Biasizzo and Kopitar-Jerala, 2020). These studies support our findings that induction of the autophagy pathway can efficiently eliminate the NLRP3 burden in AD. Glatigny et al. found that behavioral training can increase autophagy molecules in the brain (Glatigny et al., 2019) and the beclin-1 level was upregulated after the MWM and fear conditioning. Inhibiting beclin-1 in hippocampal neurons can disrupt memory performance (Glatigny et al., 2019). Also, Atsushi Sato et al. (2012) showed rapamycin, an autophagy inducer treated for 2 days could improve the social interaction and rearing in tuberous sclerosis mice. These reports demonstrate that autophagy induction is crucial for memory performance and support our approach by modulating E3 ligase expression to restore autophagy function and improve the memory performance of 3xTg-AD mice.

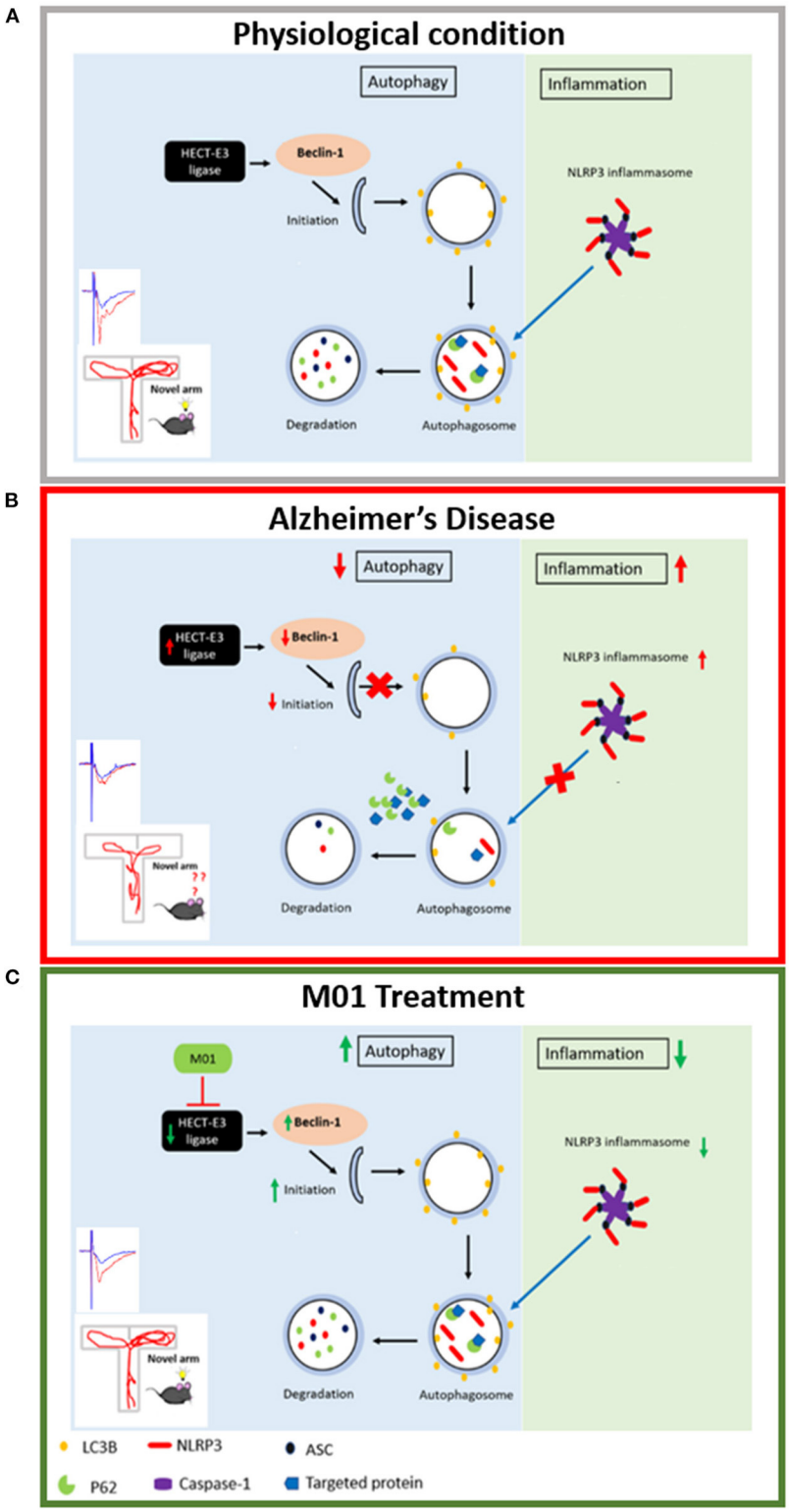

FIGURE 8
Schematic representation of the relationship between autophagy process and NLRP3 inflammasome. **(A)** Physiological condition: Under physiological condition, autophagy and NLRP3 inflammasome pathways are in a homeostatic status. **(B)** Alzheimer's disease condition: HECT-E3 ligase downregulates autophagy molecules, in turn, causes dysfunctional autophagy process and increase expression of the NLRP3 inflammasome in AD. **(C)** M01 treatment: M01 treatment rescued autophagy function and led to the degradation of the NLRP3 inflammasome proteins via autophagosomes.

In our study, we used protein docking to identify the target of M01. We found that WWP1 and NEDD4 may be the primary candidates and could be responsible for the therapeutic effect of M01 on 3xTg-AD mice. NEDD4 (Kwak et al., 2012) was increased in AD pathology. Furthermore, it has been reported that NEDD4-1 (Pei et al., 2017), NEDD4-2 (Wang et al., 2016), ITCH (Chhangani et al., 2014), and WWP1 (Sanarico et al., 2018) can regulate autophagy, either negatively or positively. These reports support our findings that modulation of E3 ligase function can induce the autophagy process. Further site-direct mutagenesis or inhibitory experiments are necessary to verify the roles of WWP1 and NEDD4 in the memory performance of 3xTg-AD mice.

Synaptic strength represents the degree of memory performance. Several studies have reported the correlation between an E3 ligase and synaptic strength. Yuen et al. (2012) showed that knockdown of the E3 ligase NEDD4-1 in the prefrontal cortex rescued the loss of glutamatergic responses and recognition memory in stressed mice. Furthermore, NEDD4-1 controls the downscaling of synaptic strength by decreasing AMPARs (Scudder et al., 2014), while knockdown of NEDD4-1 enhances AMPAR-EPSCs. These studies demonstrate that targeting the E3 ligase can alter synaptic transmission in AD. Our electrophysiological recording confirms that modulation of E3 ligases can enhance synaptic plasticity via induction of excitatory postsynaptic potential in 3xTg-AD mice.

The relationship between ubiquitination, autophagy, and the inflammatory response is dynamic and must be maintained at a homeostatic status for healthy cognitive functions in the brain (Figure 8A). Loss of this homeostasis leads to impaired memory performance in AD (Figure 8B), which can be rescued by administration of M01, the E3 ligase inhibitor (Figure 8C). Further experiments are necessary to better understand the function of individual HECT E3 ligase in enhancing autophagy processes and reducing NLRP3 inflammasome protein levels for the purpose of selecting the most promising candidates for the novel AD drug development.

Data availability statement

The original contributions presented in the study are included in the article/Supplementary material, further inquiries can be directed to the corresponding authors.

Ethics statement

The animal study was reviewed and approved by Taiwan Ministry of Science and Technology Guidelines for Animals' Ethical Treatment and Institutional Animal Care and Use Committee of Tzu Chi University, Taiwan.

Author contributions

IL and PS designed the experiments and wrote the manuscript. SJ assisted in behavioral experiments, performed immunofluorescence staining, and helped write manuscript. YY provided E3 ligase inhibitor (M01), advised in experimental design, and manuscript revision. H-JH performed and analyzed protein docking experiments. TP and PV assisted in treatment and animal experiments. C-CC advised on experimental design and hypothesis. All authors read and approved the final manuscript.

Funding

This work was funded by the Ministry of Science and Technology (MOST), Taiwan (MOST-107-2410-H320-001-MY3, MOST-110-2410-H-320-004-MY2), and Buddhist Tzu Chi Medical Foundation (TCMF-SP-108-04). This work also received partial financial support from the TMU Research Center of Cancer Translational Medicine from the Featured Areas Research Center Program within the framework of the Higher Education Sprout Project by the Ministry of Education (MOE) in Taiwan, and the Ministry of Health and Welfare (Health and Welfare Surcharge of Tobacco Products grant MOHW111-TDU-B-221-014013).

Acknowledgments

We sincerely thank Prof. Shun-Ping Huang, Hei-Jen Huang, and Hsiu Mei Hsieh-Li for experimental support. We also thank Sarayut Phasuk, Hsien-Ting Huang, Kai-Chi Liang, Dong-Rong Weih, and Dr.Ya-Wen Cheng for the helpful technique assistance. We thank Melissa Lo for the help in English Editing. We also appreciate the support provided by the Core Facility and Teaching Research Service Center (TRSC) at Tzu Chi University. The authors would like to thank the Tzu Chi University (TCU) Research Center for Big Data Teaching, Research and Statistic Consultation for providing statistic consultation assistance.

Conflict of interest

The authors declare that the research was conducted in the absence of any commercial or financial relationships that could be construed as a potential conflict of interest.

Publisher's note

All claims expressed in this article are solely those of the authors and do not necessarily represent those

of their affiliated organizations, or those of the publisher, the editors and the reviewers. Any product that may be evaluated in this article, or claim that may be made by its manufacturer, is not guaranteed or endorsed by the publisher.

Supplementary material

The Supplementary Material for this article can be found online at: https://www.frontiersin.org/articles/10.3389/fnagi.2022.916904/full#supplementary-material

References

Arqué, G., Fotaki, V., Fernández, D., De Lagrán, M. M., Arbonés, M. L., and Dierssen, M. (2008). Impaired spatial learning strategies and novel object recognition in mice haploinsufficient for the dual specificity Tyrosine-Regulated Kinase-1A (Dyrk1A). *PLoS ONE* 3:e2575. doi: 10.1371/journal.pone.0002575

Benzing, W. C., Wujek, J. R., Ward, E. K., Shaffer, D., Ashe, K. H., Younkin, S. G., et al. (1999). Evidence for glial-mediated inflammation in aged APPSW transgenic mice. *Neurobiol. Aging* 20, 581–589. doi: 10.1016/S0197-4580(99)00065-2

Biasizzo, M., and Kopitar-Jerala, N. (2020). Interplay between NLRP3 inflammasome and autophagy. *Front. Immunol.* 11:591803. doi: 10.3389/fimmu.2020.591803

Bieri, G., Lucin, K. M., O'brien, C. E., Zhang, H., Villeda, S. A., and Wyss-Coray, T. (2018). Proteolytic cleavage of Beclin 1 exacerbates neurodegeneration. *Mol. Neurodegener.* 13:68. doi: 10.1186/s13024-018-0302-4

Boland, B., Kumar, A., Lee, S., Platt, F. M., Wegiel, J., Yu, W. H., et al. (2008). Autophagy induction and autophagosome clearance in neurons: relationship to autophagic pathology in Alzheimer's disease. *J. Neurosci.* 28, 6926–6937. doi: 10.1523/JNEUROSCI.0800-08.2008

Businaro, R., Corsi, M., Asprino, R., Di Lorenzo, C., Laskin, D., Corbo, R. M., et al. (2018). Modulation of inflammation as a way of delaying Alzheimer's disease progression: the diet's role. *Curr. Alzheimer Res.* 15, 363–380. doi: 10.2174/1567205014666170829100100

Carroll, J. C., Rosario, E. R., Kreimer, S., Villamagna, A., Gentzschein, E., Stanczyk, F. Z., et al. (2010). Sex differences in β-amyloid accumulation in 3xTg-AD mice: role of neonatal sex steroid hormone exposure. *Brain Res.* 1366, 233–245. doi: 10.1016/j.brainres.2010.10.009

Chen, R.-H., Chen, Y.-H., and Huang, T.-Y. (2019). Ubiquitin-mediated regulation of autophagy. *J. Biomed. Sci.* 26:80. doi: 10.1186/s12929-019-0569-y

Chhangani, D., Upadhyay, A., Amanullah, A., Joshi, V., and Mishra, A. (2014). Ubiquitin ligase ITCH recruitment suppresses the aggregation and cellular toxicity of cytoplasmic misfolded proteins. *Sci. Rep.* 4, 5077–5077. doi: 10.1038/srep05077

Cho, M.-H., Cho, K., Kang, H.-J., Jeon, E.-Y., Kim, H.-S., Kwon, H.-J., et al. (2014). Autophagy in microglia degrades extracellular β-amyloid fibrils and regulates the NLRP3 inflammasome. *Autophagy* 10, 1761–1775. doi: 10.4161/auto.29647

Di Filippo, M., Sarchielli, P., Picconi, B., and Calabresi, P. (2008). Neuroinflammation and synaptic plasticity: theoretical basis for a novel, immune-centred, therapeutic approach to neurological disorders. *Trends Pharmacol. Sci.* 29, 402–412. doi: 10.1016/j.tips.2008.06.005

Giménez-Llort, L., Rivera-Hernández, G., Marín-Argany, M., Sánchez-Quesada, J. L., and Villegas, S. (2013). Early intervention in the 3xTg-AD mice with an amyloid β-antibody fragment ameliorates first hallmarks of Alzheimer disease. *MAbs* 5, 665–864. doi: 10.4161/mabs.25424

Glatigny, M., Moriceau, S., Rivagorda, M., Ramos-Brossier, M., Nascimbeni, A. C., Lante, F., et al. (2019). Autophagy is required for memory formation and reverses age-related memory decline. *Curr. Biol.* 29, 435–448.e8. doi: 10.1016/j.cub.2018.12.021

Griffin, W. S. T., Nicoll, J. A. R., Grimaldi, L. M. E., Sheng, J. G., and Mrak, R. E. (2000). The pervasiveness of interleukin-1 in Alzheimer pathogenesis: a role for specific polymorphisms in disease risk. *Exp. Gerontol.* 35, 481–487. doi: 10.1016/S0531-5565(00)00110-8

Hoffmann, S., Orlando, M., Andrzejak, E., Bruns, C., and Trimbuch, T. (2019). Light-activated ROS production induces synaptic autophagy. *J. Neurosci.* 39, 2163–2183. doi: 10.1523/JNEUROSCI.1317-18.2019

Holbrook, J. A., Jarosz-Griffiths, H. H., Caseley, E., Lara-Reyna, S., Poulter, J. A., Williams-Gray, C. H., et al. (2021). Neurodegenerative disease and the NLRP3 inflammasome. *Front. Pharmacol.* 12:643254. doi: 10.3389/fphar.2021.643254

Hylin, M. J., Zhao, J., Tangavelou, K., Rozas, N. S., Hood, K. N., Macgowan, J. S., et al. (2018). A role for autophagy in long-term spatial memory formation in male rodents. *J. Neurosci. Res.* 96, 416–426. doi: 10.1002/jnr.24121

Ising, C., Venegas, C., Zhang, S., Scheiblich, H., Schmidt, S. V., Vieira-Saecker, A., et al. (2019). NLRP3 inflammasome activation drives tau pathology. *Nature* 575, 669–673. doi: 10.1038/s41586-019-1769-z

Kálmán, J., Juhász, A., Laird, G., Dickens, P., Járdánházy, T., Rimanóczy, A., et al. (1997). Serum interleukin-6 levels correlate with the severity of dementia in Down syndrome and in Alzheimer's disease. *Acta Neurol. Scand.* 96, 236–240. doi: 10.1111/j.1600-0404.1997.tb00275.x

Karabeg, M. M., Grauthoff, S., Kollert, S. Y., Weidner, M., Heiming, R. S., Jansen, F., et al. (2013). 5-HTT deficiency affects neuroplasticity and increases stress sensitivity resulting in altered spatial learning performance in the Morris water maze but Not in the Barnes maze. *PLoS ONE* 8:e78238. doi: 10.1371/journal.pone.0078238

Karisetty, B. C., Bhatnagar, A., Armour, E. M., Beaver, M., Zhang, H., and Elefant, F. (2020). Amyloid-β Peptide impact on synaptic function and neuroepigenetic gene control reveal new therapeutic strategies for Alzheimer's disease. *Front. Mol. Neurosci.* 13:577622. doi: 10.3389/fnmol.2020.577622

Kwak, Y.-D., Wang, B., Li, J. J., Wang, R., Deng, Q., Diao, S., et al. (2012). Upregulation of the E3 ligase NEDD4-1 by oxidative stress degrades IGF-1 receptor protein in neurodegeneration. *J. Neurosci.* 32, 10971–10981. doi: 10.1523/JNEUROSCI.1836-12.2012

Liu, J., and Li, L. (2019). Targeting autophagy for the treatment of Alzheimer's disease: challenges and opportunities. *Front. Mol. Neurosci.* 12:203. doi: 10.3389/fnmol.2019.00203

Liu, Y.-M., Huangfu, W.-C., Huang, H.-L., Wu, W.-C., Chen, Y.-L., Yen, Y., et al. (2017). 1,4-Naphthoquinones as inhibitors of Itch, a HECT domain-E3 ligase, and tumor growth suppressors in multiple myeloma. *Eur. J. Med. Chem.* 140, 84–91. doi: 10.1016/j.ejmech.2017.09.011

Mizushima, N. (2007). Autophagy: process and function. *Genes Dev.* 21, 2861–2873. doi: 10.1101/gad.1599207

Moossavi, M., Parsamanesh, N., Bahrami, A., and Atkin, S. L. (2018). Role of the NLRP3 inflammasome in cancer. *Mol. Cancer* 17:158. doi: 10.1186/s12943-018-0900-3

Morrison, C. (2016). Hope for anti-amyloid antibodies surges, yet again. *Nat. Biotechnol.* 34, 1082–1083. doi: 10.1038/nbt1116-1082b

Nixon, R. A., Wegiel, J., Kumar, A., Yu, W. H., Peterhoff, C., Cataldo, A., et al. (2005). Extensive involvement of autophagy in Alzheimer disease: an immuno-electron microscopy study. *J. Neuropathol. Exp. Neurol.* 64, 113–122. doi: 10.1093/jnen/64.2.113

Ozcelik, S., Fraser, G., Castets, P., Schaeffer, V., Skachokova, Z., Breu, K., et al. (2013). Rapamycin attenuates the progression of tau pathology in P301S tau transgenic mice. *PLoS ONE* 8:e62459. doi: 10.1371/journal.pone.0062459

Pei, G., Buijze, H., Liu, H., Moura-Alves, P., Goosmann, C., Brinkmann, V., et al. (2017). The E3 ubiquitin ligase NEDD4 enhances killing of membrane-perturbing intracellular bacteria by promoting autophagy. *Autophagy* 13, 2041–2055. doi: 10.1080/15548627.2017.1376160

Penazzi, L., Lorengel, J., Sündermann, F., Golovyashkina, N., Marre, S., Mathis, C. M. B., et al. (2017). DMSO modulates CNS function in a preclinical Alzheimer's disease model. *Neuropharmacology* 113, 434–444. doi: 10.1016/j.neuropharm.2016.10.020

Pérez-Villegas, E. M., Pérez-Rodríguez, M., Negrete-Díaz, J. V., Ruiz, R., Rosa, J. L., De Toledo, G. A., et al. (2020). HERC1 ubiquitin ligase is required for hippocampal learning and memory. *Front. Neuroanat.* 14:592797. doi: 10.3389/fnana.2020.592797

Phasuk, S., Jasmin, S., Pairojana, T., Chang, H.-K., Liang, K.-C., and Liu, I. Y. (2021a). Lack of the peroxiredoxin 6 gene causes impaired spatial memory and abnormal synaptic plasticity. *Mol. Brain* 14:72. doi: 10.1186/s13041-021-00779-6

Phasuk, S., Pairojana, T., Suresh, P., Yang, C.-H., Roytrakul, S., Huang, S.-P., et al. (2021b). Enhanced contextual fear memory in peroxiredoxin 6 knockout mice is associated with hyperactivation of MAPK signaling pathway. *Mol. Brain* 14:42. doi: 10.1186/s13041-021-00754-1

Pickford, F., Masliah, E., Britschgi, M., Lucin, K., Narasimhan, R., Jaeger, P. A., et al. (2008). The autophagy-related protein beclin 1 shows reduced expression in early Alzheimer disease and regulates amyloid β accumulation in mice. *J. Clin. Invest.* 118, 2190–2199. doi: 10.1172/JCI33585

Pietropaolo, S., Feldon, J., and Yee, B. K. (2014). Environmental enrichment eliminates the anxiety phenotypes in a triple transgenic mouse model of Alzheimer's disease. *Cogn. Affect. Behav. Neurosci.* 14, 996–1008. doi: 10.3758/s13415-014-0253-3

Rosenzweig, N., Dvir-Szternfeld, R., Tsitsou-Kampeli, A., Keren-Shaul, H., Ben-Yehuda, H., Weill-Raynal, P., et al. (2019). PD-1/PD-L1 checkpoint blockade harnesses monocyte-derived macrophages to combat cognitive impairment in a tauopathy mouse model. *Nat. Commun.* 10:465. doi: 10.1038/s41467-019-08352-5

Saitoh, T., and Akira, S. (2016). Regulation of inflammasomes by autophagy. *J. Allergy Clin. Immunol.* 138, 28–36. doi: 10.1016/j.jaci.2016.05.009

Sanarico, A. G., Ronchini, C., Croce, A., Memmi, E. M., Cammarata, U. A., De Antoni, A., et al. (2018). The E3 ubiquitin ligase WWP1 sustains the growth of acute myeloid leukaemia. *Leukemia* 32, 911–919. doi: 10.1038/leu.2017.342

Sato, A., Kasai, S., Kobayashi, T., Takamatsu, Y., Hino, O., Ikeda, K., et al. (2012). Rapamycin reverses impaired social interaction in mouse models of tuberous sclerosis complex. *Nat. Commun.* 3:1292. doi: 10.1038/ncomms2295

Scudder, S. L., Goo, M. S., Cartier, A. E., Molteni, A., Schwarz, L. A., Wright, R., et al. (2014). Synaptic strength is bidirectionally controlled by opposing activity-dependent regulation of Nedd4-1 and USP8. *J. Neurosci.* 34, 16637–16649. doi: 10.1523/JNEUROSCI.2452-14.2014

Shi, C.-S., Shenderov, K., Huang, N.-N., Kabat, J., Abu-Asab, M., Fitzgerald, K. A., et al. (2012). Activation of autophagy by inflammatory signals limits IL-1β production by targeting ubiquitinated inflammasomes for destruction. *Nat. Immunol.* 13, 255–263. doi: 10.1038/ni.2215

Stimmell, A. C., and Baglietto-Vargas, D. (2019). Impaired spatial reorientation in the 3xTg-AD mouse model of Alzheimer's disease. 9:1311. doi: 10.1038/s41598-018-37151-z

Varinthra, P., Ganesan, K., Huang, S.-P., Chompoopong, S., Eurtivong, C., Suresh, P., et al. (2021). The 4-(Phenylsulfanyl) butan-2-one improves impaired fear memory retrieval and reduces excessive inflammatory response in triple transgenic Alzheimer's disease mice. *Front. Aging Neurosci.* 13:615079. doi: 10.3389/fnagi.2021.615079

Wang, H., Sun, R. Q., Camera, D., Zeng, X. Y., Jo, E., Chan, S. M., et al. (2016). Endoplasmic reticulum stress up-regulates Nedd4-2 to induce autophagy. *FASEB J.* 30, 2549–2556. doi: 10.1096/fj.201500119

Wang, M.-M., Feng, Y.-S., Yang, S.-D., Xing, Y., Zhang, J., Dong, F., et al. (2019a). The relationship between autophagy and brain plasticity in neurological diseases. *Front. Cell. Neurosci.* 13, 228–228. doi: 10.3389/fncel.2019.00228

Wang, W.-Y., Tan, M.-S., Yu, J.-T., and Tan, L. (2015). Role of pro-inflammatory cytokines released from microglia in Alzheimer's disease. *Ann. Transl. Med.* 3:136. doi: 10.3978/j.issn.2305-5839.2015.03.49

Wang, Y., Meng, C., Zhang, J., Wu, J., and Zhao, J. (2019b). Inhibition of GSK-3β alleviates cerebral ischemia/reperfusion injury in rats by suppressing NLRP3 inflammasome activation through autophagy. *Int. Immunopharmacol.* 68, 234–241. doi: 10.1016/j.intimp.2018.12.042

Yang, D.-S., Stavrides, P., Mohan, P. S., Kaushik, S., Kumar, A., Ohno, M., et al. (2010). Reversal of autophagy dysfunction in the TgCRND8 mouse model of Alzheimer's disease ameliorates amyloid pathologies and memory deficits. *Brain* 134, 258–277. doi: 10.1093/brain/awq341

Yuen, E. Y., Wei, J., Liu, W., Zhong, P., Li, X., and Yan, Z. (2012). Repeated stress causes cognitive impairment by suppressing glutamate receptor expression and function in prefrontal cortex. *Neuron* 73, 962–977. doi: 10.1016/j.neuron.2011.12.033

Zhang, Z., Yang, X., Song, Y.-Q., and Tu, J. (2021). Autophagy in Alzheimer's disease pathogenesis: therapeutic potential and future perspectives. *Ageing Res. Rev.* 72:101464. doi: 10.1016/j.arr.2021.101464

Zhao, S., Li, X., Wang, J., and Wang, H. (2021). The role of the effects of autophagy on NLRP3 inflammasome in inflammatory nervous system diseases. *Front. Cell Dev. Biol.* 9:657478. doi: 10.3389/fcell.2021.657478

frontiers | Frontiers in Aging Neuroscience

TYPE Original Research
PUBLISHED 12 October 2022
DOI 10.3389/fnagi.2022.892590

OPEN ACCESS

EDITED BY
Fushun Wang,
Nanjing University of Chinese Medicine, China

REVIEWED BY
Wei Wang,
University of Toronto, Canada
Boncho Ku,
Korea Institute of Oriental Medicine (KIOM), South Korea

*CORRESPONDENCE
Hae Ri Na
neuna102@paran.com
Yoo Kyoung Park
ypark@khu.ac.kr

†These authors have contributed equally to this work and share first authorship

‡These authors have contributed equally to this work

SPECIALTY SECTION
This article was submitted to Alzheimer's Disease and Related Dementias, a section of the journal Frontiers in Aging Neuroscience

RECEIVED 09 March 2022
ACCEPTED 20 September 2022
PUBLISHED 12 October 2022

CITATION
Park HK, Choi SH, Kim S, Park U, Kang SW, Jeong JH, Moon SY, Hong CH, Song H-S, Chun B-O, Lee SM, Choi M, Park KW, Kim BC, Cho SH, Na HR and Park YK (2022) Functional brain changes using electroencephalography after a 24-week multidomain intervention program to prevent dementia. *Front. Aging Neurosci.* 14:892590. doi: 10.3389/fnagi.2022.892590

Functional brain changes using electroencephalography after a 24-week multidomain intervention program to prevent dementia

Hee Kyung Park[1,2†], Seong Hye Choi[3†], SeonMyeong Kim[4], Ukeob Park[4], Seung Wan Kang[4,5], Jee Hyang Jeong[1], So Young Moon[6], Chang Hyung Hong[7], Hong-Sun Song[8], Buong-O Chun[9], Sun Min Lee[6], Muncheong Choi[10], Kyung Won Park[11], Byeong C. Kim[12], Soo Hyun Cho[12], Hae Ri Na[13*‡] and Yoo Kyoung Park[14,15*‡]

[1]Department of Neurology, Ewha Womans University School of Medicine, Seoul, South Korea, [2]Department of Mental Health Care of Older People, Division of Psychiatry, University College London, London, United Kingdom, [3]Department of Neurology, Inha University School of Medicine, Incheon, South Korea, [4]iMediSync Inc., Seoul, South Korea, [5]Data Center for Korean EEG, College of Nursing, Seoul National University, Seoul, South Korea, [6]Department of Neurology, Ajou University School of Medicine, Suwon, South Korea, [7]Department of Psychiatry, Ajou University School of Medicine, Suwon, South Korea, [8]Department of Sports Sciences, Korea Institute of Sports Science, Seoul, South Korea, [9]Graduate School of Physical Education, College of Arts and Physical Education, Myongji University, Seoul, South Korea, [10]Department of Sports and Health Science, Shinhan University, Uijeongbu-si, South Korea, [11]Department of Neurology, Dong-A University College of Medicine, Busan, South Korea, [12]Department of Neurology, Chonnam National University Medical School and Hospital, Gwangju, South Korea, [13]Department of Neurology, Bobath Memorial Hospital, Seongnam, South Korea, [14]Department of Medical Nutrition, Graduate School of East-West Medical Nutrition, Kyung Hee University, Yongin, South Korea, [15]Department of Food Innovation and Health, Graduate School of East-West Medical Nutrition, Kyung Hee University, Yongin, South Korea

Quantitative electroencephalography (QEEG) has proven useful in predicting the response to various treatments, but, until now, no study has investigated changes in functional connectivity using QEEG following a lifestyle intervention program. We aimed to investigate neurophysiological changes in QEEG after a 24-week multidomain lifestyle intervention program in the SoUth Korean study to PrEvent cognitive impaiRment and protect BRAIN health through lifestyle intervention in at-risk elderly people (SUPERBRAIN). Participants without dementia and with at least one modifiable dementia risk factor, aged 60–79 years, were randomly assigned to the facility-based multidomain intervention (FMI) (n = 51), the home-based multidomain intervention (HMI) (n = 51), and the control group (n = 50). The analysis of this study included data from 44, 49, and 34 participants who underwent EEG at baseline and at the end of the study in the FMI, HMI, and control groups, respectively. The spectrum power and power ratio of EEG were calculated. Source cortical current density and functional connectivity were estimated by standardized low-resolution brain electromagnetic tomography. Participants who received the intervention showed increases in the power of the beta1

and beta3 bands and in the imaginary part of coherence of the alpha1 band compared to the control group. Decreases in the characteristic path lengths of the alpha1 band in the right supramarginal gyrus and right rostral middle frontal cortex were observed in those who received the intervention. This study showed positive biological changes, including increased functional connectivity and higher global efficiency in QEEG after a multidomain lifestyle intervention.

Clinical trial registration: [https://clinicaltrials.gov/ct2/show/NCT03980392] identifier [NCT03980392].

KEYWORDS

cognitive impairment, biomarkers, quantitative electroencephalography, dementia, multidomain intervention

Introduction

Quantitative electroencephalography (QEEG) is a real-time, low-cost, non-invasive functional marker that reflects synaptic activity in the brain (Smailovic and Jelic, 2019). In Alzheimer's disease (AD), the hallmarks of EEG abnormalities include a shift of the power spectrum, consisting of an increase in delta power and theta power and a parallel decrease in alpha power and beta power, and along with a decrease in the coherence of fast rhythms (Jeong, 2004). Increased theta power and decreased beta power, the earliest changes in patients with AD, were also shown in amnestic mild cognitive impairment (aMCI) (Roh et al., 2011; Han et al., 2021). People with MCI who progressed to AD had lower alpha relative power and absolute power than those with stable MCI, indicating that resting state alpha activity declines gradually as cognitive functions are progressively impaired (Lejko et al., 2020). One important feature of QEEG in AD and MCI is the loss of small-world architecture (Stam et al., 2007; Zeng et al., 2015). In addition, QEEG is correlated with scores on the Mini Mental State Examination (MMSE) (Engels et al., 2015), fluid biomarkers (Jelic et al., 1998; Smailovic et al., 2018), and structural changes (Babiloni et al., 2009, 2013, 2015) in AD.

QEEG has proven useful in predicting the response to treatment. Previous studies have demonstrated that delta and theta activity were decreased by the use of acetylcholinesterase inhibitors (Kogan et al., 2001; Adler et al., 2004; Gianotti et al., 2008). Although several studies reported changes in QEEG after a single-domain intervention program such as cognitive training or physical exercise (Huang et al., 2016; Gandelman-Marton et al., 2017), the intervention studies that assessed biological changes using EEG had small sample sizes. Furthermore, until now, no study has investigated changes in functional connectivity using QEEG following a multidomain lifestyle intervention program.

The Finnish Geriatric Intervention Study to Prevent Cognitive Impairment and Disability (FINGER) study is representative of studies that aim to investigate the efficacy of a multidomain intervention program in preventing dementia. This 2-year, double-blind, randomized controlled trial found that multidomain interventions could improve cognitive function in at-risk older adults (Ngandu et al., 2015). This led to a major shift in the focus of dementia research to interventions with modifiable risk factors. However, the Multidomain Alzheimer Preventive Trial, a 3-year, randomized, placebo-controlled trial, failed to show prevention of cognitive decline (Andrieu et al., 2017). Furthermore, there were no differences in structural brain imaging between the intervention group and the control group in the FINGER study (Stephen et al., 2019), suggesting that this multidomain intervention program produced no demonstrable biological effects. The mixed results of a multidomain intervention studies with respect to dementia prevention point to the need for further investigation of the biological effects of such programs.

We demonstrated that the multidomain lifestyle intervention program designed to be suitable for older Korean individuals was feasible and effective in the SoUth Korean study to PrEvent cognitive impaiRment and protect BRAIN health through lifestyle intervention in an at-risk elderly people (SUPERBRAIN) (Park et al., 2020; Moon et al., 2021). In this study, we aimed to investigate the impact of a 24-week multidomain lifestyle intervention on functional brain changes in QEEG using data from the SUPERBRAIN. We hypothesized that there would be a difference in the electrophysiologic changes in QEEG from baseline to the study end between the intervention and control groups.

Materials and methods

Study population

A total of 152 participants aged 60–79 years from eight medical centers were enrolled in the SUPERBRAIN study, a

24-week, multicenter, outcome assessor-blinded, randomized controlled trial. Details of the study protocol have been described previously (Park et al., 2020).

The inclusion criteria were as follows: (1) 60–79 years of age; (2) at least one modifiable risk factor for dementia such as hypertension, diabetes mellitus (DM), dyslipidemia, smoking, obesity, abdominal obesity, metabolic syndrome, low level of education (≤9 years), social inactivity, and physical inactivity; (3) *z* score on the Korean MMSE (K-MMSE) above −1.5; (4) Korean Instrumental Activities of Daily Living score <0.4 (Chin et al., 2018); (5) ability to read and write; and (6) presence of a reliable informant. Participants were excluded if they had major psychiatric illnesses, dementia, substantial cognitive decline, other neurodegenerative diseases, cancer over the past 5 years, serious or unstable symptomatic cardiovascular diseases, stent insertion in coronary vessels within the previous year, and other serious medical conditions. In addition, if subjects were uncooperative or not able to take part in the intervention programs, they were excluded from this study.

Figure 1 shows a flow chart of the study. All participants were randomly assigned to three groups, consisting of the facility-based multidomain intervention (FMI, n = 51), home-based multidomain intervention (HMI, n = 51), and control group (n = 50), in a 1:1:1: ratio using a permuted block randomization method, with block sizes of three and six, through SAS macro programming, and was stratified by the participating center. The allocation sequence was known only to the independent statistical specialist. Cognitive outcome assessors remained blind to the assigned groups; they were not involved in the intervention activities. Participants were instructed not to discuss their study involvement with the outcome assessor. A total of 45, 49, and 42 participants completed the study from the FMI, HMI, and control groups, respectively. Among them, EEG was performed at baseline and at the end of the study in 45, 49, and 36 participants in the FMI, HMI, and control groups, respectively. In this study, we included one participant in the HMI group who underwent follow-up EEG at the early termination of the study. Due to bad EEG quality, 1, 1, and 2 participants in the FMI, HMI, and control groups, respectively, were excluded from the EEG analysis. Finally, the analysis of this study included data of 44, 49, and 34 participants in the FMI, HMI, and control groups, respectively (**Figure 1**). Because EEG signals are very sensitive, measurements can contain various noise signals. We considered different types of noise (vertical electrooculogram, horizontal electrooculogram, electromyography, body shaking, swallowing, etc.). Nevertheless, if noise appears strongly throughout the data, it may lose its meaning as an EEG signal. Therefore, the criteria for excluded data were determined after checking the signal quality of the raw data. More information can be found in the **Supplementary Figure 1**.

No differences in age, sex, education level, diagnosis of MCI, vascular risk factors, depression scale, and cognition were found between participants whose EEG data were analyzed (n = 127) and those who were excluded (n = 25; **Supplementary Table 1**).

Intervention and evaluation

The FMI and the HMI intervention groups received intervention consisting of five components (**Supplementary Figure 2**). Management of metabolic and vascular risk factors consisted of six sessions with a research nurse, including two sessions with an added study physician. At each session, blood pressure, height, weight, waist circumference, smoking, and alcohol drinking were assessed. Participants were given information about their vascular risk factors and were offered prescriptions if necessary. Cognitive training consisted of computerized cognitive training (in-house program) and workbooks targeting various cognitive domains, especially memory, for 50 min twice weekly. The physical exercise program, which consisted of aerobic exercise, muscle strengthening activities, balance training, and exercise to enhance flexibility, was provided for 60 min three times weekly by trained exercise professionals. Based on the Mediterranean-Dietary Approaches to Stop Hypertension diet Intervention for Neurodegenerative Delay diet, called the MIND diet, the nutritional intervention was designed by nutritionists to be familiar to older Koreans. Three individual sessions (tailored diet for the participant) and seven group sessions (education on the MIND diet, practical exercises via a cooking lessons) were provided by study nutritionists. The motivation enhancement program included four 50-min group sessions to educate the importance of lifestyle changes for the prevention of dementia. Participants were also encouraged to engage with the intervention program by watching pop-up pre-recorded video messages from family members. Achievement in the motivational program was assessed by participants themselves. The waitlist control group received a booklet that included lifestyle guidelines to prevent dementia. The multidomain intervention program was provided to the control group after the end of the study.

Demographic and clinical factors evaluated included age, sex, education, obesity, abdominal obesity, physical activity, social activity, apolipoprotein E genotype, and family history of dementia. Medical history was assessed, including hypertension, DM, dyslipidemia, cardiac disease, history of stroke, and MCI. Current smoking and current alcohol consumption were also evaluated. The K-MMSE and the Repeatable Battery for the Assessment of Neuropsychological Status (RBANS) were used as neuropsychological tests both at baseline and at the end of the study. Blood pressure, abdominal circumference, body mass index, total cholesterol, triglycerides, low-density lipoprotein (LDL) cholesterol, high-density lipoprotein (HDL) cholesterol, glucose, and hemoglobin A1c were measured at baseline and at the end of the study.

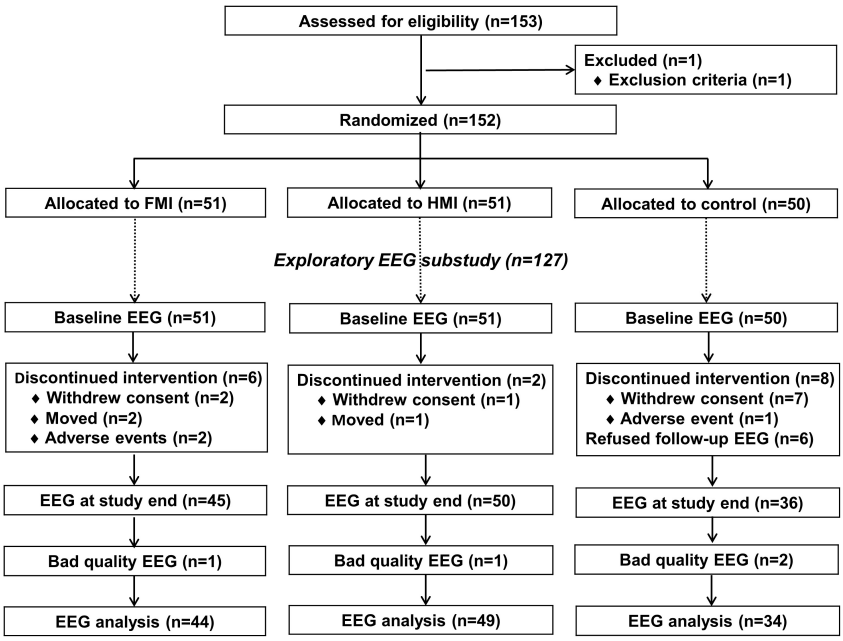

FIGURE 1
Diagram depicting the exploratory EEG substudy in the SUPERBRAIN trial. FMI, facility-based multidomain intervention; HMI, home-based multidomain intervention; EEG, electroencephalography.

Electroencephalography analysis

Resting-state EEG was recorded over a 3-min period with eyes open and another 3-min period with eyes closed using 19 electrodes based on the international 10–20 system (Fp1, Fp2, F7, F3, Fz, F4, F8, T7, C3, Cz, C4, T8, P7, P3, Pz, P4, P8, O1, and O2) at baseline and at the end of the study. The EEG signal was digitized after it was filtered with a band pass of 0.5–70 Hz.

Artifacts were removed in two steps. First, non-stationary bad epochs were totally rejected. Second, stationary bad components related to eye movement, electrocardiography, or electromyography were removed by adaptive mixture-independent component analysis (AMICA). At the sensor level, the absolute power of EEG, the square of the amplitudes, was calculated using fast Fourier transform (FFT) spectral analysis in each of the following eight frequency bands: delta (1–4 Hz); theta (4–8 Hz); alpha1 (8–10 Hz); alpha2 (10–12 Hz); beta1 (12–15 Hz); beta2 (15–20 Hz); beta3 (20–30 Hz); and gamma (30–45 Hz). To calculate the relative power, the absolute power of each frequency band was divided by the total power. The band power ratios, including the theta-to-alpha (TAR), delta-to-alpha (DAR), theta-to-beta (TBR), and theta-to-beta2 (TB2R) ratios, were calculated. In the source-level analysis, the standardized low-resolution brain electromagnetic tomography (sLORETA) was used with 68 regions of interest (ROIs) based on the Desikan-Killiany atlas. The imaginary part of coherence (iCoh) was calculated as functional connectivity among 68 ROIs at eight frequencies (Nolte et al., 2004). Every EEG feature was analyzed by the cloud-based QEEG analysis platform, iSyncBrain® (iMediSync Inc., Republic of Korea[1]).

An undirected binary network was constructed using the iCoh matrix of each frequency band taking the density of the network (25%) into consideration (Hassan et al., 2014; Liu et al., 2017). Measurements of network nodes and edges, defined as the 68 ROIs, consisted of node degree, clustering coefficient, characteristic path length, and small-worldness (Xia et al., 2013). In this study, the characteristic path length was used to measure functional integration (Rubinov and Sporns, 2010).

Ethical issues

Written informed consent was obtained from all participants by a study physician. The study protocol was approved by Inha University Hospital Institutional Review Board (IRB)(INHAUH-2018-11-022), Ewha Womans University Mokdong Hospital IRB (EUMC-2019-04-013), Ajou University Hospital IRB (AJIRB-BMR-SUR-19-070 and AJIRB-BMR-SUR-19-077), Dong-A University Hospital IRB (DAUHIRB-19-078), and Chonnam National University IRB (CNUH-2019-139) before participant enrollment in the study. The trial has been registered with ClinicalTrials.gov (NCT03980392). The study was carried out in accordance with

1 https://isyncbrain.com/

the International Conference on Harmonization Good Clinical Practice Guideline.

Statistical analysis

The modified-intention-to-treat population were used in the analysis. The chi-square test for categorical variables and one-way analysis of variance for continuous variables were used to compare baselines characteristics. Since the triglyceride level did not show a normal distribution, the Kruskal–Wallis test was used to compare the triglyceride level between groups. Analysis of covariance (ANCOVA) was used to compare the RBANS index scores among the groups, adjusted for baseline score. The independent *t*-test was used for the frequency band power of each channel on the 68 ROIs and iCoh among the 68 ROIs between the intervention and control groups. Since changes in characteristic path length of each frequency band in the 68 ROIs did not show a normal distribution, Mann-Whitney U test was used to compare changes in the characteristic path length of each frequency band between groups. And to deal with missing data, multiple imputations were performed using a fully conditional specification implemented as a MICE algorithm (van Buuren and Groothuis-Oudshoorn, 2011). We performed predictive mean matching with 20 iterations of the imputation model. For this analysis, the MICE package of R statistical software version 4.0.5 (R Foundation[2]) was used. Linear regression adjusted for

2 https://www.r-project.org

TABLE 1 Clinical characteristics of all participants in this study.

	FMI group (*N* = 44)	HMI group (*N* = 49)	Control group (*N* = 34)	*P*-value
Demographic factors				
Age at baseline, years	71.5 ± 5.0	70.9 ± 5.0	69.6 ± 4.9	0.225
Number of women	31 (70.56%)	36 (73.5%)	28 (82.4%)	0.485
Education, years	10.1 ± 4.7	9.9 ± 4.9	10.1 ± 4.9	0.976
Obesity	14 (31.8%)	23 (46.9%)	13 (40.6%)	0.318
Abdominal obesity	15 (34.1%)	20 (40.8%)	16 (47.1%)	0.507
Low physical activity	21 (47.7%)	26 (53.1%)	16 (47.1%)	0.825
Low social activity	10 (22.7%)	13 (26.5%)	11 (34.4%)	0.525
Apolipoprotein E ε4 carrier	6 (13.6%)	13 (26.5%)	5 (14.7%)	0.247
Family history of dementia	7 (15.9%)	14 (28.6%)	6 (17.6%)	0.290
Medical history				
Hypertension	21 (47.7%)	26 (53.1%)	17 (50.0%)	0.878
Diabetes mellitus	8 (18.2%)	13 (26.5%)	9 (26.5%)	0.576
Dyslipidemia	20 (45.5%)	26 (53.1%)	20 (58.8%)	0.493
Cardiac disease	4 (9.1%)	3 (6.1%)	2 (5.9%)	0.829
History of stroke	4 (9.1%)	3 (6.1%)	6 (17.6%)	0.230
Mild cognitive impairment	15 (34.1%)	15 (30.6%)	5 (14.7%)	0.144
Vascular factors				
Systolic blood pressure, mmHg	128.3 ± 16.1	127.1 ± 12.9	131.7 ± 17.3	0.402
Diastolic blood pressure, mmHg	74.5 ± 10.5	74.4 ± 10.3	74.8 ± 8.4	0.987
Total cholesterol, mg/dl	185.6 ± 38.2	189.2 ± 36.2	176.2 ± 42.2	0.322
LDL-cholesterol, mg/dl	105.1 ± 36.1	109.9 ± 33.5	98.5 ± 32.2	0.329
Triglyceride, mg/dl†	117.0 (78.0, 175.0)	113.0 (91.0, 194.0)	112.0 (82.0, 147.5)	0.875
HDL-cholesterol, mg/dl	53.8 ± 12.7	53.9 ± 14.6	52.9 ± 14.2	0.938
Body Mass Index, kg/m^2	23.7 ± 2.1	24.2 ± 3.1	25.3 ± 3.0	0.056
Abdominal circumference, cm	82.8 ± 7.2	84.5 ± 9.4	85.9 ± 8.4	0.256
Lifestyle factors				
Current smokers	2 (4.5%)	1 (2.0%)	0 (0.0%)	0.625
Current alcohol drinkers	12 (27.3%)	8 (16.3%)	10 (29.4%)	0.294
Cognition				
K-MMSE	28.2 ± 1.7	27.9 ± 1.8	27.3 ± 2.5	0.123
RBANS total scale index score	101.4 ± 19.5	101.0 ± 16.1	103.6 ± 18.2	0.795

Values are shown as the mean ± SD or *n* (%). FMI, facility-based multidomain intervention; HMI, home-based multidomain intervention; LDL, low density lipoprotein; HDL, high density lipoprotein; K-MMSE, Korean Mini-Mental State Examination; RBANS, Repeatable Battery for the Assessment of Neuropsychological Status. *P*-value was calculated from the one-way of variance for the numerical data or the chi-square test for the categorical data.
†Results are median and interquartile range and *p*-value was calculated from the Kruskal–Wallis test.

age, sex, and education was used to examine the relationship between the change in the characteristic path length of each frequency band in each of the 68 ROIs and the change in the RBANS index score in each of the FMI and HMI groups. The significance of each p value in the 68 ROIs was tested by controlling the false discovery rate (FDR) with the Benjamini-Hochberg procedure for multiple testing corrections (Benjamini and Hochberg, 1995). Statistical analyses were performed with IBM SPSS version 26 (IBM, Armonk, NY, USA). Statistical significance was set at $p < 0.05$.

Results

The baseline clinical characteristics of all participants are shown in Table 1. No differences were found in demographic factors, medical history, vascular risk factors, lifestyle factors, and cognition among the three groups. Changes in the total scale index score ($p = 0.002$) and visuoconstruction index scores ($p < 0.001$) of the RBANS between pre-intervention and post-intervention showed improvement in all intervention groups including FMI and HMI groups, compared to the control group. Compared with the control group, the RBANS total scale index score and the visuoconstruction index score were also significantly improved in each of the FMI and HMI groups (Table 2). In addition, a statistical trend toward improvement was observed in the attention index score in the HMI group ($p = 0.099$) and in the delayed memory index score in the FMI group ($p = 0.050$).

Changes in quantitative electroencephalography parameters in all intervention groups

The sensor-level analysis of EEG showed that an accelerating pattern of rhythm with alph1 decreased at F7 ($p = 0.026$), F8 ($p = 0.044$), C3 ($p = 0.049$), and T6 ($p = 0.040$) in all intervention groups, including the FMI and HMI groups, compared with the control group (Figure 2A). In addition, increases in the relative power of the beta1 band in the occipital region ($p = 0.041$) and in the absolute power of the beta3 band in the right parietal region ($p = 0.022$) were observed in all intervention groups compared with the control group (Figures 2B,C). Although these differences were not statistical significant ($p = 0.079$), the intervention groups showed an increasing tendency of occipital alpha peak frequency (mean difference = 0.017) in the O2 area, whereas the control group showed the opposite pattern (mean difference = −0.242). The functional connectivity analysis showed an increase in the iCoh of the alpha1 band, the default resting-state oscillating rhythm, in all intervention groups, whereas the control group showed the opposite results (Figure 3A). Compared to the control group,

TABLE 2 Mean changes in the index scores of the Repeatable Battery for the Assessment of Neuropsychological Status.

Index score	Baseline scores				Changes from baseline to study end				*P*-value*			
	FMI ($n = 44$)	HMI ($n = 49$)	FMI + HMI ($n = 93$)	Control ($n = 34$)	FMI ($n = 44$)	HMI ($n = 49$)	FMI + HMI ($n = 93$)	Control ($n = 34$)	FMI vs. control	HMI vs. control	FMI + HMI vs. control
Total scale	101.4 ± 19.5	101.0 ± 16.1	101.2 ± 17.7	103.6 ± 18.2	5.4 ± 7.7	5.4 ± 8.2	5.4 ± 7.9	− 0.03 ± 9.3	0.006	0.007	0.002
Immediate memory	102.2 ± 13.6	99.0 ± 14.7	100.5 ± 14.2	102.2 ± 14.5	4.7 ± 9.3	3.5 ± 12.7	4.1 ± 11.2	3.6 ± 10.3	0.603	0.655	0.995
Visuoconstruction	93.6 ± 16.8	94.2 ± 15.5	93.9 ± 16.0	93.7 ± 13.9	1.2 ± 14.2	0.8 ± 14.6	1.0 ± 14.3	− 8.5 ± 11.3	0.001	0.001	<0.001
Language	104.9 ± 15.9	108.2 ± 13.4	106.6 ± 14.7	108.7 ± 12.9	1.4 ± 12.5	1.7 ± 12.6	1.6 ± 12.5	0.6 ± 11.2	0.539	0.686	0.933
Attention	104.4 ± 18.5	102.8 ± 16.6	103.6 ± 17.5	101.8 ± 17.5	0.02 ± 8.5	2.5 ± 9.6	1.3 ± 9.1	− 0.5 ± 10.8	0.588	0.099	0.208
Delayed memory	94.5 ± 16.5	94.1 ± 14.6	94.3 ± 15.5	100.4 ± 16.4	10.3 ± 10.2	9.2 ± 12.1	9.7 ± 11.2	4.6 ± 9.3	0.050	0.383	0.139

Values are shown as the mean ± SD. RBANS, Repeatable Battery for the Assessment of Neuropsychological Status; FMI, facility-based multidomain intervention; HMI, home-based multidomain intervention.
*Analysis of covariance with each baseline score as a covariate.

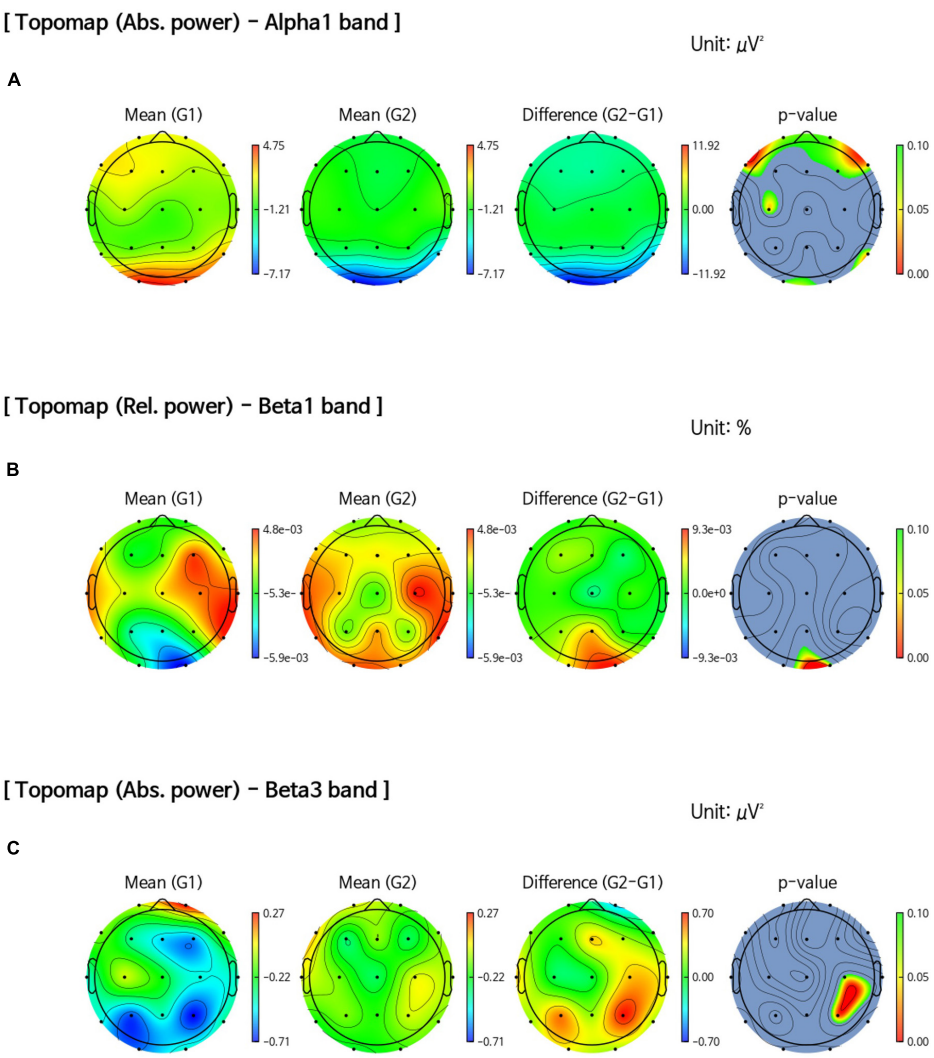

FIGURE 2
Comparison of band power changes between all intervention and control groups. **(A)** Difference between post-intervention and pre-intervention in the control group (G1) showed an increase in the absolute power of the alpha1 band in the frontal, central, and temporal regions than in all intervention groups (G2). **(B)** An increase in the relative power of the beta1 band in the occipital region (p = 0.041) after the intervention was observed in all intervention groups (G2) compared with the control group (G1). **(C)** An increase in the absolute power of the beta3 band in the right parietal region (p = 0.022) after the intervention was observed in all intervention groups (G2) compared with the control group (G1).

the characteristic path length of alpha1 band was decreased in the right supramarginal gyrus (p = 0.003) and right rostral middle frontal cortex (p = 0.003) in all intervention groups after multiple imputation for missing data (Table 3).

Changes in quantitative electroencephalography parameters in facility-based multidomain intervention group

In the FMI group compared to the control group, sensor-level analysis showed a decrease in the absolute power of the alpha2 band (p = 0.034) in the temporal area and a decrease in the relative power of the alpha1 band (p = 0.035) in the left temporal cortex (T3). Additionally, an increase in the absolute power of the beta3 band was shown in the right parietal area (P4, p = 0.038) in the FMI group compared to the control group. FMI group exhibited an increasing tendency of the occipital alpha peak frequency in the O2 area (mean difference = 0.069) compared to the controls (mean difference = −0.242), but the difference was not statistically significant (p = 0.089). The functional connectivity analysis showed an increase in the iCoh of the alpha1 band, the default resting-state oscillating rhythm, in the FMI group compared to the control group (Figure 3B). Brain network analysis showed a decreased characteristic path

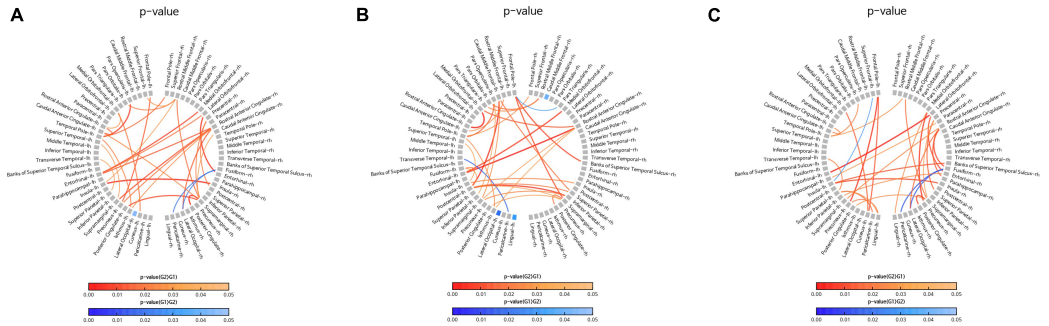

FIGURE 3
Comparison of changes in the imaginary part of coherence (iCoh) of the alpha1 band. Regions with significant differences in the iCoh changes between two groups are shown in the figures. Red lines represent a significant increase in the iCoh of the alpha1 band in the intervention group (G2) than in the control group (G1). Blue lines represent a significant increase in the iCoh of the alpha1 band in the control group (G1) than in the intervention group (G2). **(A)** Comparison of the control group (G1) with all intervention groups (G2), including facility-based multidomain intervention (FMI) and home-based multidomain intervention (HMI) groups. **(B)** Comparison of the FMI group (G2) with the control group (G1). **(C)** Comparison of the HMI group (G2) with the control group (G1).

length of alpha1 band in the right rostral middle frontal cortex (p = 0.007) in the FMI group compared to the control group (Table 3). The control group showed a decrease in characteristic path length (p = 0.002) compared with the FMI group in the right lateral occipital cortex (Table 3).

Changes in quantitative electroencephalography parameters in home-based multidomain intervention group

In a comparison between the HMI and the control groups, the HMI group showed an accelerating alpha1 brain rhythm pattern in the frontal (F7, p = 0.027; F8, p = 0.048), central (C3, p = 0.047), and temporal regions (T6, p = 0.036) decreased more than in the controls whereas the relative beta1 band in the frontal region (F3, p = 0.047) increased more in the HMI than in the control group. The functional connectivity analysis showed an increase in the iCoh of the alpha1 band in the HMI group compared to the control group (Figure 3C). Brain network analysis revealed that the characteristic path length of the alpha1 band was decreased in the right supramarginal gyrus (p = 0.009) and left temporal pole area (p = 0.007) in the HMI group compared with the control group (Table 3).

Associations between characteristic path length change and Repeatable Battery for the Assessment of Neuropsychological Status change

The improvement in the RBANS total scale index score was associated with a decrease in the characteristic path length of alpha1 band in the left medial orbitofrontal cortex in the FMI group and in the right posterior central cortex in the HMI group (Table 4). The improvement in the visuoconstruction index score of the RBANS was associated with a decrease in the characteristic path length of the alpha1 band in the left parahippocampal cortex and right frontal pole in the FMI group. There was no association between the change in the characteristic path length of the alpha1 band in each of the 68 ROIs and the change in the index score of other cognitive domains of the RBANS in the FMI group. There was no association between the change in the characteristic path length of the alpha1 band in each of the 68 ROIs and the change in the index score of all five cognitive domains of the RBANS in the HMI group.

Discussion

This is the first study that has used QEEG to investigate functional brain changes following a multidomain lifestyle intervention program to prevent dementia. This study found that the intervention group exhibited increases in the iCoh of the alpha1 band and in the relative power of the beta1 band and the absolute power of the beta3 band as well as a decrease in the characteristic path length of alpha1 band compared to the controls. Additionally, a negative association between changes of the RBANS total scale index score and changes in the characteristic path length of the alpha1 band was shown in the FMI and HMI groups, respectively.

The increased iCoh of the alpha1 band in the intervention group may be an important biological marker for improved cognition after a 24-week multidomain lifestyle intervention program. Coherence is a measure of the degree of synchronization among EEG signals from different brain regions (Hogan et al., 2003), and the iCoh has been interpreted as a measure of brain connectivity (Nolte et al., 2004).

frontiers | Research Topics

Improving memory deficits in alzheimer's disease

Edited by
Ralf J. Braun, Fushun Wang, Valentina Echeverria Moran and Shijun Xu

Published in
Frontiers in Aging Neuroscience

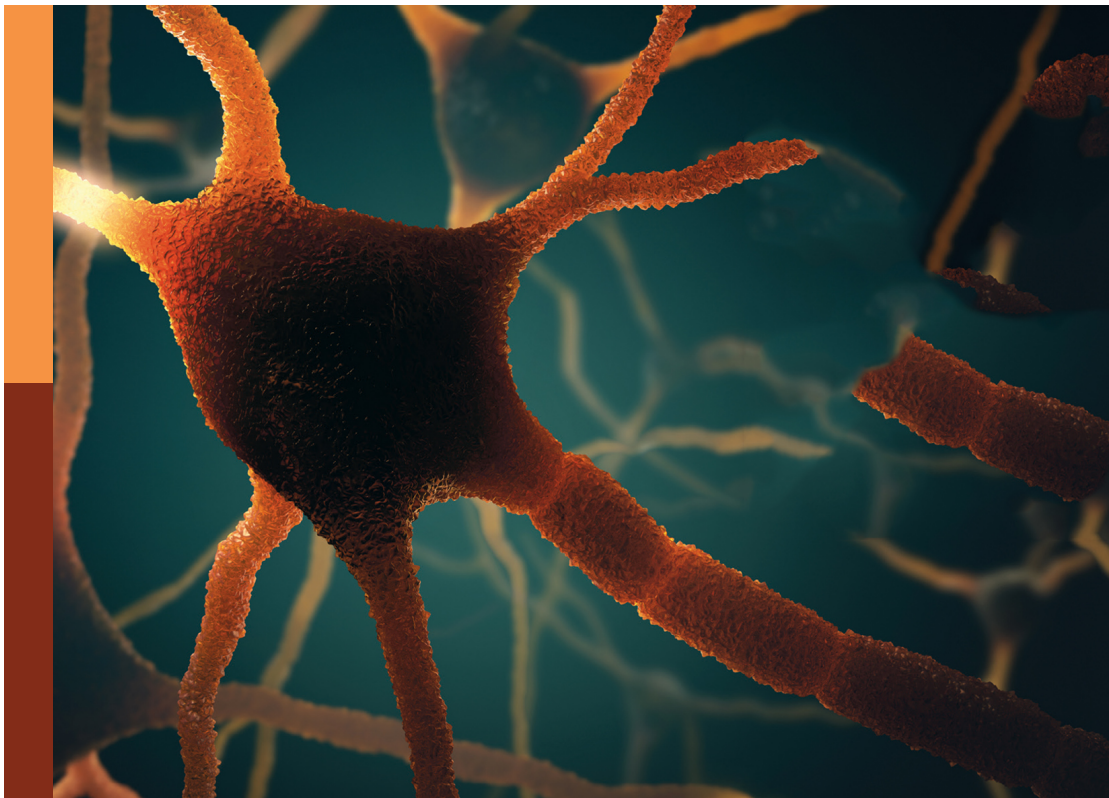

TABLE 4 Associations between changes in the characteristic path length of alpha1 band and changes in the Repeatable Battery for the Assessment of Neuropsychological Status in each intervention group.

	FMI group		HMI group
	RBANS total scale index score	Visuoconstruction index score	RBANS total scale index score
Lt. Medial orbitofrontal cortex	−0.057 (−0.086 ∼ -0.029) $p < 0.001$*	−0.022 (−0.040 ∼ -0.003) $p = 0.022$	0.003 (−0.017 ∼ 0.024) $p = 0.753$
Lt. Inferior parietal cortex	−0.009 (−0.043 ∼ 0.025) $p = 0.593$	−0.008 (−0.027 ∼ 0.011) $p = 0.407$	0.027 (0.008 ∼ 0.045) $p = 0.005$*
Lt. parahippocampal cortex	−0.010 (−0.022 ∼ 0.002) $p = 0.106$	−0.010 (−0.016 ∼ -0.003) $p = 0.004$*	0.007 (−0.003 ∼ 0.016) $p = 0.175$
Rt. Frontal pole	−0.032 (−0.077 ∼ 0.014) $p = 0.171$	−0.035 (−0.060 ∼ -0.010) $p = 0.007$*	0.020 (−0.026 ∼ 0.066) $p = 0.377$
Rt. Posterior central cortex	0.001 (−0.023 ∼ 0.026) $p = 0.919$	0.003 (−0.011 ∼ 0.017) $p = 0.653$	−0.019 (−0.035 ∼ -0.003) $p = 0.002$*

Values are shown as b (95% CI). *P*-value was calculated by linear regression analysis adjusted for age, sex, and education.
*Statistically significant after controlling the false discovery rate. RBANS, Repeatable Battery for the Assessment of Neuropsychological Status; FMI, facility-based multidomain intervention; HMI, home-based multidomain intervention; Rt., right; Lt., left.

Increased iCoh of the alpha1 band in this study implied increased connectivity of the alpha1 band, in contrast to earlier findings showing a reduction in alpha coherence in AD patients (Locatelli et al., 1998; Adler et al., 2003; Hogan et al., 2003). AD is a cortical disconnection syndrome, which refers to disruptions of structural and functional connectivity in topographically dispersed brain regions (Brier et al., 2014). In addition, the cholinergic system plays a role in the modulation of intracortical connectivity; therefore, it is not surprising that functional connectivity is disrupted in AD patients with a cholinergic deficit. Furthermore, interhemispheric coherence decreases with advanced age in normal older adults (Duffy et al., 1996; Kikuchi et al., 2000). In this regard, the increased iCoh among at-risk older adults in the intervention group suggested a positive change in functional connectivity and might be associated with improvement in the RBANS total scale index score in the intervention group. The intervention group showed a 5-point increase in the total scale index score of the RBANS and an increase in the iCoh of the alpha1 band. In contrast, the control group showed no change in the same index score and exhibited a decrease in the iCoh similar to that in normal older adults. Therefore, an increase in the iCoh of the alpha1 band may be the earliest change and may serve as a neurophysiological marker, providing evidence for biological effects on cognition in response to a multidomain lifestyle intervention.

The increase in the relative beta1 power and absolute beta3 power may be an electrophysiological marker for improvement in cognition in this study. In AD patients, a decrease in alpha power and beta power as well as an increase in theta power and delta power were shown previously (Garn et al., 2014). Furthermore, relative parietal beta1 power showed a negative correlation with amyloid deposition and a positive correlation with anterograde memory in MCI patients (Musaeus et al., 2018). Decreased relative power in the beta1 band could be a predictive marker for progression in MCI patients (Musaeus et al., 2018). In contrast to previous findings in AD and MCI patients, the present study found increased relative power in the beta1 band in the intervention group, which also showed improvement in the visuoconstruction index score on the RBANS. An increase in beta band power reflects top-down attentional modulation between brain areas by promoting feedback interactions across visual areas (Bastos et al., 2015). In addition, alterations in the beta band are associated with the resting-state EEG default mode network (DMN) (Chen et al., 2008). In this regard, increased power in the beta1 and beta3 bands might suggest functional restoration of the EEG DMN, specifically top-down attentional process.

Also of note is the decrease in the characteristic path length found in the intervention group. Quantitative analysis of complex brain networks is based on graph theory, with brain networks defined as a set of nodes or vertices and the edges or lines between them. When investigating altered features of functional brain networks, EEG provides measurement of neuronal activity with good temporal resolution (Bullmore and Sporns, 2009). AD is characterized by a loss of small-world network characteristics, as seen in the longer characteristic path length (Stam et al., 2007). As path length is defined

by the minimum number of edges, a longer path length represents lower global efficiency. An increase in path length was also shown in MCI patients, and it was negatively correlated with cognitive status (Zeng et al., 2015). In this study, we found a decrease in characteristic path length in the intervention group, but an increased path length in the control group (**Table 3**). This finding implied a positive shift toward the restoration of functional brain networks through the multidomain intervention program, in contrast to a loss of small-world network characteristics in MCI or AD patients from the perspective of a disconnection syndrome.

Finally, results showed a negative association between improvement in cognitive status and a decrease in the characteristic path length of the alpha1 band. Increased global efficiency, measured by the characteristic path length, was associated with an increase in the RBANS total scale index score in each of the FMI and HMI groups. This finding is in line with previous reports showing correlations between EEG parameters and neuropsychological test scores despite of various EEG parameters (Brunovsky et al., 2003; Babiloni et al., 2006). Specifically, the negative correlation between a cognitive marker and a marker of global efficiency in this study contrasts with previous findings showing a positive correlation between small-worldness and Montreal Cognitive Assessment scores in MCI and AD patients (Frantzidis et al., 2014; Zeng et al., 2015), suggesting the functional restoration of network organization as cognition improves.

This study has some limitations. First, a 24-week period for a multidomain lifestyle intervention program may be too short to confirm changes in EEG parameters. This study did not find an increase in the alpha band or a decrease in the delta or theta band. However, despite the intervention program's short duration, an increase in the iCoh of the alpha1 band and a decrease in the characteristic path length of the alpha1 band in the intervention group suggested very early changes in neurophysiological markers following a lifestyle modification program. Second, this study was originally planned as a feasibility study with a small sample size in contrast to previous multidomain intervention studies with large sample sizes. The small sample size may underestimate the positive results of this study when we assess the biological effects of a multidomain intervention study to prevent dementia. However, the sample size in this study was comparable to that of previous studies of single or combined intervention programs using EEG. Third, this study did not assess biomarkers of AD including amyloid and tau, so information on the subjects' pathologic status was not available. The biological changes in EEG parameters after the intervention program might vary according to pathologic status. For example, subjects with preclinical AD might be less likely to show functional changes after an intervention program than would normal older adults without amyloid deposition. Fourth, there were more participants in the control group for whom follow-up EEG was not performed than in the intervention group. It is possible that this may have influenced the study results. However, since the participants excluded from the EEG analysis in the control group were older, it is likely that it may have a more favorable effect on the results of the control group, and it is not likely that it affected the false positives of the results of this study. Additionally, the results of comparing changes in the characteristic path length of the alpha1 band between the intervention and control groups after excluding missing data were similar to those in the analysis after multiple imputation for missing data.

In summary, this study is the first study to show positive functional brain changes using QEEG after a 24-week multidomain lifestyle intervention to prevent dementia. The increased iCoh and the decreased characteristic path length of the alpha1 band in the intervention group implied increased functional brain networks with higher global efficiency following a lifestyle intervention program in at-risk older adults. Further studies with larger sample sizes and/or a longer period of intervention are needed to confirm the findings of this study.

Data availability statement

Anonymized data used in this work will be available from the corresponding authors upon request.

Ethics statement

The studies involving human participants were reviewed and approved by Inha University Hospital Institutional Review Board (IRB)(INHAUH-2018-11-022), Ewha Womans University Mokdong Hospital IRB (EUMC-2019-04-013), Ajou University Hospital IRB (AJIRB-BMR-SUR-19-070 and AJIRB-BMR-SUR-19-077), Dong-A University Hospital IRB (DAUHIRB-19-078), Chonnam National University IRB (CNUH-2019-139). The patients/participants provided their written informed consent to participate in this study.

Author contributions

HKP, SHChoi, SK, SWK, HRN, and YKP contributed to the study concept and design. HKP, SHChoi, JHJ, SYM, CHH, MC, H-SS, B-OC, SML, KWP, BCK, SHCho, HRN, and YKP participated in data collection and processing. HKP, SHChoi, SK, and UP performed the statistical analysis. HKP, SHChoi, SK, SWK, HRN, and YKP contributed to the analysis and interpretation of data and wrote the manuscript. All authors

participated in the critical revision of the manuscript and final approval of the version.

Funding

This research was supported by grants from the Korea Health Technology R&D Project through the Korea Health Industry Development Institute (KHIDI) and Korea Dementia Research Center (KDRC), funded by the Ministry of Health & Welfare and Ministry of Science and ICT (MSIT), Republic of Korea (HU21C0016) and from the National Research Council of Science & Technology (NST) Aging Convergence Research Center (CRC22011-600), the National Research Foundation of Korea (NRF) (NRF-2018M3A9F1023697), and the Institute of Information & communications Technology Planning & Evaluation (IITP) (No. 2022-0-00448) funded by the Korea government (MSIT).

Conflict of interest

Author SYM receives a research grant from Hyundai Pharmaceutical Co. Ltd. Author CHH receives research support from Eisai Korea Inc. Author JHJ receives research grants from Chong Kun Dang Pharmaceutical Corp., Jeil Pharmaceutical Co. Ltd., and Kuhnil Pharmaceutical Co. Ltd., and consults for PeopleBio Co. Ltd. Authors SYM, CHH, JHJ, YKP, HRN, and SHChoi are shareholders of Rowan Inc. Author HRN consults for Hyundai Pharmaceutical Co. Ltd. Author SHChoi consults for Hyundai Pharmaceutical Co. Ltd., and PeopleBio Co. Ltd. Authors SK, UP, and SWK received a salary from iMediSync Inc.

The remaining authors declare that the research was conducted in the absence of any commercial or financial relationships that could be construed as a potential conflict of interest.

Publisher's note

All claims expressed in this article are solely those of the authors and do not necessarily represent those of their affiliated organizations, or those of the publisher, the editors and the reviewers. Any product that may be evaluated in this article, or claim that may be made by its manufacturer, is not guaranteed or endorsed by the publisher.

Supplementary material

The Supplementary Material for this article can be found online at: https://www.frontiersin.org/articles/10.3389/fnagi.2022.892590/full#supplementary-material

References

Adler, G., Brassen, S., Chwalek, K., Dieter, B., and Teufel, M. (2004). Prediction of treatment response to rivastigmine in Alzheimer's dementia. *J. Neurol. Neurosurg. Psychiatry* 75, 292–294.

Adler, G., Brassen, S., and Jajcevic, A. (2003). EEG coherence in Alzheimer's dementia. *J. Neural Transm.* 110, 1051–1058. doi: 10.1007/s00702-003-0024-8

Andrieu, S., Guyonnet, S., Coley, N., Cantet, C., Bonnefoy, M., Bordes, S., et al. (2017). Effect of long-term omega 3 polyunsaturated fatty acid supplementation with or without multidomain intervention on cognitive function in elderly adults with memory complaints (MAPT): A randomised, placebo-controlled trial. *Lancet Neurol.* 16, 377–389. doi: 10.1016/S1474-4422(17)30040-6

Babiloni, C., Carducci, F., Lizio, R., Vecchio, F., Baglieri, A., Bernardini, S., et al. (2013). Resting state cortical electroencephalographic rhythms are related to gray matter volume in subjects with mild cognitive impairment and Alzheimer's disease. *Hum. Brain Mapp.* 34, 1427–1446. doi: 10.1002/hbm.22005

Babiloni, C., Del Percio, C., Boccardi, M., Lizio, R., Lopez, S., Carducci, F., et al. (2015). Occipital sources of resting-state alpha rhythms are related to local gray matter density in subjects with amnesic mild cognitive impairment and Alzheimer's disease. *Neurobiol. Aging* 36, 556–570. doi: 10.1016/j.neurobiolaging.2014.09.011

Babiloni, C., Frisoni, G., Steriade, M., Bresciani, L., Binetti, G., Del Percio, C., et al. (2006). Frontal white matter volume and delta EEG sources negatively correlate in awake subjects with mild cognitive impairment and Alzheimer's disease. *Clin. Neurophysiol.* 117, 1113–1129. doi: 10.1016/j.clinph.2006.01.020

Babiloni, C., Frisoni, G. B., Pievani, M., Vecchio, F., Lizio, R., Buttiglione, M., et al. (2009). Hippocampal volume and cortical sources of EEG alpha rhythms in mild cognitive impairment and Alzheimer disease. *Neuroimage* 44, 123–135. doi: 10.1016/j.neuroimage.2008.08.005

Bastos, A. M., Vezoli, J., Bosman, C. A., Schoffelen, J., Oostenveld, R., Dowdall, J. R., et al. (2015). Visual areas exert feedforward and feedback influences through distinct frequency channels. *Neuron* 85, 390–401. doi:10.1016/j.neuron.2014.12.018

Benjamini, Y., and Hochberg, Y. (1995). Controlling the false discovery rate: A practical and powerful approach to multiple testing. *J. R. Stat. Soc. Ser. B Methodol.* 57, 289–300. doi: 10.1111/j.2517-6161.1995.tb02031.x

Brier, M. R., Thomas, J. B., and Ances, B. M. (2014). Network dysfunction in Alzheimer's disease: Refining the disconnection hypothesis. *Brain Connect.* 4, 299–311. doi: 10.1089/brain.2014.0236

Brunovsky, M., Matousek, M., Edman, A., Cervena, K., and Krajca, V. (2003). Objective assessment of the degree of dementia by means of EEG. *Neuropsychobiology* 48, 19–26. doi: 10.1159/000071824

Bullmore, E., and Sporns, O. (2009). Complex brain networks: Graph theoretical analysis of structural and functional systems. *Nat. Rev. Neurosci.* 10, 186–198.

Chen, A. C., Feng, W., Zhao, H., Yin, Y., and Wang, P. (2008). EEG default mode network in the human brain: Spectral regional field powers. *Neuroimage* 41, 561–574. doi: 10.1016/j.neuroimage.2007.12.064

Chin, J., Park, J., Yang, S. J., Yeom, J., Ahn, Y., Baek, M. J., et al. (2018). Re-standardization of the Korean-instrumental activities of daily living (K-IADL): Clinical usefulness for various neurodegenerative diseases. *Dement. Neurocogn. Disord.* 17, 11–22. doi: 10.12779/dnd.2018.17.1.11

Duffy, F. H., Mcanulty, G. B., and Albert, M. S. (1996). Effects of age upon interhemispheric EEG coherence in normal adults. *Neurobiol. Aging* 17, 587–599. doi: 10.1016/0197-4580(96)00007-3

Engels, M., Stam, C. J., van der Flier, W. M., Scheltens, P., de Waal, H., et al. (2015). Declining functional connectivity and changing hub locations in

Alzheimer's disease: An EEG study. *BMC Neurol.* 15:145. doi: 10.1186/s12883-015-0400-7

Frantzidis, C. A., Vivas, A. B., Tsolaki, A., Klados, M. A., Tsolaki, M., and Bamidis, P. D. (2014). Functional disorganization of small-world brain networks in mild Alzheimer's disease and amnestic mild cognitive impairment: An EEG study using relative wavelet entropy (RWE). *Front. Aging Neurosci.* 6:224. doi: 10.3389/fnagi.2014.00224

Gandelman-Marton, R., Aichenbaum, S., Dobronevsky, E., Khaigrekht, M., and Rabey, J. M. (2017). Quantitative EEG after brain stimulation and cognitive training in Alzheimer disease. *J. Clin. Neurophysiol.* 34, 49–54. doi: 10.1097/WNP.0000000000000301

Garn, H., Waser, M., Deistler, M., Schmidt, R., Dal-Bianco, P., Ransmayr, G., et al. (2014). Quantitative EEG in Alzheimer's disease: Cognitive state, resting state and association with disease severity. *Int. J. Psychophysiol.* 93, 390–397. doi: 10.1016/j.ijpsycho.2014.06.003

Gianotti, L. R., Künig, G., Faber, P. L., Lehmann, D., Pascual-Marqui, R. D., Kochi, K., et al. (2008). Rivastigmine effects on EEG spectra and three-dimensional LORETA functional imaging in Alzheimer's disease. *Psychopharmacology* 198, 323–332. doi: 10.1007/s00213-008-1111-1

Han, S., Pyun, J., Yeo, S., Kang, D. W., Jeong, H. T., Kang, S. W., et al. (2021). Differences between memory encoding and retrieval failure in mild cognitive impairment: Results from quantitative electroencephalography and magnetic resonance volumetry. *Alzheimers Res. Ther.* 13:3. doi: 10.1186/s13195-020-00739-7

Hassan, M., Dufor, O., Merlet, I., Berrou, C., and Wendling, F. (2014). EEG source connectivity analysis: From dense array recordings to brain networks. *PLoS One* 9:e105041. doi: 10.1371/journal.pone.0105041

Hogan, M. J., Swanwick, G. R., Kaiser, J., Rowan, M., and Lawlor, B. (2003). Memory-related EEG power and coherence reductions in mild Alzheimer's disease. *Int. J. Psychophysiol.* 49, 147–163. doi: 10.1016/s0167-8760(03)00118-1

Huang, P., Fang, R., Li, B., and Chen, S. (2016). Exercise-related changes of networks in aging and mild cognitive impairment brain. *Front. Aging Neurosci.* 8:47. doi: 10.3389/fnagi.2016.00047

Jelic, V., Blomberg, M., Dierks, T., Basun, H., Shigeta, M., Julin, P., et al. (1998). EEG slowing and cerebrospinal fluid tau levels in patients with cognitive decline. *Neuroreport* 9, 157–160.

Jeong, J. (2004). EEG dynamics in patients with Alzheimer's disease. *Clin. Neurophysiol.* 115, 1490–1505.

Kikuchi, M., Wada, Y., Koshino, Y., Nanbu, Y., and Hashimoto, T. (2000). Effect of normal aging upon interhemispheric EEG coherence: Analysis during rest and photic stimulation. *Clin. Electroencephalogr.* 31, 170–174. doi: 10.1177/155005940003100404

Kogan, E. A., Korczyn, A. D., Virchovsky, R. G., Klimovizky, S. S., Treves, T. A., and Neufeld, M. Y. (2001). EEG changes during long-term treatment with donepezil in Alzheimer's disease patients. *J. Neural Transm.* 108, 1167–1173. doi: 10.1007/s007020170006

Lejko, N., Larabi, D. I., Herrmann, C. S., Aleman, A., and Ćurčić-Blake, B. (2020). Alpha power and functional connectivity in cognitive decline: A systematic review and meta-analysis. *J. Alzheimers Dis.* 78, 1047–1088. doi: 10.3233/JAD-200962

Liu, J., Li, M., Pan, Y., Lan, W., Zheng, R., Wu, F., et al. (2017). Complex brain network analysis and its applications to brain disorders: A survey. *Complexity* 2017:8362741. doi: 10.1155/2017/8362741

Locatelli, T., Cursi, M., Liberati, D., Franceschi, M., and Comi, G. (1998). EEG coherence in Alzheimer's disease. *Electroencephalogr. Clin. Neurophysiol.* 106, 229–237. doi: 10.1016/S0013-4694(97)00129-6

Moon, S. Y., Hong, C. H., Jeong, J. H., Park, Y. K., Na, H. R., Song, H., et al. (2021). Facility-based and home-based multidomain interventions including cognitive training, exercise, diet, vascular risk management, and motivation for older adults: A randomized controlled feasibility trial. *Aging* 13:15898. doi: 10.18632/aging.203213

Musaeus, C. S., Nielsen, M. S., Østerbye, N. N., and Høgh, P. (2018). Decreased parietal beta power as a sign of disease progression in patients with mild cognitive impairment. *J. Alzheimers Dis.* 65, 475–487. doi: 10.3233/JAD-180384

Ngandu, T., Lehtisalo, J., Solomon, A., Levälahti, E., Ahtiluoto, S., Antikainen, R., et al. (2015). A 2 year multidomain intervention of diet, exercise, cognitive training, and vascular risk monitoring versus control to prevent cognitive decline in at-risk elderly people (FINGER): A randomised controlled trial. *Lancet* 385, 2255–2263. doi: 10.1016/S0140-6736(15)60461-5

Nolte, G., Bai, O., Wheaton, L., Mari, Z., Vorbach, S., and Hallett, M. (2004). Identifying true brain interaction from EEG data using the imaginary part of coherency. *Clin. Neurophysiol.* 115, 2292–2307. doi: 10.1016/j.clinph.2004.04.029

Park, H. K., Jeong, J. H., Moon, S. Y., Park, Y. K., Hong, C. H., Na, H. R., et al. (2020). South Korean study to prevent cognitive impairment and protect brain health through lifestyle intervention in at-risk elderly people: Protocol of a multicenter, randomized controlled feasibility trial. *J. Clin. Neurol.* 16, 292–303. doi: 10.3988/jcn.2020.16.2.292

Roh, J. H., Park, M. H., Ko, D., Park, K., Lee, D., Han, C., et al. (2011). Region and frequency specific changes of spectral power in Alzheimer's disease and mild cognitive impairment. *Clin. Neurophysiol.* 122, 2169–2176. doi: 10.1016/j.clinph.2011.03.023

Rubinov, M., and Sporns, O. (2010). Complex network measures of brain connectivity: Uses and interpretations. *Neuroimage* 52, 1059–1069. doi: 10.1016/j.neuroimage.2009.10.003

Smailovic, U., and Jelic, V. (2019). Neurophysiological markers of Alzheimer's disease: Quantitative EEG approach. *Neurol. Ther.* 8, 37–55. doi: 10.1007/s40120-019-00169-0

Smailovic, U., Koenig, T., Kåreholt, I., Andersson, T., Kramberger, M. G., Winblad, B., et al. (2018). Quantitative EEG power and synchronization correlate with Alzheimer's disease CSF biomarkers. *Neurobiol. Aging* 63, 88–95. doi: 10.1016/j.neurobiolaging.2017.11.005

Stam, C. J., Jones, B. F., Nolte, G., Breakspear, M., and Scheltens, P. (2007). Small-world networks and functional connectivity in Alzheimer's disease. *Cereb. Cortex* 17, 92–99. doi: 10.1093/cercor/bhj127

Stephen, R., Liu, Y., Ngandu, T., Antikainen, R., Hulkkonen, J., Koikkalainen, J., et al. (2019). Brain volumes and cortical thickness on MRI in the Finnish geriatric intervention study to prevent cognitive impairment and disability (FINGER). *Alzheimers Res. Ther.* 11:53.

van Buuren, S., and Groothuis-Oudshoorn, K. (2011). mice: Multivariate imputation by chained equations in R. *J. Stat. Softw.* 45, 1–67.

Xia, M., Wang, J., and He, Y. (2013). BrainNet Viewer: A network visualization tool for human brain connectomics. *PLoS One* 8:e68910. doi: 10.1371/journal.pone.0068910

Zeng, K., Wang, Y., Ouyang, G., Bian, Z., Wang, L., and Li, X. (2015). Complex network analysis of resting state EEG in amnestic mild cognitive impairment patients with type 2 diabetes. *Front. Comput. Neurosci.* 9:133. doi: 10.3389/fncom.2015.00133

Frontiers in
Aging Neuroscience

Explores the mechanisms of central nervous system aging and age-related neural disease

The third most-cited journal in the field of geriatrics and gerontology, with a focus on understanding the mechanistic processes associated with central nervous system aging.

Discover the latest Research Topics

See more →

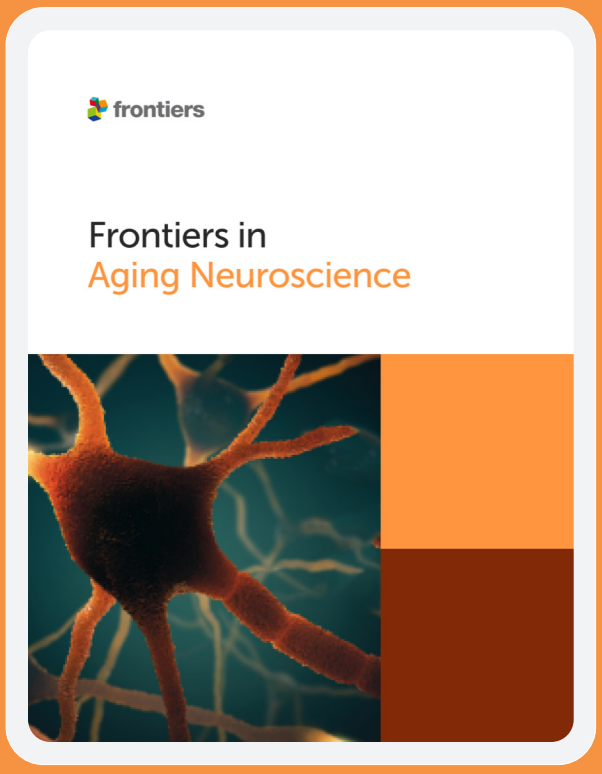

Frontiers

Avenue du Tribunal-Fédéral 34
1005 Lausanne, Switzerland
frontiersin.org

Contact us

+41 (0)21 510 17 00
frontiersin.org/about/contact